Avancées en chimie de coordination des phosphines nitroaromatiques : synthèse et chimie supramoléculaire de dérivés alkyl - aryl-carbo-benzènes

Chongwei Zhu

Université Fédérale

Toulouse Midi-Pyrénées

THÈSE

En vue de l'obtention du

DOCTORAT DE L'UNIVERSITÉ DE TOULOUSE

Délivré par :

Université Toulouse 3 Paul Sabatier (UT3 Paul Sabatier)

Présentée et soutenue par :
Chongwei ZHU
le jeudi 14 décembre 2017

Titre :

Advances in the coordination chemistry of nitroaromatic phosphines; synthesis and supramolecular chemistry of alkyl/aryl *carbo*-benzene derivatives

---

École doctorale et discipline ou spécialité :
ED SDM : Chimie organométallique de coordination - CO 043

Unité de recherche :
Laboratoire de Chimie de Coordination (UPR 8241)

Directeur/trice(s) de Thèse :

Valérie MARAVAL, Remi CHAUVIN

Jury :

Prof. Mogens Brøndsted NIELSEN,	Professeur, University of Copenhagen, Copenhagen,	**Rapporteur**
Dr. Irena STARA,	Institute of Organic Chemistry and Biochemistry, Prague,	**Rapporteur**
Dr. Philippe BLANCHARD,	Directeur de recherche, Université d'Angers, Angers,	**Examinateur**
Dr. Suzanne FERY-FORGUES,	Directeur de recherche, Université Paul Sabatier, Toulouse,	**Examinateur**
Dr. Valérie MARAVAL,	Ingénieur de recherche, CNRS, LCC, Toulouse,	**Co-Directrice**
Prof. Remi CHAUVIN,	Professeur, Université Paul Sabatier, LCC, Toulouse,	**Directeur**
Prof. Xiuling CUI	Professeur, Huaqiao University, Zhengzhou University,	**Invité**
Dr. Emmanuel GRAS	Chargé de Recherche, CNRS, LCC, Toulouse,	**Invité**

Table of Contents

Acknowledgment

Acknowledgment

Time flies so quickly, after an intensive period of thirty-nine months, my PhD career has quietly come to an end. Over the past three years, I gained tremendous acknowledge in chemistry, my experimental skill and research ability were also significantly improved. Undoubtedly, it would not be possible to conduct my research and complete my dissertation without these people who have supported and helped so much during this period. Take this opportunity, I want here to thank all of you for your great help, and the good time we spent together.

Foremost, I would first like to express my sincerest gratitude to my supervisors Dr. Valérie MARAVAL and Prof. Remi CHAUVIN for your greatest support of my PhD study and research. The door of your office was always open for us whenever I ran into trouble or had any question not only in research, but sometimes also in life.

Without you, Valérie, this thesis would not have been completed or written. Your appearance always brought me energy and hope, especially in my most difficult time when working on *carbo*-mer chemistry in the beginning and writing this thesis. I really enjoyed the time working with you, your excited expression when we determined new final products or analyzed their structures of single crystals together, deeply impressed and greatly encouraged me. At that moment, I definitely realized that research brought us happiness, I am particularly grateful to you for everything that you have done for me.

Prof. Remi Chauvin, you are one of the greatest chemist in the world, your motivation for

chemistry, enthusiasm for people, immense knowledge and meticulous working attitude have had a profound impact on me. I have learnt so much from and because of you, you always can enlighten me when I encountered difficulties. I sincerely thank you for your guidance and helping me grow as a research chemist. It has been my honor to be your PhD student.

Additionally, I would like to acknowledge my thesis committee members: Prof. Mogens Brøndsted NIELSEN (University of Copenhagen, Denmark), Dr. Irena STARA (Institute of Organic Chemistry and Biochemistry, Czech Republic), Dr. Philippe BLANCHARD (Universite d'Angers, France), Dr. Suzanne FERY-FORGUES (Université Paul Sabatier, France), Prof. Xiuling CUI (invited people, Huaqiao University and Zhengzhou University, China), and Dr. Emmanuel GRAS (invited people, LCC-CNRS, France) for their time, their encouragement, and insightful comments, which broaden my horizons in the future research.

I would like to thank the other past and present group members: Dr. Y. CANAC, many thanks to you for your help in my first year; Dr. C. LEPETIT, thank you for your concern in my first year; Prof. V. BERNARDES-GENISSON, you are a very kind lady, I always feel warm when seeing you; C. BARTHES, you always answered very patiently my questions whatever any question I asked, thank you so much for what you have done for me; K. COCQ, you are the King in *carbo*-mer chemistry, at least in my opinion. Thank you very much for sharing your experience with me and your pertinent suggestion for me; C. POIDEVIN, thank you for taking me to visit city center of Toulouse when I arrived here, and your French lesson to me despite some bad words sometimes; D. LISTUNOV, although you look serious sometimes, you are a good chemistry and warm-hearted

person, many thanks to you for discussion with me; C. D. MBOYI and A. MANKOU, You are really nice people, and helped me a lot in my first year, many thanks to both of you; M. CHAMMAM, thank you for what you have done for me, especially in my defense recently; E. M. CARVALHO, thanks for your help, man.

My appreciation also goes to our collaborators: Dr. E. GRAS, who works at LCC in Toulouse, supervised me as a co-supervisor in my first year and gave me a great support, I whole-heartedly appreciate you. Also, I want to thank Prof. H. F. HSU for the measurements of DSC, POM and PXRD experiments in Taiwan, Prof. Chun-hsien Chen for conducting STM measurement in Taiwan in *carbo*-mesogen project, Dr. A. POATER for performing the calculation for *carbo*-OPEs in Spain, Prof. J. L. MALDONADO for exploring of OPV application in Mexico.

I am also indebted to the following crystallographers: Dr. C. DUHAYON, it is so nice of you, you got involved in all the measurements and analyses of single crystals in my PhD career, I very much appreciate you. Dr. B. KAUFFMANN, who is from Bordeaux, my paper would not have been possible to be published without the high-quality data of single crystals. My appreciation also goes to Dr. N. SAFFON for attempts at picking single crystals.

I am hugely appreciative to Dr. A. SAQUET for electrochemical measurements of all the molecules in *carbo*-mer research.

I would like to thank Dr. Y. COPPEL for launching solid NMR experiment and helping resolve NMR spectra, and Dr. C. BIJANI for NMR measurements by using 500 MHz and 600

MHz spectrometer, and F. LACASSIN for carrying out ^{103}Rh NMR experiments for the Rh^{I} complexes in the first chapter of this manuscript.

Special mention goes to my M.sc supervisor Prof. X. L. CUI for coming to my defense from the distant China.

I am grateful for conversations with the following people: O. SADEK, S. AYALA-MARISCAL, A. POCINHO, W. KHODJA, A. FERNANDEZ-ALVAREZ, C. ZHANG, X. D. LIN, L. CHEN, J. R. QIU, Y. P. WANG, who all work at LCC. Many thanks also go to my friends in Toulouse: L. Q. LANG, Q. LIAO, J. H. WANG, Z. H. ZHAO, you made my free time enjoyable by playing cards and eating together at weekends.

I also want to thank LCC (CNRS) for providing a safe and comfortable workplace, and UPS for offering us various interesting and useful courses and training.

My sincere thanks go to CSC (China Scholarship Council) for my PhD scholarship. The IDEX emergence program 2014 of Toulouse is acknowledged for financial support (*carbo*-device project).

Last but not the least, I would like to thank my family for their unconditional support and encouragement in these years, I haven't been able to find more time to accompany you, in particular for my grandfather, I couldn't go back to see you last time until you left us forever. But I want to say I really love all of you, thank you.

General Introduction

General Introduction

The thesis is divided into two parts corresponding to respective topics currently recognized to rely on distinct experimental specialties, namely phosphorus/organometallic coordination chemistry on one hand (for homogeneous catalysis), and carbon-rich/acetylenic organic chemistry on the other hand (for material physics).

The two topics being long studied in parallel in the group, a research priority change in 2016 (basically for budgetary reasons) gave the opportunity to address both of them sequentially, after completion of a first study: one year on organometallics (2015), then two years on acetylenics (2016-2017). Hence the thesis content plan, made of six chapters separated into two parts of unequal lengths: one chapter *vs* five chapters, respectively.

The research versatility, formally justified by the universal "soft variations across the Periodic Table", is practically based on general common points, namely molecular synthesis with similar bench techniques (from the use of a vacuum line and Schlenk tubes to liquid-liquid extraction and column chromatography) and identical analysis methods (NMR spectroscopy in solution, IR and UV-vis absorption spectroscopy, mass spectrometry, single crystal X-ray diffractometer…).

Each chapter of the thesis is hinged around one or two published articles or (to be) submitted manuscripts reproduced as such and preceded by an introduction of the context and a summary of results.

The first part relying on general phosphorus-organometallic chemistry (Chapter 1) is deemed within the context of ligand design with the general ambition of proposing "new types" of ligands for specific applications in homogeneous catalysis. The challenge is particularly addressed in the family of weakly electron-donating ligands of redox-flexible late transition metals most frequently encountered in homogeneous pre-catalysts (Ru, Rh, Pd...), with a focus on electron-poor phosphines towards Rh(I) Lewis acidic centers. While in the family of highly electron-rich ligands, enhancement of σ-donation has long been claimed to vary in the order trialkylphosphines < aminocarbenes < phosphonium ylides in the neutral series (L or X^+),[1] followed by alkynyls < aryls < alkyls or yldiides in the anionic series (X),[2] the trend in the family of electron-poor ligands has attracted less attention and is today both more restricted and less delineated.[3] Nevertheless, the opposite order can be outlined in the P-aryl series: triarylphosphines > phosphinous esters (phosphinites) > phosphonous diesters

(phosphinites) > phosphorous triesters (posphites) ≈ fluoroarylphosphines ≈ amidi*no*phosphines (e.g. imidazo*lo*phosphines) >> imidazo*lio*phosphines.[4] The latter gap is made worth to be filled because of the thermal lability of the P-imidazolium bond in the presence of weak nucleophiles (e.g. Cl^-), preventing the use of imidazoliophosphines in catalysis.[5] As further P-impoverishment of imidazolophosphines was considered, e.g. by fluorination, one became aware that nitroaryl-phosphines were barely exemplified and their coordination chemistry unexplored. Exploration was thus initiated on the basis of a general research program in partnership with Prof. Xiuling Cui in Xiamen, China, then carried out in cooperation with Dr. Emmanuel Gras at LCC in Toulouse.

In Chapter 1,[6] challenging also the forgotten coordination of nitroaromatic phosphine ligands, N-aryl benzimidazolodiphenylphosphines nitrated at various position of the aryl and/or benzimidazolyl substituents were targeted both in the free state and as Rh(I) P-ligands (Figure 1). The global π-back donating ability of the target ligands in RhCl(CO) complexes **1a** was envisaged to be quantifiable by complementary analytical probes, i.e. the ^{103}Rh NMR shielding and the CO stretching frequency (as by the Tolman's electronic parameter from $Ni(CO)_3$ complexes).[7] The unveiled trends will be presented, along with unexpected observations and serendipity results in solvate crystallo-chemistry of dinuclear complexes **1b**.

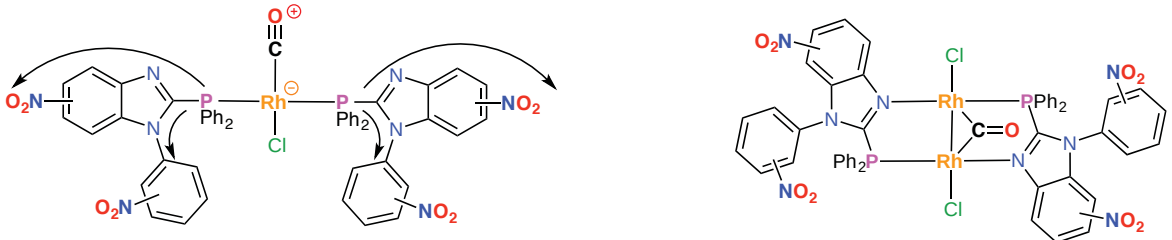

Figure 1. Devised or turned out targets of Part 1 (Chapter 1).

The second part relying on general acetylenic chemistry (Chapters 2-6) is deemed within the more general context of the chemistry of cumulene-containing macro-aromatics,[8] in particular of *carbo*-meric nature such as *carbo*-benzenes,[9] with the view to providing new fundamental knowledges and prospects of applications of *carbo*-benzene derivatives as "materials". More precisely, efforts have been dedicated to bring out the role of *supra-molecular* interactions in either local host-guest complexes or long-range *self-assemblies* of *carbo*-benzene derivatives in the broad sense. Long-range *covalent cohesion* in oligomeric

chains of *carbo*-benzene wires has also been considered. Selected targets were thus devised by combination of mental processes such as "lipidic functionalization", "homo-de-aromatizing pericondensation", and catenation (Figure 2).

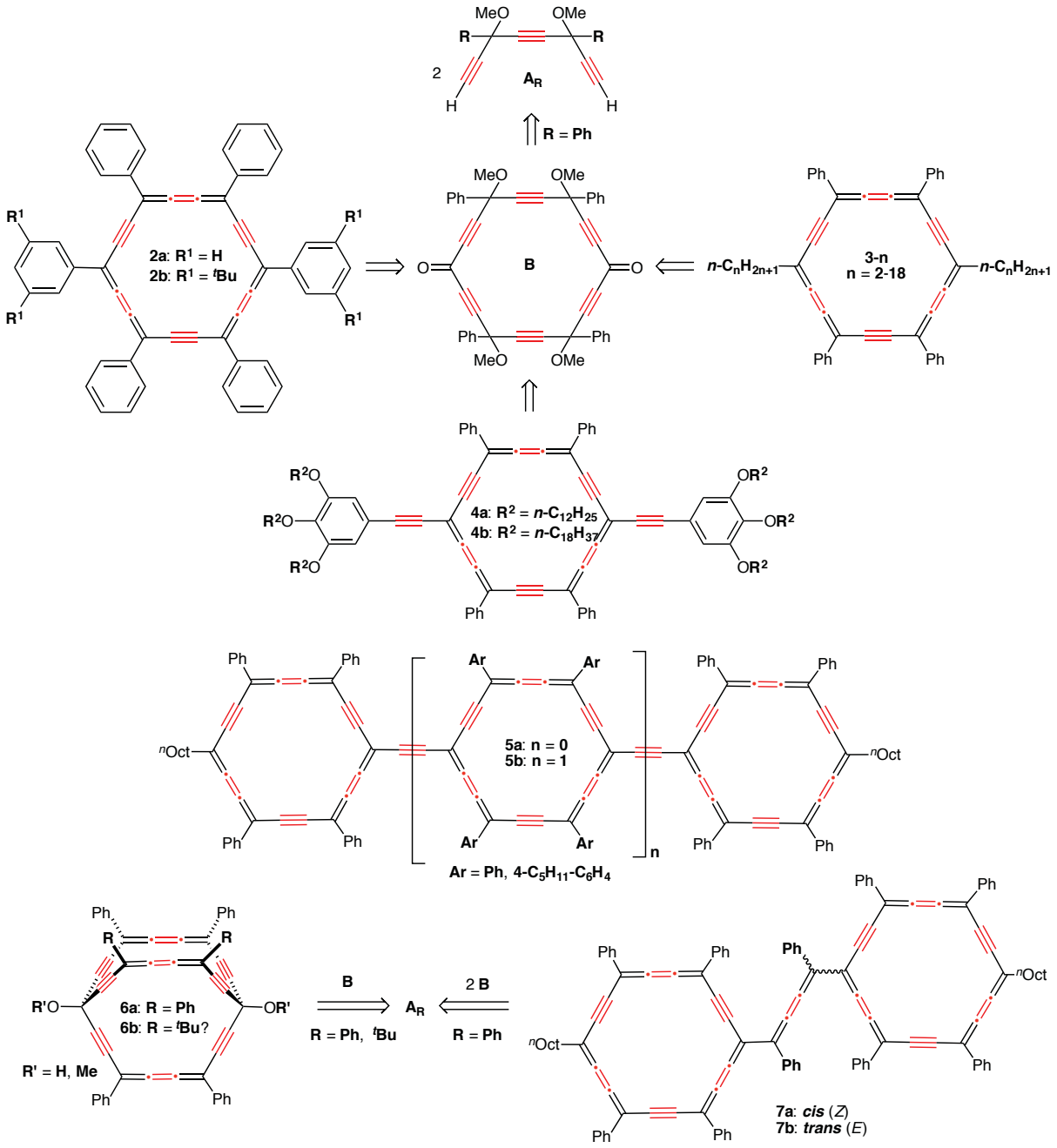

Figure 2. Targets of Part 2 (Chapters 2-6).

The first chapter (Chapter 2)[10] resumes, refines and completes characterizations of hexaaryl-*carbo*-benzenes **2**, in particular the hexaphenyl-*carbo*-benzene benchmark, regarding the efficiency of their synthesis, here carried out from the key bis-terminal triyne

$\mathbf{A_{Ph}}$ and [6]pericyclynedione **B**, [11] intrinsic solubility, structural, spectroscopical and electrochemical properties, or thin-film deposition propensity with the view to designing new donor or acceptor components of futurist photovoltaic junctions in collaboration with Profs José-Luis Maldonado and Gabriel Ramos Ortiz in Leon Guanajuato, Mexico.

In Chapter 3,[12] the limited solubility enhancement effect of alkylaryl substituents at the C_{18} *carbo*-benzene ring is suggested to be overcome by direct anchoring of two *n*-alkyl chains C_nH_{2n+1} with length varying from n = 2 to n = 20 in tetraphenyl derivatives **3**, to be from the [6]pericyclynedione **B**. In the lipidic series ($n \geq 8$), dispersive interactions between chains centro-symmetrically positioned at *para* positions could also be anticipated to drive another type of non-covalent interaction, namely the long sought direct π-π stacking between C_{18} rings, the theoretically evidenced cohesion force of the "graphityne" 3D carbon allotrope (the *carbo*-mer of graphite), having hitherto escaped the observation, even in the crystal state.

In Chapter 4, [13] "hyper-lipidic" *carbo*-benzenes of type **4**, bearing six dodecyl or octadecyl aliphatic chains and *a priori* accessible from the [6]pericyclynedione **B**, are considered for their possible mesogenic properties in discotic liquid crystals (LCs). Columnar arrangements of the hollow and rigid C_{18} mesogenic core would allow hosting molecules, salts or metal atoms, that would keep longitudinal mobility within the channels, opening prospects for axial charge transport upon doping with metallic species. Regarding the LC cohesion, the lateral dispersive interactions between the putative columns could be studied by STM imaging after freezing the flexible chains on an ordered surface of HOPG (Highly Oriented Pyrolytic Graphite). The work has been undertaken in collaboration with Taiwanese partners in Taipei, Prof. Hsiu-Fu Hsu, leading specialist in the field of liquid crystals, and Prof. Chun-hsien Chen renowned expert in STM imaging.

In Chapter 5[14] are envisaged *carbo*-meric versions of the oligophenylethynylene wires, ubiquitous in functional organic materials for their unique combination of electronic and conformational steric features. From the nomenclature standpoint, the so-called "*carbo*-OPEs" involving ethynylene tethers between aromatic C_{18} rings are skeletal *carbo*-mers of oligo-*p*-phenylenes (OPPs), starting with *carbo*-biphenyls and *carbo*-terphenyls. With the view to ensuring sufficient solubility for full characterization of the targets, *n*-octyl substituents are placed at the wire ends. Inspired by the widely exemplified efficiency of routes to tetraphenyl-mono-*carbo*-benzenes, retrosynthesis of the two types of objects **5a** and **5b** is based on a sequential catenation of tetraphenyl-hexaoxy[6]pericyclyne units, followed by a one-step total reductive aromatization. On the basis of the anticipated poor solubility of

the dodecaphenylated *carbo*-terphenyl core, an optimized target was devised by changing the four central phenyl parents into four *p*-pentylphenyl groups. After the recently disclosed synthesis and characterization of the first oligo-*carbo*-benzenic molecule, exemplified in the fused mode of a *carbo*-naphthalene,[15] the *carbo*-OPE targets are counterparts in the catenated mode, and *carbo*-terphenyls would be the first examples of molecules containing three carbo-benzene rings. The influence of catenation on the aromatic character of the C_{18} rings, according to the magnetic, structural and energetic criteria, was to be studied by DFT-based computational method, which was performed by Dr. Albert Poater, collaborator in Girona, Spain.

In Chapter 6,[16] other bis-*carbo*-benzenic derivatives are considered, and first of all upon derivation to a "homo-de-aromatized" pericondensed version, occurring in the skeletal *carbo*-mers of barrelene **6** (with two bridgehead sp^3 carbon vertices through which triple homo-conjugation of three adjacent triple bonds can occur). In spite of the large aperture of the three faces defining the inner volume of the elongated triangular bipyramid (of global nonaedral shape), the molecule is expected to act as a potential "porous cage" for H-bond donor hosts (e.g. $NH4^+$) susceptible of interacting with surrounding triple bonds as H-bond acceptors. The devised synthesis and the original idea are based on a cyclizing intramolecular double addition of the key synthon $\mathbf{A_{Ph}}$ or $\mathbf{A_{tBu}}$ to the key [6]pericyclynedione **B**. A naturally competing process is the intermolecular double addition of $\mathbf{A_R}$ to two molecules of **B**: as a spinoff, complete $SnCl_2$-mediated reduction of the latter acyclic adducts would afford skeletal *carbo*-mers of stilbene of type **7**. These butatriene (or [3]cumulene)-catenated congeners of *carbo*-biphenyl **5a** described in Chapter 5 were therefore also targeted, opening electronic and stereo-chemical natural issues, such as the chromophoric comparison with parent stilbenes, and the barrier of the *cis*/*trans* (*E*/*Z*) interconversion of the diphenyl-dialkynyl-central butatriene moiety.

In the following, the adopted "paper-stapling" presentation is completed by the corresponding Supporting Information files as experimental sections.

References

1. (a) H. Schmidbaur, *Angew. Chem. Int. Ed. Engl*., **1983**, *22*, 907-927; (b) R. Zurawinski, B. Donnadieu, M. Mikolajczyk, R. Chauvin, *Organometallics,* **200,3**, *22*, 4810-4817; (c) Y. Canac, C. Lepetit, M. Abdalilah, C. Duhayon, R. Chauvin, *J. Am Chem. Soc.,* **2008**, *130*, 8406-8413; (d) Y. Canac, C. Lepetit, R. Chauvin, *Topics Organomet. Chem*., **2010**, *30*, 1-12, and references therein.

2. (a) R. Zurawinski, C. Lepetit, Y. Canac, M. Mikolajczyk, R. Chauvin, *Inorg. Chem.,* **2009**, 48, 2147-2155; (b) B. Vabre, Y. Canac, C. Lepetit, C. Duhayon, R. Chauvin, D. Zargarian, *Chem. Eur. J*., **2015**, *21*, 17403-17414, and references therein.

3. C. Lepetit, V. Maraval, Y. Canac, R. Chauvin, *Coord. Chem. Rev*., **2016**, *308 II,* 59-75, and references therein.

4. (a) I. Abdellah, C. Lepetit, Y. Canac, C. Duhayon, R. Chauvin, *Chem. Eur. J.*, **2010**, *16*, 13095-13108; (b) Y. Canac, C. Maaliki, I. Abdellah, R. Chauvin, *New. J. Chem*., **2012**, *36*, 17-27; (c) C. Maaliki, C. Lepetit, Y. Canac, C. Bijani, C. Duhayon, R. Chauvin, *Chem. Eur. J.,* **2012**, *18*, 7705-7714; (d) S. Gaillard, J. L. Renaud, *Dalton Trans.,* **2013**, *42*, 7255-7270; (e) M. Alcarazo, *Acc. Chem. Res.,* **2016**, *49*, 1797-1805, and references therein.

5. (a) I. Abdellah, N. Debono, Y. Canac, L. Vendier R. Chauvin, *Chem*. *Asian J.,* **2010**, *5*, 1225-1231; (b) C. D. Mboyi, I. Abdellah, C. Duhayon, Y. Canac, R. Chauvin, *ChemCatChem,* **2013**, *5*, 3014-3021, and references therein.

6. C. Zhu, E. Gras, C. Duhayon, F. Lacassin, X. Cui, R. Chauvin, *Chem. Asian J*., **2017**, *12*, 2845-2856.

7. C. A. Tolman, *Chem. Rev*., **1977**, *77*, 313-348.

8. J. L. Marshall, D. Lehnherr, B. D. Lindner, R. R. Tykwinski, *ChemPlusChem,* **2017**, *82*, 967-1001, and references therein.

9. K. Cocq, C. Lepetit, V. Maraval, R. Chauvin, *Chem. Soc. Rev*., **2015**, *44*, 6535-6559, and references therein.

10. C. Zhu, C. Duhayon, D. Romero-Borja, J.-L. Maldonado, G. Ramos-Ortíz, A. Saquet, V. Maraval, R. Chauvin, *New. J. Chem*., **2017**, *41*, 3908-3914.

11. L. Leroyer, C. Zou, V. Maraval, R. Chauvin, *C. R. Chim*., **2009**, *12*, 412-419.

12. (a) C. Zhu, A. Rives, C. Duhayon, V. Maraval, R. Chauvin, *J. Org. Chem*., **2017**, 82, 925-935; (b) C. Zhu, C. Duhayon, A. Saquet, V. Maraval, R. Chauvin, *Can. J. Chem*., **2017**, *95*, 454-459.

13. C. W. Zhu, T. H. Wang, C. J. Su, S. L. Lee, A. Rives, C. Duhayon, B. Kauffmann, V. Maraval, C. h. Chen, H. F. Hsu, R. Chauvin, Chem. Commun., 2017, 53, 5902-5905.

14. C. Zhu, A. Poater, C. Duhayon, B. Kauffmann, A. Saquet, V. Maraval, R. Chauvin, *manuscript in preparation, to be submitted soon*.

15. K. Cocq, N. Saffon-Merceron, Y. Coppel, C. Poidevin, V. Maraval, R. Chauvin, *Angew. Chem. Int. Ed*., **2016**, *55*, 15133-15136.

16. (a) C. Zhu, C. Duhayon, B. Kauffmann, A. Saquet, V. Maraval, R. Chauvin, *manuscript in preparation (in-template);* (b) C. Zhu, A. Saquet, X. Cui, V. Maraval, R. Chauvin, *manuscript in preparation (in-template).*

Part I

The coordination chemistry of nitro-aromatic phosphines

Chapter 1

The forgotten nitroaromatic phosphines as weakly donating P-ligands: an N-aryl-benzimidazolyl series in RhCl(CO) complexes

Introduction & Summary

Phosphorus is an abundant element in the earth's crust, and a key element of living organisms. From the societal-industrial standpoint, organophosphorus derivatives are widely encountered amongst materials, agrochemicals, pharmaceuticals, and chemical auxiliaries or reagents for various transformations.[1] As ligands of transition metals, phosphanes thus play a crucial role in homogeneous catalysis of diverse processes such as C-H bond activation,[2] C-C cross-coupling, [3] olefin metathesis, [4] isomerization, hydrogenation or hydroformylation, [5] the electronic and steric features of phosphanes can indeed be readily adjusted for the corresponding purposes.[6]

Regarding the electronic features, ligands are commonly classified into two families: electron-rich and electron-poor. Over the past few decades, electron-rich phosphines (phosphanes with three P–C bonds) have been extensively studied and used as ligands in catalysts for C-C, C-H or C-heteroatom bond formation.[7] The P(III) atom of electron-rich phosphines and related P-ligands (such as aminophosphines) is indeed surrounded by a high electron density, providing them with a strong σ-donating character towards metal centers, allowing stabilization of the catalytic species and facilitation of oxidative addition processes in catalytic cycles. [8] Representative electron-rich P-ligands are listed below (Figure 1).

(i) Arylphosphines **1A** decorated with electron-donating groups, such as OR or NR_2.[9]

(ii) Alkylphosphines **1B**, whose design can be largely adapted to specific requirements of steric demand and/or chirality at the P-center. The strong P→metal σ-donation of alkylphosphines is also widely used to accelerate the activation of *a priori* poorly reactive aryl-Br or aryl-Cl bonds.[10]

(iii) Imidazol-2-ylidenaminophosphines **1C** (IAPs), among aminophosphines (phosphanes with at least one P-N bond) exhibiting a strong Lewis base character, were recently reported by Dielmann *et al.* to be more strongly donating than NHCs such as R_2Im's and CAACs (**1E**).[11] The P atom of these guanidinophosphines indeed undergoes the combined π-donation effects from the -N atom and -imidazol-2-yliden moiety.[6b,12] It is here noteworthy that more electronegative P-substituents with less donating lone pairs, such as alkoxy groups, exert an opposite electron-withdrawing effect on the P^{III} atom (e.g. in phosphinites or phosph(on)ites).[13]

(iv) Phosphinophosphinidenes **1D** containing a monocoordinated P(I) atom in the free state with two lone pairs and a low-lying vacant orbital, were first reported by Guy Bertrand *et al*. in 2016. As singlet aminocarbenes (**1E**), phosphinophosphinidenes have a zwitterionic character, the phosphide end making them potential electron-rich ligands. Their use in catalysis has however remained elusive.[14]

It is finally noteworthy that amongst potential C-ligands and beyond NHCs (**1E**), phophonium ylides **1F**,[15] which can be regarded as phosphane-stabilized carbenes, are endowed with three valuable characteristics: basicity, nucleophilicity, and C-donating ability. These features make them more electro-donating ligands than NHCs.[16]

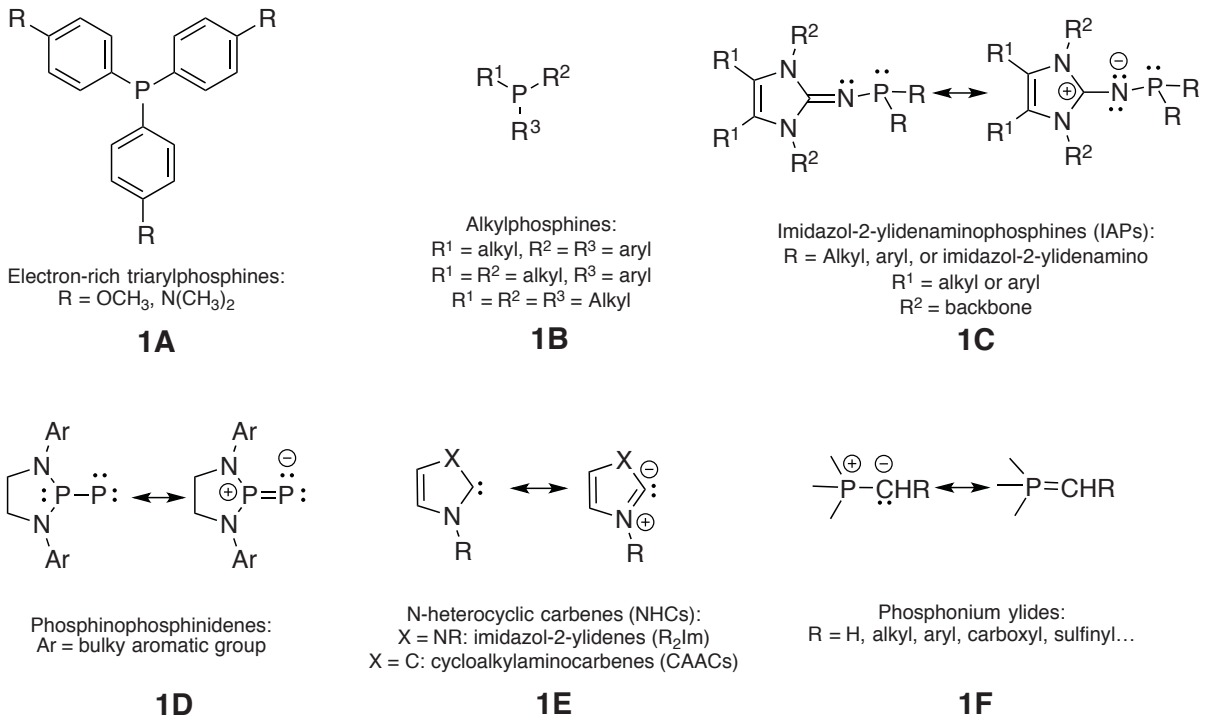

Figure 1. Examples of electron-rich P- and C-ligands.

Compared to electron-rich P-ligands, the investigation of electron-poor counterparts has remained less explored. Nonetheless, the specific efficiency of electron-deficient phosphane ligands in particular transition metal-catalyzed reactions, such as olefin metathesis or hydroformylation, has long attracted the chemists' attention.[17] On the very outset, electron-poor ligands can only be weakly coordinated to Lewis acidic centers, making the corresponding complexes prone to dissociation and exchange with possibly concomitant transformations, and thus not likely to act as efficient (pre-)catalysts.[18]

Electron-poor P-ligands are currently devised by one of the following ways (Figure 2).

(i) Substitution of triarylphosphine backbones by neutral electron-withdrawing groups, such as CF_3 or CN in **2A** and **2B**, respectively.[19]

(ii) Introduction of P–O bonds, exerting an electron-withdrawing effect on the free or coordinated P center by σ(-I)-induction, and allowing π-back-donation from a coordinated metal center to the s* orbitals of the P-O linkages. Nevertheless, phosphinous, phosphonous and phosphorous esters **2C** -i.e. phosphinites, phosphonites and phosphites, respectively- are sensitive to protic cleavage, thus restricting their catalytic use to particular cases under mild conditions.[20]

(iii) Positive chemical ionization around the P center, making the lone pair less available on the basis of simple electrostatics. a-Cationic phosphines, or carbeniophosphines, where the carbenium center in a position to the P atom is stabilized by +M donation of adjacent nitrogen lone pairs, can thus be prepared by N-alkylation of imino- or amidino-phosphines or P-substitution of a chlorophosphine by the corresponding (di)aminocarbene. Many imidazo*lio*phosphines **2D**, where the positive ~~char~~ge is delocalized over a $[RN\cdots C\cdots NR]^+$ diaminocarbyl unit, have thus been long described in the monodentate[21a-e] or symmetric chelate versions.[26f-g] Few of them also contain a second "normal" diphenylphosphino group (without any aminoalkenyl substituent) or a NHC moiety ensuring dissymmetrical chelate ability.[22] In diaminocyclopropeniophosphines **2E** or N-alkyl-pyridinio-phosphines **2F**,[23] the positive charge is further stabilized by aromatic delocalization.

More or less coordinating di-a-cationic monophosphines are also available, such as the diazaphosphepines **2G** (or "benzodiimida*zio*phosphepines" = BODIMIOPs; R = Ph, N^iPr_2)[24] and the phenyl- or *tert*-butyl-dicylopropeniophosphine **2H** (R-DCPs, R = Ph, ^{t}Bu).[25b-c] Tri-a-cationic phosphines were also exemplified as the tricyclopropeniophosphines **2I**.[29a] While cyclopropeniophosphines such as **2E** have found applications in catalysis, they are definitely less P-electron-poor that their imidazoliophosphine counterparts **2D**, which turned out to undergo decomposition in catalytic conditions:[26] both free imidazoliophosphines and complexes thereof were indeed shown to undergo C-P bond cleavage in the presence of weak nucleophiles under mild condition, such as Cl^- at 50 °C.[27] The a-cationic character of imidazoliophosphines is thus *a priori* not compatible with general catalytic conditions involving some amount of basic reagent, and the search for neutral equivalents in terms of P-electron-poorness thus appears as a natural issue. This is addressed in the next section.

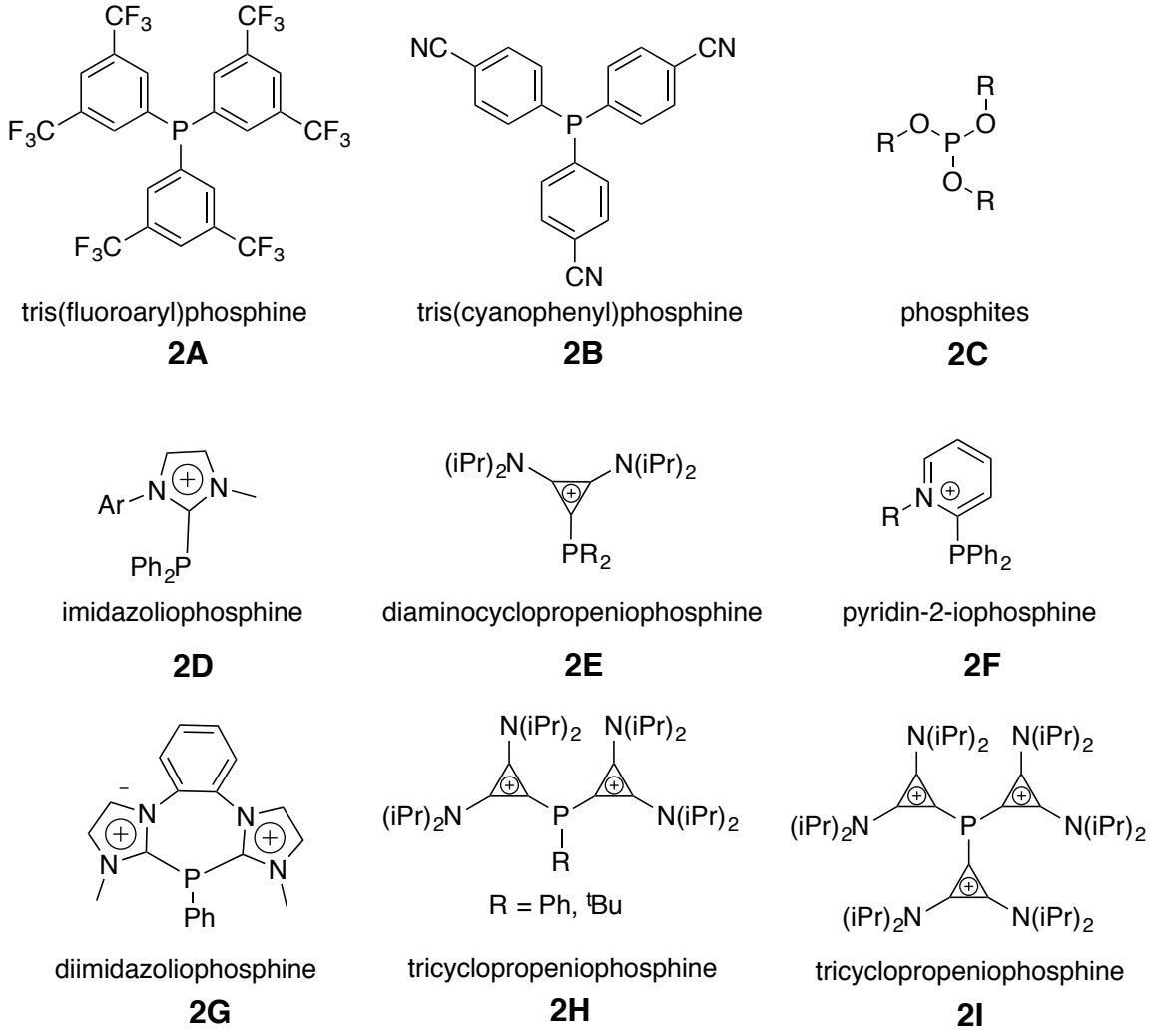

Figure 2. Representatives of electron-poor ligands: functional triarylphosphines (neutral) and carbeniophosphines (α-cationic).

(iv) Replacements of aryl P-substituents of neutral phosphines by heteroaryl groups, possibly exerting a -M electron-withdrawing effect on the P atom by π-donation of the P lone pair into the antibonding π* orbitals of the heterocycle, if lower in energy than in carboaryl groups (e.g. $E(\pi^*) = E(\text{LUMO}) = -0.026$ Ha for pyridine (B_2), *vs* 0.000 Ha for benzene (E_{2u}), at the DFT level B3PW91/6-31G(d,p)). Simple hetero-aromatic phosphines were thus exemplified for more or less π-accepting five-membered heterocycles such furan in **3Aa**,[28] thiophene in **3Ab**, [29] or pyrrole in **3Ac**[30a] (Figure 3). The case of diazoles has attracted more attention, e. g. with N-methyl-imidazole in the tris(imidazolyl)phosphine **3B** (TIMP),[30b] and N-aryl/alkyl-imidazoles, N-aryl-benzimidazoles or oxadiazole in the mono-diazolyl-phosphines **3C**,[30c] **3D**[22a] or **3E**,[30c] respectively.[30]

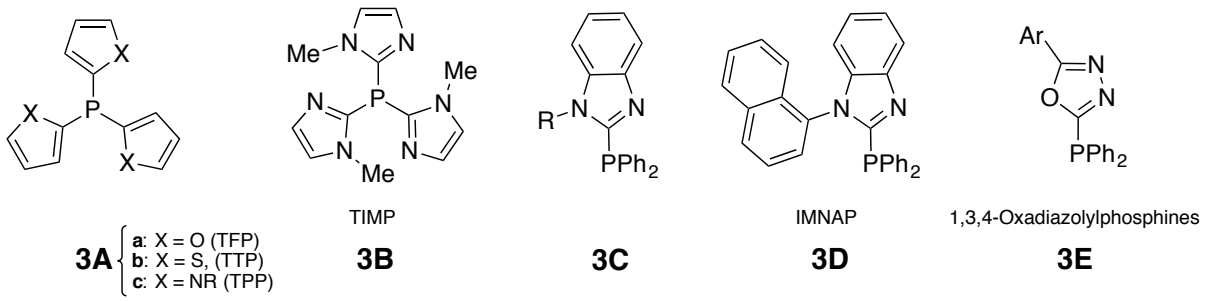

Figure 3. Examples of neutral heteroaryl-monophosphines.

The electron density at P atom actually varies not only with the nature of the heterocycle, but also with its position on a given heterocycle. The steric demand towards the P atom can also be modulated by anchoring suitable substituents at suitable positions. From a more practical standpoint, the synthetic routes to heteroaryl phosphines are more versatile than in the carboaryl series. In particular, the CH vertex in α-position to the endocyclic heteroatom is quite acidic, and can be regio-selectively substituted by the phosphinyl or selected decorating groups under mild conditions.[31]

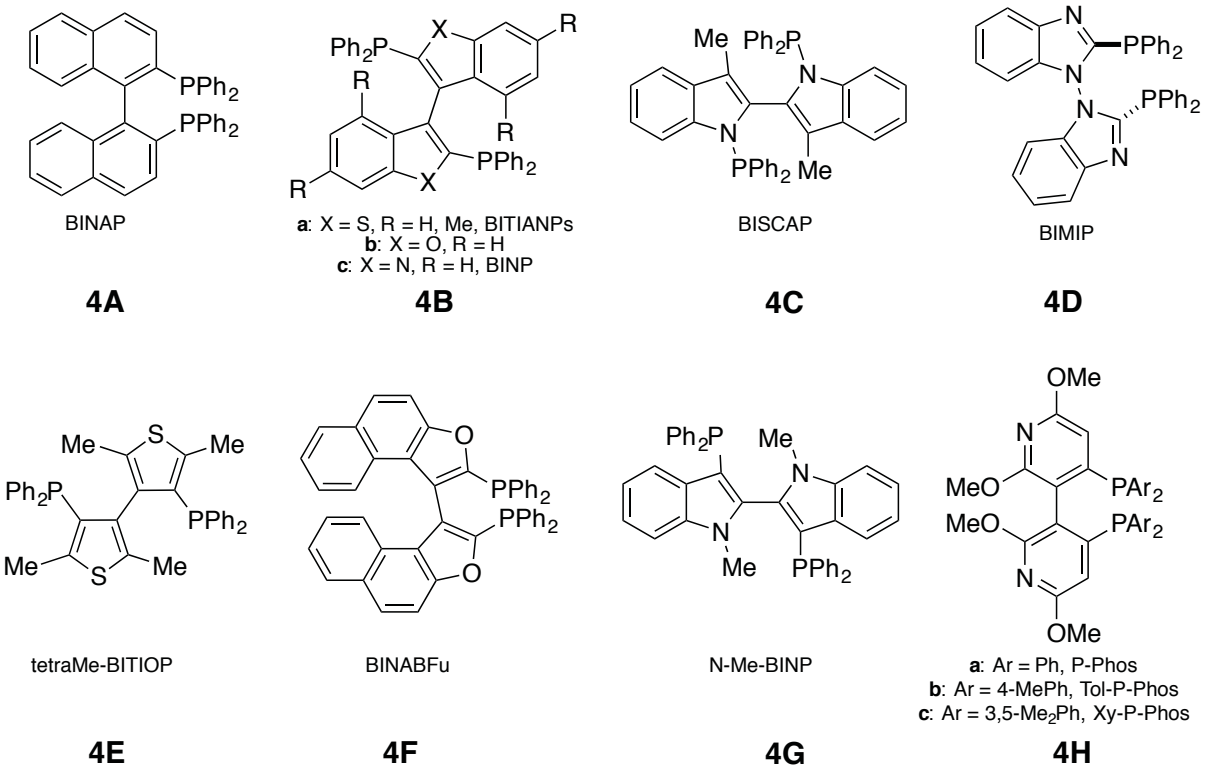

Figure 4. Representative C_2-symmetric diheteroaryl-diphosphine ligands.

Quite early, in 1995, inspired by the in-time challenging development of C_2-symmetric diphosphines,[32,33] initiated by the discovery of BINAP **4A** in 1980,[34] Sannicolò *et al*. reported the first example of C_2-symmetric diheteroaryl-diphosphine, BITIANP **4B**,[35] followed the

next year, by BISCAP **4C** where the P(III) atoms are directly bound to endocyclic nitrogen atoms (Figure 4).[36] Simultaneously, the first atropo-chiral diheteroaryl-diphosphine BIMIP **4D**, based on the *N,N'*-bisbenzimidazolyl scaffold, was prepared in enantiomeric pure form: on this occasion, the authors highlighted the paradox between the electron-poor character of BIMIP and its coordinating ability towards metal centers.[37] In 2000 was reported the four-step synthesis of tetramethyl-bithiophene diphosphine, tetraMe-BITIOP **4E**.[38] On the basis of these results, a large number of atropochiral diheteroaryl-diphosphine ligands were then devised, as illustrated by BINAPFu **4F**,[39] N-Me-BINP **4G**,[40] or P-Phos **4H**.[41] C_1-symmetric aryl-heteroaryl-diphosphines were also considered, such as BINATIP **5A** (Figure 5).[42] Congeners **5B-5H** were subsequently developed for their efficiency in the catalysis of Diels-Alder, hydrogenation and allylation reactions, including in the asymmetric version using enantio-enriched ligands such as (+)- or (–)-BIMINAP **5H**.[26,43]

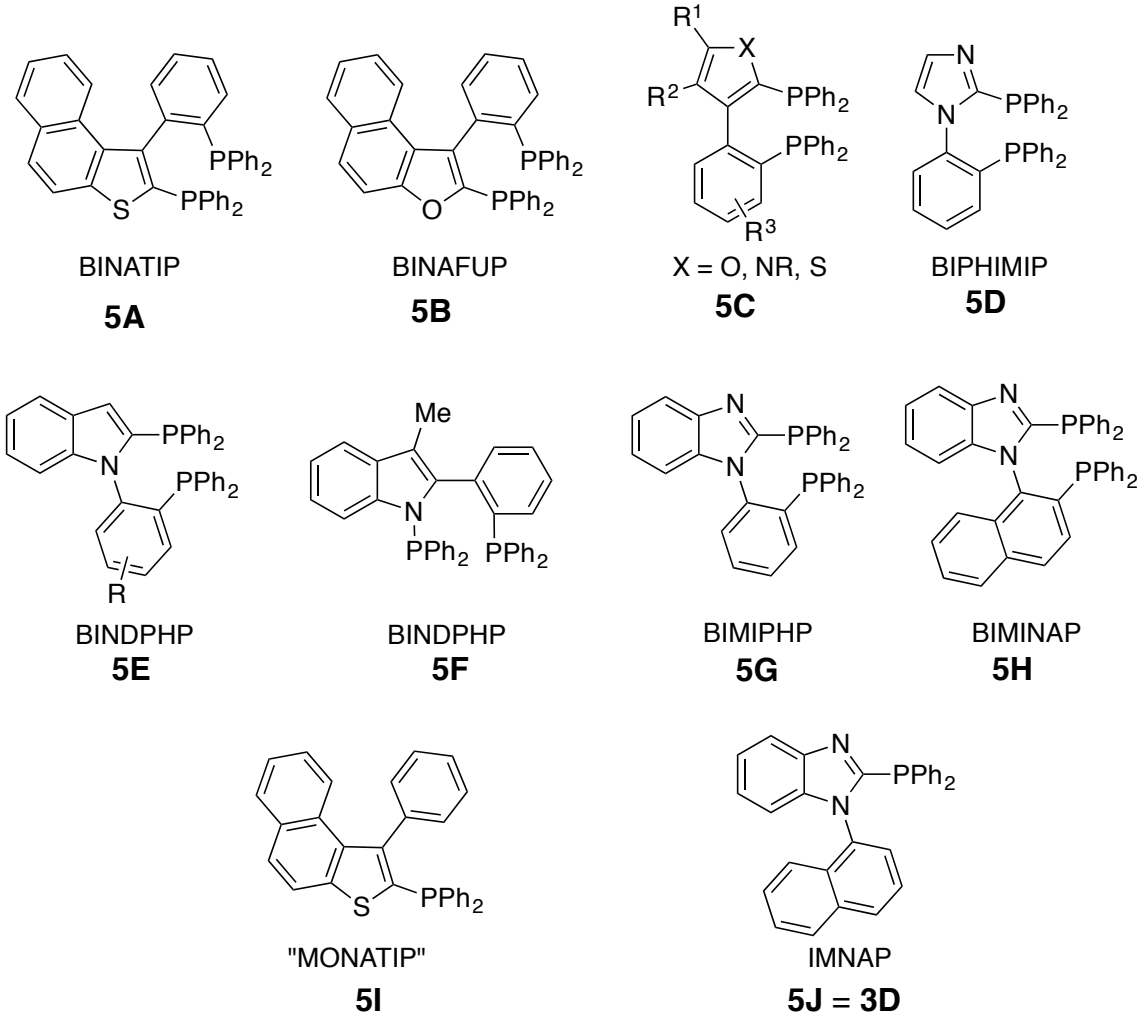

Figure 5. Selected examples of aryl-heteroaryl-diphosphines (**5A-H**), and aryl-heteroaryl-monophosphines (**5I-J**).

The mono-phosphine versions "MONATIP" **5I** and IMNAP **5J** (actually **3D**, Figure 3), of **5A** and **5H** respectively, deserve emphasis as particularly rigid aryl-heteroaryl monophoshines.

With the view to enhancing further the P-electron-poor character of heteroaryl-phosphines while keeping their electric neutrality, substitution by electron-withdrawing substituents was considered. Beside the widely used groups in the carboaryl-phosphine series (F, CF_3, CN, COR, SO_2CF_3 (triflone)... See Figure 2), one became aware that the NO_2 group has remained unexplored, likely because of a possible redox incompatibility with the P^{III} center. However, the electron-withdrawing effect of NO_2 through an aromatic system is *a priori* much stronger than that of CF_3 or CN, and deserves some attention. The challenge was thus addressed by designing a set of nitro-substituted (*N*-phenyl-benzimidazol-1-yl)diphenylphosphines, and targeting their complexes at a Rh(CO)Cl center, where the C=O IR stretching frequency and ^{103}Rh NMR chemical shift could serve as probes of the (weak) electron-donating character of the P-ligand.

In conclusion, a series of (*N*-phenyl-benzimidazol-1-yl)diphenylphosphines bearing a variable number of nitro groups at N-phenyl ring or/and benzimidazol core were prepared in the presence of optimized base LDA, and their corresponding *trans*-$L_2Rh^ICl(CO)$ complexes were also obtained through two strategies. (See Scheme 1.) The systematic variations of IR ν_{CO} and ^{103}Rh NMR revealed the weakly σ-donating electronic properties of these nitro-substituted phosphines compared to the non-nitrated parent and cationic N-methyl-benzimidazolium counterpart. Additionally, Dinuclear (μ-CO)$(LRhCl)_2$ clathrate with a high content (6.7:1) of dichoromenthane in crystal state was observed in nitro-substituted series.

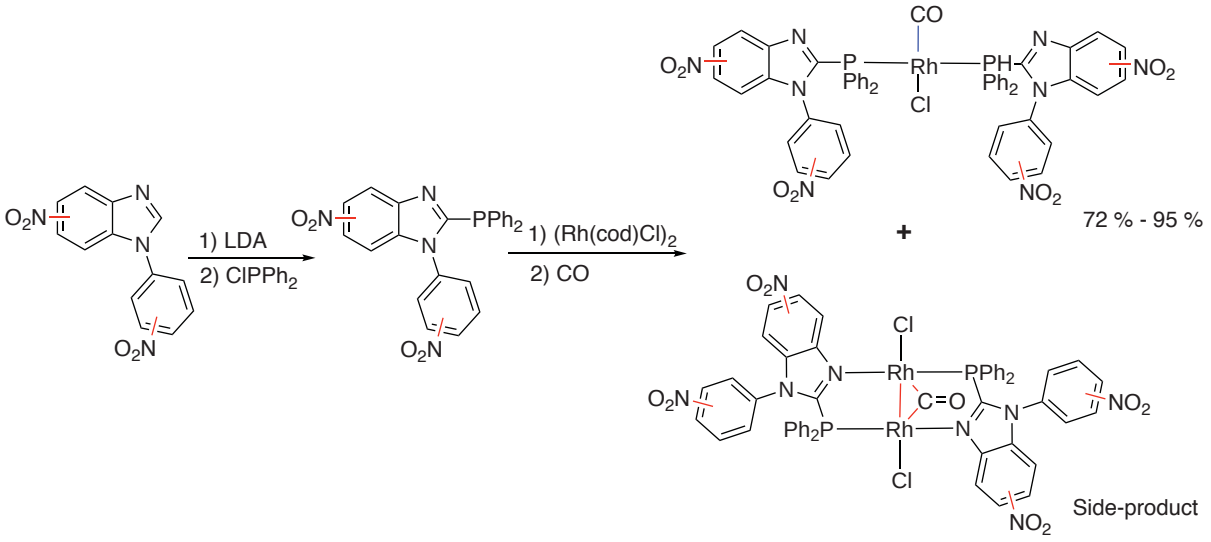

Scheme 1. The employed route for preparation of nitro-substituted (*N*-phenyl-benzimidazol-1-yl)diphenylphosphines and corresponding Rh^I complexes.

Reference

1. a). E. Macia, *Chem. Soc. Rev*., **2005**, 34, 691-701; b). M. Guino, K. K. (Mimi)Hii, *Chem. Soc. Rev*., **2007**, 36, 608-617; c). R. Martin, S. L. Buchwald, *Acc. Chem. Res*., **2008**, *41*, 1461-1473; d). R. Raz, *Clin. Microbiol. Infect*., **2011**, *18*, 4-7; e). M. Kazemi, A. M. Tahmasbi, R. Valizadeh, A. A. Naserian, A. Soni, *Agric. Sci. Res. J.*, **2012**, *2*, 512-522; f). Y. M. He, Y. Feng, Q. H. Fan, *Acc. Chem. Res*., **2014**, *47*, 2894-2906; g). M. P. Duffy, W. Delaunay, P. A. Bouit, M. Hissler, *Chem. Soc. Rev*., **2016**, *45*, 5296-5310; h). A. M. Caminade, *Chem. Soc. Rev*., **2016**, *45*, 5174-5186.

2. C. C. C. Johansson, T. J. Colacot, *Angew. Chem. Int. Ed.*, **2010**, *49*, 676-707; *Angew. Chem.*, **2010**, *122*, 686-718.

3. a). A. F. Littke, G. C. Fu, *Angew. Chem. Int. Ed*., **2002**, *41*, 4176-4211; *Angew. Chem.*, **2002**, *114*, 4350-4386; b). R. Martin, S. L. Buchwald, *Acc. Chem. Res*., **2008**, *41*, 1461-1473.

4. J. Czaban, C. Torborg, K. Grela, *Sustainable Catalysis* (Ed.: P. J. Dunn), John Wiley & Sons, Inc., Hoboken, New Jersey, **2013**, p.163-214.

5. J. K. MacDougall, M. C. Simpson, M. J. Green, D. J. Cole-Hamilton, *J. Chem. Soc. Dalton Trans*., **1996**, 1161-1172.

6. a). C. A. Tolman, *Chem. Rev.*, **1977**, *77*, 313-348. b). M. A. Winsche, P. Mehlmann, T. Witteler, F. Bu, P. Rathmann, F. Dielmann, *Angew. Chem. Int. Ed.*, **2015**, *54*, 11857-11860.

7. a). R. L. Pruettan, D. J. A. Smith, *J. Org. Chem*., **1969**, *34*, 327-330; b). C. A. Tolman, *Chem. Rev*., **1977**, *77*, 313-348; c). W. S. Knowles, *Acc. Chem. Res*., **1983**, *16*, 106-112; d). J. P. Wolfe, R. A. Singer, B. H. Yang, S. L. Buchwald, *J. Am. Chem. Soc*., **1999**, *121*, 9550-9561; e). A. Aranyos, D. W. Old, A. Kiyomori, J. P. Wolfe, J. P. Sadighi, S. L. Buchwald, *J. Am. Chem. Soc*., **1999**, *121*, 4369-4378; f). A. F. Littke, G. C. Fu, *J. Org. Chem*., **1999**, *64*, 10-11; g). J. P. Wolfe, S. L. Buchwald, *Angew. Chem. Int. Ed*., **1999**, *38*, 2413-2416; h). C. J. Li *Chem. Rev*., **2005**, *105*, 3095-3165; i). K. H. Shaughnessy, *Eur. J. Org. Chem*., **2006**, 1827-1835; j). S. Ito, K. Munakata, A. Nakamura, K. Nozaki, *J. Am. Chem. Soc*., **2009**, *131*, 14606-14607; k). S. Diez-Gonzalez, N. Marion, S. P. Nolan, *Chem. Rev*., **2009**, *109*, 3612-3676; l). P. Yang, L. H. Lim, P. Chuanprasit, H. Hirao, J. R. Zhou, *Angew. Chem. Int. Ed*., **2016**, *55*, 12083-12087.

8. Y. Canac, C. Lepetit, M. Abdalilah, C. Duhayon, R. Chauvin, *J. Am. Chem. Soc*., **2008**, *130*, 8406-8413.

9. a). R. Schmid, M. Cereghetti, B. Heiser, P. Schonholzer, H. J. Hansen, *Helv. Chim. Acta.*, **1988**, *71*, 897-929; b). H. Jendralln, C. H. Li, E. Paulus, *Tetrahedron: Asymmetry*, **1994**, *5*, 1297-1320; c). P. Kocovsky, S. Vyskocil, M. Smrcina, *Chem. Rev*., **2003**, *103*, 3213-3245; d). H. Shimizu, I. Nagasaki, T. Saito, *Tetrahedron*, **2005**, *61*, 5405-5432; e). Z, Freixa, P. W.N.M. van Leeuwen, *Coord. Chem. Rev*., **2008**, *252*, 1755-1786.

10. a) M. Bacci, S. Midollini, P. Stoppioni, L. Sacconi, *Inorg. Chem.,* **1973**, *12*, 1801-1805; b) J. R. Görlich, R. Schmutzler, *Phosphorus Sulfur Silicon Relat. Elem*., **1995**, *102*, 211-215; **1993**, *81*, 141-148; c) M. J. Burk, J. E. Feaster, W. A. Nugent, R. L. Harlow, *J. Am. Chem. Soc*., **1993**, *115*, 10125-10138; d) W. H. Hu, C. C. Pai, C. C. Chen, G. P. Xue, A. S. C. Chan, *Tetrahedron: Asymmetry,* **1998**, *9*, 3241-3246; e) A. Aranyos, D. W. Old, A. Kiyomori, J. P. Wolfe, J. P. Sadighi, S. L. Buchwald, *J. Am. Chem. Soc.,* **1999**, *121*, 4369-4378; f). K. H. Shaughnessy, R. S. Booth, *Org. Lett*., **2001**, *3*, 2757-2759; g) J. S. You, J. G. Verkade, *J. Org. Chem.*, **2003**, *68*, 8003-8007; h) J. S. Huang, G. A. Yu, J. Xie, N. Y. Zhu, C. M. Che, *Inorg. Chem*., **2006**, *45*, 5724-5726; i) A. J. Kendall, L. N. Zakharov, D. R. Tyler, *Inorg. Chem*., **2016**, *55*, 3079-3090; j) M. Dutartre, J. Bayardon, S. Juge, *Chem. Soc. Rev.*, **2016**, *45*, 5771-5794.

11. a). D. Bourissou, O. Guerret, F. P. Gabbai, G. Bertrand, *Chem. Rev*., **2000**, *100*, 39-91; b). Y. Canac, M. Soleilhavoup, S. Conejero, G. Bertrand, *J. Organomet. Chem*., **2004**, *689*, 3857-3865; c). J. Vignolle, X. Cattoen, D. Bourissou, *Chem. Rev.*, **2009**, *109*, 3333-3384; i). P. L. Arnold, I. J. Casely, *Chem. Rev*., **2009**, *109*, 3599-3611; e). O. Schuster, L. R. Yang, H. G. Raubenheimer, M. Albrecht, *Chem. Rev*., **2009**, *109*, 3445-3478; d). D. J. Nelson, S. P. Nolan, *Chem. Soc. Rev.*, **2013**, *42*, 6723-6753; f). F. E. Hahn, M. C. Jahnke, *Angew. Chem. Int. Ed*., **2008**, *47*, 3122-3172; g). V. Charra, P. Frémont, P. Braunstein, *Coord. Chem. Rev*., **2017**, *341*, 53-176.

12. X. Wu, M. Tamm, *Coord. Chem. Rev*., **2014**, *260*, 116-138.

13. a). M. P. Magee, W. Luo, W. H. Hersh, *Organometallics*, **2002**, *21*, 362-372; b). R. A. Baber, M. L. Clarke, K. M. Heslop, A. C. Marr, A. G. Orpen, P. G. Pringle, A. Ward, D. E. Zambrano-Williams, *Dalton Trans.*, **2005**, 1079-1085.

14. L. Liu, D. A. Ruiz, D. Munz, G. Bertrand, *Chem.*, **2016**, *1*, 147-153.

15. a). H. Schmidbaur, *Angew. Chem. Int. Ed. Engl*., **1983**, *22*, 907-927; b). J. Vicente, M. T. Chicote, *Coord.Chem. Rev*., **1999**, *193-195*, 1143-1161; c). L. R. Falvello, J. C. Gines, J. J. Carbo, A. Lledos, R. Navarro, T. Soler, E. P. Urriolabeitia, *Inorg.Chem*., **2006**, *45*, 6803-6815; d). Y. Canac, C. Duhayon, R. Chauvin, *Angew. Chem. Int. Ed.*, **2007**, *46*, 6313-6315.

16. a). O. I. Kolodiazhny, *Tetrahedron*, **1996**, *52*, 1855-1929; b). Y. Canac, C. Duhayon, R. Chauvin, *Angew. Chem. Int. Ed*., **2007**, *46*, 6313-6315; c). Y. Canac, C. Lepetit, M. Abdalilah, C. Duhayon, R. Chauvin, *J. Am. Chem. Soc*., **2008**, *130*, 8406-8413.

17. a). M. P. Magee, W. Luo, W. H. Hersh, *Organometallics*, **2002**, *21*, 362-372; b). R. A. Baber, M. L. Clarke, K. M. Heslop, A. C. Marr, A. G. Orpen, P. G. Pringle, A. Ward, D. E. Zambrano-Williams, *Dalton Trans*., **2005**, 1079-1085; c). Q. Liu, L. P. Wu, I. Fleischer, D. Selent, R. Franke, R. Jackstell, M. Beller, *Chem. Eur. J.*, **2014**, *20*, 6888-6894.

18. D. B. Grotjahn, Y. Gong, L. Zakharov, J. A. Golen, A. L. Rheingold, *J. Am. Chem. Soc*., **2006**, *128*, 438-453.

19. a). M. Pomerantz, M. S. Terrazas, Y. Cheng, X. M. Gu, *Phosphorus. Sulfur and Silicon*, **1996**, *109-110*, 505-508; b). F. Berhal, O. Esseiva, C. H. Martin, H. Tone, J. P. Genet, T. Ayad, V. Ratovelomanana-Vidal, *Org. Lett.*, **2011**, *13*, 2806-2809; c). M. H. Shaw, R. A. Croft, W. G. Whittingham, J. F. Bower, *J. Am. Chem. Soc.*, **2015**, *137*, 8054-8057; d). M. J. Stark, M. J. Shaw, A. Fadamin, N. P. Rath, E. B. Bauer, *J. Organomet. Chem.*, **2017**, *847*, 41-53.

20. a) Y. Canac, N. Debono, L. Vendier, R. Chauvin, *Inorg. Chem*., **2009**, *48*, 5562-5568; b) D. Parmar, E. Sugiono, S. Raja, M. Rueping, *Chem. Rev*., **2014**, *114*, 9047-9153.

21. See for examples: a) U. Zoller, *Tetrahedron,* **1988**, *44*, 7413-7426; b) N. Kuhn, M. Goehner, G. Henkel, *Z. Anorg. Allg. Chem*., **1999**, *625*, 1415-1416; c) M. Azouri, J. Andrieu, M. Picquet, P. Richard, B. Hanquet, I. Tkatchenko, *Eur. J. Inorg. Chem*., **2007**, 4877-4883; d) A. A. Tolmachev, A. A. Yurchenko, A. S. Merculov, M. G. Semenova, E. V. Zarudnitskii, V. V. Ivanov, A. M. Pinchuk, *Heteroatom Chem*., **1999**, *10*, 585-597; e) C. Maaliki, C. Lepetit, C. Duhayon, Y. Canac, R. Chauvin, *Chem. Eur. J*., **2012**, *18*, 16153-16160; f) C. Barthes, C. Lepetit, Y. Canac, C. Duhayon, D. Zargarian, R. Chauvin, *Inorg. Chem*., **2013**, *52*, 48-58; g) Y. Canac, C. Bijani, C. Duhayon, R. Chauvin, *Organometallics,* **2013**, *32*, 4054-4057.

22. See for example: a) N. Debono, Y. Canac, C. Duhayon, R. Chauvin, *Eur. J. Inorg. Chem*., **2008**, *2008*, 2991-2999; b) B. Vabre, Y. Canac, C. Duhayon, R. Chauvin, D. Zargarian, *Chem. Commun*., **2012**, *48*, 10446-10448; c) I. Abdellah, Y. Canac, C. D. Mboyi, C. Duhayon, R. Chauvin, *J. Organomet. Chem.,* **2015**, *776*, 149-152; d) L. Dubrulle, C. Poidevin, C. Maaliki, Y. Canac, C. Lepetit, C. Duhayon, R. Chauvin, *Eur. J. Inorg. Chem*., **2016**, 313-321.

23. H. Tinnermann, C. Wille, M. Alcarazo, *Angew. Chem., Int. Ed*., **2014**, *53*, 8732-8736.

24. a) C. Maaliki, C. Lepetit, Y. Canac, C. Bijani, C. Duhayon, R. Chauvin, *Chem. Eur. J*., **2012**, *18*, 7705-7714; b) C. Maaliki, Y. Canac, C. Lepetit, C. Duhayon, R. Chauvin, *RSC*

Advances, **2013**, *3*, 20391-20398; c) A. Mankou Makaya, Y. Canac, C. Bijani, C. Duhayon, R. Chauvin, *Phosphorus Sulfur Silicon Relat. Elem*., **2015**, *190*, 789-802; d) A. Mankou Makaya, *Nouveaux Potentiels du Noyaux Imidazole en Chimie de Coordination de Ligands Phospho-Carbonés : Effets de Charges et Versions Chirales*, Ph. D. Thesis, Chapt. 1, pp 31-97, University of Toulouse, Toulouse 3-Paul Sabatier, July 12, **2016**, Toulouse, France.

25. a) J. Petuškova, M. Patil, S. Holle, C. W. Lehmann, W. Thiel, M. Alcarazo, *J. Am. Chem. Soc*., **2011**, *133*, 20758-20760; b) C. D. Mboyi, C. Maaliki, A. M. Makaya, Y. Canac, C. Duhayon, R. Chauvin, *Inorg. Chem*., **2016**, *55*, 11018-11027; c) G. Mehler, P. Linowski, J. Carreras, A. Zanardi, J. W. Dube, M. Alcarazo, *Chem. Eur. J.,* **2016**, *22*, 15320-15327.

26. See for example: I. Abdellah, N. Debono, Y. Canac, L. Vendier, R. Chauvin, *Chem. Asian J*., **2010**, *5*, 1225-1231.

27. a) I. Abdellah, C. Lepetit, Y. Canac, C. Duhayon, R. Chauvin, *Chem. Eur. J.*, **2010**, *16*, 13095-13108; b) S. Gaillard, J. L. Renaud, *Dalton Trans.*, **2013**, *42*, 7255-7270; c) M. Alcarazo, *Chem. Eur. J.*, **2014**, *20*, 7868-7877; d) M. Alcarazo, *Acc. Chem. Res.*, **2016**, *49*, 1797-1805.

28. V. Farina, B. Krishnan, *J. Am. Chem. Soc*., **1991**, *113*, 9585-9595.

29. K. Issleib, A. Brack, *Zeitschrift fuer Anorganische und Allgemeine Chemie,* **1957**, *292*, 245-253.

30. a). V. Farina, B. Krishnan, *J. Am. Chem. Soc*., **1991**, *113*, 9585-9595; b). A. A. Tolmachev, A. A. Yurchenko, A. S. Merculov, M. G. Semenova, E. V. Zarudnitskii, V. V. Ivanov, A. M. Pinchuk, *Heteroatom Chem*., **1999**, *10*, 585-597; c). L. H. Zou, Z. B. Dong, C. Bolm, *Synlett*, **2012**, *23*, 1613-1616.

31. a). T. Benincori, S. Rizzo, F. Sannicolò, *J. Heterocyclic Chem.*, **2002**, *39*, 471-485. b). T. L. Au-Yeung, A. S. C. Chan, *Coord. Chem. Rev*., **2004**, *248*, 2151-2164.

32. a). N. Sakai, S. Mano, K. Nozaki, H. Takaya, *J. Am. Chem. Soc*., **1993**, *115*, 7033-7034; b). E. B. Kaloun, R. Merdes, J. P. Genet, J. Uziel, S. Juge, *J. Organomet. Chem.*, **1997**, *529*, 455-463; c). W. M. Dai, K. K. Y. Yeung, J. T. Liu, Y. Zhang, I. D. Williams, *Org. Lett*., **2002**, *4*, 1615-1618; d). P. Kocovsky, S. Vyskocil, M. Smrcina, *Chem. Rev*., **2003**, *103*, 3213-3245; e). H. Shimizu, I. Nagasaki, T. Saito, *Tetrahedron*, **2005**, *61*, 5405-5432; f). Z. Freixa, P. W. N. M. van Leeuwen, *Coord. Chem. Rev.*, **2008**, *252*, 1755-1786.

33. T. T. L. Au-Yeung, A. S. C. Chan, *Coord. Chem. Rev*., **2004**, *248*, 2151-2164.

34. a). A. Miyashita, A. Yasuda, H. Takaya, K. Toriumi, T. Ito, T. Souchi, R. Noyori, *J. Am. Chem. Soc*., **1980**, *102*, 7932-7934. b) A. Miyashita, H. Takaya, T. Souchi, R. Noyori, *Tetrahedron*, **1984**, *40*, 1245-1253.

35. a). P. Antognazza, T. Benincori, E. Brenna, E. Cesarotti, F. Demartin, T. Pilati, F. Sannicolò, L. Trimarco, *J. Org. Chem.*, **1996**, *61*, 6244-6251; b). T. Benincori, E. Brenna, F. Sannicolò, L. Trimarco, P. Antognazza, E. Cesarotti, F. Demartin, T. Pilati, *J. Org. Chem*., **1996**, *61*, 6244-6251; c). U. Berensa, J. M. Brown, J. Long, R. Seike, *Tetrahedron: Asymmetry*, **1996**, *7*, 285-292.

36. T. Benincori, E. Brenna, F. Sannicolo, L. Trimarco, P. Antognazza, E. Cesarotti, F. Demartin, T. Pilati, G. Zotti, *J. Organomet. Chem.*, **1997**, *529*, 445-453.

37. P. Antognazza, T. Benincori, S. Mazzoli, F. Sannicolò, T. Pilati, *Phosphorus. Sulfur and Silicon*, **1999**, *144-146*, 405-408.

38. T. Benincori, E. Cesarotti, O. Piccolo, F. Sannicolò, *J. Org. Chem*., **2000**, *65*, 2043-2047.

39. a). N. G. Andersen, M. Parvez, B. A. Keay, *Org. Lett*., **2000**, *2*, 2817-2820; b). N. G. Andersen, M. Parvez, R. McDonald, B. A. Keay, *Can. J. Chem.*, **2004**, *82*, 145-161.

40. T. Benincori, O. Piccolo, S. Rizzo, F. Sannicolò, *J. Org. Chem*., **2000**, *65*, 8340-8347.

41. C. C. Pai, C. W. Lin, C. C. Lin, C. C. Chen, A. S. C. Chan, *J. Am. Chem. Soc*., **2000**, *122* 11513-11514.

42. T. Benincori, S. Gladiali, S. Rizzo, F. Sanncolò, *J. Org. Chem*., **2001**, *66*, 5940-5942.

43. a) F. Sannicolò, T. Benincori, S. Rizzo, S. Gladiali, S. Pulacchini, G. Zotti, *Synthesis*, **2001**, *15*, 2327-2336; b) N. V. Artemova, M. N. Chevykalova, Y. N. Luzikov, I. E. Nifant'ev, E. E. Nifant'ev, *Tetrahedron*, **2004**, *60*, 10365-10370.

Article 1

ACES Asian Chemical Editorial Society

DOI: 10.1002/asia.201701078

CHEMISTRY AN ASIAN JOURNAL Full Paper

Rhodium Carbonyl Complexes

The Forgotten Nitroaromatic Phosphines as Weakly Donating P-ligands: An *N*-Aryl-benzimidazolyl Series in RhCl(CO) Complexes

Chongwei Zhu,[a, b] Emmanuel Gras,*[a, b] Carine Duhayon,[a, b] Francis Lacassin,[a, b] Xiuling Cui,[c] and Remi Chauvin*[a, b, c]

Dedicated to Professor Marian Mikolajczyk on the occasion of his 80th birthday

Abstract: The coordination chemistry of a priori weakly σ-donating nitroaromatic phosphines is addressed through a series of nitro-substituted (*N*-phenyl-benzimidazol-1-yl)diphenylphosphines in Rh^{I} complexes. From a set of seven such phosphines $L = L_{xyz}^{(')}$ (*x*, *y*, *z* = 0 or 1 = number of NO_2 substituents at the 5, 6 and N-Ph *para* positions, respectively), including the non-nitrated parent L_{000} and its dicationic N-methyl counterpart L_{000}', three LRhCl(COD) and seven L_2RhCl(CO) complexes have been obtained in 72–95% yield. Despite of a *cis* orientation of the L and CO ligands, the C=O IR stretching frequency ν_{CO} varies in the expected sense, from $1967 \pm 1\ cm^{-1}$ for L_{xy0} to $1978 \pm 1\ cm^{-1}$ for L_{xy1}, and $2005\ cm^{-1}$ for L_{000}'. The ^{103}Rh NMR chemical shift δ_{Rh} varies from −288 ppm for L_{000} to -316 ± 1 ppm for L_{10z} or L_{01z}, and −436 ppm for L_{000}'. The ν_{CO} and δ_{Rh} probes thus reveal moderate but systematic variations, and act as "orthogonal" spectroscopic indicators of the presence of nitro groups on the N-Ph group and the benzimidazole core, respectively. For the dicationic ligand L_{000}', a tight electrostatic sandwiching of the Rh-Cl bond by the benzimidazole moities is evidenced by X-ray crystallography ($RhCl^{\delta-}\cdots CN_2^{+} \approx 3.01$ Å). Along with the LRhCl(CO) complexes, dinuclear side-products $(\mu\text{-CO})(RhClL)_2$ were also obtained in low spectroscopic yield: for the dinitro ligand $L = L_{011}$, a unique 1:6.7 clathrate structure, with dichloromethane as solvate, is also revealed by X-ray crystallography.

Introduction

In the continuing debate on the fundamental nature of the coordination bond,[1] the ligands of some reference Lewis acids (LAs) are commonly classified between the electron-rich and electron-poor categories: for transition metal LAs, this prebonding characteristic makes it possible to predict strong or weak ligand-to-metal charge transfer. Beside the long studied class of electron-rich ligands, ranging from alkylphosphines to diaminocarbenes and onium ylides,[2] the class of electron-poor phosphane counterparts has attracted less systematic attention but remains challenging for appraising coordination limits while decreasing the strength of σ-donation.[3] The need for electron-poor ligands is, however, more practically motivated by catalysis issues for rate-determining steps requiring a relatively low electron density at a metal center balanced by sufficient stability of the complex. Even weak σ-donation can indeed be compensated by strong π-back bonding, as it happens with phosphites identified as ligands of choice for catalytic transformations such as hydroformylation.[4] As esters of phosphorous acid, phosphites are however sensitive to P–O bond protolysis, and two main kinds of more robust electron-deficient triarylphosphine ligands can be distinguished: the electron-poor neutral phosphines, mainly represented by fluoroarylphosphine,[5] *N*-heteroarylphosphines (e.g., imidazolo-phosphines),[6] and the highly electron-poor α-cationic phosphines, such as imidazolio-, diaminocyclopropenio-, or pyridinio-phosphines.[6a,7,8] These carbenio-phosphines, optimally described as carbene–phosphenium adducts,[9] have been shown to exhibit P-donating ability in ternary C→P→LA coordination motifs,[7a] even in the case of the extremely electron-poor α-diationic dicyclopropeniophosphines.[10] While cyclopropenio-phosphines give particularly stable Pd complexes acting as efficient catalysts (e.g., for cycloisomerization of enynes),[7d,11] imidazolio-phosphines and their complexes are more reactive, un-

[a] C. Zhu, Dr. E. Gras, Dr. C. Duhayon, F. Lacassin, Prof. R. Chauvin
CNRS
LCC (Laboratoire de Chimie de Coordination)
205 route de Narbonne, BP44099, 31077 Toulouse Cedex 4 (France)
Fax: (+33) 561-553-003
E-mail: emmanuel.gras@lcc-toulouse.fr
chauvin@lcc-toulouse.fr

[b] C. Zhu, Dr. E. Gras, Dr. C. Duhayon, F. Lacassin, Prof. R. Chauvin
Université de Toulouse
UPS, ICT-FR 2599, 31062 Toulouse Cedex 9 (France)

[c] Prof. X. Cui, Prof. R. Chauvin
Engineering Research Center of Molecular Medicine, Ministry of Education, Key Laboratory of Xiamen Marine and Gene Drugs, Institutes of Molecular Medicine and School of Biomedical Sciences
Huaqiao University
Xiamen, 361021 (P.R. China)

Supporting information and the ORCID identification number(s) for the author(s) of this article can be found under https://doi.org/10.1002/asia.201701078.

dergoing P–C bond cleavage in the presence of weak nucleophiles (such as Cl^-), thus restricting the scope of possible applications.[9,12]

With the view to enhancing the electron-deficiency of the parent imidazolophosphines without the detrimental effect of the α-positive charge, N-methylation of the former (CH_3^+ N-coordination) could be replaced by CH-substitution with neutral electron-withdrawing groups (Figure 1). Examination of this issue drew the author's attention to the fact that an a priori simple way to make a triarylphosphine ligand more electron-deficient while remaining neutral seems to have been forgotten: alternative to fluorination, nitration should indeed be particularly efficient. Indeed, considering Hammett constants σ_p and σ_m as crude means of comparison of the electron-withdrawing effect of a substituent through an aromatic system,[13] one of the largest values is attained for NO_2 ($\sigma_m = 0.71$, $\sigma_p = 0.78$), standing close to that of the cationic substituent $^+NMe_3$ ($\sigma_m = 0.88$, $\sigma_p = 0.82$), and much higher than those of other neutral substituents such as F ($\sigma_m = 0.34$, $\sigma_p = 0.06$), CF_3 ($\sigma_m = 0.43$, $\sigma_p = 0.54$) or CN ($\sigma_m = 0.56$, $\sigma_p = 0.66$).[14]

Prior to any coordination chemistry considerations, the oxymoronic redox nature of nitro-substituted arylphosphines can be considered as a basic challenge,[15] at least from the thermodynamic standpoint (the nitro-nitroso isomerization 4-NO_2-C_6H_4-PPh_2→4-NO-C_6H_4-P(O)Ph_2 is calculated to be exothermic by $\Delta ZPE = -23.2$ kcal mol^{-1}; see the Supporting Information).[16] Direct nitration of aryl-phosphines are prevented by the P-oxidizing potency of the nitronium ion,[17] and most of related synthetic efforts have focused on oxidized P=O or P=S precursors.[18] Coordination complexes of nitroarylphosphines are actually limited to the formal cases of such P→O or P→S derivatives: to the best of the our knowledge, indeed, no experimental example of corresponding P→metal complexes has ever been reported,[19] thus unveiling a quite general challenge. While the basic triphenylphosphine series will deserve a natural attention, in particular for the reference (4-nitrophenyl)-diphenylphosphine (see Conclusion),[15b,20] the forgotten nitration strategy for lowering further the electron deficiency of aromatic phosphine ligands is hereafter addressed within the above-summarized concern in the benzimidazolyl phosphine series (Figure 1 a).

While modern routes to arylphosphines consist in Cu-, Ni- or Pd-catalyzed Ar-P coupling reactions from Ar-X + E-PPh_2 (X = I, Br, OTf; E = H, Ph, S*n*Bu_3, Cl), nitro-ArX substrates are rarely exemplified,[21] and have even been claimed to be incompatible with generally efficient conditions.[22] Yet, the most employed approach to tertiary phosphines remains based on nucleophilic substitution processes at P centers with lithium or Grignard reactants, as also illustrated in the arene/heteroarene series,[23] in particular for imidazole and benzimidazole representatives.[6e,12b] For the present objective, (*N*-aryl-*1H*-benzoimidazol-2-yl)diphenylphosphines have thus been targeted from the more or less nitrated *NH*,N_2*CH* benzimidazole precursors **1a–d** by substitution of $ClPPh_2$ with lithium salts of *N*-aryl-N_2*CH* derivatives **2a–h** (Figure 1 b). The propensity of nitro-arene/heteroarene substrates to undergo addition or redox processes in the presence of lithium reagents has indeed been reported for alkyl lithiums only.[24] Moreoever, since *N*-methyl-5-nitro-*1H*-benzoimidazol-2-yl lithium has been shown to undergo selective electrophilic chlorination with NCS,[25] reaction of the 1*N*-phenyl congener **2b** with the analogous Ph_2P-Cl electrophile appears as a natural possibility to prepare the set of eight

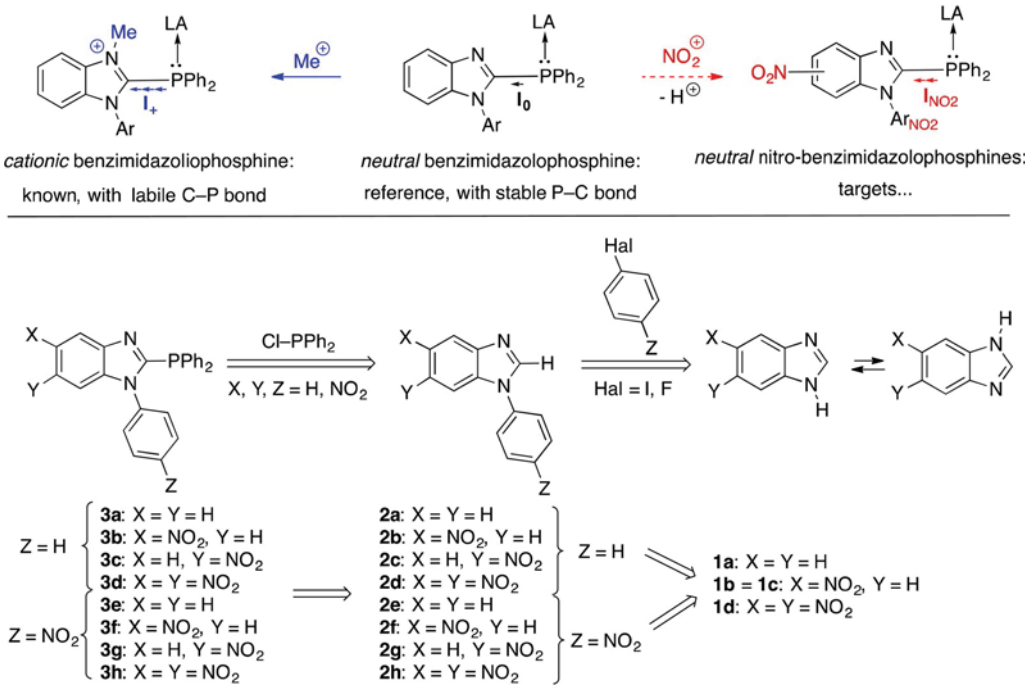

Figure 1. a) top: alternative manners to tune the P-σ-donating ability of benzimidazolophosphines towards a Lewis acid (LA): C-nitration vs. N-alkylation (expected order of inductive effects: $I_0 < I_{NO2} < I_+$); b) bottom: selected targets and synthetic approach.

more or less nitrated *N*-aryl-*1H*-benzoimidazolophosphines **3a**–**h** (Figure 1). Their coordinating properties were then envisaged to be compared by the ν_{CO} stretching frequencies of carbonyl complexes thereof (LA = $Ni(CO)_3$ in Figure 1a).[26] Instead of $Ni(CO)_3$ serving to define the Tolman's electronic parameters, LA = RhCl(CO) is here preferred for the sake of comparison with former results on related complexes of chelating bisimidazolophosphines,[27] and more generally because of the added value of the complementary ^{103}Rh NMR probe for rhodium-phosphine complexes.[28]

Results and Discussion

Synthesis of nitro-benzimidazolophosphines

The four *NH*,N_2*CH* benzimidazole precursors **1a**–**d** were provided either as commercially available for **1a**, or prepared following known procedures; the nitro derivative **1b** or **1c** (in tautomeric equilibrium) was thus elaborated from 4-nitro-1,2-benzenediamine by condensation of triethylorthoester in the presence of a catalytic amount of $TiCl_4$ and the dinitro derivative **1d** was obtained by nitration of **1b**,**c** with fuming HNO_3 in concentrated H_2SO_4 (see the Experimental Section and cited references).

N-Phenylation of **1a** and **1b**,**c** was implemented by copper-catalyzed C-N coupling from iodobenzene under conditions reported by Buchwald et al.,[29] yielding **2a** in 90% yield,[30] and the isomers **2b** and **2c** in 64% and 23% yield, respectively, after separation by column chromatography.[31] The method however failed to produce **2d** from **1d**, in correlation with the very low N-nucleophilicity of **1d** resulting from the cooperative effect of the two nitro groups.

N-*p*-Nitrophenylation of **1a**–**c** was carried out by S_NAr of 4-fluoro-nitrobenzene, affording the known nitro derivative **2e** in 95% yield,[30] and the isomers **2f** and **2g** in 53% and 34% yield, respectively.[32] Using the same procedure from **1d**, the trinitro derivative **2h** was isolated in 86% yield (Scheme 1).

Phosphinylation of the lithium salts of **2a**–**c**-**2e**–**h** by nucleophilic substitution of $ClPPh_2$ required optimization of the initial deprotonation step. Inspired by the above-mentioned report on the selective deprotonation and reactivity of the N-methyl congener of **2b**,[25] the use of lithium diisopropylamide (LDA) as a base in THF was envisaged, with a strict control of the temperature at −78 °C.[33] Applied to **2b**, these conditions indeed allowed isolation of **3b** in 83% yield, in the absence of any oxyazobenzene side-product (Scheme 2).[33] The same procedure gave access in 56% yield to the reference non-nitrated benzimidazolophosphine **3a**, previously reported to be available in 20% yield only under metal-free conditions (in the presence of NEt_3 as a base).[34] In summary, application of the LDA procedure to **2a**–**c**-**2e**–**g** afforded **3a**–**c**-**3e**–**g** in 45–83% yield, while only trace amounts of **3h** were obtained from the trinitro substrate **2h**. The phosphinylation selectivity was first evidenced by NMR spectroscopy by the disappearance of the amidine C^1*H* singlet signal at 8.10–8.90 ppm and the appearance of a $^{31}P\{^1H\}$ singlet signal in the range −21.3/−24.5 ppm.

Single crystals of **3b**, **3c**, **3e** and **3f** deposited from solvent mixtures of pentane and dichloromethane (DCM) were found suitable for X-ray diffraction (XRD) analysis (see the Supporting Information).[35] Notably, the structure of the 5-nitrobenzimidazolophosphine **3b** was resolved in the uncommon $P6_1$ space group of the hexagonal system. In all the structures, the C–P distances are virtually identical (1.83 ± 0.01 Å) and the torsion angles between the N-Ar and benzimidazole mean planes have a median value of 68.5 ± 1.3°. The amidine sp^2-C1 atom is found slightly pyramidalized, with a tilting angle of the C–P bond axis versus the imidazole ring mean plane of ca. 4.7 ± 0.3° for **3c** and **3e**-**f**, but reaching 11.3° for **3b**.

Coordination complexes of nitro-benzimidazolophosphines

With the view to comparing the coordinating properties of the benzimidazolophosphines through IR ν_{CO} values of RhCl(CO), complexes of type **4** (Scheme 3), **3a**–**c** and **3e**–**h** were first sequentially reacted with $[Rh(COD)Cl]_2$ (for cleavage of the μ-Cl

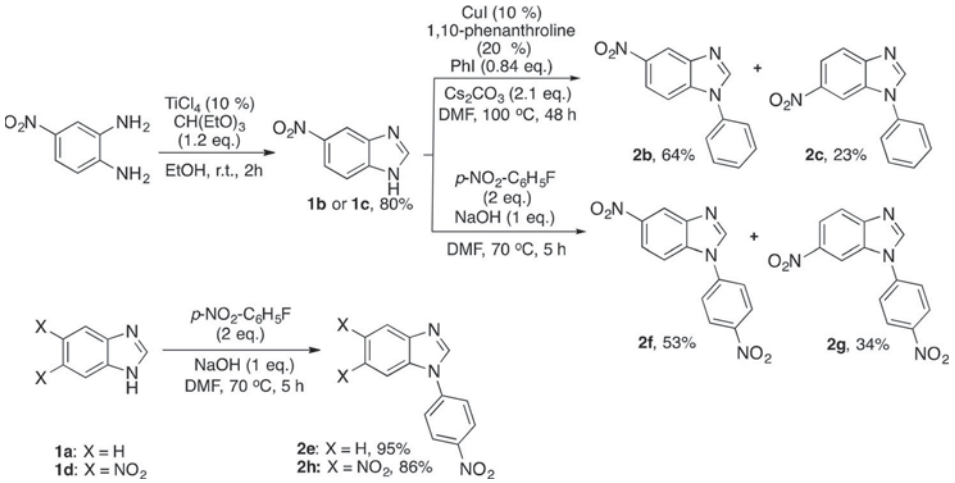

Scheme 1. Syntheses of nitro-functionalized benzimidazoles (for the 4,5-X_2 isomer of **1d**, **1d′**, see the Supporting Information).

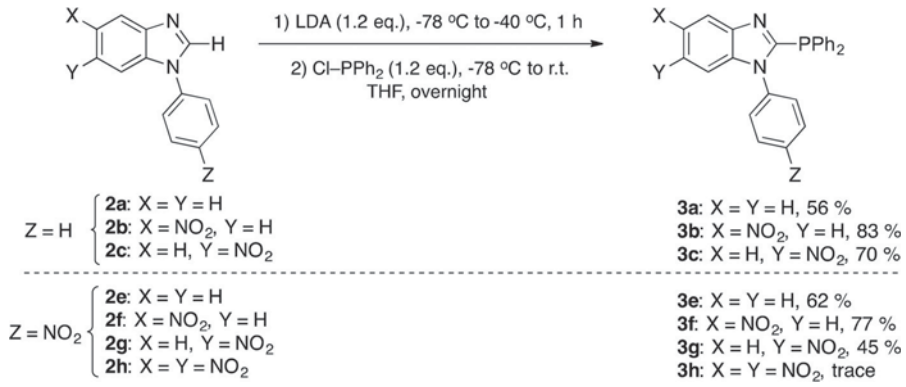

Scheme 2. Selective C-phosphinylation of nitro-functionalized benzimidazoles.

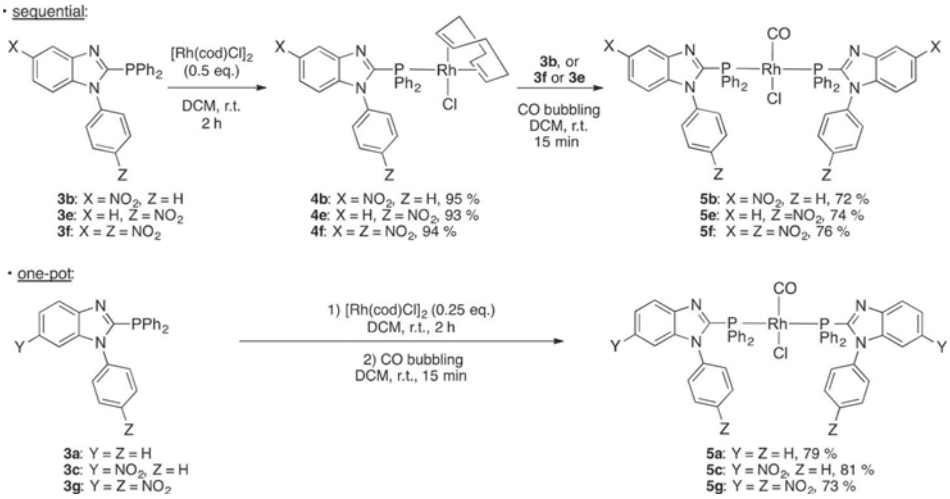

Scheme 3. Sequential and one-pot, two-step syntheses of RhCl(CO) complexes of nitro-substituted benzimidazolophosphines. From **6x**, initially non-identified side-products denoted as **6x** (***x*** = **b**,**c** **e**–**g**) were also obtained (see Figure 3).

bridges; COD = 1,5-cyclooctadiene) before displacement of the COD ligand by a second equivalent of the phosphine and a carbonyl ligand.

Reaction of **3b** with half an equivalent of $[Rh(COD)Cl]_2$ in DCM for 2 h at room temperature led to the COD complex **4b** in 95% yield. P-Rh coordination was established by the change of the $^{31}P\{^1H\}$ NMR signal, shifting from −22.88 to +19.00 ppm, and splitting from a singlet to a doublet with a coupling constant of 150.7 Hz characteristic of a $^1J_{PRh}$ coupling. Moving the nitro group from the benzimidazole core in **3b** to the Ar N-substituent in **3e** did not alter the reactivity with the Rh^I dimer, giving **4e** in 93% yield. Likewise, reaction of the dinitro benzimidazolophosphine **3f** with $[Rh(COD)Cl]_2$ gave **4f** in a similar 94% yield. Further displacement of the COD ligand of **4b**, **4e** and **4f** was achieved by adding one additional equivalent of the respective phosphines **3b**, **3e** and **3f**, followed by CO bubbling for 15 min, thus affording the diphosphine RhCl(CO) complexes **5b**, **5e** and **5f** in 74±2% yield (Scheme 3). In each case, another phosphine-rhodium complex numbered as **6b**, **6e** or **6f** was concomitantly formed as an initially non-identified side-product, the structural assignment of which could be achieved by crystallographic analysis only (see below, Figure 3).

A one-pot procedure was also attempted, providing the target complexes with slightly higher overall yields, as illustrated from **3a**, **3c** and **3g** (Scheme 3). Two equivalents of **3c** were thus treated with half an equivalent of $[Rh(COD)Cl]_2$ in DCM for 2 h at r.t., and subsequently with bubbling carbon monoxide for 15 min., affording **5c** in 81% yield. The same treatment from **3a** and **3g** provided directly **5a** and **5g** in 79% and 73% yield, respectively. In all cases involving a nitro ligand (not in the case of **5a**), the side-product of initially unknown structure **6x** (***x*** = **b**,**c**, **e**–**g**) was also observed (see below).

For the sake of reference to the original concern, the RhCl(CO) complex **5a′** of the cationic benzimidazoliophosphine **3a′** was also targeted. Treatment of **3a** with one equivalent of methyl triflate (MeOTf) in DCM at −78 °C actually led to the N-methylated target product **3a′** in mixture with the P-methylated isomer **3a″** in a 5:1 ratio, as evidenced by the disappearance of the ^{31}P NMR signal of **3a** (−24.49 ppm) and appearance of two signals at −15.48 and +14.36 ppm consistent

with the structures of **3a**′ and **3a**′′, respectively. This lack of N/P selectivity in the reaction of the hard methylating agent MeOTf with imidazolophosphine is unprecedented, but correlated with the absence of a second P center in the monophosphine **3a** as compared to the cases of the *N*-aryl benzimidazolo- and imidazolo-diphosphines BIMINAP (2-(diphenylphosphanyl)-1-[2-(diphenylphosphanyl)naphthalen-1-yl]-1*H*-1,3-benzodiazole) and BIPHIMIP (2-(diphenylphosphanyl)-1-[2-(diphenylphosphanyl)phenyl-1*H*-imidazole).[6e,12b,36] Under the same conditions, treatment of the 5-nitrobenzimidazolophosphine **3b** with MeOTf gave a mixture of the N- and P-methylated isomers **3b**′ and **3b**′′ in a 3:2 ratio according to NMR analysis (see the Supporting Information): this further lowering of N/P selectivity can be interpreted by the electron-withdrawing effect of the nitro group decreasing the electron density of the N atom more than that of the more remote P atom.

As the two cations **3a**′ and **3a**′′ could not be efficiently separated, the 5:1 mixture was used in coordination experiments. Treatment of this mixture with 0.25 mol. equivalent of $[Rh(COD)Cl]_2$ with respect to **3a**′, before bubbling carbon monoxide for 15 min allowed the complex **5a**′ to be isolated in a high 85% yield after removal of **3a**′′ by washing the DCM-containing residue with cold pentane (Scheme 4).

The $P_2RhCl(CO)$ complexes of type **5** have been characterized by ^{1}H, ^{13}C, ^{31}P and ^{103}Rh NMR and IR spectroscopies (see below). Remarkably, no MS method, among ESI, APCI and MALDI, was found suitable to produce molecular peaks of the complexes, preventing structural confirmation by HRMS: the lability of primary cationic species generated in the MS chamber is actually correlated with the weak donating ability of the monodentate ligands. The structures of **5a–c**, **5f–g** and **5a**′ were more precisely determined by XRD analysis of single crystals grown slowly from DCM solutions (Table 1, Figure 2). Notably, the structure of the dinitro ligand complex **5f** was resolved with the chiral space group $P2_12_12_1$. In the crystal state, all the complexes were found to exhibit a square planar-like geometry, with a *trans* arrangement of the two phosphine ligands, and an occupation disorder of the facing Cl and CO ligands, except for **5f** and **5a**′. While the Rh–Cl and Rh–C distances vary in the ranges 2.38 ± 0.03 Å and 1.81 ± 0.02 Å, respectively, the C–P distances remain close to 2.31 ± 0.01 Å. The C–O distance, varying in the range 1.14 ± 0.03 Å (Table 1), appears not to be a significant indicator of the global electron-donating ability of the phosphine ligand.[37a] This can be ascribed to the *cis*-orientation of the P-Rh-CO bonds, and to the long recognized considerably weaker geometrical *cis*-influence of a P ligand on the lengthening of a geminal Rh-L bond (with an

Table 1. Crystallographic data for the complexes **5a–c**, **5f,g** and **5a**′.

	5a	**5b**	**5c**	**5f**	**5g**	**5a**′	**6f**
CCDC no	1496162	1496160	1496161	1496163	1496164	1496165	1496166
Empirical formula	$C_{51}H_{38}ClN_4OP_2Rh$	$C_{55}H_{44}Cl_9N_6O_5P_2Rh$	$C_{51}H_{36}ClN_6O_5P_2Rh$	$C_{53}H_{38}Cl_5N_8O_9P_2Rh$	$C_{53}H_{38}Cl_5N_8O_9P_2Rh$	$C_{58.5}H_{51}Cl_8F_6N_4O_7P_2RhS_2$	$C_{57.7}H_{47.4}Cl_{15.4}N_8O_9P_2Rh_2$
M_r	923.19	1352.92	1013.19	1273.05	1273.05	1548.67	1810.59
Cryst. system	monoclinic	triclinic	triclinic	orthorhombic	orthorhombic	triclinic	triclinic
Space group	$P2_1/n$	$P\bar{1}$	$P\bar{1}$	$P2_12_12_1$	*Pbca*	$P\bar{1}$	$P\bar{1}$
T [K]	100	100	100	100	120	100	100
a [Å]	10.704(3)	9.5819(3)	8.8037(4)	14.0668(9)	15.9457(5)	14.7172(11)	10.5619(3)
b [Å]	11.496(4)	10.7141(4)	10.9560(6)	16.7870(13)	11.2917(3)	15.0289(11)	17.8643(6)
c [Å]	17.080(4)	14.7256(6)	12.0990(6)	22.524(2)	29.2082(11)	18.4532(14)	19.6796(7)
α [°]	90	98.0370(16)	87.651(2)	90	90	91.977(3)	97.7610(16)
β [°]	99.466(9)	102.8561(16)	79.310(2)	90	90	109.881(2)	90.9492(15)
γ [°]	90	102.9773(16)	69.853(2)	90	90	117.436(2)	104.4739(14)
V [Å^3]	2073.1(5)	1407.26(6)	1076.24(9)	5318.8(5)	5259.08(19)	3316.0(4)	3557.48(13)
D_c	1.479	1.596	1.563	1.590	1.608	1.551	1.690
Z	2	1	1	4	4	2	2
$\mu(Mo_{K\alpha})$ [mm^{-1}]	0.599	0.842	0.593	0.698	0.706	0.761	1.146
Refl. measured	31654	86814	52472	79662	76783	106296	180292
Refl. unique/R_{int}	4800/0.143	12318/0.026	4759/0.038	13763/0.058	7694/0.098	21412/0.030	24511/0.035
Refl. [$I > 3\sigma(I)$]	2792	10661	4427	11405	4876	16438	18966
Nb parameters	274	403	313	704	352	811	928
R	0.0560	0.0389	0.0266	0.0309	0.0621	0.0560	0.0348
R_w	0.0609	0.0348	0.0233	0.0312	0.0751	0.0540	0.0366
S = GooF	1.121	1.049	1.073	1.093	0.999	1.030	1.077
$\Delta\rho_{max}/\Delta\rho_{min}$ [e Å^{-3}]	1.20/−1.99	0.98/−0.67	0.41/−0.72	0.57/−0.41	0.95/−1.03	2.40/−0.96	2.10/−1.27

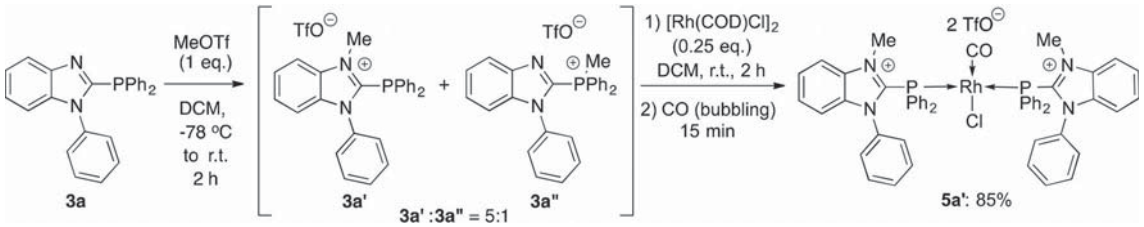

Scheme 4. N- vs. P-methylation of the benzimidazolophosphine **3a**, and P-coordination of the benzimidazoliophosphine product **3a**′ at a RhCl(CO) center.

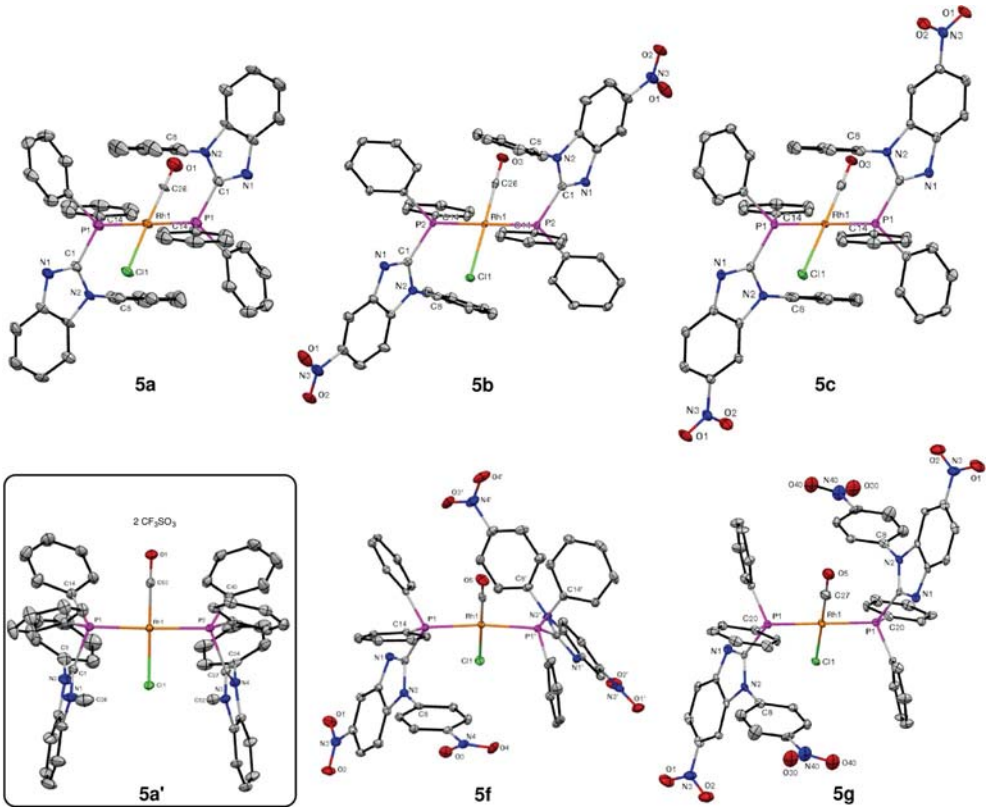

Figure 2. XRD molecular views of **5a–c**, **5f–g** and **5a′**. Thermal ellipsoids at the 50% probability level. For clarity, hydrogen atoms are omitted. The ellipsoid diagrams of the triflate anions of **5a"** are also omitted. The N-Ph and P-Ph *ipso* atoms reveal a π-stacking interaction: C8–C14 ≈3.26 Å (**5a**), 3.20 Å (**5b**, **5c**), 3.18 Å (**5f**), 3.14 Å (**5a′**); C8–C20 ≈2.24 Å (**5g**); C34–C40 ≈3.14 Å (**5a′**). In the dication **5a′**, the sandwiching of the Cl atom by the benzimidazolium moieties is indicated by the short distances: Cl1–C1 ≈Cl1–C27 = 3.01 ± 0.01 Å, Cl1–N1 ≈Cl1–N3 = 3.20 Å, Cl1–N2 ≈Cl1–N4 = 3.41 ± 0.00 Å Cl1–C26 ≈Cl1–C52 = 3.55 ± 0.05 Å.

even weaker correlated influence on the C=O bond length for L = CO) as compared to the corresponding *trans*-influences.[37b] For the a priori least donating dicationic ligand **3a′**, the intermediate C–O distance value of 1.14 Å is, however, also correlated with the unique conformational features of the complex **5a′**. In the neutral complexes **5a–c**, **5f–g**, indeed, the $ImPh_2P$-(Rh)-PPh_2Im unit adopts a staggered conformation, with perfectly *anti*-periplanar imidazolyl groups in **5a–c** and **5g** (Im-P-P-Im dihedral angles = 180°), and synclinal-gauche imidazolyl groups wrapping the Rh–Cl bond in **5f** (Im-P···P-Im dihedral angle = 45°, N_2C···Cl ≈3.28 Å). In contrast, the dicationic complex **5a′** exhibits a perfectly eclipsed conformation of the Rh–Cl bond with both the *syn*-periplanar imidazolyl groups (Im-P···P-Im dihedral angle = 2.8°); the shortness of the N_2C^+···$Cl^{\delta-}$ distances (3.01 ± 0.01 Å) is attributed to the electrostatic effect.

Tentative analysis of coordination properties of nitro-benzimidaz*olo*phosphines

Disregarding the classical broadness of the ^1H signals of the cyclooctadiene ligand in complexes **4**, all the other signals of NMR spectra of complexes **4** and **5** recorded at room temperature are particularly sharp (see the Supporting Information, section 2, pp. 32–51), ruling out any slow equilibrium between a main *trans* form (found in the crystal state) and significant proportion of the putative *cis* isomer. The latter is indeed expected to be thermodynamically highly disfavored by the bulkiness of the P environment. Notably, the ^{31}P coordination shift $\Delta\delta_{^{31}P}(\boldsymbol{x}) = \delta_{^{31}P}(\mathbf{5x}) - \delta_{^{31}P}(\mathbf{3x})$ (***x*** = **a–g**, **a′**) is found larger for the cationic ligand ($\Delta\delta_{^{31}P}(\mathbf{a'}) = 53.6$ ppm) than for the neutral ligands, for which $\Delta\delta_{^{31}P}$ is found to depend on the presence of NO_2 groups on the benzimidazole core only (Table 2): $\Delta\delta_{^{31}P}$ ≈45.5 ± 0.1 ppm for a non-nitrated benzimidazole core (***x*** = **a**, **e**), $\Delta\delta_{^{31}P}$ ≈46.6 ± 0.3 ppm otherwise (***x*** = **b**, **c**, **f**, **g**). At last, the $^1J_{RhP}$ coupling constant does not vary significantly remaining in the range 129.6 ± 1.5 Hz for all the neutral complexes, and just reaching 132.8 Hz for the dicationic complex **5a′**.

In a more classical approach, the IR stretching frequency of the CO co-ligand (ν_{CO}) and ^{103}Rh, ^{31}P NMR chemical shifts ($\delta_{^{103}Rh}$, $\delta_{^{31}P}(\mathbf{5x})$) of the $(\mathbf{3x})_2RhCl(CO)$ complexes **5x** in CD_2Cl_2 solutions were selected for appraising the coordinating properties of **3x**, ***x*** = **a–g**, **a′** (Table 2). The "pre-coordinating" properties of the latter was also tentatively envisaged to be revealed by its ^{31}P NMR chemical shift in the free state, $\delta 31_P(\mathbf{3x})$.

As previously observed in related RhX(COD)(phosphine) complexes,[28] no correlation is observed between $\delta_{^{103}Rh}(\mathbf{5x})$ and either $\delta_{^{31}P}(\mathbf{5x})$ or $\delta_{^{31}P}(\mathbf{3x})$. P-Coordination to non-metal hard Lewis acids such an oxygen atom is the singlet spin state (promoted oxygen, O*) was also envisaged in the corresponding phosphine oxides **3xO**, ***x*** = **a–g**, generated by treatment of **3x** with H_2O_2 (**3aO** and **3bO** were also isolated and character-

Table 2. Selected IR, NMR spectroscopic or crystallographic data for the ligands **3a–c**, **3f,g**, **3a′** or complexes thereof.[a,b]

charge	Z	*x*[a]	ν_{CO} (**5x**)[c] [cm^{-1}]	$\delta 103_{Rh}$ (**5x**)[f,d]	[ppm][e]	$\delta 31_P$ (**5x**) [ppm]	$\Delta\delta 31_P(x)$[g] [ppm]	$^1J_{RhP}$ [Hz]	$\delta 31_P$ (**3x**) [ppm]	$\delta 31_P$ (**3xO**) [ppm]	$d_{C\text{-}O}$ (**5x**)[h] [Å]
0	H	**a**	1966	−8586	−288	20.9	45.4	129.6	−24.5	17.0	1.110(14)
0	H	**b**	1968	−8613	−316	23.7	46.7	129.6	−23.0	17.6	1.138(4)
0	H	**c**	1969	−8612	−315	23.9	46.4	131.2	−22.5	17.4	1.160(5)
0	NO_2	**e**	1979	n.d.		22.3	45.7	128.3	−23.4	18.1	–
0	NO_2	**f**	1978	n.d.		25.0	46.9	129.6	−21.9	17.9	1.157(3)
0	NO_2	**g**	1980	−8612	−315	25.0	46.3	129.6	−21.3	17.9	1.161(16)
+1	H	**a′**	2005	−8733	−436	38.1	53.6	132.8	−15.5	–	1.141(3)

[a] Substitution pattern (***x***=**a–g**, **a′**) of N-phenyl-benzimidazole core as defined in Figure 1 (X, Y, Z=H, NO_2) and Scheme 4 (for **a′**). [b] NMR spectra of solutions in CD_2Cl_2; [c] from IR spectra in the solid state recorded by the ATR (attenuated total reflection) technique; [d] chemical shift with respect $Rh(acac)_3$ with the frequency ratio Ξ'= 3.186447%; [e] chemical shift for the formal frequency ratio Ξ=3.160000%; [f] the $^1J_{Rh\text{-}P}$ coupling constants remain similar, varying from 128.3 Hz for **5e** to 132.8 Hz for **5a′**; [g] coordination shift: $\Delta\delta_{^{31}P}(x)=\delta_{^{31}P}(\mathbf{5x})-\delta_{^{31}P}(\mathbf{3x})$; [h] from X-ray diffraction data (see Table 2 and the Supporting Information).

for the dicationic complex **5a′** are out of range, but relatively consistent with the expected effects of "electronegative" substituents on the global donating character of the P atom towards the RhCl(CO) center.

The sensitivity of the ν_{CO} value to *p*-nitro-substitution at the N-phenyl group is remarkable (+ 10 cm^{-1} for a remote NO_2 group, nine-bond away from the CO ligands), in particular with regard to the vanishing effect of nitro substitution at the benzimidazole core in spite of π-conjugation with the coordinating P center. Whatever the electronic process at stake (partial π-conjugation and/or σ-inductive attraction through the N-Ar bond), the observation is in line with former observations of a marked effect of *N*-nitroaryl and *N*-fluoroaryl substitution on intrinsic π-accepting ability or catalytic properties of imidazol-2-ylidene ligands.[38]

ized: see the Supporting Information); the ^{31}P NMR shifts of **3xO** remain, however, almost constant at 17.5±0.5 ppm.

The ν_{CO} and $\delta_{^{103}Rh}$ parameters thus appear to play complementary roles for appraising the effects of nitro substituents on either the benzimidazole core or pending N-phenyl group, respectively.

Whatever the nitro-decoration of the benzimidazole core, indeed, an N-phenylated ligand gives ν_{CO}=1968±1 cm^{-1} (**5a–c**) and an N-*p*-nitrophenylated ligand gives ν_{CO}=1979±1 cm^{-1} (**5e–g**). Using the ^{103}Rh NMR probe (see the Experimental Section), whatever the N-aryl substituent, the presence of a nitro substituent on the benzimidazole core (at either position 5 or 6) gives $\delta_{^{103}Rh}$=−315 ppm, vs. $\delta_{^{103}Rh}$=−288 ppm for the non-nitrated reference **5a** (the value for **5e** could, however, not be determined due to solubility issues). The ν_{CO} and $\delta_{^{103}Rh}$ values

Dinuclear nitro-benzimidazolophosphine side products: CH_2Cl_2-clathrate complexes

Each of the nitro-containing complexes **5b,c**, **5e-.g** (Scheme 3) was actually obtained in mixture with a side-product containing a Rh–P bond, as evidenced by ^{31}P NMR spectroscopy of the crude material, and denoted as **6b,c**, **6e–g** (see the Experimental Section). The exact structure of these complexes could, however, not be assessed by spectroscopic methods. In the case of the dinitro ligand **3f**, however, crystals of **6f** deposited from a DCM solution of the residue obtained from the supernatant of crystals of **5f** after reaction of **3f** with **4f** (Scheme 3). X-ray diffraction analysis showed a dinuclear structure, where the two Rh centers are in distorted bipyramidal environments, coordinated by a μ-CO and two P,N-bridging ligands **3f** (Figure 3). The corresponding structures are assigned

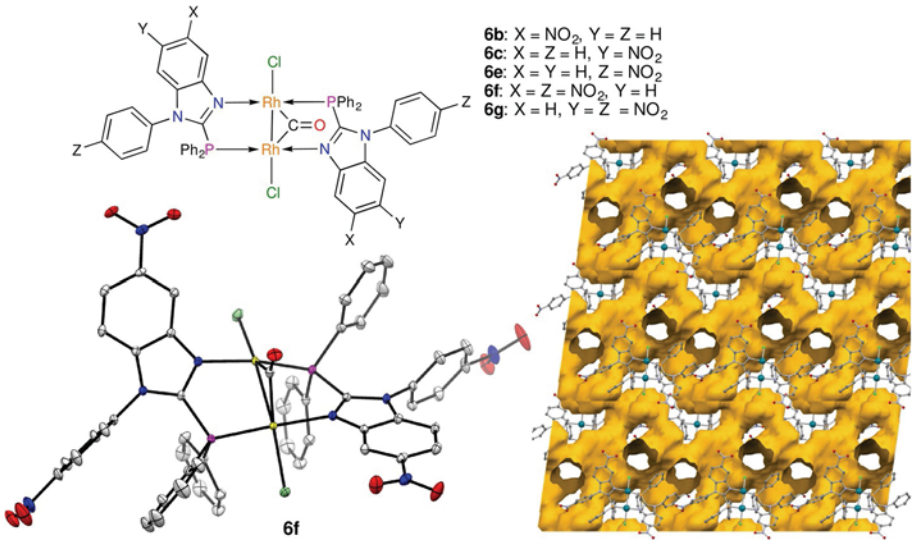

Figure 3. Lewis structure of the dinuclear side-products formed along with the target complexes **5b,c**, **5e–g** (Scheme 3; top), crystallographic molecular view of **6f** with thermal ellipsoids at the 50% probability level (bottom left), and free van der Waals gallery available for hosting DCM solvent molecules within the network of molecules of **6f** (bottom right).

to the side-products **6b**, **6c**, **6e** and **6g** obtained from **4b**, **4c**, **4e** and **4g**, respectively.

A search in the CCDC database for similar complexes featuring such a $[Rh_2(\mu\text{-}CO)Cl_2]$ core gave 18 related examples, five of them featuring P,N coordination to the Rh centers, with Rh–Rh bonding distances ranging from 2.57 Å to 3.01 Å.[39] The Rh–Rh distance of 2.63 Å measured in **6f** is thus quite short, smaller than the average value of 2.68 Å over the series. The Rh–Cl bonds of **6f** (bent from the Rh–Rh axis by ca. 163°) are significantly shorter than all the corresponding bonds within the CCDC sampling (2.36 Å vs. 2.42 to 2.45 Å). The C–O distance of 1.17 Å measured in **6f** is identical to the average value over the CCDC series. The Rh–P bonds of **6f** are found to be quite short (2.21–2.22 Å), and much shorter than in the parent complex **5f** (2.31 Å). The Rh–N bonds are, however, found to be consistently shorter (2.08–2.10 Å).

The crystals of **6f** are actually clathrates, with 6.7 DCM molecules per molecule of **6f**. The high solvent content was first suspected after observing disintegration of isolated crystals in polyisobutene blend oils used as cryo-protectants for XRD analysis (PARATONE or PARABAR 10312; the use of a perfluoropolyether oil, PFO-XR 75, was finally required). The solvate molecules are spread over 12 positions, eight of them being partially occupied and forming a chain with short distances between positions strongly occupied by Cl atoms (Cl···Cl ≈3.5 Å), thus suggesting that the chain cohesion is due to halogen bonding,[40a] today widely invoked in crystal engineering.[40b,c] Chains of DCM molecules were also proposed to occur in a related dirhodium complex, [39i] but the extended van der Waals gallery within the crystal network of **6f** (Figure 3) meets more general challenges in the search for metal–organic inclusion compounds of the clathrate type or porous coordination polymers,[41a] in particular for DCM guest molecules which are more currently found hosted by organic lattices.[41b–e] Within the family of the Werner clathrates, based on a discrete packing of MX_2L_4 complexes (M = divalent transition metal ion, X = small anionic ligand, L = pyridine ligand),[41f] and related Hoffmann clathrates based on a grid of CN-bridged coordination polymer (initiated by the cadmium(II)-CCl_4 clathrate),[41g,h] one may cite the Werner DCM-clathrate $[Ni(NCS)_2(3\text{-cyanopyridine})_4]\cdot 2CH_2Cl_2$.[41i] More particular examples are the recently described dinuclear clathrates $[Cd_2I_2(\mu\text{-}L)_2]\cdot CH_2Cl_2$ (L = 4,4′-bis(2-methylimidazol-1-ylmethyl)biphenyl),[41j] and $[Ag(NO_3)_2Pt(\mu\text{-}$benzothiadiazol-4-ylethynyl)(4-diphenylaminopyridine)$]\cdot CH_2Cl_2$.[41k]

Conclusion

The disclosed strategy, upstream based on the use of LDA as the optimal base for the deprotonation of more or less nitrated *N*-aryl benzimidazole precursors dedicated to react with $ClPPh_2$, allowed a pioneering exploration of the coordination chemistry of nitroaromatic phosphines as neutral electron-poor ligands with decreased σ-donating ability. The approach and results open natural prospects in organometallic chemistry such as the synthesis of tri- or tetra-nitro counterparts of the ligands **3**, the design of chelating diphosphine congeners, and the comparison with possible analogous complexes of nitrated triphenylphosphines such as $(4\text{-}NO_2\text{-}C_6H_4)_3P$ standing as a paradigm. As a preliminary analysis, reduction of the P atom of known *p*-nitrophenylphosphine oxides with the classical $HSiCl_3$ reagent is, however, expected to be tricky: in spite of an early report,[15e] recent results indeed indicate that competing reduction of the nitro group by $HSiCl_3$ could occur, even under milder conditions.[42] In an alternative strategy, (4-nitrophenyl)-diphenylphosphine, partly described 40 years ago,[15b,20] was targeted from 4-nitro-iodobenzene and $ClPPh_2$ but could not be isolated, and further efforts in this direction are naturally envisaged. Nevertheless, targeting the particular category of the benzimidazolyllphosphine complexes **4** and **5** gave the opportunity of evidencing unique features such as: (i) empirical binary "orthogonal spectroscopic indicators" of the presence or not of nitro groups on distinct parts of the ligand (the benzimidazole core and the N-aryl substituent), based on an observed contrast between two ranges of values separated by ca. 5 times the spectroscopic resolutions: 10 cm^{-1} and 30 ppm, respectively, for the ν_{CO} and δ_{Rh} probes at the RhCl(CO) center; (ii) in the dicationic complex **5a′**, an electrostatic sandwiching of a chloro ligand by two imidazolium rings resulting from a packing effect, and possibly balanced by enhanced polarization of the Rh-Cl bond; (iii) serendipitous finding of an organic–organometallic clathrate of high solvent content (the DCM solvate complex **6f**). A more general occurrence of such features could be sought for in other systems involving other transition metals (Ni, Pd, Pt) and ligands or co-ligands thereof. Finally, beyond coordination chemistry, the results are naturally aimed at exploring the use such complexes in homogeneous catalysis.

Experimental Section

General remarks

THF and diethyl ether were dried and distilled over sodium-benzophenone. Pentane and dichloromethane (DCM) were dried with a PureSolv-MD-5 Innovative Technology system for the purification of solvents. $[Rh(COD)Cl]_2$ and other reagents were employed as received from commercial sources, in particular, solutions of *n*BuLi were 2.5 M in hexane. All reactions were carried out under an argon atmosphere by using Schlenk and vacuum line techniques. Column chromatography was carried out on silica gel (60 Å, C.C 70–200 μm). Previously reported procedures were used for the preparation of the phosphines and their precursors, in particular for the previously described compounds **1b** and **1c**,[43] **1d** and **1e**,[44] **2a**,[45] and **3a**.[6e,29b]

Procedures for the preparation of new compounds

For the characterization of the reported compounds by ^1H, ^{31}P,^{13}C NMR and IR spectroscopies, by mass spectrometry, and by melting point, see the Supporting Information.

Preparation of 2b and 2c.[44] A mixture of **1b** (2.69 g, 16.5 mmol), Cu^I (0.263 g, 1.38 mmol), 1,10-phenanthroline (0.48 g, 2.76 mmol), Cs_2CO_3 (9.42 g, 28.9 mmol) was evacuated twice and back-filled with argon in a dried Schlenk tube, then iodobenzene (1.52 mL, 13.8 mmol) and DMF (20 mL) was added with a syringe. The reaction mixture was stirred at 100 °C for 48 h. After the mixture was cooled down to ambient temperature, the solution was filtered on

silica gel, extracted with EtOAc, dried over $MgSO_4$ and concentrated under reduced pressure. The residue was purified by column chromatography on silica gel eluted with a 3/2 EtOAc/pentane mixture to deliver **2b** (2.108 g, 8.8 mmol, 64%) and **2c** (0.75 g, 3.1 mmol, 23%) as yellow solids.

Preparation of 2f and 2g.[46] A mixture of **1b** (1.63 g, 10 mmol) and NaOH (0.40 g, 10 mmol) in 20 mL DMF was treated with 4-nitrofluorobenzene (2.12 mL, 20 mmol) at room temperature under argon. The mixture was stirred at 70 °C for 5 h before addition of water. The resulting suspension was extracted with EtOAc (3× 40 mL), and the organic layers were combined, dried over $MgSO_4$ and concentrated to dryness under reduced pressure. Column chromatography of the residue on silica gel eluted with a 3/2 EtOAc/pentane mixture afforded the corresponding products **2f** (1.51 g, 5.3 mmol, 53%) and **2g** (0.97 g, 3.4 mmol, 34%) as yellow solids.

The same procedure from **1e** afforded **2e** as a yellow solid in 95% yield. Starting from **1h**, and changing the chromatographic eluting system to a 1/1 EtOAc/pentane mixture, **2h** was obtained as a yellow solid in 86% yield.

General procedure for preparation of the nitroaromatic phosphines 3b,c, 3e–h

A solution of **2a–c**, **2e–h** (1 equiv) in THF was treated with a solution of freshly prepared LDA (1.2 equiv) at −78 °C. The mixture was slowly warmed up to −40 °C, then stirred for 1 h at this temperature. After cooling back to −78 °C, chlorodiphenylphosphine was added dropwise and the solution was slowly warmed up, then stirred at r.t. for 4 h. After addition of a saturated aqueous NH_4Cl solution and dilution with DCM, the aqueous layer was separated and the organic layer was dried over $MgSO_4$ and concentrated to dryness under reduced pressure. The residue was purified by column chromatography on silica gel eluted with a 3/1 DCM/pentane mixture to give the corresponding products as yellow solids (for more details, see the Supporting Information): **3a** (78%), **3b** (83%), **3c** (70%), **3e** (62%), **3f** (77%), **3g** (45%), **3h** (<5%).

General procedure for generation of the phosphine oxides 3xO (x = a-c, e-g)

The phosphine oxides were generated according to a previously reported procedure,[47] by treatment of a solution **3x** in THF with H_2O_2 (3 equiv) at room temperature under TLC monitoring. After addition of $NaHCO_3$ and $Na_2S_2O_3$ solutions, the reaction mixture was separated, and the aqueous layer was extracted with DCM. The combined organic layer was dried over Na_2SO_4 and concentrated under reduced pressure affording the corresponding phosphine oxide in quantitative ^{31}P NMR spectroscopic yield without further purification. The products were analyzed by ^{31}P NMR spectroscopy only (see Table 2), except for **3aO** and **3bO** which were more completely characterized (see the Supporting Information).

General procedures for the preparation of rhodium complexes

Method A. A solution of **3x** (***x*** = **b**, **f**, **e**) and $[Rh(cod)Cl]_2$ (0.5 equiv) in DCM was stirred at r. t. for 4 h. After concentration under reduced pressure, the residue was washed with pentane and dried to afford the corresponding rhodium complex as brown solids: **4b** (95%), **4e** (93%), **4f** (94%).

A solution of **4x** and the corresponding phosphine **3x** (1 equiv) in DCM was treated with bubbling carbon monoxide for 15 min. After concentration under reduced pressure, the residue was washed with diethyl ether (or a DCM/pentane mixture) to give the corresponding rhodium complex **5b** (60%), **5e** (74%), **5f** (76%). Minor amounts of the dimeric rhodium complex **6b** (18%), **6e** (14%) or **6f** (15%) were also detected by ^{31}P NMR spectroscopy of the crude material (approximate spectroscopic yields given). Crystals of **6f** deposited from a DCM solution could be characterized by XRD analysis (see below and the Supporting Information).

Method B. A solution of **3x** (***x*** = **a**, **c**, **g**) and $[Rh(cod)Cl]_2$ (0.25 equiv) in DCM was stirred at r. t. for 4 h. Carbon monoxide was then bubbled through the solution for 15 min. After evaporation of the solvent under reduced pressure, the crude mixture was washed with diethyl ether (or a DCM/pentane mixture) to give the corresponding rhodium complex **5a** (79%), **5c** (81%) or **5g** (73%) as a yellow solid. Minor amounts of the dimeric rhodium complex **6c** (4%) or **6g** (13%) were also detected by ^{31}P NMR spectroscopy of the crude material (approximate spectroscopic yields given).

Rhodium complex 5a′. To a solution of **3a** (152 mg, 0.4 mmol) in DCM (4 mL) at −90 °C was added methyl trifluoromethanesulfonate (45 μL, 0.4 mmol). The mixture was slowly warmed up to −40 °C and stirred for 2 h. After evaporation of the solvent under reduced pressure, the residue was washed with cold pentane, dried under reduced pressure and then analyzed as a 5:1 N^+Me:P^+Me mixture of the methylation products of **3a**, which could not be separated. To a solution of this mixture in DCM (10 mL) was added $[Rh(cod)Cl]_2$ (41 mg, 0.083 mmol), and stirring was pursued at r. t. for 4 h. Carbon monoxide was then bubbled through the solution for 15 min. The solvent was evaporated under reduced pressure, and the residue was washed with diethyl ether to afford **5a′** (130 mg, 68%) as a yellow solid.

^{103}Rh NMR spectroscopy

$^{103}Rh/^{31}P\{^1H\}$ HMQC spectra were recorded on a Bruker AV400 spectrometer, equipped with a three-canal probe H{P}{X}-TBI 5 mm using saturated solutions of **5x** in CD_2Cl_2 (in the cases of **5e** and **5f**, saturated concentration did not allow achieving sufficient acquisition in available time). A preliminary search for the ^{103}Rh resonances was performed through $^{31}P\{^1H\}$ experiments with ^{103}Rh inversion using a sequence adapted from the literature giving a narrow range for ^{103}Rh chemical shifts.[48] In this range, precise chemical shifts of ^{103}Rh were measured via an inverse correlation HMQC using both ^{103}Rh-^{31}P coupling constants. The exact spectrometer ^1H frequency of $\nu_0 = 400.1318$ MHz corresponds to the resonance of tetramethylsilane. The ^{103}Rh frequency ratio Ξ can be assigned to either the formal value Ξ = 3.16% (for which rhodium metal is just an approximate reference giving $\delta_{^{103}Rh} \approx 0$ ppm),[49] or to the observable value Ξ′ = 3.186447% defined from the real reference $Rh(acac)_3$ (for which $\delta_{^{103}Rh} = 0$ ppm if saturated in $CDCl_3$ solution).[50] Each frequency ratio defines its own chemical shift scale in ppm: $\delta = (\nu - \Xi\nu_0)/(\Xi\nu_0)\ 10^6$ and $\delta' = (\nu - \Xi'\ \nu_0)/(\Xi'\ \nu_0)\ 10^6$, where ν is the physical resonance frequency observed for the nominal field of the spectrometer. By elimination of ν, the scales are related by the equation: $\delta = \delta'\xi + (\xi - 1)\ 10^6$, where $\xi = \Xi'/\Xi = 1.008369$ (giving $\delta(Rh(acac)_3) = 8369 \approx 8358$ ppm for $\delta'(Rh(acac)_3) = 0$).[49a] The $\delta_{^{103}Rh}$ values in Table 2 are given in both scales.

Crystallographic studies

Intensity X-ray diffraction data from single crystals were collected at low temperature on an Apex2 Bruker diffractometer equipped with a 30 W air-cooled microfocus source ($\lambda = 0.71073$ Å) or on an Oxford-Diffraction Gemini ($\lambda = 0.71073$ or 1.54180 Å). The structures

were solved using direct methods or SUPERFLIP, and refined by means of least-squares procedures on *F* using the programs of the PC version of CRYSTALS. Atomic scattering factors were taken from the International Tables for X-Ray Crystallography.[51] All non-hydrogen atoms were refined anisotropically. Hydrogen atoms were refined using a riding model. Absorption corrections were introduced using the program MULTISCAN. For the free phosphines **3 b** and **3 f**, it was not possible to resolve diffuse electron-density residuals (enclosed solvent molecules). Treatment with the SQUEEZE facility from PLATON resulted in a smooth refinement.[52]

Supporting Information

It includes yields, spectroscopic and other characterizations of all new compounds. ^{1}H, ^{31}P, ^{13}C,^{103}Rh-$^{31}P\{^{1}H\}$ HMQC NMR spectra and crystallographic data are also provided.

Acknowledgements

C.Z. thanks the China Scholarship Council for financial support. R.C. thanks the CNRS for half a teaching sabbatical in 2014–2015 and 2015–2016. A determining support was also indirectly provided by the ANR program (ANR-11-BS07-016-01). The authors are also indebted to Dr. Valérie Maraval for efficient logistic management.

Conflict of interest

The authors declare no conflict of interest.

Keywords: coordination bond · nitroaromatic chemistry · nitroarylphosphines · P ligands · phosphines · rhodium carbonyl complexes

[1] C. Lepetit, V. Maraval, Y. Canac, R. Chauvin, *Coord. Chem. Rev.* **2016**, *308*, 59 – 75.

[2] a) D. J. Nelson, S. P. Nolan, *Chem. Soc. Rev.* **2013**, *42*, 6723 – 6753; b) M. Melaimi, M. Soleilhavoup, G. Bertrand, *Angew. Chem. Int. Ed.* **2010**, *49*, 8810 – 8849; *Angew. Chem.* **2010**, *122*, 8992 – 9032; c) "Late transition metal complexes of neutral η^1-carbon ligands": G. van Koten in *Top. Organomet. Chem.* (Eds.: R. Chauvin, Y. Canac), Springer, Heidelberg, **2010**; d) J. Vignolle, X. Cattoën, D. Bourissou, *Chem. Rev.* **2009**, *109*, 3333 – 3384; e) S. Díez-González, N. Marion, S. P. Nolan, *Chem. Rev.* **2009**, *109*, 3612 – 3676; f) F. E. Hahn, M. C. Jahnke, *Angew. Chem. Int. Ed.* **2008**, *47*, 3122 – 3172; *Angew. Chem.* **2008**, *120*, 3166 – 3216; g) Y. Canac, M. Soleihavoup, S. Conejero, G. Bertrand, *J. Organomet. Chem.* **2004**, *689*, 3857 – 3865.

[3] C. Maaliki, C. Lepetit, Y. Canac, C. Bijani, C. Duhayon, R. Chauvin, *Chem. Eur. J.* **2012**, *18*, 7705 – 7714.

[4] See for example: a) R. L. Pruett, J. A. Smith, *J. Org. Chem.* **1969**, *34*, 327 – 330; b) K. Nozaki, T. Nanno, H. Takaya, *J. Organomet. Chem.* **1997**, *527*, 103 – 108; c) R. A. Baber, M. L. Clarke, K. M. Heslop, A. C. Marr, A. G. Orpen, P. G. Pringle, A. Ward, D. E. Zambrano-Williams, *Dalton Trans.* **2005**, 1079 – 1085; d) F. Doro, J. N. H. Reek, P. W. N. M. van Leeuwen, *Organometallics* **2010**, *29*, 4440 – 4447; e) Q. Liu, L. Wu, I. Fleischer, D. Selent, R. Franke, R. Jackstell, M. Beller, *Chem. Eur. J.* **2014**, *20*, 6888 – 6894.

[5] See for example: a) M. F. Ernst, D. M. Roddick, *Inorg. Chem.* **1989**, *28*, 1624 – 1627; b) M. Brookhart, W. A. Chandler, A. C. Pfister, C. C. Santini, P. S. White, *Organometallics* **1992**, *11*, 1263 – 1274; c) D. C. Smith, Jr., E. D. Stevens, S. P. Nolan, *Inorg. Chem.* **1999**, *38*, 5277 – 5281; d) D. R. Palo, C. Erkey, *Organometallics* **2000**, *19*, 81 – 86; e) F. Berhal, O. Esseiva, C. H. Martin, H. Tone, J.-P. Genet, T. Ayad, V. Ratovelomanana-Vidal, *Org. Lett.* **2011**, *13*, 2806 – 2809; f) B. G. Anderson, J. L. Spencer, *Chem. Eur. J.* **2014**, *20*, 6421 – 6432.

[6] a) I. V. Komarov, M. Y. Kornilov, A. A. Tolmachev, A. A. Yurchenko, E. B. Rusanov, A. N. Chernega, *Tetrahedron* **1995**, *51*, 11271 – 11280; b) M. Enders, O. Fritz, H. Pritzkow, *Z. Anorg. Allg. Chem.* **2004**, *630*, 1501 – 1506; c) P. Antognazza, T. Benincori, S. Mazzoli, F. Sannicolo, T. Pilati, *Phosphorus Sulfur Silicon Relat. Elem.* **1999**, *144*, 405 – 408; d) T. Benincori, E. Brenna, F. Sannicolo, L. Trimarco, P. Antognazza, E. Cesarotti, F. Demartin, T. Pilati, G. Zotti, *J. Organomet. Chem.* **1997**, *529*, 445 – 453; e) N. Debono, Y. Canac, C. Duhayon, R. Chauvin, *Eur. J. Inorg. Chem.* **2008**, 2991 – 2999; f) I. Abdellah, N. Debono, Y. Canac, L. Vendier, R. Chauvin, *Chem. Asian J.* **2010**, *5*, 1225 – 1231.

[7] For pioneering works, see: a) U. Zoller, *Tetrahedron* **1988**, *44*, 7413 – 7426; b) N. Kuhn, J. Fahl, D. Blaeser, R. Boese, *Z. Anorg. Allg. Chem.* **1999**, *625*, 729 – 734; c) N. Kuhn, M. Goehner, G. Henkel, *Z. Anorg. Allg. Chem.* **1999**, *625*, 1415 – 1416; d) J. Sirieix, M. Obberger, B. Betzemeier, P. Knochel, *Synlett* **2000**, *11*, 1613 – 1615; e) M. Azouri, J. Andrieu, M. Picquet, P. Richard, B. Hanquet, I. Tkatchenko, *Eur. J. Inorg. Chem.* **2007**, 4877 – 4883.

[8] For reviews, see: a) Y. Canac, C. Maaliki, I. Abdellah, R. Chauvin, *New. J. Chem.* **2012**, *36*, 17 – 27; b) S. Gaillard, J. L. Renaud, *Dalton Trans.* **2013**, 7255 – 7270; c) M. Alcarazo, *Chem. Eur. J.* **2014**, *20*, 7868 – 7877; d) M. Alcarazo, *Acc. Chem. Res.* **2016**, *49*, 1797 – 1805.

[9] I. Abdellah, C. Lepetit, Y. Canac, C. Duhayon, R. Chauvin, *Chem. Eur. J.* **2010**, *16*, 13095 – 13108.

[10] a) C. Mboyi, C. Maaliki, A. Mankou Makaya, Y. Canac, C. Duhayon, R. Chauvin, *Inorg. Chem.* **2016**, *55*, 11018 – 11027; b) G. Mehler, P. Linowski, J. Carreras, A. Zanardi, J. W. Dube, M. Alcarazo, *Chem. Eur. J.* **2016**, *22*, 15320 – 15327.

[11] J. Petuskova, H. Bruns, M. Alcarazo, *Angew. Chem. Int. Ed.* **2011**, *50*, 3799 – 3802; *Angew. Chem.* **2011**, *123*, 3883 – 3886.

[12] a) B. Vabre, Y. Canac, C. Duhayon, R. Chauvin, D. Zargarian, *Chem. Commun.* **2012**, *48*, 10446 – 10448; b) I. Abdellah, Y. Canac, C. D. Mboyi, C. Duhayon, R. Chauvin, *J. Organomet. Chem.* **2015**, *776*, 149 – 162; c) B. Vabre, Y. Canac, C. Lepetit, C. Duhayon, R. Chauvin, D. Zargarian, *Chem. Eur. J.* **2015**, *21*, 17403 – 17414.

[13] C. Hansch, A. Leo, R. W. Taft, *Chem. Rev.* **1991**, *91*, 165 – 195.

[14] Generalization of the Hammett equation, originally defined for X/H-substitution (-H⟶-X), to aza-analogation (=CH-⟶=*N*-) and protoaza-analogation (=CH-⟶=NH^+-) gives the following values for the corresponding constants: $\sigma_{m(N)}=0.45$, $\sigma_{p(N)}=0.76$, $\sigma_{m(NH+)}=2.09$ and $\sigma_{p(NH+)}=2.34$. Comparison with the NO_2/H-substitution values ($\sigma_m=0.71$, $\sigma_p=0.78$) indicates that neutral azalogation has a significant, albeit weaker, electron-withdrawing effect, but suggests that *N*-protonation (representative of *N*-alkylation) has a twice stronger effect ($\sigma_{m(NH+)}-\sigma_{m(N)}=1.64$, $\sigma_{p(NH+)}-\sigma_{p(N)}=1.58$). See: C. D. Jonhson, *The Hammet Equation*, pp. 99 – 101, Cambridge University Press, London, **1973**.

[15] a) A. Stachlewska-Wroblowa, K. Okon, *Bull. Acad. Pol. Sci. Ser. Sci. Chim.* **1961**, *9*, 297 – 301; b) G. P. Schiemenz, *Chem.Ber.* **1966**, *99*, 514 – 519; c) G. P. Schiemenz, K. Roehlk, *Chem.Ber.* **1971**, *104*, 1219 – 1233; d) J. I. G. Cadogan, D. J. Sears, D. M. Smith, *J. Chem. Soc. C* **1969**, 1314 – 1318; e) G. P. Schiemenz, P. Nielsen, *Phosphorus Sulfur Relat. Elem.* **1985**, *21*, 259 – 266.

[16] DFT calculations at the B3PW91/6-31G(d,p) level, without solvent correction (vacuum), using the Firefly software (see SI): a) A. A. Granovsky, Firefly version 8, (http://classic.chem.msu.su:gran:firefly:index.html) which is partially based on the GAMESS (US) source code; b) M. W. Schmidt, K. K. Baldridge, J. A. Boatz, S. T. Elbert, M. S. Gordon, J. H. Jensen, S. Koseki, N. Matsunaga, K. A. Nguyen, S. Su, T. L. Windus, M. Dupuis, J. A. Montgomery, *J. Comput. Chem.* **1993**, *14*, 1347 – 1363.

[17] G. A. Olah, B. G. B. Gupta, S. C. Narang, *J. Am. Chem. Soc.* **1979**, *101*, 5317 – 5322.

[18] a) M. Makosza, M. Paszewski, D. Sulikowski, *Synlett* **2008**, 2938 – 2940; b) J. Xu, P. B. Zhang, Y. Z. Gao, Y. Y. Chen, G. Tang, Y. F. Zhao, *J. Org. Chem.* **2013**, *78*, 8176 – 8183; c) M. Hayashi, T. Matsuura, I. Tanaka, H. Ohta, Y. Watanabe, *Org. Lett.* **2013**, *15*, 628 – 631; d) H. Zhang, X. Y. Zhang, D. Q. Dong, Z. L. Wang, *RSC. Adv.* **2015**, *5*, 52824 – 52831; e) D. V. Aleksanyan, Z. S. Klemenkova, A. A. Vasil'ev, A. Y. Gorenberg, Y. V. Nelyubina, V. A. Kozlov, *Dalton Trans.* **2015**, *44*, 3216 – 3226.

[19] Model nitroaryl-phosphine ligands in Rh^{II}, Ru^{II} or Fe^{II} complexes have however been calculated at the DFT level of theory: a) P. Hirva, P. Lahuerta, J. Perez-Prieto, *Theor. Chem. Acc.* **2005**, *113*, 63 – 68; b) P. Hirva, E. Julio, J. Lloret, P. Lahuerta, J. Perez-Prieto, *Inorg. Chem.* **2007**, *46*, 2619 – 2626; c) E. Pump, L. Cavallo, C. Slugovc, *Monatsh. Chem.* **2015**, *146*, 1131 – 1141; d) B. Mondal, F. Neese, S. Ye, *Inorg. Chem.* **2016**, *55*, 5438 – 5444.
[20] G. P. Schiemenz, M. Finzenhagen, *Liebigs Ann. Chem.* **1976**, 2126 – 2135.
[21] a) N. F. Blank, J. R. Moncarz, T. J. Brunker, C. Scriban, B. J. Anderson, O. Amir, D. S. Glueck, L. N. Zakharov, J. A. Golen, C. D. Incarvito, A. L. Rheingold, *J. Am. Chem. Soc.* **2007**, *129*, 6847 – 6858; b) N. Nowrouzi, S. Keshtgar, E. B. Jahromi, *Tetrahedron Lett.* **2016**, *57*, 348 – 350.
[22] a) F. Y. Kwong, C. W. Lai, Y. Tian, K. S. Chan, *Tetrahedron Lett.* **2000**, *41*, 10285 – 10289; b) S. E. Martin, M. Bonaterra, R. A. Rossi, *J. Organomet. Chem.* **2002**, *664*, 223 – 227.
[23] For recent examples in the aryl-heteroaryl series, see: a) N. V. Artemova, M. N. Chevykalova, Y. N. Luzikov, I. E. Nifant'ev, E. E. Nifant'ev, *Tetrahedron* **2004**, *60*, 10365 – 10370; b) D. M. Zink, D. Volz, T. Baumann, M. Mydlak, H. Flügge, J. Friedrichs, M. Nieger, S. Bräse, *Chem. Mater.* **2013**, *25*, 4471 – 4486.
[24] a) G. Bartoli, *J. Chem. Soc. Perkin Trans. 2* **1989**, 573 – 578; b) G. Bartoli, M. Bosco, R. Dalpozzo, L. Grossi, *NATO ASI Ser. Ser. C* **1989**, *257*, 489 – 502.
[25] G. Piersanti, L. Giorgi, F. Bartoccini, G. Tarzia, P. Minetti, G. Gallo, F. Giorgi, M. Castorina, O. Ghirardi, P. Carminati, *Org. Biomol. Chem.* **2007**, *5*, 2567 – 2571.
[26] C. A. Tolman, *Chem. Rev.* **1977**, *77*, 313 – 348.
[27] a) Y. Canac, N. Debono, L. Vendier, R. Chauvin, *Inorg. Chem.* **2009**, *48*, 5562 – 5568; b) C. Barthes, C. Lepetit, Y. Canac, C. Duhayon, D. Zargarian, R. Chauvin, *Inorg. Chem.* **2013**, *52*, 48 – 58.
[28] C. J. Elsevier, B. Kowall, H. Kragten, *Inorg. Chem.* **1995**, *34*, 4836 – 4839.
[29] a) A. Klapars, J. C. Antilla, X. Huang, S. L. Buchwald, *J. Am. Chem. Soc.* **2001**, *123*, 7727 – 7729; b) S. Harkal, F. Rataboul, A. Zapf, C. Fuhrmann, T. Riermeier, A. Monsees, M. Beller, *Adv. Synth. Catal.* **2004**, *346*, 1742 – 1748.
[30] L. Zhu, L. Cheng, Y. Zhang, R. Xie, J. You, *J. Org. Chem.* **2007**, *72*, 2737 – 2743.
[31] The regioisomers are markedly distinguished by the amidine CH ^{1}H NMR chemical shift, at 8.70 ppm for **2b** and 8.39 ppm for **2c**, vs. 8.35 ppm for **2a**: assuming that the substituent effect (vs. H in **2a**) is first determined by the shortest bond path to the NO_2 group, the C5 path of **2b** appears more efficient than the C3NC path of **2c**.
[32] The dinitro compounds **2f** and **2g** could be separated by column chromatography, but their lack of solubility in organic solvent happened to be detrimental to their isolation in highly pure form. Noteworthy, the Buchwald's procedure from **1b**,**c** and 4-iodonitrobenzene was found much less efficient, giving **2f** and **2g** in 25% and 12% yield, respectively.
[33] At a higher temperature of −40 °C, LDA was indeed reported to reduce nitroarenes to aminoarenes and oxyazoarenes via single electron transfer (SET): A. L. Wang, E. Biehl, *ARKIVOC* **2002**, 71 – 75.
[34] L. H. Zou, Z. B. Dong, C. Bolm, *Synlett* **2012**, *23*, 1613 – 1616.
[35] CCDC 1496156 (**3b**), 1496157 (**3c**), 1496158 (**3f**), 1496159 (**3e**), 1496162 (**5a**), 1496160 (**5b**), 1496161 (**5c**), 1496163 (**5f**), 1496164 (**5g**), 1496165 (**5a′**) and 1496166 (**6f**) contain the supplementary crystallographic data for this paper. These data can be obtained free of charge from The Cambridge Crystallographic Data Centre.
[36] N-alkyl congeners of *N*-phenyl imidazolo-monophosphines (non-benzannelated analogues of **3a**) were reported to undergo selective N-methylation with Me_2SO_4 or $[Me_3O][BF_4]$, and selective P-methylation with MeI: A. A. Tolmachev, A. A. Yurchenko, A. S. Merculov, M. G. Semenova, E. V. Zarudnitskii, V. V. Ivanov, A. M. Pinchuk, *Heteroat. Chem.* **1999**, *10*, 585 – 597.
[37] Even in the neutral ligand sub-series, the C – O distance takes the smallest value of 1.11 Å in **5a** for the a priori most electron-donating representative **3a** and significantly greater values of ca. 1.16 Å in **5c** and **5f**–**g** for the corresponding nitro-ligands **3c** and **3f**-**g** (Table 1); F. R. Hartley, *Chem. Soc. Rev.* **1973**, *2*, 163 – 179.
[38] See, for example: a) T. Vorfalt, S. Leuthußer, H. Plenio, *Angew. Chem. Int. Ed.* **2009**, *48*, 5191 – 5194; *Angew. Chem.* **2009**, *121*, 5293 – 5296; b) T. Sato, Y. Hirose, D. Yoshioka, S. Oi, *Organometallics* **2012**, *31*, 6995 – 7003; c) Z.-Q. Zhu, M.-Y. Jiang, J.-H. Lin, C.-P. Zhang, X.-C. Hang, C.-G. Zheng, Q.-Y. Chen, J.-C. Xiao, *Synlett* **2009**, 2305 – 2308; d) T. Ritter, M. W. Day, R. H. Grubbs, *J. Am. Chem. Soc.* **2006**, *128*, 11768 – 11769; e) M. G. Hobbs, C. J. Knapp, P. T. Welsh, J. Borau-Garcia, T. Ziegler, R. Roesler, *Chem. Eur. J.* **2010**, *16*, 14520 – 14533 and references therein; f) D. A. J. Harding, E. G. Hope, K. Singh, G. A. Solan, *Organometallics* **2012**, *31*, 1518 – 1523 and references therein.
[39] a) R. J. Haines, N. D. C. T. Steen, *J. Chem. Soc. Chem. Commun.* **1981**, 407 – 408; b) R. J. Haines, N. D. C. T. Steen, *J. Chem. Soc. Dalton Trans.* **1983**, 2229 – 2234; c) N. C. Yang, H. Shou, T. Wang, J. Masnovi, *J. Am. Chem. Soc.* **1980**, *102*, 6654 – 6656; d) J. P. Farr, M. M. Olmstead, C. H. Hunt, A. L. Balch, *Inorg. Chem.* **1981**, *20*, 1182 – 1187; e) H. Braunschweig, M. Forster, K. Radacki, *Angew. Chem. Int. Ed.* **2006**, *45*, 2132 – 2134; *Angew. Chem.* **2006**, *118*, 2187 – 2189; f) F. A. Cotton, C. T. Eagle, A. C. Price, *Inorg. Chem.* **1988**, *27*, 4362 – 4368; g) R. Y. Haines, M. Laing, E. Meintjies, F. Sommerville, *J. Organomet. Chem.* **1981**, *215*, C17 – C19; h) F. E. Wood, M. M. Olmstead, A. L. Balch, *J. Am. Chem. Soc.* **1983**, *105*, 6334 – 6335; i) R. E. Marsh, M. M. Olmstead, W. P. Schaefer, V. Schomakert, *Inorg. Chem.* **1993**, *32*, 4658 – 4659; j) L. A. Oro, M. A. Ciriano, B. E. Villarroya, A. Tiripicchio, F. J. Lahoz, *J. Chem. Soc. Chem. Commun.* **1984**, 521 – 522; k) B. R. Sutherland, M. Cowie, *Inorg. Chem.* **1984**, *23*, 1290 – 1297; l) A. L. Balch, L. A. Fossett, R. R. Guimerans, M. M. Olmstead, *Organometallics* **1985**, *4*, 781 – 788; m) L. Gelmini, D. W. Stephan, *Inorg. Chim. Acta* **1985**, *98*, L3 – L6; n) R. H. Dawson, M. M. Harding, S. Maginn, A. K. Smith, *Inorg. Chim. Acta* **1988**, *149*, 281 – 284; o) S. Jääskeläinen, M. Haukka, H. Riihimäki, J. T. Pursiainen, T. A. Pakkanen, *J. Organomet. Chem.* **2004**, *689*, 1064 – 1070; p) B. T. Heaton, C. Jacob, J. T. Sampanthar, *J. Chem. Soc. Dalton Trans.* **1998**, 1403 – 1410; q) L. A. Oro, M. A. Ciriano, B. E. Villarroya, A. Tiripicchio, F. J. Lahoz, *J. Chem. Soc. Dalton Trans.* **1985**, 1891 – 1898; r) H. Song, R. C. Haltiwanger, M. R. DuBois, *Organometallics* **1987**, *6*, 2022 – 2028.
[40] For a recent general review, see: a) G. Cavallo, P. Metrangolo, R. Milani, T. Pilati, A. Priimagi, G. Resnati, G. Terraneo, *Chem. Rev.* **2016**, *116*, 2478 – 2601; b) *Halogen Bonding in Crystal engineering, fundamentals and applications*, *Cryst. Growth Des.* virtual issue, **2012**, Volume *vi* (8), http://pubs.acs.org/page/cgdefu/vi/8; c) F. M. Amombo Noa, S. A. Bourne, L. R. Nassimbeni, *Cryst. Growth Des.* **2015**, *15*, 3271 – 3279.
[41] a) S. Kitagawa, K. Uemura, *Chem. Soc. Rev.* **2005**, *34*, 109 – 119; b) F. Bottino, P. Finocchiaro, J. Lipkowski, A. Mamo, S. Pappalardo, K. Suwinska, *J. Inclusion Phenom. Mol. Recognit. Chem.* **1991**, *11*, 41 – 48; c) A. R. Albunia, R. Graf, *Soft Mater.* **2011**, *9*, 183 – 198; d) B. T. Ibragimov, *CrystEngComm* **2007**, *9*, 111 – 118; e) V. G. Saraswatula, M. A. Bhat, S. Bhattacharya, B. K. Saha, *J. Chem. Sci.* **2014**, *126*, 1265 – 1273; see for example: f) D. V. Soldatov, *J. Chem. Crystallogr.* **2006**, *36*, 747 – 768; g) T. Kitazawa, S. Nishikiori, R. Kuroda, T. Iwamoto, *Chem. Lett.* **1988**, 1729 – 1732; see for example: h) K. Vellingiri, A. Deep, K.-H. Kim, *ACS Appl. Mater. Interfaces* **2016**, *8*, 29835 – 29857; i) M. L. Kilkenny, L. R. Nassimbeni, *J. Chem. Soc. Dalton Trans.* **2001**, 3065 – 3068; j) T. Jacobs, L. J. Barbour, *CrystEngComm* **2013**, *15*, 1512 – 15414; k) Z. Dai, A. J. Metta-Magana, J. E. Nunez, *Inorg. Chem.* **2014**, *53*, 7188 – 7196.
[42] a) M. Orlandi, F. Tosi, M. Bonsignore, M. Benaglia, *Org. Lett.* **2015**, *17*, 3941 – 3943; b) M. Orlandi, M. Benaglia, F. Tosi, R. Annunziata, F. Cozzi, *J. Org. Chem.* **2016**, *81*, 3037 – 3041.
[43] Z. H. Zhang, L. Yin, Y. M. Wang, *Catal. Commun.* **2007**, *8*, 1126 – 1131.
[44] a) G. A. Zhumabaeva, S. K. Kotovskaya, N. M. Perova, V. N. Charushin, O. N. Chupakhin, *Russ. Chem. Bull.* **2006**, *55*, 1243 – 1247; b) K. Kincaid, J. Beckman, A. Zivkovic, R. L. Halcomb, J. W. Engels, R. D. Kuchta, *Nucleic Acids Res.* **2005**, *33*, 2620 – 2628.
[45] L. B. Zhu, P. Guo, G. C. Li, J. B. Lan, R. G. Xie, J. S. You, *J. Org. Chem.* **2007**, *72*, 8535 – 8538.
[46] C. B. Liu, H. Wang, X. Xing, Y. Xu, J. A. Ma, B. Zhang, *Tetrahedron Lett.* **2013**, *54*, 4649 – 4652.
[47] Y. Unoh, T. Satoh, K. Hirano, M. Miura, *ACS Catal.* **2015**, *5*, 6634 – 6639.
[48] A. Bax, *J. Magn. Reson.* **1983**, *52*, 76 – 80.
[49] a) B. E. Mann in *NMR of Newly Accessible Nuclei, Vol. 2* (Ed.: P. Laszlo), Academic Press, New York, **1983**, Chap. 11, pp. 301 – 318; b) J. M. Ernsting, S. Gaemers, C. J. Elsevier, *Magn. Reson. Chem.* **2004**, *42*, 721 – 736.
[50] a) R. Benn, A. Rufinska, *Angew. Chem. Int. Ed. Engl.* **1986**, *25*, 861 – 881; *Angew. Chem.* **1986**, *98*, 851 – 871; b) R. K. Harris, E. D. Becker, S. M. Cab-

ral de Mennezes, R. Goodfellow, P. Granger, *Pure Appl. Chem.* **2001**, *73*, 1795 – 1818; c) R. K. Harris, E. D. Becker, S. M. Cabral de Mennezes, P. Granger, R. E. Hoffman, K. H. Zilm, *Pure Appl. Chem.* **2008**, *80*, 59 – 84.
[51] J. A. Ibers, W. C. Hamilton, *International Tables for X-Ray Crystallography, Vol. IV*, Kynoch, Birmingham, **1974**.
[52] P. V. D. Sluis, A. L. Spek, *Acta Crystallogr. Sect. A* **1990**, *46*, 194 – 201.

Manuscript received: July 28, 2017
Accepted manuscript online: August 28, 2017
Version of record online: October 12, 2017

CHEMISTRY
AN ASIAN JOURNAL

Supporting Information

The forgotten nitro-aromatic phosphines as weakly donating P-ligands: a N-aryl-benzimidazolyl series in RhCl(CO) complexes[†]

Chongwei Zhu,[a,b] Emmanuel Gras,[a,b]* Carine Duhayon,[a,b] Francis Lacassin,[a,b]

Xiuling Cui,[c] Remi Chauvin[a,b,c] *

[a] *CNRS, LCC (Laboratoire de Chimie de Coordination), 205 route de Narbonne, BP44099, 31077 Toulouse Cedex 4 (France)*. Fax: (+33)5 61 55 30 03. E-mail: emmanuel.gras@lcc-toulouse.fr, *chauvin@lcc-toulouse.fr*.
[b] *Université de Toulouse, UPS, ICT-FR 2599, 31062 Toulouse Cedex 9 (France)*
[c] *Engineering Research Center of Molecular Medicine, Ministry of Education, Key Laboratory of Xiamen Marine and Gene Drugs, Institutes of Molecular Medicine and School of Biomedical Sciences, Huaqiao University, Xiamen, 361021 (China).*

asia_201701078_sm_miscellaneous_information.pdf

[†] The paper is dedicated to Prof. Marian Mikolajczyk on the occasion of his 80th birthday.

Table of contents

1. Lists of experimental characterizations

See general procedures used in the main text (sections 4.1 and 4.2.).

The following analytical instruments were used, ^{1}H, ^{13}C, ^{31}P and ^{103}Rh NMR: Avance 300, Avance 400, Avance 400 HD and Avance 500. NMR chemical shifts δ are given in ppm, with positive values to high frequency relative to the tetramethylsilane reference for ^{1}H and ^{13}C, with respect to the H_3PO_4 reference for ^{31}P, and with respect to the formal reference of the frequency ratio Ξ = 3.16 % (for values with respect to the $Rh(acac)_3$ reference of the frequency ratio Ξ'= 3.186447 %, see Table 2 and section 4.3 in the article); coupling constants J are given in Hertz (Hz). UV-visible absorption: Perkin-Elmer UV-Vis Win-Lab Lambda 950. UV-visible extinction molar coefficients ε are given in $L \cdot mol^{-1} \cdot cm^{-1}$ and wavelengths λ in nm. Mass spectra were obtained on a Perkin Elmer Sciex spectrometer (MS/MS API-365). Abreviations: M.p. = Melting point; M.-D.p. = Melting-decomposition point.

1b or 1c. 5-nitro-1*H*-benzo[*d*]imidazole

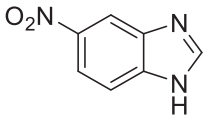

Brown solid (5.22 g, 32 mmol, 80 %); prepared from 4-nitro-o-phenylenediamine (6.32 g, 40 mmol), $HC(OC_2H_5)_3$ (6.8 ml, 48 mmol) and $TiCl_4$ (0.44 ml, 4 mmol) in EtOH (80 mL). **M.p.** = 210-212 °C. **^{1}H NMR** (300 MHz, acetone-d_6) δ: 12.21 (s, 1H), 8.57 (d, J = 2.3 Hz, 1H), 8.48 (s, 1H), 8.17 (dd, J = 8.9, 2.2 Hz, 1H), 7.81 (d, J = 8.9 Hz, 1H). **^{13}C{^{1}H} NMR** (101 MHz, DMSO-d_6) δ: 147.29, 143.08, 142.03, 139.00, 118.11, 115.33, 113.18.

1d. 5,6-dinitro-1*H*-benzo[*d*]imidazole

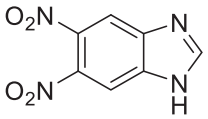

White solid (1.34 g, 6.4 mmol, 66 %); prepared from **1b** (1.6 g, 9.8 mmol) in fuming H_2SO_4 (30 mL) and HNO_3 (15 mL). **M.p.** = 253-255 °C. **^{1}H NMR** (400 MHz, acetone-d_6) δ: 8.71 (s, 1H), 8.40 (s, 2H). **^{13}C{^{1}H} NMR** (101 MHz, acetone-d^6) δ: 148.78, 139.07, 113.65.

1d'. 4,5-dinitro-1*H*-benzo[*d*]imidazole

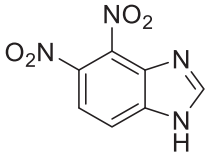

Yellow solid (0.63 g, 3.0 mmol, 31 %); prepared from **1c** (1.6 g, 9.8 mmol) in fuming H_2SO_4 (30 mL) and HNO_3 (15 mL). **M.p.** = 249-251 °C. **^{1}H NMR** (400 MHz, DMSO-d_6) δ: 8.93 (dd, J = 2.0, 0.7 Hz, 1H), 8.80 (d, J = 2.0 Hz, 1H), 8.73 (s, 1H). **^{13}C{^{1}H} NMR** (101 MHz, DMSO) δ: 149.51, 141.87, 133.24, 121.40, 114.71.

2a. 1-phenyl-1*H*-benzo[*d*]imidazole

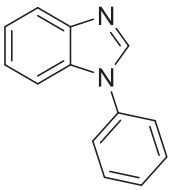

Colorless liquid (2.1 g, 10.8 mmol, 90 %); prepared from the mixture of benzimidazole (1.42 g, 12 mmol), iodobenzene (2.04 g, 10 mmol), CuI (0.38 g, 2 mmol), 1,10-phenanthroline (0.72 g, 4 mmol) and Cs_2CO_3 (6.85 g, 21 mmol) in DMF (20 mL).**^{1}H NMR** (400 MHz, $CDCl_3$) δ: 8.07 (s, 1H), 7.91-7.83 (m, 1H), 7.55-7.47 (m, 3H), 7.46-7.38 (m, 3H), 7.33-7.25 (m, 2H). **^{13}C{^{1}H} NMR** (101 MHz, $CDCl_3$) δ: 144.08, 142.26, 136.31, 133.66, 130.00, 127.98, 123.96, 123.67, 122.77, 120.59, 110.46.

2b. 5-nitro-1-phenyl-1*H*-benzo[*d*]imidazole

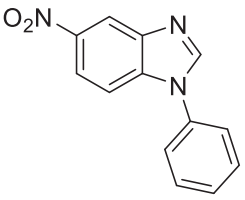

Yellow solid (2.11 g, 8.8 mmol, 64%); prepared from a mixture of **1b** (2.69 g, 16.5 mmol), iodobenzene (2.82 g, 13.8 mmol), CuI (0.26 g, 1.4 mmol), 1,10-phenanthroline (0.50 g, 2.8 mmol) in Cs_2CO_3 (9.42 g, 28.9 mmol) in DMF (30 mL). **M.p.** = 160-162 °C. **^{1}H NMR** (400 MHz, $CDCl_3$) δ: 8.69 (dd, J = 2.2, 0.5 Hz, 1H), 8.26 (s, 1H), 8.19 (dd, J = 9.0, 2.2 Hz, 1H), 7.60-7.64 (m, 2H), 7.57-7.48 (m, 4H). **^{13}C{^{1}H} NMR** (101 MHz, $CDCl_3$) δ: 145.71, 143.98, 143.35, 137.75, 135.17, 130.41, 129.13, 124.26, 119.36, 117.25, 110.60. **HRMS** (ES+) calcd. for $C_{13}H_9N_3O_2$: $[M+H]^+$, 240.0773, found: m/z 240.0773.

2c. 6-nitro-1-phenyl-1*H*-benzo[*d*]imidazole

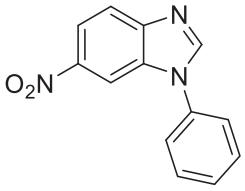

White solid (0.75 g, 3.1 mmol, 23 %); prepared from a mixture of **1c** (2.69 g, 16.5 mmol), iodobenzene (2.82 g, 13.8 mmol), CuI (0.26 g, 1.4 mmol), 1,10-phenanthroline (0.50 g, 2.8 mmol) in Cs_2CO_3 (9.42 g, 28.9 mmol) in DMF (30 mL). **M.p.** = 162-164 °C. **^{1}H NMR** (400 MHz, $CDCl_3$ δ: 8.39 (d, *J* = 2.2 Hz, 1H), 8.31 (s, 1H), 8.19 (dd, *J* = 8.9, 2.2 Hz, 1H), 7.88 (d, *J* = 8.9 Hz, 1H), 7.61-7.64 (m, 2H), 7.55-7.48 (m, 3H). **^{13}C{^{1}H} NMR** (101 MHz, $CDCl_3$) δ: 148.18, 146.67, 144.39, 135.03, 133.19, 130.47, 129.15, 124.26, 120.75, 118.46, 107.56. **HRMS** (ES+) calcd. for $C_{13}H_9N_3O_2$: $[M+H]^+$, 240.0773, found: m/z 240.0779.

2e. 1-(4-nitrophenyl)-1*H*-benzo[*d*]imidazole

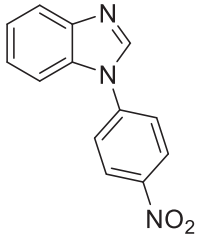

Yellow solid (1.81 g, 7.6 mmol, 95 %); prepared from benzoimidazole (0.94 g, 4 mmol), 1-fluoro-4-nitrobenzene (2.26 g, 8 mmol) and NaOH (0.32 g, 4 mmol) in DMF (10 mL). **M.p.** = 183-185 °C. **^{1}H NMR** (400 MHz, $CDCl_3$) δ: 8.50-8.39 (m, 2H), 8.17 (s, 1H), 7.94 – 7.83 (m, 1H), 7.78-7.68 (m, 2H), 7.65-7.55 (m, 1H), 7.44-7.32 (m, 2H). **^{13}C{^{1}H} NMR** (101 MHz, $CDCl_3$) δ: 146.48, 144.42, 141.68, 141.60, 132.77, 125.81, 124.56, 123.69, 123.61, 121.14, 110.29. **HRMS** (ES+) calcd. for $C_{13}H_9N_3O_2$: $[M+H]^+$, 240.0773, found: m/z 240.0778.

2f. 5-nitro-1-(4-nitrophenyl)-1*H*-benzo[*d*]imidazole

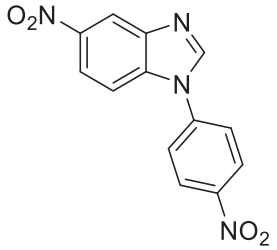

Yellow solid (1.51 g, 5.3 mmol, 53 %); prepared from **1b** (1.63 g, 10.0 mmol), 1-fluoro-4-nitrobenzene (2.82 g, 20 mmol) and NaOH (0.40 g, 10.0 mmol) in DMF (20 mL). **M.p.** = 262-264 °C. **^{1}H NMR** (400 MHz, acetone-d_6) δ: 8.83 (s, 1H), 8.68 (d, *J* = 2.2 Hz, 1H), 8.57 (d, *J* = 8.7 Hz, 2H), 8.33 (dd, *J* = 9.1, 2.2 Hz, 1H), 8.14 (d, *J* = 8.8 Hz, 2H), 7.97 (d, *J* = 9.0 Hz, 1H). **^{13}C{^{1}H} NMR** (101 MHz, acetone) δ: 146.49, 144.11, 140.88, 138.95, 125.59, 124.94, 124.51, 119.33, 116.49, 113.73, 111.38. **HRMS** (ES+) calcd. for $C_{13}H_9N_4O_4$: $[M+H]^+$, 285.0624, found: m/z 285.0634.

2g. 6-nitro-1-(4-nitrophenyl)-1*H*-benzo[*d*]imidazole

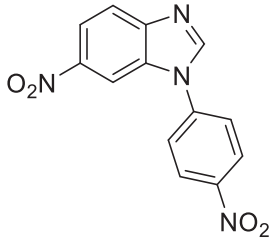

Light yellow solid (0.97 g, 3.4 mmol, 34 %); prepared from **1c** (1.63 g, 10.0 mmol), 1-fluoro-4-nitrobenzene (2.82 g, 20 mmol) and NaOH (0.40 g, 10.0 mmol) in DMF (20 mL). **M.p.** = 159-161 °C. **^{1}H NMR** (400 MHz, acetone-d_6) δ: 8.90 (s, 1H), 8.64 – 8.55 (m, 3H), 8.33 – 8.26 (m, 1H), 8.17 (d, *J* = 9.0 Hz, 2H), 8.00 (d, *J* = 9.0 Hz, 1H). **^{13}C{^{1}H} NMR** (101 MHz, acetone-d_6) δ: 147.58, 146.49, 125.69, 124.93, 124.51, 120.78, 119.33, 118.48, 116.49, 111.38, 107.69. **HRMS** (ES+) calcd. for $C_{13}H_9N_4O_4$: $[M+H]^+$, 285.0624, found: m/z 285.0631.

2h. 5,6-dinitro-1-(4-nitrophenyl)-1*H*-benzo[*d*]imidazole

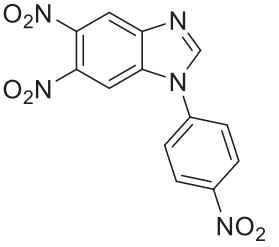

Yellow solid (1.00 g, 3.0 mmol, 86 %); prepared from **1d** (0.74 g, 3.6 mmol), 1-fluoro-4-nitrobenzene (1.01 g, 7.2 mmol) and NaOH (0.14 g, 3.6 mmol) in DMF (7 mL). **^{1}H NMR** (300 MHz, acetone-d_6) δ: 9.07 (s, 1H), 8.60-8.56 (m, 3H), 8.53 (s, 1H), 8.23-8.18 (m, 2H). **^{13}C{^{1}H} NMR** (75 MHz, acetone-d_6) δ: 149.49, 125.64, 125.59, 117.95, 109.69. **HRMS** (ES+) calcd. for $C_{13}H_7N_5O_6$: $[M+H]^+$, 330.0475, found: m/z 330.0478.

3a. 2-(diphenylphosphanyl)-1-phenyl-1*H*-benzo[*d*]imidazole

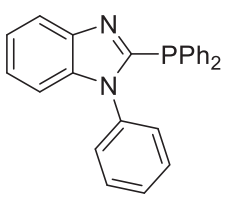

White solid (0.88 g, 2.3 mmol, 56 %); prepared from **2a** (1.37 g, 7.1 mmol), LDA (10.6 mmol in 10 ml THF) and $ClPPh_2$ (1.9 ml, 10.6 mmol) in THF (50 mL). **M.p.** = 157-159 °C. **^{1}H NMR** (400 MHz, $CDCl_3$) δ: 7.91 (d, *J* = 8.1 Hz, 1H), 7.56-7.48 (m, 4H), 7.46-7.40 (m, 3H), 7.39-7.20 (m, 10H), 7.18 (d, *J* = 7.9

Hz, 1H). **^{13}C{^{1}H} NMR** (101 MHz, $CDCl_3$) δ: 154.87 (d, J_{CP} = 10.1 Hz, C), 144.18 (d, J_{CP} = 2.0 Hz, C), 137.70, 136.14 (d, J_{CP} = 2 Hz, C), 134.36, 134.30, 134.15, 129.32 (d, J_{CP} = 2.0 Hz, CH), 128.79, 128.50 (d, J_{CP} = 7.1 Hz, CH), 127.92 (d, J_{CP} = 3.0 Hz, C), 123.48, 122.43, 120.46, 110.26. **^{31}P{^{1}H} NMR** (162 MHz, $CDCl_3$) δ: -24.50. **HRMS** (ES+) calcd. for $C_{25}H_{19}N_2P$: $[M+H]^+$, 379.1364, found: m/z 379.1364.

3aO. 2-(diphenylphosphoroso)-1-phenyl-1*H*-1,3-benzodiazole

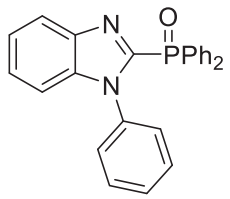

White solid. **^{1}H NMR** (400 MHz, CD_2Cl_2) δ 7.91-7.85 (m, 1H), 7.80-7.74 (m, 4H), 7.55 (m, 2H), 7.45 (m, 4H), 7.40-7.34 (m, 5H), 7.31-7.25 (m, 2H), 7.22 – 7.16 (m, 1H). **^{13}C{^{1}H} NMR** (101 MHz, CD_2Cl_2) δ 148.28(d, J_{CP} = 139.4 Hz, C), 142.76(d, J_{CP} = 17.2 Hz, C), 137.73(d, J_{CP} = 3.0 Hz, C), 135.46, 134.32(d, J_{CP} = 21.4 Hz, C), 132.14(d, J_{CP} = 3.0 Hz, CH), 131.88(d, J_{CP} = 10.1 Hz, CH), 131.08, 128.98, 128.90, 128.35(d, J_{CP} = 12.1 Hz, CH), 127.94, 125.23, 123.35, 120.99, 111.08. **^{31}P{^{1}H} NMR** (162 MHz, CD_2Cl_2) δ 17.23. **HRMS** (ES+) calcd. $C_{25}H_{19}N_2OP$: $[M+H]^+$, 395.1313, found: m/z 395.1316.

3b. 2-(diphenylphosphanyl)-5-nitro-1-phenyl-1*H*-benzo[*d*]imidazole

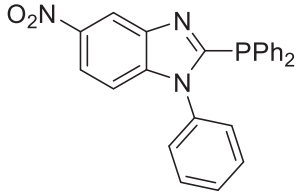

Yellow solid (0.35 g, 0.8 mmol, 83 %); prepared from **2b** (0.24 g, 1.0 mmol), LDA (1.2 mmol in 2 mL of THF) and $ClPPh_2$ (0.36 ml, 2 mmol) in THF (15 mL). **M.p.** = 129-132 °C. **^{1}H NMR** (400 MHz, $CDCl_3$) δ: 8.78 (d, *J* = 2.2 Hz, 1H), 8.15 (dd, *J* = 9.0, 2.2 Hz, 1H), 7.55-7.43 (m, 7H), 7.40-7.31 (m, 6H), 7.20-7.15 (m, 3H). **^{13}C{^{1}H} NMR** (101 MHz, $CDCl_3$) δ: 160.26 (d, J_{CP} = 16.2 Hz, C), 143.83, 143.31 (d, J_{CP} = 2.0 Hz, C), 141.61, 135.03 (d, J_{CP} = 2.0 Hz, C), 134.46 (d, J_{CP} = 21.2 Hz, CH), 133.05 (d, J_{CP} = 5.1 Hz, C), 129.82, 129.71, 129.58, 128.71 (d, J_{CP} = 8.1 Hz, CH), 127.70 (d, J_{CP} = 3.0 Hz, CH), 119.16, 117.00, 110.12. **^{31}P{^{1}H} NMR** (162 MHz, $CDCl_3$) δ: -22.88. **HRMS** (ES+) calcd. for $C_{25}H_{18}N_3O_2P$: $[M+H]^+$, 424.1215, found: m/z 424.1213.

3bO. 2-(diphenylphosphoroso)-5-nitro-1-phenyl-1*H*-1,3-benzodiazole

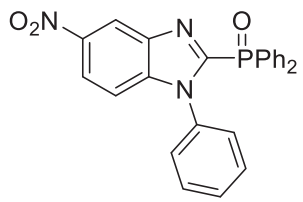

Light yellow solid. **^{1}H NMR** (400 MHz, $CDCl_3$) δ 8.81 (t, J = 1.8 Hz, 1H), 8.19 (dt, J = 9.1, 2.4 Hz, 1H), 7.79 (m, 4H), 7.53 (m, 2H), 7.46-7.34 (m, 7H), 7.24-7.18 (m, 3H). **^{13}C{^{1}H} NMR** (101 MHz, $CDCl_3$) δ 152.58(d, J_{CP} = 132.3 Hz, C), 144.44, 141.85(d, J_{CP} = 17.2 Hz, C), 141.26(d, J_{CP} = 4.0 Hz, C), 134.35, 132.57(d, J_{CP} = 3.0 Hz, CH), 131.80 (d, J_{CP} = 10.1 Hz, CH), 130.95, 129.84, 129.74, 129.37, 128.56(d, J_{CP} = 12.1 Hz, CH), 127.80, 120.57, 118.23, 111.34. **^{31}P{^{1}H}** NMR (162 MHz, $CDCl_3$) δ 17.32. **HRMS** (ES^+) calcd. for $C_{25}H_{19}N_3O_3P$: $[M+H]^+$, 440.1164, found: m/z 440.1166.

3c. 2-(diphenylphosphanyl)-6-nitro-1-phenyl-1*H*-benzo[*d*]imidazole

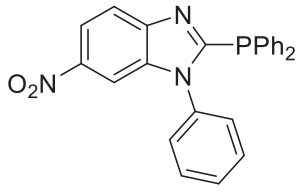

Yellow solid (0.30 g, 0.7 mmol, 70 %); prepared from **2c** (0.24 g, 1.0 mmol), LDA (1.2 mmol in 2 mL of THF) and $ClPPh_2$ (0.22 ml, 1.2 mmol) in THF (15 mL). **M.p.** = 160-163 °C. **^{1}H NMR** (400 MHz, $CDCl_3$) δ: 8.20 (dd, *J* = 8.9, 2.2 Hz, 1H), 8.08 (d, *J* = 2.1 Hz, 1H), 7.91 (d, *J* = 9.0 Hz, 1H), 7.53 – 7.45 (m, 7H), 7.38 (m, 6H), 7.20 (dt, *J* = 8.2, 1.3 Hz, 2H). **^{13}C{^{1}H} NMR** (101 MHz, $CDCl_3$) δ: 161.74 (d, J_{CP} = 17.2 Hz, C), 148.11 (d, J_{CP} = 2.0 Hz, C), 144.11, 137.23, 134.87 (d, J_{CP} = 1.0 Hz, C), 134.49 (d, J_{CP} = 22.2 Hz, CH), 133.05 (d, J_{CP} = 6.1 Hz, C), 129.85, 129.81, 129.68, 128.74 (d, J_{CP} = 8.1 Hz, CH), 127.74 (d, J_{CP} = 3.0 Hz, CH), 120.36, 118.24, 107.12. **^{31}P{^{1}H} NMR** (162 MHz, $CDCl_3$) δ: -22.33. **HRMS** (ES+) calcd. for $C_{25}H_{18}N_3O_2P$: $[M+H]^+$, 424.1215, found: m/z 424.1221.

3e. 2-(diphenylphosphanyl)-1-(4-nitrophenyl)-1*H*-benzo[*d*]imidazole

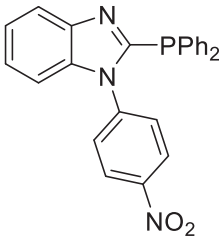

Yellow solid (0.26 g, 0.6 mmol, 62 %); prepared from **2e** (0.24 g, 1.0 mmol), LDA (1.2 mmol in 2 mL of THF) and $ClPPh_2$ (0.36 ml, 2 mmol) in THF (15 mL). **M.p.** = 175-178 °C. **^{1}H NMR** (400 MHz, CD_2Cl_2) δ: 8.30-8.22 (m, 2H), 7.84-7.79 (m, 1H), 7.49-7.27 (m, 14H), 7.23-7.17 (m, 1H). **^{13}C{^{1}H} NMR** (101 MHz, $CDCl_3$) δ: 154.56 (d, J_{CP} = 13.1 Hz, C), 147.33, 144.28, 141.89, 136.92, 134.30 (d, J_{CP} = 21.2 Hz, CH), 133.40 (d, J_{CP} = 4.1 Hz, CH), 129.74, 128.72 (d, J_{CP} = 8.1 Hz, CH), 128.54 (d, J_{CP} = 19.2 Hz, C), 124.80, 124.21, 123.18, 120.85, 109.74. **^{31}P{^{1}H} NMR** (162 MHz, CD_2Cl_2) δ: -23.39. **HRMS** (ES+) calcd. for $C_{25}H_{18}N_3O_2P$: $[M+H]^+$, 424.1215, found: m/z 424.1212.

3f. 2-(diphenylphosphanyl)-5-nitro-1-(4-nitrophenyl)-1*H*-benzo[*d*]imidazole

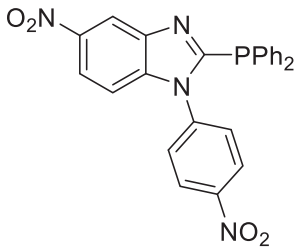

Yellow solid (0.46 g, 0.9 mmol, 77 %); prepared from **2f** (0.35 g, 1.2 mmol), LDA (1.4 mmol in 2 mL of THF) and $ClPPh_2$ (0.25 ml, 1.4 mmol) in THF (20 mL). **M.p.** = 190-192 °C. **^{1}H NMR** (400 MHz, CD_2Cl_2) δ: 8.72 (d, J = 2.2 Hz, 1H), 8.31-8.24 (m, 2H), 8.20 (dd, J = 9.0, 2.2 Hz, 1H), 7.48-7.39 (m, 8H), 7.39-7.32 (m, 4H), 7.22 (dd, J = 8.9, 0.5 Hz, 1H). **^{13}C{^{1}H} NMR** (101 MHz, CD_2Cl_2) δ: 159.94 (d, J_{CP} = 19.2 Hz, C), 147.88, 144.24, 140.98, 140.58, 134.57 (d, J_{CP} = 21.2 Hz, CH), 132.26 (d, J_{CP} = 6.1 Hz, C), 131.77 (d, J_{CP} = 10.1 Hz, C), 130.09, 128.78 (d, J_{CP} = 8.1 Hz, CH), 128.66 (d, J_{CP} = 4.0 Hz, CH), 124.97, 119.55, 116.64, 109.88. **^{31}P{^{1}H} NMR** (162 MHz, CD_2Cl_2) δ: -21.89. **HRMS** (ES+) calcd. for $C_{25}H_{17}N_4O_4P$: $[M+H]^+$, 469.1066, found: m/z 469.1067. C.

3g. 2-(diphenylphosphanyl)-6-nitro-1-(4-nitrophenyl)-1*H*-benzo[*d*]imidazole

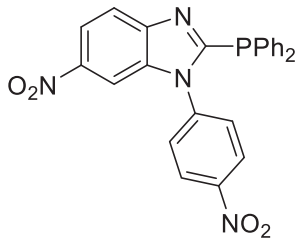

Yellow solid (0.38 g, 0.8 mmol, 45 %); prepared from **2g** (0.50 g, 1.8 mmol), LDA (2.2 mmol in 5 mL of THF) and $ClPPh_2$ (0.43 ml, 2.2 mmol) in THF (30 mL). **M.p.** = 172-174 °C. **^{1}H NMR** (300 MHz, CD_2Cl_2) δ: 8.33-8.25 (m, 2H), 8.23 (dd, J = 8.9, 2.2 Hz, 1H), 8.07 (dd, J = 2.1, 0.6 Hz, 1H), 7.90 (dd, J = 8.9, 0.6 Hz, 1H), 7.49-7.31 (m, 12H). **^{13}C{^{1}H}** NMR (101 MHz, CD_2Cl_2) δ: 161.50 (d, J_{CP} = 19.2 Hz, C), 148.04 (d, J_{CP} = 2.0 Hz, C), 147.93, 144.42, 140.40, 136.68, 134.59 (d, J_{CP} = 21.2 Hz, CH), 132.20 (d, J_{CP} = 5.1 Hz, C), 131.77 (d, J_{CP} = 10.1 Hz, C), 130.10, 128.78 (d, J_{CP} = 8.1 Hz, CH), 128.71 (d, J_{CP} = 4.0 Hz, CH), 125.05, 120.29, 118.68, 106.64. **^{31}P{^{1}H} NMR** (121 MHz, CD_2Cl_2) δ: -21.34. **HRMS** (ES+) calcd. for $C_{25}H_{17}N_4O_4P$: $[M+H]^+$, 469.1066, found: m/z 469.1048.

3h. 2-(diphenylphosphanyl)-5,6-dinitro-1-(4-nitrophenyl)-1*H*-benzo[*d*]imidazole

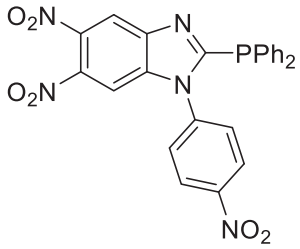

Yellow solid (trace, < 5%); prepared from **2g** (0.14 g, 0.4 mmol), LDA (0.5 mmol in 2 ml of THF) and $ClPPh_2$ (0.1 ml, 0.5 mmol) in THF (40 mL). **^{1}H NMR** (400 MHz, CD_2Cl_2) δ: 8.38 (s, 1H), 8.31-8.24 (m, 2H), 7.68 (s, 1H), 7.45-.41 (m, 6H), 7.39-7.36 (m, 6H). **^{13}C{^{1}H} NMR** (101 MHz, CD_2Cl_2) δ: 148.32, 144.78, 138.00, 134.68 (d, J_{CP} = 21.2 Hz, CH), 132.64, 132.45, 131.26 (d, J_{CP} = 5.1 Hz, C), 130.43, 129.02, 128.93 (d, J_{CP} = 9.1 Hz, CH), 128.66 (d, J_{CP} = 3.0 Hz, CH), 128.55 (d, J_{CP} = 7.1 Hz, C), 125.24, 117.68, 107.80. **^{31}P{^{1}H} NMR** (162 MHz, CD_2Cl_2) δ: -20.19. **HRMS** (ES+) calcd. for $C_{25}H_{16}N_5O_6P$: $[M+H]^+$, 514.0912, found: m/z 514.0916.

4b. RhCl(η^2-C_8H_{12})(3b)

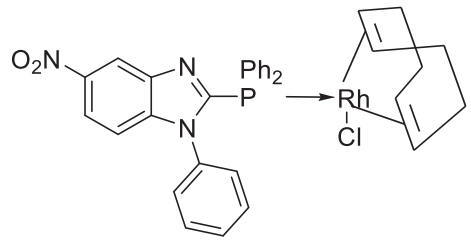

Brown solid (101 mg, 0.18 mmol, 95 %); prepared from **3b** (80 mg, 0.19 mmol) and $[Rh(cod)Cl]_2$ (47 mg, 0.09 mmol) in CH_2Cl_2 (4 mL). **^{1}H NMR** (400 MHz, CD_2Cl_2) δ: 8.71 (d,

J = 2.2 Hz, 1H), 8.16 (dd, *J* = 9.1, 2.2 Hz, 1H), 7.84 – 7.74 (m, 5H), 7.57 – 7.53 (m, 3H), 7.44 (dt, *J* = 7.4, 4.2 Hz, 2H), 7.36 (td, *J* = 7.7, 2.4 Hz, 5H), 7.10 (d, *J* = 9.0 Hz, 1H), 5.38 (brs, 2H, CH_{cod}) , 3.82 – 3.23 (brs, 2H, CH_{cod}), 2.30 – 2.18 (brs, 4H, $CH_{2\ cod}$), 1.93 (brs, 4H, $CH_{2\ cod}$). **$^{13}C\{^1H\}$ NMR** (101 MHz, CD_2Cl_2) δ: 144.14, 142.13, 141.85 (d, J_{CP} = 10.1 Hz, CH), 135.53, 135.29 (d, J_{CP} = 12.1 Hz, CH), 130.78 (d, J_{CP} = 3.1 Hz, C), 130.53, 130.09, 129.74, 129.54, 128.92, 128.20 (d, J_{CP} = 11.1 Hz, C), 119.51, 116.96, 111.08, 105.27 (brs, CH_{cod}), 78.63 (brs, CH_{cod}), 70.92 (brs, CH_{cod}), 32.50 (brs, $CH_{2\ cod}$), 30.85 (brs, $CH_{2\ cod}$), 29.67 (brs, $CH_{2\ cod}$). **$^{31}P\{^1H\}$ NMR** (162 MHz, CD_2Cl_2) δ: 19.00 (d, J_{PRh} = 150.7 Hz).

4e. RhCl(η²-C_8H_{12})(3e)

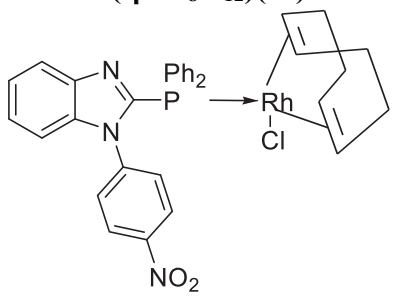

Brown solid (84 mg, 0.15 mmol, 93 %); prepared from **3e** (69 mg, 0.16 mmol) and $[Rh(cod)Cl]_2$ (40 mg, 0.08 mmol) in CH_2Cl_2 (4 mL). **^1H NMR** (400 MHz, CD_2Cl_2) δ: 8.35-8.18 (m, 2H), 7.83 (ddd, *J* = 10.3, 7.9, 1.8 Hz, 5H), 7.79-7.69 (m, 2H), 7.45-7.38 (m, 2H), 7.38-7.25 (m, 6H), 7.11 (dd, *J* = 7.3, 1.8 Hz, 1H), 5.32 (brs, 2H, CH_{cod}), 3.43 (brs, 2H, CH_{cod}), 2.37-2.15 (brs, 4H, $CH_{2\ cod}$), 1.95 (brs, 4H, $CH_{2\ cod}$). **$^{13}C\{^1H\}$ NMR** (101 MHz, CD_2Cl_2) δ: 148.76 (d, J_{CP} = 62.6 Hz, C), 147.45, 142.96 (d, J_{CP} = 11.1 Hz, C), 142.09, 137.39, 135.35 (d, J_{CP} = 12.1 Hz, CH), 131.76 (d, J_{CP} = 10.1 Hz, C), 130.78 (d, J_{CP} = 3.0 Hz, CH), 130.32, 129.60, 128.22 (d, J_{CP} = 10.1 Hz, CH), 124.77, 124.43, 123.50, 120.55, 110.52, 105.57 (brs, CH_{cod}), 78.59 (brs, CH_{cod}), 71.34 (brs, CH_{cod}), 32.48 (brs, $CH_{2\ cod}$), 30.87 (brs, $CH_{2\ cod}$), 28.84 (brs, $CH_{2\ cod}$). **$^{31}P\{^1H\}$ NMR** (162 MHz, CD_2Cl_2) δ: 18.81 (d, J_{PRh} = 150.7 Hz).

4f. RhCl(η²-C_8H_{12})(3f)

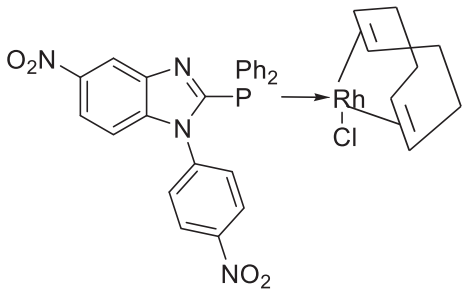

Brown solid (114 mg, 0.19 mmol, 94 %); prepared from **3f** (94 mg, 0.20 mmol) and $[Rh(cod)Cl]_2$ (49 mg, 0.10 mmol) in CH_2Cl_2 (4 mL). **^1H NMR** (400 MHz, CD_2Cl_2) δ: 8.76 (d, *J* = 2.2 Hz, 1H), 8.33-8.29 (m, 2H), 8.21 (dd, *J* = 9.0, 2.2 Hz, 1H), 7.81-7.75 (m, 6H), 7.49-7.44 (m, 2H), 7.40-7.33 (m, 4H), 7.17 (d, *J* = 9.0 Hz, 1H), 5.38 (brs, 2H, CH_{cod}), 3.48 (brs, 2H, CH_{cod}), 2.49 (brs, 4H, $CH_{2\ cod}$), 2.32-2.17 (brs, 4H, $CH_{2\ cod}$). **$^{13}C\{^1H\}$ NMR** (101 MHz, CD_2Cl_2) δ: 147.97, 144.51, 142.18 (d, J_{CP} = 8.9 Hz, C), 141.07 (d, J_{CP} = 6.1 Hz, C), 137.83, 135.23 (d, J_{CP} = 12.1 Hz, CH), 131.80, 131.11 (d, J_{CP} = 3.0 Hz, CH), 129.50, 128.63, 128.45 (d, J_{CP} = 10.1 Hz, CH), 124.56, 120.05, 117.21, 110.78, 105.96 (brs, CH_{cod}), 78.66 (brs, CH_{cod}), 71.52 (brs, CH_{cod}), 32.72 (brs, $CH_{2\ cod}$), 30.86 (brs, $CH_{2\ cod}$), 28.56 (brs, $CH_{2\ cod}$). **$^{31}P\{^1H\}$ NMR** (162 MHz, CD_2Cl_2) δ: 20.14 (d, J_{PRh} = 152.3 Hz).

5a. RhCl(CO)(3a)₂

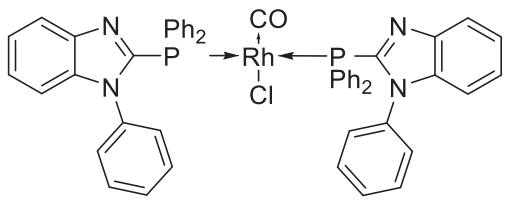

Yellow solid (146 mg, 0.16mmol, 79 %); prepared from 3a (151 mg, 0.4 mmol), $[Rh(cod)Cl]_2$ (49 mg, 0.10 mmol) and CO (bubbling for 15 min) in CH_2Cl_2 (10 mL). **M.-D.p.** = 215-217 °C. **^1H NMR** (400 MHz, CD_2Cl_2) δ: 7.81 (dt, *J* = 8.1, 1.0 Hz, 1H), 7.78-7.74 (m, 3H), 7.50-7.45 (m, 2H), 7.40-7.37 (m, 4H), 7.33-7.18 (m, 4H), 7.16-7.09 (m, 2H), 7.00-6.89 (m, 3H). **$^{13}C\{^1H\}$ NMR** (101 MHz, CD_2Cl_2) δ: 149.39, 142.74 (t, J_{CP} = 5.1 Hz, J_{CP} = 6.1 Hz, C), 138.50, 135.40, 135.16 (t, J_{CP} = 7.1 Hz, J_{CP} = 6.1 Hz, CH), 130.66, 128.91 (d, J_{CP} = 18.1 Hz, CH), 128.65, 128.16 (t, J_{CP} = 5.1 Hz, J_{CP} = 6.1 Hz, CH), 125.71, 124.06, 122.71, 122.43, 120.18, 110.54. The ^{13}C of CO can't be observed due to poor solubility. **$^{31}P\{^1H\}$ NMR** (162 MHz, CD_2Cl_2) δ: 20.85 (d, J_{PRh} = 129.6 Hz). **$^{103}Rh\{^1H\}$ NMR** (12.64 MHz, CD_2Cl_2) δ: –288. **IR:** ν = 1966 cm^{-1} (CO), 742 cm^{-1}, 688 cm^{-1}.

5b. RhCl(CO)(3b)₂

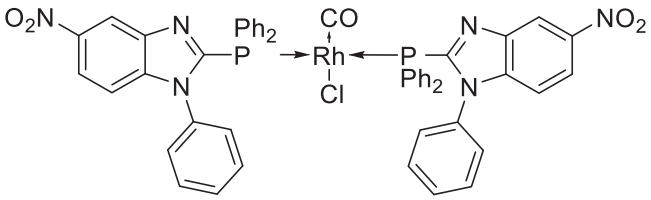

Yellow solid (131 mg, 0.13 mmol, 72 %); prepared from **4b** (101 mg, 0.18 mmol), **3b** (76 mg, 0.18 mmol) and CO (bubbling for 15 min) in CH_2Cl_2 (10 mL). **M.-D.p.** = 226-228 °C. **^{1}H NMR** (400 MHz, CD_2Cl_2) δ: 8.73 (d, *J* = 2.1 Hz, 1H), 8.11 (dd, *J* = 9.0, 2.2 Hz, 1H), 7.78-7.78 (m, 4H), 7.56-7.48 (m, 2H), 7.41 (tt, *J* = 7.1, 1.6 Hz, 4H), 7.30-7.25 (m, 1H), 7.14-7.06 (m, 2H), 7.01 (d, *J* = 9.0 Hz, 1H), 6.98-6.90 (m, 2H). **^{13}C{^{1}H} NMR** (101 MHz, CD_2Cl_2) δ: 144.08, 142.36, 135.08 (t, J_{CP} = 6.1 Hz, J_{CP} = 7.1 Hz, CH), 134.40, 131.09, 129.36, 129.25, 128.95, 128.58, 128.44 (t, J_{CP} = 6.1 Hz, J_{CP} = 5.1 Hz, CH), 125.22, 119.56, 116.90, 115.36, 110.68; no ^{13}*C*O signal was observed due to poor solubility. **^{31}P{^{1}H} NMR** (162 MHz, CD_2Cl_2) δ: 23.71 (d, J_{PRh} = 129.6 Hz). **^{103}Rh{^{1}H} NMR** (12.64 MHz, CD_2Cl_2) δ: –316. **IR:** ν = 1968 cm^{-1} (CO), 1517 cm^{-1}, 1495 cm^{-1}, 1426 cm^{-1}, 1340 cm^{-1}, 1279 cm^{-1}, 1096 cm^{-1}, 1064 cm^{-1}, 1003 cm^{-1}, 922 cm^{-1}, 890 cm^{-1}, 821 cm^{-1}, 807 cm^{-1}, 733 cm^{-1}, 694 cm^{-1}.

5c. RhCl(CO)(3c)$_2$

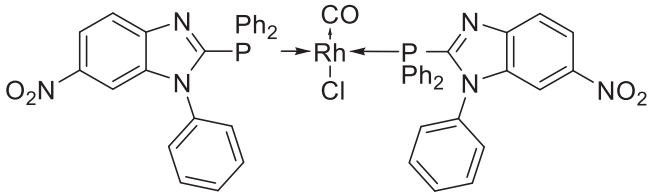

Yellow solid (82 mg, 0.08 mmol, 81 %); prepared from **3c** (85 mg, 0.2 mmol), $[Rh(cod)Cl]_2$ (25 mg, 0.05 mmol) and CO (bubbling for 15 min) in CH_2Cl_2 (5 mL). **M.-D.p.** = 283-285 °C. **^{1}H NMR** (500 MHz, CD_2Cl_2) δ: 8.16 (dd, *J* = 9.0, 2.2 Hz, 1H), 7.90 (d, *J* = 9.0 Hz, 1H), 7.86 (d, *J* = 2.2 Hz, 1H), 7.77-7.73 (m, 4H), 7.54 – 7.49 (m, 2H), 7.41 (dd, *J* = 8.4, 7.0 Hz, 4H), 7.32-7.27 (m, 1H), 7.13-7.09 (m, 2H), 6.96 (dd, *J* = 8.3, 7.5 Hz, 2H). **^{13}C{^{1}H} NMR** (101 MHz, CD_2Cl_2) δ: 146.42, 144.58, 137.82, 135.09 (t, J_{CP} = 7.1 Hz, J_{CP} = 6.1 Hz, CH), 134.21, 131.12, 129.46, 129.34, 128.90, 128.63, 128.46 (t, J_{CP} = 5.1 Hz, J_{CP} = 6.1 Hz, CH), 120.44, 118.30, 113.12, 107.50. ^{13}*C*O signal was not observed due to poor solubility. **^{31}P{^{1}H} NMR** (162 MHz, CD_2Cl_2) δ: 23.88 (d, J_{PRh} = 131.2 Hz). **^{103}Rh{^{1}H} NMR** (12.64 MHz, CD_2Cl_2) δ: –315. **IR:** ν = 1969 cm^{-1} (CO), 1514 cm^{-1}, 1494 cm^{-1}, 1424 cm^{-1}, 1334 cm^{-1}, 1064 cm^{-1}, 873 cm^{-1}, 831 cm^{-1}, 734 cm^{-1}, 687 cm^{-1}.

5e. RhCl(CO)(3e)$_2$

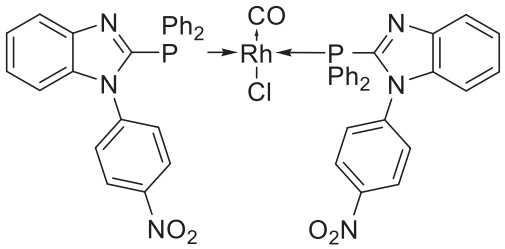

Brown solid (112mg, 0.11 mmol, 74 %); prepared from **4e** (84 mg, 0.15 mmol), **3e** (36 mg, 0.15 mmol) and CO (bubbling for 15 min) in CH_2Cl_2 (5 mL). **M.-D.p.** = 252-254 °C. **^{1}H NMR** (300 MHz, CD_2Cl_2) δ: 7.87 (dt, J = 8.2, 0.9 Hz, 1H), 7.78-7.62 (m, 6H), 7.60-7.51 (m, 2H), 7.47-7.41 (m, 4H), 7.37-7.29 (m, 3H), 7.26 (dd, *J* = 7.2, 1.3 Hz, 1H), 7.02-6.93 (m, 1H). **^{13}C{^{1}H} NMR** (101 MHz, CD_2Cl_2) δ: 186.24 (tt, J_{CP} = 15.2 Hz, J_{CRh} = 73.7 Hz, CO), 148.79 (t, J_{CP} = 35.4 Hz, C), 147.46, 142.84 (t, J_{CP} = 6.1 Hz, C), 140.91, 137.82, 134.79 (t, J_{CP} = 7.1 Hz, J_{CP} = 6.1 Hz, CH), 131.22, 129.93, 129.48, 128.57 (t, J_{CP} = 6.1 Hz, J_{CP} = 5.1 Hz, CH), 124.75, 124.19, 123.36, 120.56, 110.14. **^{31}P{^{1}H} NMR** (121 MHz, CD_2Cl_2) δ: 22.29 (d, J_{PRh} = 128.3 Hz). **IR:** ν = 1979 cm^{-1} (CO), 1525 cm^{-1}, 1497 cm^{-1}, 1435 cm^{-1}, 1349 cm^{-1}, 1095 cm^{-1}, 854 cm^{-1}, 820 cm^{-1}, 746 cm^{-1}, 689 cm^{-1}.

5f. RhCl(CO)(3f)$_2$

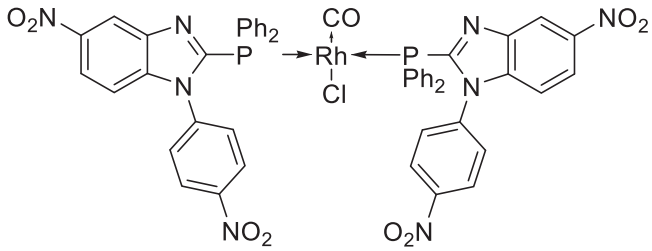

Yellow solid (154 mg, 0.14 mmol, 76 %); prepared from **4f** (114 mg, 0.19 mmol), **3f** (89 mg, 0.19 mmol) and CO (bubbling for 15 min) in CH_2Cl_2 (10 mL). **M.-D.p.** = 280-282 °C. **^{1}H NMR** (400 MHz, CD_2Cl_2) δ: 8.77 (d, *J* =

2.1 Hz, 1H), 8.16 (dd, J = 9.0, 2.2 Hz, 1H), 7.77 – 7.72 (m, 4H), 7.69-7.66 (m, 2H), 7.63-7.58 (m, 2H), 7.47 (ddd, J = 8.7, 4.9, 1.6 Hz, 4H), 7.33 – 7.30 (m, 2H), 7.02 (d, J = 9.0 Hz, 1H). **^{13}C{^{1}H} NMR** (101 MHz, CD_2Cl_2) δ: 185.82 (tt, J_{CP} = 16.2 Hz, J_{CRh} = 72.7 Hz, CO), 153.33 (t, J_{CP} = 33.3 Hz, C), 147.95, 144.46, 141.96 (t, J_{CP} = 6.1 Hz, C), 141.41, 139.71, 134.78 (t, J_{CP} = 7.1 Hz, J_{CP} = 6.1 Hz, CH), 131.68, 129.97, 128.87 (t, J_{CP} = 5.1 Hz, J_{CP} = 6.1 Hz, CH), 128.48, 124.39, 120.15, 117.18, 110.37. **^{31}P{^{1}H} NMR** (162 MHz, CD_2Cl_2) δ: 24.98 (d, J_{PRh} = 129.6 Hz). **IR:** ν = 1980 cm^{-1} (CO), 1593 cm^{-1}, 1520 cm^{-1}, 1497 cm^{-1}, 1436 cm^{-1}, 1339 cm^{-1}, 1278 cm^{-1}, 1094 cm^{-1}, 1068 cm^{-1}, 988 cm^{-1}, 886 cm^{-1}, 854 cm^{-1}, 820 cm^{-1}, 736 cm^{-1}, 688 cm^{-1}

5g. RhCl(CO)(3g)$_2$

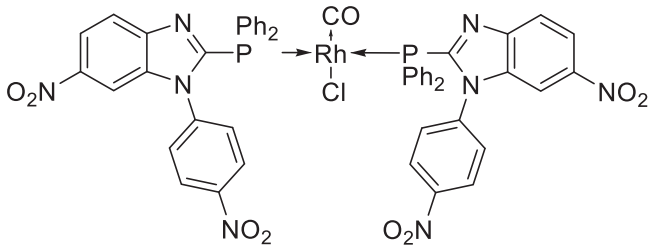

Yellow solid (161 mg, 0.15mmol, 73 %); prepared from **3g** (188 mg, 0.4 mmol), $[Rh(cod)Cl]_2$ (49 mg, 0.10 mmol) and CO (bubbling for 15 min) in CH_2Cl_2 (10 mL). **M.-D.p.** = 285-287 °C. **^{1}H NMR** (400 MHz, CD_2Cl_2) δ: 8.22 (dd, J = 9.0, 2.2 Hz, 1H), 7.96 (d, J = 9.0 Hz, 1H), 7.86 (d, J = 2.2 Hz, 1H), 7.81 – 7.70 (m, 4H), 7.69 – 7.63 (m, 2H), 7.63 – 7.55 (m, 2H), 7.46 (ddt, J = 9.0, 7.5, 1.6 Hz, 4H), 7.33 – 7.26 (m, 2H). **^{13}C{^{1}H} NMR** (101 MHz, CD_2Cl_2) δ: 184.24 (CO), 148.00, 146.44, 144.93, 139.51, 137.20, 134.79 (t, J_{CP} = 7.1 Hz, CH), 131.71, 130.03, 128.87 (t, J_{CP} = 5.1 Hz, CH), 128.66, 128.42, 124.45, 120.89, 118.87, 107.07. **^{31}P{^{1}H} NMR** (162 MHz, CD_2Cl_2) δ: 25.01 (d, J_{PRh} = 129.6 Hz). **^{103}Rh{^{1}H} NMR** (12.64 MHz, CD_2Cl_2) δ: –315. **IR:** ν = 1978 cm^{-1} (CO), 1811 cm^{-1}, 1594 cm^{-1}, 1517 cm^{-1}, 1426 cm^{-1}, 1338 cm^{-1}, 1278 cm^{-1}, 1094 cm^{-1}, 1063 cm^{-1}, 988 cm^{-1}, 887 cm^{-1}, 854 cm^{-1}, 819 cm^{-1}, 734 cm^{-1}, 687 cm^{-1}.

5a'. RhCl(CO)(3a')$_2$

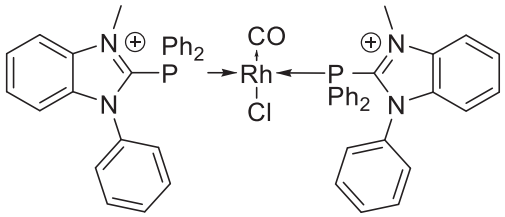

Yellow solid (130 mg, 0.14 mmol, 68 %); prepared from **3a** (151 mg, 0.4 mmol), MeOTf (45 µL, 0.4 mmol), $[Rh(cod)Cl]_2$ (41 mg, 0.08 mmol) and CO (bubbling for 15 min) in CH_2Cl_2 (10 mL). **M.-D.p.** = 240-242 °C. **^{1}H NMR** (400 MHz, CD_2Cl_2) δ: 8.02 – 7.85 (m, 5H), 7.70 (t, J = 7.8 Hz, 1H), 7.57 (dd, J = 15.0, 7.4 Hz, 3H), 7.53 – 7.40 (m, 5H), 7.35 – 7.22 (m, 4H), 7.03 (d, J = 8.4 Hz, 1H), 4.09 (s, 3H, -CH_3). **^{13}C{^{1}H} NMR** (101 MHz, CD_2Cl_2) δ: 183.67 (tt, J_{CP} = 17.2 Hz, J_{CRh} = 70.7 Hz, CO), 146.19 (t, J_{CP} = 13.1 Hz, J_{CP} = 14.1 Hz, C), 135.63 (t, J_{CP} = 8.1 Hz, CH), 135.03, 133.52, 133.02, 132.02, 131.51, 130.22 (t, J_{CP} = 6.1 Hz, CH), 128.28 (d, J_{CP} = 56.6 Hz, CH), 125.73, 124.52 (t, J_{CP} = 24.2 Hz, J_{CP} = 25.3 Hz, C), 122.53, 119.34, 116.15, 113.36 (d, J_{CP} = 3.0 Hz, CH), 36.55 (t, J_{CP} = 2.0 Hz, CH_3). **^{31}P{^{1}H} NMR** (162 MHz, CD_2Cl_2) δ: 38.14 (d, J_{PRh} = 132.8 Hz). **^{103}Rh{^{1}H} NMR** (12.64 MHz, CD_2Cl_2) δ: –436. **IR:** ν = 2005 cm^{-1} (CO), 1438 cm^{-1}, 1256 cm^{-1}, 1149 cm^{-1}, 1088 cm^{-1}, 1028 cm^{-1}, 742 cm^{-1}, 694 cm^{-1}.

6b-c,e-g: respective dinuclear side-products of 5b-c,e-g

Characterized only by ^{31}P NMR spectroscopy of the crude final reaction mixture (approximate spectroscopic yields given), and by X-ray crystallography for **6f**:

6b (18 %): ^{31}P{^{1}H} NMR (162 MHz, CD_2Cl_2) δ: 43.29 (d, J_{PRh} = 149.0 Hz).

6c (4 %): ^{31}P{^{1}H} NMR (162 MHz, CD_2Cl_2) δ: 43.52 (d, J_{PRh} = 147.4 Hz).

6e (14 %): ^{31}P{^{1}H} NMR (162 MHz, CD_2Cl_2) δ: 41.10 (d, J_{PRh} = 147.4 Hz).

6f (15 %): $^{31}P\{^{1}H\}$ NMR (162 MHz, CD_2Cl_2) δ: 43.61 (d, J_{PRh} = 149.0 Hz). XRD analysis: see section 3.11 of the S.I. below.

6g (13 %): $^{31}P\{^{1}H\}$ NMR (162 MHz, CD_2Cl_2) δ: 43.86 (d, J_{PRh} = 148.8 Hz).

2. Crystallographic data

Molecular views below are given for thermal ellipsoids at the 30 % probability level. They are complementary to the corresponding molecular views of Figure 2 and 3 in the main Text. See also Table 1 and the experimental section 4.4 (Crystallographic studies) in the main text.

2.1. Crystal data for 3b (CCDC 1496156)

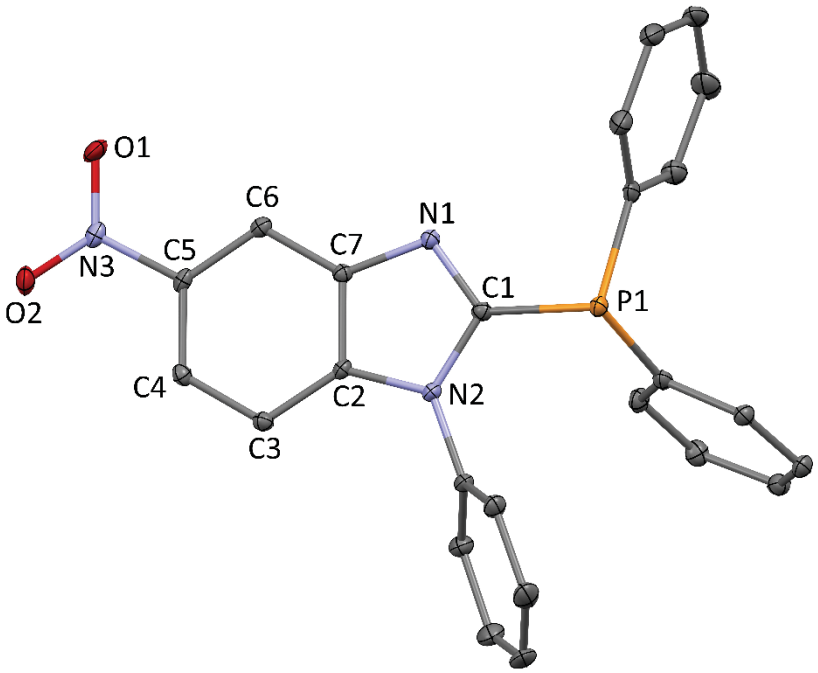

a = 23.7536(4) Å α = 90°
b = 23.7536(4) Å β = 90°
c = 6.57812(13) Å γ = 120°

Volume	3214.32(10) Å³	Crystal Class	hexagonal
Space group	P 6_1	Z =	6
Formula	C_{25} H_{18} N_3 O_2 P_1	M_r	423.41
Cell determined from	15092 reflections	Cell θ range =	4 - 71°
Temperature	120K		
Shape	block		
Colour	colorless	Size	0.10 × 0.15 × 0.20 mm
D_x	1.31	F000	1320.000
μ	1.356 mm^{-1}		
Absorption correction	multi-scan		
T_{min}	0.82	T_{max}	0.87

Data Collection

Diffractometer	multi-scan
Scan type	φ and ω scans
Reflections measured	33620
Independent reflections	4085
Rint	0.0506
θ_{max}	70.9379
h =	-24 → 0
k =	0 → 29
l =	-8 → 8

Refinement

$\Delta\rho_{min}$ =	-0.24 e Å^{-3}
$\Delta\rho_{max}$ =	0.20 e Å^{-3}
Reflections used	3766
Cutoff: I >	3.00σ(I)
Parameters refined	281
S =	1.08
R-factor	0.031
weighted R-factor	0.038
Δ/σ_{max}	0.0006
Flack parameter	-0.035(6)
Refinement on	F
w =	$w' \times [1 - (\Delta F_{obs} / 6 \times \Delta F_{est})^2]^2$
w′ =	$[P_0T_0'(x) + P_1T_1'(x) + ...P_{n-1}T_{n-1}'(x)]^{-1}$, where P_i are the coefficients of a Chebychev series in $t_i(x)$, and $x = F_{calc}/F_{calcmax}$.
P_0 - P_{n-1} =	14.1 -6.88 11.2

2.2. Crystal data for 3c (CCDC 1496157)

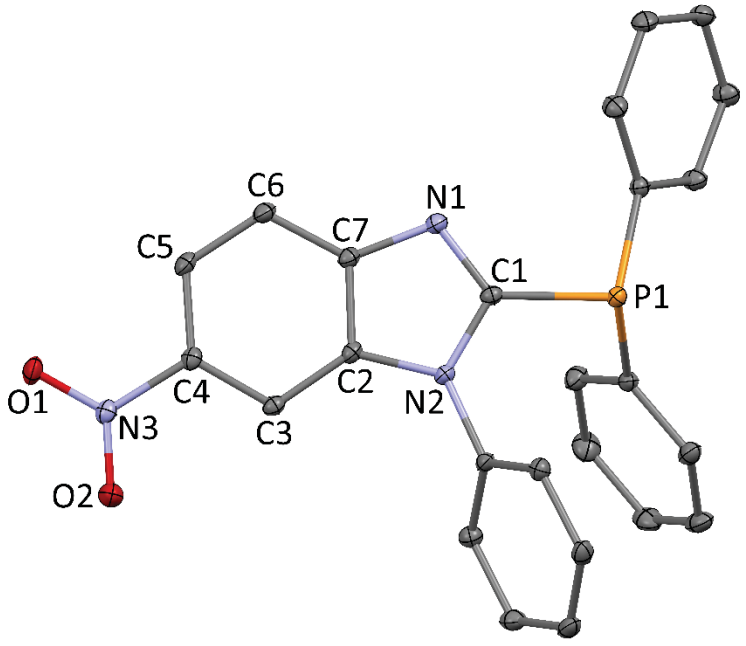

a = 11.97328(18) Å α = 90°
b = 5.99825(12) Å β = 93.6851(14)°
c = 28.3117(4) Å γ = 90°

Volume	2029.10(6) Å³	Crystal Class	monoclinic
Space group	P 2_1/c	Z =	4
Formula	C_{25} H_{18} N_3 O_2 P_1	M_r	423.41
Cell determined from	15870 reflections	Cell θ range =	4 - 71°
Temperature	120K		
Shape	block		
Colour	orange	Size	0.18 × 0.20 × 0.25 mm
D_x	1.39	F000	880.000
μ	1.432 mm^{-1}		
Absorption correction	multi-scan		
T_{min}	0.52	T_{max}	0.77

Data Collection

Diffractometer	multi-scan
Scan type	φ and ω scans
Reflections measured	25992
Independent reflections	3885
Rint	0.0197
θ_{max}	70.5594
h =	-14 → 14
k =	-7 → 6
l =	-34 → 34

Refinement

$\Delta\rho_{min}$ =	-0.32 e $Å^{-3}$
$\Delta\rho_{max}$ =	0.32 e $Å^{-3}$
Reflections used	3767
Cutoff: I >	3.00σ(I)
Parameters refined	281
S =	1.05
R-factor	0.031
weighted R-factor	0.038
Δ/σ_{max}	0.0029
Refinement on	F
w =	$w' \times [1 - (\Delta F_{obs} / 6 \times \Delta F_{est})^2]^2$
w′ =	$[P_0T_0'(x) + P_1T_1'(x) + ...P_{n-1}T_{n-1}'(x)]^{-1}$, where P_i are the coefficients of a Chebychev series in $t_i(x)$, and $x = F_{calc}/F_{calcmax}$.
P_0 - P_{n-1} =	6.53 3.71 4.86 1.05

2.3. Crystal data for 3e (CCDC 1496159)

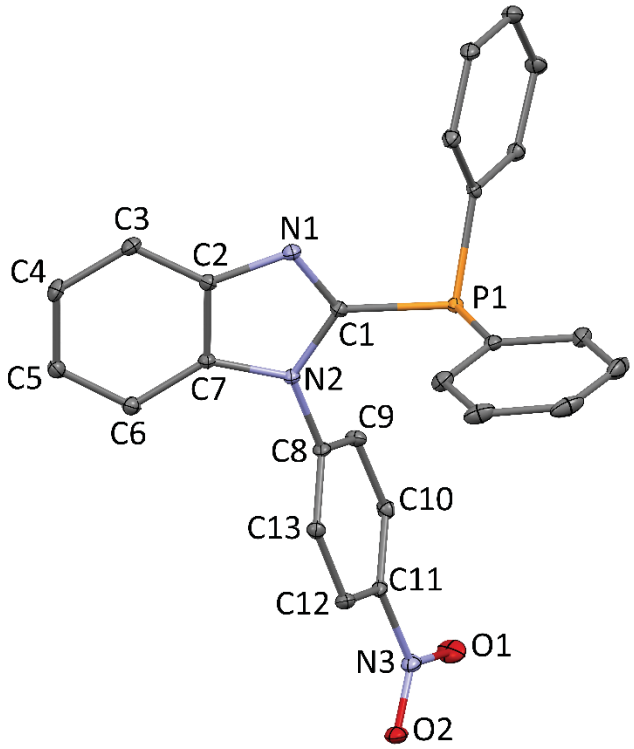

a = 8.3080(2) Å α = 70.855(3)°
b = 10.7343(3) Å β = 79.535(3)°
c = 14.5679(6) Å γ = 74.248(3)°

Volume	1175.09(5) Å³	Crystal Class	triclinic
Space group	P -1	Z =	2
Formula	C_{26} H_{20} Cl_2 N_3 O_2 P_1	M_r	508.34
Cell determined from	9918 reflections	Cell θ range =	3 - 28°
Temperature	100K		
Shape	planar		
Colour	colorless	Size	0.02 × 0.15 × 0.15 mm
D_x	1.44	F000	524.000
μ	0.375 mm^{-1}		
Absorption correction	multi-scan		
T_{min}	0.92	T_{max}	0.99

Data Collection

Diffractometer	multi-scan
Scan type	φ and ω scans
Reflections measured	38869
Independent reflections	4780
Rint	0.0723
θ_{max}	29.7781
h =	-11 → 11
k =	-14 → 14
l =	-20 → 20

Refinement

$\Delta\rho_{min}$ =	-0.47 e Å^{-3}
$\Delta\rho_{max}$ =	0.52 e Å^{-3}
Reflections used	9580
Cutoff: I >	3.00σ(I)
Parameters refined	308
S =	1.05
R-factor	0.058
weighted R-factor	0.053
Δ/σ_{max}	0.0005
Refinement on	F
w =	$w' \times [1 - (\Delta F_{obs} / 6 \times \Delta F_{est})^2]^2$
w′ =	$[P_0T_0'(x) + P_1T_1'(x) + ...P_{n-1}T_{n-1}'(x)]^{-1}$, where P_i are the coefficients of a Chebychev series in $t_i(x)$, and $x = F_{calc}/F_{calcmax}$.
P_0 - P_{n-1} =	3.50 0.147 2.16 0.747

2.4. Crystal data for 3f (CCDC 1496158)

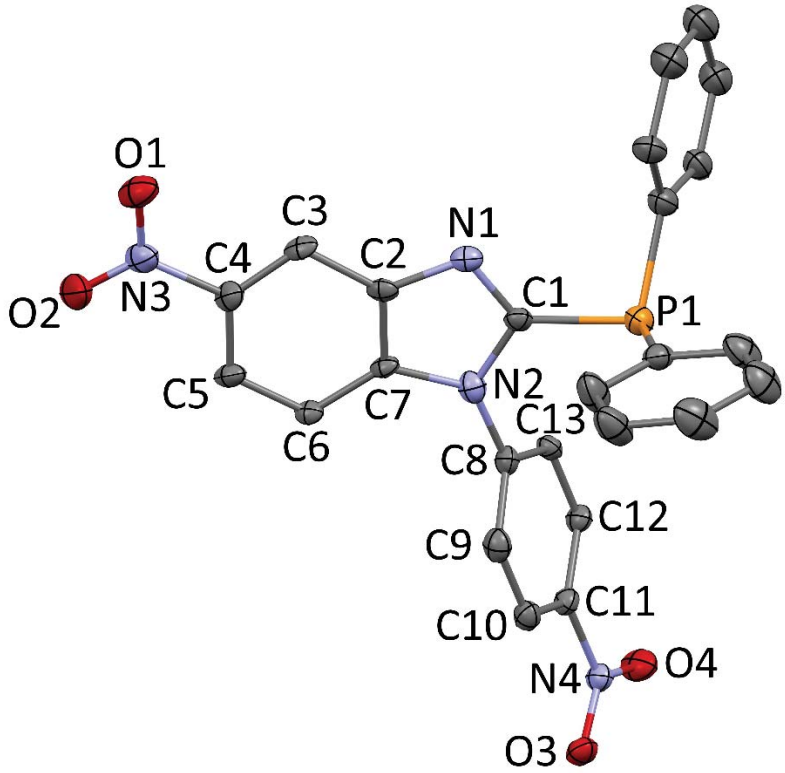

a = 8.1470(4) Å α = 90°
b = 31.0776(15) Å β = 93.6216(15)°
c = 11.2413(6) Å γ = 90°

Volume	2840.49(15) Å^3	Crystal Class	monoclinic
Space group	P 2_1/n	Z =	4
Formula	C_{25} H_{17} N_4 O_4 P_1	M_r	468.41
Cell determined from	9798 reflections	Cell θ range =	3 - 26°
Temperature	100K		

Shape	block		
Colour	colorless	Size	0.12 × 0.15 × 0.25 mm
D_x	1.10	F000	968.000
μ	0.129 mm^{-1}		
Absorption correction	multi-scan		
T_{min}	0.89	T_{max}	0.98

Data Collection

Diffractometer	multi-scan
Scan type	φ and ω scans
Reflections measured	61693
Independent reflections	5906
Rint	0.0483
θ_{max}	26.5681
h =	-10 → 10
k =	0 → 38
l =	0 → 14

Refinement

$\Delta\rho_{min}$ =	-0.80 e $Å^{-3}$
$\Delta\rho_{max}$ =	1.06 e $Å^{-3}$
Reflections used	5052
Cutoff: I >	3.00σ(I)
Parameters refined	307
S =	1.05
R-factor	0.147
weighted R-factor	0.152
Δ/σ_{max}	0.0001
Refinement on	F
w =	$w' \times [1 - (\Delta F_{obs} / 6 \times \Delta F_{est})^2]^2$
w′ =	$[P_0T_0'(x) + P_1T_1'(x) + ...P_{n-1}T_{n-1}'(x)]^{-1}$, where P_i are the coefficients of a Chebychev series in $t_i(x)$, and $x = F_{calc}/F_{calcmax}$.
P_0 - P_{n-1} =	0.703 0.570 0.233

2.5. Crystal data for 5a (CCDC 1496162)

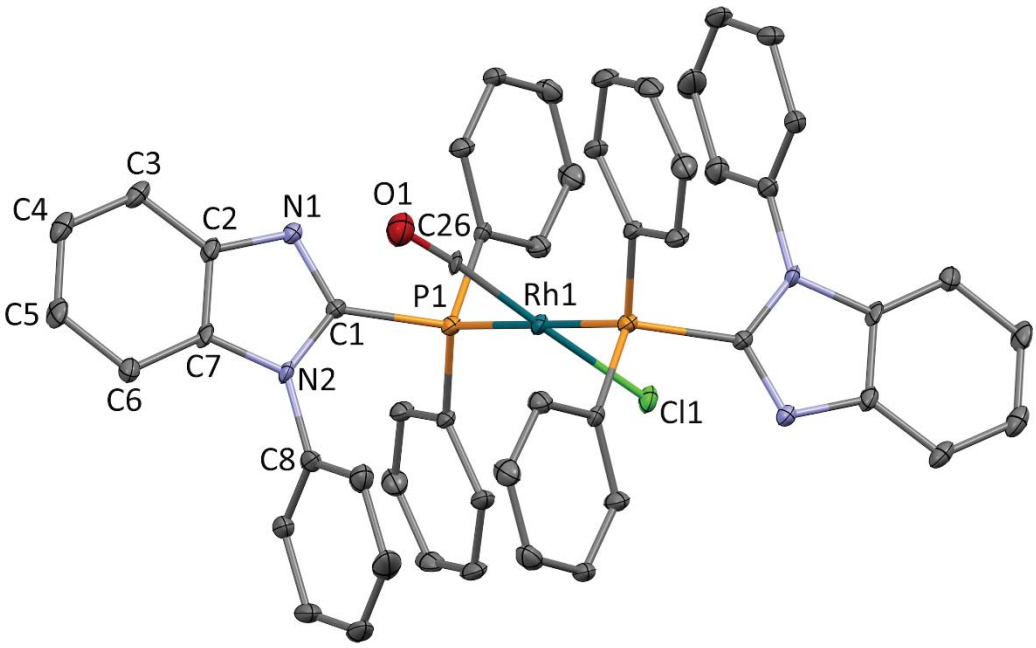

a = 10.704(3) Å α = 90°
b = 11.496(4) Å β = 99.466(9)°
c = 17.080(4) Å γ = 90°

Volume	2073.1(5) Å³	Crystal Class	monoclinic
Space group	P 2_1/n	Z =	2
Formula	C_{51} H_{38} Cl_1 N_4 O_1 P_2 Rh_1	M_r	923.19
Cell determined from	4387 reflections	Cell θ range =	2 - 23°
Temperature	100K		
Shape	block		
Colour	pale yellow	Size	0.05 × 0.10 × 0.10 mm
D_x	1.48	F000	944.000
μ	0.599 mm^{-1}		
Absorption correction	multi-scan		
T_{min}	0.87	T_{max}	0.97

Data Collection

Diffractometer	multi-scan
Scan type	φ and ω scans
Reflections measured	31654
Independent reflections	4800
Rint	0.1428
θ_{max}	27.8628
h =	-13 → 13
k =	-15 → 15
l =	-17 → 22

Refinement

$\Delta\rho_{min}$ =	-1.99 e Å^{-3}
$\Delta\rho_{max}$ =	1.20 e Å^{-3}
Reflections used	2792
Cutoff: I >	3.00σ(I)
Parameters refined	274
S =	1.12
R-factor	0.056
weighted R-factor	0.061
Δ/σ_{max}	0.0008
Refinement on	F
w =	$w' \times [1 - (\Delta F_{obs} / 6 \times \Delta F_{est})^2]^2$
w′ =	$[P_0T_0'(x) + P_1T_1'(x) + ...P_{n-1}T_{n-1}'(x)]^{-1}$, where P_i are the coefficients of a Chebychev series in $t_i(x)$, and $x = F_{calc}/F_{calcmax}$.
P_0 - P_{n-1} =	0.769 0.399 0.531

2.6. Crystal data for 5b (CCDC 1496160)

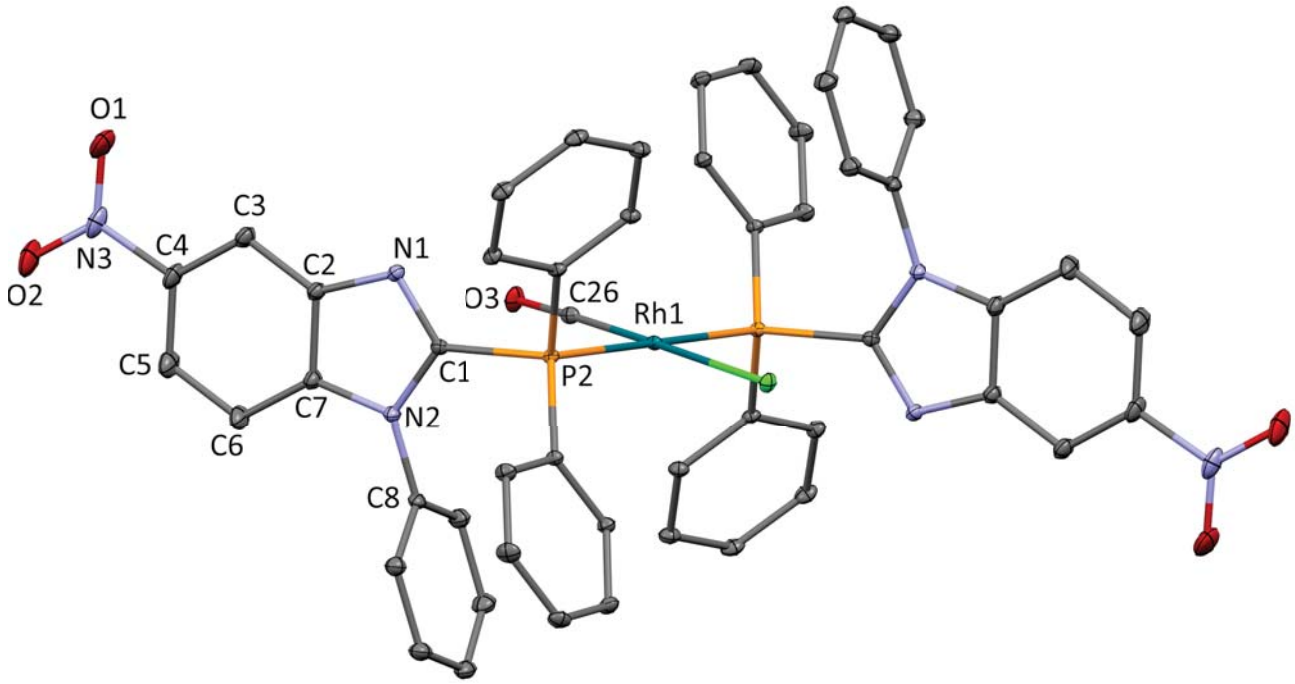

a = 9.5819(3) Å α = 98.0370(16)°
b = 10.7141(4) Å β = 102.8561(16)°
c = 14.7256(6) Å γ = 102.9773(16)°

Volume	1407.26(6) Å^3	Crystal Class	triclinic
Space group	P -1	Z =	1
Formula	C_{55} H_{44} Cl_9 N_6 O_5 P_2 Rh_1	M_r	1352.92

Cell determined from	9518 reflections	Cell θ range =	2 - 37°
Temperature	100K		
Shape	plate		
Colour	pale yellow	Size	0.08 × 0.22 × 0.25 mm
D_x	1.60	F000	684.000
μ	0.842 mm^{-1}		
Absorption correction	multi-scan		
T_{min}	0.77	T_{max}	0.93

Data Collection

Diffractometer	multi-scan
Scan type	φ and ω scans
Reflections measured	86814
Independent reflections	12318
Rint	0.0257
θ_{max}	41.0868
h =	-17 → 14
k =	-16 → 19
l =	-26 → 22

Refinement

$\Delta\rho_{min}$ =	-0.67 e $Å^{-3}$
$\Delta\rho_{max}$ =	0.98 e $Å^{-3}$
Reflections used	10661
Cutoff: I >	3.00σ(I)
Parameters refined	403
S =	1.05
R-factor	0.039
weighted R-factor	0.035
Δ/σ_{max}	0.0005
Refinement on	F
w =	$w' \times [1 - (\Delta F_{obs} / 6 \times \Delta F_{est})^2]^2$
w′ =	$[P_0T_0'(x) + P_1T_1'(x) + ...P_{n-1}T_{n-1}'(x)]^{-1}$, where P_i are the coefficients of a Chebychev series in $t_i(x)$, and $x = F_{calc}/F_{calcmax}$.
P_0 - P_{n-1} =	0.411 0.375 0.271

2.7. Crystal data for 5c (CCDC 1496161)

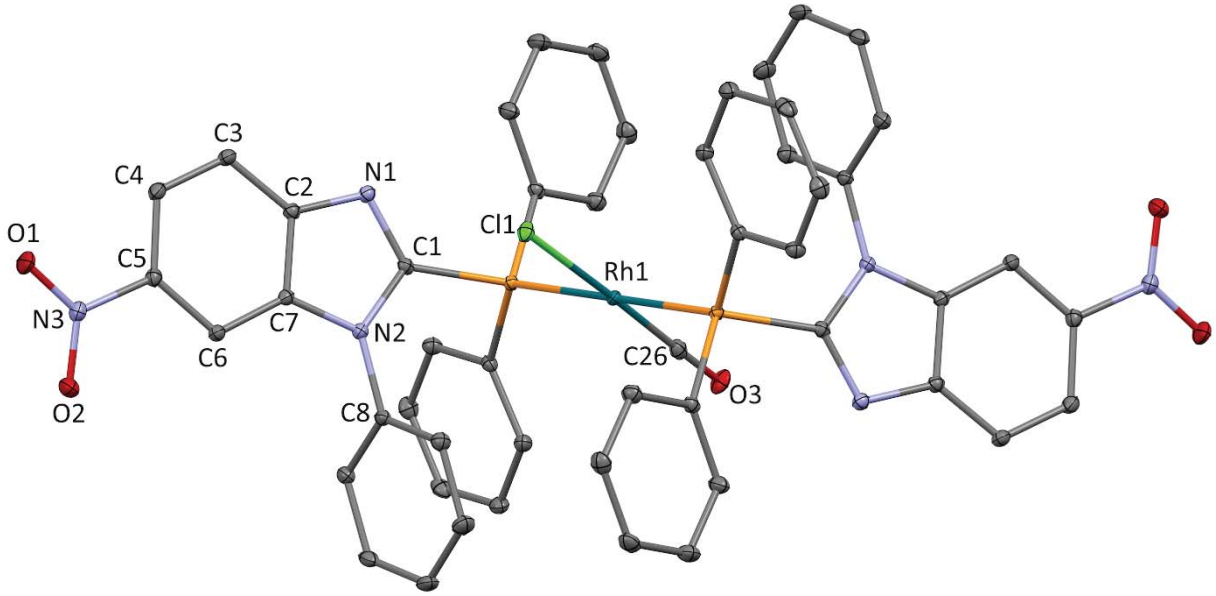

a = 8.8037(4) Å α = 87.651(2)°
b = 10.9560(6) Å β = 79.310(2)°
c = 12.0990(6) Å γ = 69.853(2)°

Volume	1076.24(9) Å³	Crystal Class	triclinic
Space group	P -1	Z =	1
Formula	C_{51} H_{36} Cl_1 N_6 O_5 P_2 Rh_1	M_r	1013.19
Cell determined from	9742 reflections	Cell θ range =	3 - 37°
Temperature	100K		
Shape	block		
Colour	colorless	Size	0.10 × 0.20 × 0.20 mm
D_x	1.56	F000	516.000
μ	0.593 mm^{-1}		
Absorption correction	multi-scan		
T_{min}	0.83	T_{max}	0.94

Data Collection

Diffractometer	multi-scan
Scan type	φ and ω scans
Reflections measured	52472
Independent reflections	4759
Rint	0.0375
θ_{max}	27.1267
h =	-11 → 11
k =	-14 → 14
l =	-15 → 15

Refinement

$\Delta\rho_{min}$ =	-0.72 e Å^{-3}
$\Delta\rho_{max}$ =	0.41 e Å^{-3}
Reflections used	4427
Cutoff: I >	3.00σ(I)
Parameters refined	313
S =	1.07
R-factor	0.027
weighted R-factor	0.023
Δ/σ_{max}	0.0004
Refinement on	F
w =	$w' \times [1 - (\Delta F_{obs} / 6 \times \Delta F_{est})^2]^2$
w′ =	$[P_0T_0'(x) + P_1T_1'(x) + ...P_{n-1}T_{n-1}'(x)]^{-1}$, where P_i are the coefficients of a Chebychev series in $t_i(x)$, and $x = F_{calc}/F_{calcmax}$.
P_0 - P_{n-1} =	0.321 0.277 0.224

2.8. Crystal data for 5f (CCDC 1496163)

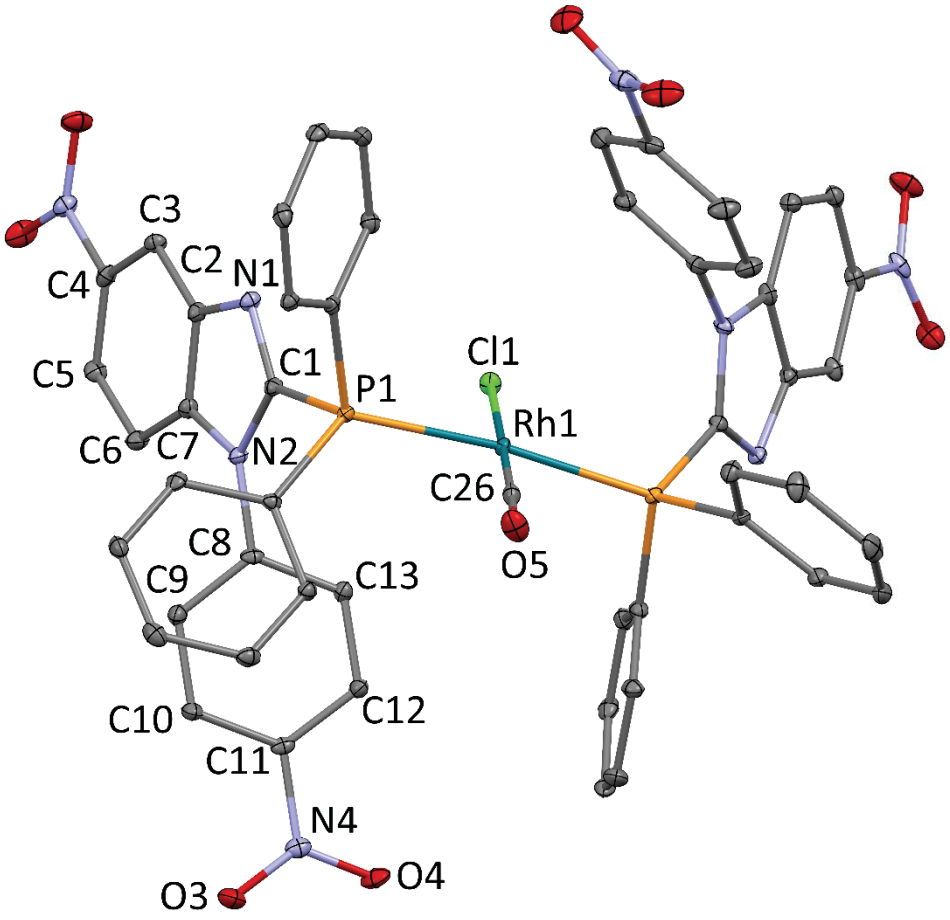

a = 14.0668(9) Å α = 90°
b = 16.7870(13) Å β = 90°
c = 22.524(2) Å γ = 90°

Volume	5318.8(5) Å^3	Crystal Class	orthorhombic
Space group	P 2_1 2_1 2_1	Z =	4

Formula	C_{53} H_{38} Cl_5 N_8 O_9 P1' Rh_1	M_r	1273.05
Cell determined from 9907 reflections		Cell θ range =	2 - 28°
Temperature	100K		
Shape	stick		
Colour	pale yellow	Size	0.05 × 0.05 × 0.20 mm
D_x	1.59	F000	2576.000
μ	0.698 mm^{-1}		
Absorption correction	multi-scan		
T_{min}	0.97	T_{max}	0.97

Data Collection

Diffractometer	multi-scan
Scan type	φ and ω scans
Reflections measured	79662
Independent reflections	13763
Rint	0.0577
θ_{max}	28.8741
h =	-18 → 19
k =	-22 → 22
l =	-30 → 30

Refinement

$\Delta\rho_{min}$ =	-0.41 e $Å^{-3}$
$\Delta\rho_{max}$ =	0.57 e $Å^{-3}$
Reflections used	11405
Cutoff: I >	3.00σ(I)
Parameters refined	704
S =	1.09
R-factor	0.031
weighted R-factor	0.031
Δ/σ_{max}	0.0030
Flack parameter	-0.020(15)
Refinement on	F
w =	$w' \times [1 - (\Delta F_{obs} / 6 \times \Delta F_{est})^2]^2$
w′ =	$[P_0T_0'(x) + P_1T_1'(x) + ...P_{n-1}T_{n-1}'(x)]^{-1}$, where P_i are the coefficients of a Chebychev series in $t_i(x)$, and $x = F_{calc}/F_{calcmax}$.
P_0 - P_{n-1} =	0.201 0.396E-01 0.750E-01

2.9. Crystal data for 5g (CCDC 1496164)

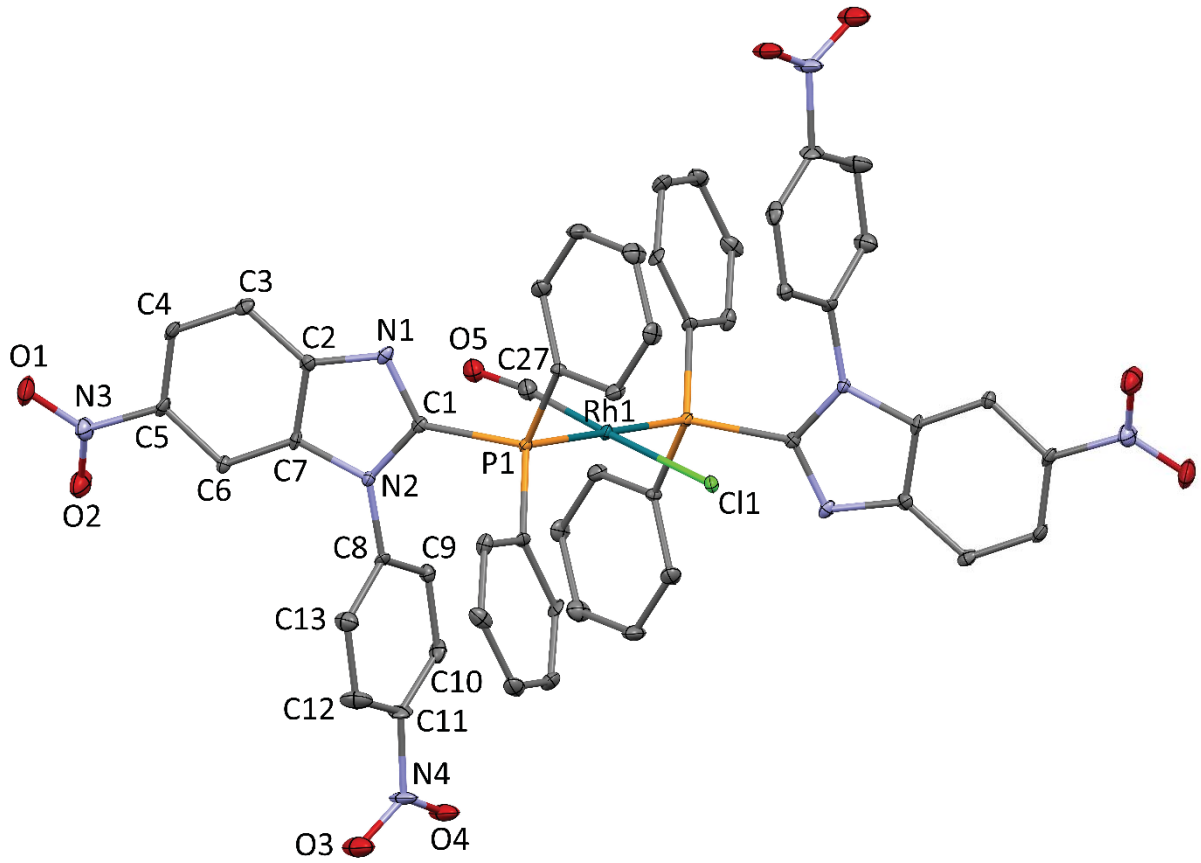

a = 15.9457(5) Å α = 90°
b = 11.2917(3) Å β = 90°
c = 29.2082(11) Å γ = 90°

Volume	5259.08(19) Å³	Crystal Class	orthorhombic
Space group	P b c a	Z =	4
Formula	C_{53} H_{38} Cl_5 N_8 O_9 P_2 Rh_1	M_r	1273.05
Cell determined from	9450 reflections	Cell θ range =	3 - 30°
Temperature	120K		
Shape	planar		
Colour	colorless	Size	0.02 × 0.20 × 0.25 mm
D_x	1.61	F000	2576.000
μ	0.706 mm^{-1}		
Absorption correction	multi-scan		
T_{min}	0.86	T_{max}	0.99

Data Collection

Diffractometer	multi-scan
Scan type	φ and ω scans
Reflections measured	76783
Independent reflections	7694

Rint	0.0981
θ_{max}	30.7129
h =	-21 → 22
k =	-15 → 16
l =	-41 → 40

Refinement

$\Delta\rho_{min}$ =	-1.03 e Å^{-3}
$\Delta\rho_{max}$ =	0.95 e Å^{-3}
Reflections used	4876
Cutoff: I >	3.00σ(I)
Parameters refined	352
S =	1.00
R-factor	0.062
weighted R-factor	0.075
Δ/σ_{max}	0.0036
Refinement on	F
w =	1

2.10. Crystal data for 5a' (CCDC 1496165)

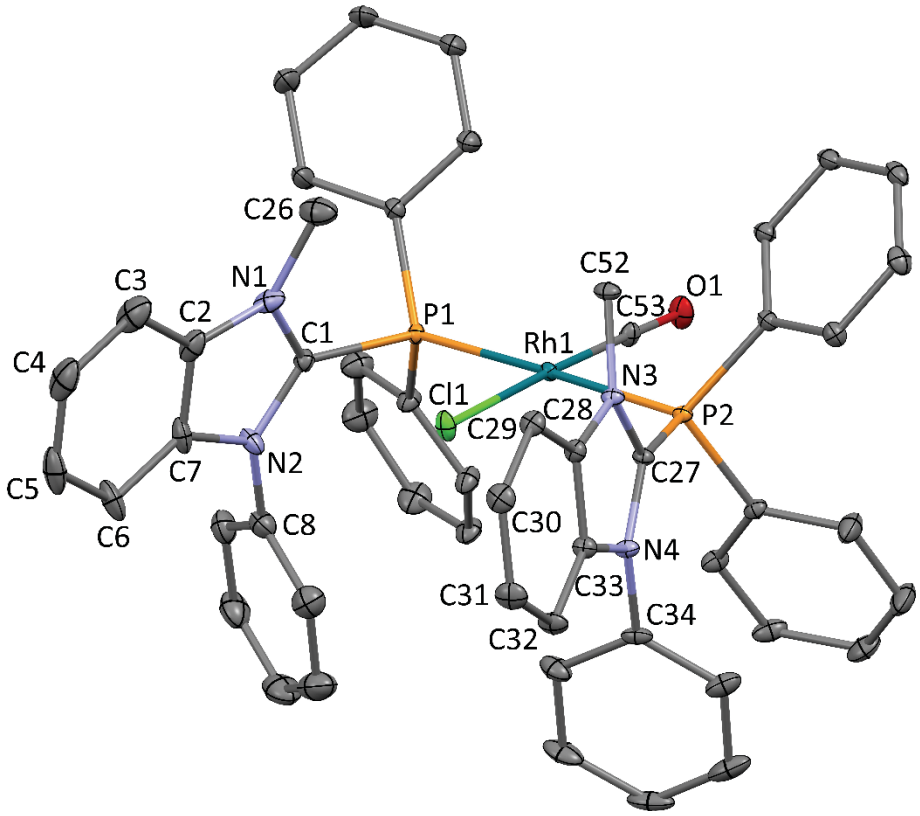

a = 14.7172(11) Å α = 91.977(3)°
b = 15.0289(11) Å β = 109.881(2)°

c = 18.4532(14) Å γ = 117.436(2)°

Volume	3316.0(4) Å³	Crystal Class	triclinic
Space group	P -1	Z =	2
Formula	$C_{58.50}$ H_{51} Cl_8 F_6 N_4 O_7 P_2 Rh_1 S_2	M_r	1548.67
Cell determined from	9030 reflections	Cell θ range =	2 - 32°
Temperature	100K		
Shape	block		
Colour	pale yellow	Size	0.15 × 0.15 × 0.20 mm
D_x	1.55	F000	1566.000
μ	0.761 mm^{-1}		
Absorption correction	multi-scan		
T_{min}	0.79	T_{max}	0.89

Data Collection

Diffractometer	multi-scan
Scan type	φ and ω scans
Reflections measured	106296
Independent reflections	21412
Rint	0.0296
θ_{max}	32.1035
h =	-21 → 21
k =	-19 → 22
l =	-26 → 26

Refinement

$\Delta\rho_{min}$ =	-0.96 e $Å^{-3}$
$\Delta\rho_{max}$ =	2.40 e $Å^{-3}$
Reflections used	16438
Cutoff: I >	3.00σ(I)
Parameters refined	811
S =	1.03
R-factor	0.056
weighted R-factor	0.054
Δ/σ_{max}	0.0012
Refinement on	F
w =	$w' \times [1 - (\Delta F_{obs} / 6 \times \Delta F_{est})^2]^2$
w′ =	$[P_0T_0'(x) + P_1T_1'(x) + ...P_{n-1}T_{n-1}'(x)]^{-1}$, where P_i are the coefficients of a Chebychev series in $t_i(x)$, and $x = F_{calc}/F_{calcmax}$.
P_0 - P_{n-1} =	0.511 0.531 0.282

2.11. Crystal data for 6f (CCDC 1496166)

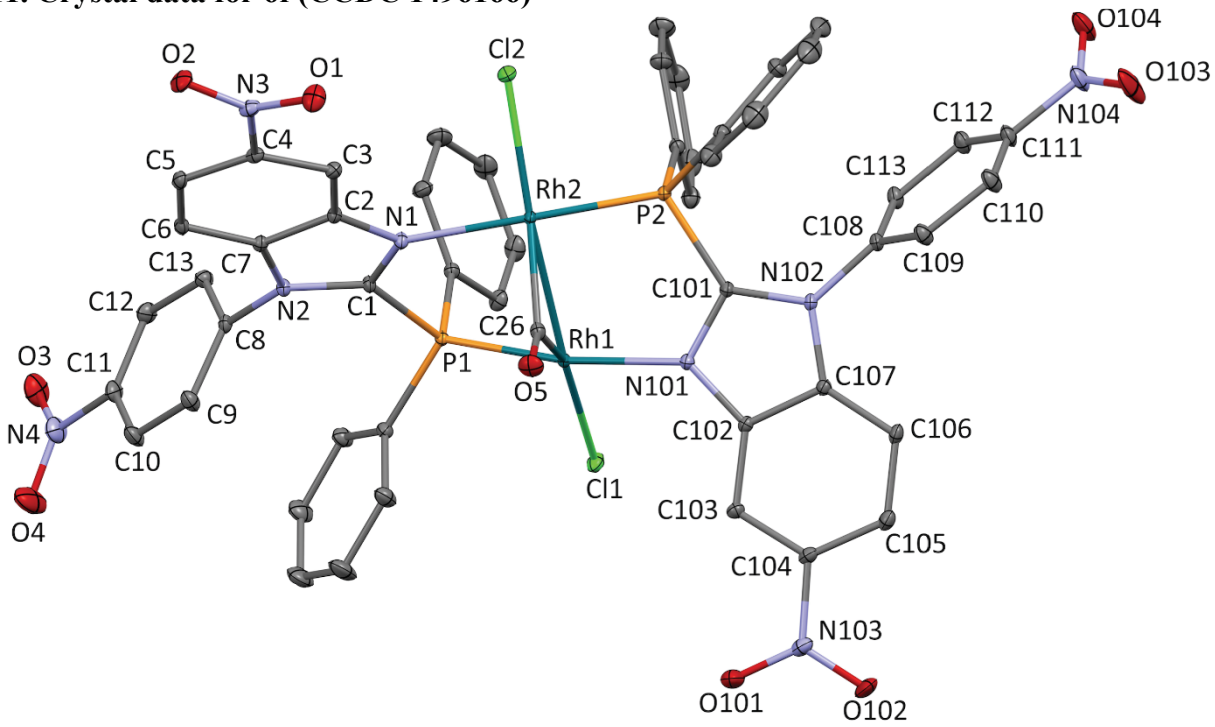

a = 10.5619(3) Å α = 97.7610(16)°
b = 17.8643(6) Å β = 90.9492(15)°
c = 19.6796(7) Å γ = 104.4739(14)°

Volume	3557.48(13) Å³	Crystal Class	triclinic
Space group	P -1	Z =	2
Formula	$C_{57.70}$ $H_{47.40}$ $Cl_{15.40}$ N_8 O_9 P_2 Rh_2	M_r	1810.59
Cell determined from	9441 reflections	Cell θ range =	2 - 33°
Temperature	100K		
Shape	planar		
Colour	orange	Size	0.06 × 0.22 × 0.22 mm
D_x	1.69	F000	1806.800
μ	1.146 mm^{-1}		
Absorption correction	multi-scan		
T_{min}	0.83	T_{max}	0.93

Data Collection

Diffractometer	multi-scan
Scan type	φ and ω scans
Reflections measured	180292
Independent reflections	24511

Rint	0.0345
θ_{max}	33.2151
h =	-16 → 15
k =	-26 → 26
l =	-29 → 29

Refinement

$\Delta\rho_{min}$ =	-1.27 e Å^{-3}
$\Delta\rho_{max}$ =	2.10 e Å^{-3}
Reflections used	18966
Cutoff: I >	3.00σ(I)
Parameters refined	928
S =	1.08
R-factor	0.035
weighted R-factor	0.037
Δ/σ_{max}	0.0039
Refinement on	F
w =	$w' \times [1 - (\Delta F_{obs} / 6 \times \Delta F_{est})^2]^2$
w′ =	$[P_0T_0'(x) + P_1T_1'(x) + ...P_{n-1}T_{n-1}'(x)]^{-1}$, where P_i are the coefficients of a Chebychev series in $t_i(x)$, and $x = F_{calc}/F_{calcmax}$.
P_0 - P_{n-1} =	0.226 0.938E-01 0.740E-01

3. Output data of DFT calculations (see note 16 in the main text)

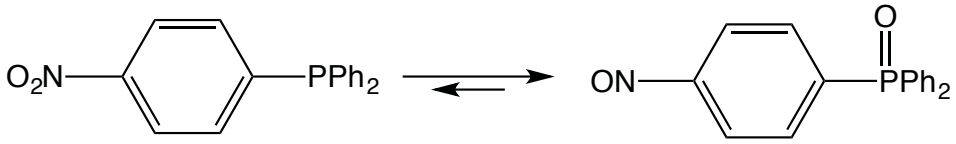

O_2NP **ONPO**

DFT calculations have been performed at the B3PW91/6-31G(d,p) level, without solvent correction (vacuum), using the Firefly software: a) A. A. Granovsky, *Firefly version 8,* http://classic.chem.msu.su:gran:firefly:index.html) which is partially based on the GAMESS (US) source code; b) M. W. Schmidt, K. K. Baldridge, J. A. Boatz, S. T. Elbert, M. S. Gordon, J. H. Jensen, S. Koseki, N. Matsunaga, K. A. Nguyen, S. Su, T. L. Windus, M. Dupuis, J. A. Montgomery, *J. Comput. Chem*. **1993**, *14*, 1347-1363.

3.1. Geometry and thermochemistry of O_2NP

3.1.1. Input file and optimized geometry of O_2NP

Input	**Optimized geometry Cartesian coordinates (Å)** **NUCLEAR ENERGY = 1757.3639467317 Ha** **ELECTRONIC ENERGY = -2997.7953133640 Ha** **TOTAL ENERGY = -1240.4313666323 Ha**
! File created by MacMolPlt 7.7	ATOM X Y Z

```
 $CONTRL SCFTYP=RHF RUNTYP=OPTIMIZE
DFTTYP=B3PW91 MAXIT=50 ICHARG=0
MULT=1
   MOLPLT=.TRUE. NPRINT=7 $END
 $SYSTEM mwords=64 timlim=2000 $END
 $BASIS GBASIS=N31 NGAUSS=6 NDFUNC=1
NPFUNC=1 $END
 $SCF DIRSCF=.TRUE. $END
 $STATPT OPTTOL=0.0001 NSTEP=500 $END
 $data
PPh2C6H4NO2
C1
C     6  0.4240844181 -0.3337009813 -0.0333218485
C     6 -0.2476711169  0.6572786240 -0.7397225623
C     6 -1.6382737419  0.6233698878 -0.7833480811
C     6 -2.3530685118 -0.3826247559 -0.1176493830
C     6 -1.6375948937 -1.3943853147  0.5488232652
C     6 -0.2505845845 -1.3832981443  0.5849782149
N     7  1.8825978405 -0.2582531890  0.0946404852
H     1  0.3215310832  1.4387397878 -1.2329773108
H     1 -2.1828182642  1.3897330225 -1.3243240719
H     1 -2.1747820493 -2.1840658984  1.0669767226
H     1  0.3167926845 -2.1512753003  1.0972645220
P    15 -4.1771792979 -0.3228157761  0.1231498582
O     8  2.4473068207  0.7026943698 -0.4171071235
O     8  2.4479680545 -1.1537271692  0.7135777840
C     6 -6.1540368153 -2.0628372313 -0.6745406355
C     6 -4.8005640341 -1.7437443755 -0.8596229671
C     6 -4.0304417252 -2.5312209120 -1.7244188542
C     6 -4.6024331748 -3.6226290057 -2.3771726891
C     6 -5.9526809851 -3.9192472150 -2.1989749876
C     6 -6.7302012340 -3.1277463715 -1.3530048260
H     1 -6.7632977985 -1.4633589870 -0.0002699932
H     1 -3.9937949177 -4.2331110414 -3.0377048777
H     1 -6.4000733051 -4.7634320578 -2.7170015437
H     1 -7.7842372663 -3.3478927049 -1.2141503985
C     6 -4.7953330668  2.3591633647 -0.1745113397
C     6 -4.7187904509  1.1382957817 -0.8618321833
C     6 -5.1145315221  1.0995825946 -2.2073951779
C     6 -5.5736824484  2.2548496663 -2.8401161419
C     6 -5.6184805519  3.4665546052 -2.1520391009
C     6 -5.2243955445  3.5184706572 -0.8168861535
H     1 -4.5148393223  2.4024899069  0.8748148182
H     1 -5.8960219453  2.2085440372 -3.8767640054
H     1 -5.9742956131  4.3661351233 -2.6478509355
H     1 -5.2610880663  4.4557166362 -0.2673481971
H     1 -5.0780126751  0.1649116775 -2.7621119568
H     1 -2.9849859786 -2.2950233108 -1.8970283247
 $END
```

```
-------------------------------------------------------------
C   0.3278830205 -0.4243358423 -0.0785576368
C  -0.3240270009  0.6169779716 -0.7285157790
C  -1.7133112027  0.6754392957 -0.6766190069
C  -2.4475813111 -0.2940698432  0.0200951862
C  -1.7531033345 -1.3240436076  0.6791772332
C  -0.3689832832 -1.4018379929  0.6275851861
N   1.7896732105 -0.4971766724 -0.1374300608
H   0.2582130415  1.3554898919 -1.2670179051
H  -2.2306036034  1.4805159745 -1.1880899373
H  -2.3058268021 -2.0754413099  1.2369479345
H   0.1792083458 -2.1932166400  1.1245517791
P  -4.2807582648 -0.2475664815  0.2248155029
O   2.3782222768  0.3739808187 -0.7677972489
O   2.3361267643 -1.4267620726  0.4458292236
C  -6.0957202998 -2.2023474117 -0.5307385069
C  -4.8128254812 -1.6953509082 -0.7845327099
C  -4.0220753078 -2.3198960000 -1.7588600424
C  -4.5051126609 -3.4224818562 -2.4615909583
C  -5.7859216106 -3.9100236097 -2.2080421048
C  -6.5825052426 -3.2950438975 -1.2434234197
H  -6.7131493325 -1.7393913682  0.2352658910
H  -3.8782912193 -3.9002997331 -3.2095744080
H  -6.1596269412 -4.7704668627 -2.7556795696
H  -7.5793844372 -3.6738441052 -1.0361099770
C  -4.9378376052  2.4209107441 -0.1515069630
C  -4.7722447090  1.1945248867 -0.8113869220
C  -5.0091129563  1.1317087977 -2.1908037916
C  -5.3913125877  2.2726495418 -2.8934638769
C  -5.5368367473  3.4905552597 -2.2300858125
C  -5.3081744710  3.5636973550 -0.8571811300
H  -4.7805466003  2.4766273284  0.9231029651
H  -5.5758428336  2.2100793790 -3.9624019793
H  -5.8341338735  4.3784413346 -2.7811233815
H  -5.4288701747  4.5074891170 -0.3328629530
H  -4.9013090234  0.1859804526 -2.7139573226
H  -3.0222077416 -1.9493319334 -1.9649874979
```

3.1.2 Hessian calculation output for O_2NP

```
 ---------------------------------
 • O2NP THERMOCHEMISTRY AT T=    0.00 K
 ---------------------------------

USING IDEAL GAS, RIGID ROTOR, HARMONIC NORMAL MODE APPROXIMATIONS.
P=  1.01325E+05 PASCAL.
ALL FREQUENCIES ARE SCALED BY   1.00000
THE MOMENTS OF INERTIA ARE (IN AMU*BOHR**2)
   5410.35773    10216.56550    13838.00476
```

THE ROTATIONAL SYMMETRY NUMBER IS 1.0
THE ROTATIONAL CONSTANTS ARE (IN GHZ)
0.33327 0.17649 0.13030
THE HARMONIC ZERO POINT ENERGY IS (SCALED BY 1.000)
0.277144 HARTREE/MOLECULE 60826.013696 CM**-1/MOLECULE
173.910475 KCAL/MOL 727.641426 KJ/MOL

	Q	LN Q
ELEC.	1.00000E+00	0.000000
TRANS.	4.35749E-06	-12.343615
ROT.	6.08123E-02	-2.799963
VIB.	1.00000E+00	0.000000
TOT.	2.64989E-07	-15.143579

	E	H	G	CV	CP	S
	KJ/MOL	KJ/MOL	KJ/MOL	J/MOL-K	J/MOL-K	J/MOL-K
ELEC.	0.000	0.000	0.000	0.000	0.000	0.000
TRANS.	0.000	0.000	0.000	12.472	20.786	-81.844
ROT.	0.000	0.000	0.000	12.472	12.472	-10.808
VIB.	727.641	727.641	727.641	0.000	0.000	0.000
TOTAL	727.641	727.641	727.642	24.943	33.258	-92.652

	E	H	G	CV	CP	S
	KCAL/MOL	KCAL/MOL	KCAL/MOL	CAL/MOL-K	CAL/MOL-K	CAL/MOL-K
ELEC.	0.000	0.000	0.000	0.000	0.000	0.000
TRANS.	0.000	0.000	0.000	2.981	4.968	-19.561
ROT.	0.000	0.000	0.000	2.981	2.981	-2.583
VIB.	173.910	173.910	173.910	0.000	0.000	0.000
TOTAL	173.910	173.910	173.911	5.962	7.949	-22.144

• O_2NP THERMOCHEMISTRY AT T= 298.15 K

USING IDEAL GAS, RIGID ROTOR, HARMONIC NORMAL MODE APPROXIMATIONS.
P= 1.01325E+05 PASCAL.
ALL FREQUENCIES ARE SCALED BY 1.00000
THE MOMENTS OF INERTIA ARE (IN AMU*BOHR**2)
5410.35773 10216.56550 13838.00476
THE ROTATIONAL SYMMETRY NUMBER IS 1.0
THE ROTATIONAL CONSTANTS ARE (IN GHZ)
0.33327 0.17649 0.13030
THE HARMONIC ZERO POINT ENERGY IS (SCALED BY 1.000)
0.277144 HARTREE/MOLECULE 60826.013696 CM**-1/MOLECULE
173.910475 KCAL/MOL 727.641426 KJ/MOL

	Q	LN Q
ELEC.	1.00000E+00	0.000000
TRANS.	2.11506E+08	19.169765
ROT.	9.90019E+06	16.108065
VIB.	4.18821E+07	17.550370
TOT.	8.76991E+22	52.828199

	E	H	G	CV	CP	S
	KJ/MOL	KJ/MOL	KJ/MOL	J/MOL-K	J/MOL-K	J/MOL-K
ELEC.	0.000	0.000	0.000	0.000	0.000	0.000
TRANS.	3.718	6.197	-47.521	12.472	20.786	180.171
ROT.	3.718	3.718	-39.931	12.472	12.472	146.401
VIB.	768.643	768.643	684.135	272.569	272.569	283.442
TOTAL	776.080	778.559	596.683	297.512	305.827	610.014

	E	H	G	CV	CP	S

```
       KCAL/MOL  KCAL/MOL  KCAL/MOL CAL/MOL-K CAL/MOL-K CAL/MOL-K
ELEC.     0.000     0.000     0.000     0.000     0.000     0.000
TRANS.    0.889     1.481   -11.358     2.981     4.968    43.062
ROT.      0.889     0.889    -9.544     2.981     2.981    34.991
VIB.    183.710   183.710   163.512    65.146    65.146    67.744
TOTAL   185.488   186.080   142.611    71.107    73.094   145.797
......END OF NORMAL COORDINATE ANALYSIS......

CPU       TIME:   STEP =      0.05 ,  TOTAL =    47074.8 SECONDS (  784.6 MIN)
WALL CLOCK TIME:   STEP =      0.04 ,  TOTAL =    83566.4 SECONDS ( 1392.8 MIN)
CPU UTILIZATION:   STEP =    125.25%,  TOTAL =      56.33%
AN INPUT FILE FOR -MOLPLT- HAS BEEN PUNCHED.
   3738091 WORDS OF    DYNAMIC MEMORY USED
   2720862 BYTES OF    HEAP MEMORY    USED,      109399 BYTES REMAIN IN USE

WARNING! THIS VERSION OF FIREFLY IS PROBABLY OUTDATED!
PLEASE CHECK FIREFLY HOMEPAGE FOR INFORMATION ON UPDATES!

EXECUTION OF FIREFLY TERMINATED NORMALLY  1:04:31 21-JUL-2017
```

3.2. Geometry and thermochemistry of ONPO

3.2.1. Input file and optimized geometry of ONPO

Input

```
!  File created by MacMolPlt 7.7
 $CONTRL SCFTYP=RHF RUNTYP=OPTIMIZE
DFTTYP=B3PW91    MAXIT=50    ICHARG=0
MULT=1
   MOLPLT=.TRUE. NPRINT=7 $END
 $SYSTEM mwords=64 timlim=6000 $END
 $BASIS GBASIS=N31 NGAUSS=6 NDFUNC=1
NPFUNC=1 $END
 $SCF DIRSCF=.TRUE. $END
 $STATPT OPTTOL=0.0001 NSTEP=500 $END
 $data
OPPh2C6H4NO
C1
C    6    0.32788   -0.42434   -0.07856
C    6   -0.32403    0.61698   -0.72852
C    6   -1.71331    0.67544   -0.67662
C    6   -2.44758   -0.29407    0.02010
C    6   -1.75310   -1.32404    0.67918
C    6   -0.36898   -1.40184    0.62759
N    7    1.78967   -0.49718   -0.13743
H    1    0.25821    1.35549   -1.26702
H    1   -2.23060    1.48052   -1.18809
H    1   -2.30583   -2.07544    1.23695
H    1    0.17921   -2.19322    1.12455
P   15   -4.28076   -0.24757    0.22482
O    8    2.37822    0.37398   -0.76780
C    6   -6.09572   -2.20235   -0.53074
C    6   -4.81283   -1.69535   -0.78453
C    6   -4.02208   -2.31990   -1.75886
C    6   -4.50511   -3.42248   -2.46159
C    6   -5.78592   -3.91002   -2.20804
C    6   -6.58251   -3.29504   -1.24342
```

Optimized geometry Cartesian coordinates (Å)

NUCLEAR ENERGY = 1794.8106068056 Ha
ELECTRONIC ENERGY = -3035.2774428743 Ha
TOTAL ENERGY = -1240.4668360686 Ha

ATOM	X	Y	Z
C	0.3644979457	-0.4309783089	0.0229663210
C	-0.2799847197	0.1640451238	-1.0668879355
C	-1.6647492891	0.2358049264	-1.0752875752
C	-2.4070913018	-0.2932459226	-0.0052887136
C	-1.7494952793	-0.8688639207	1.0884384592
C	-0.3604714302	-0.9403566003	1.1009169137
N	1.7960127395	-0.5563772184	0.1268698204
H	0.3254756136	0.5626026112	-1.8750047063
H	-2.1749815046	0.7199511510	-1.9035682762
H	-2.3381347156	-1.2387804012	1.9226450034
H	0.1826934230	-1.3815347909	1.9316538419
P	-4.2392744428	-0.2768572087	0.0735414971
O	2.4147876503	-0.1119004535	-0.8221452050
C	-5.9759670404	-2.3268242090	-0.4950136449
C	-4.7884943624	-1.7106865770	-0.9092692144
C	-4.1008156048	-2.2103794674	-2.0218533895
C	-4.6089136509	-3.3006458169	-2.7252116684
C	-5.7989796567	-3.9012551272	-2.3170497720
C	-6.4785734039	-3.4172690745	-1.1999832247
H	-6.4846541418	-1.9530449219	0.3890234645
H	-4.0702908413	-3.6863098623	-3.5861871640
H	-6.1914174514	-4.7536310628	-2.8643835212
H	-7.3980972133	-3.8939769626	-0.8729133771
C	-5.0616070766	2.3460670708	-0.0571997216
C	-4.7762999293	1.2130055325	-0.8293731780
C	-4.9278694550	1.2666274215	-2.2201119117
C	-5.3389685246	2.4487410684	-2.8326095616
C	-5.6095869637	3.5776777008	-2.0605415748
C	-5.4750995740	3.5242779181	-0.6736767865
H	-4.9759816193	2.2834679548	1.0238311289
H	-5.4590195132	2.4838999711	-3.9116785104

H	1	-6.71315	-1.73939	0.23527	H	-5.9362434923	4.4964326826 -2.5396179608
H	1	-3.87829	-3.90030	-3.20957	H	-5.6996342748	4.3995769707 -0.0708744455
H	1	-6.15963	-4.77047	-2.75568	H	-4.7484539461	0.3818158943 -2.8247691565
H	1	-7.57938	-3.67384	-1.03611	H	-3.1598069810	-1.7641895608 -2.3320152883
C	6	-4.93784	2.42091	-0.15151	O	-4.7355999725	-0.3124065298 1.4890890337
C	6	-4.77224	1.19452	-0.81139			
C	6	-5.00911	1.13171	-2.19080			
C	6	-5.39131	2.27265	-2.89346			
C	6	-5.53684	3.49056	-2.23009			
C	6	-5.30817	3.56370	-0.85718			
H	1	-4.78055	2.47663	0.92310			
H	1	-5.57584	2.21008	-3.96240			
H	1	-5.83413	4.37844	-2.78112			
H	1	-5.42887	4.50749	-0.33286			
H	1	-4.90131	0.18598	-2.71396			
H	1	-3.02221	-1.94933	-1.96499			
O	8	-4.80705	-0.22443	1.72724			
$END							

3.2.2 Hessian calculation output for ONPO

• ONPO THERMOCHEMISTRY AT T= 0.00 K

USING IDEAL GAS, RIGID ROTOR, HARMONIC NORMAL MODE APPROXIMATIONS.
P= 1.01325E+05 PASCAL.
ALL FREQUENCIES ARE SCALED BY 1.00000
THE MOMENTS OF INERTIA ARE (IN AMU*BOHR**2)
5778.87772 9097.20772 11995.56906
THE ROTATIONAL SYMMETRY NUMBER IS 1.0
THE ROTATIONAL CONSTANTS ARE (IN GHZ)
0.31201 0.19820 0.15031
THE HARMONIC ZERO POINT ENERGY IS (SCALED BY 1.000)
0.275771 HARTREE/MOLECULE 60524.649792 CM**-1/MOLECULE
173.048831 KCAL/MOL 724.036309 KJ/MOL

	Q	LN Q
ELEC.	1.00000E+00	0.000000
TRANS.	4.35749E-06	-12.343615
ROT.	5.52173E-02	-2.896478
VIB.	1.00000E+00	0.000000
TOT.	2.40609E-07	-15.240094

	E	H	G	CV	CP	S
	KJ/MOL	KJ/MOL	KJ/MOL	J/MOL-K	J/MOL-K	J/MOL-K
ELEC.	0.000	0.000	0.000	0.000	0.000	0.000
TRANS.	0.000	0.000	0.000	12.472	20.786	-81.844
ROT.	0.000	0.000	0.000	12.472	12.472	-11.611
VIB.	724.036	724.036	724.036	0.000	0.000	0.000
TOTAL	724.036	724.036	724.036	24.943	33.258	-93.455

	E	H	G	CV	CP	S
	KCAL/MOL	KCAL/MOL	KCAL/MOL	CAL/MOL-K	CAL/MOL-K	CAL/MOL-K
ELEC.	0.000	0.000	0.000	0.000	0.000	0.000
TRANS.	0.000	0.000	0.000	2.981	4.968	-19.561
ROT.	0.000	0.000	0.000	2.981	2.981	-2.775
VIB.	173.049	173.049	173.049	0.000	0.000	0.000
TOTAL	173.049	173.049	173.049	5.962	7.949	-22.336

• ONPO THERMOCHEMISTRY AT T= 298.15 K

USING IDEAL GAS, RIGID ROTOR, HARMONIC NORMAL MODE APPROXIMATIONS.
P= 1.01325E+05 PASCAL.
ALL FREQUENCIES ARE SCALED BY 1.00000
THE MOMENTS OF INERTIA ARE (IN AMU*BOHR**2)
5778.87772 9097.20772 11995.56906
THE ROTATIONAL SYMMETRY NUMBER IS 1.0
THE ROTATIONAL CONSTANTS ARE (IN GHZ)
0.31201 0.19820 0.15031
THE HARMONIC ZERO POINT ENERGY IS (SCALED BY 1.000)
0.275771 HARTREE/MOLECULE 60524.649792 CM**-1/MOLECULE
173.048831 KCAL/MOL 724.036309 KJ/MOL

	Q	LN Q
ELEC.	1.00000E+00	0.000000
TRANS.	2.11506E+08	19.169765
ROT.	8.98934E+06	16.011550
VIB.	4.34784E+07	17.587775
TOT.	8.26655E+22	52.769089

	E	H	G	CV	CP	S
	KJ/MOL	KJ/MOL	KJ/MOL	J/MOL-K	J/MOL-K	J/MOL-K
ELEC.	0.000	0.000	0.000	0.000	0.000	0.000
TRANS.	3.718	6.197	-47.521	12.472	20.786	180.171
ROT.	3.718	3.718	-39.692	12.472	12.472	145.598
VIB.	765.903	765.903	680.437	276.743	276.743	286.652
TOTAL	773.339	775.818	593.225	301.687	310.001	612.422

	E	H	G	CV	CP	S
	KCAL/MOL	KCAL/MOL	KCAL/MOL	CAL/MOL-K	CAL/MOL-K	CAL/MOL-K
ELEC.	0.000	0.000	0.000	0.000	0.000	0.000
TRANS.	0.889	1.481	-11.358	2.981	4.968	43.062
ROT.	0.889	0.889	-9.487	2.981	2.981	34.799
VIB.	183.055	183.055	162.628	66.143	66.143	68.511
TOTAL	184.833	185.425	141.784	72.105	74.092	146.372

.....END OF NORMAL COORDINATE ANALYSIS.....

CPU TIME: STEP = 0.04 , TOTAL = 48660.7 SECONDS (811.0 MIN)
WALL CLOCK TIME: STEP = 0.04 , TOTAL = 48672.0 SECONDS (811.2 MIN)
CPU UTILIZATION: STEP = 100.95%, TOTAL = 99.98%
AN INPUT FILE FOR -MOLPLT- HAS BEEN PUNCHED.
3738091 WORDS OF DYNAMIC MEMORY USED
2720862 BYTES OF HEAP MEMORY USED, 109399 BYTES REMAIN IN USE

WARNING! THIS VERSION OF FIREFLY IS PROBABLY OUTDATED!
PLEASE CHECK FIREFLY HOMEPAGE FOR INFORMATION ON UPDATES!

EXECUTION OF FIREFLY TERMINATED NORMALLY 15:13:53 20-JUL-2017

Part II

Synthesis and supramolecular chemistry of alkyl/ aryl *carbo*-benzene derivatives

Chapter 2

Hexaaryl-*carbo*-benzenes revisited: a novel synthetic route, crystallographic data, and prospects of electrochemical behavior

Introduction & Summary

The carbon element is of paramount importance for the "chemical construction" of life on Earth and is also the basis of organic chemistry. About 10^7 different organic molecules and polymers have been synthesized by chemists, their structural diversity being based on stable C-C and C-X bonds, and is accompanied by varieties of chemical and physical properties. Most of them were found to have widespread applications ranging from drugs to materials. Regarding all-carbon molecules and materials, each discovery of a new carbon allotrope was a revolution for materials science, due to their extraordinary electronic and structural properties.[1]

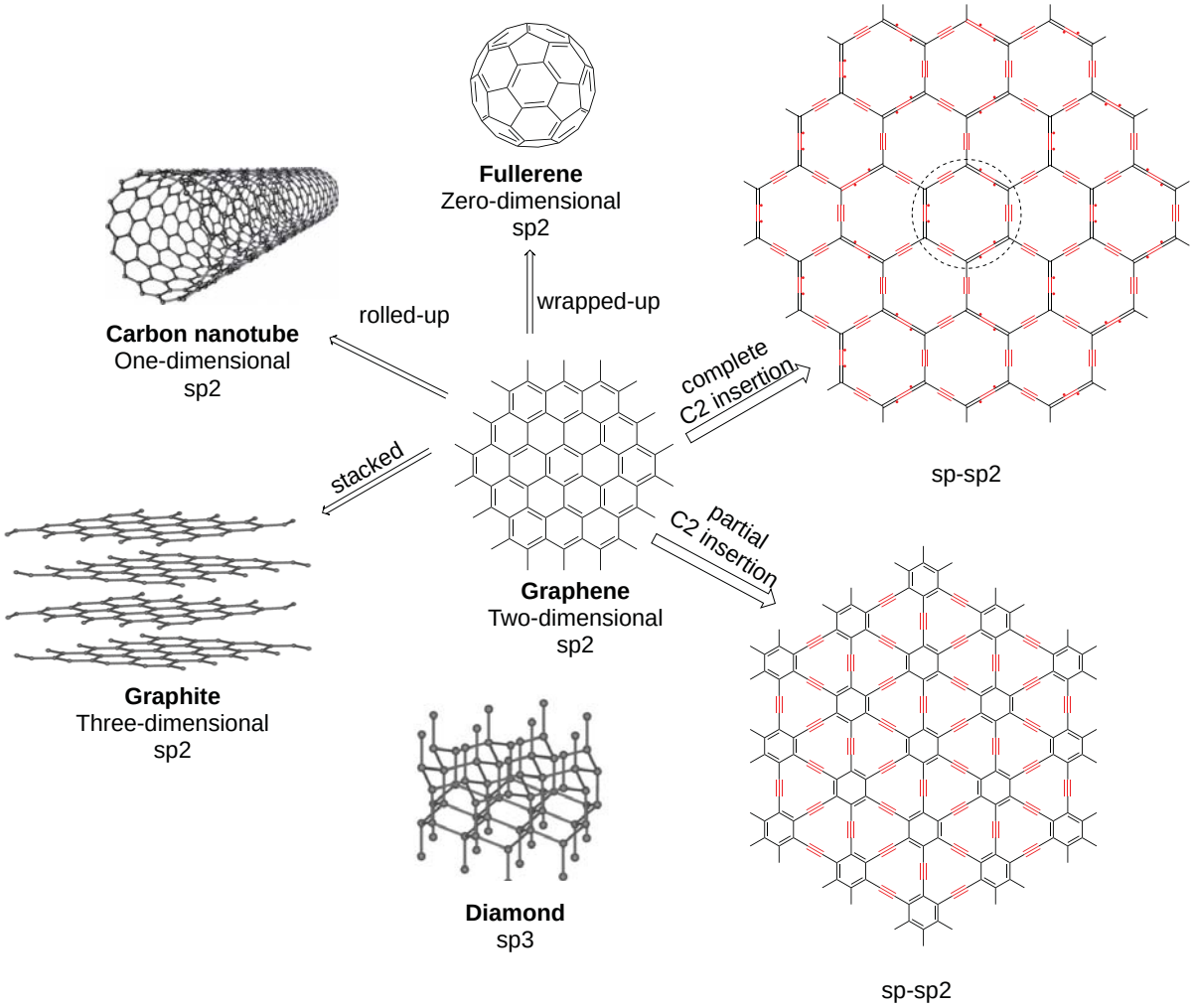

Figure 1. Representative allotropic carbon materials with differently hybridized carbon atoms. The α-graphyne was proposed and studied at the theoretical level only, while all the other carbon allotropes depicted in this figure are known.

Early studies on carbon materials mainly focused on two carbon allotropes: graphite and diamond, which consist of networks of sp^2 and sp^3 hybridized carbon atoms, respectively. The

three-dimensional, layered structure of graphite makes it suitable to be used as a solid lubricant and as a reinforcing additive in carbon fibers.[2] Diamond, featuring the properties of hardness and high refractive index, is mainly used in jewelry and in drilling heads for geological exploration.[1b] Their different applications, based on their distinct chemical and physical properties, drew the attention of the scientific community towards the development of novel carbon materials.

In 1985, Kroto and co-workers disclosed a third allotropic form of carbon, namely, the zero-dimensional Buckminster fullerene or C_{60}, made of 60 equivalent sp^2 hybridized carbon atoms, which was fabricated by laser irradiation of graphite.[3] Subsequently, systematic investigations of this new carbon allotrope by chemical methods, such as UV-visible, IR spectroscopies, and mass spectrometry, were reported by Krätschmer *et al*..[4] Fullerene can be considered as a wrapped-up graphene sheet (Figure 1), since these two materials have the same arrangement of carbon atoms. One-dimensional carbon nanotubes, first prepared by Lijima in 1991 using an arc-discharge evaporation method, also exhibit the same sp^2-hybridized carbon network, and can be regarded as a rolled-up graphene sheet.[5] More recently, the parent of these zero- and one-dimensional carbon allotropes, a graphene sheet, was first obtained by mechanical exfoliation by Geim *et al*.. This flat monolayer of carbon atoms densely packed into a honeycomb lattice was described as a two-dimensional material on the basis of investigations of its electronic properties (see Figure 1).[6]

All these sp^2-hybridized carbon allotropes became attractive for scientists not only for their aesthetically fascinating structure, but also for their prominent properties. Indeed, the π-electron-rich conjugated systems of fullerene, carbon nanotubes and graphene confer them unique and outstanding electronic, mechanical, and thermal properties.[7] For example, functionalized fullerenes were applied as highly efficient electron acceptors in photovoltaic devices.[8] They were also shown to exhibit non-linear optical properties[9] or to act as mesogens for the formation of liquid crystal mesophases[10]. Water-soluble fullerenes decorated with hydrophilic groups were also found to efficiently inhibit HIV-1 protease.[11] Carbon nanotubes were considered for their appealing properties possibly correlated with their helicity, such as their semiconducting or metallic character, which can be potentially used in fine materials, and also their gas storage ability.[12,1d] Although graphene has been developed for only a decade, its unique electronic properties could give rise to applications in integrated circuits,[13] in the domain of energy,[14] and even in anticancer therapy.[15]

The development of new carbon allotropes, having new types of scaffolds made of sp^2-sp or sp^3-sp hybridized carbon atoms, is thus a topic of high interest.

The structures of graphynes, made of sp^2- and sp-hybridized carbon atoms, were proposed in 1987 by Baughman as new bidimensional carbon allotropes.[16] These carbon allotropes have been largely studied at the theoretical level, in particular for their promising electronic and mechanical properties.[17] These expanded graphenic structures are formally obtained by insertion of C_2 units into all the covalent bonds of graphene (α-graphyne) or a part of them (γ-graphyne) (see Figure 1). This expansion process can be related to the *carbo*-

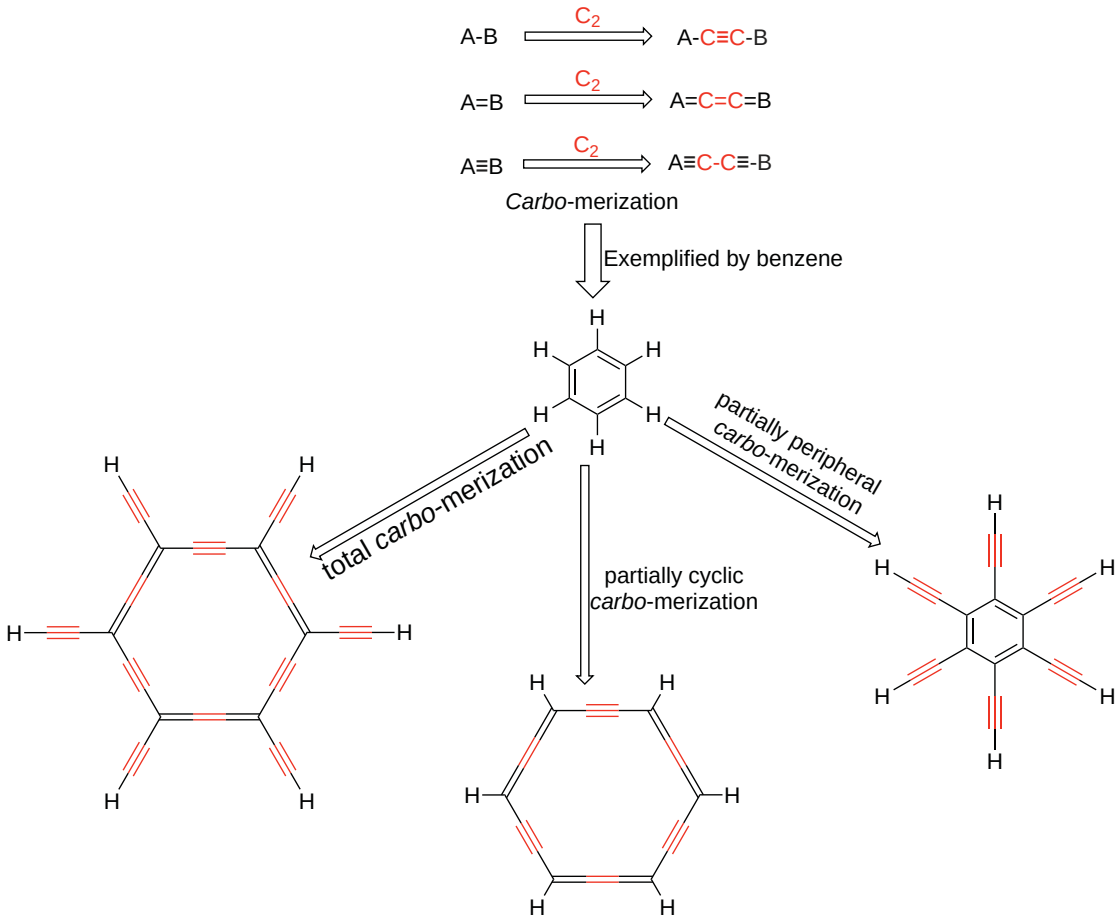

Figure 2. *Carbo*-merization process illustrated in the case of the benzene molecule.

merization process defined by R. Chauvin in 1995, and consisting of the formal insertion of C_2 units into all the covalent bonds, or a topologically defined type of bonds, of any parent Lewis structure (Figure 2).[18] α-Graphyne can thus be also viewed as the *carbo*-mer of graphene, or *carbo*-graphene, its basic constitutive motif is a *carbo*-benzene ring, whose synthesis has been largely studied in our group over the past 20 years (Figure 1).[19] The intrinsic characteristics and properties (stability, aromaticity…) of *carbo*-benzenes, and *carbo*-mers in general, have been largely studied at the theoretical level,[20] and motivate the

synthetic efforts to prepare such expanded molecules. The D_{6h}-symmetry, hollow discotic character (diameter ≈ 0.8 nm), magnetic aromaticity, and conjugated π-electron-rich system of the *carbo*-benzene ring makes it attractive for possible applications in various fields, such as nonlinear optics, electrical conductivity, or liquid crystals. Although the unsubstituted *carbo*-benzene $C_{18}H_6$ still remains unknown today, more than thirty examples of diversely substituted ring *carbo*-mers of benzene have been described.[19]

All the *carbo*-benzenes are prepared from their corresponding hexaoxy[6]pericyclyne precursors. The term pericyclyne was proposed by L. T. Scott, who described the first fully hydrocarbon representatives in the 1980's (Figure 3. A).[21] A large variety of other cyclic oligoacetylenes have been synthesized,[22] among which are oxygen-substituted pericyclynes (Figure 3, C)[23] or pericycldiynes (Figure 3. B, D, E),[24] cyclic hexaphenylacetylene (Figure 3. G),[25] γ-graphdiyne units (Figure 3. F).[26]

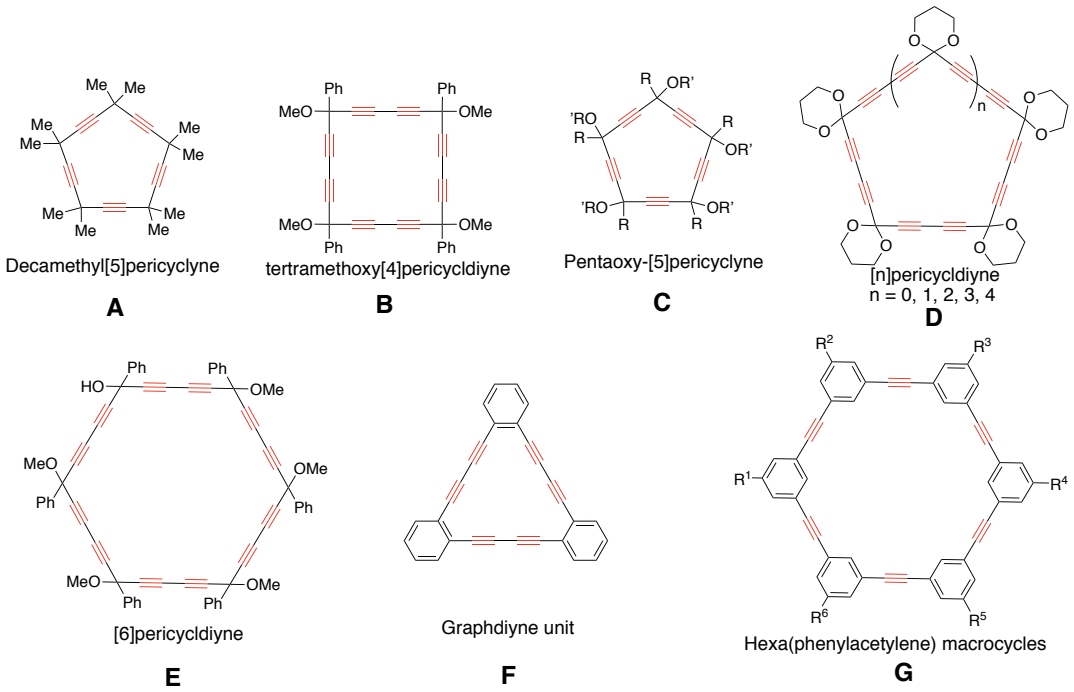

Figure 3. Examples of cyclic oligoacetylenes. **F**, **G** are phenylene and acetylene hybrid macrocycles.

The preparation of *carbo*-benzenes calls for the synthesis of hexaoxy[6]pericyclyne precursors, whose six hydroxyl or alkoxyl groups are finally removed under reductive and acidic conditions to afford the aromatic C_{18} macrocycle of *carbo*-benzenes. Several routes were envisioned to prepare these hexaoxy[6]pericyclynes, all of them being based on a key macrocyclization step between a dinucleophile X and a dielectrophile Y, the corresponding macrocyclization being then denoted as [X+Y] (Figure 4).

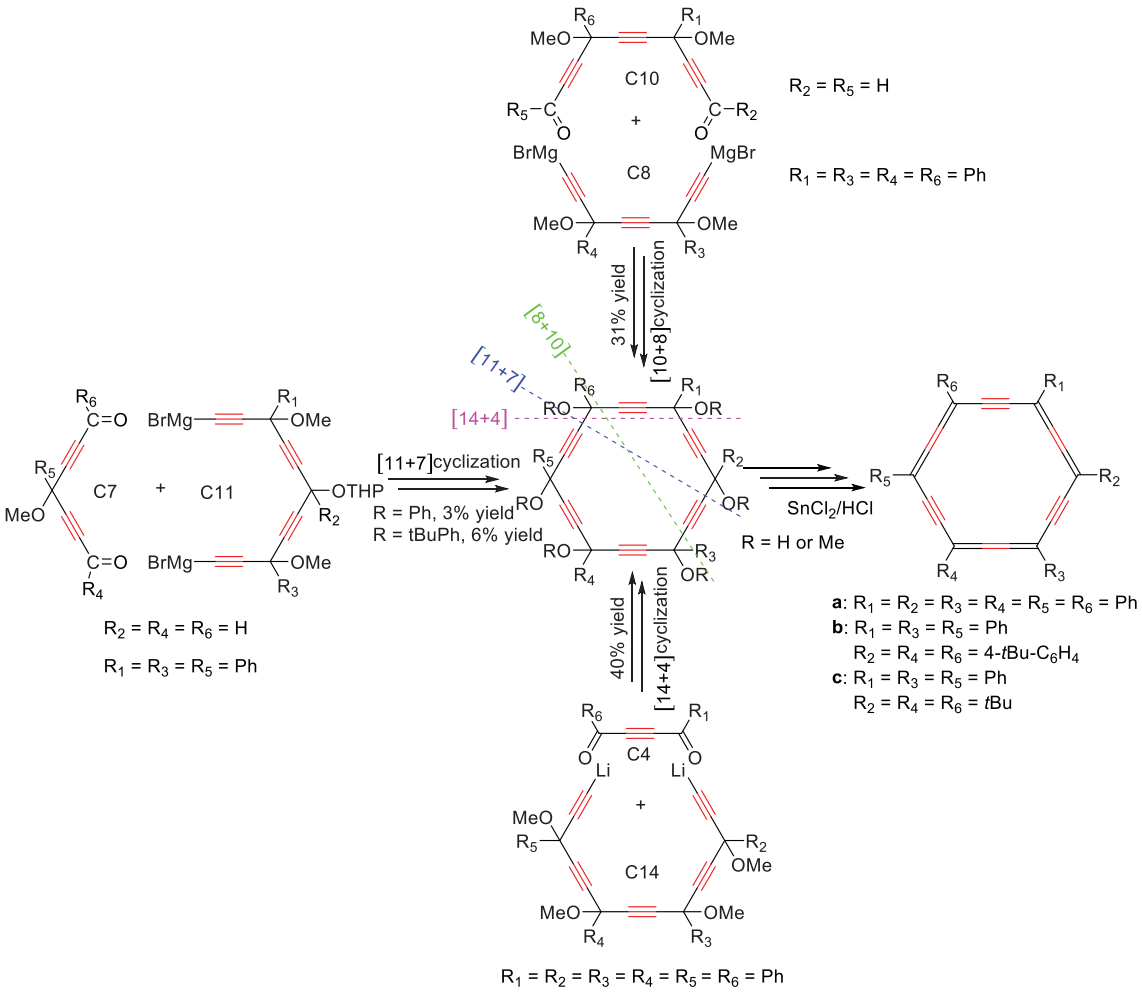

Figure 4. Different macrocyclization strategies developed for the synthesis of hexaoxy[6]pericyclyne precursors of *carbo*-benzenes.

The first examples of *carbo*-benzenes were reported by Ueda *et al.*,[27] and their hexaoxy[6]pericyclyne precursors were prepared through a [11+7] macrocyclization process. Three octupolar *carbo*-benzenes **a-c** were prepared with this way, including the hexaphenyl-*carbo*-benzene **a**, obtained in 15 steps with a 1% global yield (Figure 4).

In 2007, a new synthetic route based on [14+4] cyclization was proposed for the preparation of the hexaphenyl-*carbo*-benzene **a** in 8 steps and 12% overall yield.[28] The [8 +10] macrocyclization approach was later shown to be the most efficient route to prepare quadrupolar *carbo*-benzenes, through the synthesis of a key [6]pericyclynediol precursor **d**, isolated in about 30 % yield by cyclic addition of a C_8 triyne dinucleophile and a C_{10} triynedial dielectrophile.[29] Very recently, the yield of this key macrocyclization step was significantly improved up to 48 % by a fine tuning of the concentration, speed of addition of the two reagents, and temperature of the reaction mixture.[30] The [6]pericyclynedione **e**

resulting from the oxidation of [6]pericyclynediol **d** with MnO_2, can readily react with various nucleophiles R-X (X= Li, or MgBr), thus leading, after a subsequent reductive aromatization step, to a large number of quadrupolar *carbo*-benzenes **f-o** (see Scheme 1). Some of these quadrupolar molecules were found to exhibit remarkable properties, such as, the high single molecular conductance (SMC) of the *p*-dianilinyl-*carbo*-benzene **g**,[31] or one- and two-photon absorption properties (OPA and TPA) of the *p*-difluorenyl-*carbo*-benzenes **n** and **o**.[32] Among the reported *carbo*-benzenes in the past years, almost half of them were obtained by this method.

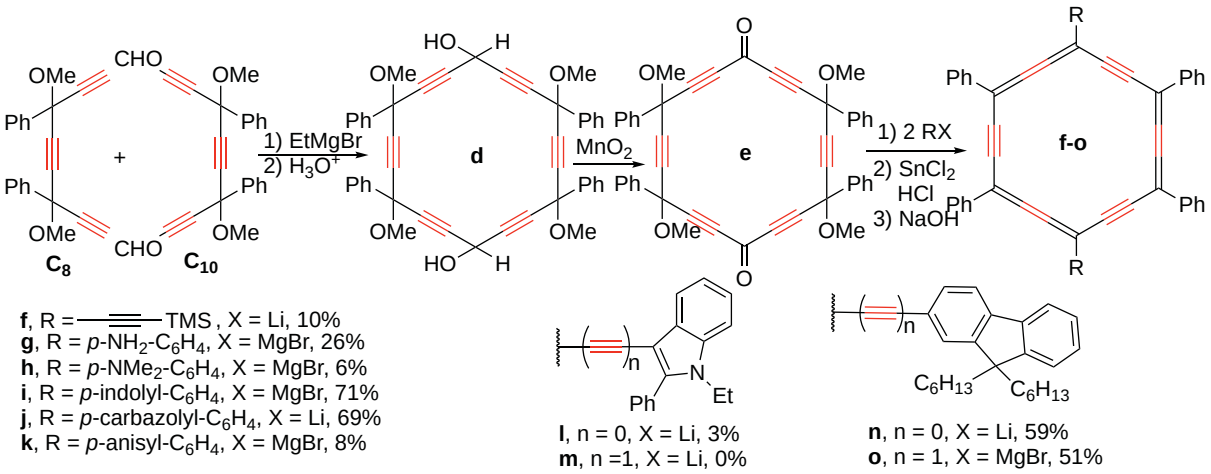

Scheme 1. Examples of quadrupolar *carbo*-benzenes **f-o** prepared from the [6]pericyclynedione **e**.

However, most of the *carbo*-benzenes suffer from a very limited solubility, thus restricting the scope of potential applications of this new family of compounds. The search for substituents allowing to increase the solubility of these carbon-rich molecules is thus becoming today of crucial importance. The hexaphenyl-*carbo*-benzene as a reference compound **a** was thus first re-prepared and modified in order to improve the solubility. It was also an opportunity to complete its characterization, which was only partially described by Ueda, Kuwatani *et al.*[27] The synthetic route to the known hexaphenyl-*carbo*-benzene **a** was here envisaged by the classically used double addition of two different nucleophiles ($Ph^-Li^+$and Ph^-MgBr^+) to the key [6]pericyclynedione **e**. The original synthesis by Ueda *et al*. could thus be improved by shortening the synthetic route (from 15 to 12), and the global yield was increased from 1% to 8%. The synthesis of the expectedly soluble analogue **p** bearing two di-*tert*-butylphenyl substituents was also described and these two hexaaryl-*carbo*-benzenes **a** and **p** could be fully characterized, including by X-ray diffraction analysis and

electrochemistry. The charge transport properties of the hexaphenyl-*carbo*-benzene **a** were also investigated regarding possible applications in organic photovoltaic devices. The extremely low solubility of **a**, however, prevented the formation of thin films of sufficient quality for the measurement of charge transport properties, further evidencing the drawback of the low solubility of *carbo*-benzenes. The replacement of two phenyl groups of **a** with two di-*tert*-butylphenyl groups in **p** was however shown to only slightly increase the solubility of *carbo*-benzene. Nevertheless, efficient solubilizing substituents were recently found, and the synthesis and properties of the corresponding *carbo*-benzenes are described in the Chapter 3 of this manuscript.

Reference

1. a). H. W. Kroto, A. W. Allaf, S. P. Balm, *Chem. Rev*., **1991**, *91*, 1213-1235; b). F. Diederich, Y. Rubin, *Angew. Chem. Int. Ed. Engl*. **1992**, *31*, 1101-1123; c). A. H. Castro Neto, F. Guinea, N. M. R. Peres, K. S. Novoselov, A. K. Geim, *Rev. Mod. Phys*., **2009**, *81*, 109-162; d). A. Hirsch, *Nat. Mater*., **2010**, *9*, 868-871.

2. E. Fitzer, *Carbon*, **1989**, *27*, 621-645.

3. H. W. Kroto, J. R. Heath, S. C. O'Brien, R. F. Curl, R. E. Smalley, *Nature*, **1985**, *318*, 162 −163.

4. W. Kratschmer, L. D. Lamb, K. Fostiropoulos, D. R. Huffman, *Nature*, **1990**, *347*, 354-358.

5. S. Lijima, *Nature*, **1991**, *354*, 56-58.

6. K. S. Novoselov, A. K. Geim, S. V. Morozov, D. Jiang, Y. Zhang, S. V. Dubonos, I. V. Grigorieva, A. A. Firsov, *Science*, **2004**, *306*, 666−669.

7. W. Zhou, X. Bai, E. Wang, S. Xie, *Adv. Mater*., **2009**, *21*, 4565−4583.

8. G. Dennler, M. C. Scharber, C. J. Brabec, *Adv. Mater*., **2009**, *21*, 1323–1338.

9. E. Koudoumas, M. Konstantaki, A. Mavromanolakis, S. Couris, M. Fanti, F. Zerbetto, K. Kordatos, M. Prato, *Chem. Eur. J*., **2003**, *9*, 1529-1534.

10. S. Campidelli, T. Brandmuller, A. Hirsch, I. M. Saez, J. W. Goodby, R. Deschenaux, *Chem. Commun*., **2006**, 4282–4284.

11. S. H. Friedman, D. L. Decamp, R. P. Sijbesma, G. Srdanov, F. Wudl, G. L. Kenyon, *J. Am. Chem. Soc*., **1993**, *115*, 6506-6509.

12. a). C. Liu, Y. Y. Fan, M. Liu, H. T. Cong, H. M. Cheng, M. S. Dresselhaus, *science*, **1999**, *286*, 1127-1129; b). R. T. Yang, *carbon*, **2000**, *38*, 623-641; c). P. Poncharal, Z. L. Wang, D. Ugarte, W. A. de Heer, *science*, **1999**, *283*, 1513-1516.

13. R. R. Nair, P. Blake, A. N. Grigorenko, K. S. Novoselov, T. J. Booth, T. Stauber, N. M. R. Peres, A. K. Geim, *science*, **2008**, *320*, 1308.

14. X. M. Li, H. W. Zhu, K. L. Wang, A. Y. Cao, J. Q. Wei, C. Y. Li, Y. Jia, Z. Li, X. Li, D. H. Wu, *Adv. Mater.*, **2010**, *22*, 2743–2748.

15. M. Fiorillo, A. F. Verre, M. Iliut, M. Peiris-Pagés, B. Ozsvari, R. Gandara, A. R. Cappello, F. Sotgia, A. Vijayaraghavan, M. P. Lisanti, *Oncotarget*, **2015**, *6*, 3353-3562.

16. R. H. Baughman, H. Eckhardt, M. Kertesz, *J. Chem. Phys*., **1987**, *87*, 6687-6699.

17. a). S. Iijima, *Nature*, **1991**, *354*, 56-58; b). D. Malko, C. Neiss, F. Vines, A. Gorling, *Phys. Rev. Lett*., **2012**, *108*, 086804.

18. R. Chauvin, *Tetrahedron Lett*., **1995**, *36*, 397-400; *Tetrahedron Lett*., **1995**, *36*, 401-404.

19. a). L. Leroyer, V. Maraval, R. Chauvin, *Chem. Rev*., **2012**, *112*, 1310-1343; b). K. Cocq, C. Lepetit, V. Maraval, R. Chauvin, *Chem. Soc. Rev*., **2015**, *44*, 6535-6559.

20. a). B. G. Kim, H. J. Choi, *Phys. Rev. B*, **2012**, *87*, 11543; b). J. M. Ducere, C. Lepetit, R. Chauvin, *J. Phys. Chem. C*, **2013**, *117*, 21671-21681.

21. a). L. T. Scott, G. J. DeCicco, J. L. Hyunn, G. Reinhardt, *J. Am. Chem. Soc*., **1983**, *105*, 7760-7761; b). K. N. Houk, L. T. Scott, N. G. Rondan, D. C. Spellmeyer, G. Reinhardt, J. L. Hyun, G. J. DeCicco, R. Weiss, M. H. M. Chen, L. S. Bass, J. Clardy, F. S. Jorgensen, T. A. Eaton, V. Sarkosi, C. M. Petit, L. Ng, K. D. Jordan, *J. Am. Chem. Soc*., **1985**, *107*, 6556-6562.

22. a). F. Diederich, *Nature*, **1994**, *369*, 199-207; b). V. Maraval, R. Chauvin, *Chem. Rev*., **2006**, *106*, 5317-5343.

23. c). L. Maurette, C. Tedeschi, E. Sermot, M. Soleilhavoup, F. Hussain, B. Donnadieu, R. Chauvin, *Tetrahedron*, **2004**, *60*, 10077-10098.

24. a). M. Brake, V. Enkelmann, U. H. F. Bunz, *J. Org. Chem*., **1996**, *61*, 1190-1191. b). H. L. Anderson, R. Faust, Y. Rubin, F. Diederich, *Angew. Chem. Int. Ed. Engl*., **1994**, *33*, 1366-1368; c). C. Zou, C. Lepetit, Y. Coppel, R. Chauvin, *Pure Appl. Chem.*, **2006**, *78*, 791-811; c). P. Manini, W. Amrein, V. Gramlich, F. Diederich, Angew. Chem. Int. Ed., 2002, 41, 4339-4343.

25. J. S. Zhang, J. S. Moore, *J. Am. Chem. Soc*., **1992**, *114*, 9702-9704.

26. M. M. Haley, S. C. Brand, J. J. Pak, *Angew. Chem. Int. Ed. Engl*., **1997**, *36*, 835-838.

27. a). Y. Kuwatani, N. Watanabe, l. Ueda, *Tetrahedron Lett*., **1995**, *36*, 119-122. b). R. Suzuki, H. Tsukuda, N. Watanabe, Y. Kuwatani, l. Ueda, *Tetrahedron*, **1998**, *54*, 2477-2496.

28. C. Saccavini, C. Tedeschi, L. Maurette, C. Sui-Seng, C. Zou, M. Soleilhavoup, L. Vendier, R. Chauvin, *Chem. Eur. J*., **2007**, *13*, 4895-4913.

29. L. Leroyer, C. H. Zou, V. Maraval, R. Chauvin, *C. R. Chimie*, **2009**, *12*, 412-429.

30. K. Cocq, V. Maraval, R. Chauvin, unpublished results.

31. Z. H. Li, M. Smeu, A. Rives, V. Maraval, R. Chauvin, M. A. Ratner, E. Borguet, *Nat. Commun*., **2015**, *6*, 6321.

32. I. Baglai, M. Anda-Villa, R. M. Barba-Barba, C. Poidevin, G. Ramos-Ort, V. Maraval, C. Lepetit, N. Saffon-Merceron, J. L. Maldonado, R. Chauvin, *Chem. Eur. J*., **2015**, *21*, 14186-14195.

Article 2

NJC

PAPER

View Article Online
View Journal | View Issue

Cite this: *New J. Chem.*, 2017, 41, 3908

Hexaaryl-*carbo*-benzenes revisited: a novel synthetic route, crystallographic data, and prospects of electrochemical behavior†

Chongwei Zhu,[ab] Carine Duhayon,[ab] Daniel Romero-Borja,[c] José-Luis Maldonado,[c] Gabriel Ramos-Ortíz,[c] Alix Saquet,[ab] Valerie Maraval*[ab] and Remi Chauvin*[ab]

Received 3rd January 2017,
Accepted 29th March 2017

DOI: 10.1039/c7nj00028f

rsc.li/njc

An improved 12-step synthetic route and full characterization of hexaphenyl-*carbo*-benzene (**4**, 8%) and the *p*-bis-3,5-di-*tert*-butylphenyl homologue (**11**, 4%), are described. The *carbo*-benzene reference **4** is now accurately described in the crystal state by X-ray diffraction analysis in the chiral space group $P2_12_12_1$, and in comparison to the less symmetric derivative **11** exhibiting a centro-symmetric packing. According to cyclic voltammetry, both hexaaryl-*carbo*-benzenes **4** and **11** can behave as both reversible potent electron acceptors and standard electron donors, with respective potentials of −0.73 ± 1 V and +1.17 ± 2 V/SCE, respectively. Due to their extremely low solubility, solid films of **11** fabricated using the "wet method", with the initial view of studying charge transport properties, were found to display high roughness.

1 Introduction

By January 1995, the title term "*carbo*-benzene" was proposed for **1**, as a putative example of Hückel-aromatic *carbo*-mer,[1] namely a structure devised by D_{6h} symmetry-preserving C_2-expansion of the benzene molecule (Fig. 1).[2] In spite of an attempt of synthesis *via* the hexaoxy-[6]pericyclynediol **2** (itself targeted *via* a [9+9] macro-cyclization route from the triynal **3**),[3] the "bare" *carbo*-benzene **1** could not be obtained and remains hitherto experimentally unknown.[4] Exactly at the same time, Ueda *et al.* communicated the synthesis of 3,6,9,12,15,18-hexaphenyldodecadehydro[18]-annulene **4** and a few congeners,[5] standing as the first examples of *carbo*-benzene derivatives, in tri- or hexa-substituted versions (Scheme 1). The highly chromophoric compound **4** and its [6]pericyclynetriol precursor **5** were described in more details by the same authors in 1998.[6] The employed route was based on a [11+7] macro-cyclization step, where the bis-terminal tetrayne **6** reacts as a dinucleophile with the skipped bis-ynal **7** as a dielectrophile. The original synthetic route thus consisted of 15 steps, with 1% overall yield, and 59% yield for the **5** → **4** reductive aromatization step.[5,6] In 2007, the same hexaphenyl-*carbo*-benzene **4** was reported to be also accessible by reductive aromatization of the [6]pericyclynediol **8** or [6]pericyclynetetraol **9**, in 12 or 22% yield, respectively.[7] The precursors **8** and **9** were themselves obtained through [14+4] macro-cyclization processes, in nine steps with 11% overall yield, and eight steps with 12% overall yield, respectively.[8]

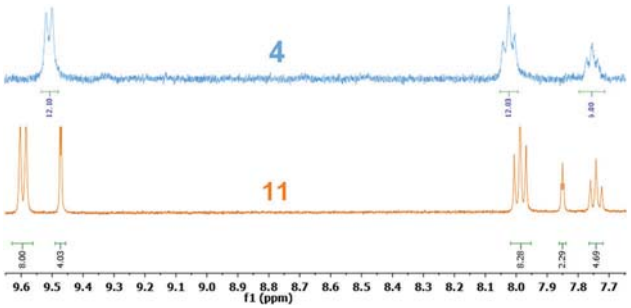

Fig. 1 Aromatic region of the ^{1}H NMR spectra of **4** and **11** in highly diluted $CDCl_3$ solutions (400 MHz, 12 h acquisition time).

A much shorter alternative route would be based on a [8+10] macro-cyclization process and a key [6]pericyclynedione **10**,[9] which more recently proved to be efficient for the synthesis of centro-symmetric tetraphenyl-*carbo*-benzene targets.[10] Application of this method to the preparation of the *carbo*-benzene paradigm **4** is hereafter described, along with the synthesis of the *a priori* more lipophilic *p*-bis-(di-3,5-*tert*-butylphenyl) derivative **11**.

[a] *CNRS, LCC (Laboratoire de Chimie de Coordination), 205 route de Narbonne, BP 44099, 31077 Toulouse Cedex 4, France. E-mail: valerie.maraval@lcc-toulouse.fr, chauvin@lcc-toulouse.fr*

[b] *Université de Toulouse, UPS, ICT-FR 2599, 118 route de Narbonne, 31062 Toulouse Cedex 9, France*

[c] *Centro de Investigaciones en Óptica A.P. 1-948, 37000 León, Gto., Mexico*

† Electronic supplementary information (ESI) available: ^{1}H and ^{13}C NMR spectra, XRD data, SWV and CV voltammograms. CCDC 1503931 and 1518487. For ESI and crystallographic data in CIF or other electronic format see DOI: 10.1039/c7nj00028f

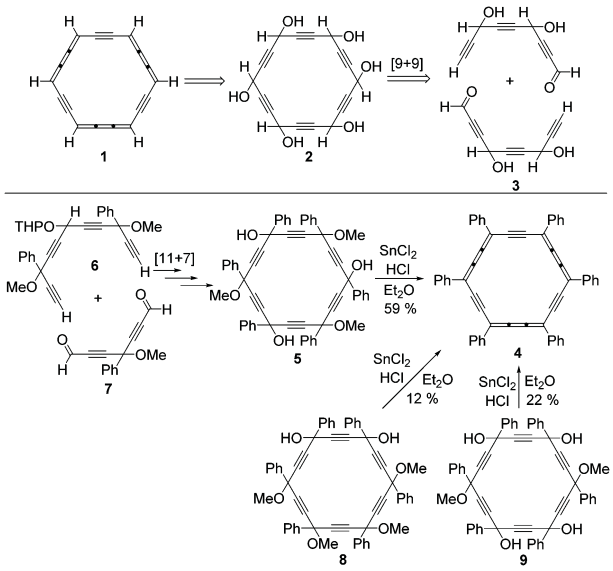

Scheme 1 Strategies envisaged for the preparation of the unsubstituted *carbo*-benzene **1** (top); known syntheses of hexaphenyl-*carbo*-benzene **4** (bottom).

In the 1998 pioneer report,[6] X-ray diffraction (XRD) analysis of a single crystal of **4** allowed confirmation of the quasi-D_{6h} symmetric structure and provided information on bond distances and bond angles. Nevertheless, the quality of the crystallographic structure was likely not sufficient for deposition of a coordinate listing at the CCDC, where no corresponding cif file is currently available. The challenge of gaining accurate crystallographic data to make a cif file of **4** available at the CCDC is particularly addressed below.

2 Results and discussion

The *carbo*-benzene targets **4** and **11** were thus envisaged by reductive aromatization of the [6]pericyclynediols **12** and **13**. The latter were targeted from the known [6]pericyclynedione **10**, respectively, obtainable by oxidation of the corresponding secondary [6]pericyclynediol **14** (Scheme 2).[9] An optimal procedure

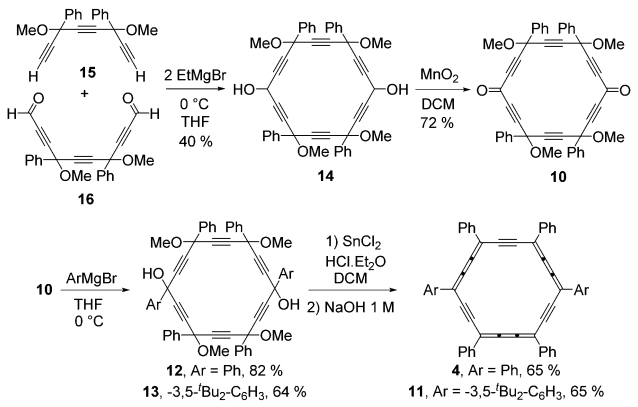

Scheme 2 Synthesis of *carbo*-benzene targets *via* a [8+10] macrocyclization route.

for the synthesis of **14** is based on a [8+10] macro-cyclization step involving the C_8 triyne **15** and C_{10} dialdehyde **16**. As compared to the previously used [11+7] and [14+4] strategies (see the Introduction), the advantage of the [8+10] strategy is its late divergence character: the sensitive dialdehyde **16** is indeed readily obtained from the triyne **15** just before the macro-cyclization step, providing the [6]pericyclynediol **14** in *ca.* 40% yield (see the ESI† for a detailed comparison of the original and improved synthesis strategies).[9] The key [6]pericyclynedione **10** is then obtained by oxidation of **14** with MnO_2. From **10**, the targets **4** and **11** were prepared in two steps following a procedure previously experienced for the synthesis of other *carbo*-benzenes.[10] The addition of two equivalents of either PhLi or PhMgBr to diketone **10** was thus attempted. Treatment of **10** with PhLi was found to induce opening of the C_{18} ring, allowing access to the diadduct **12** in a trace amount only. In contrast, the use of PhMgBr allowed isolation of **12** with a remarkably high 82% yield (Scheme 2). The Grignard reagent was thus also used for anchoring two 3,5-di-*tert*-butylphenyl groups to **10**, providing the [6]pericyclynediol **13** with 64% yield.

Using a classical procedure,[10] reductive aromatization of **12** and **13** in dichloromethane (DCM) solution with 10 equivalents of $SnCl_2$ and 20 equivalents of $HCl{\cdot}Et_2O$, followed by neutralization with 1 M aqueous NaOH, gave the targets **4** and **11** with the same 65% yield. This procedure differs from the original one by the nature of the solvent and the hydrolysis conditions.[6] The results confirm recent observations that the use of DCM as a solvent instead of diethyl ether, along with milder hydrolytic conditions (1 M instead of 10 M NaOH), provides higher yields in *carbo*-benzenes, essentially by enhancement of the solubility of both reagents and products.[10] In comparison with the original method,[5,6] not only the yield in **4** of the last reductive elimination step has been improved from 59 to 65%, but also the total number of steps has been reduced from 15 to 12, while the global yield has been increased from about 1% to 8% (see the ESI† for comparative synthesis schemes).

The hexa-aryl-*carbo*-benzenes **4** and **11** have been isolated as poorly soluble dark red solids. The introduction of two *tert*-butyl groups on two phenyl substituents of **4** thus appears to have a limited effect on the solubility of such rigid carbon-rich compounds. Indeed, the solubility of **11** was determined to be *ca.* 0.46 ± 0.03 mg mL^{-1}, namely less than twice the solubility of **4** of *ca.* 0.29 ± 0.03 mg mL^{-1}, in spite of the presence of four *tert*-butyl groups on two of the aromatic substituents of **11**. For comparison, direct anchoring of aliphatic chains at two vertices the C_{18} macrocycle was recently reported to be much more efficient with the view of increasing the solubility of *carbo*-benzenes.[13]

In spite of this, accurate spectroscopic data could be obtained for both **4** and **11** (^{1}H NMR, ^{13}C NMR, UV-vis), thus confirming the data ranges of Ueda *et al.* for **4**.[5,6] In particular, ^{1}H NMR spectra of **4** and **11** reveal the characteristic deshielding of the *ortho*-^{1}H nuclei of the aryl substituents resulting from the magnetic anisotropy induced by the strong diatropic C_{18} ring current (Fig. 1).[1,5–7,10]

The UV-vis absorption spectrum of **4** in chloroform solution confirms the λ_{max} value of 472 nm previously reported (Fig. 2).[6]

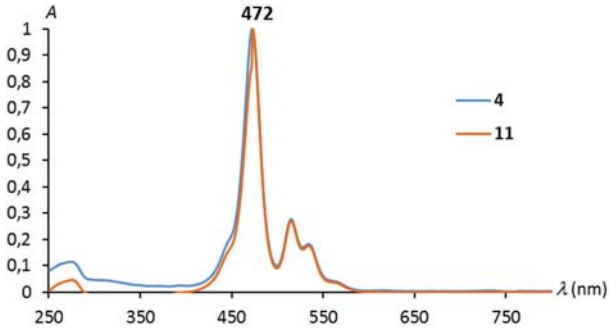

Fig. 2 Normalized absorption spectra of **4** and **11** in chloroform solution.

Carbo-benzene **11** exhibits an identical spectral profile with the same λ_{max} value. The molar extinction coefficient of **4** was however measured to be lower than the value initially reported (234 000 *vs.* 363 000 L mol^{-1} cm^{-1}).[6] The absorption spectra of **4** and **11** are classical for *carbo*-benzenes, and their common maximum absorption wavelength λ_{max} = 472 nm is a median value of all the reported values, varying from 424 nm for the octupolar triphenyl-*carbo*-benzene,[5,6] to 521 nm for the quadrupolar *para*-*N*,*N*-dimethylanilinyl-tetraphenyl-*carbo*-benzene.[10b]

The structures of **4** and **11** were confirmed by XRD analysis of single crystals deposited from chloroform solutions (Fig. 3 and Table 1).[14] Contrary to the pioneer crystallographic data,[6] the quality of the present crystals of **4** proved to be sufficient for refined resolution, having allowed a new deposition at the CCDC.[14] The same solvate allotropic variety, involving one $CHCl_3$ molecule per molecule of **4**, was obtained. Noteworthily, the highly planar centro-symmetric molecule **4** thus crystallizes in the Sohncke chiral space group $P2_12_12_1$. Crystallization of a highly symmetrical achiral molecule such as **4** in a chiral space group is not common, but examples have been previously reported for other rigid compounds.[15]

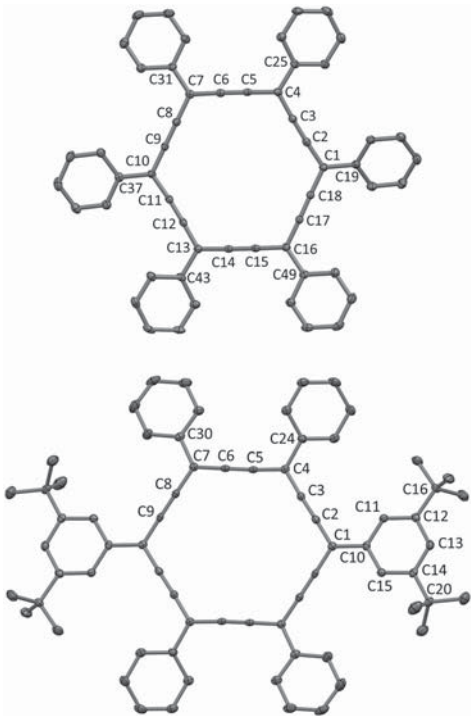

Fig. 3 Molecular views of the X-ray crystal structures of *carbo*-benzenes **4** (top) and **11** (bottom). Numbering of non-equivalent C atoms is indicative of the crystal symmetry. For clarity, hydrogen atoms and solvent molecules are omitted.

Table 1 Selected crystallographic data for **4** and **11**[14]

	4	**11**
Empirical formula	$C_{54}H_{30}$, $CHCl_3$	$C_{70}H_{62}$, 2($CHCl_3$)
Formula mass	798.21	1142.02
Crystal system	Orthorhombic	Triclinic
Space group	$P2_12_12_1$ (CCDC 1231497)	$P\bar{1}$
T [K]	100	120
a [Å]	12.4948(5)	10.1720(5)
b [Å]	16.0972(6)	11.8006(8)
c [Å]	20.2765(9)	12.8576(7)
α [°]	90	90.105(5)
β [°]	90	101.559(5)
γ [°]	90	94.484(5)
V [Å^3]	4078.24(18)	1507.20(8)
D_c	1.300	1.258
Z	4	1
μ [mm^{-1}]	0.263	0.327
Refl. Measured	97 066	23 700
Refl. unique/R_{int}	9935/0.048	6699/0.045
Refl. with $I > 3\sigma(I)$	7863	4214
Nb parameters	560	379
R	0.0351	0.045
R_w	0.0369	0.0516
Flack parameter	0.05(5)	—
Nb Friedel-pairs	4448	—
$\Delta\rho_{max}/\Delta\rho_{min}$ [e Å^{-3}]	0.66/−0.58	0.50/−0.33

Geometrical features of the macrocycle of **4** are typical of generic *carbo*-benzenes, with average sp^{2}C–spC and spC–spC bond lengths of 1.39 and 1.22 Å, respectively. The average angle at the sp^2 vertices of the macrocycle is 118.9°. The C_{18} ring is slightly distorted: the maximum deviation from planarity is 0.11 Å, while the globally hexagonal shape is not regular, the diameters (between facing sp^2 vertices) varying from 7.79 Å to 8.17 Å. Torsion angles between the phenyl mean planes and the macrocycle mean plane vary from 2.9° to 29.8°. In the crystal of **11**, the molecules pack in a parallel fashion, the distance between the mean planes of two successive *carbo*-benzene macrocycles being 3.62 Å, *i.e.* much larger than in the recently reported first examples of π-stacked *carbo*-benzenes.[13a] No π-stacking is indeed observed here between two C18 rings, or between a C18 ring and any C6 ring of the aryl substituents. Instead of a chlorine atom of the chloroform molecule co-crystallized with **4** (see above), one of the methyl groups of a *tert*-butyl substituent of **11** pointing towards the center of the C_{18} ring of the nearest neighbouring molecule: the closest H atom of this methyl group resides 1.43 Å away from the centroid and 1.38 Å from the mean plane of the neighboring C_{18} ring (Fig. 4).

The electrochemical behavior of **4** and **11** has also been studied (Table 2). Cyclic (CV) and square-wave (SWV) voltammograms were recorded for **4** and **11** in chloroform solutions (see the ESI†). More conventional DCM solutions could indeed not be used because of an extremely low solubility in this solvent. For a reference dibutyl-*carbo*-benzene exhibiting sufficient solubility

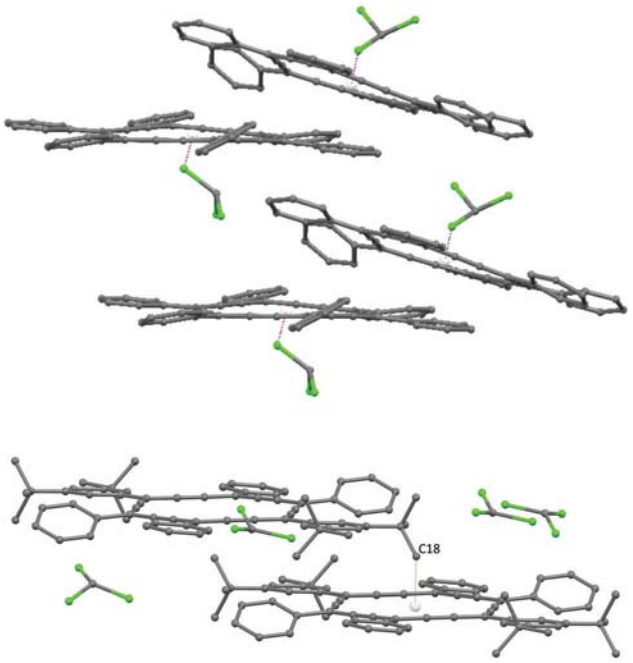

Fig. 4 Views of the crystalline molecular packing of **4** (top) and **11** (bottom) evidencing both the absence of π-stacking between the C_{18} rings, and interactions with solvent molecules (for **4**) and between two *carbo*-benzene molecules (for **11**).

in either solvents, such a solvent change was recently shown to make redox processes less reversible, but keep the redox potential values almost unchanged, thus allowing a comparison between data obtained from either DCM or chloroform solutions.[13b]

While the first reduction process was found to occur reversibly at similar potentials (−0.72 V for **4**, −0.74 V for **11**), the second reduction was found to be irreversible for both compounds (Table 2). These values are consistent with previous values reported for other *para*-diaryl-tetraphenyl-*carbo*-benzenes, the first reduction occurring between −0.75 and −0.85 V depending on the nature of the aryl groups.[10a,b] This process is however made easier upon substitution of the C_{18} ring by acetylenic substituents: the lowest reduction potential (in absolute value) of −0.60 V observed to date for any *carbo*-benzene was indeed measured for a *para*-bis-fluorenylethynyl-substituted representative.[10f] In the oxidation regime, the first peak potentials of the two *carbo*-benzenes have comparable values (1.14 V for **4** and 1.19 V for **11**), but the process was found reversible for **11** only: the oxidation product of **4** indeed undergoes polymerization, leading to a deposit on the electrode. A second non-reversible oxidation process was also observed for **11**. *Carbo*-benzenes generally undergo irreversible oxidation, most of them leading to a polymeric film on the electrode after the first oxidation process, the latter occurring at potentials between +0.51 and +0.90 V for donor-substituted hexaaryl-*carbo*-benzenes,[10a,b] and reaching +1.17 V for a fluorenylethynyl-substituted derivative exhibiting a more extended π-conjugation.[10f]

The low first reduction potential value of **4** and **11** (*ca.* −0.73 V) suggests their possible use as electron acceptors, thus as possible alternatives to C_{60} (and PCBM) for photovoltaics (the first reduction potential of C_{60} is −0.55 V in chloroform).[16] The accessible and possibly reversible character of the first oxidation of **11** (at 1.19 V) might also be compatible with its use as an organic electron donor. However, the very low solubility of these hexaaryl-*carbo*-benzenes, even that of the slightly more soluble derivative **11**, did not allow preparation of highly regular thin solid films using the "wet method", thus preventing measurement of their efficiency for charge transport.[17] Indeed, while microscopic optical images clearly show the non-uniformity of the films, AFM measurements showed a film roughness of *ca.* 355 nm (Fig. 5). This entails a poor optical quality of the films, as evidenced by

Table 2 CV and SWV data for the *carbo*-benzenes **4** and **11** in chloroform solutions

	Reductions			Oxidations		
Product	$E^1_{1/2}$ [a] (ΔE_P)[b]	RI_P [c]	E_P^{2red} [d]	$E^3_{1/2}$ [a] (ΔE_P)[b]	RI_P [c]	E_P^{4ox} [d]
4	−0.72[e] (0.44)	0.58	−1.15[f]			1.14[f]
11	−0.74[e] (0.59)	1.01	−1.30	1.19[e] (0.53)	0.68	1.70

[a] Half-wave potential $E_{1/2} = (E_P^{red} + E_P^{ox})/2$, in V/SCE. [b] Separation between the two peak potentials: $\Delta E_P = |E_P^{red} - E_P^{ox}|$, in V. [c] Peak current ratio $RI_P = |I_P^{ox}/I_P^{red}|$. [d] E_P values measured from CV in V/SCE. [e] Reversibility observed at a high scan rate only. [f] The compound underwent polymerization and deposited on the electrode.

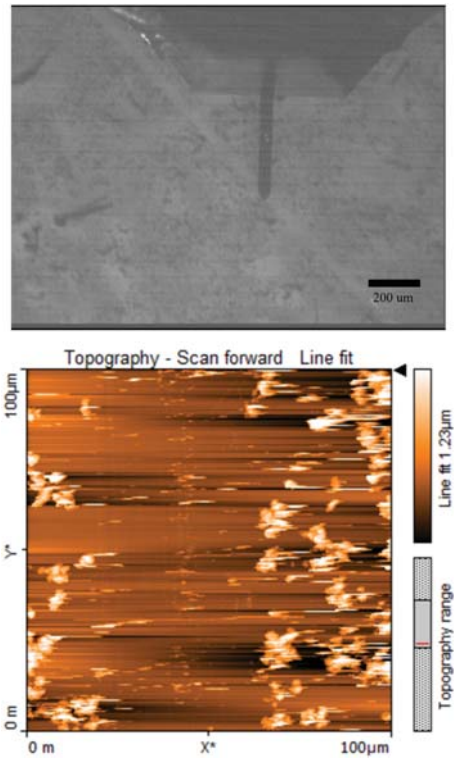

Fig. 5 Morphology of spin-casted films of **11** (blended with $PC_{71}BM$: 1 : 1, w/w ratio) on a glass substrate: microscopic optical image taken using a digital camera installed on the AFM instrument used (top), and the AFM image showing the film roughness (rms) ~355 nm (bottom). An additional AFM image is available in the ESI.†

their UV-vis absorption spectra exhibiting large light scattering competing with absorption (see the ESI†).

3 Conclusions

Hexaphenyl-*carbo*-benzene **4** is a fully symmetrical paradigm and model of the *carbo*-benzene family: 20 years after its first description, its synthetic accessibility has been significantly improved through the implementation of a [8+10] macro-cyclization strategy, and its characterization has been completed by accurate crystallographic and electrochemical data. The expected enhancement of solubility upon substitution of **4** by four *tert*-butyl groups was found to be limited, preventing the use of thin films of **11** for charge transport in organic photovoltaics. Nevertheless, the much higher solubility of recently described *p*-dialkyltetraphenyl-*carbo*-benzenes[13] allows consideration of their possible use for such applications. The results of the envisaged studies will be communicated in due course.

4 Experimental

4.1 General remarks

THF, diethyl ether (Et_2O), pentane and dichloromethane (DCM) were dried using a PureSolv-MD-5 Innovative Technology system for the purification of solvents. All other reagents were used as commercially available. In particular, solutions of PhLi were 1.9 M in dibutyl ether, solutions of PhMgBr were 3 M in diethyl ether, and solutions of HCl were 2 M in diethyl ether. All reactions were carried out under an argon atmosphere using Schlenk and vacuum line techniques. Column chromatography was carried out on silica gel (60 Å, C.C 70–200 μm). Silica gel thin layer chromatography plates (60F254, 0.25 mm) were revealed under UV-light and/or by treatment with an ethanolic solution of phosphomolybdic acid (20%). The following analytical instruments were used, ^{1}H and ^{13}C NMR: Avance 400 and Avance 400 HD spectrometers; mass spectroscopy: a Quadrupolar Nermag R10-10H spectrometer; UV-visible: a Perkin-Elmer UV-vis Win-Lab Lambda 950; and NMR chemical shifts are given in ppm with positive values to high frequency relative to the tetramethylsilane reference. Coupling constants *J* are in Hertz. The UV-visible extinction molar coefficient ε is in L mol^{-1} cm^{-1} and wavelengths λ in nm.

4.2 Experimental procedures and characterization

4.2.1 Hexaphenylcyclooctadeca-1,2,3,7,8,9,13,14,15-nonaen-5,11,17-triyne (4). A solution of [6]pericyclynediol **12** (77 mg, 0.087 mmol) in DCM (50 mL) was treated with $SnCl_2$ (165 mg, 0.87 mmol) and HCl (0.87 ml, 1.74 mmol, 2 M in Et_2O) at −78 °C. The mixture was stirred at −78 °C for 10 min, then at room temperature for 25 min. After the addition of aqueous 1 M NaOH (1.74 mL) and filtration through celite®, the organic layer was washed with brine three times, dried over $MgSO_4$, and concentrated under reduced pressure. The residue was purified by washings with Et_2O (3 × 5 mL) and pentane (3 × 5 mL) to obtain **4** as a dark violet solid with 65% yield (38 mg, 0.057 mmol). ^{1}H NMR (400 MHz, $CDCl_3$) δ 9.48 (d, J = 7.3 Hz, 12H, *o*-C_6H_5), 8.01 (t, J = 7.7 Hz, 12H, *m*-C_6H_5), 7.74 (t, J = 7.4 Hz, 6H, *p*-C_6H_5). ^{13}C{^{1}H} NMR (101 MHz, $CDCl_3$) δ 140.25 (i-C_6H_5), 130.56 (*o*-C_6H_5), 129.92 (*m*-C_6H_5), 129.44 (*p*-C_6H_5), 118.46 (=*C*=*C*=, –*C*≡*C*–), 104.53 (=*C*Ph–). HRMS (MALDI-TOF/DCTB): *m*/*z*: $[M + Na]^+$ calculated for $C_{54}H_{30}Na$: 701.2245, found: 701.2225. UV-vis ($CHCl_3$): λ_{max} = 472 nm (ε = 234 000 L mol^{-1} cm^{-1}). Melting-decomposition temperature: 221 °C.

4.2.2 1,10-Bis(3,5-di-*tert*-butylphenyl)-4,7,13,16-tetraphenylcyclooctadeca-1,2,3,7,8,9,13,14,15-nonaen-5,11,17-triyne (11). A solution of [6]pericyclynediol **13** (130 mg, 0.123 mmol) in DCM (100 mL) was treated with $SnCl_2$ (233 mg, 1.23 mmol) and HCl (1.3 mL, 2.453 mmol, 2 M in Et_2O) at −78 °C. The mixture was stirred at −78 °C for 20 min, then at room temperature for 15 min. After the addition of 1 M aqueous NaOH (2.6 mL) and filtration through celite®, the organic layer was washed with brine three times, dried over $MgSO_4$ and concentrated under reduced pressure. The residue was purified by washings with Et_2O (3 × 5 mL) and pentane (3 × 5 mL) to obtain **11** as a dark red solid with 65% yield (47 mg, 0.052 mmol). ^{1}H NMR (400 MHz, $CDCl_3$) δ 9.59−9.55 (m, 8H, *o*-C_6H_5), 9.45 (d, J = 1.7 Hz, 4H, *o*-C_6H_3), 7.96 (dd, J = 8.1, 7.2 Hz, 8H, *m*-C_6H_5), 7.83 (t, J = 1.7 Hz, 2H, *p*-C_6H_3), 7.72 (t, J = 7.3 Hz, 4H, *p*-C_6H_5), 1.78 (s, 36H, –C(CH_3)$_3$). ^{13}C{^{1}H} NMR (101 MHz, $CDCl_3$) δ 152.55 (*m*-C_6H_3), 140.39 (i-C_6H_5), 130.50 (*o*-C_6H_5), 129.85 (*m*-C_6H_5), 129.34 (*p*-C_6H_5), 127.05 (i-C_6H_3), 125.02 (*o*-C_6H_3), 124.22 (*p*-C_6H_3), 118.17 (=*C*=*C*=, –*C*≡*C*–), 105.63 (=*C*Ph–), 35.55 (–*C*(CH$_3$)$_3$), 31.88 (–C(*C*H$_3$)$_3$). HRMS (MALDI-TOF/DCTB): *m*/*z*: $[M]^{+\bullet}$ calculated for $C_{70}H_{62}$ 902.4852, found: 902.4787. UV-vis ($CHCl_3$): λ_{max} = 472 nm (ε = 248 000 L mol^{-1} cm^{-1}). Melting-decomposition temperature: 230 °C.

4.2.3 4,7,13,16-Tetramethoxy-1,4,7,10,13,16-hexaphenylcyclooctadeca-2,5,8,11,14,17-hexayne-1,10-diol (12). A solution of [6]pericyclynedione **10** (86 mg, 0.126 mmol) in THF (20 mL) was treated with PhMgBr (0.1 mL, 0.291 mmol) at 0 °C. The reaction mixture was stirred for 1 h at this temperature and 0.5 h at room temperature. After the addition of a saturated aqueous solution of NH_4Cl, the aqueous layer was separated and extracted with Et_2O. The combined organic layers were dried over $MgSO_4$ and concentrated under reduced pressure. The residue was purified by chromatography on silica gel (pentane : ethyl acetate 4 : 1) to obtain **12** as a yellow oil with 82% yield (87 mg, 0.104 mmol). ^{1}H NMR (400 MHz, $CDCl_3$) δ 7.89–7.62 (m, 12H, *o*-C_6H_5), 7.49–7.27 (m, 18H, *m*-, *p*-C_6H_5), 3.71–3.35 (m, 12H, –OCH_3), 3.35–3.05 (m, 2H, –O*H*). ^{13}C{^{1}H} NMR (101 MHz, $CDCl_3$) δ 140.90–140.69 (i-C_6H_5–C(OH)<), 139.49–139.24 (i-C_6H_5–C(OCH$_3$)<), 129.13–128.92 (*p*-C_6H_5), 128.73–128.49 (*m*-C_6H_5), 126.56–126.40 (*o*-C_6H_5–C(OCH$_3$)<), 125.78–125.74 (*o*-C_6H_5–C(OH)<), 87.22–86.63, 84.65–84.37, 82.96–82.57 (–*C*≡*C*–), 72.02–71.91 (>*C*(OH)Ph), 65.10, 65.07 (>*C*(OCH$_3$)Ph), 53.48, 53.45 (–O*C*H$_3$). HRMS (MALDI-TOF/DCTB): *m*/*z*: $[M]^{+\bullet}$ calculated for $C_{58}H_{44}O_6$ 836.3138, found: 836.3015.

4.2.4 1,10-Bis(3,5-di-*tert*-butylphenyl)-4,7,13,16-tetramethoxy-4,7,13,16-tetraphenylcyclooctadeca-2,5,8,11,14,17-hexayne-1,10-diol (13). A solution of [6]pericyclynedione **10** (165 mg, 0.243 mmol) in THF (20 mL) was treated with 3,5-di-*tert*butyl-C_6H_3MgBr

(0.625 mmol in 1 mL THF) at 0 °C. The reaction mixture was stirred for 1.5 h at this temperature and 0.5 h at room temperature. After the addition of a saturated aqueous solution of NH_4Cl, the aqueous layer was separated and extracted with Et_2O. The organic layers were combined, dried over $MgSO_4$ and concentrated under reduced pressure. The residue was purified by chromatography on silica gel (pentane : ethyl acetate 4 : 1) to obtain **13** as a yellow oil with 64% yield (165 mg, 0.156 mmol). ^{1}H NMR (400 MHz, CD_2Cl_2) δ 7.93–7.54 (m, 12H, *o*-C_6H_5), 7.54–7.24 (m, 14H, *m*, *p*-C_6H_5, *p*-C_6H_3), 3.70–3.40 (m, 12H, –OCH_3), 3.36–3.17 (m, 2H, –O*H*), 1.41–1.22 (m, 36H, –$C(CH_3)_3$). ^{13}C{^{1}H} NMR (101 MHz, CD_2Cl_2) δ 151.41–151.34 (*m*-C_6H_3), 139.88–139.68 (i-C_6H_5), 139.62–139.52 (i-C_6H_3) 129.08–128.94 (*p*-C_6H_5), 128.56–128.46 (*m*-C_6H_5), 126.45–126.26 (*o*-C_6H_5), 123.34, 123.25 (*p*-C_6H_3), 120.24–120.10 (*o*-C_6H_3), 87.24–86.94, 84.63–84.37, 82.65–82.54 (–*C*≡*C*–), 72.02–71.81 (>*C*(OH)Ph), 65.77–65.70 (>*C*(OCH_3)Ph), 53.37–53.19 (–O*C*H_3), 34.96, 34.93 (–*C*$(CH_3)_3$), 31.20–31.10 (–C(*C*$H_3)_3$). HRMS (MALDI-TOF/DCTB): *m*/*z*: $[M + Na]^+$ calculated for $C_{74}H_{76}O_6Na$: 1083.5540, found: 1083.5476.

4.3 Crystal structure determination

Intensity data were collected at low temperature on an Apex2 Bruker diffractometer equipped with a 30 W air-cooled microfocus source or on an Oxford-Diffraction Gemini (λ_{Mo} = 0.71073 Å). The structures were solved using SUPERFLIP, and refined by means of least-squares procedures on *F* using the programs of the PC version of CRYSTALS.[11] Atomic scattering factors were taken from the International Tables for X-ray Crystallography.[12] For **4**, the asymmetric unit consists in a whole *carbo*-benzene molecule. For **11**, it contains half a molecule. Both asymmetric units contain a disordered $CHCl_3$ solvent molecule. All non-hydrogen atoms were refined anisotropically. Hydrogen atoms were refined using a riding model. Absorption corrections were introduced using the program MULTISCAN.

4.4 Voltammetric measurements

Voltammetric measurements were carried out using a potentiostat Autolab PGSTAT100 controlled by GPES 4.09 software. Experiments were performed at room temperature in a home-made airtight three-electrode cell connected to a vacuum/argon line. The reference electrode consisted of a saturated calomel electrode (SCE) separated from the solution by a bridge compartment. The counter electrode was a platinum wire of *ca.* 1 cm^2 apparent surface. The working electrode was a Pt microdisk (0.5 mm diameter). The supporting electrolyte [*n*-Bu_4N][PF_6] was used as received (Fluka, 99% electrochemical grade) and simply degassed under argon. The chloroform solutions used in the electrochemical study was 10^{-3} M in *carbo*-benzene and 0.1 M in the supporting electrolyte. Before each measurement, the solutions are degassed by bubbling argon, and the working electrode was polished using a polishing machine (Presi P230). Typical instrumental parameters for recording square-wave voltammograms were: SW frequency f = 20 Hz, SW amplitude E_{sw} = 20 mV, and scan increment ΔE = 5 mV.

4.5 Solid film fabrication and AFM measurements

Glass substrates were cleaned with ethanol in an ultrasonic bath and were rubbed with alcohol-wetted cotton. Substrates were then dried with clean and dry air and kept at 85 °C over 15 min. Before deposition of the compound layers by spin-casting (blend of 11:PCBM) from a chlorobenzene solution (at 30 mg mL^{-1}), substrates were treated with UV oxygen plasma for 5 min. The solution was stirred for 4 h and deposited by spin-coating at 1500 rpm for 30 s in a N_2 glovebox. Morphology, roughness and thickness were analyzed by means of atomic force microscopy (AFM) using a microscope easyscan2 from Nanosurf, with a maximum square scanning area of 110 μm, operating in contact mode under ambient conditions (see the ESI†).

Acknowledgements

C. Z. thanks the China Scholarship Council for his PhD scholarship. The Toulouse IDEX Emergence program 2014 is acknowledged for funding (*Carbo*-device project). R. C. Thanks the Centre National de la Recherche Scientifique (CNRS) for half a teaching sabbatical in 2015–2016. The authors thank the French-Mexican International Associated Laboratory (LIA) ''Molecular Chemistry with Applications in Materials and Catalysis'' funded by the CNRS and the CONACyT.

Notes and references

1 (*a*) R. Chauvin, *Tetrahedron Lett.*, 1995, **36**, 397–400; (*b*) V. Maraval and R. Chauvin, *Chem. Rev.*, 2006, **106**, 5317–5343; (*c*) K. Cocq, C. Lepetit, V. Maraval and R. Chauvin, *Chem. Soc. Rev.*, 2015, **44**, 6535–6559.

2 In simple words, a *carbo*-mer is a molecular structure derived from a parent Lewis covalent structure by systematic insertion of one dicarbon unit in each original covalent bond (single, double, triple) of given type (*e.g.* any bond, or C–C bond only).

3 The [9+9] macrocyclization under basic conditions was not attempted because of the instability of the triynal precursor **3**, which prevented its isolation. For more details, see: R. Chauvin, *Tetrahedron Lett.*, 1995, **36**, 401–404.

4 The structure of **1** has however been extensively studied at the theoretical level, in both the ground state and excited states by DFT and TDDFT calculations, respectively. (*a*) C. Godard, C. Lepetit and R. Chauvin, *Chem. Commun.*, 2000, 1833–1834; (*b*) C. Lepetit, C. Godard and R. Chauvin, *New J. Chem.*, 2001, **25**, 572–580; (*c*) C. Lepetit, B. Silvi and R. Chauvin, *J. Phys. Chem. A*, 2003, **107**, 464–473; (*d*) C. Zou, C. Lepetit, Y. Coppel and R. Chauvin, *Pure Appl. Chem.*, 2006, **78**, 791–811; (*e*) A. Soncini, P. W. Fowler, C. Lepetit and R. Chauvin, *Phys. Chem. Chem. Phys.*, 2008, **10**, 957–964; (*f*) R. Chauvin, C. Lepetit, V. Maraval and L. Leroyer, *Pure Appl. Chem.*, 2010, **82**, 769–800; (*g*) C. Poidevin, C. Lepetit, N. Ben Amor and R. Chauvin, *J. Chem. Theory Comput.*, 2016, **12**, 3727–3740.

5 Y. Kuwatani, N. Watanabe and I. Ueda, *Tetrahedron Lett.*, 1995, **36**, 119–122.

6 R. Suzuki, H. Tsukude, N. Watanabe, Y. Kuwatani and I. Ueda, *Tetrahedron*, 1998, **54**, 2477–2496.
7 C. Saccavini, C. Sui-Seng, L. Maurette, C. Lepetit, S. Soula, C. Zou, B. Donnadieu and R. Chauvin, *Chem. – Eur. J.*, 2007, **13**, 4914–4931.
8 C. Saccavini, C. Tedeschi, L. Maurette, C. Sui-Seng, C. Zou, M. Soleilhavoup, L. Vendier and R. Chauvin, *Chem. – Eur. J.*, 2007, **13**, 4895–4913.
9 (*a*) L. Maurette, C. Tedeschi, E. Sermot, M. Soleilhavoup, F. Hussain, B. Donnadieu and R. Chauvin, *Tetrahedron*, 2004, **60**, 10077–10098; (*b*) L. Leroyer, C. Zou, V. Maraval and R. Chauvin, *C. R. Chim.*, 2009, **12**, 412–429; for early references on pericyclynes see: (*c*) L. T. Scott, G. J. DeCicco, J. L. Hyun and G. Reinhardt, *J. Am. Chem. Soc.*, 1983, **105**, 7760–7761; (*d*) L. T. Scott, G. J. DeCicco, J. L. Hyun and G. Reinhardt, *J. Am. Chem. Soc.*, 1985, **107**, 6546–6555; (*e*) C. Zou, V. Maraval and R. Chauvin, *C. R. Chim.*, 2009, **12**, 412–429.
10 (*a*) L. Leroyer, C. Lepetit, A. Rives, V. Maraval, N. Saffon-Merceron, D. Kandaskalov, D. Kieffer and R. Chauvin, *Chem. – Eur. J.*, 2012, **18**, 3226–3240; (*b*) A. Rives, I. Baglai, V. Malytskiy, V. Maraval, N. Saffon-Merceron, Z. V. Voitenko and R. Chauvin, *Chem. Commun.*, 2012, **48**, 8763–8765; (*c*) I. Baglai, V. Maraval, C. Bijani, N. Saffon-Merceron, Z. Voitenko, Y. M. Volovenko and R. Chauvin, *Chem. Commun.*, 2013, **49**, 8374–8376; (*d*) K. Cocq, V. Maraval, N. Saffon-Merceron and R. Chauvin, *Chem. Rec.*, 2015, **15**, 347–361; (*e*) K. Cocq, V. Maraval, N. Saffon-Merceron, A. Saquet, C. Poidevin, C. Lepetit and R. Chauvin, *Angew. Chem., Int. Ed.*, 2015, **54**, 2703–2706; (*f*) I. Baglai, M. de Anda-Villa, R. M. Barba-Barba, C. Poidevin, G. Ramos-Ortíz, V. Maraval, C. Lepetit, N. Saffon-Merceron, J.-L. Maldonado and R. Chauvin, *Chem. – Eur. J.*, 2015, **21**, 14186–14195; (*g*) I. Baglai, V. Maraval, Z. Voitenko, Y. Volovenko and R. Chauvin, *Fr.-Ukr. J. Chem.*, 2013, **1**, 48–53; (*h*) K. Cocq, N. Saffon-Merceron, A. Poater, V. Maraval and R. Chauvin, *Synlett*, 2016, 2105–2112.
11 P. W. Betteridge, J. R. Carruthers, R. I. Cooper, K. Prout and D. J. Watkin, *J. Appl. Crystallogr.*, 2003, **36**, 1487.
12 J. A. Ibers and W. C. Hamilton, *International Tables for X-ray Crystallography*, Kynoch Press, Birmingham, England, 1974, vol. IV.
13 (*a*) C. Zhu, A. Rives, C. Duhayon, V. Maraval and R. Chauvin, *J. Org. Chem.*, 2017, **82**, 925–935; (*b*) C. Zhu, C. Duhayon, A. Saquet, V. Maraval and R. Chauvin, *Can. J. Chem.*, DOI: 10.1139/cjc-2016-0629.
14 CCDC 1503931 (**4**) and 1518487 (**11**).
15 E. Pidcock, *Chem. Commun.*, 2005, 3457–3459.
16 I. Noviandri, R. D. Bolskar, P. A. Lay and C. A. Reed, *J. Phys. Chem. B*, 1997, **101**, 6350–6358.
17 (*a*) D. Barreiro-Argüelles, G. Ramos-Ortiz, J. L. Maldonado, E. Pérez-Gutiérrez, D. Romero-Borja and A. Álvarez-Fernández, *IEEE J. Photovolt.*, 2017, **7**, 191–198; (*b*) E. Pérez-Gutiérrez, D. Barreiro-Argüelles, J. L. Maldonado, M. A. Meneses-Nava, O. Barbosa-García, G. Ramos-Ortíz, M. Rodríguez and C. Fuentes-Hernández, *ACS Appl. Mater. Interfaces*, 2016, **8**, 28763–28770.

SUPPLEMENTARY INFORMATION

Hexaphenyl-*carbo*-benzene revisited: novel synthetic route, crystallographic data, and prospects of electrochemical behavior

Chongwei Zhu,[a,b] Carine Duhayon,[a,b] Daniel Romero-Borja,[c] José-Luis Maldonado,[c] Gabriel Ramos-Ortíz,[c] Alix Saquet,[a,b] Valérie Maraval[a,b]* and Remi Chauvin[a,b]*

[a] *CNRS, LCC (Laboratoire de Chimie de Coordination), 205 route de Narbonne, BP 44099, 31077 Toulouse Cedex 4, France.*

[b] *Université de Toulouse, UPS, ICT-FR 2599, 118 route de Narbonne, 31062 Toulouse Cedex 9, France.*

[c] *Centro de Investigaciones en Óptica A.P. 1-948, 37000 León, Gto., México.*

E-mail adresses: valerie.maraval@lcc-toulouse.fr, chauvin@lcc-toulouse.fr

Table of contents

1. Crystallographic data

1.1. Crystallographic data and refinement parameters for the *carbo*-benzene 4

a = 12.4948(5) Å α = 90°
b = 16.0972(6) Å β = 90°
c = 20.2765(9) Å γ = 90°

Volume	4078.24(18) Å³	Crystal Class	orthorhombic
Space group	P 2_1 2_1 2_1	Z =	4
Formula	C_{55} H_{31} Cl_3	M_r	798.21
Cell determined from	9793 reflections	Cell θ range =	2 - 27°
Temperature	100K		
Shape	block		
Colour	red	Size	0.12 × 0.15 × 0.15 mm
D_x	1.30	F000	1648.000
μ	0.263 mm^{-1}		
Absorption correction	multi-scan		
T_{min}	0.94	T_{max}	0.97

Data Collection

Diffractometer	multi-scan
Scan type	φ and ω scans
Reflections measured	97066
Independent reflections	9935
Rint	0.0481
θ_{max}	28.0845
h =	-16 → 16
k =	-21 → 21
l =	-26 → 26

Refinement

$\Delta\rho_{min}$ =	-0.58 e $Å^{-3}$
$\Delta\rho_{max}$ =	0.66 e $Å^{-3}$
Reflections used	7863
Cutoff: I >	3.00σ(I)
Parameters refined	560
S =	1.11
R-factor	0.035
weighted R-factor	0.037
Δ/σ_{max}	0.0009

Flack parameter	0.05(5)
Refinement on	F
w =	$w' \times [1 - (\Delta F_{obs} / 6 \times \Delta F_{est})^2]^2$
	$[P_0T_0'(x) + P_1T_1'(x) + ...P_{n-1}T_{n-1}'(x)]^{-1}$,
w′ =	where P_i are the coefficients of a Chebychev series in $t_i(x)$, and x = $F_{calc}/F_{calcmax}$.
P_0 - P_{n-1} =	0.141 0.867E-01 0.374E-01

1.2. Crystallographic data and refinement parameters for the *carbo*-benzene 11

a = 10.1720(5) Å α = 90.105(5)°
b = 11.8006(8) Å β = 101.559(5)°
c = 12.8576(7) Å γ = 94.484(5)°

Volume	1507.20(8) Å³	Crystal Class	triclinic
Space group	P -1	Z =	1
Formula	C_{72} H_{64} Cl_6	M_r	1142.02
Cell determined from	4578 reflections	Cell θ range =	4 - 28°
Temperature	120K		
Shape	stick		
Colour	red	Size	0.10 × 0.10 × 0.25 mm
D_x	1.26	F000	598.000
μ	0.327 mm^{-1}		
Absorption correction	multi-scan		
T_{min}	0.79	T_{max}	0.97

Data Collection

Diffractometer	multi-scan
Scan type	φ and ω scans
Reflections measured	23700
Independent reflections	6699
Rint	0.0452
θ_{max}	28.7271
h =	-13 → 13
k =	-15 → 15
l =	-17 → 17

Refinement

$\Delta\rho_{min}$ =	-0.33 e $Å^{-3}$
$\Delta\rho_{max}$ =	0.50 e $Å^{-3}$
Reflections used	4214

Cutoff: I >	$3.00\sigma(I)$
Parameters refined	379
S =	1.11
R-factor	0.044
weighted R-factor	0.052
Δ/σ_{max}	0.0004
Refinement on	F
w =	$w' \times [1 - (\Delta F_{obs} / 6 \times \Delta F_{est})^2]^2$
w′ =	$[P_0T_0'(x) + P_1T_1'(x) + ...P_{n-1}T_{n-1}'(x)]^{-1}$, where P_i are the coefficients of a Chebychev series in $t_i(x)$, and $x = F_{calc}/F_{calcmax}$.
P_0 - P_{n-1} =	9.96 -2.07 7.52

2. SWV and CV voltammograms for 4 and 11

Voltammetric measurements were carried out with a potentiostat Autolab PGSTAT100 controled by GPES 4.09 software. Experiments were performed at room temperature in a home-made airtight three-electrode cell connected to a vacuum/agon line. The reference electrode consisted of a saturated calomel electrode (SCE) separated from the solution by a bridge compartment. The counter electrode was a platinum wire of *ca* 1 cm^2 apparent surface. The working electrode was a Pt microdisk (0.5 mm diameter). The supporting electrolyte [*n*-Bu_4N][PF_6] was used as received (Fluka, 99 % electrochemical grade) and simply degassed under argon. The chloroform solutions used in the electrochemical study was 10^{-3} M in *carbo*-benzene and 0.1 M in supporting electrolyte. Before each measurement, the solutions are degassed by bubbling argon, and the working electrode was polished with a polishing machine (Presi P230). Typical instrumental parameters for recording square-wave voltammograms were: SW frequency f = 20 Hz, SW amplitude E_{sw} = 20 mV, scan increment *dE* = 5 mV.

2.1. Voltammogramms of 4

- SWV voltammogramms of **14**

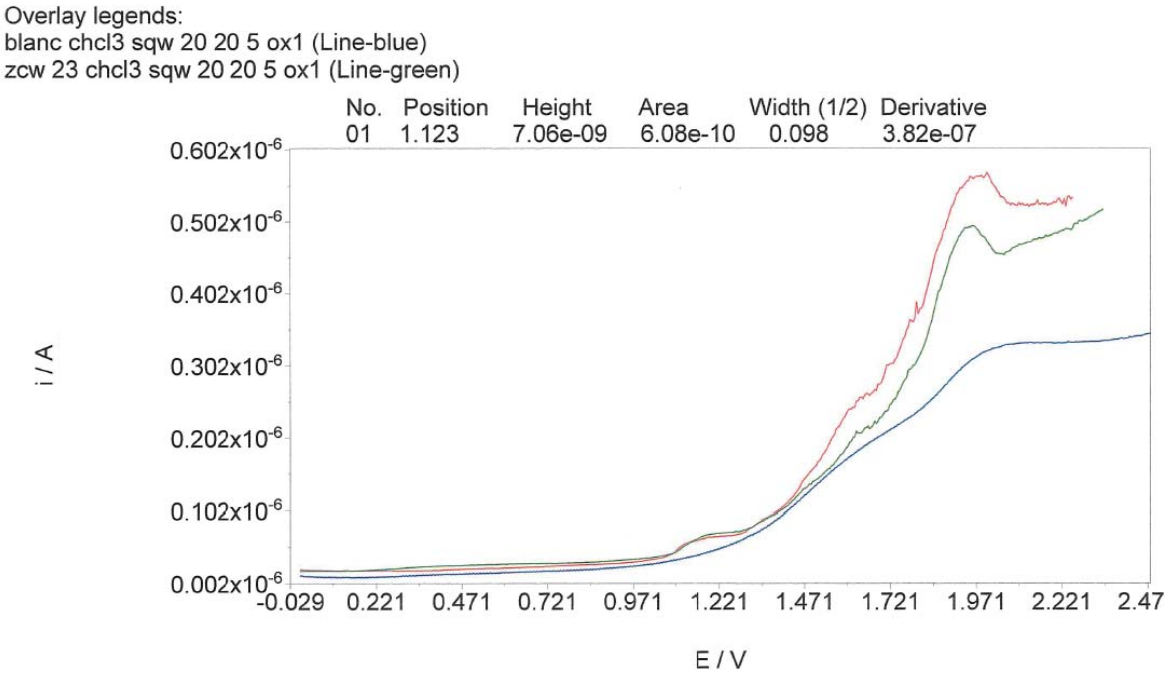

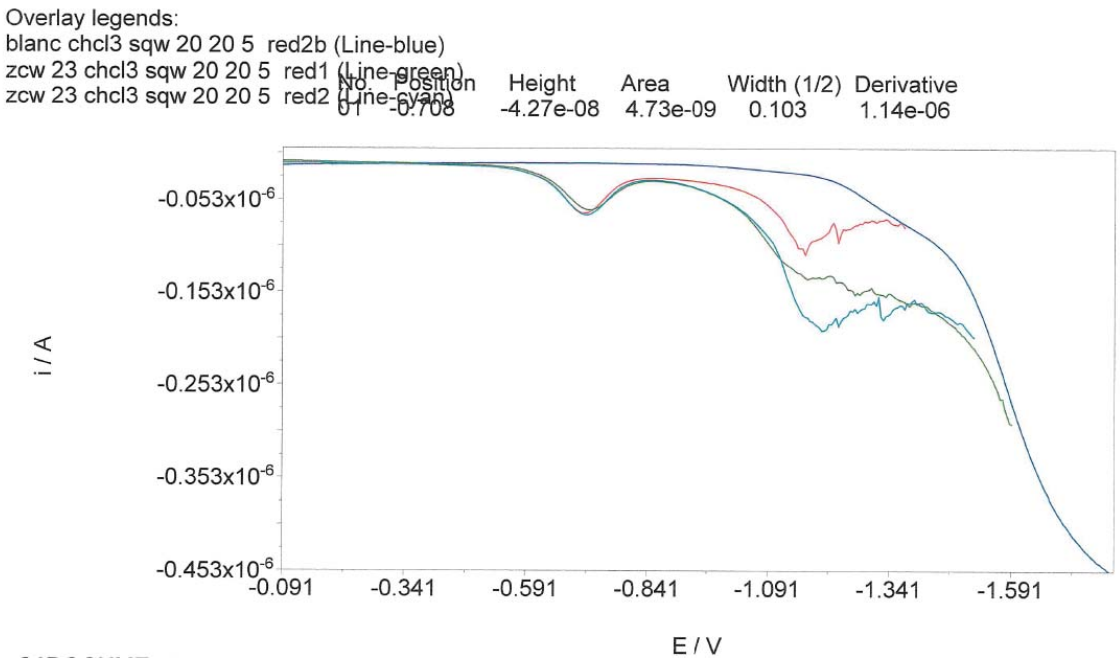

- CV voltammogramm of **4**

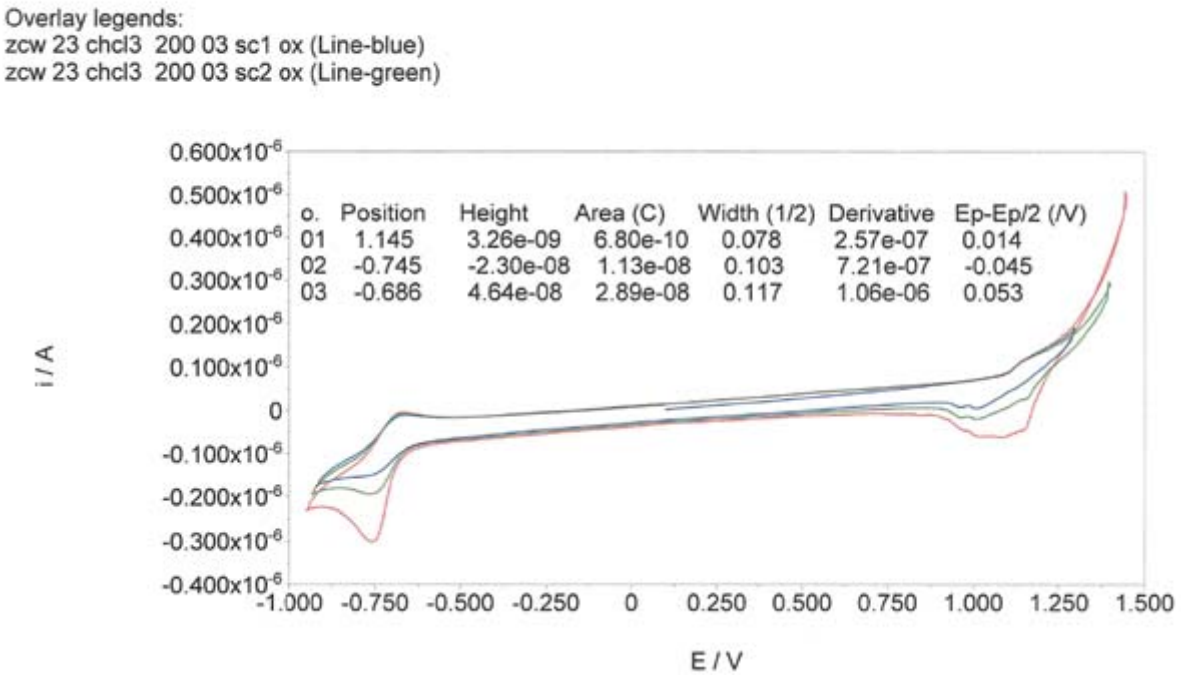

2.1. Voltammogramms of 11

- SWV voltammogramms of **11**

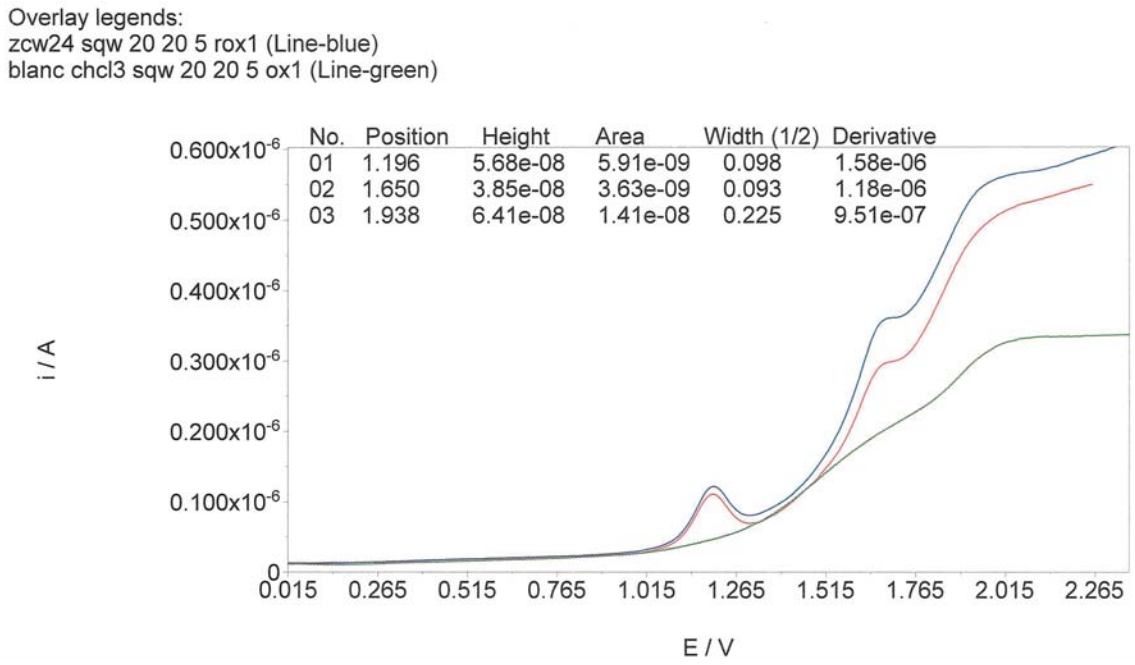

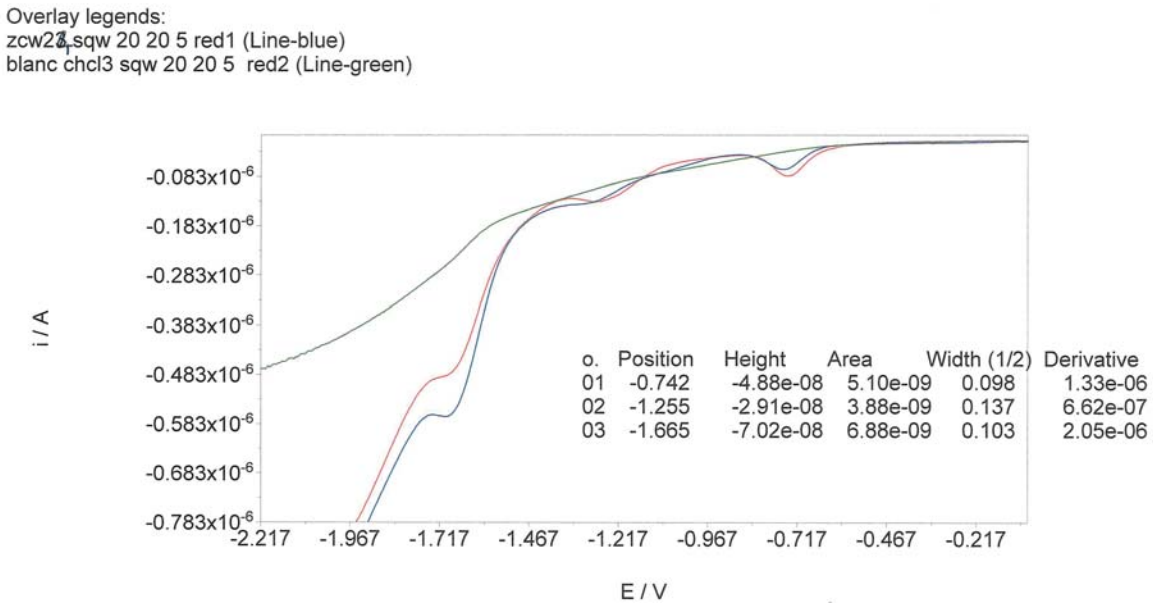

- CV voltammogramm of **11**

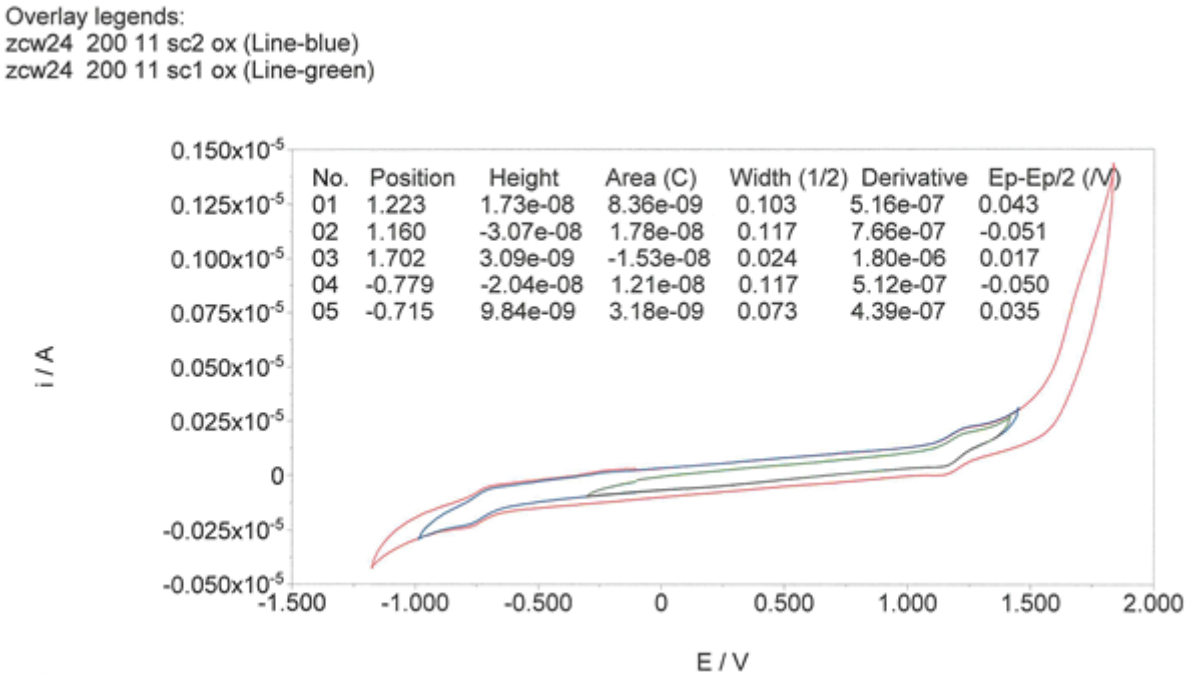

3. Comparison of the Ueda's original method with the proposed alternative method

While the original synthetic approach described by Ueada, Kuwatani *et al.* was achieved with a 1 % overall yield (0.8 % exactly), the alternative approach gave a 8 % overall yield.

• Synthesis of intermediates prior to the [11+7] and [8+10] macro-cyclization processes

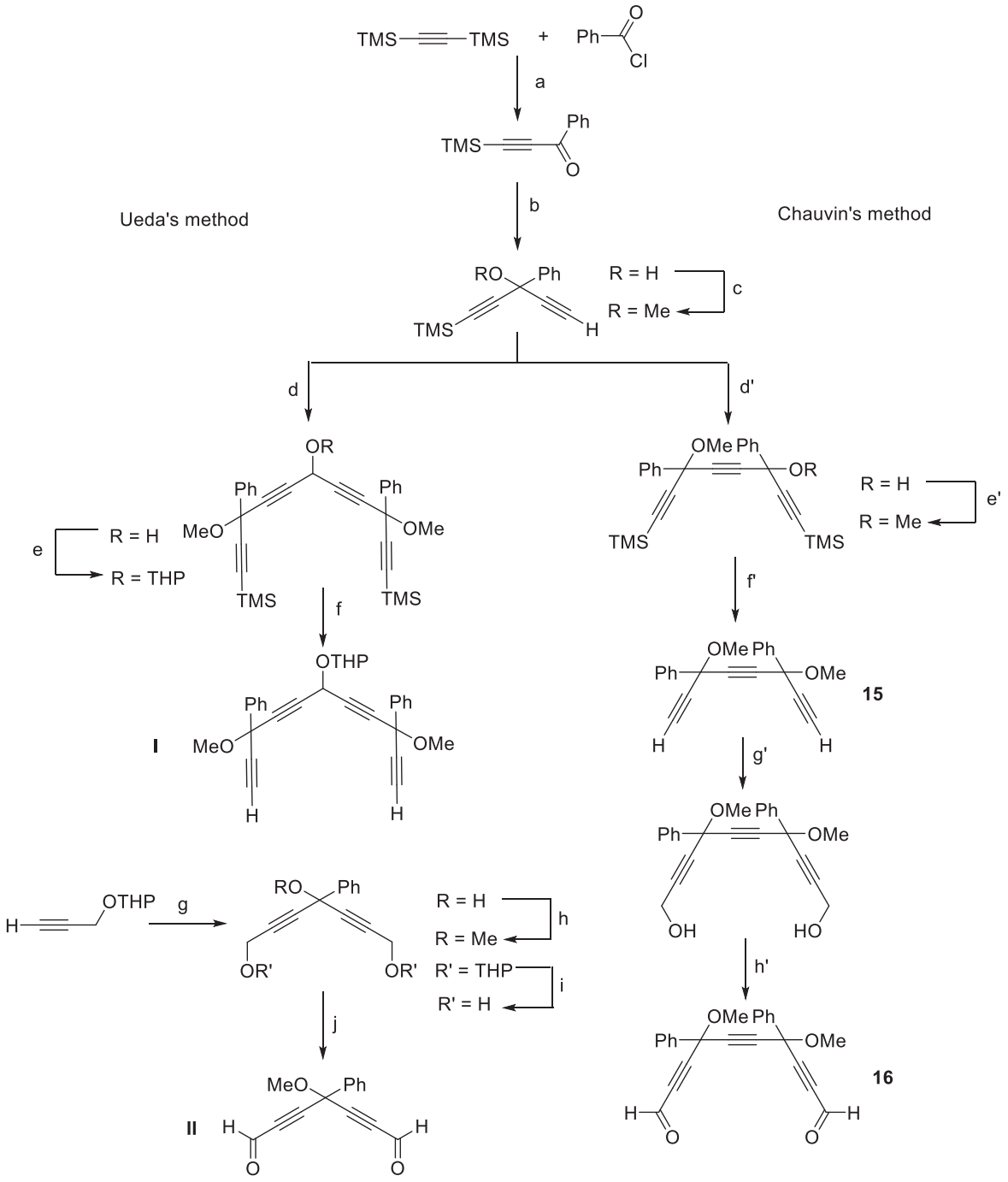

Reagents and conditions: a) $AlCl_3$, DCM, 0 °C, 94 % , b) HCCMgBr, THF, 0 °C, 97 %, c) 1) n-BuLi, THF, -78 °C, 2) MeI, DMSO, - 25 °C, 95 %, d) 1) EtMgBr, THF, 0 °C, 2) HCO_2Me, THF, 0 °C, 90 %, e) DHP/PPTS, DCM, rt, 97 %, f) TBAF, THF/H_2O, rt, 95 %, g) 1) EtMgBr, THF, 0 °C, 2) PhCOCl, 77 %, h) NaH, MeI, THF, 0 °C, 90 %, i) PPTS, MeOH, 55 °C, 95 %, j) Dess-Martin, DCM, rt, 86 %.
d') 1) EtMgBr, THF, 0 °C, 2) TMS-CC-C(O)Ph, 90 %, e') 1) n-BuLi, THF, - 78 °C, 2) MeI, DMSO, - 25 °C, 97 %, f') K_2CO_3, MeOH, 100 %, g') 1) n-BuLi, THF, - 78 °C, 2) $(CH_2O)n$, 85 %, h') IBX, DCE, 83 %.

• [11+7] and [8+10] macro-cyclization, oxidation, addition, and aromatization processes

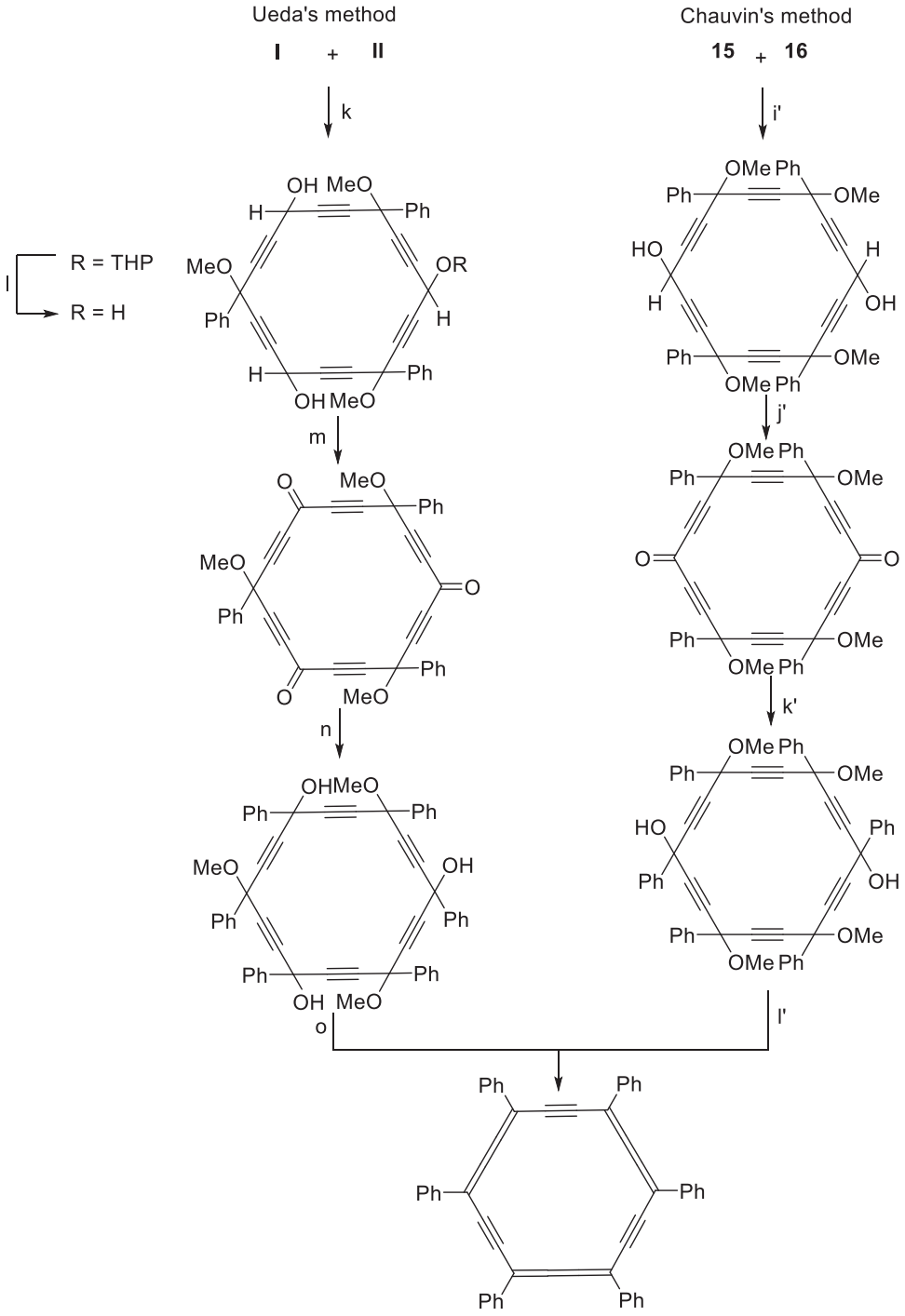

Reagents and conditions: k) 1) EtMgBr, THF, 0°C, 2) $CeCl_3$, 6 %, l) PPTS, MeOH, 55 °C, 86 %, m) Dess-Martin reagent, DCM, 70 %, n) PhMgBr, THF, 0 °C, o) $SnCl_2$/HCl, Et_2O, 0 °C, 59 %.
i') EtMgBr, 0 °C, 40 %, j') MnO_2, DCM, 72 %, k') PhMgBr, THF, 0 °C, 82 %, l') 1) $SnCl_2$/HCl, DCM, - 78 °C, 2) NaOH 1M, 65 %.

4. AFM images of thin films based on the *carbo*-benzene 11

In the spin-coated films on glass substrates **11** is blended with $PC_{71}BM$ in a 1/1 w/w ratio.

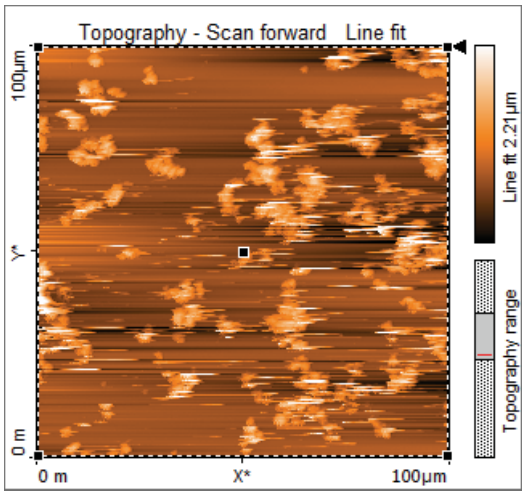

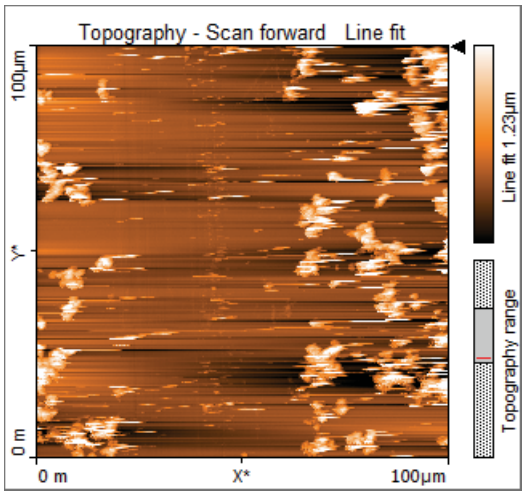

=> average roughness = 355 nm

5. UV-vis absorption spectra of thin films based on the *carbo*-benzene 11

In the spin-coated films on glass substrates **11** is blended with $PC_{71}BM$ in a 1/1w/w ratio**.**

Thermal annealing at 80 °C (in red) did not influence the aspect of the absorption/scattering spectra.

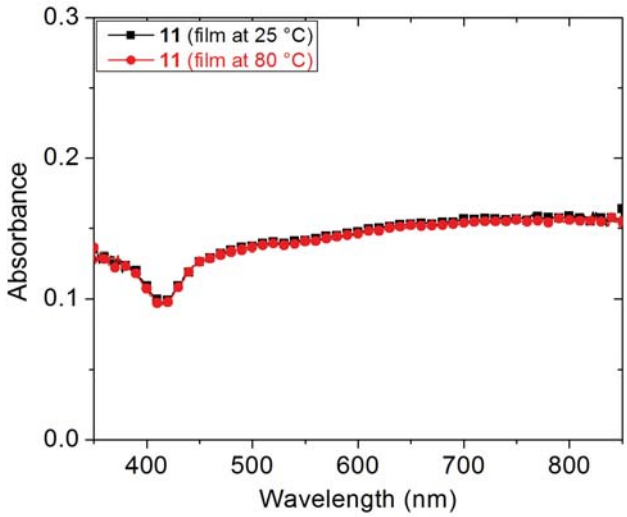

Chapter 3

Lipidic *carbo*-benzenes: molecular probes of magnetic anisotropy and stacking properties of α-graphyne

Introduction & Summary

The key [6]pericyclynedione precursor of *para*-disubstituted *carbo*-benzenes is today easily prepared through a nine-step procedure involving a [8+10] macrocyclization reaction between a C_8 triyne and a C_{10} triynedial.[1] A series of quadrupolar *carbo*-benzenes bearing various substituents at their *para*-positions, such as anisyl-, [2] fluorenyl-, [3] trimethylsilylethynyl-,[1b, 4] and anilinyl-, [5] have been synthesized in two steps from this common [6]pericyclynedione precursor. The intrinsic structural and electronic features of the C_{18} aromatic ring provide *carbo*-benzenes with remarkable properties and prospects of applications.

Up to now, all the *carbo*-benzenes that were shown to possess outstanding physicochemical properties are quadrupolar representatives, and exhibited single molecule conductance or two-photon absorption properties, depending on the substituents at their *para*-positions.[3,6] Very recently, the use of hexaphenyl-*carbo*-benzene as an electron-acceptor in organic photovoltaics, in replacement of the classically used PCBM C_{60} derivative, was also envisaged.[7] However, the extremely poor solubility of this *carbo*-benzene made impossible the preparation of thin films of sufficient quality to be applied in organic photovoltaic devices.[8] The quite low solubility of *carbo*-benzenes generally not only prevents their use in some attractive domains of applications, but also makes them difficult to purify and characterize in solution.

The search for efficient solubilizing substituents appeared therefore to be an inescapable task, which started to be addressed recently in the context of the synthesis of a *carbo*-naphthalene. Indeed, this rigid bis-macrocycle, anticipated to be very poorly soluble, was targeted with eight *para*-pentylphenyl substituents, but their solubilizing effect was shown to be quite limited (Figure 1. D).[9] Similarly, the introduction of two di-*tert*-butylphenyl groups at the *para*-positions of a *carbo*-benzene failed to enhance its solubility (Figure 1, A).[7] The introduction of alkyl groups onto the phenyl substituents of *carbo*-benzenes being poorly efficient to increase their solubility, the direct insertion of aliphatic chains onto the C_{18} macrocycle was envisaged. Ueda *et al*. early reported on the synthesis of an octupolar *carbo*-benzene bearing three *tert*-butyl groups alternating with three phenyl groups on the hexagonal C_{18} macrocycle (Figure 1. B),[10] and more recently, a series of representatives bearing two, four or six *tert*-butyl groups were prepared, and these substituents were shown to significantly improve the solubility of *carbo*-benzenes in organic solvents. [11] The synthesis of a *p*-diisopropyl-tetraphenyl-*carbo*-benzene was also recently described, and it was found to be

very poorly soluble, the isopropyl groups thus appearing to be much less efficient than *tert*-butyl groups for increasing the solubility (Figure 2. C).[12]

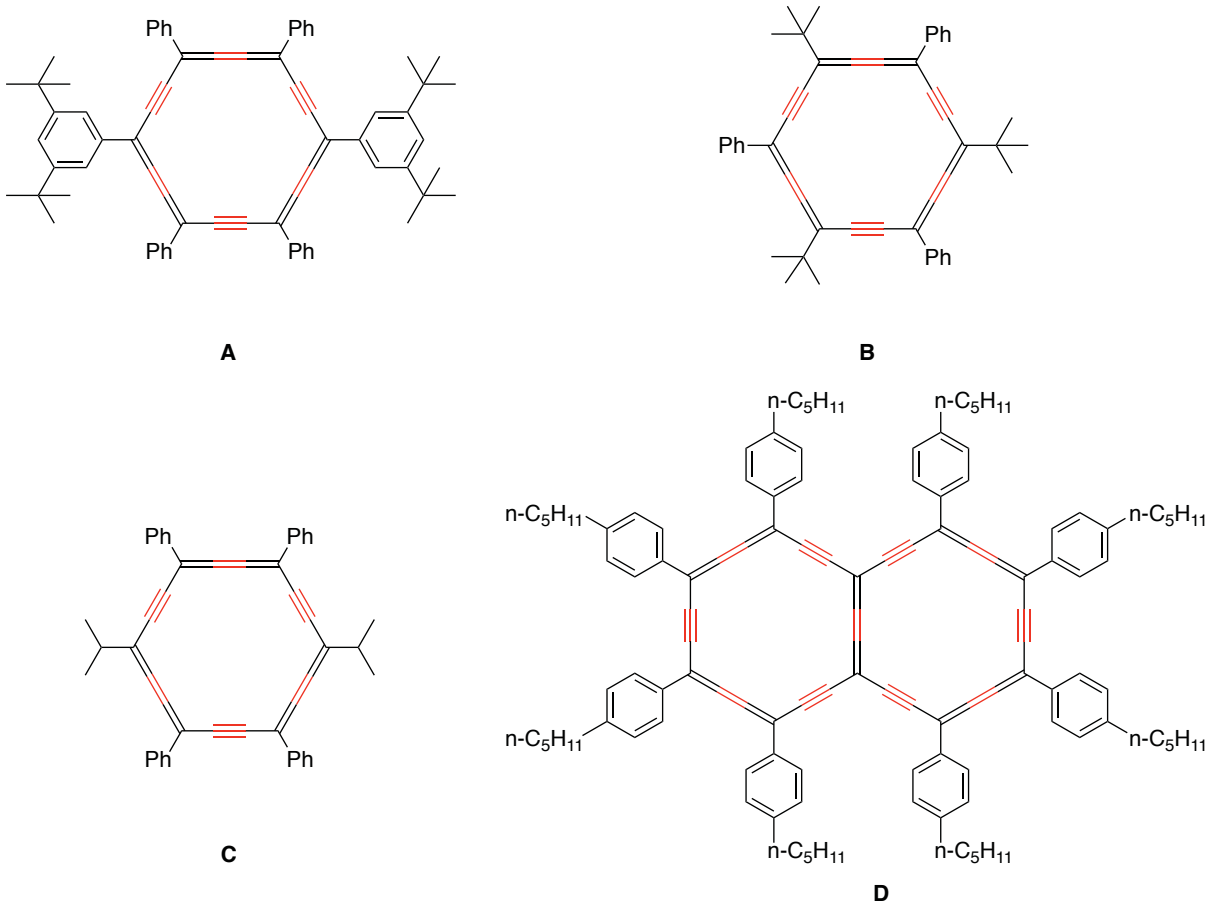

Figure 1. Examples of *carbo*-benzene derivatives bearing various alkyl groups.

On the basis of these preliminary results, the direct attachment of linear alkyl chains of variable lengths at the *para*-positions of *carbo*-benzenes was envisaged as a novel approach aiming at improving the solubility of these molecules (see Scheme 1.). A set of lengths of *n*-alkyl chains (n = 2, 4, 8, 14, 20) were proposed, and the preparation of the corresponding *carbo*-benzenes was addressed through the classical two-step procedure from the [6]pericyclynedione. The use of alkyl magnesium bromide reagents led to the generation of mixtures of the targeted di-adduct and the reduced mono-adducts, thus allowing for the parallel preparation of series of dialkyl- and mono-alkyl-*carbo*-benzenes respectively. The outcome of the reaction depending on the nature of the nucleophile was also explored in order to determine which reagent gives the highest selectivity in the targeted di-adducts and corresponding quadrupolar *carbo*-benzenes. Three types of alkyl nucleophiles were attempted: alkyl lithium (C^-Li^+), alkyl halogenomagnesium (C^-MgX^+, X = Cl, Br), and alkyl cerium chloride ($C^-CeCl_2^+$), the latter

giving the di-adduct in higher yield, without the reduced product. The physicochemical properties of the obtained *p*-dialkyl-tetraphenyl-*carbo*-benzenes were studied and discussed as a function of the chain length, including solubility, melting-decomposition point, absorption properties, electrochemical behavior and crystal packing.

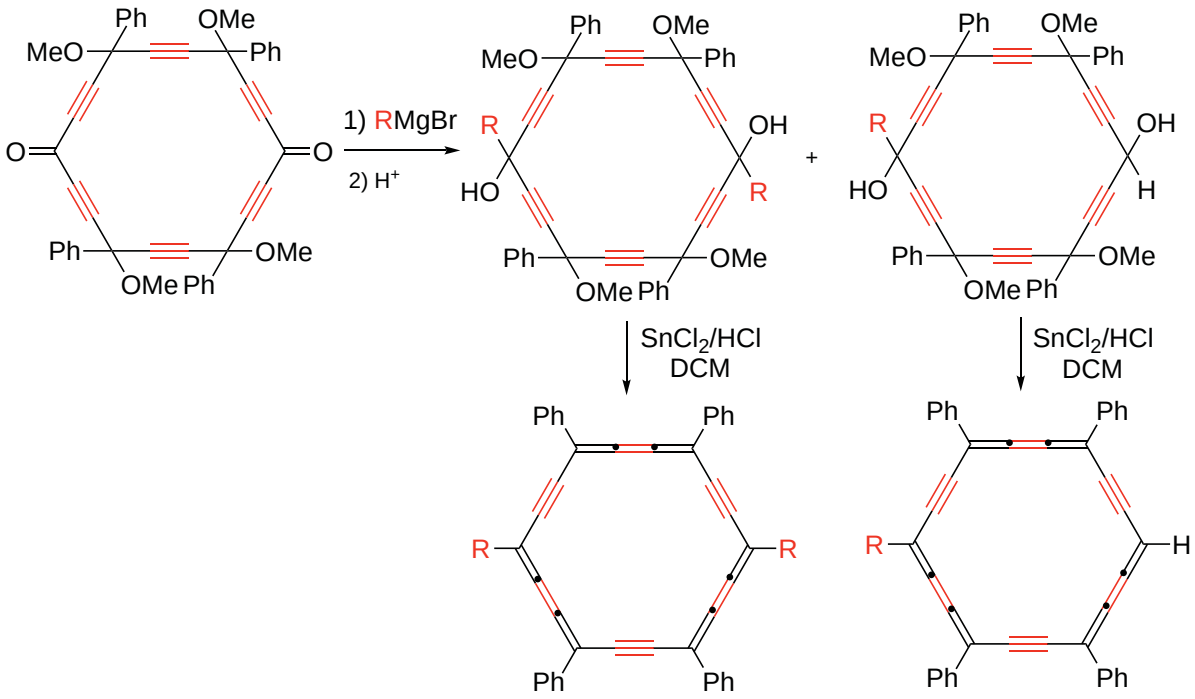

Scheme 1. The synthetic route based on a [6]pericyclynedione for preparation of dialkyl- and monoalkyl-*carbo*-benzenes by using RMgBr as a base.

Reference

1. a). L. Leroyer, C. H. Zou, V. Maraval, R. Chauvin, *C. R. Chimie*, **2009**, *12*, 412-429; b). C. Saccavini, C. Tedeschi, L. Maurette, C. Sui-Seng, C. H. Zou, M. Soleilhavoup, L. Vendier, R. Chauvin, *Chem. Eur. J.*, **2007**, *13*, 4895-4913. For general references on *carbo*-mers see : c) V. Maraval, R. Chauvin, *Chem. Rev.,* **2006**, *106*, 5317-5343 ; d) L. Leroyer, C. Lepetit, V. Maraval, R. Chauvin, *Chem. Soc. Rev*., **2015**, *44*, 6535-6559.

2. L. Leroyer, C. Lepetit, A. Rives, V. Maraval, N. Saffon-Merceron, D. Kandaskalov, D. Kieffer, R. Chauvin, *Chem. Eur. J*., **2012**, *18*, 3226-3240.

3. I. Baglai, M. Anda-Villa, R. M. Barba-Barba, C. Poidevin, G. Ramos-Ort, V. Maraval, C. Lepetit, N. Saffon-Merceron, J. L. Maldonado, R. Chauvin, *Chem. Eur. J*., **2015**, *21*, 14186-14195.

4. C. Saccavini, C. Sui-Seng, L. Maurette, C. Lepetit, S. Soula, C. H. Zou, B. Donnadieu, R. Chauvin, *Chem. Eur. J*., **2007**, *13*, 4914-4931.

5. I. Baglai, V. Maraval, C. Bijani, N. Saffon-Merceron, Z. Voitenko, Y. M. Volovenko, R. Chauvin, *Chem. Commun*., **2013**, *49*, 8374-8376.

6. Z. H. Li, M. Smeu, A. Rives, V. Maraval, R. Chauvin, M. A. Ratner, E. Borguet, *Nat. Commun*., **2015**, *6*, 6321.

7. C. Zhu, C. Duhayon, D. Romero-Borja, J.-L. Maldonado, G. Ramos-Ortiz, A. Saquet, V. Maraval, R. Chauvin, *New J. Chem.,* **2017**, *41*, 3908-3914.

8. a). D. Barreiro-Arguelles, G. Ramos-Ortiz, J. L. Maldonado, E. Perez-Gutierrez, D. Romero-Borja, A. Alvarez-Fernandez, *IEEE J. Photovolt*., **2017**, *7*, 191-198; b). E. Perez-Gutierrez, D. Barreiro Arguelles, J. L. Maldonado, M. A. Meneses-Nava, O. Barbosa-Garcia, G. Ramos-Ortiz, M. Rodriguez, C. Fuentes-Hernandez, *ACS Appl. Mater. Interfaces*, **2016**, *8*, 28763-28770.

9. K. Cocq, N. Saffon-Merceron, Y. Coppel, C. Poidevin, V. Maraval, R. Chauvin, *Angew. Chem. Int. Ed*., **2016**, *55*, 15133-15136.

10. a). Y. Kuwatani, N. Watanabe, l. Ueda, *Tetrahedron Lett*., **1995**, *36*, 119-122. b). R. Suzuki, H. Tsukuda, N. Watanabe, Y. Kuwatani, l. Ueda, *Tetrahedron*, **1998**, *54*, 2477-2496.

11. D. Listunov, C. Duhayon, A. Poater, S. Mazères, A. Saquet, V. Maraval, R. Chauvin, submitted for publication.

12. K. Cocq, N. Saffon-Merceron, A. Poater, V. Maraval, R. Chauvin, *Synlett*., **2016**, *27*, 2105-2112.

Article 3

JOC The Journal of Organic Chemistry

Article

pubs.acs.org/joc

Lipidic *Carbo*-benzenes: Molecular Probes of Magnetic Anisotropy and Stacking Properties of α-Graphyne

Chongwei Zhu,[†,‡] Arnaud Rives,[†,‡] Carine Duhayon,[†,‡] Valérie Maraval,*[,†,‡] and Remi Chauvin*[,†,‡]

[†]CNRS, LCC (Laboratoire de Chimie de Coordination), 205 route de Narbonne, BP 44099, 31077 Toulouse Cedex 4, France

[‡]Université de Toulouse, UPS, ICT-FR 2599, 118 route de Narbonne, 31062 Toulouse Cedex 9, France

Supporting Information

ABSTRACT: Solubilization of the C_{18} fundamental circuit of α-graphyne has been envisaged by decoration with aliphatic chains R = *n*-C_nH_{2n+1}. The synthesis and characterization of *p*-dialkyl-tetraphenyl-*carbo*-benzenes (*n* = 2, 8, 14, 20) are thus presented and compared to the monoalkyl series produced concomitantly. In both series, a dramatic enhancement of solubility in organic solvents (CH_2Cl_2, $CHCl_3$) is observed for $n \geq 8$, and in the dialkyl series, the melting−decomposition temperature of the solid products is shown to decrease linearly from 208 °C for *n* = 2 to 149 °C for *n* = 20. Fluoroalkyl analogues with R = *n*-$C_8H_4F_{13}$ are also described. The products display classical UV−vis electronic spectra of *carbo*-benzenes in solution (λ_{max} = 445.5 ± 1 nm, $\varepsilon \approx 200\,000$ L·mol^{-1}·cm^{-1}). They are also characterized by UV−vis absorption in the solid state, which is found to be correlated with the color and crystal packing. The methylene groups of R provide an experimental probe of the magnetic anisotropy and aromaticity of the C_{18} ring through the progressive NMR shielding of the ^{1}H nuclei from ca. 4.70 to 1.25 ppm going away from the border of the ring (as far as 8 Å away). All alkyl-*carbo*-benzenes were also found to be highly crystalline. Seven of them have been characterized by X-ray diffraction analysis and the C_{18} columnar packing compared in a systematic manner. Crystals of the diethyl and bistetradecyl derivatives, containing no solvent molecule, provided the first examples of direct π-stacking of *carbo*-benzene rings, with inter-ring distances very close to calculated interlayer distances in AB and ABC α-graphityne (3.255 and 3.206 Å vs 3.266 and 3.201 Å, respectively).

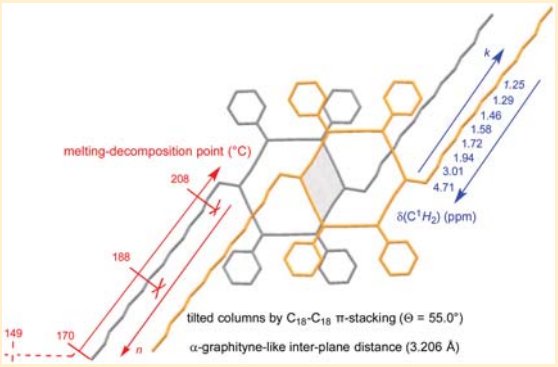

1. INTRODUCTION

Within the continually growing family of π-conjugated carbon allotropes, two main types can be distinguished: the graphenic type based on sp^2-C atoms only, exemplified by fullerenes, carbon nanotubes (CNTs) and graphene, and the graphynic type based on mixed sp^2- and sp-C atoms,[1] exemplified by graphdiyne[2] and the yet unknown α-, β-, γ-, or 6,6,12-graphynes.

Molecular fragments of either known or unknown, 2D or 3D carbon allotropes, including graphene or α-graphyne, graphite, or α-graphityne,[3] are targeted for property promises inherited from the parent pure-carbon material with the view to designing devices made of diverse components (photovoltaic cells, organic light-emitting diodes, field-effect transistors...). In contrast to the nonselective methods employed for the preparation of mixtures of graphenic nanocarbons (arc discharge, laser ablation, chemical vapor deposition),[4] the bottom-up organic synthesis approach allows access to atomically defined molecular fragments containing oligocyclic carbon cores formally extruded from either CNTs and graphene,[5] γ-graphyne,[6] γ-graphdiyne,[7] or α-graphyne.[8] The decrease of solubility vs the size of the all-carbon core is however a recurring issue requiring recourse to solubilizing substituents of sp^2 vertices at the core periphery. As no substituent can be attached to sp-C atoms, the case of graphynic cores is thus particularly challenging. In the case of α-graphyne, the primary carbon core is the *carbo*-mer of the C_6 ring of graphene,[9] i.e. a ca. three-times larger C_{18} ring with a circumscribed nuclear diameter of ca. 8 Å and a van der Waals hole diameter of ca. 5 Å. The corresponding molecular fragments are *carbo*-benzene derivatives **1** (Figure 1), generally poorly soluble in organic solvents, except in chloroform (albeit to a limited extent).[9b,10] This lack of solubility has prevented systematic studies of chemical properties of *carbo*-benzenes. For synthesis and yield issues, indeed, most of the *carbo*-benzenes reported to date are of the type **1a**, bearing at least four phenyl substituents, the remaining two vertices being either unsubstituted (CH) or substituted by other aryl or alkynyl groups. More or less soluble related *carbo*-meric structures have also been investigated.[10c] Partial saturation of the *carbo*-benzenic C_{18} ring to *carbo*-cyclohexadiene rings or release of its macrocyclic stiffness in *carbo*-butadienes **3** was thus shown to induce a higher solubility (Figure 1).[10c,d] Although **2** and **3** are easier to handle and characterize, the macro/*carbo*-aromatic character of *carbo*-benzenes **1a**, extensively investigated at the

Received: October 1, 2016
Published: December 14, 2016

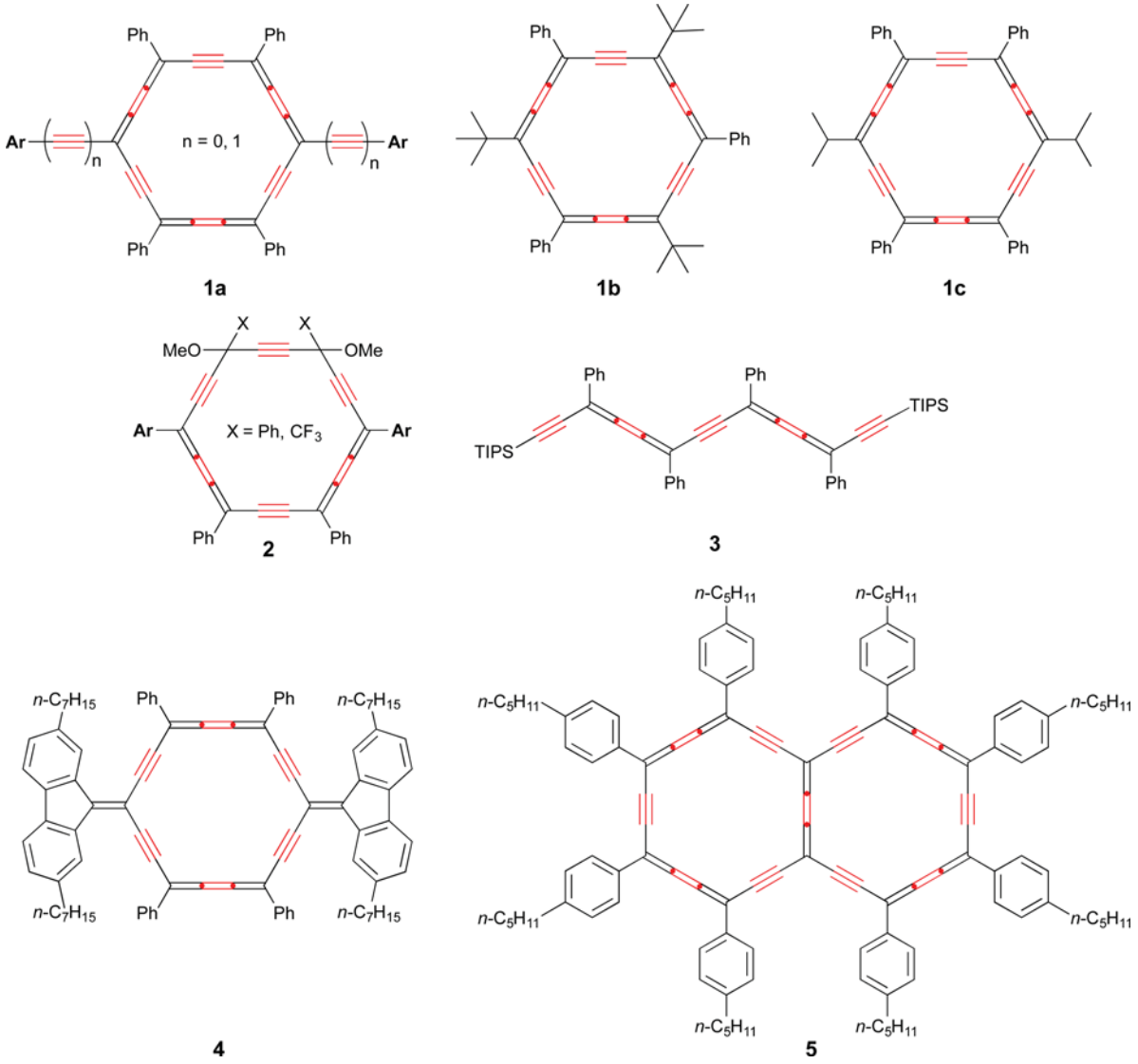

Figure 1. Examples of π-conjugated *carbo*-meric molecules of variable solubility.

theoretical level,[9b,10c] is crucial to provide them with various properties such as unprecedented single-molecule conductance (106 nS with Ar = 4-NH_2−C_6H_4, n = 0; vs 2.7 nS for the acyclic analogue **3**),[11] high two-photon absorption cross-section (656 GM at 800 nm with Ar = 9,9-dihexyl-9*H*-fluoren-2-yl, n = 1),[12] or chemical reversibility of the reduction to pro-aromatic *carbo*-quinoids such as **4** (Ar = 9-hydroxy-2,7-diheptyl-9*H*-fluoren-9-yl, n = 0; Ar is here aromatic but not aryl).[13] In the two latter cases and in the case of the *carbo*-naphthalene **5**,[8] attachment of alkyl chains on the fluorenyl(idene) or phenyl substituents was required to secure some solubility. Replacement of bare phenyl substituents by alkyl-phenyl groups (alkyl = ^{n}C_5H_{11}, ^{t}Bu) was however observed to have a minor solubilizing effect.[8,10a,b,14] Direct attachment of alkyl chains on the C_{18} core while removing two aryl substituents should be a priori a more efficient method with the view to enhancing the solubility of *carbo*-benzene derivatives. Only two alkyl-substituted *carbo*-benzenes have been described to date: an octupolar tri(*tert*-butyl) derivative **1b**[10b] and very recently a quadrupolar di(isopropyl) derivative **1c**:[15] with branched short (C_2) alkyl chains, however, none of them is lipidic in nature, and the gain in solubility remains weak. Lipidic *carbo*-benzenes were therefore envisaged in the quadrupolar series with two *n*-alkyl chains at the para positions (substitution pattern of **1a** and **1c**). Their synthesis and physicochemical properties (solubility, magnetic aromaticity, light absorption, crystal packing) are hereafter described and discussed.

2. RESULTS AND DISCUSSION

2.1. Synthesis of Mono- and Dialkyl-*carbo*-benzenes.

The target *p*-di-*n*-alkyl-*carbo*-benzenes were envisaged by reductive aromatization of the corresponding [6]periyclyne-diols **6a**−**e** (Scheme 1), themselves envisaged from the [6]pericyclynedione **7**,[16] that proved to be a relevant last-but-one pivotal precursor of most quadrupolar *carbo*-benzenes known to date (but not **1c**).[9b,10c] Following an optimized procedure, the diketone **7** is obtained as a statistical mixture of five diastereoisomers in 10 steps and ca. 10% global yield from benzoyl chloride and bis-trimethylsilylacetylene, the C_{18} ring being formed in a [8 + 10] cyclization step from a C_8 diterminal triyne and the corresponding C_{10} triyndial.[16a] The alkyl groups were then introduced by double-nucleophilic attack of **7** with two equivalents of the corresponding alkyl Grignard reagents (in the presence of an optimized excess of three equivalents):

DOI: 10.1021/acs.joc.6b02397
J. Org. Chem. 2017, 82, 925−935

Scheme 1. Synthesis of Mono- and Dialkyl-*carbo*-benzenes by Addition of Alkyl or Fluoroalkyl Grignard Reactants to the [6]Pericyclynedione 7, Followed by Reductive Aromatization of the [6]Pericyclynediol Products 6 and 8 Using Anhydrous $SnCl_2$[a]

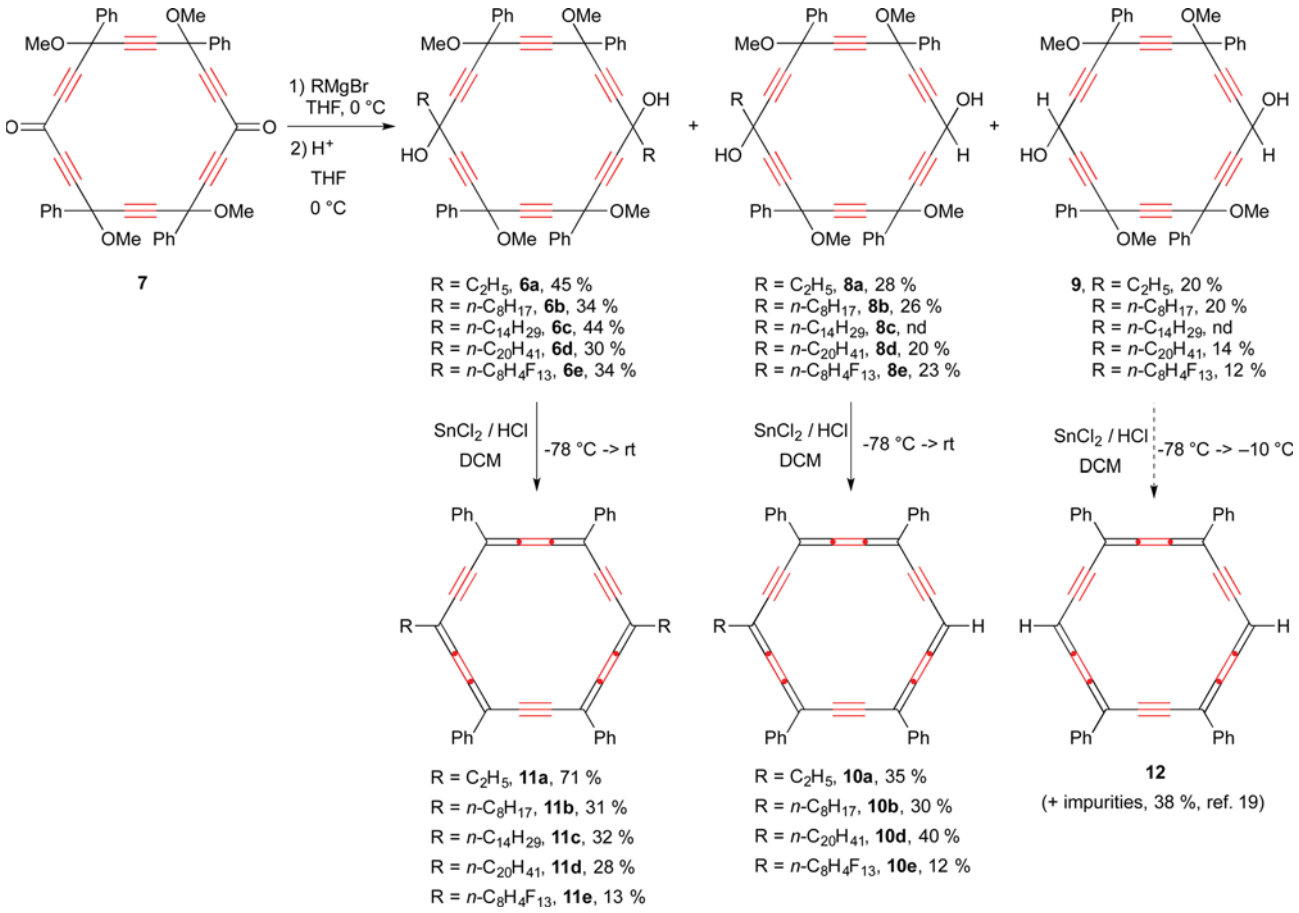

[a]The nonalkylated *carbo*-benzene **12** was previously described, including by X-ray crystallography.

aryl Grignard congeners indeed proved to be optimal nucleophiles for **7**, giving higher yields than the lithium counterparts.[10c] Four alkyl chains R = n-C_nH_{2n+1} differing by a minimal C_6 increment were selected: n = 2, 8, 14, 20. The C_8 chain was also considered in the partially fluorinated version R = n-$C_8H_4F_{13}$. While ethyl and tetradecyl magnesium bromides were used from commercially available solutions, the other Grignard reactants were prepared from the corresponding bromoalkanes. In all cases, the Grignard reaction with **7** led to two main products, always obtained in comparable ratios as mixtures of isomers (Scheme 1). The major product is the diadduct **6a**–**e** (isolated in 30–45% yield), while the minor one is the monoadduct **8a**–**e** resulting from the reduction of one of the keto groups of **7** to a carbinol vertex (and isolated in 20–28% yield). Smaller quantities of the known double-reduction product **9** were also obtained in 6–20% yield.[16a] The reducing ability of alkyl Grignard reagents, in particular toward hindered ketones, is due to the presence of a H atom in the β-position, allowing β-elimination leading to the corresponding terminal olefin and "HBr + Mg^0" as a formal reducing agent. The exact mechanism of the reduction has been largely studied,[17] and several procedures were proposed to enhance the selectivity in addition vs reduction.[18] The recommended use of apolar solvents such as toluene, or additives such as $CeCl_3$ have been attempted but proved to be inefficient on dialkynylketone substrates such as **7**. Nevertheless, taking advantage of this, isolation of an extended library of both monoalkyl-[6]-pericyclynediols **8a**–**e** and dialkyl-[6]pericyclynediols **6a**–**e** offered the opportunity to target both the dissymmetrical monoalkyl-*carbo*-benzenes **10a**–**e** and the symmetrical dialkyl-*carbo*-benzenes **11a**–**e**.

Using a classical treatment with anhydrous $SnCl_2$ and etheral HCl, the [6]pericyclynediols **6a**–**e** and **8a,b,d,e** were converted to the corresponding *carbo*-benzenes **11a**–**e** and **10a,b,d,e**, isolated in 13–71% yield and 12–40% yield, respectively (Scheme 1).[9b,10a–c] By comparison, the aromatization of **9** was previously reported to give the unsubstituted tetraphenyl-*carbo*-benzene **12**, along with an HCl adduct thereof.[19] The present products were obtained as dark blue-violet solids, giving orange solutions in chloroform. The solubility of the mono- and diethyl representatives **11a** and **10a** in any organic solvent happens to be very low, preventing full characterization of **11a** in solution. As anticipated in the hydrocarbon series, the solubility was found to increase with the chain length from C_2 to C_{14} and then to decrease back for C_{20}. In contrast, no significant effect on the solubility was observed upon fluorination of the C_8 chain of **11b** into **11e**.

2.2. NMR Characterization of Mono- and Dialkyl-*carbo*-benzenes. The mono- and dialkyl-*carbo*-benzenes were characterized by NMR spectroscopy in solution, except **11a**, the poor solubility of which required recourse to the CP-MAS

DOI: 10.1021/acs.joc.6b02397
J. Org. Chem. 2017, 82, 925–935

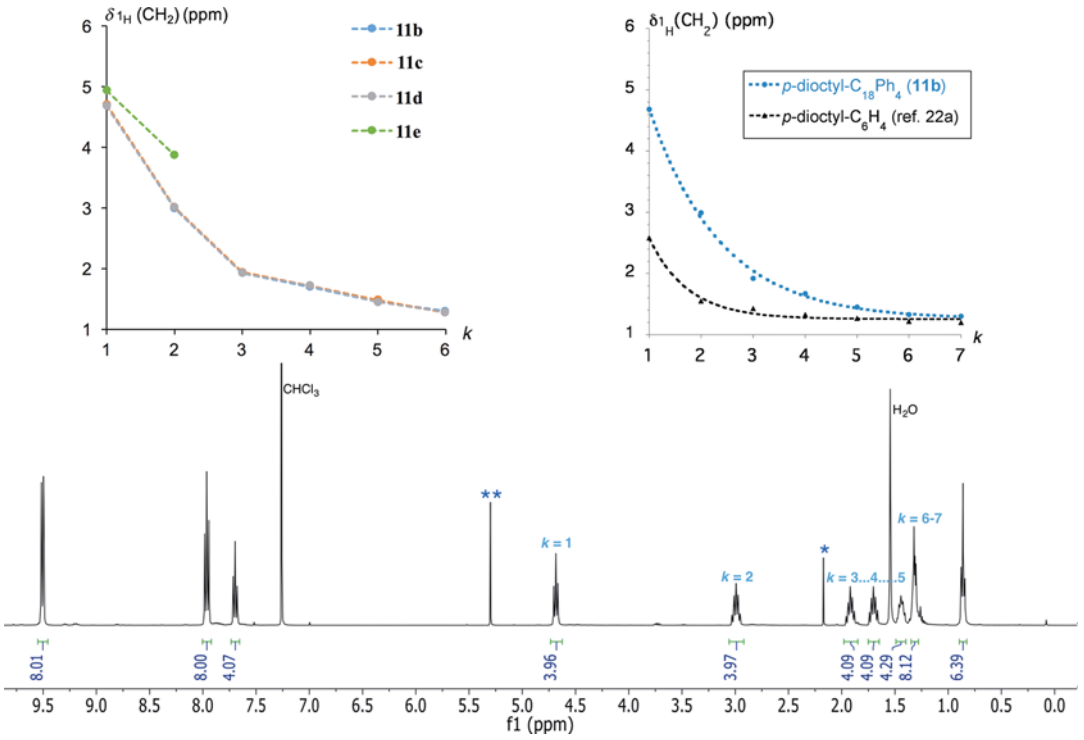

Figure 2. Variation of the ^{1}H NMR chemical shifts of the CH_2 groups of the alkyl chains of **11b–e** vs the CH_2 rank (top left), variation of the ^{1}H NMR chemical shifts of the CH_2 groups of the alky chains of **11b** and parent 1,4-dioctylbenzene[22a] vs the CH_2 rank (top right),[23] and full ^{1}H NMR spectrum of the dioctyl-*carbo*-benzene **11b** in $CDCl_3$ (bottom); (*) acetone; (**) CH_2Cl_2.

technique to record the ^{13}C NMR spectrum in the solid state (see SI).

The symmetrical *carbo*-benzenes **11a–e** display comparable ^{1}H NMR spectral profiles in the aromatic region, with highly deshielded signals for the two *ortho*-C*H* nuclei of the four equivalent phenyl substituents resonating at 9.52 ± 0.1 ppm for **11a–d** and 9.44 ppm for the fluorinated derivative **11e**. The ^{1}H NMR deshielding outside the macrocycle is experimental evidence of the strong diatropic ring current of *carbo*-benzenes. The corresponding magnetic anisotropy has long been established by calculation of nucleus-independent chemical shifts NICS(x),[20] x Å above the centroid of the C_{18} ring on the normal to the ring mean plane passing through this center (NICS(0) = −17.9 ppm for unsubstituted *carbo*-benzene vs −8.0 ppm for benzene).[21] According to the Biot–Savart law, the magnetic deshielding should decrease versus the distance from the ring border, and the aliphatic chains of **11a–e** directly anchored to this border provide a unique experimental probe to appraise the distance effect through the variation of the ^{1}H chemical shifts of the CH_2 groups along the chains. In **11b–d**, containing at least six CH_2 groups in almost identical local environments, the progressive shielding of the $C^{1}H_2$ signals away from the C_{18} macrocycle is the same for the three compounds and highly regular (Figure 2). The first methylene group (directly connected to the *carbo*-benzene ring and numbered as k = 1) thus resonates at very low field, at ca. 4.7 ppm in **11a–d** (4.72 ppm in **11a**; 4.68 ppm in **11b** vs 2.58 ppm in the parent 1,4-dioctylbenzene),[22] while the chemical shift of the next groups (numbered as k = 2, 3,...) undergoes an exponential decay down to ca. 1.25 ppm.[23] With six or seven methylene groups having significantly different ^{1}H chemical shifts, the dioctyl derivative **11b** bears the shortest aliphatic chain serving as an experimental probe of the magnetic anisotropy of the aromatic *carbo*-benzene macrocycle away from the C_{18} ring border (as far as 7.7 Å for k = 6, 8.9 Å for k = 7: see Figure 2 and X-ray crystal structure of **11b**, section 4 and SI).

In **11e**, the two first methylene protons are further deshielded by the neighboring fluorine atoms. The amplitude of the main curve (**11a–d**) shows that the alkyl protons are highly sensitive to the aromatic (diatropic) ring current. No such deshielding effect is observed on the ^{13}C and ^{19}F nuclei of the CH_2 and CF_2 groups along the alkyl substituents in **11a–d** or **11e**, the corresponding chemical shifts remaining almost unchanged upon aromatization of the [6]pericyclynediol precursors **6a–e**. This is in accordance with earlier recognition of the lower sensitivity of ^{19}F and ^{13}C nuclei to ring current effects, as compared to ^{1}H nuclei.[24] Although ring current effects in ^{13}C NMR have been evidenced in particular cases,[25] the ^{19}F NMR chemical shifts have been more generally considered to be more sensitive to steric than to electronic effects.[26]

In the dissymmetrical monoalkyl series **10a,b,d,e**, ^{1}H and ^{13}C NMR chemical shifts of the CH_2 groups are identical to those observed for the dialkyl counterparts. The ^{1}H nucleus directly connected to the C_{18} macrocycle resonates at 9.81 ± 0.03 ppm, which is comparable to the chemical shift of 9.87 ppm for the corresponding nuclei in the unsubstituted tetraphenyl-*carbo*-benzene **12**.[19]

2.3. Absorption Spectroscopy of Mono- and Dialkyl-*carbo*-benzenes. The mono- and dialkyl-*carbo*-benzenes **10a,b,d,e** and **11a–e** are highly chromophoric, with molar extinction coefficients in chloroform solution always around 200 000 L·mol^{-1}·cm^{-1}, all the measured values being in the range 185 000 < ε < 219 000 L·mol^{-1}·cm^{-1}. Their UV–vis absorption spectra in $CHCl_3$ are almost perfectly super-

DOI: 10.1021/acs.joc.6b02397
J. Org. Chem. 2017, 82, 925–935

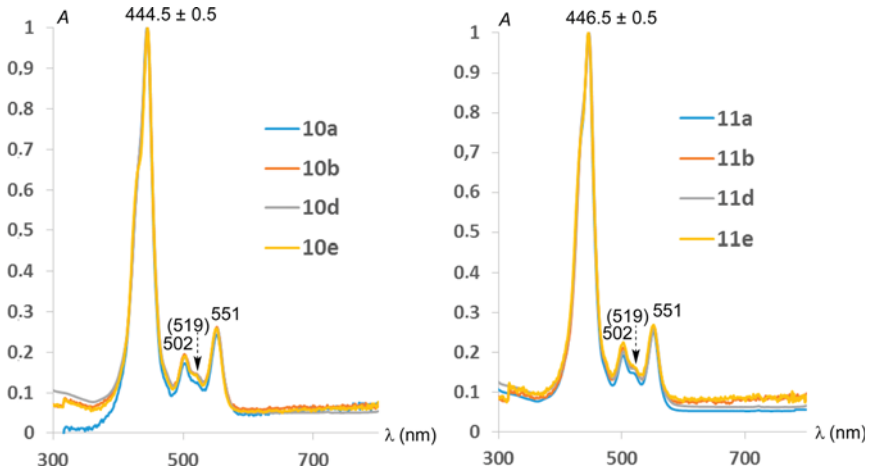

Figure 3. Normalized UV−vis absorption spectra of the monoalkyl-*carbo*-benzenes **10a,b,d,e** (left) and dialkyl-*carbo*-benzenes **11a,b,d,e** (right) in chloroform solution.

Table 1. Selected Crystallographic Data for 11a−d

molecule	**11a**	**11b**	**11c**[a]	**11d**	**11d**[b]	**12**[b,c]
R	C_2H_5	C_8H_{17}	$C_{14}H_{29}$	$C_{20}H_{41}$	$C_{20}H_{41}$	H
crystallization solvent	$CHCl_3$	$CHCl_3$	$CHCl_3$	DCM	$CHCl_3$	DCM
cocrystallized solvent	no	yes	no	yes	yes	no
melting−decomposition point (°C)	208	188	170	149		
deviation from C_{18} ring planarity (Å)	0.058(2)	0.045(1)	0.036(3)	0.035(5)	0.049	0.032
angle between C_{18} and alkyl planes (deg)	40.2(2)	6.6(1)	22.0(1)	3.3(1)	7.8	
angle between the C_{18} and Ph planes (deg)	10.99(4)	1.63(2)	8.31(7)	7.50(11)	5.4	10.8
	8.18 (4)	3.27(2)	7.07(7)	3.54(13)	1.9	18.5
	11.03(4)	5.88(3)		4.54(10)		
	8.33(4)	8.46(2)		1.53(11)		
distance between closest C_{18} planes (Å)	3.255	3.215	3.206[a]	3.398	3.277	2.984
Θ (deg)	57.7	65.9	55.0[a]	71.5	74.4	71.6
space group	$P2_1/c$	P-1	$P2_1/n$	P-1	P-1	$P2_1/c$
no. of axes, angle between them (deg)	2, 64.5(1)	1	2, 70.07(2)	1		
diameter (maximum C···C distance, Å)	12.269(4)	27.711(2)	39.930(7)	57.435(11)	57.367	16.7

[a]Chemical vertical overlap of successive C_{18} rings (see Figure 5). [b]Crystals of **11d** obtained from a $CHCl_3$ solution; approximate values (without esd) determined from the Mercury interface (3.8 version). [c]From ref 19.

imposable and exhibit the classical pattern of *carbo*-benzenes (Figure 3):[9b,10c,12,19] a main band at λ_{max} = 446.5 ± 0.5 nm in the dialkyl series **11a−e**, 444.5 ± 0.5 nm in the monoalkyl series **10a,b,d,e**, accompanied by three smaller bands at 502.0 ± 0.5, 519.0 ± 0.5 (sh), and 551.5 ± 0.5 nm. The presence of one or two alkyl substituents on the C_{18} macrocycle has thus a negligible effect on the absorption properties in solution, but the dialkyl-*carbo*-benzenes have different colors in the solid state. For comparison, the UV−vis spectrum of the unsubstituted tetraphenyl-*carbo*-benzene **12** is virtually identical (with λ_{max} = 444 nm).[19] As previously demonstrated,[12] the main one-photon absorption band of *carbo*-benzenes, whatever their substitution pattern, corresponds to two transitions centered on the C_{18} rings, analyzable by the Gouterman four-orbital model devised for porphyrins.[27]

The dialkyl-*carbo*-benzenes displaying different colors in the solid state (**11a** and **11c** are dark blue, **11b** is dark violet, and **11d** and **11e** are dark red), the solid UV−vis absorption spectra of the solids were also recorded and found consistent with the observed colors despite the broadness of the bands, with one or two maxima in the range 450−650 nm (analogous spectral shapes are observed for the solid monoalkyl congeners **10a,b,d,e**: see SI). In spite of the structural similarity of the molecules, different intermolecular interactions in the solid state should thus be invoked to explain the color variation: related crystallochromy, i.e., correlation of the solid state color with the crystal packing as a function of the length of alkyl substituents, was recently reported for a series of tetraalkyltetracenes.[28] A correlation between the crystal packing of **11a−e** and their color in the solid state is tentatively sought for hereafter.

2.4. Crystal Properties of Lipidic *Carbo*-benzenes. Beyond their lipidic nature, both mono- and dialkyl-*carbo*-benzenes proved to be highly crystalline. Seven representatives, **10b,d** and **11a−e**, could thus be characterized by X-ray diffraction (XRD) analysis of single crystals deposited from DCM or $CHCl_3$ solutions (Table 1, Figure 4; for **10b** and **10d**, see Figure S1 in the SI).[29] The weak diffracting power of crystals of the fluorinated dioctyl-*carbo*-benzene **11e** limited the acquisition of data but allowed qualitative confirmation of the structure (see SI, Figure S2).

In the dialkyl series **11a−d**, the C_{18} ring exhibits a classical quasi-planar quasi-hexagonal conformation (with a maximal deviation of 0.058(2) Å for **11a**) and classical bond lengths (spC≡spC ≈ 1.22−1.23 Å, sp^2C≡spC ≈ 1.37−1.39 Å).[9b,10c] The alkyl carbon chains, stretched in a planar zigzag arrangement,

DOI: 10.1021/acs.joc.6b02397
J. Org. Chem. 2017, 82, 925−935

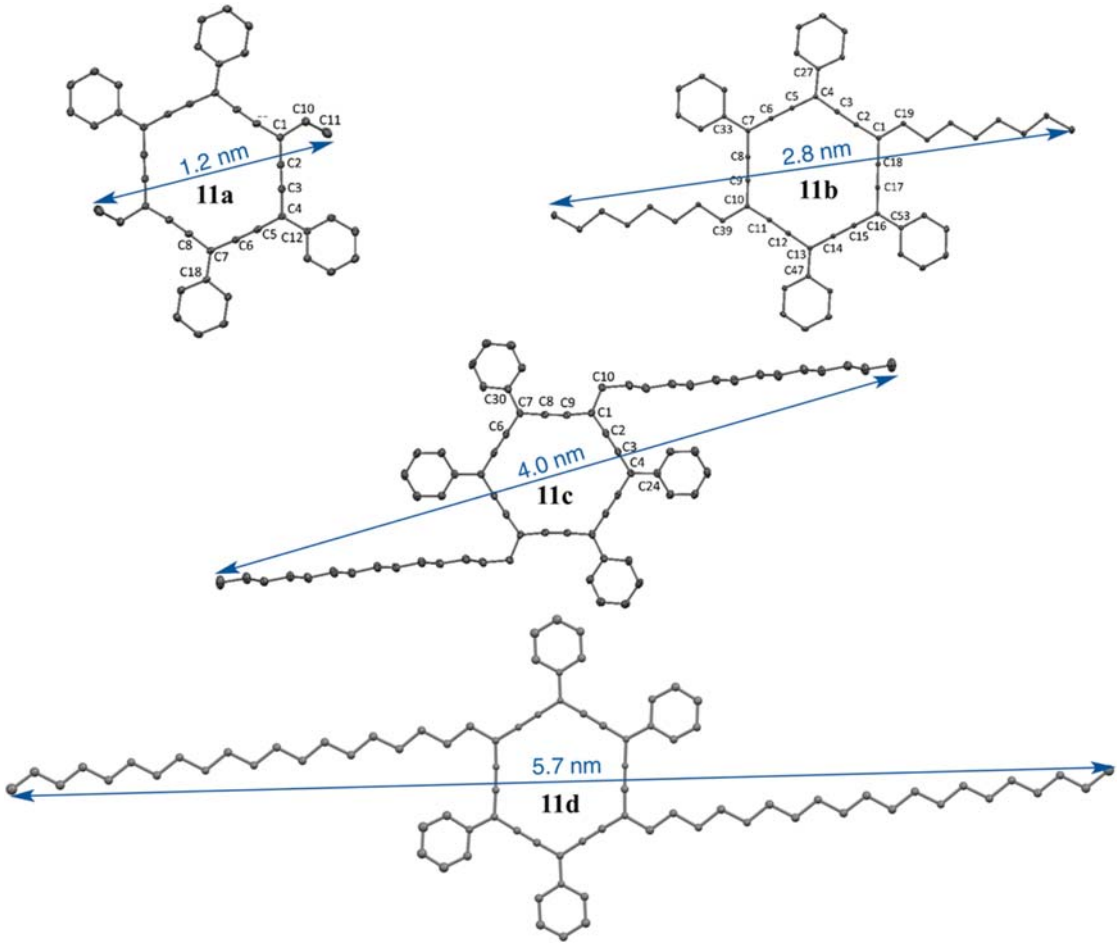

Figure 4. Molecular views of the X-ray crystal structures of the dialkyl-*carbo*-benzenes **11a–d**. Numbering of nonequivalent C atoms indicative of the crystal symmetry. Thermal ellipsoids at the 50% probability level. For clarity, hydrogen atoms and solvent molecules (for **11b** and **11d**) are omitted (for more details, see SI).

can be coplanar with the C_{18} macrocycle (dihedral angles of 6.6(1)° for **11b**, 3.3(1)° for **11d**) or not (dihedral angle of 40.2(2)° for **11a**, 22.0(1)° for **11c**). With two fully stretched eicosyl chains, the *carbo*-benzene **11d** is the largest *carbo*-benzenic structure ever described, with a distance of 57.435(11) Å between the two carbon atoms of the CH_3 ends (Table 1).

In the crystal state, the macrocycles of **11a–d** form slanting columnar arrangements, where the distance between the C_{18} mean planes of two successive *carbo*-benzene molecules varies from 3.206 to 3.398 Å. The deviation from "columnar verticality" (Θ = tilting angle between the column axis and the normal to the mean planes) varies from 55.0° for **11c** to 71.5° for **11d**. The first examples of π-stacking between *carbo*-benzene rings are observed in the crystal structures of **11a** and **11c** (Figure 5), where the small Θ values allow partial vertical overlap of successive C_{18} macrocycles separated by distances very close to those calculated for ABC or AB α-graphityne (2.201–3.266 Å).[3] The maximal extent of vertical overlap is thus attained in crystals of **11c** (top Figure 5), where the distance between the C_{18} mean planes (3.206 Å) corresponds to the shortest internuclear distances of ca. 3.36 and 3.41 Å occurring between pairs sp-C and sp^2-C(Ph) vertices of successive C_{18} rings, respectively. π-Stacking between phenyl substituents, even at low overlap extent, can also significantly contribute to the stabilization of the tilted columnar arrangement.[30] Nevertheless, the molecular packing indicates significant dispersive intermolecular interactions between tetradecyl chains arranged in a parallel manner: six alternating methylene groups of one chain interact with their closest congeners in the neighboring molecule through C···C distances in the range 4.50–4.58 Å, revealing an intermolecular van der Waals contact between ideally located H atoms (internuclear H···H distances of ca. 2.8 Å). The π-stacking between *carbo*-benzene rings is however not merely driven by the London forces between the C_{14} alkyl chains of **11c**: the same configuration is also observed for the much shorter (not interacting) C_2 alkyl chains of **11a**, with a slightly larger deviation from columnar verticality (Θ = 57.7°) and shortest internuclear distances of ca. 3.29 and 3.55 Å between pairs of sp-C and sp^2-C(Ph) vertices in successive C_{18} rings, respectively.

The π-stacking of C_{18} rings in crystals of **11a** and **11c** is actually correlated with the absence of cocrystallized solvent molecule. No such stacking is observed in crystals of **11b** (Θ = 65.9°) and **11d** (Θ = 71.5°) containing $CHCl_3$ and DCM molecules, respectively. In crystals of the dioctyl-*carbo*-benzene **11b**, an interaction between each C_{18} ring and one $CHCl_3$ molecule is revealed by a short spC_2···ClC contact (ca. 3.41 Å), with a spC_2···Cl–C angle of ca. 150.8°: this arrangement is indicative of a σ-hole-directed C–Cl···π halogen bond, previously evidenced and analyzed in the *carbo*-mer series.[10c,31]

As observed earlier for *o*-tetraphenyl-*carbo*-benzenes,[19] the Cl

DOI: 10.1021/acs.joc.6b02397
J. Org. Chem. 2017, 82, 925–935

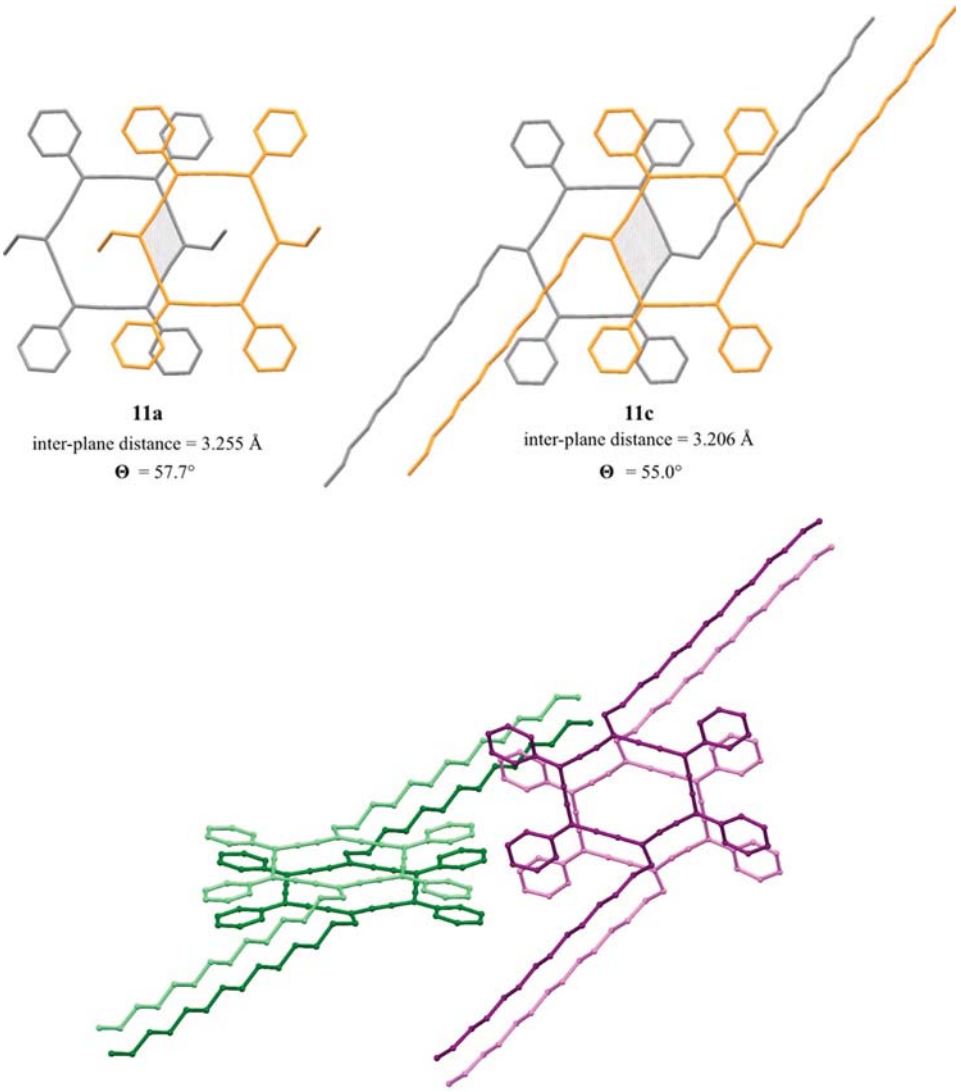

Figure 5. Views perpendicular to the C_{18} mean planes of **11a** and **11c** in the crystal (top), and perspective view of the 55°-tilted columnar packing of **11c** (bottom), showing the "vertical" overlap of successive C_{18} rings illustrative of the one calculated in AB or ABC α-graphityne.[3]

atom lies very close to the centroid of the C_{18} ring (by ca. 1.08 Å). Likewise, no π-stacking of C_{18} rings occurs in other crystals of **11d** containing $CHCl_3$ molecules (Θ = 74.4°): a σ-hole-directed C−Cl···π halogen bond between the C_{18} ring and one $CHCl_3$ molecule is revealed by a short spC_2···ClC contact (ca. 3.40 Å), where the middle of the spC≡spC bond is almost aligned with the Cl−C bond axis (spC_2···Cl−C ≈ 173.3°), the Cl atom lying quite close to the centroid of the C_{18} ring (by ca. 1.78 Å). In crystals deposited from DCM, no C−Cl···π halogen bond is observed between DCM and *carbo*-benzene molecules (**10b**, **10d**, **11d**).

On the basis of these analyses, a tentative correlation between the intermolecular interactions and the colors of the dialkyl-*carbo*-benzenes **11a−d** in the solid state can be proposed. The common blue color of solid **11a** and **11c** can be correlated with the comparable extent of π-stacking interactions between the C_{18} macrocycles ($\Theta \approx 55°$). Furthermore, the C_2 and C_{14} alkyl chains of these two *carbo*-benzenes stretch out of the C_{18} ring mean planes, while the carbon chains and the macrocycle are coplanar in all other cases. Also noteworthy, crystals of **11d** and **11b**, red and violet, with and without π-stacking between phenyl substituents, respectively, exhibit the same space group (*P*-1). The decrease of π-stacking efficiency from **11a** and **11c** to **11d** and **11b** is also correlated with their different colors and UV−vis absorption spectra, the wavelength of the right edge of the broad band decreasing in the same order of magnitude: from ca. 700 nm for **11a** and **11c** to ca. 675 and 660 nm for **11d** and **11b**, respectively (see SI).

As a macroscopic crystal property, the variation of the melting point of the dialkyl-*carbo*-benzenes **11a−e** has been investigated. Although the dark color of the crystals prevented visual monitoring of the melting process, melting−decomposition temperature values could be determined (Table 1). While detectable melting−decomposition points of most nonlipidic *carbo*-benzenes are in the range 200−250 °C,[10c] a regular decrease of this temperature with the chain length *n* is observed: from 208 °C for *n* = 2 to 149 °C for *n* = 20 (Figure 6). Noteworthy, the melting−decomposition temperature of the fluorooctyl derivative **11e** is just slightly higher (196 °C) than that of the octyl analogue **11b** (188 °C). In the hydrocarbon series, extrapolation of the linear fit to very long chains ($n > 20$) suggests possible thermotropic behavior at temperatures compatible with molecular stability.

DOI: 10.1021/acs.joc.6b02397
J. Org. Chem. 2017, 82, 925−935

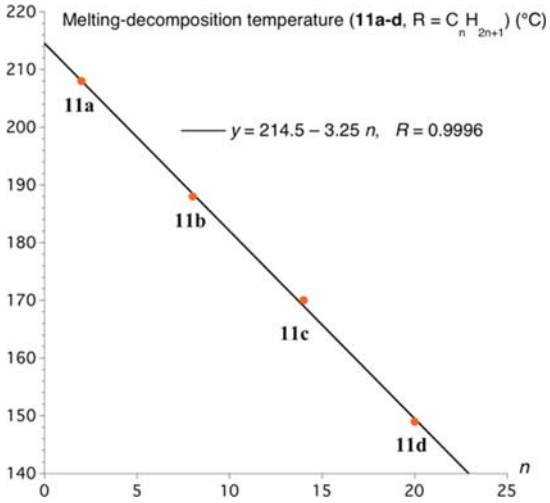

Figure 6. Variation of detectable melting−decomposition temperatures of dialkyl-*carbo*-benzenes vs the chain length *n*.

3. CONCLUSION

The disclosed series of *carbo*-benzenes combining oxymoronic features of lipidic and aromatic/chromophoric hydrocarbons opens new prospects in the context of *carbo*-benzene and futurist α-graphyne chemistry.

The dioctyl derivative **11b** bearing the shortest alkyl chain serves as an experimental ^{1}H NMR probe of the magnetic aromaticity of the *carbo*-benzene macrocycle, as far as ca. 8 Å away from the C_{18} ring border. The octyl chains of **11b** also provide sufficient solubility to allow future studies of the chemical reactivity of the *carbo*-benzene ring, in particular toward metallic ions or small π-electron-rich organic guests to form π-inclusion complexes of various types.[32] The analogue **11e** is the first example of a fluorinated *carbo*-benzene derivative.

The diethyl and bistetradecyl derivatives **11a** and **11c** afford first examples of π-stacking of *carbo*-benzene rings, thus providing experimental evidence of the possible cohesion of α-graphyne layers in α-graphityne. The maximum overlap extent is attained in crystals of **11c**, where the distance of 3.206 between stacked C_{18} ring planes fits with the calculated interlayer distances of 3.266 and 3.201 Å in AB and ABC α-graphitynes, respectively.[3]

The biseicosyl derivative **11d** exhibits the lowest melting−decomposition temperature ever reported for a *carbo*-benzene derivative (149 °C). At lower temperature and possibly greater chain lengths ($n > 20$), reversible thermotropic behavior might be envisaged. The columnar packing of dialkyl-*carbo*-benzenes in the crystalline state suggests that liquid crystal properties of putative *carbo*-benzenic mesogens might involve discotic assemblies.

4. EXPERIMENTAL SECTION

4.1. General Remarks. THF, diethyl ether (Et_2O), pentane, and dichloromethane (DCM) were dried by filtration under dry argon over two alumina-containing columns. All other reagents were used as commercially available. In particular, commercial solutions of *n*-BuLi were 2.5 M in hexane, solutions of ethylmagnesium bromide were 3 M in THF, and solutions of HCl were 2 M in Et_2O. [6]Pericyclynedione **7** was prepared according to previously published procedures.[16a] All reactions were carried out under an argon atmosphere using Schlenk tubes and vacuum line techniques. Column chromatography was carried out on silica gel (60 Å, CC 70−200 μm). Silica gel thin layer chromatography plates (60F254, 0.25 mm) were revealed by treatment with an ethanolic solution of phosphomolybdic acid (20%). NMR chemical shifts are given in ppm with positive values to high frequency relative to the tetramethylsilane reference. Coupling constants *J* are given in Hertz; wavelengths λ in nanometers, and UV−vis extinction molar coefficients ε in $L{\cdot}mol^{-1}{\cdot}cm^{-1}$.

4.2. Experimental Procedures. *4.2.1. General Procedure for the Preparation of Grignard Reagents RMgBr, R = n-C_nH_{2n+1} (n = 2, 8, 14, 20), n-$C_8H_4F_{13}$.* To a solution of magnesium metal (0.441 mmol, 1 equiv) in THF (0.5 mL) a solution of alkyl bromide (0.530 mmol, 1.2 equiv) was added dropwise at room temperature. The mixture was stirred for 2 h at 50 °C and then cooled to room temperature. The resulting solution of alkylbromomagnesium bromides RMgBr was used directly without any further purification.

*4.2.2. General Procedure for the Preparation of Lipidic [6]-Pericyclynediols **6a−e** and **8a−e**.* A solution of [6] pericyclynedione **7** (100 mg, 0.147 mmol) in THF (30 mL) at −10 °C was treated with a freshly prepared solution of RMgBr (0.441 mmol in 0.5 mL of THF). The mixture was stirred at −10 °C for 4 h. After treatment with saturated aqueous solution of NH_4Cl, the aqueous layer was separated and extracted by diethyl ether, the organic layers were combined, then dried over $MgSO_4$, and concentrated to dryness under reduced pressure. The residue was purified by chromatography on silica gel to afford the diadduct **6**, the monoadduct **8**, and the double-reduction product **9** as yellow oils.

*4.2.3. General Procedure for Preparation of Lipidic Carbo-benzenes **10a,b,d,e** and **11a−e**.* A solution of [6]pericyclynediol **6** or **8** in DCM was treated with anhydrous $SnCl_2$ (10 equiv) and HCl (20 equiv; 2 M in Et_2O) at −78 °C. The mixture was stirred at −78 °C for 10 min and then at room temperature for 20 min. After treatment with 1 M aqueous NaOH (20 equiv) and filtration through Celite, the organic layer was separated, washed with brine (3×), dried over $MgSO_4$, and concentrated to dryness under reduced pressure. The residue was purified by chromatography on silica gel to give the *carbo*-benzene **11** or **10** as a strongly colored solid.

4.3. Analytical Characterization. *4.3.1. Details for the Pericyclynediols **6a**, **8a**, and **9**.* [6]Pericyclynedione **7** (0.147 mmol, 100 mg) was reacted with commercial C_2H_5MgBr (0.441 mmol, 3 M in THF) in THF (30 mL). Chromatography on silica gel eluted with pentane:EtOAc = 4:1 and then 3:1 gave **6a** (0.067 mmol, 50 mg, 45%) and **8a** (0.042 mmol, 30 mg, 28%) as yellow oils, along with the known bis-secondary [6]pericyclynediol **9** (0.028 mmol, 19 mg, 20%).[16a]

*1,10-Diethyl-4,7,13,16-tetramethoxy-4,7,13,16-tetraphenylcyclooctadeca-2,5,8,11,14,17-hexayne-1,10-diol (**6a**).* ^{1}H NMR (300 MHz, $CDCl_3$) δ 7.89−7.57 (m, 8H), 7.51−7.28 (m, 12H), 3.69−3.20 (m, 12H), 3.07−2.38 (m, 2H), 2.15−1.85 (m, 4H), 1.27−1.08 (m, 6H).

$^{13}C\{^1H\}$ NMR (101 MHz, $CDCl_3$) δ 139.3, 129.1, 129.0, 128.5−128.4, 126.5−126.4, 87.0−86.8, 84.5−84.4, 81.1−81.0, 71.9−71.8, 64.4, 64.3, 53.3−53.2, 36.6−36.4, 9.1−8.9.

HRMS (MALDI-TOF/DCTB): *m/z* $[M]^{+\bullet}$ calcd for $C_{50}H_{44}O_6$ 740.3132, found 740.3099.

*1-Ethyl-4,7,13,16-tetramethoxy-4,7,13,16-tetraphenylcycloctadeca-2,5,8,11,14,17-hexayne-1,10-diol (**8a**).* ^{1}H NMR (400 MHz, $CDCl_3$) δ 7.76−7.67 (m, 8H), 7.40−7.32 (m, 12H), 5.44−5.22 (m, 1H), 3.65−3.31 (m, 12H), 3.03−2.23 (m, 2H), 2.11−1.93 (m, 2H), 1.20−1.06 (m, 3H).

$^{13}C\{^1H\}$ NMR (101 MHz, $CDCl_3$) δ 139.6−139.2, 129.1−129.0, 128.5−128.4, 126.5−126.4, 87.2−86.9, 84.70−83.5, 82.2−81.9, 81.2−81.1, 71.8−71.7, 64.4−64.3, 53.4−53.3, 52.4−52.3, 36.7−36.5, 9.1−8.8.

HRMS (MALDI-TOF/DCTB): *m/z* $[M + H]^+$ calcd for $C_{48}H_{41}O_6$ 713.2897, found 713.2919.

*4,7,13,16-Tetramethoxy-4,7,13,16-tetraphenylcyclooctadeca-2,5,8,11,14,17-hexayne-1,10-diol (**9**).*[16a] Yellow oil. Spectral characteristics identical to those of an authentic sample.[1] ^{1}H NMR (400 MHz, $CDCl_3$) δ 7.81−7.62 (m, 8H), 7.44−7.28 (m, 12H), 5.31 (m, 2H), 3.66−3.32 (m, 12H), 3.05−2.62 (m, 2H).

*4.3.2. Details for the Pericyclynediols **6b** and **8b**.* [6]-Pericyclynedione **7** (0.147 mmol, 100 mg) was reacted with *n*-

DOI: 10.1021/acs.joc.6b02397
J. Org. Chem. 2017, 82, 925−935

$C_8H_{17}MgBr$ (0.441 mmol in 0.5 mL of THF) in THF (30 mL). Chromatography over silica gel eluted with pentane:EtOAc 4:1 and then 3:1 afforded **6b** as a yellow oil (0.101 mmol, 92 mg, 34%), **8b** as a yellow oil as well (0.038 mmol, 30 mg, 26%), and the known bis-secondary [6]pericyclynediol **9** (0.029 mmol, 20 mg, 20%).[16a]

*4,7,13,16-Tetramethoxy-1,10-dioctyl-4,7,13,16-tetraphenylcyclooctadeca-2,5,8,11,14,17-hexayne-1,10-diol (**6b**).* ^{1}H NMR (400 MHz, $CDCl_3$) δ 7.81−7.65 (m, 8H), 7.44−7.31 (m, 12H), 3.63−3.34 (m, 12H), 3.31−2.57 (m, 2H), 2.00 (m, 4H), 1.87−1.47 (m, 4H), 1.34−1.18 (m, 20H), 0.88 (m, 6H).

$^{13}C\{^1H\}$ NMR (101 MHz, $CDCl_3$) δ 139.4, 129.1−128.9, 128.6−128.4, 126.6−126.4, 87.4−86.9, 84.5−84.4, 81.2, 81.0, 71.9, 71.8, 63.7, 53.4−53.3, 43.3−43.1, 31.9, 30.3−29.2, 24.6−24.5, 22.7, 14.1.

HRMS (MALDI-TOF/DCTB): m/z $[M + Na]^+$ calcd for $C_{62}H_{68}O_6Na$ 931.4908, found 931.4994.

*4,7,13,16-Tetramethoxy-1-octyl-4,7,13,16-tetraphenylcyclooctadeca-2,5,8,11,14,17-hexayne-1,10-diol (**8b**).* ^{1}H NMR (400 MHz, $CDCl_3$) δ 7.81−7.61 (m, 8H), 7.39−7.33 (m, 12H), 5.39−5.26 (m, 1H), 3.64−3.34 (m, 12H), 2.96−2.30 (m, 2H), 2.05−1.96 (m, 2H), 1.73−1.55 (m, 2H), 1.28 (m, 10H), 0.91−0.85 (m, 3H).

$^{13}C\{^1H\}$ NMR (101 MHz, $CDCl_3$) δ 139.4, 129.1−129.0, 128.5, 126.5−126.4, 87.2−80.9, 71.8, 63.7, 53.4, 53.3, 52.32−52.26, 43.2, 31.9, 29.5−29.2, 24.5, 22.7−22.6, 14.1.

HRMS (MALDI-TOF/DCTB): m/z $[M + H]^+$ calcd for $C_{54}H_{53}O_6$ 797.3836, found 797.3879.

*4.3.3. Details for the Pericyclynediol **6c**.* [6]Pericyclynedione **7** (0.29 mmol, 200 mg) was reacted with n-$C_{14}H_{29}MgBr$ (0.65 mmol in 0.5 mL of THF) in THF (30 mL). Chromatography over silica gel eluted with pentane/EtOAc 95:5 and then 9:1 afforded **6c** as a pale brown oil (0.13 mmol, 140 mg, 44%).

*4,7,13,16-Tetramethoxy-1,10-ditetradecyl-4,7,13,16-tetraphenylcyclooctadeca-2,5,8,11,14,17-hexayne-1,10-diol (**6c**).* ^{1}H NMR (300 MHz, $CDCl_3$) δ 7.78−7.69 (m, 8H). 7.42−7.35 (m, 12H), 3.63−3.41 (m, 12H), 2.02 (m, 4H), 1.65 (bs, 4H), 1.28 (bs, 44 H), 0.91 (t, $^3J_{HH}$ = 6.9 Hz, 6H).

$^{13}C\{^1H\}$ NMR (75 MHz, $CDCl_3$) δ 139.5−139.2, 129.2−129.0, 128.6−128.3, 126.5−126.3, 87.4−87.2, 84.4, 81.0−80.8, 71.8, 63.7, 52.4−52.3, 43.0, 31.9, 29.7−29.3, 22.7, 14.1.

HRMS (MALDI-TOF/DCTB): m/z [M + Na] calcd for $C_{74}H_{92}O_6Na$ 1099.6786, found 1099.6793.

*4.3.4. Details for the Pericyclynediols **6d** and **8d**.* [6]-Pericyclynedione **7** (0.147 mmol, 100 mg) was reacted with $C_{20}H_{41}MgBr$ (0.441 mmol in 1 mL of THF) in THF (30 mL). Chromatography over silica gel eluted with pentane/EtOAc 8:1, then 4:1, and then 3:1 afforded **6d** (0.043 mmol, 54 mg, 30%) and **8d** (0.029 mmol, 28 mg, 20%) as yellow oils, along with the known bis-secondary [6]pericyclynediol **9** (0.021 mmol, 14 mg, 14%).[16a]

*1,10-Diicosyl-4,7,13,16-tetramethoxy-4,7,13,16-tetraphenylcyclooctadeca-2,5,8,11,14,17-hexayne-1,10-diol (**6d**).* ^{1}H NMR (400 MHz, $CDCl_3$) δ 7.83−7.62 (m, 8H), 7.42−7.29 (m, 12H), 3.61−3.33 (m, 12H), 3.14−2.68 (m, 2H), 2.05−1.93 (m, 4H), 1.78−1.48 (m, 8H), 1.27 (bs, 64H), 0.89 (t, $^3J_{HH}$ = 6.7 Hz, 6H).

$^{13}C\{^1H\}$ NMR (101 MHz, $CDCl_3$) δ 139.6−139.4, 129.1−129.0, 128.5−128.4, 126.5−126.4, 87.4−87.0, 84.5−84.3, 81.1−80.8, 71.9, 71.8, 63.7, 53.4−53.2, 43.3−43.1, 32.8, 31.9, 29.7−29.4, 22.7, 14.1.

HRMS (MALDI-TOF/DCTB): m/z $[M + Na]^+$ calcd for $C_{86}H_{116}O_6Na$ 1267.8664, found 1267.8710.

*1-Icosyl-4,7,13,16-tetramethoxy-4,7,13,16-tetraphenylcyclooctadeca-2,5,8,11,14,17-hexa-yne-1,10-diol (**8d**).* ^{1}H NMR (400 MHz, $CDCl_3$) δ 7.82−7.62 (m, 8H), 7.39−7.34 (m, 12H), 5.41−5.25 (m, 1H), 3.63−3.35 (m, 12H), 3.04−2.38 (m, 2H), 1.99−1.96 (m, 2H), 1.62 (m, 4H), 1.26 (s, 32H), 0.88 (t, $^3J_{HH}$ = 6.8 Hz, 3H).

$^{13}C\{^1H\}$ NMR (101 MHz, $CDCl_3$) δ 139.4−139.3, 129.1−128.5, 128.5, 126.5−126.4, 87.2, 84.6−83.6, 82.1, 80.9−80.4, 71.8, 63.7, 53.4−53.3, 52.4−52.3, 43.2, 43.1, 31.9, 30.3−29.3, 24.5, 22.7, 14.1.

HRMS (MALDI-TOF/DCTB): m/z $[M]^+$ calcd for $C_{66}H_{76}O_6$ 964.5636, found 964.5598.

*4.3.5. Details for the Fluorinated Pericyclynediols **6e** and **8e**.* [6]Pericyclynedione **7** (0.147 mmol, 100 mg) was reacted with n-$C_8H_4F_{13}MgBr$ (0.441 mmol in 1 mL of THF) in THF (30 mL). Chromatography over silica gel eluted with pentane:EtOAc = 5:1 and then 3:1 afforded **6e** (0.049 mmol, 68 mg, 34%) and **8e** (0.034 mmol, 35 mg, 23%) as yellow oils, along with the known bis-secondary [6]pericyclynediol **9** (0.017 mmol, 12 mg, 12%).[16a]

*4,7,13,16-Tetramethoxy-4,7,13,16-tetraphenyl-1,10-bis-(3,3,4,4,5,5,6,6,7,7,8,8,8-tridecafluorooctyl)cyclooctadeca-2,5,8,11,14,17-hexayne-1,10-diol (**6e**).* ^{1}H NMR (400 MHz, $CDCl_3$) δ 7.82−7.58 (m, 8H), 7.46−7.32 (m, 12H), 3.77−3.31 (m, 12H), 3.05−2.66 (m, 2H), 2.49−2.30 (m, 8H).

$^{13}C\{^1H\}$ NMR (101 MHz, $CDCl_3$) δ 139.1, 139.0, 129.3−129.2, 128.7−128.6, 126.4−126.2, 85.3−85.1, 84.4, 84.3, 82.3−82.1, 71.7, 62.2, 53.3−53.2, 34.2, 29.7. In the absence of $\{^{19}F\}$ decoupling, the signals of the fluorinated carbon atoms, expected to be multiplets of high order, are not observed.

^{19}F NMR (376 MHz, $CDCl_3$) δ −80.7 to −80.8, −113.8 to −113.9, −121.9 to −122.0, −122.9, −123.4, −123.5, −126.1 to −126.3.

HRMS (MALDI-TOF/DCTB): m/z $[M + Na]^+$ calcd for $C_{62}H_{42}O_6F_{26}Na$ 1399.2458, found 1399.2584.

*4,7,13,16-Tetramethoxy-4,7,13,16-tetraphenyl-1-(3,3,4,4,5,5,6,6,7,7,8,8,8-tridecafluorooctyl)cyclooctadeca-2,5,8,11,14,17-hexayne-1,10-diol (**8e**).* ^{1}H NMR (400 MHz, $CDCl_3$) δ 7.81−7.58 (m, 8H), 7.45−7.31 (m, 12H), 5.45−5.30 (m, 1H), 3.63−3.31 (m, 12H), 3.26−2.63 (m, 2H), 2.46−2.25 (m, 4H).

$^{13}C\{^1H\}$ NMR (101 MHz, $CDCl_3$) δ 139.2−139.0, 129.2−129.1, 128.6−128.5, 126.5−126.2, 85.4−81.9, 71.2, 62.2, 53.4−53.2, 52.4−52.3, 34.1, 26.6. In the absence of $\{^{19}F\}$ decoupling, the signals of the fluorinated carbon atoms, expected to be multiplets of high order, are not observed.

^{19}F NMR (376 MHz, $CDCl_3$) δ −80.7 to −80.8, −113.8 to −113.9, −121.8 to −122.0, −122.8 to −122.9, −123.4 to −123.5, −126.1 to −126.2.

HRMS (MALDI-TOF/DCTB): m/z $[M + Na]^+$ calcd for $C_{54}H_{39}O_6F_{13}Na$ 1053.2431, found 1053.2498.

*4.3.6. Details for the Monolipidic Carbo-benzenes **10a,b,d,e**. 7-Ethyl-1,4,10,13-tetraphenylcyclooctadeca-1,2,3,7,8,9,13,14,15-nonaen-5,11,17-triyne (**10a**).* [6]Pericyclynediol **8a** (0.042 mmol, 30 mg), anhydrous $SnCl_2$ (0.42 mmol, 80 mg), HCl (0.84 mmol, 2 M in Et_2O), and CH_2Cl_2 (15 mL) were mixed. Chromatography over silica gel eluted with pentane:DCM 3:1 afforded **10a** as a dark violet solid (0.015 mmol, 10 mg, 35%).

^{1}H NMR (400 MHz, $CDCl_3$) δ 9.78 (s, 1H), 9.59−9.47 (m, 8H), 7.99−7.95(m, 8H), 7.74−7.67 (m, 4H), 4.74 (q, $^3J_{HH}$ = 7.5 Hz, 2H), 2.51 (t, $^3J_{HH}$ = 7.5 Hz, 3H).

$^{13}C\{^1H\}$ NMR (101 MHz, $CDCl_3$) δ 139.9−139.6, 130.2, 130.1, 129.9−129.8, 129.6−129.7, 123.1−116.0, 108.7, 105.2, 103.1, 87.2, 37.1, 16.2.

HRMS (MALDI-TOF/DCTB): m/z $[M]^+$ calcd for $C_{44}H_{26}$ 554.1999, found 554.2043.

UV−vis ($CHCl_3$): λ_{max} = 444 nm (ε = 185 000 L·mol^{-1}·cm^{-1}).

Melting−decomposition temperature: 201 °C.

*7-Octyl-1,4,10,13-tetraphenylcyclooctadeca-1,2,3,7,8,9,13,14,15-nonaen-5,11,17-triyne (**10b**).* [6]Pericyclynediol **8b** (0.038 mmol, 30 mg), anhydrous $SnCl_2$ (0.38 mmol, 72 mg), HCl (0.753 mmol, 2 M in Et_2O), and CH_2Cl_2 (20 mL) were mixed. Chromatography over silica gel eluted with pentane:DCM 3:1 afforded **10b** as a dark violet solid (0.011 mmol, 7 mg, 30%).

^{1}H NMR (400 MHz, CD_2Cl_2) δ 9.84 (s, 1H), 9.60−9.48 (m, 8H), 8.01−7.71 (m, 8H), 7.77−7.69 (m, 4H), 4.74 (t, $^3J_{HH}$ = 7.6 Hz, 2H), 3.07−2.97 (quint, $^3J_{HH}$ = 7.6 Hz, 2H), 1.99−1.90 (quint, $^3J_{HH}$ = 7.6 Hz, 2H), 1.72 (quint, $^3J_{HH}$ = 7.6 Hz, 2H), 1.47 (quint, $^3J_{HH}$ = 7.6 Hz, 2H), 1.39−1.29 (m, 4H), 0.86 (t, $^3J_{HH}$ = 7.6 Hz, 3H).

$^{13}C\{^1H\}$ NMR (75 MHz, CD_2Cl_2) δ 139.6, 139.3, 130.0, 129.8, 129.8, 129.7, 129.6, 122.9, 121.8, 119.7, 119.3, 116.2, 115.6, 108.0, 105.1, 103.1, 87.3, 40.9, 31.9, 31.9, 29.7, 29.6, 29.3, 22.7, 13.9.

HRMS (MALDI-TOF/DCTB): m/z $[M]^+$ calcd for $C_{50}H_{38}$ 638.2968, found 638.3018.

UV−vis ($CHCl_3$): λ_{max} = 445 nm (ε = 189 000 L·mol^{-1}·cm^{-1}).

Melting−decomposition temperature: 166 °C.

*7-Icosyl-1,4,10,13-tetraphenylcyclooctadeca-1,2,3,7,8,9,13,14,15-nonaen-5,11,17-triyne (**10d**).* [6]Pericyclynediol **8d** (0.029 mmol, 28 mg), anhydrous $SnCl_2$ (0.290 mmol, 55 mg), HCl (0.580 mmol, 2 M

DOI: 10.1021/acs.joc.6b02397
J. Org. Chem. 2017, 82, 925−935

in Et_2O), and CH_2Cl_2 (30 mL) were mixed. Chromatography over silica gel eluted with pentane:DCM 7:2 afforded **10d** as a dark violet solid (0.012 mmol, 9 mg, 40%).

^{1}H NMR (400 MHz, CD_2Cl_2) δ 9.84 (s, 1H), 9.56−9.53 (2d, $^3J_{HH}$ = 7.6 Hz, 8H), 8.00 (t, $^3J_{HH}$ = 7.6 Hz, 8H), 7.76−7.70 (m, 4H), 4.74 (t, $^3J_{HH}$ = 7.6 Hz, 2H), 3.07−2.98 (quint; $^3J_{HH}$ = 7.6 Hz, 2H), 1.98−1.90 (quint;$^3J_{HH}$ = 7.6 Hz, 2H), 1.76−1.69 (quint; $^3J_{HH}$ = 7.6 Hz, 2H), 1.49−1.43 (quint; $^3J_{HH}$ = 7.6 Hz, 2H), 1.23 (bs, 28H), 0.89−0.83 (t, $^3J_{HH}$ = 7.6 Hz, 3H).

^{13}C{^{1}H} NMR (101 MHz, $CDCl_3$) δ 139.9, 139.6, 130.1, 129.9, 129.8, 129.7, 129.6, 129.4, 123.1, 122.0, 120.0, 119.6, 116.5, 115.9, 107.6, 105.2, 103.1, 87.2, 41.0, 31.9, 30.9, 29.8−29.3, 22.7, 14.1.

HRMS (MALDI-TOF/DCTB): m/z [M]$^+$ calcd for $C_{62}H_{62}$ 806.4852, found 806.4829; m/z [M + Na]$^+$ calcd for $C_{62}H_{62}Na$ 829.4749, found 829.4828.

UV−vis ($CHCl_3$): λ_{max} = 445 nm (ε = 194 000 L·mol^{-1}·cm^{-1}).

Melting−decomposition temperature: 163 °C.

*1,4,10,13-Tetraphenyl-7-(3,3,4,4,5,5,6,6,7,7,8,8,8-tridecafluorooctyl)cyclooctadeca-1,2,3,7,8,9,13, 14,15-nonaen-5,11,17-triyne (**10e**).* [6]Pericyclynediol **8e** (0.034 mmol, 35 mg), anhydrous $SnCl_2$ (0.34 mmol, 65 mg), HCl (0.68 mmol, 2 M in Et_2O), and CH_2Cl_2 (20 mL) were mixed. Chromatography over silica gel eluted with pentane:DCM 5:1 afforded **10e** as a dark red solid (0.006 mmol, 5 mg, 12%).

^{1}H NMR (400 MHz, $CDCl_3$) δ 9.80 (s, 1H), 9.54−9.48 (2d, $^3J_{HH}$ = 7.3 Hz, 8H), 7.97 (t, $^3J_{HH}$ = 7.3 Hz, 8H), 7.72 (td, $^3J_{HH}$ = 7.3 Hz, $^4J_{HH}$ = 1.5 Hz, 4H), 5.05−4.96 (m, 2H), 4.01−3.83 (m, 2H).

^{13}C{^{1}H} NMR (101 MHz, $CDCl_3$) δ 139.5, 139.4, 130.2, 129.9, 129.8, 129.7, 123.3−116.4, 105.6, 103.8, 101.5, 87.8, 31.2, 29.7. In the absence of {^{19}F} decoupling, the signals of the fluorinated carbon atoms, expected to be multiplets of high order, are not observed.

^{19}F NMR (376 MHz, $CDCl_3$) δ −80.6, −113.5 to −113.6, −121.5, −122.6, −123.0 to −123.1, −125.9 to −126.0.

HRMS (MALDI-TOF/DCTB): m/z [M]$^+$ calcd for $C_{50}H_{25}F_{13}$ 872.1749, found 872.1754; m/z [M + Na]$^+$ calcd for $C_{50}H_{25}F_{13}Na$ 895.1646, found 895.1623.

UV−vis ($CHCl_3$): λ_{max} = 445 nm (ε = 219 000 L·mol^{-1}·cm^{-1}).

Melting−decomposition temperature: 192 °C.

*4.3.7. Details for the Doubly Lipidic Carbo-benzenes **11a−e**.*

*1,10-Diethyl-4,7,13,16-tetraphenylcyclooctadeca-1,2,3,7,8,9,13,14,15-nonaen-5,11,17-triyne (**11a**).* [6]Pericyclynediol **6a** (0.048 mmol, 50 mg), $SnCl_2$ (0.48 mmol, 128 mg), anhydrous HCl (0.95 mmol, 2 M in Et_2O), and CH_2Cl_2 (40 mL) were mixed. Purification by washing on glass cotton with DCM and pentane afforded **11a** as a dark blue solid (0.034 mmol, 20 mg, 71%).

^{1}H NMR (400 MHz, $CDCl_3$) δ 9.53 (d, $^3J_{HH}$ = 8.0 Hz, 8H), 7.99 (pseudo-t, $^3J_{HH}$ = 8.0 Hz, 8H), 7.72 (t, $^3J_{HH}$ = 8.0 Hz, 4H), 4.75 (q, $^3J_{HH}$ = 7.6 Hz, 4H), 2.53 (t, $^3J_{HH}$ = 7.6 Hz, 6H).

CP/MAS ^{13}C NMR (100 MHz) δ 137.3, 127.1, 118.1, 114.1, 102.5, 100.3, 27.9, 8.6.

HRMS (MALDI-TOF/DCTB): m/z [M]$^+$ calcd for $C_{46}H_{30}$ 582.2342, found 582.2326.

UV−vis ($CHCl_3$): λ_{max} = 446 nm (ε = 187 000 L·mol^{-1}·cm^{-1}).

Melting−decomposition temperature: 208 °C.

*1,10-Dioctyl-4,7,13,16-tetraphenylcyclooctadeca-1,2,3,7,8,9,13,14,15-nonaen-5,11,17-triyne (**11b**).* [6]Pericyclynediol **6b** (0.099 mmol, 90 mg), anhydrous $SnCl_2$ (0.99 mmol, 188 mg), HCl (1.98 mmol, 2 M in Et_2O), and CH_2Cl_2 (50 mL) were mixed. Chromatography over silica gel eluted with pentane:DCM 3:1 afforded **11b** as a dark violet solid (0.031 mmol, 23 mg, 31%).

^{1}H NMR (400 MHz, $CDCl_3$) δ 9.54 (dd, $^3J_{HH}$ = 8.2 Hz, $^4J_{HH}$ = 1.2 Hz, 8H), 7.96 (pseudo-t, $^3J_{HH}$ = 8.2 Hz, 8H), 7.73 (t, $^3J_{HH}$ = 8.2 Hz, 4H), 4.68 (t, $^3J_{HH}$ = 7.5 Hz, 4H), 2.99 (quint, $^3J_{HH}$ = 7.5 Hz, 4H), 1.92 (quint, $^3J_{HH}$ = 7.5 Hz, 4H), 1.67 (quint, $^3J_{HH}$ = 7.5 Hz, 4H), 1.45 (m, 4H), 1.35−1.28 (m, 8H), 0.86 (t, $^3J_{HH}$ = 7.5 Hz, 6H).

^{13}C{^{1}H} NMR (101 MHz, $CDCl_3$) δ 139.9, 129.9, 129.8, 129.3, 122.1, 119.4, 116.0, 106.6, 103.0, 40.7, 32.0, 31.8, 29.7, 29.6, 29.3, 22.7, 14.1.

HRMS (MALDI-TOF/DCTB): m/z [M]$^+$ calcd for $C_{58}H_{54}$ 750.4220, found 750.4240.

UV−vis ($CHCl_3$): λ_{max} = 446.5 nm (ε = 196 000 L·mol^{-1}·cm^{-1}).

Melting−decomposition temperature: 188 °C.

*1,4,10,13-Tetraphenyl-7,16-ditetradecylcyclooctadeca-1,2,3,7,8,9,13,14,15-nonaen-5,11,17-triyne (**11c**).* [6]Pericyclynediol **6c** (0.037 mmol, 40 mg), anhydrous $SnCl_2$ (0.370 mmol, 71 mg), HCl (0.740 mmol, 2 M in Et_2O), and CH_2Cl_2 (20 mL) were mixed. Chromatography over silica gel eluted with pentane:DCM 95:5 afforded **11c** as a dark blue solid (0.012 mmol, 11 mg, 32%).

^{1}H NMR (400 MHz, $CDCl_3$) δ 9.51 (dd, $^3J_{HH}$ = 7.7, $^4J_{HH}$ = 1.3 Hz, 8H), 7.96 (t, $^3J_{HH}$ = 7.7 Hz, 8H), 7.69 (t, $^3J_{HH}$ = 7.7 Hz, 4H), 4.69 (t, $^3J_{HH}$ = 7.3 Hz, 4H), 3.01 (quint, $^3J_{HH}$ = 7.3 Hz, 4H), 1.94 (quint, $^3J_{HH}$ = 7.3 Hz, 4H), 1.72 (quint, $^3J_{HH}$ = 7.3 Hz, 4H), 1.46−1.39 (m, 4H), 1.22 (bs, 32H), 0.85 (t, $^3J_{HH}$ = 7.3 Hz, 6H).

^{13}C{^{1}H} NMR (75 MHz, CD_2Cl_2) δ 139.9, 129.8, 129.7, 129.3, 122.1, 119.4, 116.0, 106.6, 103.1, 40.7, 31.9, 31.8, 29.6−29.8, 29.4, 22.7, 14.1.

HRMS (MALDI-TOF/DCTB): m/z [M]$^+$ calcd for $C_{70}H_{78}$ 918.6098, found 918.6088.

UV−vis ($CHCl_3$): λ_{max} = 446 nm (ε = 206 000 L·mol^{-1}·cm^{-1}).

Melting−decomposition temperature: 170 °C.

*1,10-Diicosyl-4,7,13,16-tetraphenylcyclooctadeca-1,2,3,7,8,9,13,14,15-nonaen-5,11,17-triyne (**11d**).* [6]Pericyclynediol **6d** (0.040 mmol, 50 mg), anhydrous $SnCl_2$ (0.400 mmol, 76 mg), HCl (0.800 mmol, 2 M in Et_2O), and CH_2Cl_2 (20 mL) were mixed. Chromatography over silica gel eluted with pentane:DCM 4:1 afforded **11d** as a dark red solid (0.011 mmol, 12 mg, 28%).

^{1}H NMR (400 MHz, $CDCl_3$) δ 9.59−9.45 (d, $^3J_{HH}$ = 7.7 Hz, 8H), 7.96 (t, $^3J_{HH}$ = 7.7 Hz, 8H), 7.70 (t, $^3J_{HH}$ = 7.7, 4H), 4.68 (t, $^3J_{HH}$ = 7.5 Hz, 4H), 3.08−2.91 (quint, $^3J_{HH}$ = 7.5 Hz, 4H), 1.92 (quint, $^3J_{HH}$ = 7.5 Hz, 4H), 1.76−1.66 (quint, $^3J_{HH}$ = 7.5 Hz, 4H), 1.48−1.41 (m, 4H), 1.39−1.18 (bs, 56H), 0.90−0.85 (t, $^3J_{HH}$ = 7.5 Hz, 6H).

^{13}C{^{1}H} NMR (101 MHz, $CDCl_3$) δ 139.9, 129.9, 129.7, 129.3, 122.0, 119.4, 116.0, 106.6, 103.0, 40.7, 31.9, 31.8, 29.8−29.4, 22.7, 14.1.

HRMS (MALDI-TOF/DCTB): m/z [M + Na]$^+$ calcd for $C_{82}H_{102}Na$ 1109.7873, found 1109.7874.

UV−vis ($CHCl_3$): λ_{max} = 446.6 nm (ε = 196 000 L·mol^{-1}·cm^{-1}).

Melting−decomposition temperature: 149 °C.

*1,4,10,13-Tetraphenyl-7,16-bis(3,3,4,4,5,5,6,6,7,7,8,8,8-tridecafluorooctyl)cyclooctadeca-1,2,3,7,8,9,13,14,15-nonaen-5,11,17-triyne (**11e**).* [6]Pericyclynediol **6e** (0.044 mmol, 60 mg), anhydrous $SnCl_2$ (0.44 mmol, 83 mg), HCl (0.87 mmol, 2 M in Et_2O), and CH_2Cl_2 (30 mL) were mixed. Chromatography over silica gel eluted with pentane/DCM 4:1 afforded **11e** as a dark red solid (0.006 mmol, 7 mg, 13%).

^{1}H NMR (400 MHz, $CDCl_3$) δ 9.50 (d, $^3J_{HH}$ = 7.7 Hz, 8H), 7.96 (t, $^3J_{HH}$ = 7.7 Hz, 8H), 7.73 (t, $^3J_{HH}$ = 7.7 Hz, 4H), 5.01−4.87 (m, 4H), 3.98−3.77 (m, 4H).

^{13}C{^{1}H} NMR (101 MHz, $CDCl_3$) δ 139.4, 129.9, 129.9, 129.8, 121.1, 119.7, 116.4, 104.1, 101.1, 32.8, 31.0. In the absence of {^{19}F} decoupling, the signals of the fluorinated carbon atoms, expected to be multiplets of high order, are not observed

^{19}F NMR (376 MHz, $CDCl_3$) δ −80.6 to −80.7, −113.5 to −113.6, −121.5, −121.6, −122.6, −123.0 to −123.1, −125.9 to −126.0.

HRMS (MALDI-TOF/DCTB): m/z [M]$^+$ calcd for $C_{58}H_{28}F_{26}$ 1218.1776, found 1218.1691.

UV−vis ($CHCl_3$): λ_{max} = 446 nm (ε = 201 000 L·mol^{-1}·cm^{-1}).

Melting−decomposition temperature: 196 °C.

■ ASSOCIATED CONTENT

Supporting Information

The Supporting Information is available free of charge on the ACS Publications website at DOI: 10.1021/acs.joc.6b02397.

^{1}H, ^{13}C, and ^{19}F NMR spectra for all new compounds, crystallographic data of **11a−d**, **10b**, **10d**, and **11e**, UV−vis spectra of **10a**, **10b**, **10d**, **10e**, and **11a−d** in the solid state (PDF)

(CIF)

DOI: 10.1021/acs.joc.6b02397
J. Org. Chem. 2017, 82, 925−935

AUTHOR INFORMATION

Corresponding Authors

*E-mail: valerie.maraval@lcc-toulouse.fr.

*E-mail: chauvin@lcc-toulouse.fr.

ORCID

Remi Chauvin: 0000-0002-4491-6390

Notes

The authors declare no competing financial interest.

ACKNOWLEDGMENTS

C.Z. thanks the China Scholarship Council for his Ph.D. scholarship. The ANR program (ANR-11-BS07-016-01) is acknowledged for the postdoctoral fellowship of A.R. and for funding. R.C. thanks the Centre National de la Recherche Scientifique (CNRS) for half a teaching sabbatical in 2015−2016. The authors also thank Dr. Yannick Coppel for the CP-MAS NMR analysis of **11a** and Dr. Nathalie Saffon-Merceron for the X-ray diffraction analysis of **11c**.

REFERENCES

(1) (a) Baughman, R. H.; Eckhardt, H.; Kertesz, M. *J. Chem. Phys.* **1987**, *87*, 6687−6699. (b) Malko, D.; Neiss, C.; Vines, F.; Gorling, A. *Phys. Rev. Lett.* **2012**, *108*, 086804. (c) Kim, B. G.; Choi, H. J. *Phys. Rev. B: Condens. Matter Mater. Phys.* **2012**, *86*, 115435. (d) Ivanovskii, A. L. *Prog. Solid State Chem.* **2013**, *41*, 1−19. (e) Han, N.; Liu, H.; Zhou, S.; Zhao, J. *J. Phys. Chem. C* **2016**, *120*, 14699−14705.

(2) Li, Y.; Xu, L.; Liu, H.; Li, Y. *Chem. Soc. Rev.* **2014**, *43*, 2572−2586.

(3) Ducere, J.-M.; Lepetit, C.; Chauvin, R. *J. Phys. Chem. C* **2013**, *117*, 21671−21681.

(4) In *Carbon Nanotubes: Synthesis, Properties and Applications*; Dresselhaus, M., Dresselhaus, G., Avouris, P., Eds; Springer, 2001.

(5) Segawa, Y.; Ito, H.; Itami, K. *Nat. Mater.* **2016**, *1*, 15002.

(6) (a) Kehoe, J. M.; Kiley, J. H.; English, J. J.; Johnson, C. A.; Petersen, R. C.; Haley, M. M. *Org. Lett.* **2000**, *2*, 969−972. (b) Yoshimura, T.; Inaba, A.; Sonoda, M.; Tahara, K.; Tobe, Y.; Williams, R. V. *Org. Lett.* **2006**, *8*, 2933−2936. (c) Johnson, C. A., II; Lu, Y.; Haley, M. M. *Org. Lett.* **2007**, *9*, 3725−3728. (d) Haley, M. M. *Pure Appl. Chem.* **2008**, *80*, 519−532.

(7) (a) Wan, W. B.; Haley, M. M. *J. Org. Chem.* **2001**, *66*, 3893−3901. (b) Marsden, J. A.; Haley, M. M. *J. Org. Chem.* **2005**, *70*, 10213−10226.

(8) Cocq, K.; Saffon-Merceron, N.; Coppel, Y.; Poidevin, C.; Maraval, V.; Chauvin, R. *Angew. Chem., Int. Ed.* **2016**, *55*, 15133−15136.

(9) (a) Chauvin, R. *Tetrahedron Lett.* **1995**, *36*, 397−400. (b) Maraval, V.; Chauvin, R. *Chem. Rev.* **2006**, *106*, 5317−5343.

(10) (a) Kuwatani, Y.; Watanabe, N.; Ueda, I. *Tetrahedron Lett.* **1995**, *36*, 119−122. (b) Suzuki, R.; Tsukuda, H.; Watanabe, N.; Kuwatani, Y.; Ueda, I. *Tetrahedron* **1998**, *54*, 2477−2496. (c) Cocq, K.; Lepetit, C.; Maraval, V.; Chauvin, R. *Chem. Soc. Rev.* **2015**, *44*, 6535−6559. (d) Barthes, C.; Rives, A.; Maraval, V.; Chelain, E.; Brigaud, T.; Chauvin, R. *French-Ukrainian J. Chem.* **2015**, *3*, 60−65.

(11) Li, Z.; Smeu, M.; Rives, A.; Maraval, V.; Chauvin, R.; Ratner, M. A.; Borguet, E. *Nat. Commun.* **2015**, *6*, 6321−6329.

(12) Baglai, I.; de Anda-Villa, M.; Barba-Barba, R. M.; Poidevin, C.; Ramos-Ortíz, G.; Maraval, V.; Lepetit, C.; Saffon-Merceron, N.; Maldonado, J.-L.; Chauvin, R. *Chem. - Eur. J.* **2015**, *21*, 14186−14195.

(13) Cocq, K.; Maraval, V.; Saffon-Merceron, N.; Saquet, A.; Poidevin, C.; Lepetit, C.; Chauvin, R. *Angew. Chem., Int. Ed.* **2015**, *54*, 2703−2706.

(14) Zhu, C.; Duhayon, C.; Maraval, V.; Chauvin, R. Unpublished results.

(15) Cocq, K.; Saffon-Merceron, N.; Poater, A.; Maraval, V.; Chauvin, R. *Synlett* **2016**, *27*, 2105−2112.

(16) (a) Saccavini, C.; Tedeschi, C.; Maurette, L.; Sui-Seng, C.; Zou, C.; Soleilhavoup, M.; Vendier, L.; Chauvin, R. *Chem. - Eur. J.* **2007**, *13*, 4895−4913. (b) Leroyer, L.; Zou, C.; Maraval, V.; Chauvin, R. *C. R. Chim.* **2009**, *12*, 412−429. For early references on pericyclynes, see: (c) Scott, L. T.; DeCicco, G. J.; Hyun, J. L.; Reinhardt, G. *J. Am. Chem. Soc.* **1983**, *105*, 7760−7761. (d) Scott, L. T.; DeCicco, G. J.; Hyun, J. L.; Reinhardt, G. *J. Am. Chem. Soc.* **1985**, *107*, 6546−6555.

(17) (a) Morrison, J. D.; Tomaszewski, J. E.; Mosher, H. S.; Dale, J.; Miller, D.; Elsenbaumer, R. L. *J. Am. Chem. Soc.* **1977**, *99*, 3167−3168. (b) Ashby, E. C.; Goel, A. B. *J. Am. Chem. Soc.* **1981**, *103*, 4983−4985.

(18) (a) Canonne, P.; Foscolos, G.; Caron, H.; Lemay, G. *Tetrahedron* **1982**, *38*, 3563−3568. (b) Imamoto, T.; Takiyama, N.; Nakamura, K.; Hatajima, T.; Kamiya, Y. *J. Am. Chem. Soc.* **1989**, *111*, 4392−4398.

(19) Cocq, K.; Maraval, V.; Saffon-Merceron, N.; Chauvin, R. *Chem. Rec.* **2015**, *15*, 347−361.

(20) Schleyer, P. v. R.; Maerker, C.; Dransfeld, A.; Jiao, H. J.; Hommes, J. R. V. *J. Am. Chem. Soc.* **1996**, *118*, 6317−6318.

(21) Lepetit, C.; Godard, C.; Chauvin, R. *New J. Chem.* **2001**, *25*, 572−580.

(22) (a) For di-*n*-octyl-benzene, see: Bramborg, A.; Linker, T. *Adv. Synth. Catal.* **2010**, *352*, 2195−2199. (b) For di-*n*-tetradecyl-benzene, see: Huang, W. Y.; Gao, W.; Kwei, T. K.; Okamoto, Y. *Macromolecules* **2001**, *34*, 1570−1578.

(23) If n denotes the rank of the CH_2 group (starting from $n = 1$ in α position to the C_{18} ring), for **11b** a curve fit with an exponential decay gives $\delta_H \approx 1.256 + 4.995 \exp[-1.333n]$ ppm, $R \approx 0.994$; for the parent dioctylbenzene,[22a] the curve fit gives $\delta_H \approx 1.250 + 7.184 \exp[-0.734n]$ ppm, $R \approx 0.999$.

(24) Balci, M. *Basic ^{1}H-^{13}C NMR Spectroscopy*; Elsevier: Amsterdam, 2005. On p 285 it is stated "In the ^{13}C NMR spectroscopy, the ring current effect is less important [than in the ^{1}H NMR spectroscopy], as it contributes only a little to the total shielding (2 ppm), which is generally hidden by other larger effects". In absolute value, this effect is in the same range as the one operating in ^{1}H NMR (2−3 ppm). The relative weakness of the ring current effect in ^{13}C NMR (also observed in ^{19}F NMR) can thus also be related to the larger width of the chemical shift windows (220 ppm for ^{13}C, 350 ppm for ^{19}F) as compared to the ^{1}H nucleus (15 ppm).

(25) (a) Gunter, H.; Schmickler, H. In *The Chemistry of Nonbenzenoid Aromatic Compounds II*; Kreher, R., Darmstadt, T. H., Eds.; Butterworth Co. Ltd.: London, 1975; pp 807−828 and references therein. (b) du Vernet, R.; Boekelheide, V. *Proc. Natl. Acad. Sci. U. S. A.* **1974**, *71*, 2961−2964.

(26) Dolbier, W. R. *Guide to Fluorine NMR for Organic Chemists*; Wiley: New York, 2009.

(27) Gouterman, M. *J. Mol. Spectrosc.* **1961**, *6*, 138−163.

(28) Kitamura, C.; Abe, Y.; Ohara, T.; Yoneda, A.; Kawase, T.; Kobayashi, T.; Naito, H.; Komatsu, T. *Chem. - Eur. J.* **2010**, *16*, 890−898.

(29) CCDC 1494584−1494589 (**11a**−**11d**·CH_2Cl_2, **10b**, **10d**) and 1494840 (**11d**·$CHCl_3$) and 1501523 (**10b**, allotrope) contain the supplementary crystallographic data for this paper. The data can be obtained free of charge from the Cambridge Crystallographic Data Centre via http://www.ccdc.cam.ac.uk/getstructures.

(30) Ninković, D. B.; Andrić, J. M.; Malkov, S. N.; Zarić, S. D. *Phys. Chem. Chem. Phys.* **2014**, *16*, 11173−11177.

(31) Shishkin, O. V.; Zubatyuk, R. I.; Dyakonenko, V. V.; Lepetit, C.; Chauvin, R. *Phys. Chem. Chem. Phys.* **2011**, *13*, 6837−6848.

(32) Turias, F.; Poater, J.; Chauvin, R.; Poater, A. *Struct. Chem.* **2016**, *27*, 249−259.

Article 4

NRC Research Press

ARTICLE

Selective access to *p*-dialkyl-*carbo*-benzenes from a [6]pericyclynedione: the *n*-butyl nucleophile model for a metal switch study

Chongwei Zhu, Carine Duhayon, Alix Saquet, Valérie Maraval, and Remi Chauvin

Abstract: The synthesis, spectroscopic properties, comparative electrochemical behavior in $CHCl_3$ vs CH_2Cl_2, and X-ray crystal structure of *p*-di-*n*-butyl-tetraphenyl-*carbo*-benzene are described. The selectivity of preparation of the ultimate [6]pericyclynediol precursor has been examined by comparing the reactivity of the [6]pericyclynedione substrate with four *n*-Bu-MX_n nucleophiles involving more or less halogenated metal centers MX_n ($0 \le n \le 2$): Li, MgBr, MgCl, $CeCl_2$/LiCl. The cerium reagent is found to be the most efficient, giving approximately twice the yield given by Grignard reagents in the target diadduct (90% vs 51%–53%). The dibutyl-*carbo*-benzene product happens to be soluble in both $CHCl_3$ and CH_2Cl_2: cyclic voltammograms of either solution exhibit almost identical peak potentials with reduced reversibility of the redox processes in $CHCl_3$.

Key words: alkylcerium, alkyne, aromatics, *carbo*-benzene, *carbo*-mer.

Résumé : Nous décrivons la synthèse du *p*-di-*n*-butyl-tétraphényl-*carbo*-benzène, ainsi que ses propriétés spectroscopiques, son comportement électrochimique comparatif dans le $CHCl_3$ p/r au CH_2Cl_2 et sa structure cristalline, déterminée par radiocristallographie. Nous avons examiné la sélectivité de la synthèse du dernier précurseur, le [6]péricyclynediol, en comparant les réactivités d'un substrat précurseur, une [6]péricyclynedione, avec quatre nucléophiles de formule *n*-Bu-MX_n dont les centres métalliques M sont plus ou moins halogénés, où MX_n ($0 \le n \le 2$) = Li, MgBr, MgCl, $CeCl_2$/LiCl. Le réactif à base de cérium s'est révélé le plus efficace, le rendement en diadduit cible étant d'environ le double des rendements obtenus avec les réactifs de Grignard (90 % p/r à 51–53 %). Il se trouve que le dibutyl-*carbo*-benzène généré est soluble tant dans le $CHCl_3$ que dans le CH_2Cl_2 : les diagrammes de voltampérométrie cyclique des deux solutions présentent des potentiels de crête presque identiques, la réversibilité des processus rédox étant toutefois réduite dans le cas du $CHCl_3$. [Traduit par la Rédaction]

Mots-clés : alkylcérium, alcyne, aromatiques, *carbo*-benzène, *carbo*-mère.

Introduction

Among π-conjugated carbon allotropes and beyond the foremost graphene type, graphynic materials, composed of both sp^2-C and sp-C atoms, have been considered at the theoretical level[1] but have been more sparingly studied at the experimental level. Nevertheless, several molecular fragments of γ-graphyne,[2] γ-graphdiyne,[3] and even α-graphyne[4] have been described. A key issue in the synthesis and study of such carbon-rich compounds is their limiting solubility, approaching that of graphite upon increase of the size of the carbon core within a C–H bond periphery. As a solution, peripheral decoration by lipophilic groups is currently envisaged. This can be illustrated by the recent report of a ring *carbo*-mer of naphthalene,[5] with eight *p*-pentylphenyl substituents of the C_{32} core having allowed full characterization of this first example of fused polycyclic α-graphyne fragment, in or from solutions in $CHCl_3$.[4] However, the solubilizing effect of the *p*-pentylphenyl groups appeared limited, even on the smaller *carbo*-benzene congener $C_{18}(4\text{-}n\text{-}C_5H_{11}\text{-}C_6H_4)_6$. The *carbo*-benzene C_{18} ring is actually the smallest cyclic primitive motif of α-graphyne, and most of the derivatives reported hitherto bear only H, aryl, or alkynyl substituents.[6] Very recently, direct anchoring of alkyl chains at the sp^2 vertices of the C_{18} ring was envisaged in a series of *p*-dialkyl-tetraphenyl-*carbo*-benzenes **1a–1e**, which could be obtained in two steps, namely by addition of alkylmagnesium bromides to the [6]pericyclynedione **2** followed by reductive aromatization of the [6]pericyclynediol products **3a–3e** (Scheme 1).[7] However, the Grignard approach was not found to be selective, and beside the diadducts **3a–3e**, the single and double reductions products **4a–4e** (resulting from the monoadduct) and **5** are also formed. The reducing power of alkyl Grignard reagents is actually known to be due to the presence of a H atom in β position of the Mg atom,[8] but several recommended methods to overcome this effect, e.g., through the change of solvent, failed to improve the reaction outcome. The use of alternative or additive metals should thus be envisaged.

In general nucleophilic addition of Nu–MX_n to carbonyl groups, beyond lithium (M = Li, $n = 0$) and magnesium (M = Mg, $n = 1$, X = Br, Cl, I) cations, cerium cations (M = Ce, $n = 2$, X = Cl) have also been reported to provide higher selectivity under smooth conditions.[9] In the present context, targeting the [6]pericyclynediols **6a–6b** from the bis-terminal tetrayne **7a–7b** and dialdehyde **8**, while reactions of the $MgBr^+$ salts alone appeared almost unproductive (0%–6%),[6a,6b,6h] addition of $CeCl_3$ was shown to improve the yield to 12%–14%, likely via the corresponding $CeCl_2^+$ salts (Scheme 2).

Received 1 December 2016. Accepted 9 January 2017.

C. Zhu, C. Duhayon, A. Saquet, V. Maraval, and R. Chauvin. CNRS, LCC (Laboratoire de Chimie de Coordination), 205 route de Narbonne, BP 44099, 31077 Toulouse Cedex 4, France; Université de Toulouse, UPS, ICT-FR 2599, 118 route de Narbonne, 31062 Toulouse Cedex 9, France.

Corresponding authors: Valérie Maraval (email: valerie.maraval@lcc-toulouse.fr) and Remi Chauvin (email: chauvin@lcc-toulouse.fr).

This paper is part of a Special issue to honor Professor Reginald Mitchell.

Dedicated to Prof. Reginald H. Mitchell on the occasion of its retirement and prospect of a long remaining life in inspiring the design and study of novel aromatic compounds.

Scheme 1. Last two steps of previous syntheses of *p*-dialkyl-*carbo*-benzenes. The intermediates **2–5** were used as mixtures of stereoisomers.

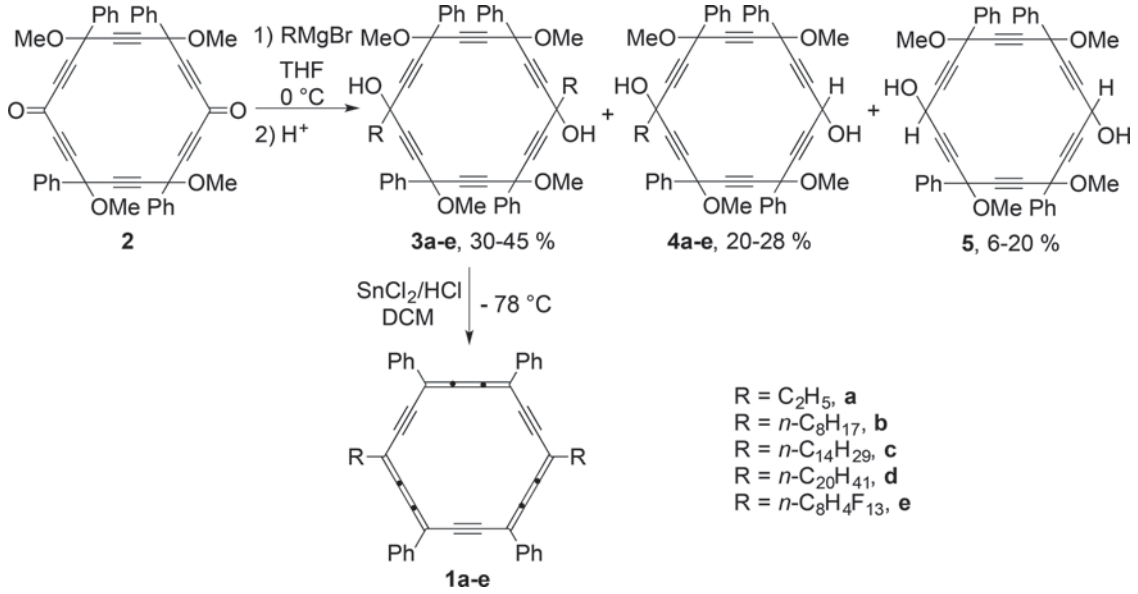

Scheme 2. Improvement of a [11+7] macrocyclization from a C11 tetrayne and a C7 dialdehyde through the use of a cerium(III) reagent.

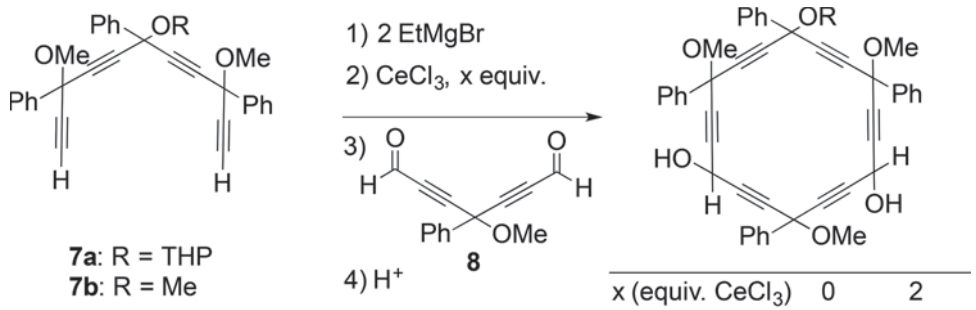

x (equiv. $CeCl_3$)	0	2
6a: R = THP	6 %	14 %
6b: R = Me	0%	12 %

As part of ongoing efforts to improve access efficiency to *carbo*-benzene molecules, the study of the metal effect on the double nucleophilic addition to the diketone **2** has been undertaken for Nu = *n*-Bu, a model nucleophile of intermediate length, with the view to obtaining the hitherto unknown representative *p*-di-*n*-butyl-tetraphenyl-*carbo*-benzene **1f**. This target, bearing both aliphatic and aromatic substituents, is also devised to serve as a standard for electrochemical studies in the *carbo*-benzene series.

Experimental

General

THF was dried with a PureSolv MD5 Innovative Technology system for the purification of solvents. All other reagents were used as commercially available. In particular, commercial solutions of *n*-BuLi were 2.5 mol/L in hexane, and solutions of HCl were 2 mol/L in diethyl ether. All reactions were carried out under argon atmosphere using Schlenk tube and vacuum line techniques. Column chromatography was carried out on silica gel (60 Å, 70–200 μm). Silica gel thin layer chromatography plates (60F254, 0.25 mm) were revealed under UV light and (or) by treatment with an ethanolic solution of phosphomolybdic acid (20%). The following analytical instruments were used: ^{1}H and ^{13}C NMR spectroscopy: Avance 300, Avance 400, and Avance 400 HD; mass spectrometry: Quadrupolar Nermag R10–10H; UV–vis absorption: Perkin-Elmer UV–vis Win-Lab Lambda 950; X-ray diffraction: Apex2 Bruker, micro-focus X-ray source (Mo Kα radiation). NMR chemical shifts are given in ppm with positive values to high frequency relative to the tetramethylsilane reference. Coupling constants (*J*) are given in Hertz. UV–vis absorption wavelengths (λ) are given in nanometers, and the corresponding maximum extinction molar coefficient (ε) is given in L mol^{-1} cm^{-1}.

Crystal structure determination

Intensity diffraction data for **1f** were collected at 100 K. The structure was solved by direct methods using SIR92 and refined by full-matrix least-square procedures on *F* using the programs of the PC version of CRYSTALS.[10] Atomic scattering factors were taken from the International Tables for X-ray Crystallography.[11] All non-hydrogen atoms were refined anisotropically. Hydrogen atoms were refined using a riding model. Absorption corrections were introduced using the program MULTISCAN.

Voltammetric measurements

Voltammetric measurements were carried out with a potentiostat Autolab PGSTAT100 controlled by GPES 4.09 software. Experiments were performed at room temperature in a homemade, air-tight, three-electrode cell connected to a vacuum/argon line. The reference electrode consisted of a saturated calomel electrode (SCE) separated from the solution by a bridge compartment. The counter electrode was a platinum wire of approximately 1 cm^2

Published by NRC Research Press

apparent surface. The working electrode was a Pt microdisk (diameter, 0.5 mm). The supporting electrolyte [n-Bu_4N][PF_6] was used as received (Fluka, 99% electrochemical grade) and simply degassed under argon. The solutions used in the electrochemical study were 10^{-3} mol/L in *carbo*-benzene and 0.1 mol/L in supporting electrolyte. Before each measurement, the solutions were degassed by bubbling argon, and the working electrode was polished with a polishing machine (Presi P230). Typical instrumental parameters for recording square-wave voltammograms were as follows: SW frequency (f) = 20 Hz, SW amplitude (E_{sw}) = 20 mV, and scan increment (dE) = 5 mV.

Experimental characterizations and procedures of new products

Characterization of 1,10-dibutyl-4,7,13,16-tetraphenylcyclooctadeca-1,2,3,7,8,9,13,14,15-nonaen-5,11,17-triyne (1f)

A solution of [6]pericyclynediol **3f** (50 mg, 0.063 mmol) in dichloromethane (DCM, 30 mL) was treated with $SnCl_2$ (120 mg, 0.63 mmol) and HCl (1.26 mmol, 2 mol/L in Et_2O) at –78 °C. The mixture was stirred at –78 °C for 10 min and then at room temperature for 20 min. After treatment with 1 mol/L aqueous NaOH (1.26 mL) and filtration through Celite®, the organic layer was washed with brine (three times), dried over $MgSO_4$, and concentrated under reduced pressure. The residue was purified by chromatography on silica gel (pentane:DCM, 4:1) to give **1f** as a dark red solid (25 mg, 0.04 mmol, 63% yield).

^{1}H NMR (400 MHz, $CDCl_3$) δ 9.51 (dd, $^3J_{HH}$ = 8.0, $^4J_{HH}$ = 1.2 Hz, 8H, *o*-C_6H_5), 7.97 (dd, $^3J_{HH}$ = 8.2, 7.2 Hz, 8H, *m*-C_6H_5Pr), 7.73–7.66 (m, 4H, *p*-C_6H_5), 4.69 (t, $^3J_{HH}$ = 7.5 Hz, 4H, CH_2Pr), 3.04–2.92 (m, 4H, CH_2CH_2Me), 2.02–1.91 (m, 4H, CH_2Me), 0.91–0.82 (m, 6H, CH_3).

^{13}C{^{1}H} NMR (101 MHz, $CDCl_3$) δ 139.9 (*i*-C_6H_5), 129.8 (*o*-C_6H_5), 129.8 (*m*-C_6H_5), 129.3 (*p*-C_6H_5), 122.1, 119.4, 116.0 (=*C*=*C*=, *C*≡*C*), 106.5 (*C*–Bu), 103.0 (*C*–Ph), 40.4 (CH_2Pr), 34.0 (CH_2Et), 22.8 (CH_2Me), 14.3 (CH_3).

HRMS (MALDI-TOF/DCTB) (*m*/*z*): [M]$^+$ calcd for $C_{50}H_{38}$, 638.2974; found, 638.3000; [M+Na]$^+$ calcd for $C_{50}H_{38}Na$, 661.2871; found, 661.2931.

UV–vis ($CHCl_3$): λ_{max} = 446.45 nm (ε = 208 000 L mol^{-1} cm^{-1}).

Melting–decomposition temperature: 188 °C.

Characterization of 1-butyl-4,7,13,16-tetramethoxy-4,7,13,16-tetraphenylcyclooctadeca-2,5,8,11,14, 17-hexayne-1,10-diol (4f), a side product obtained during the preparation of 3f

^{1}H NMR (400 MHz, $CDCl_3$) δ 7.81–7.64 (m, 8H, *o*-C_6H_5), 7.45–7.31 (m, 12H, *m*-, *p*-C_6H_5), 5.43–5.24 (m, 1H, *CH*OH), 3.64–3.33 (m, 12H, O*CH*$_3$), 2.91–2.31 (m, 2H, O*H*), 2.07–1.95 (m, 2H, CH_2Pr), 1.76–1.60 (m, 2H, CH_2Et), 1.41–1.30 (m, 2H, CH_2Me), 0.93–0.82 (m, 3H, CH_3).

^{13}C{^{1}H} NMR (101 MHz, $CDCl_3$) δ 139.48 (*i*-C_6H_5), 129.10 (*p*-C_6H_5), 128.53 (*m*-C_6H_5), 126.46 (*o*-C_6H_5), 87.10, 84.67, 82.91 (*C*≡*C*), 75.96, 72.98 (*C*(OMe)Ph), 63.71 (*C*(OH)Bu), 53.36–53.31 (O*CH*$_3$), 53.26 (*CH*OH), 42.82 (CH_2Pr), 26.66 (CH_2Et), 22.35 (CH_2Me), 11.41 (CH_2CH_3).

HRMS (MALDI-TOF/DCTB) (*m*/*z*): [M+Na]$^+$ calcd for $C_{50}H_{44}O_6Na$, 763.3036; found, 763.3085.

Characterization of 1,10-dibutyl-4,7,13,16-tetramethoxy-4,7,13,16-tetraphenylcyclooctadeca-2,5,8,11,14,17-hexayne-1,10-diol (3f)

Procedure for the preparation of **3f** *with* n-*BuMgBr*

To a suspension of magnesium turnings (3.2 mg, 0.13 mmol) in THF (0.5 mL) at room temperature was added dropwise *n*-BuBr (0.06 mL, 0.53 mmol). The mixture was stirred for 2 h at room temperature. A solution of [6]pericyclynedione **2** (30 mg, 0.04 mmol) in THF (5 mL) at 0 °C was treated with the freshly prepared solution of *n*-BuMgBr. The mixture was stirred at 0 °C for 3 h before treatment with a saturated aqueous solution of NH_4Cl. The aqueous layer was extracted with diethyl ether, and the combined organic layers were dried over $MgSO_4$ and concentrated under reduced pressure. The residue was purified by chromatography on silica gel (pentane:EtOAc, 5:1, then 3:1) to give the diadduct **3f** (18 mg, 0.0226 mmol, 51% yield), the monoadduct **4f** (9 mg, 0.012 mmol, 28% yield), and the known di-reduction diol product **5** (5 mg, 0.007 mmol, 16% yield),[6h,11] as yellow oils.

Procedure for the preparation of **3f** *with* n-*BuMgCl*

A solution of [6]pericyclynedione **2** (40 mg, 0.06 mmol) in THF (6 mL) at 0 °C was treated with commercial *n*-BuMgCl (0.18 mmol, 2 mol/L in diethyl ether). The mixture was stirred at 0 °C for 1 h and then at room temperature for 3 h before treatment with a saturated aqueous solution of NH_4Cl. The aqueous layer was extracted with diethyl ether, and the combined organic layers were dried over $MgSO_4$ and concentrated under reduced pressure. The residue was purified by chromatography on silica gel (pentane:EtOAc, 5:1, then 3:1) to give the diadduct **3f** as a yellow oil (25 mg, 53% yield).

Procedure for the preparation of **3f** *with* n-*BuLi*

A solution of [6]pericyclynedione **2** (40 mg, 0.06 mmol) in THF (6 mL) at –78 °C was treated with *n*-BuLi (0.12 mmol, 2.5 mol/L in hexane). The mixture was stirred while slowly warming up to –30 °C over 1.5 h before addition of an aqueous solution of NH_4Cl. The aqueous layer was extracted with diethyl ether, and the combined organic layers were dried over $MgSO_4$ and concentrated under reduced pressure. The residue was purified by chromatography on silica gel (pentane:EtOAc, 5:1) to give **3f** as a yellow oil (33 mg, 0.04 mmol, 70% yield).

Procedure for the preparation of **3f** *with* n-*BuLi and* $CeCl_3$

To a suspension of $CeCl_3$ (37 mg, 0.15 mmol) in THF (10 mL) at –78 °C was added *n*-BuLi (0.15 mmol, 2.5 mol/L in hexane), and the resulting mixture was stirred for 0.5 h at this temperature. After treatment with a solution of [6]pericyclynedione **2** (50 mg, 0.0735 mmol) in THF (8 mL) at –78 °C, the mixture was slowly warmed up to –20 °C during 2 h before addition of an aqueous solution of NH_4Cl. The aqueous layer was extracted with diethyl ether, and the combined organic layers were dried over $MgSO_4$ and concentrated under reduced pressure. The residue was purified by chromatography on silica gel (pentane:EtOAc, 5:1) to give **3f** as a yellow oil (53 mg, 0.07 mmol, 90% yield).

^{1}H NMR (300 MHz, $CDCl_3$) δ 7.81–7.64 (m, 8H, *o*-C_6H_5), 7.45–7.30 (m, 12H, *m*-, *p*-C_6H_5), 3.73–3.21 (m, 12H, OCH_3), 3.04–2.51 (m, 2H, O*H*), 2.10–1.89 (m, 4H, CH_2Pr), 1.78–1.51 (m, 4H, CH_2Et), 1.39–1.23 (m, 4H, CH_2Me), 1.00–0.81 (m, 6H, CH_2CH_3).

^{13}C{^{1}H} NMR (75 MHz, $CDCl_3$) δ 139.6–139.3 (*i*-C_6H_5), 129.1–129.0 (*p*-C_6H_5), 128.5–128.4 (*m*-C_6H_5), 126.5–126.4 (*o*-C_6H_5), 87.4–87.0, 84.5–84.3, 81.2–80.1 (*C*≡*C*), 71.9–71.8 (*C*(OMe)Ph), 63.7 (*C*(OH)Bu), 53.4–53.3 (O*CH*$_3$), 43.0–42.8 (CH_2Pr), 26.8–26.5 (CH_2Et), 22.4–22.3 (CH_2Me), 14.2–13.9 (CH_2CH_3).

HRMS (MALDI-TOF/DCTB) (*m*/*z*): [M+H]$^+$ calcd for $C_{54}H_{53}O_6$, 797.3842; found, 797.3771.

Results and discussion

p-Di-*n*-butyl-tetraphenyl-*carbo*-benzene **1f** was targeted through the "classical" route, i.e., by reductive aromatization of the corresponding [6]pericyclynediol **3f**, itself envisaged from the [6]pericyclynedione **2** and various *n*-Bu-MX_n reagents, MX_n = MgBr, MgCl, Li, $CeCl_2$ (Scheme 3).[12]

Following previous experiences (Scheme 1), addition of two equivalents of *n*-butylmagnesium bromide to **2** gave **3f** in 51% yield, along with the reduced monoadduct **4f** and the known bis-secondary [6]pericyclynediol **5**,[6h,13] isolated in yields of 28% and 16%, respectively.

Replacing *n*-BuMgBr by *n*-BuMgCl led to the diadduct **3f** with a similar 53% yield but without reduction side product, as indicated by the absence of any *CH*OH ^{1}H NMR signal in the range of 5–6 ppm. This change in nucleophilic vs redox selectivity can be attributed to the electronegativity-driven higher nucleophilic reactivity of the chlorinated magnesium salt compared with the brominated congener. Traces of the non-reduced mono-ketone

Scheme 3. En route and access to *p*-di-*n*-butyl-tetraphenyl-*carbo*-benzene.

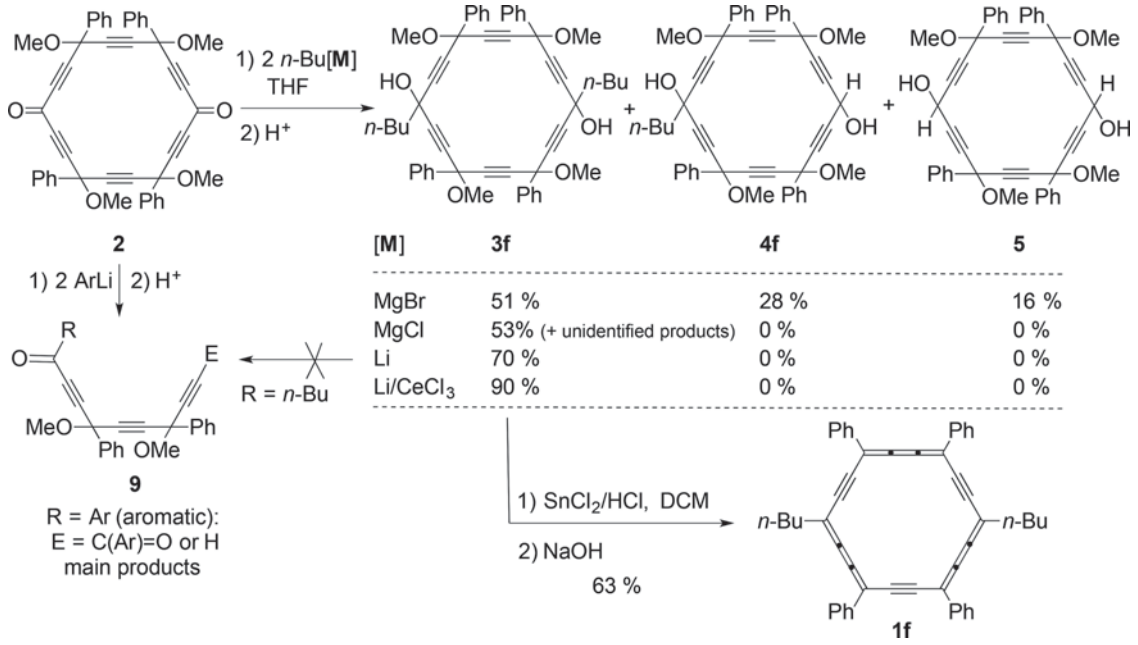

monoadduct were detected by ^{1}H NMR spectroscopy but could not be separated from other unidentified products, which were likely polymeric in nature.

Addition of two equivalents of *n*-butyllithium to **2** followed by aqueous quenching at –30 °C was found to proceed selectively, allowing the diadduct **3f** to be isolated in 70% yield. This result contrasts with the poor efficiency of the addition of aryllithium reagents to the same diketone **2**, the intermediate lithium alkoxide evolving by retro-additive opening of the macrocycle towards stabilized arylketones such as **9** (Scheme 3).[14] Such a ring opening was not observed with *n*-BuLi, provided that the reaction mixture was quenched at –30 °C.

Finally, the addition of two equivalents of *n*-butylcerium dichloride, assumed to be formed in situ from *n*-BuLi and dry $CeCl_3$, to **2** was found to proceed very selectively, affording the [6]pericyclynediol **3f** with a 90% isolated yield. This result is in line with the results disclosed above (M = Li > Mg, X = Cl > Br) and with previous reports on the general use of cerium reagents.[6a,6b,9]

The target **1f** was finally obtained by classical reductive treatment of the [6]pericyclynediol **3f** with $SnCl_2$ and HCl in DCM.[6] It was isolated with 63% yield as a stable, dark red solid, soluble in chlorinated organic solvents (chloroform and DCM).

Single crystals of **1f** deposited from a DCM solution were analyzed by X-ray diffraction, confirming the anticipated structure (Fig. 1). The C_{18} macrocycle of **1f** is quasi-planar with a quasi-regular hexagonal shape, with the maximal deviation from planarity being 0.028 Å. The measured bond lengths in the C_{18} ring are classical for a *carbo*-benzene (*sp*C–*sp*C ≈ 1.22–1.23 Å, sp^2C–*sp*C ≈ 1.37–1.38 Å). The *n*-butyl chains exhibit a zigzag arrangement almost perfectly coplanar with the C_{18} ring, as previously observed for a few other dialkyl-*carbo*-benzenes.[7a] Two of the phenyl substituents are also quasi-coplanar with the C_{18} ring, whereas the two other substituents adopt a torsion angle of approximately 25°. The distance between two successive C_{18} mean planes is 3.45 Å, which is longer than the shortest corresponding distance of 3.21 Å measured for the bis-tetradecyl-*carbo*-benzene: no direct π–π stacking between C_{18} rings of **1f** is observed in the crystal, where co-crystallized DCM molecules prevent van der Waals contact between nearest macrocycles.[7a]

The dibutyl-*carbo*-benzene **1f** was also characterized by ^{1}H and ^{13}C NMR in $CDCl_3$ solution. The ^{1}H NMR spectral profile is similar

Fig. 1. Molecular view of the X-ray crystal structure of **1f**. Thermal ellipsoids at the 50% probability level. For clarity, hydrogen atoms are omitted.

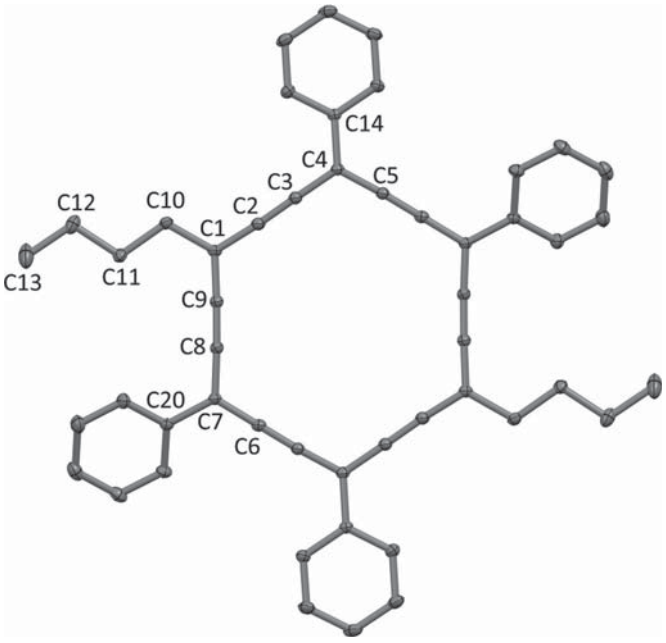

to those reported for other dialkyl-*carbo*-benzenes, with a strong deshielding at 9.51 ppm of the *o*-C*H* nuclei of the four equivalent phenyl substituents.[7a] This effect reveals the strength of the diatropic C_{18} ring current, which also progressively affects the ^{1}H signals of the *n*-butyl chain versus the distance of the CH_2 groups to the C_{18} ring border, as previously analyzed for other *n*-alkyl-*carbo*-benzenes (Supplementary Fig. S1).[7a]

The UV–vis absorption pattern of **1f** in chloroform solution is typical for dialkyl-tetraphenyl-*carbo*-benzenes (λ_{max} = 446 ± 0.5 nm), with one main band at 446 nm, accompanied by three smaller bands at higher wavelengths (Supplementary Fig. S2).[7a] The chro-

Published by NRC Research Press

Table 1. Voltammetric data for **1f** in DCM and chloroform solutions.

	Reductions			Oxidations		
Redox event no.	$E_{1/2}$ (ΔE_P)	RI_P	E_P^{red}	$E_{1/2}$ (ΔE_P)	RI_P	E_P^{ox}
DCM						
First	−0.82 (68)	0.97		1.15 (78)	1.04	
Second	−1.26 (63)	0.97		1.63 (107)	1.15	
Third			−1.98			2.06
$CHCl_3$						
First	−0.82[a] (59)	1.01		1.18[a] (53)	0.68	
Second			−1.32[b]			1.69
Third						2.05

Note: Supporting electrolyte: solvent + 0.1 mol/L [TBA][PF_6]; scan rate: 0.2 V/s. The half-wave potential ($E_{1/2}$) = (E_P^{red} + E_P^{ox})/2, in V/SCE. The separation between the two peak potentials was calculated as follows: $\Delta E_P = |E_P^{red} - E_P^{ox}|$, in V. The peak current ratio (RI_P) = $|I_P^{ox}/I_P^{red}|$. E_P values are measured from CV, in V/SCE.

[a]Reversibility is observed at high scan rates only.

[b]The third reduction cannot be observed in $CHCl_3$ because the solvent is reduced at this potential.

mophoric intensity of **1f** is also classical in this series, with a maximum extinction coefficient of 208 000 L mol^{-1} cm^{-1}.

The title target **1f** has been selected as a model for an analysis of the solvent effect on the electrochemical behavior of *carbo*-benzene derivatives, which might be not soluble enough in DCM to allow the study of redox properties in this solvent, requiring the use of chloroform instead.[15] For the sake of comparison, solutions of **1f** in both chloroform and DCM were thus investigated by square wave (SW) and cyclic (CV) voltammetry (Table 1).

In the reference DCM solvent, **1f** lends itself to three successive reduction processes, two of them being reversible at $E_{1/2}^{red}$ = −0.82 V and −1.26 V, these values being comparable with the values previously reported for other *carbo*-benzene derivatives.[6f,6i,15] The aromaticity of the C_{18} ring indeed attenuates its sensitivity to substituents.[6f] In chloroform, the two first reductions occur at similar potentials (albeit turning less reversible at −0.82 V and −1.32 V), whereas the third reduction peak occurring at E_P^{red} = −1.98 V in DCM cannot be detected because of the narrower electrochemical observation window of $CHCl_3$, which is reduced at this potential. These results also show that replacement of two aryl substituents by alkyl counterparts has a weak but electronically consistent effect on the reduction potential values (−0.72 V and −1.15 V for hexaphenyl-*carbo*-benzene).[15]

In both solvents, three oxidation processes are also observed at comparable potentials, with a loss of reversibility of the second wave observed in DCM ($E_{1/2}^{ox2}$ = +1.63 V) by passing to chloroform (E_P^{ox2} = +1.69 V).

The influence of the solvent on the redox potentials is thus limited, but affects the reversibility of the processes, possibly because of the higher viscosity and lower dielectric constant of chloroform ($\eta(CHCl_3)$ = 0.537 mPa·s > η(DCM) = 0.413 mPa·s, $\varepsilon(CHCl_3)$ = 4.81 < ε(DCM) = 8.93). A high dielectric constant indeed favors charge dissociation thus enhancing the conductivity of the electrolytic solution.

Conclusion

The metal switch study of the reaction of a model alkyl nucleophile with the [6]pericyclynedione **2** brings out the dichlorocerium(III) reagent as the most selective for the production of **3f**. The improvement is particularly eloquent by comparison with the bromomagnesium reagent affording also the double reduction product **5** and the single addition–reduction product **4f** (that could, however, be profitably used for a *carbo*-benzene library purpose).[7a] The synthesis results provide a global increase of the yield of preparation of *p*-di-*n*-butyl-tetraphenyl-*carbo*-benzene **1f** from 32% to 57% over the two last steps. The cerium method can thus henceforth be envisaged for the synthesis of other alkyl-*carbo*-benzenes.

The disclosed voltammetry results, the first ones in the alkyl-*carbo*-benzene series, indicate that the electrochemical behavior of *carbo*-benzenes is little sensitive to solvent (DCM vs chloroform) and substituent (alkyl vs aryl) effects. More generally, the "hybrid" member of the *carbo*-benzene family **1f**, with two alkyl chain and four phenyl ring substituents, could now serve as a soluble standard for other comparative studies.

Supplementary data

Supplementary data are available with the article through the journal Web site at http://nrcresearchpress.com/doi/suppl/10.1139/cjc-2016-0629.

Acknowledgements

C.Z. thanks the China Scholarship Council for his Ph.D. scholarship. The ANR program (ANR-11-BS07-016-01) is acknowledged for funding. R.C. thanks the Centre National de la Recherche Scientifique (CNRS) for half a teaching sabbatical in 2015–2016.

References

(1) (a) Baughman, R. H.; Eckhardt, H.; Kertesz, M. *J. Chem. Phys.* **1987**, *87*, 6687. doi:10.1063/1.453405; (b) Malko, D.; Neiss, C.; Viñes, F.; Görling, A. *Phys. Rev. Lett.* **2012**, *108*, 086804. doi:10.1103/PhysRevLett.108.086804; (c) Kim, B. G.; Choi, H. J. *Phys. Rev. B* **2012**, *86*, 115435. doi:10.1103/PhysRevB.86.115435; (d) Ducéré, J.-M.; Lepetit, C.; Chauvin, R. *J. Phys. Chem. C* **2013**, *117*, 21671. doi:10.1021/jp4067795; (e) Ivanovskii, A. L. *Prog. Solid State Chem.* **2013**, *41*, 1. doi:10.1016/j.progsolidstchem.2012.12.001; (f) Han, N.; Liu, H.; Zhou, S.; Zhao, J. *J. Phys. Chem. C* **2016**, *120*, 14699. doi:10.1021/acs.jpcc.6b04384.

(2) (a) Kehoe, J. M.; Kiley, J. H.; English, J. J.; Johnson, C. A.; Petersen, R. C.; Haley, M. M. *Org. Lett.* **2000**, *2*, 969. doi:10.1021/ol005623w; (b) Yoshimura, T.; Inaba, A.; Sonoda, M.; Tahara, K.; Tobe, Y.; Williams, R. V. *Org. Lett.* **2006**, *8*, 2933. doi:10.1021/ol060781u; (c) Johnson, C. A., II; Lu, Y.; Haley, M. M. *Org. Lett.* **2007**, *9*, 3725. doi:10.1021/ol7014253; (d) Haley, M. M. *Pure Appl. Chem.* **2008**, *80*, 519. doi:10.1351/pac200880030519.

(3) (a) Wan, W. B.; Haley, M. M. *J. Org. Chem.* **2001**, *66*, 3893. doi:10.1021/jo010183n; (b) Marsden, J. A.; Haley, M. M. *J. Org. Chem.* **2005**, *70*, 10213. doi:10.1021/jo050926v.

(4) Cocq, K.; Saffon-Merceron, N.; Coppel, Y.; Poidevin, C.; Maraval, V.; Chauvin, R. *Angew. Chem. Int. Ed.* **2016**, *55*, 15133. doi:10.1002/anie.201608300.

(5) (a) Chauvin, R. *Tetrahedron Lett.* **1995**, *36*, 397. doi:10.1016/0040-4039(94)02275-G; (b) Maraval, V.; Chauvin, R. *Chem. Rev.* **2006**, *106*, 5317. doi:10.1021/cr050964e.

(6) For references on *carbo*-benzenes see: (a) Kuwatani, Y.; Watanabe, N.; Ueda, I. *Tetrahedron Lett.* **1995**, *36*, 119. doi:10.1016/0040-4039(94)02181-A; (b) Suzuki, R.; Tsukude, H.; Watanabe, N.; Kuwatani, Y.; Ueda, I. *Tetrahedron* **1998**, *54*, 2477. doi:10.1016/S0040-4020(98)00011-8; (c) Saccavini, C.; Sui-Seng, C.; Maurette, L.; Lepetit, C.; Soula, S.; Zou, C.; Donnadieu, B.; Chauvin, R. *Chem. Eur. J.* **2007**, *13*, 4914. doi:10.1002/chem.200601193; (d) Zou, C.; Duhayon, C.; Maraval, V.; Chauvin, R. *Angew. Chem. Int. Ed.* **2007**, *46*, 4337. doi:10.1002/anie.200605262; (e) Leroyer, L.; Lepetit, C.; Rives, A.; Maraval, V.; Saffon-Merceron, N.; Kandaskalov, D.; Kieffer, D.; Chauvin, R. *Chem. Eur. J.* **2012**, *18*, 3226. doi:10.1002/chem.201102993; (f) Rives, A.; Baglai, I.; Malytskyi, V.; Maraval, V.; Saffon-Merceron, N.; Voitenko, Z.; Chauvin, R. *Chem. Commun.* **2012**, *48*, 8763. doi:10.1039/c2cc34176j; (g) Baglai, I.; Maraval, V.; Bijani, C.; Saffon-Merceron, N.; Voitenko, Z.; Volovenko, Y. M.; Chauvin, R. *Chem. Commun.* **2013**, *49*, 8374. doi:10.1039/c3cc43204a; (h) Cocq, K.; Maraval, V.; Saffon-Merceron, N.; Chauvin, R. *Chem. Rec.* **2015**, *15*, 347. doi:10.1002/tcr.201402091; (i) Cocq, K.; Lepetit, C.; Maraval, V.; Chauvin, R. *Chem. Soc. Rev.* **2015**, *44*, 6535. doi:10.1039/C5CS00244C; (j) Baglai, I.; de Anda-Villa, M.; Barba-Barba, R. M.; Poidevin, C.; Ramos-Ortíz, G.; Maraval, V.; Lepetit, C.; Saffon-Merceron, N.; Maldonado, J.-L.; Chauvin, R. *Chem. Eur. J.* **2015**, *21*, 14186. doi:10.1002/chem.201500482; (k) Cocq, K.; Saffon-Merceron, N.; Maraval, V.; Chauvin, R. *Synlett* **2016**, *27*, 2105. doi:10.1055/s-0035-1562720.

(7) (a) Zhu, C.; Rives, A.; Duhayon, C.; Maraval, V.; Chauvin, R. *J. Org. Chem.* **2017**, *82*, 925. doi:10.1021/acs.joc.6b02397. For references on pericyclynes see: (b) Scott, L. T.; DeCicco, G. J.; Hyun, J. L.; Reinhardt, G. *J. Am. Chem. Soc.* **1983**, *105*, 7760. doi:10.1021/ja00364a057; (c) Scott, L. T.; DeCicco, G. J.; Hyun, J. L.; Reinhardt, G. *J. Am. Chem. Soc.* **1985**, *107*, 6546. doi:10.1021/ja00309a021.

(8) (a) Morrisson, J. D.; Tomaszewski, J. E.; Mosher, H. S.; Dale, J.; Miller, D.; Elsenbaumer, R. L. *J. Am. Chem. Soc.* **1977**, *99*, 3167. doi:10.1021/ja00451a054; (b) Ashby, E. C.; Goel, A. B. *J. Am. Chem. Soc.* **1981**, *103*, 4983. doi:10.1021/ja00406a070.

(9) For early references see: (a) Imamoto, T.; Kusumoto, T.; Yokoyama, M. *J. Chem. Soc., Chem. Commun.* **1982**, 1042. doi:10.1039/c39820001042; (b) Imamoto, T.; Sugiura, Y.; Takiyama, N. *Tetrahedron Lett.* **1984**, *25*, 4233. doi:10.1016/S0040-

4039(01)81404-0. For a recent review see: (c) Bartoli, G.; Marcantoni, E.; Marcolini, M.; Sambri, L. *Chem. Rev.* **2010**, *110*, 6104. doi:10.1021/cr100084g.
(10) Betteridge, P. W.; Carruthers, J. R.; Cooper, R. I.; Prout, K.; Watkin, D. J. *J. Appl. Cryst.* **2003**, *36*, 1487. doi:10.1107/S0021889803021800.
(11) *International Tables for X-ray Crystallography*; Kynoch: Birmingham, England, 1974; Vol. 4.
(12) (a) Maurette, L.; Tedeschi, C.; Sermot, E.; Soleilhavoup, M.; Hussain, F.; Donnadieu, B.; Chauvin, R. *Tetrahedron* **2004**, *60*, 10077. doi:10.1016/j.tet.2004.07.052; (b) Leroyer, L.; Zou, C.; Maraval, V.; Chauvin, R. *C. R. Chimie* **2009**, *12*, 412. doi:10.1016/j.crci.2008.09.018.
(13) Saccavini, C.; Tedeschi, C.; Maurette, L.; Sui-Seng, C.; Zou, C.; Soleilhavoup, M.; Vendier, L.; Chauvin, R. *Chem. Eur. J.* **2007**, *13*, 4895. doi:10.1002/chem.200601191.
(14) Zhu, C.; Maraval, V; Chauvin, R., unpublished results.
(15) Zhu, C.; Duhayon, C.; Romero-Borja, D.; Maldonado, J.-L.; Ramos-Ortíz, G.; Saquet, A.; Maraval, V.; Chauvin, R., submitted for publication.

Published by NRC Research Press

SUPPORTING INFORMATION

Lipidic *carbo*-benzenes:

molecular probes of magnetic anisotropy and stacking properties of *a*-graphyne

Chongwei Zhu,[a,b] Arnaud Rives,[a,b] Carine Duhayon,[a,b] Valérie Maraval,[a,b*] Remi Chauvin[a,b*]

[a] *CNRS, LCC (Laboratoire de Chimie de Coordination), 205 route de Narbonne, BP 44099, 31077 Toulous,, France*

[b] *Université de Toulouse, UPS, ICT-FR 2599, 118 route de Narbonne, 31062 Toulouse Cedex 9, France*

E-mail: valerie.maraval@lcc-toulouse.fr, chauvin@lcc-toulouse.fr

Contents

1. Crystallographic data of 11a-d, 10b, 10d, 11e

Crystals of **11a-e**, **10b** and **10d** and were obtained from DCM or chloroform by slow evaporation of the solvent at room temperature. For **10b**, two crystallization processes from the same solvent (DCM) gave allotropic crystals, **10b1** and **10b2**, both triclinic but differing by the content of the asymmetric unit.

1.1. Crystal structure determination

Intensity data were collected at low temperature on a diffractometer equipped with a 30W air-cooled microfocus source (λ = 0.71073 Å). The structures were solved using SUPERFLIP, and refined by means of least-squares procedures on *F* using the programs of the PC version of CRYSTALS.[1] Atomic scattering factors were taken from the International Tables for X-Ray Crystallography.[2] The asymmetric unit consists in a whole *carbo*-benzene molecule (with or without solvent), excepting for **10b1** (2 molecules per asymmetric unit), for **11b**, **11c** and **11d•CHCl$_3$** (0.5 molecule per asymmetric unit), and for **10b2** (3 molecules per asymmetric unit). Except for **11d•CH$_2$Cl$_2$** (poorly diffracting), all non-H atoms were refined anisotropically. Crystals of **10b2** were found to be twinned, and data were treated with ROTAX which gave the twin law between the two components (0.75:0.25). Hydrogen atoms were refined using a riding model. Absorption corrections were introduced using the program MULTISCAN.

References: [1] Betteridge, P. W.; Carruthers, J. R.; Cooper, R. I.; Prout, K.; Watkin, D. J., *J. Appl. Cryst.* **2003**, *36*, 1487.
[2] *International Tables for X-ray Crystallography*, vol. IV, Kynoch Press, Birmingham, England (1974).

1.2. Crystallographic data and refinement parameters for dialkyl-*carbo*-benzenes (11a-d)

	11a	**11b**	**11c**	**11d•CH$_2$Cl$_2$**	**11d•CHCl$_3$**
CCDC no	1494584	1494585	1494586	1494587	1494840
Empirical formula	$C_{46}H_{30}$	$C_{59}H_{55}Cl_3$	$C_{70}H_{78}$	$C_{84}H_{106}Cl_4$	$C_{84}H_{104}Cl_6$
Formula mass	582.74	870.44	919.39	1257.57	1326.46
Crystal system	Monoclinic	Triclinic	Monoclinic	Triclinic	Triclinic
Space group	*P2$_1$/c*	*P-1*	*P2$_1$/n*	*P-1*	*P-1*
T [K]	100	100	193	100	100
a [Å]	16.8971(10)	13.1786(5)	18.391(3)	12.3283(9)	10.5493(7)
b [Å]	6.0972(4)	13.3182(5)	5.5876(9)	17.5410(13)	12.2119(8)
c [Å]	16.0454(10)	14.4208(6)	26.892(5)	18.7671(13)	16.3716(12)
a [°]	90	92.0053(16)	90	70.412(2)	76.044(4)
b [°]	106.6094(17)	110.5356(15)	90.190(6)	89.193(2)	78.422(4)
g [°]	90	91.6484(16)	90	70.980(2)	64.554(3)
V [Å^3]	1584.10(10)	2366.50(10)	2763.4(5)	3594.1(2)	1836.90(13)
D_c	1.222	1.221	1.105	1.162	1.199
Z	2	2	2	2	1
μ [mm^{-1}]	0.069	0.232	0.062	0.208	0.278

crystal data contd'	**11a**	**11b**	**11c**	**11d•CH_2Cl_2**	**11d•$CHCl_3$**
Refl. measured	20507	123166	49708	69045	82354
Refl. unique/R_{int}	4476/0.035	17221/0.032	4630/0.161	17697/0.118	9202/0.063
Refl. with $I > ns(I)$	2814 (n=3)	12269 (n=3)	1897 (n=3)	4555 (n=3)	5929 (n=3)
Nb parameters	208	559	316	373	406
R	0.0492	0.0380	0.0459	0.0639	0.0393
R_w	0.0508	0.0408	0.0475	0.0644	0.0399
GooF	1.08	1.06	1.05	1.05	1.09
Dr_{max}/Dr_{min} [e.Å^{-3}]	0.34/-0.34	0.52/-0.35	0.19/-0.19	0.96/-0.46	0.40/-0.35

1.3. Crystallographic data and refinement parameters for monoalkyl-*carbo*-benzenes (10b,d)

	10b1	**10b2**	**10d**
CCDC no	1494588	1501523	1494589
Empirical formula	$C_{51}H_{40}Cl_2$	$C_{50.67}H_{39.33}Cl_{1.33}$	$C_{64}H_{66}Cl_4$
Formula mass	723.78	695.47	977.04
Crystal system	Triclinic	Triclinic	Monoclinic
Space group	*P-1*	*P-1*	$P2_1/c$
T [K]	100	100	100
a [Å]	13.0609(14)	16.195(2)	10.7200(5)
b [Å]	14.0494(16)	19.407(3)	45.197(2)
c [Å]	22.454(3)	20.992(3)	12.0719(5)
α [°]	77.832(3)	69.639(4)	90
β [°]	75.363(3)	68.618(4)	114.6957(14)
γ [°]	85.051(3)	82.046(4)	90
V [Å^3]	3894.6(4)	5759.3(7)	5314.0(2)
D_c	1.234	1.203	1.221
Z	4	6	4
μ [mm^{-1}]	0.202	0.157	0.263
Refl. measured	109361	201324	118107
Refl. unique/R_{int}	12499/0.075	19589/0.080	10849/0.065
Refl. with $I > ns(I)$	9607 (n=2.6)	15746 (n=3)	6334 (n=3)
Nb parameters	955	1406	631
R	0.0620	0.0860	0.0414
R_w	0.0603	0.0829	0.0408
GooF	1.09	1.02	1.10
Dr_{max}/Dr_{min} [e.Å^{-3}]	0.57/-0.43	0.80/-1.11	0.38/-0.56

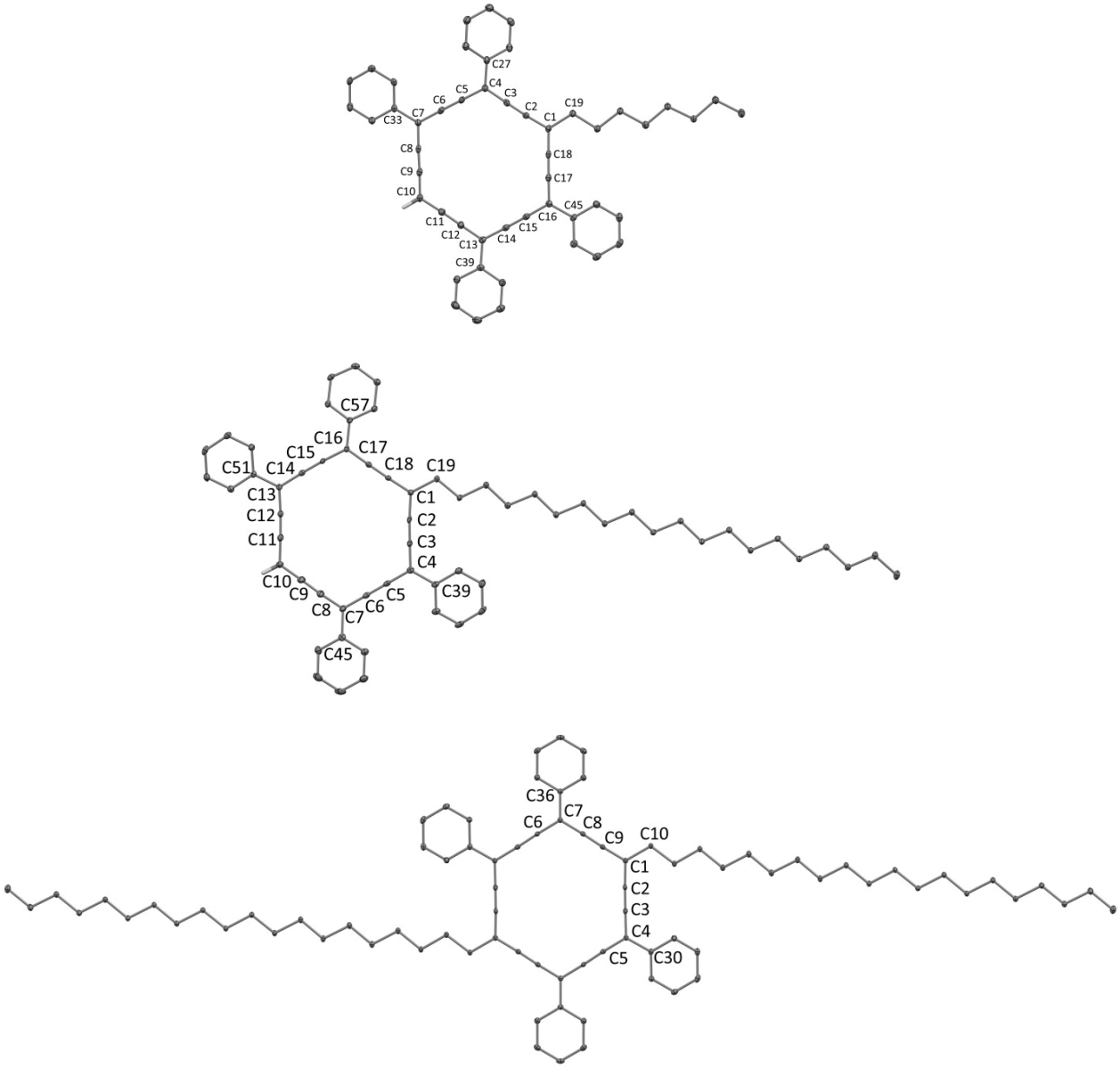

Figure S1. Molecular views of the X-ray crystal structures of the *carbo*-benzenes **10b1** (*top*), **10d** (*middle*) and **11d•CHCl$_3$** (*bottom*). 30 % Probability level for the thermal ellipsoids. For clarity, solvent molecules are omitted. All hydrogen atoms are also omitted, except those bonded to the C_{18} macrocycle (see full-page figures in Section 2.14, pp 136-142).

1.4. Crystallographic data and refinement parameters for a fluoroalkyl-*carbo*-benzene (11e)

Crystals of the *carbo*-benzene **11e** were also obtained from a dichloromethane solution, but the crystals were very small and poorly diffracting. A draft of the structure was obtained in the $P2_1/c$ space group (a = 4.7492(5), b = 30.0592(10), c = 47.2671(14) Å, β = 94.950(3) °, V = 20877.7(6) Å^3), with four molecules in the asymmetric unit, making very large the number of parameters to refine, while the

number of measured intensities was very low. The refinement of the model was thus not achieved, but a figure is given, with R = 33 % (Figure S2).

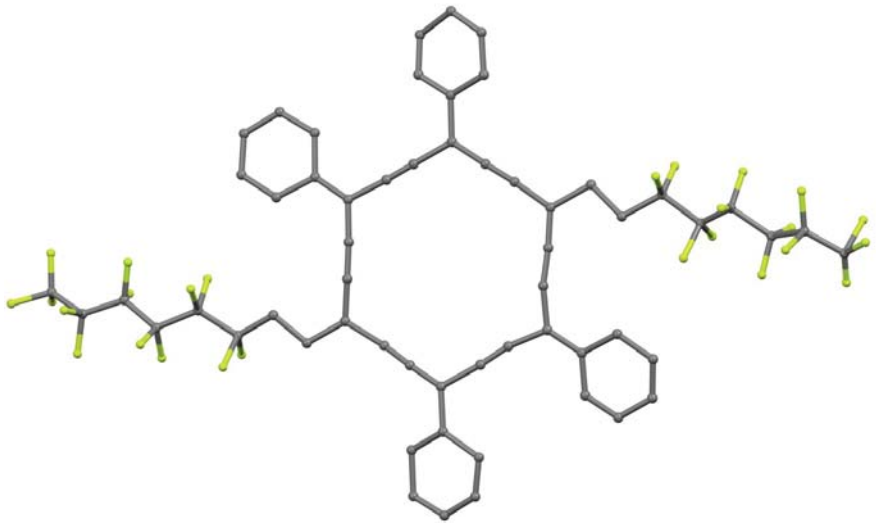

Figure S2. Molecular view of the X-ray crystal structure of **11e**. R = 33 %.

1.5. Complete crystal data for 10b1

a = 13.0609(14) Å α = 77.832(3)°
b = 14.0494(16) Å β = 75.363(3)°
c = 22.454(3) Å γ = 85.051(3)°

Volume	3894.6(4) Å³	Crystal Class	triclinic
Space group	P -1	Z =	4
Formula	C_{51} H_{40} Cl_2	M_r	723.78
Cell determined from	9982 reflections	Cell θ range =	2 - 24°
Temperature	100K		
Shape	block		
Colour	red	Size	0.15 × 0.15 × 0.20 mm
D_x	1.23	F000	1519.990
μ	0.202 mm^{-1}		
Absorption correction	multi-scan		
T_{min}	0.91	T_{max}	0.97

Data Collection

Diffractometer	multi-scan
Scan type	φ and ω scans
Reflections measured	109361
Independent reflections	12499
Rint	0.0754

θ_{max}	24.3781
h =	-15 → 15
k =	-16 → 16
l =	-26 → 25

Refinement

$\Delta\rho_{min}$ =	-0.43 e Å^{-3}
$\Delta\rho_{max}$ =	0.57 e Å^{-3}
Reflections used	9607
Cutoff: I >	2.60σ(I)
Parameters refined	955
S =	1.09
R-factor	0.062
weighted R-factor	0.060
Δ/σ_{max}	0.0009
Refinement on	F
w =	$w' \times [1 - (\Delta F_{obs} / 6 \times \Delta F_{est})^2]^2$
w′ =	$[P_0T_0'(x) + P_1T_1'(x) + ...P_{n-1}T_{n-1}'(x)]^{-1}$, where P_i are the coefficients of a Chebychev series in $t_i(x)$, and $x = F_{calc}/F_{calcmax}$.
P_0 - P_{n-1} =	0.246 0.281 0.860E-01

1.6. Complete crystal data for 10b2

a = 16.195(2) Å α = 69.639(4)°
b = 19.407(3) Å β = 68.618(4)°
c = 20.992(3) Å γ = 82.046(4)°

Volume	5759.3(7) Å^3	Crystal Class	triclinic
Space group	P -1	Z =	6
Formula	$C_{50.67}$ $H_{39.33}$ $Cl_{1.33}$	M_r	695.47
Cell determined from	9776 reflections	Cell θ range =	2 - 25°
Temperature	100 K		
Shape	block		
Colour	red	Size	0.15 × 0.15 × 0.18 mm
D_x	1.20	F000	2195.995
μ	0.157 mm^{-1}		
Absorption correction	multi-scan		
T_{min}	0.85	T_{max}	0.98

Data Collection

Diffractometer	multi-scan
Scan type	φ and ω scans
Reflections measured	201324
Independent reflections	19589
Rint	0.0795

θ_{max}	24.7606
h =	-19 → 19
k =	-22 → 22
l =	-24 → 24

Refinement

$\Delta\rho_{min}$ =	-1.11 e Å^{-3}
$\Delta\rho_{max}$ =	0.80 e Å^{-3}
Reflections used	15745
Cutoff: I >	3.00σ(I)
Parameters refined	1406
S =	1.02
R-factor	0.086
weighted R-factor	0.083
Δ/σ_{max}	0.0004
Refinement on	F
w =	$w' \times [1 - (\Delta F_{obs} / 6 \times \Delta F_{est})^2]^2$
w′ =	$[P_0 T_0'(x) + P_1 T_1'(x) + ...P_{n-1} T_{n-1}'(x)]^{-1}$, where P_i are the coefficients of a Chebychev series in $t_i(x)$, and $x = F_{calc}/F_{calcmax}$.
P_0 - P_{n-1} =	0.220 0.223 0.518E-01

1.7. Complete crystal data for 10d

a = 10.7200(5) Å α = 90°
b = 45.197(2) Å β = 114.6957(14)°
c = 12.0719(5) Å γ = 90°

Volume	5314.0(2) Å^3	Crystal Class	monoclinic
Space group	P 1 2_1/c 1	Z =	4
Formula	C_{64} H_{66} Cl_4	M_r	977.04
Cell determined from	9351 reflections	Cell θ range =	21 - 26°
Temperature	100K		
Shape	block		
Colour	red	Size	0.15 × 0.15 × 0.20 mm
D_x	1.22	F000	2072.00
μ	0.263 mm^{-1}		0
Absorption correction	multi-scan		
T_{min}	0.88	T_{max}	0.96

Data Collection

Diffractometer	multi-scan
Scan type	φ and ω scans
Reflections measured	118107
Independent reflections	10849
Rint	0.0653
θ_{max}	26.3725
h =	-13 → 13
k =	-56 → 56

l =	-15 → 15

Refinement

$\Delta\rho_{min}$ =	-0.56 e Å^{-3}
$\Delta\rho_{max}$ =	0.38 e Å^{-3}
Reflections used	6334
Cutoff: I >	3.00σ(I)
Parameters refined	631
S =	1.10
R-factor	0.041
weighted R-factor	0.041
Δ/σ_{max}	0.0008
Refinement on	F
w =	$w' \times [1 - (\Delta F_{obs} / 6 \times \Delta F_{est})^2]^2$
w' =	$[P_0T_0'(x) + P_1T_1'(x) + ...P_{n-1}T_{n-1}'(x)]^{-1}$
	where P_i are the coefficients of a Chebychev series in $t_i(x)$, and $x = F_{calc}/F_{calcmax}$.
P_0 - P_{n-1} =	0.196 0.196 0.788E-01

1.8. Complete crystal data for 11a

a = 16.8971(10) Å α = 90°
b = 6.0972(4) Å β = 106.6094(17)°
c = 16.0454(10) Å γ = 90°

Volume	1584.10(10) Å^3	Crystal Class	monoclinic
Space group	P 2_1/c	Z =	2
Formula	C_{46} H_{30}	M_r	582.74
Cell determined from	5584 reflections	Cell θ range =	3 - 30°
Temperature	100K		
Shape	needle		
Colour	red	Size	0.05 × 0.05 × 0.15 mm
D_x	1.22	F000	612.000
μ	0.069 mm^{-1}		
Absorption correction	multi-scan		
T_{min}	0.92	T_{max}	1.00

Data Collection

Diffractometer	multi-scan
Scan type	φ and ω scans
Reflections measured	20507
Independent reflections	4476
Rint	0.0347
θ_{max}	30.0206
h =	-23 → 23

k =	-8 → 8
l =	-22 → 22

Refinement

$\Delta\rho_{min}$ =	-0.34 e Å^{-3}
$\Delta\rho_{max}$ =	0.34 e Å^{-3}
Reflections used	2814
Cutoff: I >	3.00σ(I)
Parameters refined	208
S =	1.08
R-factor	0.049
weighted R-factor	0.051
Δ/σ_{max}	0.0002
Refinement on	F
w =	$w' \times [1 - (\Delta F_{obs} / 6 \times \Delta F_{est})^2]^2$

$w' = [P_0T_0'(x) + P_1T_1'(x) + ...P_{n-1}T_{n-1}'(x)]^{-1}$,

where P_i are the coefficients of a Chebychev series in $t_i(x)$, and $x = F_{calc}/F_{calcmax}$.

P_0 - P_{n-1} =	0.213 0.171 0.691E-01

1.9. Complete crystal data for 11b

a = 13.1786(5) Å α = 92.0053(16)°

b = 13.3182(5) Å β = 110.5356(15)°

c = 14.4208(6) Å γ = 91.6484(16)°

Volume	2366.50(10) Å³	Crystal Class	triclinic
Space group	P -1	Z =	2
Formula	C_{59} H_{55} Cl_3	M_r	870.44
Cell determined from	9808 reflections	Cell θ range =	2 - 27°
Temperature	100K		
Shape	block		
Colour	dark red	Size	0.15 × 0.15 × 0.20 mm
D_x	1.22	F000	920.000
μ	0.232 mm^{-1}		
Absorption correction	multi-scan		
T_{min}	0.88	T_{max}	0.97

Data Collection

Diffractometer	multi-scan
Scan type	φ and ω scans
Reflections measured	123166
Independent reflections	17221
Rint	0.0321
θ_{max}	37.4984
h =	-18 → 19
k =	-19 → 22
l =	-20 → 20

Refinement

$\Delta\rho_{min}$ =	-0.35 e Å^{-3}
$\Delta\rho_{max}$ =	0.52 e Å^{-3}
Reflections used	12269
Cutoff: I >	3.00σ(I)
Parameters refined	559
S =	1.06
R-factor	0.038
weighted R-factor	0.041
Δ/σ_{max}	0.0006
Refinement on	F
w =	$w' \times [1 - (\Delta F_{obs} / 6 \times \Delta F_{est})^2]^2$
w′ =	$[P_0T_0'(x) + P_1T_1'(x) + ...P_{n-1}T_{n-1}'(x)]^{-1}$, where P_i are the coefficients of a Chebychev series in $t_i(x)$, and $x = F_{calc}/F_{calcmax}$.
P_0 - P_{n-1} =	0.175 0.150 0.517E-01

1.10. Complete crystal data for 11c

a = 18.391(3) Å α = 90°
b = 5.5876(9) Å β = 90.190(6)°
c = 26.892(5) Å γ = 90°

Volume	2763.4(5) Å^3	Crystal Class	monoclinic
Space group	P 1 2_1/n 1	Z =	2
Formula	C_{70} H_{78}	M_r	919.39
Cell determined from	7232 reflections	Cell θ range =	3 - 24°
Temperature	193K		
Shape	needle		
Colour	red	Size	0.01 × 0.04 × 0.52 mm
D_x	1.10	F000	996.000
μ	0.062 mm^{-1}		
Absorption correction	multi-scan		
T_{min}	0.95	T_{max}	1.00

Data Collection

Diffractometer	multi-scan
Scan type	φ and ω scans
Reflections measured	49708
Independent reflections	4630
Rint	0.1614
θ_{max}	24.7531
h =	-21 → 21
k =	-6 → 6
l =	-31 → 30

Refinement

$\Delta\rho_{min}$ =	-0.19 e $Å^{-3}$
$\Delta\rho_{max}$ =	0.19 e $Å^{-3}$
Reflections used	1897
Cutoff: I >	3.00σ(I)
Parameters refined	316
S =	1.05
R-factor	0.046
weighted R-factor	0.048
Δ/σ_{max}	0.0007
Refinement on	F
w =	$w' \times [1 - (\Delta F_{obs} / 6 \times \Delta F_{est})^2]^2$
w′ =	$[P_0T_0'(x) + P_1T_1'(x) + ...P_{n-1}T_{n-1}'(x)]^{-1}$, where P_i are the coefficients of a Chebychev series in $t_i(x)$, and $x = F_{calc}/F_{calcmax}$.
P_0 - P_{n-1} =	0.435 0.374 0.237

1.11. Complete crystal data for 11d•CH_2Cl_2

a = 12.3283(9) Å α = 70.412(2)°
b = 17.5410(13) Å β = 89.193(2)°
c = 18.7671(13) Å γ = 70.980(2)°

Volume	3594.1(2) Å³	Crystal Class	triclinic
Space group	P -1	Z =	2
Formula	C_{84} H_{106} Cl_4	M_r	1257.57
Cell determined from	6777 reflections	Cell θ range =	2 - 28°
Temperature	100K		
Shape	block		
Colour	red	Size	0.10 × 0.20 × 0.20 mm
D_x	1.16	F000	1356.000
μ	0.208 mm^{-1}		
Absorption correction	multi-scan		
T_{min}	0.87	T_{max}	0.98

Data Collection

Diffractometer	multi-scan
Scan type	φ and ω scans
Reflections measured	69045
Independent reflections	17697
Rint	0.1182
θ_{max}	28.4987
h =	-16 → 16
k =	-23 → 23
l =	-25 → 20

Refinement

$\Delta\rho_{min}$ =	-0.51 e $Å^{-3}$
$\Delta\rho_{max}$ =	0.90 e $Å^{-3}$
Reflections used	4555
Cutoff: I >	3.00σ(I)
Parameters refined	373
S =	1.04
R-factor	0.063
weighted R-factor	0.064
Δ/σ_{max}	0.0003
Refinement on	F
w =	$w' \times [1 - (\Delta F_{obs} / 6 \times \Delta F_{est})^2]^2$
w′ =	$[P_0T_0'(x) + P_1T_1'(x) + ...P_{n-1}T_{n-1}'(x)]^{-1}$, where P_i are the coefficients of a Chebychev series in $t_i(x)$, and $x = F_{calc}/F_{calcmax}$.
P_0 - P_{n-1} =	0.190 0.170 0.838E-01 0.344E-01 0.759E-02

1.12. Complete crystal data for 11d•$CHCl_3$

a = 10.5493(7) Å α = 76.044(4)°
b = 12.2119(8) Å β = 78.422(4)°
c = 16.3716(12) Å γ = 64.554(3)°

Volume	1836.90(13) Å³	Crystal Class	triclinic
Space group	P -1	Z =	1
Formula	C_{84} H_{104} Cl_6	M_r	1326.46
Cell determined from	9996 reflections	Cell θ range = 2 - 28°	
Temperature	100K		
Shape	block		
Colour	red	Size	0.05 × 0.10 × 0.20 mm
D_x	1.20	F000	710.000
μ	0.278 mm^{-1}		
Absorption correction	multi-scan		
T_{min}	0.90	T_{max}	0.99

Data Collection

Diffractometer	multi-scan
Scan type	φ and ω scans
Reflections measured	82354
Independent reflections	9202
Rint	0.0627
θ_{max}	28.4313
h =	-14 → 14
k =	-16 → 15
l =	-21 → 21

Refinement

$\Delta\rho_{min}$ =	-0.35 e $Å^{-3}$
$\Delta\rho_{max}$ =	0.40 e $Å^{-3}$
Reflections used	5929
Cutoff: I >	3.00σ(I)
Parameters refined	406

1.13. Complete crystal data for 11e

a = 14.7492(5) Å α = 90°
b = 30.0592(10) Å β = 94.950(3)°
c = 47.2671(14) Å γ = 90°

Volume	20877.7(6) Å³	Crystal Class	monoclinic
Space group	P 2_1/c	Z =	16
Formula	$C_{58.25}$ $Cl_{0.50}$ F_{26} $O_{0.25}$	M_r	1215.32
Cell determined from	0 reflections	Cell θ range =	0 - 0°
Temperature	293K		
D_x	1.55	F000	9504.000
μ	0.181 mm^{-1}		
Absorption correction	none		
T_{min}	0.73	T_{max}	1.00

Data Collection

Diffractometer	none
Scan type	φ and ω scans
Reflections measured	249256
Independent reflections	45723
Rint	0.4750
θ_{max}	28.7636
h =	-19 → 19
k =	-23 → 40
l =	-62 → 60

Refinement

$\Delta\rho_{min}$ =	-2.18 e $Å^{-3}$
$\Delta\rho_{max}$ =	2.80 e $Å^{-3}$
Reflections used	24079
Cutoff: I >	3.00σ(I)
Parameters refined	1373
S =	2.03
R-factor	0.319
weighted R-factor	0.338
Δ/σ_{max}	4.8922
Refinement on	F
w =	1

1.14. Thermal ellipsoid plots of 10b, 10b2, 10d, 11a, 11b,

11c, 11d. 10b (30 % probability level for the thermal ellipsoids)

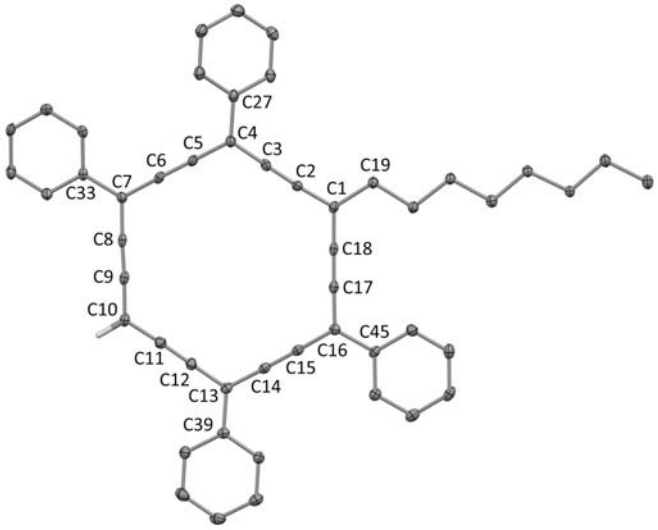

10b2 (30 % probability level for the thermal ellipsoids)

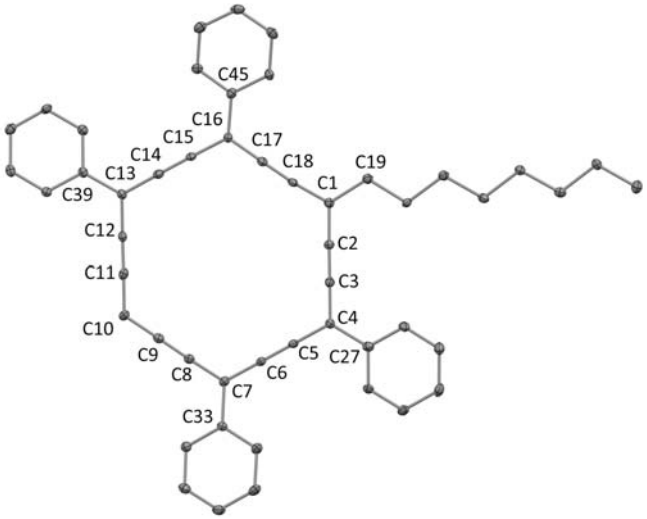

10d (30 % probability level for the thermal ellipsoids)

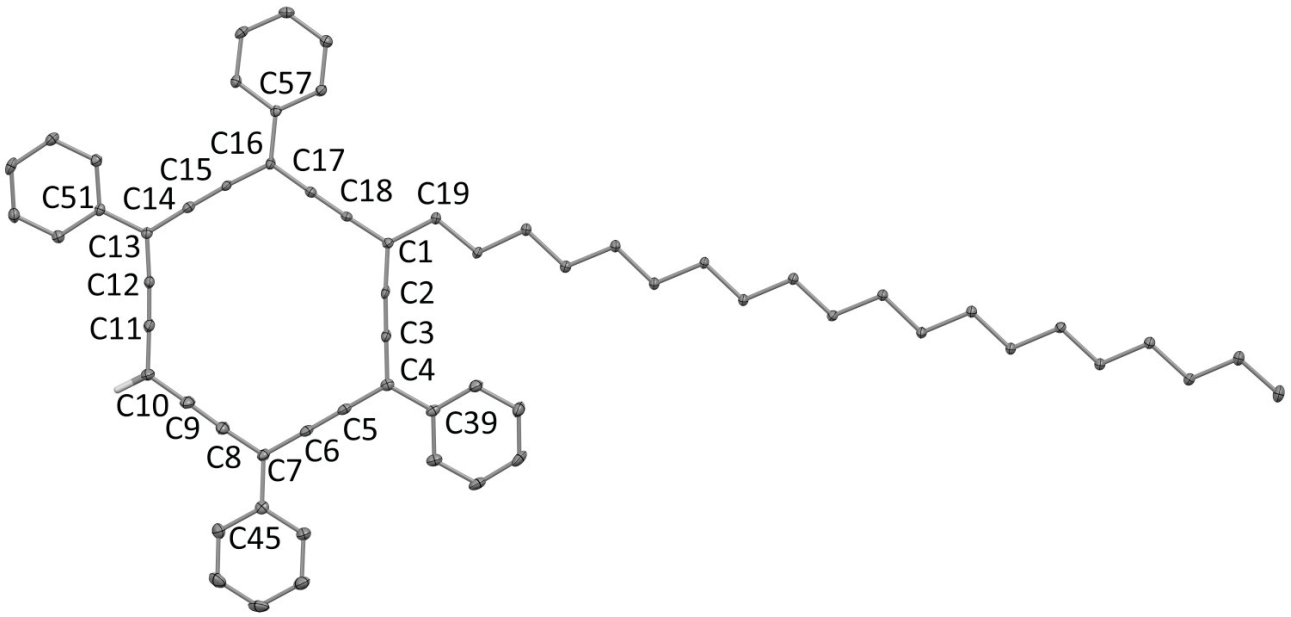

11a (30 % probability level for the thermal ellipsoids)

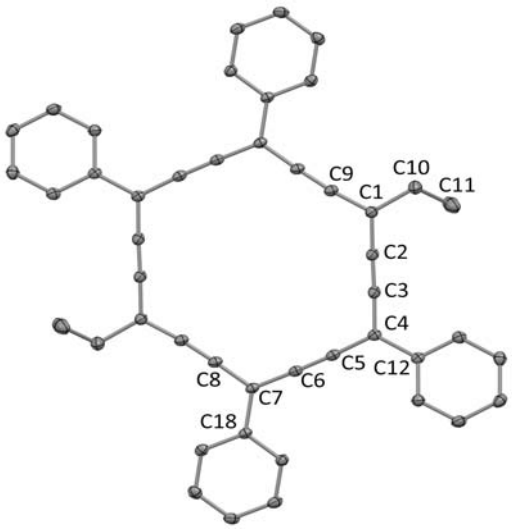

11b (30 % probability level for the thermal ellipsoid

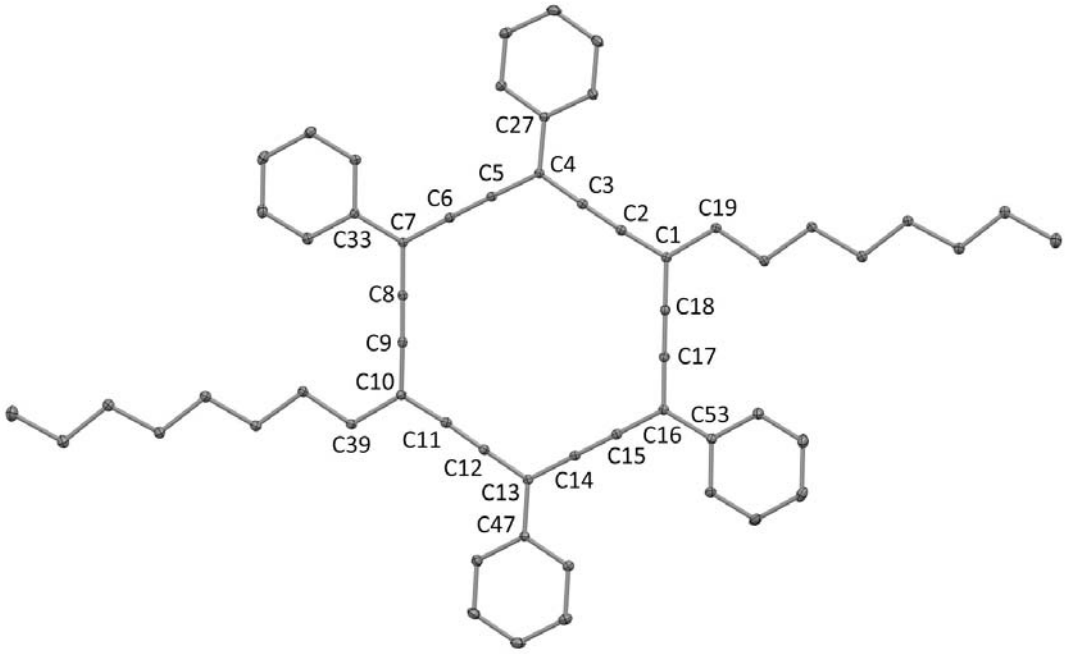

11c (30 % probability level for the thermal ellipsoids)

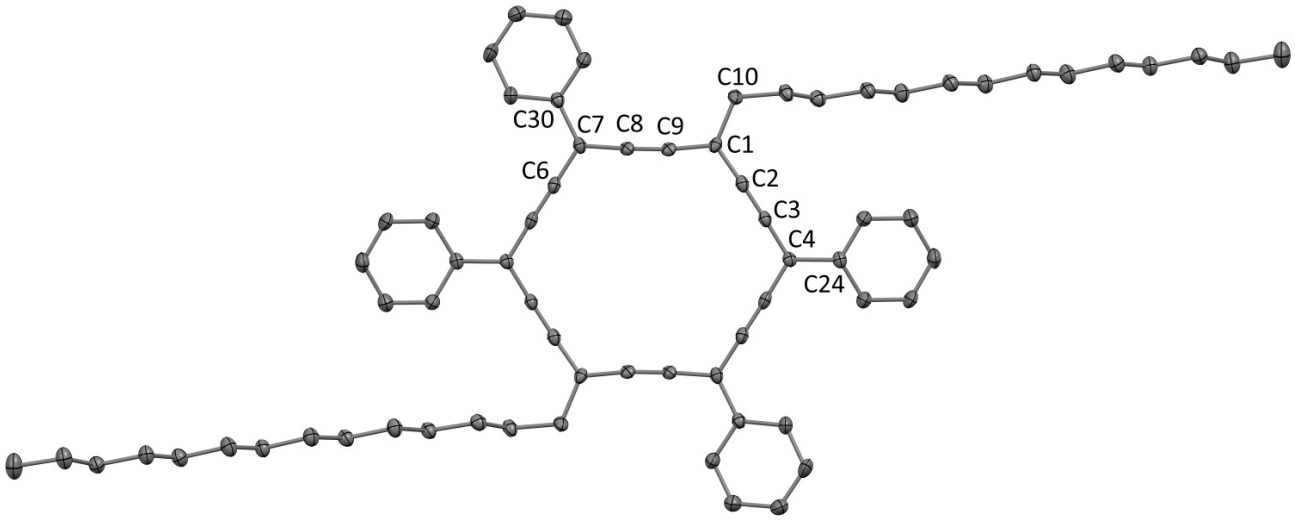

11d•$CHCl_3$ (30 % probability level for the thermal ellipsoids)

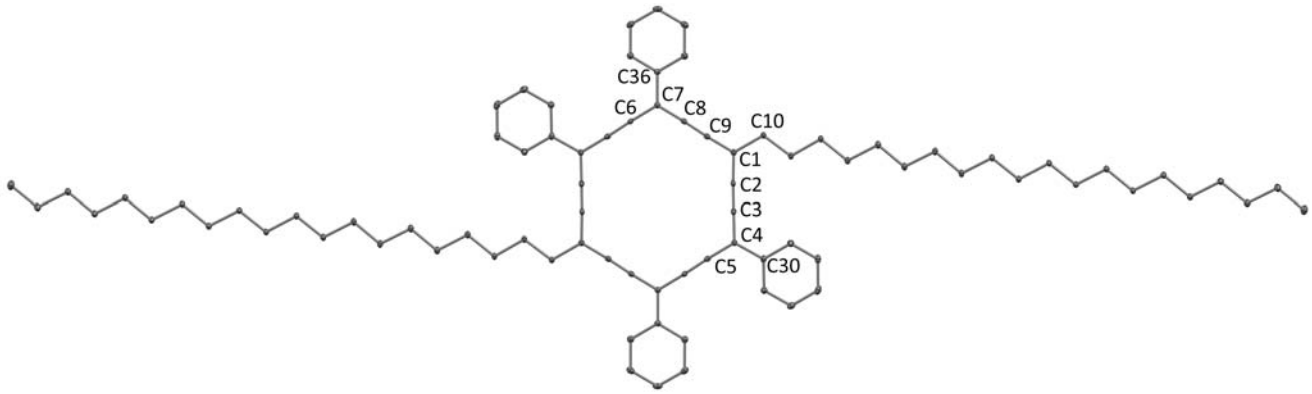

11d•CH_2Cl_2 = 11d in the main text (30 % probability level for isotropic thermal "ellipsoids")

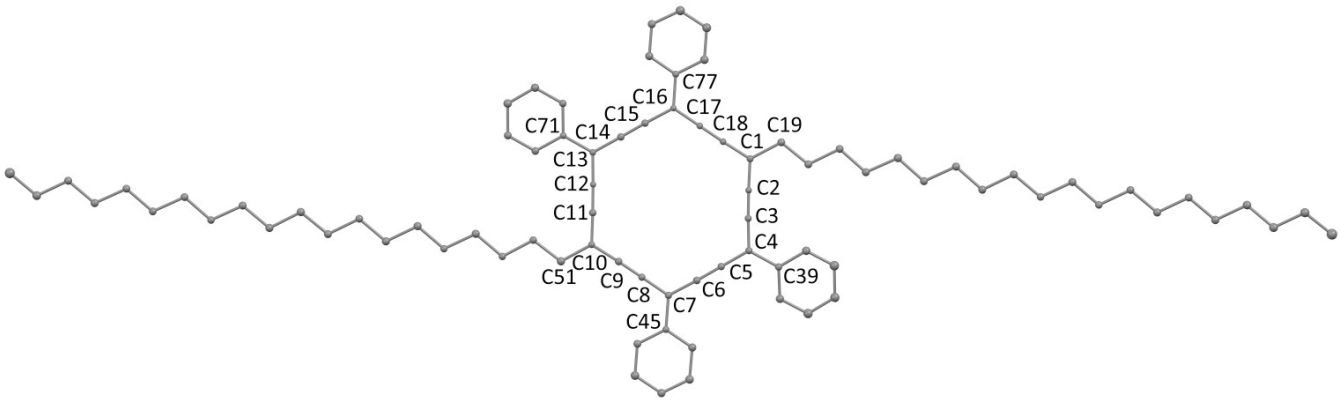

11e (30 % probability level for isotropic thermal "ellipsoids": see Figure S2)

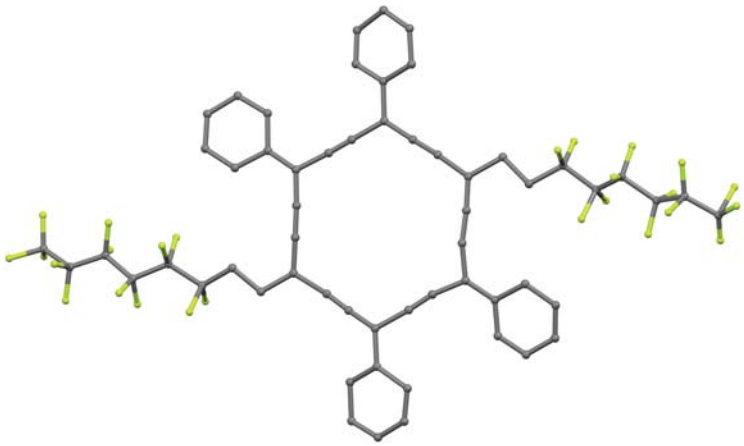

1.15. Solid UV-visible absorption spectra (absorbance *vs* wave length in nm).

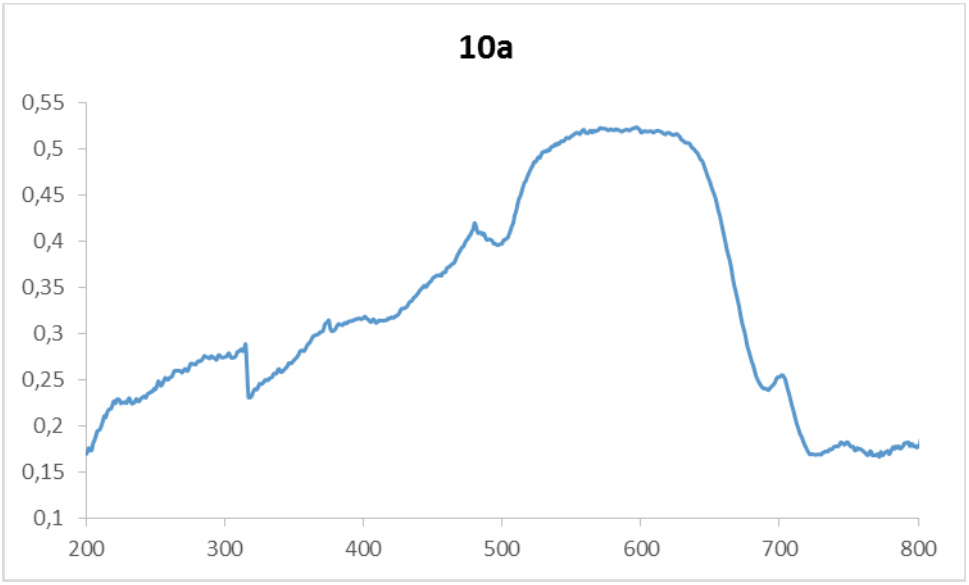

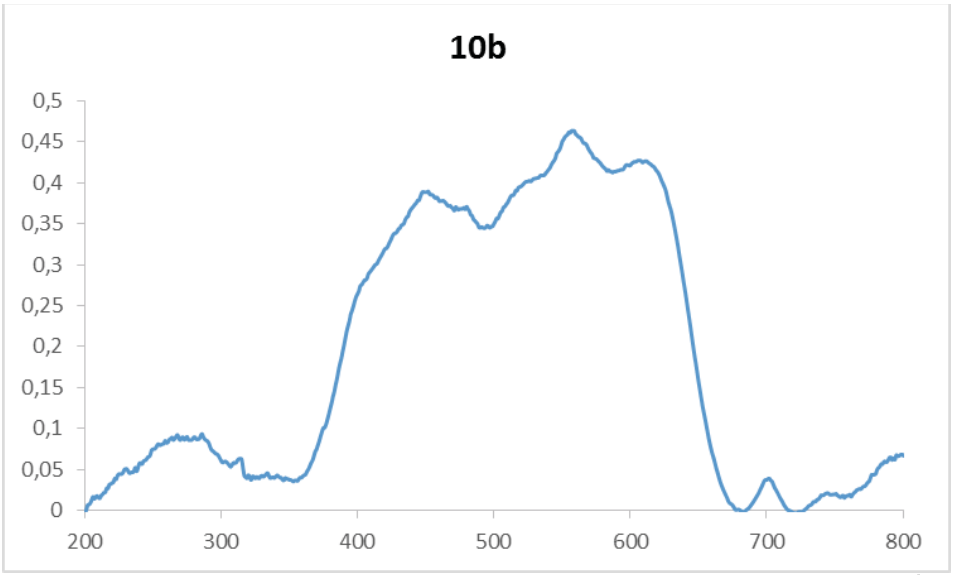

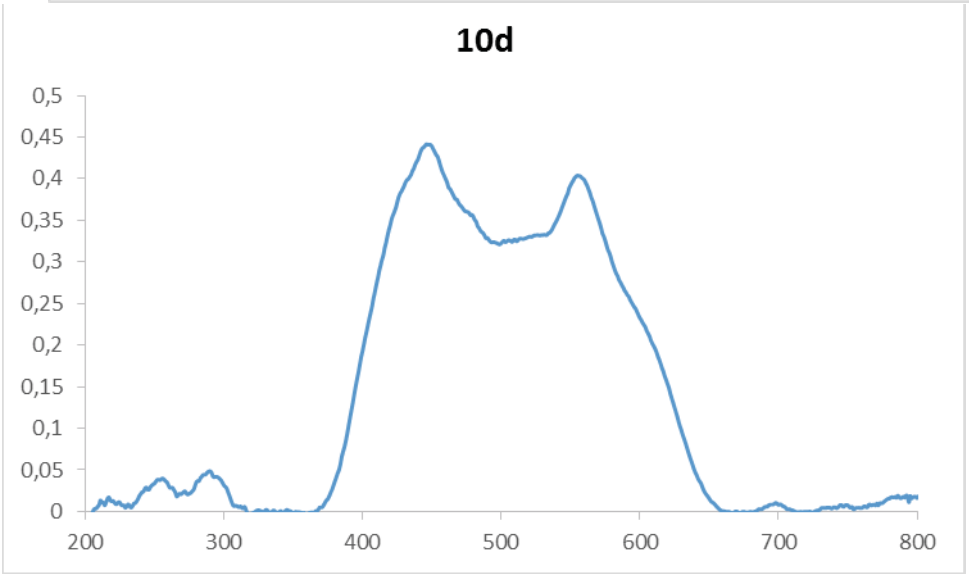

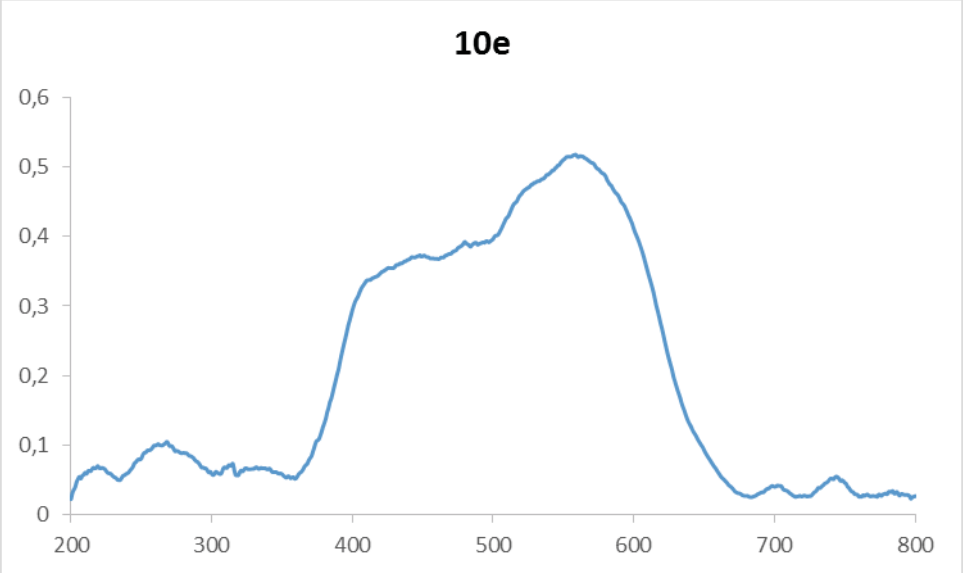
10e
0,6
0,5
0,4
0,3
0,2
0,1
0
200
300
400
500
600
700
800

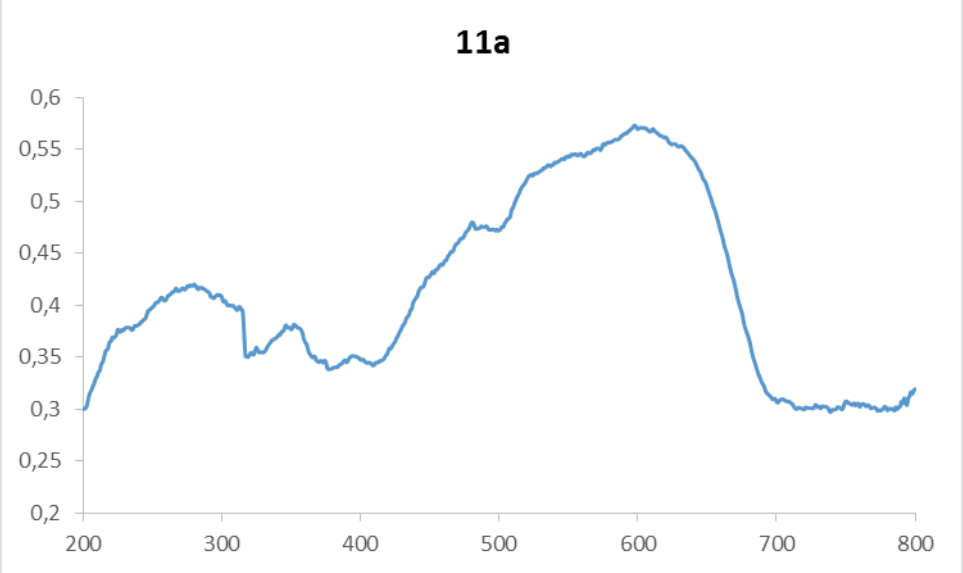
11a
0,6
0,55
0,5
0,45
0,4
0,35
0,3
0,25
0,2
200
300
400
500
600
700
800

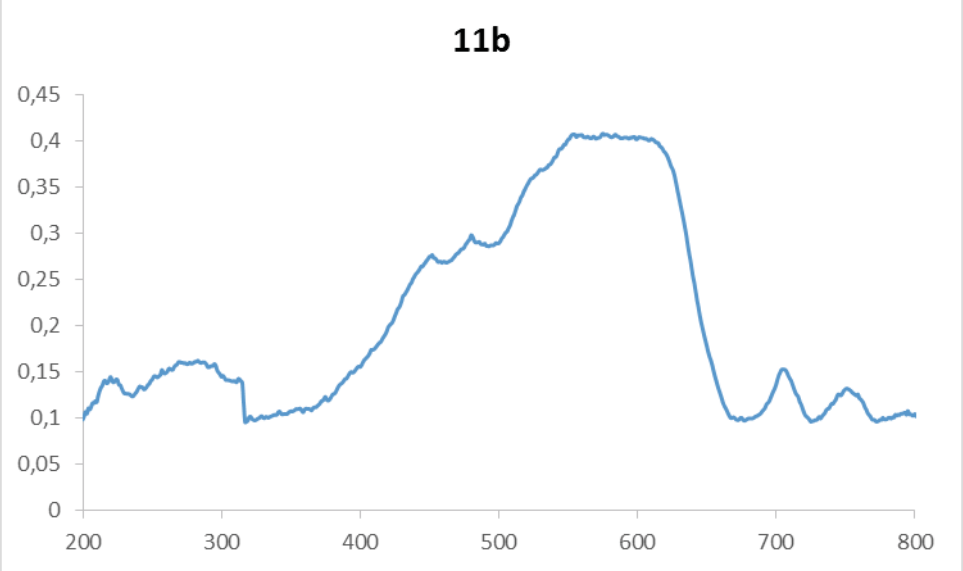
11b
0,45
0,4
0,35
0,3
0,25
0,2
0,15
0,1
0,05
0
200
300
400
500
600
700
800

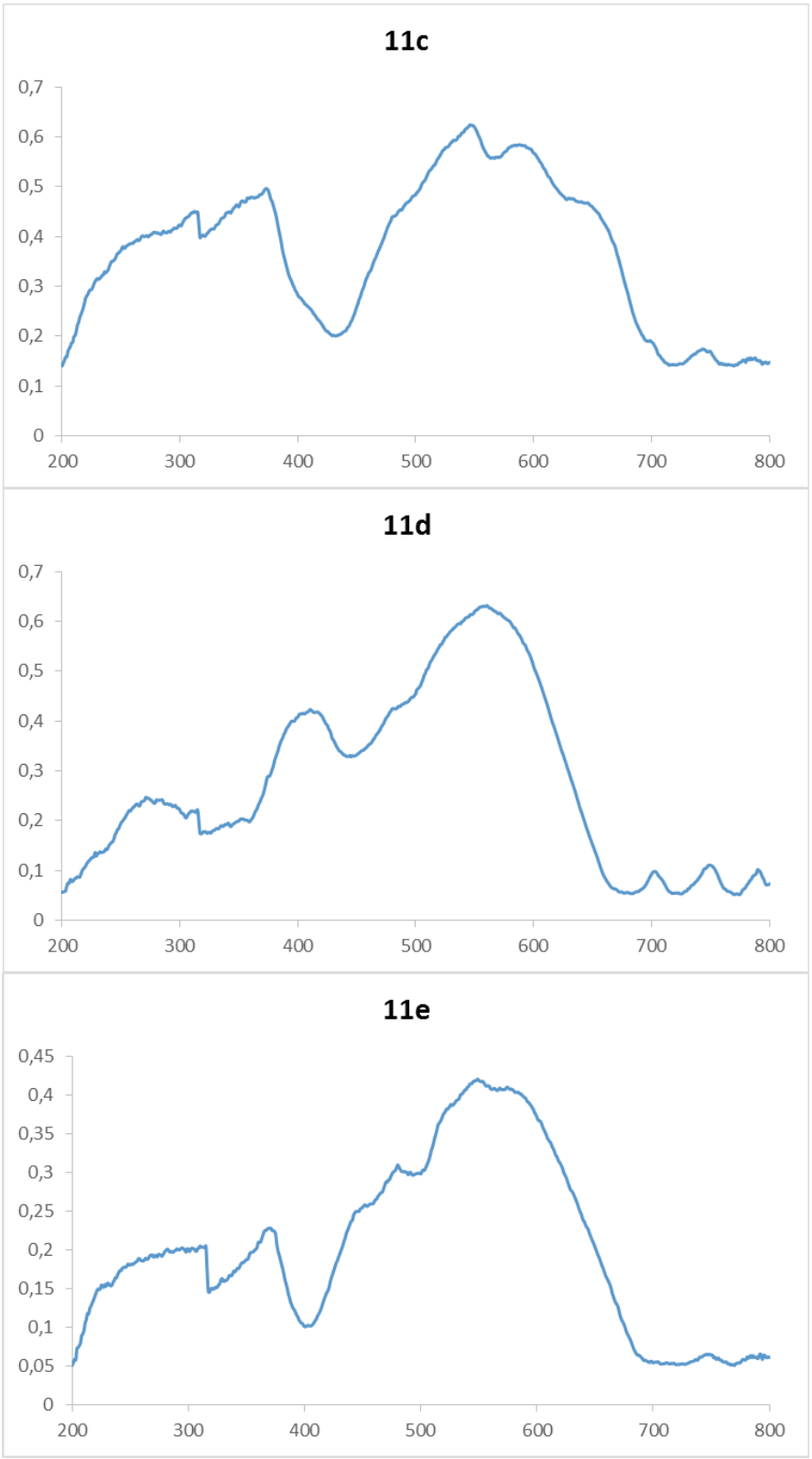
11c
0,7
0,6
0,5
0,4
0,3
0,2
0,1
0
200
300
400
500
600
700
800
11d
0,7
0,6
0,5
0,4
0,3
0,2
0,1
0
200
300
400
500
600
700
800
11e
0,45
0,4
0,35
0,3
0,25
0,2
0,15
0,1
0,05
0
200
300
400
500
600
700
800

1.16. UV-vis absorption spectrum of 1f in $CHCl_3$:

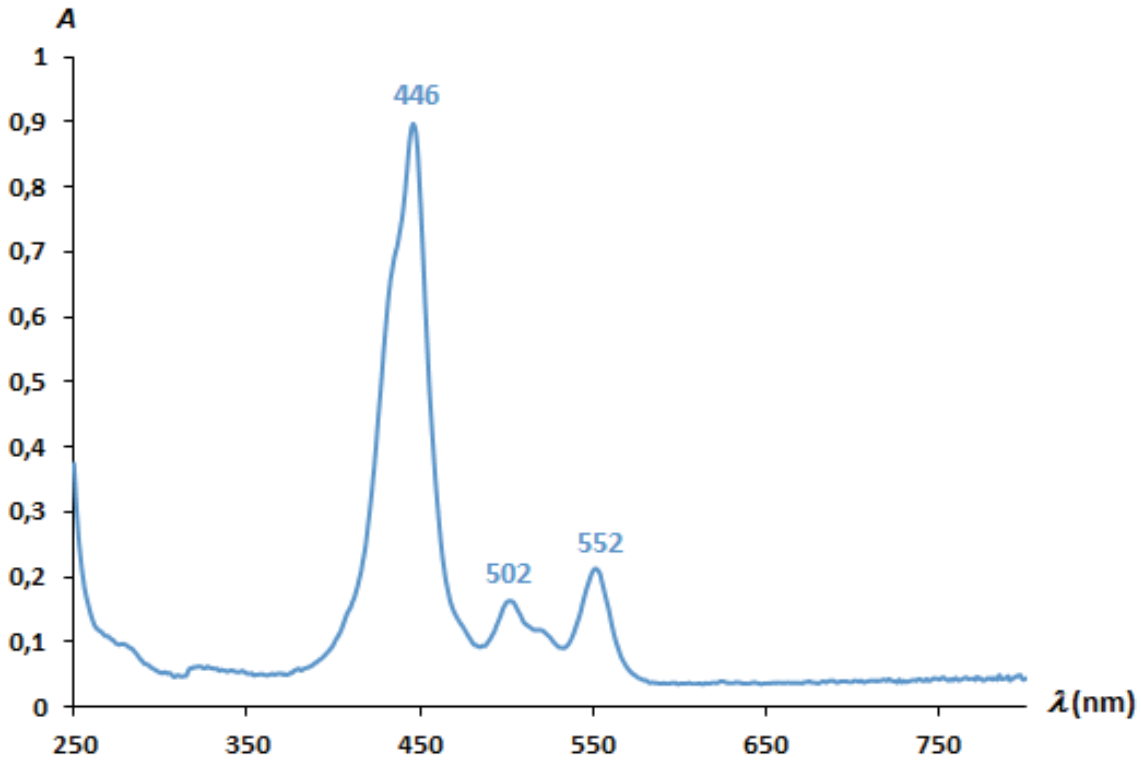

Chapter 4

3D and 2D supramolecular assemblies and thermotropic behaviour of a *carbo*-benzenic mesogen

Introduction & Summary

Liquid crystals (LCs) are extensively applied in various electronic devices that are part of our daily life, such as smartphones, laptops, flat panel TVs. The LC phase, an intermediate state between a crystal state and an amorphous state, is formed by the spontaneous self-organization of mesogenic molecules. Depending on the shape of mesogenic molecules, LCs are commonly classified into two categories: calamitic (rod-like) LCs[1] and discotic (disk-like) LCs.[2] The rod-like mesophase, was first described by Reinitzer at the end of the 19th century.[3] Since then, the LCs behavior of linear rod-like shape mesogens have been widely studied and started to lead to applications, in particular in liquid crystal displays (LCDs).[4]

Disk-like liquid crystals (DLCs) have been known only for 40 years, since Chandrasekhar first reported on the formation of discotic mesophases from benzene-hexa-*n*-alkanoate mesogens in 1977.[5] Recently, intense research efforts have been devoted to the development of DLCs due to their potential applications in organic field effect transistors (OFETs), organic light emitting diodes (OLEDs), and organic photovoltaic devices (OPVs).[2, 6] Discotic mesogen molecules typically possess a flat and rigid aromatic core decorated with several flexible aliphatic chains, and allow the formation of two main types of mesophases: nematic and columnar.[2, 4] Lamellar mesophases, whose structure remain still ambiguous today, can also be formed from discotic mesogens.[7] The nematic phase, the simplest and less-ordered LC phase in which the discotic molecules are orientationally arranged with no long-range translational order, already produced industrial applications as optical compensating films aiming to increase the angle of view in LCDs. [8 ,6b] When the discotic mesogens arrange into parallel columns, it gives columnar mesophases, [2] whose formation is assumed to be cooperatively induced by central aromatic cores and peripheral side chains of the mesogen. In this mesophase, the core-core intracolumnar distance is quite short (usually 3.5 Å), thus allowing an overlap of the π-orbitals of two adjacent mesogens, whereas the intercolumnar distance is generally longer (about 20-40 Å), depending on the length of the flexible side chains.

The most common aromatic cores for columnar LCs are: macrocyclic or polycyclic compounds possibly containing heteroatoms (N, O, S), such as porphyrins, phthalocyanines, and hexaazatriphenylenes (HATs), [9] triphenylenes or hexa-peri-hexabenzocoronenes (HBCs) (as shown in Figure 1. A-E).[10] Generally, large planar aromatic cores allowing for an extended π-

orbital overlap, are prone to reinforce the stability of the columnar arrangement and the supramolecular order. The dispersive chains attached to the central core also play a significant role in the formation of columnar mesophases. The nature, the number and the position of the chains on the mesogenic core can indeed strongly affect the phase transition temperatures, the solubility of the mesogenic molecules, the intercolumnar distances and the intracolumnar order of the mesophases. The most used flexible side chains for columnar mesogenic molecules cover linear and branched alkyl, alkylphenyl (or alkoxyphenyl) and carboxyl chains.

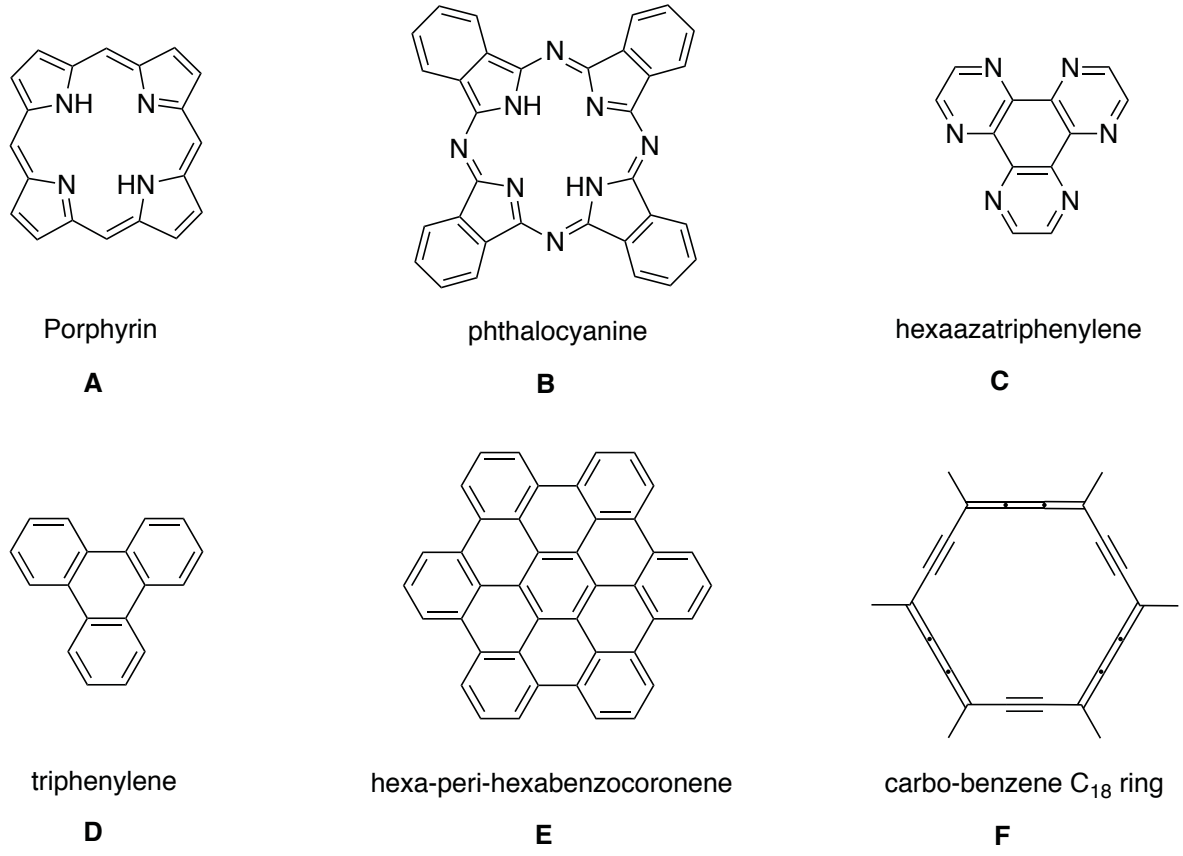

Figure 1. **A-E**: examples of typical polyclic mesogenic cores for columnar LCs. **F**: the *carbo*-benzene ring as first macro-monocyclic newly investigated mesogenic core.

While macro-poly-heterocyclic aromatics, such as porphyrins, were extensively studied as mesogenic cores, no specific attention has been paid to macro-mono-cyclic aromatics. In particular, the *carbo*-benzene C_{18} ring, whose macro-aromatic character was often compared to that of the 18-π-electrons $C_{16}N_2$ circuits of porphyrins, had not been envisaged as a mesogenic

core before this work. The 18-π-electron conjugated *carbo*-benzene ring, three-fold expanded analogue of benzene, with its all-carbon composition, aromatic core, flatness, and strong magnetic anisotropy, represents an attractive new core for the design of DLCs (see Figure 1. F). Furthermore, the hexagonal shape of *carbo*-benzenes makes them an ideal platform for the design of novel series of mesogens, with a possibility to anchor alkyl chains at different positions of the macrocycle. Recently, lipidic *p*-dialkyl-tetraphenyl-*carbo*-benzenes bearing two *n*-alkyl chains of discrete lengths (n = 2, 8, 14, and 20) were reported, but none of them was found to exhibit a LC behavior,[11] suggesting that the presence of only two alkyl chains attached to an aromatic C_{18} macrocycle is not sufficient to induce the formation of mesophases. Moreover, the melting point (or decomposition point) of most of the *carbo*-benzenes is higher than 200 ^{o}C, which is not consistent with the formation of mesophases. The melting point of the recently reported *p*-dialkyl-*carbo*-benzenes was shown to linearly decrease upon increasing the chain lengths, thus implying that the increase of the number of alkyl chains on *carbo*-benzene core could induce a LC behavior. Consequently, two *para*-trialkoxyphenylethynyl-*carbo*-benzenes of different chain lengths (*n*-$C_{12}H_{25}$ and *n*-$C_{18}H_{37}$) were prepared, and the mesogenic behavior of one of them was studied (see Figure 2.). The formation of a rectangular columnar mesophase at 115 °C was observed, and evidenced by polarized optical microscopy (POM), differential scanning calorimetry (DSC), powder X-Ray diffraction (PXRD) and scanning tunneling microscopy (STM). The lattice constants determined for the 3D lattice were found to be in good agreement with the 2D STM images of the *carbo*-benzene deposited on an HOPG surface.

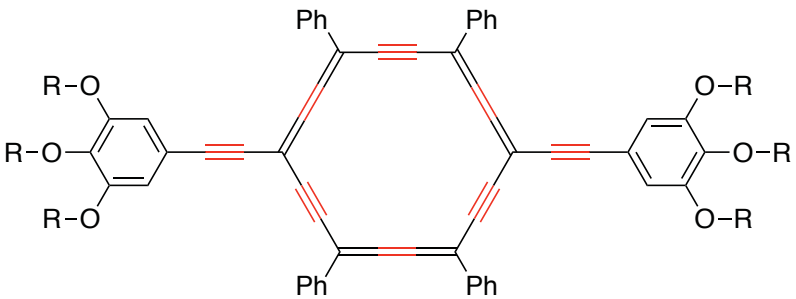

R = $C_{12}H_{25}$ or R = $C_{18}H_{37}$

Figure 2. Two designed "*carbo*-mesogen" molecules bearing different chain lengths.

Reference

1. M. Hird, *Chem. Soc. Rev*. **2007**, *36*, 2070-2095.

2. T. Wöhrle, I. Wurzbach, J. Kirres, A. Kostidou, N. Kapernaum, J. Litterscheidt, J. C. Haenle, P. Staffeld, A. Baro, F. Giesselmann, S. Laschat, *Chem. Rev.* **2016**, *116*, 1139-1241.

3. D. Vorländer, *Ber. Dtsch. Chem. Ges*. **1907**, *40*, 1970-1972.

4. S. Laschat, A. Baro, N. Steinke, F. Giesselmann, C. Hägele, G. Scalia, R. Judele, E. Kapatsina, S. Sauer, A. Schreivogel, M. Tosoni, *Angew. Chem. Int. Ed*., **2007**, *46*, 4832-4887.

5. S. Chandrasekhar, B. K. Sadashiva, K. A. Suresh, *Pramana*, **1977**, *9*, 471-480.

6. a). S. Sergeyev, W. Pisula, Y. H. Geerts, *Chem. Soc. Rev*., **2007**, *36*, 1902-1929; b). R. J. Bushby, K. Kawata, *Liq. Cryst*. **2011**, *38*, 1415-1426.

7. For a recent example, see: C. W. Ong, Y.-C. Chan, M.-C. Yeh, H.-Y. Lin, H.-F. Hsu, *RSC Adv*. **2013**, *3*, 8657-8659.

8. H. Bengs, O. Karthaus, H. Ringsdorf, C. Baehr, M. Ebert, J. H. Wendorff, *Liq. Cryst*., **1991**, *10*, 161-168.

9. C. M. Drain, A. Varotto, I. Radivojevic, *Chem. Rev*., **2009**, *109*, 1630-1658; b). B. Roy, N. De, K. C. Majumdar, *Chem. Eur. J.*, **2012**, *18*, 14560-14588.

10. a). S. Kumar, *Liq. Cryst*. **2004**, *31*, 1037-1059. b) W. Pisula, X. Feng, K. Müllen, *Adv. Mater*. **2010**, *22*, 3634-3649.

11. C. W. Zhu, A. Rives, C. Duhayon, V. Maraval, R. Chauvin, *J. Org. Chem*., **2017**, *82*, 925-935.

Article 5

ChemComm

COMMUNICATION

View Article Online
View Journal | View Issue

Cite this: *Chem. Commun.*, 2017, 53, 5902

Received 29th March 2017,
Accepted 9th May 2017

DOI: 10.1039/c7cc02430d

rsc.li/chemcomm

3D and 2D supramolecular assemblies and thermotropic behaviour of a *carbo*-benzenic mesogen†

Chongwei Zhu,[ab] Tsai-Hui Wang,[c] Chien-Jhang Su,[c] Shern-Long Lee,[d] Arnaud Rives,[ab] Carine Duhayon,[ab] Brice Kauffmann,[e] Valérie Maraval,*[ab] Chun-hsien Chen,*[d] Hsiu-Fu Hsu*[c] and Remi Chauvin*[ab]

Hexaalkoxy-di(phenylethynyl)-tetraphenyl-*carbo*-benzenes bearing six C_nH_{2n+1} aliphatic chains (n = 12, 18) have been synthesized and characterized, including by single crystal XRD analysis. For n = 12, a liquid crystal behaviour was observed in the range of 109–130 °C. DSC, POM and PXRD analyses evidenced a rectangular columnar mesophase at 115 °C. The determined 3D lattice constants are consistent with 2D STM images of the so-called "*carbo*-mesogen" deposited on an HOPG surface.

Since the early report by S. Chandrasekhar *et al.* describing mesomorphic properties of a hexasubstituted benzene derivative,[1] a large variety of disc-like π-conjugated rigid cores have been envisaged for the design of discotic-type liquid crystal (LC) mesogens. Such cores have been diversely substituted by two, three, four, six or more dispersion groups, conferring them the self-assembling properties governing the mesophase formation. In the case of extended cores such as discoid polycyclic aromatic hydrocarbons (PAHs), or heterocyclic counterparts, nanosegregation between the aromatic cores and outer aliphatic chains has been shown to act as a driving force for the formation of columnar mesophases.[2] The discoid symmetry order (so) of these cores varies from so = 3 for triangular triphenylene[3] and its expanded hexadehydrobenzo[12]annulene (DBA) counterparts,[4] to so = 4 for tetragonal porphin,[5] and up to so = 6 for hexagonal hexabenzocoronene (HBC).[6] Most of the latter are thus condensed polycycles, where the peripheral macrocycle encompasses smaller rings filling the discoid interior (*e.g.* 5 and 13 primitive rings in porphin and HBC, respectively). In contrast, due to the decrease of aromaticity *vs.* ring size, the mesogenic properties of macro-monocycles have been sparsely investigated beyond the case of DBA,[4] where rigidity is restored by both double insaturations and benzannelation, albeit for moderate size (C_{12} ring) and discoid character (so = 3). This challenge actually meets former designs of discotic LCs based on larger shape-persistent primitive macrocyclic cores of the oligo-phenylacetylene type.[7] A "tubular" discotic LC devised from a hollow phenylacetylene macrocycle (PAM C_{30} ring) decorated with six dispersion groups providing the mesogen with a regular hexagonal discoid character (so = 6) has thus been evidenced in the range of 144–110 °C.[7a] A larger mesogenic core (C_{58} ring) filled with intra-annular polar groups was shown to give stable columnar mesophases which were fully characterized at 120 °C or 110 °C.[7b] With the view of gaining insight into the mesogenic properties of truly monocyclic (non-benzannelated) macro-aromatics, the *carbo*-benzene ring of **1** appears to be a relevant candidate (Scheme 1), both in terms of size (C_{18}, diameter ≈ 0.8 nm) and discoid character (so = 6). As a three-fold expanded *carbo*-meric version of benzene,[8] the 18-π-electron *carbo*-benzene ring is aromatic just as the 6-π-electron parent is.[9] This C_{18} core also possesses other remarkable features, such as an all-carbon composition, an extended flexible flatness, a strong magnetic anisotropy, and a structural/chromophoric analogy with the $C_{16}N_2$ porphyrin core, thus providing *carbo*-benzene derivatives with unique properties.[10] The same features make the same C_{18} core also attractive for LC design upon anchoring of selected dispersion groups. Lipidic *carbo*-benzenes *p*-$(C_nH_{2n+1})_2C_{18}Ph_4$ bearing two *n*-alkyl chains of various lengths (n = 2, 8, 14, and 20) at the *para*-positions were recently described,[11] but none of them was found to display any LC behaviour. An increase of the number of dispersion groups is thus here envisaged by anchoring two pyrogallol ether groups at the same *para* positions, and more precisely two long-chain trialkoxyphenylethynyl groups.

The synthesis of the targets **1a** and **1b** was intended from the [6]pericyclynedione **2**,[12] following a method widely used for the

[a] *CNRS, LCC (Laboratoire de Chimie de Coordination), 205 route de Narbonne, BP44099, 31077 Toulouse Cedex 4, France*
[b] *Université de Toulouse, UPS, ICT-FR 2599, 31062 Toulouse Cedex 9, France. E-mail: valerie.maraval@lcc-toulouse.fr, chauvin@lcc-toulouse.fr*
[c] *Department of Chemistry, Tamkang University, 251 Taipei, Taiwan. E-mail: hhsu@mail.tku.edu.tw*
[d] *Department of Chemistry and Center for Emerging Material and Advanced Devices, National Taiwan University, 106 Taipei, Taiwan. E-mail: chhchen@ntu.edu.tw*
[e] *Université de Bordeaux, CNRS, INSERM, UMS3033/US001, Institut Européen de Chimie et Biologie, F-33607 Pessac, France*

† Electronic supplementary information (ESI) available. CCDC 1546671. For ESI and crystallographic data in CIF or other electronic format see DOI: 10.1039/c7cc02430d

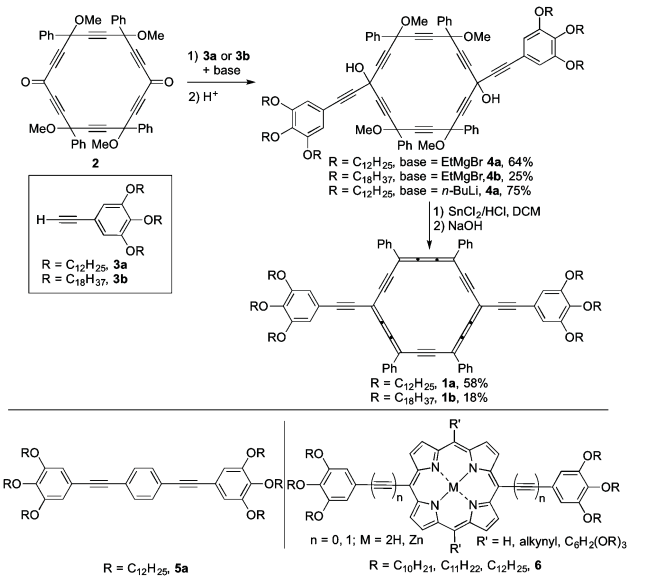

Scheme 1 Synthesis of the hexaalkyloxy-di(ethynylphenyl)-tetraphenyl-*carbo*-benzenes **1a** and **1b**, and previously reported reference congeners **5a** and **6**.

preparation of other *para*-disubstituted tetraphenyl-*carbo*-benzenes.[8b,c,11] The precursors of the selected dispersion groups classically used in LC design, the ethynylpyrogallol ethers **3a** and **3b** with alkyl chain lengths of n = 12 and 18, respectively, were prepared from commercially available 5-bromo-1,2,3-trimethoxybenzene.[13] The addition of two equivalents of the bromomagnesium salt of **3a** or **3b** to the diketone **2** afforded the expected [6]pericyclynediols **4a** and **4b** as mixtures of diastereoisomers in 64 and 25% yields, respectively. The low isolated yield of **4b** was due to the tricky procedure required for the purification of such a highly paraffinic molecule. The reaction of **2** with the lithium salt of **3a** (generated with *n*-BuLi) was also attempted, allowing the diadduct **4a** to be obtained in up to 75% yield (Scheme 1). After the treatment of **4a** and **4b** with $SnCl_2$ and HCl, the *carbo*-benzenes **1a** and **1b** were finally obtained in 58% and 18% yields, respectively (Scheme 1). The two products were isolated as dark blue-violet solids, giving red-violet dichloromethane (DCM) or chloroform solutions. The dodecyl derivative **1a** was however found to be much more soluble than the octadecyl homologue **1b**, the latter dissolving in chloroform only and at a very low concentration. Both ^{1}H and ^{13}C NMR spectra of **1b** could however be recorded in $CDCl_3$ solution at 320 K. A signature of the presence of the aromatic C_{18} macrocycle of **1a** and **1b** is the diatropic ring current-induced deshielding of the *ortho*-^{1}H nuclei of the phenyl substituents at *ca.* 9.5 ppm, as observed for all aryl-substituted *carbo*-benzenes. Both **1a** and **1b** also exhibit similar UV-vis absorption spectra in chloroform solution, with the same maximum absorption wavelength at 490 nm. In most cases, whatever the solvents and conditions employed, **1a** and **1b** were found to give thin hair-like crystals, or incidentally bipyramidal crystals (see photographs in the ESI†), of extremely low diffracting power. Nevertheless, after many attempts, single crystals suitable for XRD analysis were obtained from a chloroform solution of **1a**,

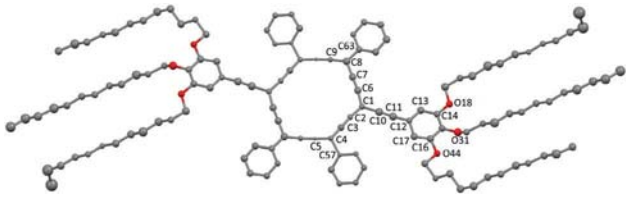

Fig. 1 Molecular view of the X-ray crystal structure of **1a**, with thermal ellipsoids drawn at the 30% probability level. For clarity, hydrogen atoms are omitted.

thus allowing confirmation of the structure (Fig. 1).[14] Due to weak diffraction intensities and low resolution, non-hydrogen atoms could only be refined with isotropic displacement parameters, but in the absence of any solvate molecule, no disorder is found in the structure, in particular in the dodecyl chains aligned in a parallel manner in parallel triads (approximately along the *a* axis and the *ab* plane).

Mesophases of **1a**, more soluble and available in a larger amount than **1b**, could also be analysed in detail. As a literature reference, the oligophenyleneethynylene (OPE) derivative **5a**, *carbo*-meric parent of **1a** (Scheme 1), was recently reported for its self-assembling properties in solution, but the possible thermotropic LC behaviour of the pure substance was not mentioned.[15] Porphyrinic analogues of type **6** with two or four trialkoxyaryl dispersion groups (Scheme 1) were also reported to exhibit LC behaviour at low temperature.[16]

The phase behaviour of **1a** was investigated by the combination of polarizing optical microscopy (POM), differential scanning calorimetry (DSC), and powder X-ray diffraction (PXRD). Under POM, a viscous birefringent liquid was observed upon heating between 100 and 130 °C (Fig. 2). Further heating was found to give a dark image, indicating either decomposition of **1a** or formation of its isotropic phase, which remained the same upon cooling even to room temperature. The birefringent texture of the viscous liquid upon heating (usually not as indicative as natural textures obtained by cooling a perfect liquid phase, since solid state attributes can remain and interfere) does not show characteristic features for an explicit identification of phases. In the DSC thermogram between 0 and 120 °C, signals can be detected upon

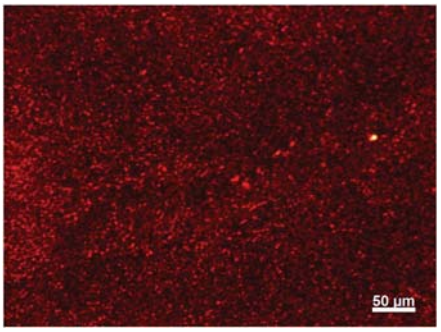

Fig. 2 Polarizing micrograph of **1a** at 109 °C on heating as a viscous liquid showing birefringent textures indicating the phase to be liquid crystalline (the identity of the LC phase cannot be determined from the POM texture only). Scale: white box length = 50 µm.

heating only, and a phase transition at 109 °C is in accordance with POM observations. Further heating leads to an exothermic signal starting at *ca.* 130 °C, interpretable as the signature of either a recrystallization or a decomposition process.

As no signal is observed in the second or third heating/cooling runs, the initial exothermic signal at 136 °C is ascribed to thermal decomposition. The lowest reported melting–decomposition temperature for a tetraaryl-*carbo*-benzene is just 12 °C higher (148 °C for *p*-dieicosyl-tetraphenyl-*carbo*-benzene),[11] and although most hexaaryl- and dialkynyltetraaryl-*carbo*-benzenes reported to date have been shown to melt or decompose above 200 °C, the "π-frustration" brought by the trialkoxyphenylethynyl groups onto the π-electron-rich C_{18} core of **1a** can account for a specific thermal instability.[17] When the DSC thermogram of **1a** is recorded between 0 and 115 °C to avoid thermal decomposition, the non-reproducibility of the signal at 109 °C is ascribed to the thermal history of the virgin crystals (powders). However, after one night annealing at room temperature, a new signal at 55.1 °C appears on heating and a signal at 27.8 °C can be observed on cooling. These DSC data for two cycles between 0 and 115 °C are consistent with POM observations (see the ESI†).

The LC behaviour of **1a** was confirmed by PXRD, allowing investigation of molecular packing patterns in different states. Upon heating the crystalline phase at temperatures above 109 °C and below 130 °C, a wide angle broad halo at 4.7 Å of molten chains evolved, indicating the fluid phase formation.[18] In the small angle regime, signals are simplified by comparison to the complicated patterns of the crystalline phase. The PXRD pattern at 115 °C (Fig. 3) can be indexed to a columnar rectangular (Col_{rec}) phase. Detailed analysis of the PXRD data allowed the determination of the two-dimensional lattice constants of the Col_{rec} phase at 115 °C (Table 1): a = 48.5 Å, b = 45.0 Å, and Z = 3 (Z: number of molecules in a unit cell). No signal could be attributed to the intracolumnar correlation along the c axis.

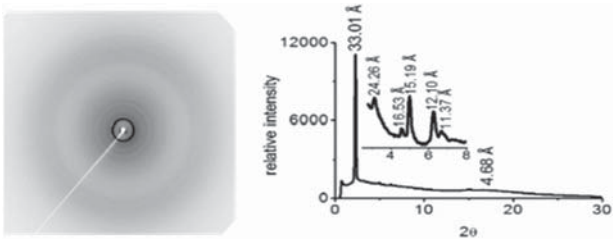

Fig. 3 Powder X-ray diffractogram of **1a** at 115 °C in the LC phase range indicating a columnar rectangular geometry. Left: 2D-XRD; right: 1D-XRD.

Table 1 PXRD data of **1a** at 115 °C (see Fig. 3)

	d-Spacing (Å)			
Phase	Obsd	Calcd	Miller indices	Lattice constants (Å)
Col_{rec}	33.01	33.01	11	a = 48.52
	24.26	24.26	20	b = 45.04
	16.53	16.51	22	Z = 3
	15.19	15.22	31	
	12.10	12.13	40	
	11.37	11.71	41	
	4.68		(Alkyl)	

The 2D lattice constants of the LC phase are consistent with a specific domain in STM images of **1a**, which is primarily revealed as a macrocycle decorated by six phenyl-like groups (Fig. 4). Although the 2D packing is not perfectly regular and compact, it clearly shows a 48 × 43 Å rectangular pattern analogous to the one determined by PXRD analysis. The distances between neighbouring molecules of **1a** are found to be *ca.* 16, 21, 24, and 25 Å. As observed in the single crystal along the a axis,[18] the alkyl chains are aligned in a parallel manner with the [0110] direction of the underlying graphite substrate, and are interdigitated between neighbouring molecules, thus locking rotation of the mesogen about the column axes.

A schematic molecular packing deduced from PXRD and STM investigations is shown in Fig. 5. For the 2D lattice, STM resolves 3 chains per molecule of **1a** while the other chains are presumably fluxional in the solution. This is a common packing pattern for alkane-decorated aromatics because of the limited space and insufficient attractions from the substrate.[19] For the 3D columnar phase, the fluxional chains inferred from STM images are likely coplanar with the molecular plane due to van der Waals interactions between alkyl chains of the nearest upper and lower layers (*vide infra*, Fig. 5c).[18]

The macrocyclic cores thus stack face-to-face into columns by π–π interactions, assisted by nanosegregation of domains of interdigitated molten side-chains and π–π interaction of the peripheral phenyl/phenylethynyl groups. The alkyl chains are arranged in a *trans* manner with respect to the *para*-dialkynyl axis, thus driving an anisotropic in-plane packing by chain interdigitation.

The extended aromatic core of the *carbo*-benzene **1a** (58 sp^2- or sp-C atoms) is embedded in a 34% more extended oxyparaffinic surrounding (78 sp^3-CH_2 or O centers). This balance allows a LC behaviour of the pure substance in a rectangular columnar mesophase resulting from unprecedented differential supramolecular associations around C_{18} macro-monocycles. These results open natural prospects for a new generation of functional tubular discotic LCs based on such a type of rigid cores.

C. Z. thanks the China Scholarship Council for his PhD scholarship. The ANR program (ANR-11-BS07-016-01) is acknowledged for the postdoctoral fellowship of A. R. and for funding of working facilities. R. C. thanks the Centre National de la Recherche

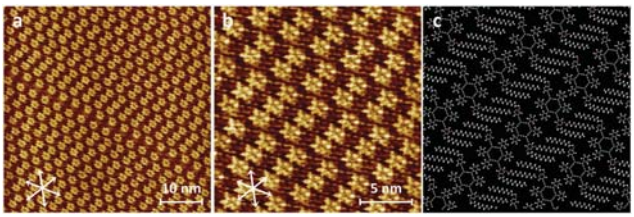

Fig. 4 STM images of **1a**. (a) STM image showing the in-plane molecular packing into ordered arrays; (b) high resolution STM image exhibiting the macrocycle organization by intermolecular chain interdigitation framing a rectangular pattern of 48 × 43 $Å^2$ tiles (see TOC scheme or Fig. 5c); (c) proposed packing for panel b. Conditions: substrate, HOPG (highly oriented pyrolytic graphite); solvent, 1,2,4-trichlorobenzene; concentration, *ca.* 0.1 mM; E_{bias}, −800 mV; $i_{tunneling}$, 0.18 nA; room temperature.

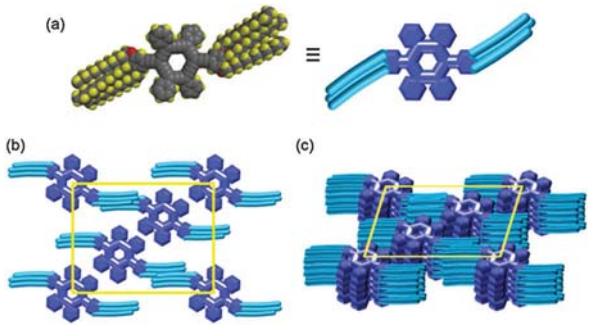

Fig. 5 Molecular packing patterns based on PXRD and STM investigations of **1a**. (a) Spaced-filled model and to-scale cartoon representation. (b) Top view cartoon representation of the columnar rectangular lattice. (c) Side-view cartoon representation of the columnar molecular packing.

Scientifique (CNRS) for half a teaching sabbatical in 2015–2016. The authors also thank Dr Nathalie Saffon-Merceron for her efforts in trying to solve the structure of **1a** by X-ray diffraction analysis of single crystals thereof. In the framework of the CNRS ЯÉCIPROCS network, this work has benefited from the X-ray facility of the Biophysical and Structural Chemistry platform at IECB, CNRS UMS3033, INSERM US001, Bordeaux University. C.-h. C. and H.-F. H. would like to thank Ministry of Science and Technology for financial support.

Notes and references

1 S. Chandrasekhar, B. K. Sadashiva and K. A. Suresh, *Pramana*, 1977, **9**, 471–480.
2 T. Wöhrle, I. Wurzbach, J. Kirres, A. Kostidou, N. Kapernaum, J. Litterscheidt, J. C. Haenle, P. Staffeld, A. Baro, F. Giesselmann and S. Laschat, *Chem. Rev.*, 2016, **116**, 1139–1241.
3 (*a*) S. H. Seo, T. V. Jones, H. Seyler, J. O. Peters, T. H. Kim, J. Y. Chang and G. N. Tew, *J. Am. Chem. Soc.*, 2006, **128**, 9264–9265; (*b*) S.-I. Kato, N. Takahashi, H. Tanaka, A. Kobayashi, T. Yoshihara, S. Tobita, T. Yamanobe, H. Uehara and Y. Nakamura, *Chem. – Eur. J.*, 2013, **19**, 12138–12151.
4 K. Tahara, Y. Yamamoto, D. E. Gross, H. Kozuma, Y. Arikuma, K. Ohta, Y. Koizumi, Y. Gao, Y. Shimizu, S. Seki, K. Kamada, J. S. Moore and Y. Tobe, *Chem. – Eur. J.*, 2013, **19**, 11251–11260.
5 C. M. Drain, A. Varotto and I. Radivojevic, *Chem. Rev.*, 2009, **109**, 1630–1658.
6 O. F. Aebischer, B. Alameddine and T. A. Jenny, *Chimia*, 2008, **62**, 967–973.
7 (*a*) O. Y. Mindyuk, M. R. Stetzer, P. A. Heiney, J. C. Nelson and J. S. Moore, *Adv. Mater.*, 1998, **10**, 1363–1366; (*b*) M. Fischer, G. Lieser, A. Rapp, I. Schnell, W. Mamdouh, S. De Feyter, F. C. De Schryver and S. Höger, *J. Am. Chem. Soc.*, 2004, **126**, 214–222.
8 (*a*) R. Chauvin, *Tetrahedron Lett.*, 1995, **36**, 397–400; (*b*) V. Maraval and R. Chauvin, *Chem. Rev.*, 2006, **106**, 5317–5343; (*c*) K. Cocq, C. Lepetit, V. Maraval and R. Chauvin, *Chem. Soc. Rev.*, 2015, **44**, 6535–6559.
9 (*a*) C. Godard, C. Lepetit and R. Chauvin, *Chem. Commun.*, 2000, 1833–1834; (*b*) C. Lepetit, C. Godard and R. Chauvin, *New J. Chem.*, 2001, **25**, 572–580; (*c*) C. Lepetit, B. Silvi and R. Chauvin, *J. Phys. Chem. A*, 2003, **107**, 464–473; (*d*) A. Soncini, P. W. Fowler, C. Lepetit and R. Chauvin, *Phys. Chem. Chem. Phys.*, 2008, **10**, 957–964; (*e*) R. Chauvin, C. Lepetit, V. Maraval and L. Leroyer, *Pure Appl. Chem.*, 2010, **82**, 769–800.
10 For two-photon absorption properties of *carbo*-benzenes see: (*a*) I. Baglai, M. de Anda-Villa, R. M. Barba-Barba, C. Poidevin, G. Ramos-Ortíz, V. Maraval, N. Saffon-Merceron, J.-L. Maldonado and R. Chauvin, *Chem. – Eur. J.*, 2015, **21**, 14186–14195. For single molecule conductance properties of *carbo*-benzenes see: (*b*) Z. Li, M. Smeu, A. Rives, V. Maraval, R. Chauvin, M. A. Ratner and E. Borguet, *Nat. Commun.*, 2015, **6**, 6321.
11 C. Zhu, A. Rives, C. Duhayon, V. Maraval and R. Chauvin, *J. Org. Chem.*, 2017, **82**, 925–935.
12 (*a*) L. Maurette, C. Tedeschi, E. Sermot, M. Soleilhavoup, F. Hussain, B. Donnadieu and R. Chauvin, *Tetrahedron*, 2004, **60**, 10077–10098; (*b*) L. Leroyer, C. Zou, V. Maraval and R. Chauvin, *C. R. Chim.*, 2009, **12**, 412–429. For references on pericyclynes see: (*c*) L. T. Scott, G. J. DeCicco, J. L. Hyun and G. Reinhardt, *J. Am. Chem. Soc.*, 1983, **105**, 7760–7761; (*d*) L. T. Scott, G. J. DeCicco, J. L. Hyun and G. Reinhardt, *J. Am. Chem. Soc.*, 1985, **107**, 6546–6555.
13 J. Wu, M. D. Warson, L. Zhang, Z. Wang and K. Müllen, *J. Am. Chem. Soc.*, 2004, **126**, 177–186.
14 $C_{130}H_{174}O_6$, pink red plate, M = 1832.81 g mol^{-1}, monoclinic, a = 49.45(2) Å, b = 15.293(11) Å, c = 7.3526(14) Å, $\alpha = \gamma = 90°$, β = 91.49(3)°, V = 5558(2) Å^3, T = 100 K, space group $P2_1/c$, Z = 2, μ(Cu K$_\alpha$) = 0.490 mm^{-1}; 13 385 reflections measured and 4780 unique ($2\theta_{max}$ = 102.6°, R_{int} = 0.086), 2434 reflections [$I > 2.5\sigma(I)$] used in all calculations; R = 0.2493, R_w = 0.2680 (more details in ESI†). CCDC 1546671.
15 M. J. Mayoral, C. Rest, J. Schellheimer, V. Stepanenko and G. Fernández, *Chem. – Eur. J.*, 2012, **18**, 15607–15611.
16 (*a*) D. Koszelewski, A. Nowak-Król, M. Drobizhev, C. J. Wilson, J. E. Haley, T. M. Cooper, J. Romiszewski, E. Górecka, H. L. Anderson, A. Rebane and D. T. Gryko, *J. Mater. Chem. C*, 2013, **1**, 2044–2053; (*b*) M. Salamończyk, D. Pociecha, A. Nowak-Król, D. Koszelewski, D. T. Gryko and E. Górecka, *Chem. – Eur. J.*, 2015, **21**, 7384–7388.
17 I. Baglai, V. Maraval, C. Bijani, N. Saffon-Merceron, Z. Voitenko, Y. M. Volovenko and R. Chauvin, *Chem. Commun.*, 2013, **49**, 8374–8376.
18 Similar distances occur in the single crystal, where the shortest distance between C atoms of parallel sections of nearest dodecyl chains varies in the range 4.5–4.8 Å in intramolecular triads (approximately along the *b* axis), and in the range 4.1–4.3 Å between intercalated molecules (approximately along the *c* axis).
19 (*a*) S.-L. Lee, H.-J. Wu, Y.-J. Hsu, H.-H. Chen, H.-F. Hsu and C.-h. Chen, *Chem. Commun.*, 2014, **50**, 14093–14096; (*b*) S.-L. Lee, Y.-J. Hsu, H.-J. Wu, H.-A. Lin, H.-F. Hsu and C.-h. Chen, *Chem. Commun.*, 2012, **48**, 11748–11750.

SUPPORTING INFORMATION

3D and 2D Supramolecular Assemblies and Thermotropic Behavior of a *Carbo*-benzenic Mesogen

Chongwei Zhu,[a] Tsai-Hui Wang,[b] Chien-Jhang Su,[b] Shern-Long Lee,[c] Arnaud Rives,[a] Carine Duhayon,[a] Brice Kauffmann,[d] Valérie Maraval,*[a] Chun.-hsien Chen,*[c] Hsiu-Fu Hsu,*[b] and Remi Chauvin*[a]

[a] *CNRS, LCC (Laboratoire de Chimie de Coordination)*
205 route de Narbonne, BP44099, 31077 Toulouse Cedex 4 (France)
Université de Toulouse, UPS, ICT-FR 2599, 31062 Toulouse Cedex 9 (France).
E-mail: valerie.maraval@lcc-toulouse.fr, chauvin@lcc-toulouse.fr
[b] *Department of Chemistry, Tamkang University, 251 Taipei (Taiwan).*
E-mail: hhsu@mail.tku.edu.tw
[c] *Department of Chemistry and Center for Emerging Material and Advanced Devices, National Taiwan University, 106 Taipei (Taiwan).*
E-mail: chhchen@ntu.edu.tw
[d] *Institut Européen de Chimie et Biologie, 2, Rue Robert Escarpit, 33607 Pessac (France).*

Table of Contents

1. General remarks

THF, diethyl ether (Et_2O), pentane and dichloromethane (DCM) were dried with a PureSolv-MD-5 Innovative Technology system for the purification of solvents. All other reagents were used as commercially available. In particular, solutions of *n*-BuLi were 1.6 M or 2.5 M in hexane, solutions of EtMgBr were 3 M in THF, solutions of HCl were 2 M in diethyl ether. All reactions were carried out under argon atmosphere using Schlenk and vacuum line techniques. Column chromatography was carried out on silica gel (60 Å, 70-200 µm). Silica gel thin layer chromatography plates (60F254, 0.25 mm) were revealed under UV-light and/or by treatment with an ethanolic solution of phosphomolybdic acid (20%). The following analytical instruments were used, ^{1}H and ^{13}C NMR: Avance 400 and Avance 400 HD spectrometers; mass spectroscopy: TSQ 7000 Thermo Electron and Voyager DE-ST Perseptive Biosystems spectrometers; UV-Visible: Perkin-Elmer UV-Vis Win-Lab Lambda 35; IR: Perkin Elmer 1725. NMR chemical shifts are given in ppm with positive values to high frequency relative to the tetramethylsilane reference. Coupling constants J are in Hertz. UV-Visible extinction molar coefficient ε is in $L.mol^{-1}.cm^{-1}$ and wavelengths λ in nm. Liquid crystalline properties measurements were conducted by the followings. Differential scanning calorimetry (DSC) was measured on a Perkin-Elmer Pyris1 DSC with heating and cooling rates of 5 and 10 °C min^{-1}. Polarizing optical microscopy (POM) was carried out on a Zeiss Axio Imager A1m with a Mettler FP90/FP82HT hot stage system. X-ray powder diffraction data were collected on the wiggler beam line BL17A of the National Synchrotron Radiation Research Center (NSRRC), Taiwan, using a triangular bent Si(111) monochromator and a wavelength of 1.320662 Å. The sample in a 1-mm capillary was mounted on the Huber 5020 diffractometer. An air stream heater is equipped at BL17A beamline and the temperature controller is programmable by a PC with a PID feedback system. Single crystal X-ray diffraction data were collected on a high flux microfocus Rigaku FRX rotating anode at the copper kα wavelength equipped with a Dectris Pilatus 200K hybrid detector.

2. Synthesis procedures and characterization of all new compounds

- Synthesis of the *carbo*-benzenes **1a** and **1b**

1,4,10,13-tetraphenyl-7,16-bis((3,4,5-tris(dodecyloxy)phenyl)ethynyl)cyclooctadeca-1,2,3,7,8,9,13,14,15-nonaen-5,11,17-triyne (1a)

A solution of **4a** (130 mg, 0.065 mmol) in DCM (100 mL) was treated with $SnCl_2$ (124 mg, 0.653 mmol) and HCl (0.65 mL, 1.31 mmol) at -78 °C. The reaction mixture was stirred for 10 min at -78 °C and for 20 min at rt. After treatment with aqueous 1 M NaOH (1.31 mL) and filtration through celite®, the organic layer was washed with brine three times, dried over $MgSO_4$ and evaporated under reduced pressure. The residue was purified by chromatography on silica gel (Pentane/DCM 3 : 1) to give the **1a** as a dark blue-violet solid (70 mg, 0.038 mmol, 58%).

^{1}H NMR (400 MHz, CD_2Cl_2) δ 9.45 (d, J = 7.8 Hz, 8H), 7.95 (t, J = 7.8 Hz, 8H), 7.73 (m, 4H), 7.31 (s, 4H), 4.24 (t, J = 6.5 Hz, 8H), 4.13 (t, J = 6.5 Hz, 4H), 1.97 (m, 8H), 1.91 – 1.77 (m, 4H), 1.69 – 1.54 (m, 12H), 1.49 (m, 8H), 1.44 – 1.22 (m, 88H), 0.89 (m, 18H).

^{13}C{^{1}H} NMR (101 MHz, CD_2Cl_2) δ 153.5, 140.4, 139.0, 130.0, 129.9, 129.8, 120.4, 119.7, 117.1, 113.8, 110.5 (*o*-C_6H_2), 104.8, 99.6, 89.7, 84.5, 73.7, 69.4, 32.0 – 22.7 (m), 13.9.

HRMS (MALDI-TOF): *m/z* calcd for $C_{130}H_{174}O_6$ $[M]^+$: 1831.3310, found: 1831.3165.

UV-Visible ($CHCl_3$): λ_{max} = 488 nm (ε = 203000 L·mol^{-1}·cm^{-1}).

1,4,10,13-tetraphenyl-7,16-bis((3,4,5-tris(octadecyloxy)phenyl)ethynyl)cyclooctadeca-1,2,3,7,8,9,13,14,15-nonaen-5,11,17-triyne (1b)

A solution of **4b** (60 mg, 0.024 mmol) in DCM (50 mL) was treated with $SnCl_2$ (46 mg, 0.24 mmol) and HCl (0.24 mL, 0.48 mmol) at -78 °C. The reaction mixture was stirred for 10 min at -78 °C and for 50 min at rt. After treatment with aqueous 1 M NaOH (1.00 mL) and filtration through celite®, the organic layer was washed with brine three times, dried over $MgSO_4$ and evaporated under reduced pressure. The residue was washed three times with diethyl ether to give the **1b** as a dark blue-violet solid (10 mg, 0.004 mmol, 18%).

^{1}H NMR (500 MHz, 318 K, $CDCl_3$) δ 9.48 (d, J = 7.1 Hz, 8H), 7.97 (t, J = 7.1 Hz, 8H), 7.72 (t, J = 7.1 Hz, 4H), 7.32, (s, 4H), 4.27 (t, J = 6.4 Hz, 8H), 4.19 (t, J = 6.4 Hz, 4H), 2.00 (m, 8H), 1.90 (m, 4H), 1.64 (m, 12H), 1.51 (m, 12H), 1.39-1.29 (m, 156H), 0.91 (m, 18H).

^{13}C{^{1}H} NMR (125 MHz, $CDCl_3$) δ 153.5, 140.8, 139.4, 130.1, 129.7, 120.9, 119.0, 117.3, 114.3, 111.2, 104.9, 99.3, 89.9, 84.8, 73.8, 69.7, 31.9-29.3 (m), 26.2, 26.2, 22.6, 22.6, 14.0, 14.0.

HRMS (MALDI-TOF): *m/z* calcd for $C_{166}H_{246}O_6$ $[M]^+$: 2335.8944, found: 2335.8909.

UV-Visible ($CHCl_3$): λ_{max} = 488 nm (ε = 187000 L·mol^{-1}·cm^{-1}).

- Synthesis of the tris-alkoxy-5-ethynylbenzene derivatives **3a** and **3b**

The 1,2,3-tris-octadecyloxy-5-ethynylbenzene **3b** was prepared according to the procedure previously described for the synthesis of the 3,4,5- tris-dodecyloxy-5-ethynylbenzene **3a** (Scheme S1).[1]

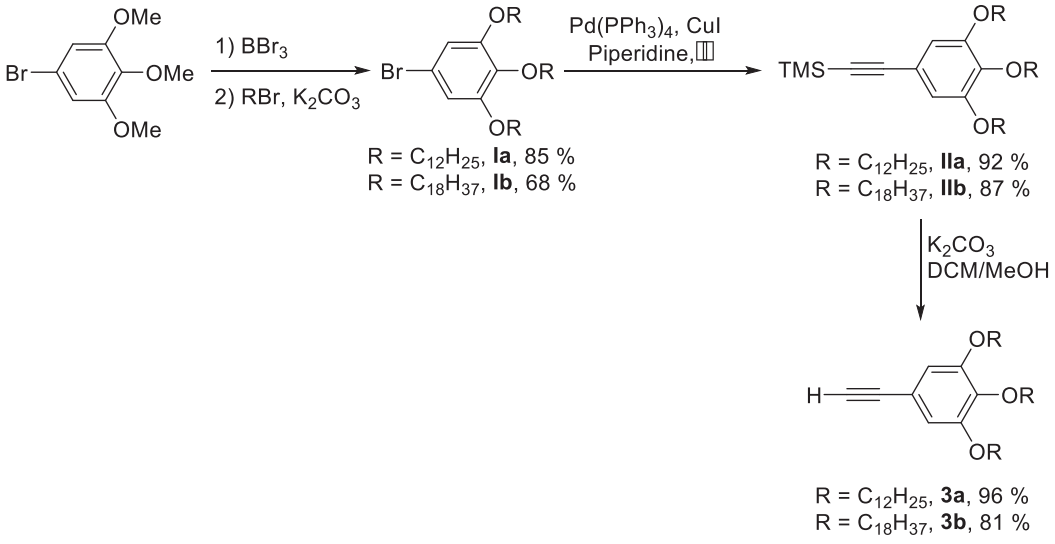

Scheme S1. Synthesis of the trialkoxy-phenylacetylenes **3a** and **3b**.

5-Bromo-1,2,3-tris(dodecyloxy)benzene (Ia)

^{1}H NMR (400 MHz, CD_2Cl_2) δ 6.68 (s, 2H), 3.96 (t, J = 6.5 Hz, 4H), 3.92 (t, J = 6.5 Hz, 2H), 1.90 – 1.82 (m, 2H), 1.82 – 1.75 (m, 4H), 1.69 (m, 2H), 1.51 – 1.40 (m, 8H), 1.28 (m, 42H), 0.91 – 0.87 (t, J = 6.5 Hz, 9H).

5-Bromo-1,2,3-tris(octadecyloxy)benzene (Ib)

^{1}H NMR (300 MHz, $CDCl_3$) δ 6.68 (s, 2H), 3.96-3.90 (m, 6H), 1.85-1.71 (m, 6H), 1.47 (m, 6H), 1.30 (bs, 84H), 0.90 (t, J = 6.5 Hz, 9H).
^{13}C{^{1}H} NMR (400 MHz, C_6D_6) *d* 154.3, 138.1, 115.6, 110.3, 73.1, 68.8, 32.0, 30.6, 29.9, 29.8, 29.8, 29.5, 29.4, 29.3, 26.4, 26.1, 22.8, 14.0.
HRMS (MALDI-TOF): *m/z* calcd for $C_{60}H_{113}O_3Br$ [M^+]: 960.7873, found: 960.7908.

Trimethyl((3,4,5-tris(dodecyloxy)phenyl)ethynyl)silane (IIa)

^{1}H NMR (300 MHz, CD_2Cl_2) δ 6.65 (s, 2H), 3.93 (td, J = 6.5, 3.2 Hz, 6H), 1.78 (dt, J = 8.3, 6.4 Hz, 4H), 1.69 (dt, J = 8.6, 6.6 Hz, 2H), 1.53 – 1.42 (m, 6H), 1.29 (bs, 48H), 0.92 – 0.86 (m, 9H), 0.24 (s, 9H).

Trimethyl((3,4,5-tris(octadecyloxy)phenyl)ethynyl)silane (IIb)

^{1}H NMR (300 MHz, $CDCl_3$) δ 6.69 (s, 2H), 3.97 (m, 6H), 1.84-1.75 (m, 6H), 1.52-1.47 (m, 6H), 1.30 (bs, 84H), 0.92 (t, J = 6.5 Hz, 9H), 0.27 (s, 9H).

^{13}C{^{1}H} NMR (101 MHz, $CDCl_3$) δ 152.9, 139.3, 117.5, 110.5, 105.5, 92.4, 73.4, 69.1, 32.0, 30.3, 29.8, 29.8, 29.7, 29.7, 29.4, 29.4, 26.1, 26.1, 22.7, 14.1, 0.0.

HRMS (MALDI-TOF): *m/z* calcd for $C_{65}H_{122}O_3Si$ [M^+]: 978.9163, found: 978.9242.

1,2,3-Tris(dodecyloxy)-5-ethynylbenzene (3a)

^{1}H NMR (400 MHz, CD_2Cl_2) δ 6.69 (s, 2H), 3.93 (m, 6H), 3.04 (s, 1H), 1.78 (m, 4H), 1.70 (m, 2H), 1.46 (m, 6H), 1.28 – 1.32 (m, 48H), 0.91 – 0.86 (t, J = 6.5 Hz, 9H).

1,2,3-Tris(dodecyloxy)-5-ethynylbenzene (3b)

^{1}H NMR (300 MHz, $CDCl_3$) δ 6.71 (s, 2H), 3.97 (m, 6H), 3.01 (s, 1H), 1.84-1.75 (m, 6H), 1.48-1.45 (m, 6H), 1.28 (bs, 84H), 0.90 (m, 9H).

^{13}C{^{1}H} NMR (75 MHz, $CDCl_3$) δ 152.9, 139.5, 116.4, 110.7, 84.0, 75.7, 73.5, 69.1, 31.9, 30.3, 29.8, 29.7, 29.6, 29.6, 29.4, 29.3, 26.1, 26.1, 22.7, 14.1.

HRMS (MALDI-TOF): *m/z* calcd for $C_{62}H_{114}O_3$ [M^+]: 906.8768, found: 906.8758.

- Synthesis of the [6]pericyclynediols **4a** and **4b**

3,6,12,15-Tetramethoxy-3,6,12,15-tetraphenyl-9,18-bis((3,4,5-tris(dodecyloxy) phenyl)ethynyl)cyclooctadeca-1,4,7,10,13,16-hexayne (4a)

A solution of **3a** (174 mg, 0.26 mmol) in THF (40 mL) was treated with *n*-BuLi (0.09 mL, 0.22 mmol) at -78 °C. The mixture was stirred for 20 min at -78 °C and 20 min at rt, before dropwise addition at -78 °C of a solution of **2** (60 mg, 0.09 mmol) in THF (4 mL). The reaction mixture was allowed to warm up to room temperature slowly and then stirred for 8 h. After treatment with an aqueous saturated solution of NH_4Cl, the aqueous layer was extracted with diethyl ether. The combined organic layers were washed with brine, dried over $MgSO_4$, and evaporated under reduced pressure. The residue was purified by chromatography on silica gel (Pentane/EtOAc 10 : 1, then 4 : 1) to give **4a** as a yellow oil (132 mg, 0.066 mmol, 75%).

^{1}H NMR (400 MHz, CD_2Cl_2) δ 7.79 – 7.67 (m, 8H), 7.46 – 7.35 (m, 12H), 6.76 – 6.61 (m, 4H), 4.05 – 3.83 (m, 12H), 3.66 – 3.36 (m, 14H), 1.78 (m, 8H), 1.73 – 1.66 (m, 4H), 1.51 – 1.42 (m, 12H), 1.29 (m, 96H), 0.88 (t, J = 6.7 Hz, 18H).

^{13}C{^{1}H} NMR (101 MHz, CD_2Cl_2) δ 153.0, 139.8, 139.5 – 139.1 (m), 129.2 – 129.1 (m), 128.6 – 128.5 (m), 126.5 – 115.1 (m), 110.2, 84.5 – 83.6 (m), 80.5 – 80.4 (m), 73.5, 71.7, 69.1, 54.7 – 53.3(m), 32.0 – 22.3(m), 22.6, 22.3, 13.4.
HRMS (MALDI-TOF): *m/z* calcd for [M^+] $C_{134}H_{188}O_{12}$: 1989.4101, found: 1989.4075.

3,6,12,15-Tetramethoxy-3,6,12,15-tetraphenyl-9,18-bis((3,4,5-tris(octadecyloxy) phenyl)ethynyl)cyclooctadeca-1,4,7,10,13,16-hexayne (4b)

A solution of **3b** (300 mg, 0.33 mmol) in THF (30 mL) was treated with EtMgBr (0.11 mL, 0.33 mmol) at 0 °C. The mixture was stirred for 20 min at 0 °C and 2 h at rt, before dropwise addition at 0 °C of a solution of **2** (100 mg, 0.147 mmol) in THF (5 mL). The reaction mixture was allowed to warm up slowly to rt and then stirred overnight. After treatment with an aqueous saturated solution of NH_4Cl, the aqueous layer was extracted with diethyl ether. The combined organic layers were washed with brine, dried over $MgSO_4$, and evaporated under reduced pressure. The residue was purified by chromatography on silica gel (Hexane/EtOAc 9 : 1) to give **4b** as a yellow oil (90 mg, 0.036 mmol, 25%).

^{1}H NMR (300 MHz, $CDCl_3$) d 7.81-7.74 (m, 8H), 7.40-7.37 (m, 12H), 6.72 (m, 4H), 4.00-3.97 (m, 12H), 3.69-3.42 (m, 14H), 1.83-1.77 (m, 12H), 1.49 (m, 12H), 1.29 (bs, 168H), 0.91 (m, 18H).

^{13}C{^{1}H} NMR (75 MHz, $CDCl_3$) δ 153.0, 139.5-138.8 (), 129.2, 128.6-128.4 (m), 126.7-126.5 (m), 115.4, 110.5, 84.6-84.3 (m), 84.0-83.7 (m), 80.6-80.2 (m), 73.5, 71.9, 69.2, 53.6, 53.5, 32.0, 29.7-29.6 (m), 29.4-29.3 (m), 26.1, 22.7, 14.1.
MS (MALDI-TOF): *m/z* 2495 [M-H]$^+$ (20), 2519 [M+Na]$^+$ (25), 2535 [M+K]$^+$ (100).

3. Absorption spectra of 1a and 1b

Combined normalized UV spectra of **1a** and **1b** in chloroform solution

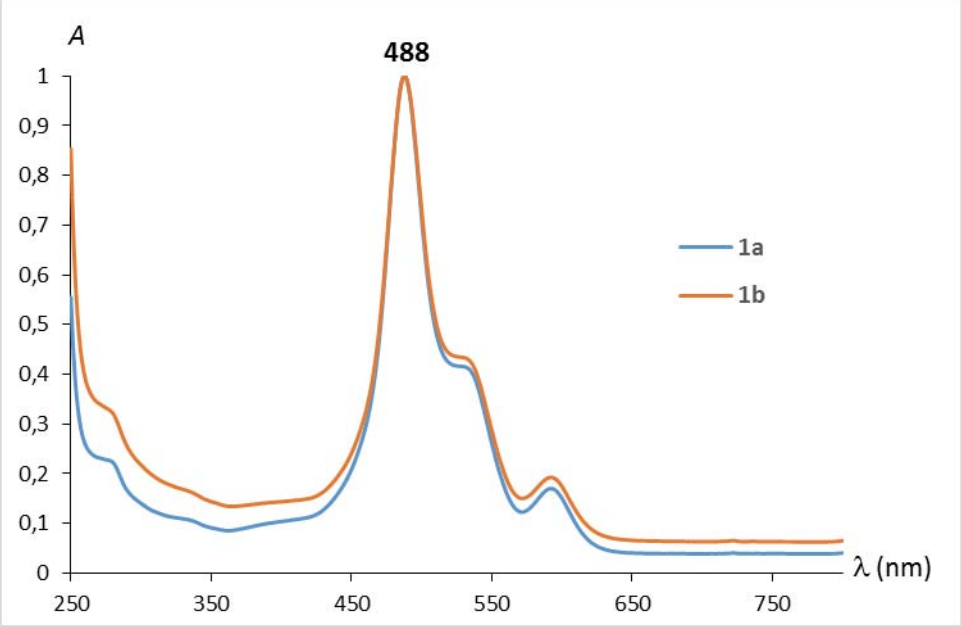

4. DSC thermograms of 1a

From top to bottom: 1st and 2nd cycles between 25 and 200 ºC; 1st, 2nd cycles between 0 and 115 °C, and 3rd cycle (annealed at rt for one night) between - 35 and 115 ºC.
With heating up to 115 ºC, the signal at 109 ºC observed in the first heating is not reproducible. This is ascribed to the thermal history of the virgin crystals (powders). However, after one night annealing at room temperature, a new signal at 55.1 ºC appears on heating and a signal at 27.8 ºC can be observed on cooling. POM observations between 0 and 115 ºC for two cycles are consistent with the DSC data.

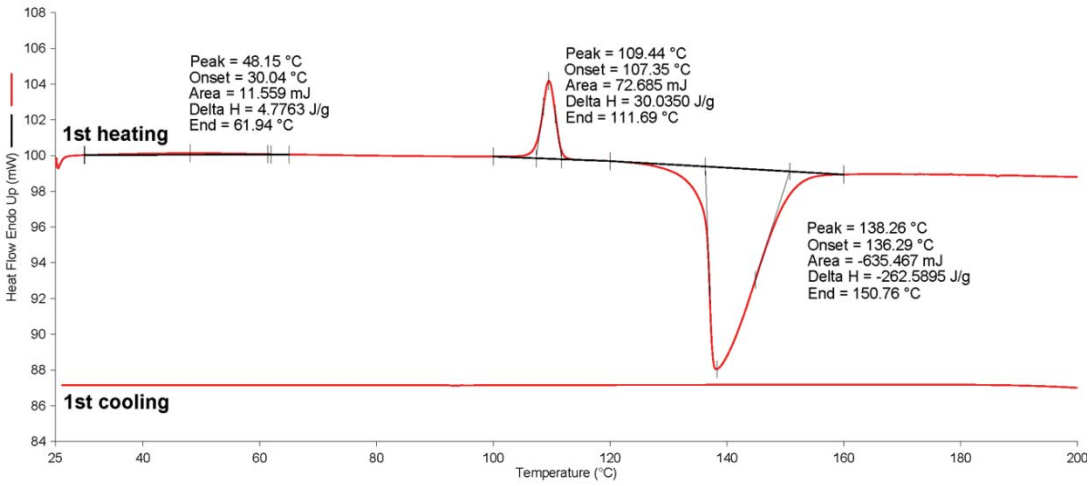

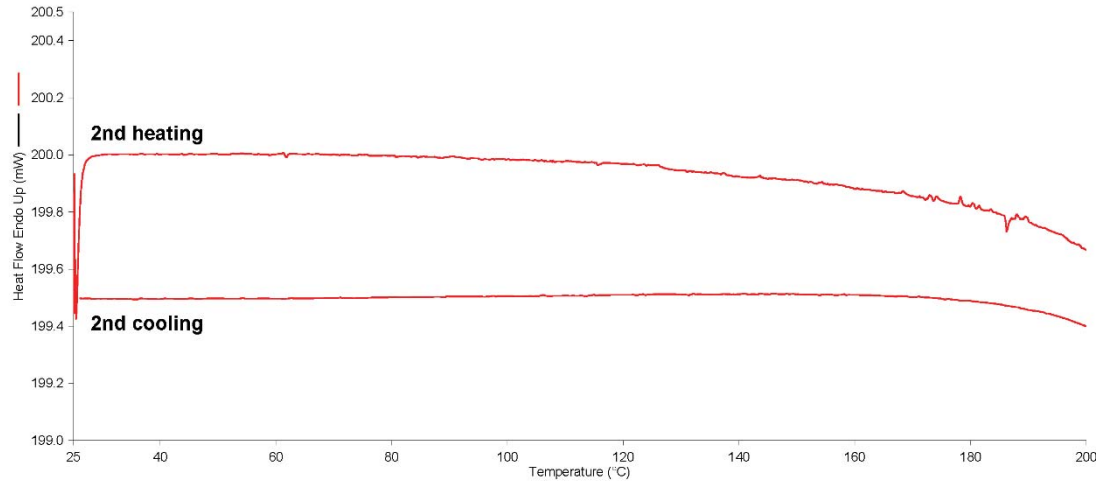
2nd heating
2nd cooling
Heat Flow Endo Up (mW)
Temperature (°C)

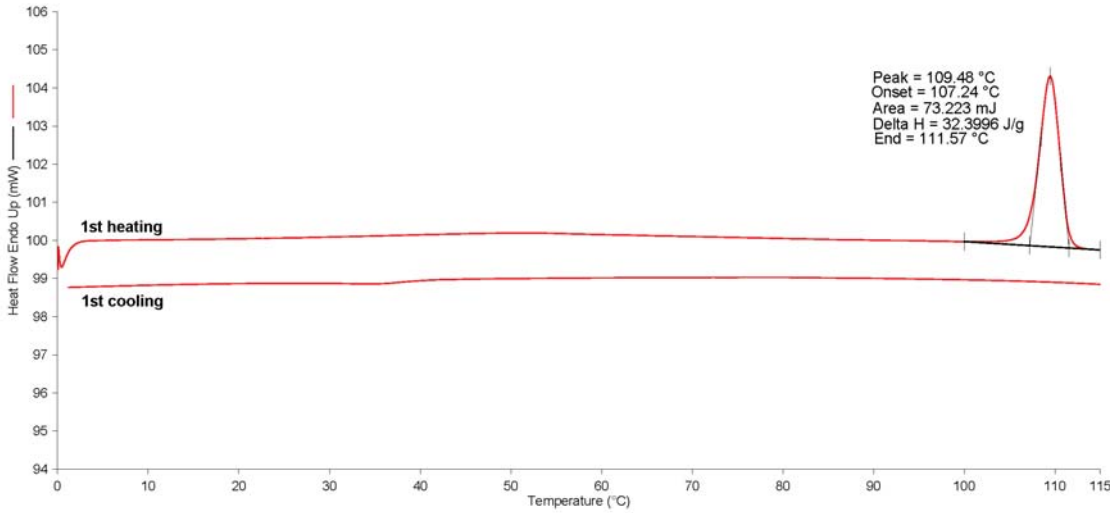
Peak = 109.48 °C
Onset = 107.24 °C
Area = 73.223 mJ
Delta H = 32.3996 J/g
End = 111.57 °C
1st heating
1st cooling
Heat Flow Endo Up (mW)
Temperature (°C)

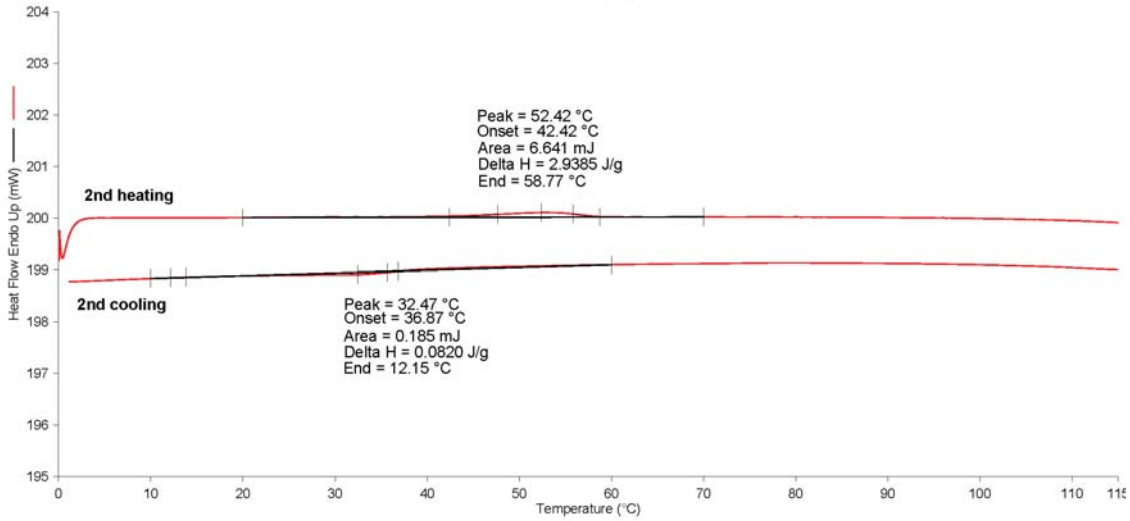
Peak = 52.42 °C
Onset = 42.42 °C
Area = 6.641 mJ
Delta H = 2.9385 J/g
End = 58.77 °C
2nd heating
2nd cooling
Peak = 32.47 °C
Onset = 36.87 °C
Area = 0.185 mJ
Delta H = 0.0820 J/g
End = 12.15 °C
Heat Flow Endo Up (mW)
Temperature (°C)

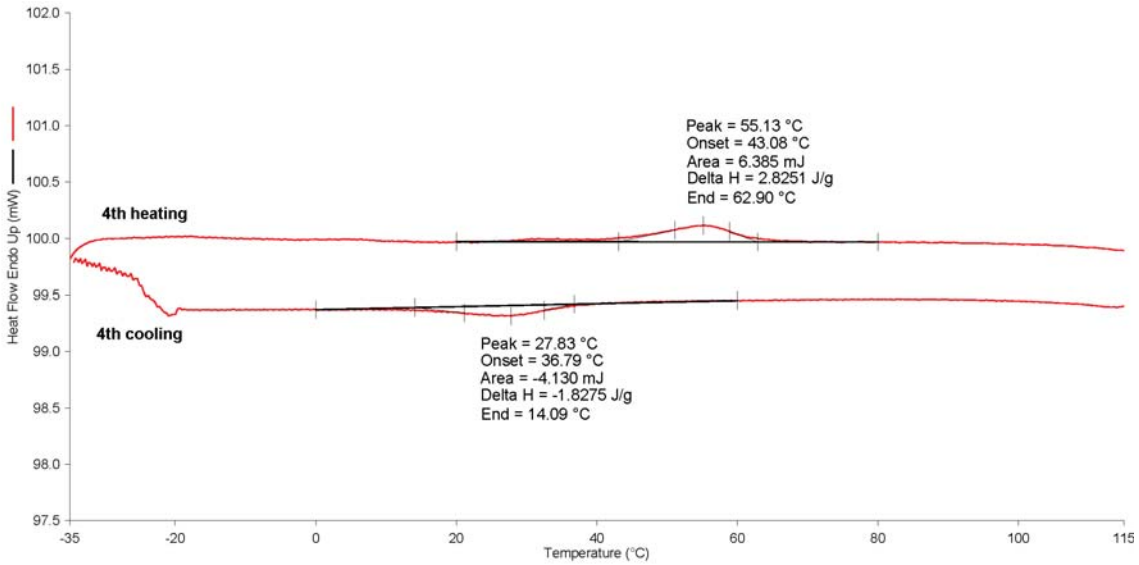
Heat Flow Endo Up (mW)
Temperature (°C)
4th heating
4th cooling
Peak = 55.13 °C
Onset = 43.08 °C
Area = 6.385 mJ
Delta H = 2.8251 J/g
End = 62.90 °C
Peak = 27.83 °C
Onset = 36.79 °C
Area = -4.130 mJ
Delta H = -1.8275 J/g
End = 14.09 °C

5. Variable temperature powder X-ray diffractograms of 1a upon heating (left: 2D; right: 1D)

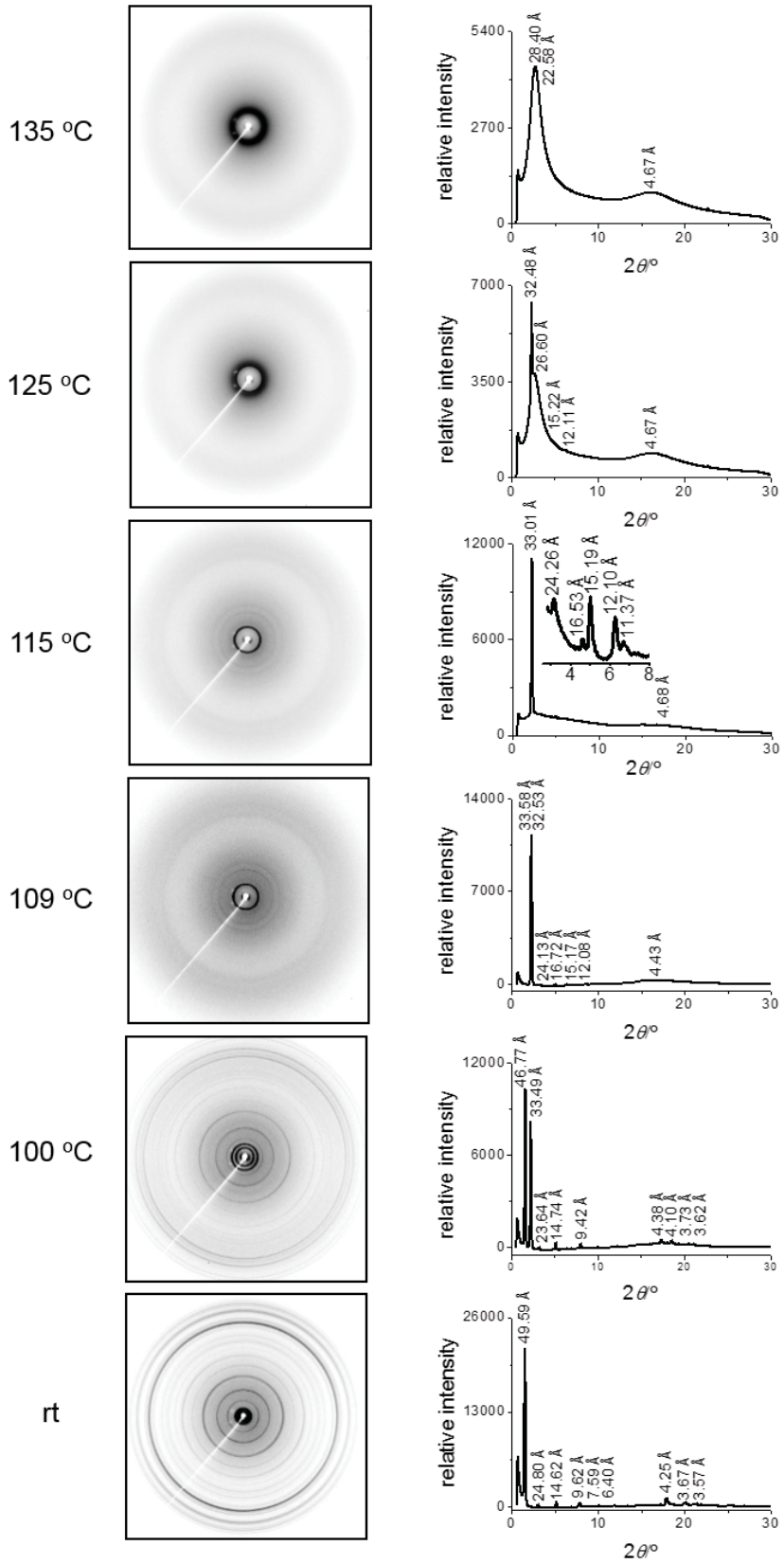

6. Photographs of crystals of 1a

These bipyramidal crystals were obtained by slow evaporation of the solvent from a chloroform solution, but in spite of their relatively large size they proved unsuitable for XRD analysis with standard diffractometers (see section 8).

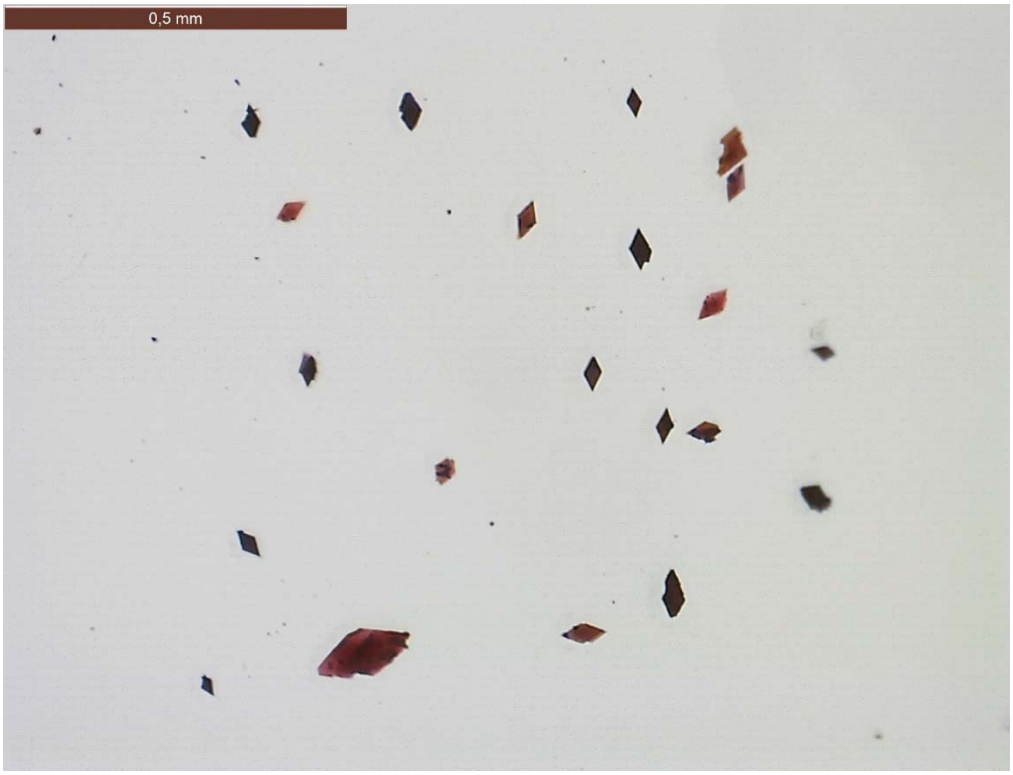

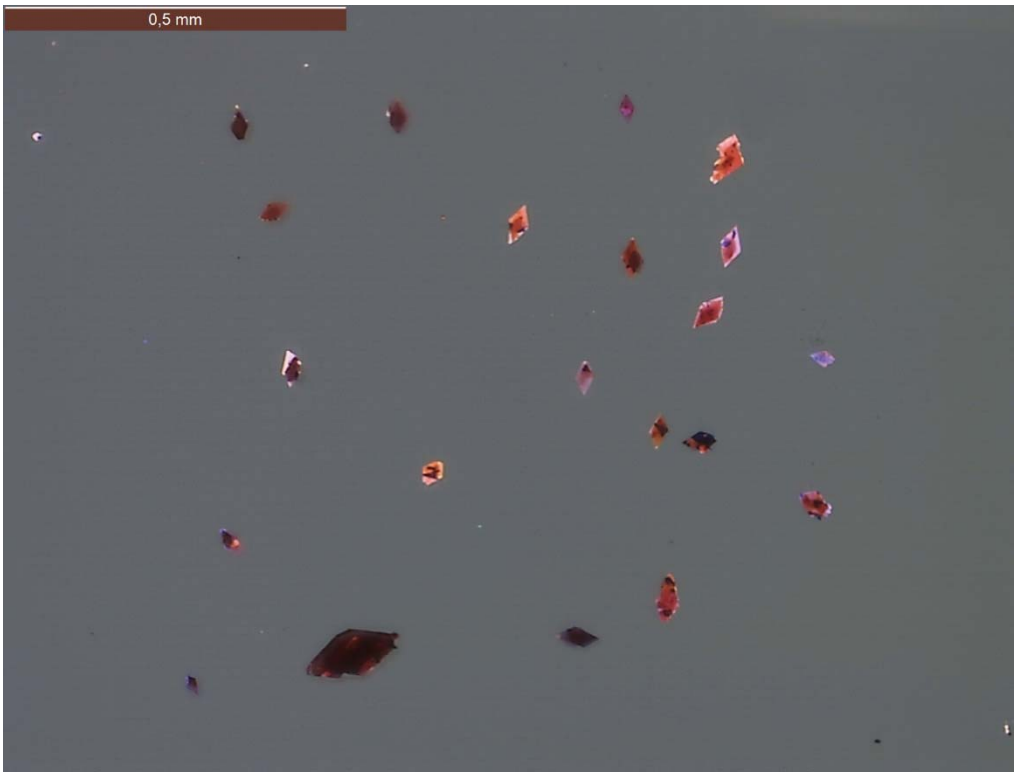

7. Crystallographic data for 1a

Small crystalline plates of poor quality were obtained from a chloroform solution of **1a**. Due to the low diffractive power of the crystals, data collections were performed on a high flux microfocus Rigaku FRX rotating anode at the copper kα wavelength equipped with a Dectris Pilatus 200K hybrid detector at 100 K. The diffractive power was quite low for crystals of poor quality. The structure was solved direct methods and refined by means of least-square procedure on *F* by using CRYSTALS. Absorption correction was performed by using a multiscan procedure. Due to the weak diffraction intensities and low resolution, non-hydrogen atoms could be refined only with isotropic displacement parameters. *Phenyl* were refined as rigid groups. Surprisingly, the compound crystallizes without any interstitial solvent molecule. Crystals were found to be inherently twinned. Data were treated with ROTAX which gave the twin law between the two components (0.87 : 0.13).[2] Refinement of the final model led to an imperfect but reasonable solution and confirmed the structure of **1a** (Figure 1 below).

$C_{130}H_{174}O_6$, pink red plate, M = 1832.81 g.mol^{-1}, monoclinic, a = 49.45(2), b = 15.293(11), c = 7.3526(14) Å, β = 91.49(3), V = 5558(2) Å^3, T = 100 K, space group $P2_1/c$, Z = 2, μ(Cu K$_\alpha$) = 0.490 mm^{-1}, 13385 reflections measured and 4780 unique ($2\theta_{max}$ = 102.6°, R_{int} = 0.086), 2434 reflexions [$I > 2.5\ \sigma(I)$] used in all calculations. R = 0.2493, R_w = 0.2680.
CCDC 1546671 contains the supplementary crystallographic data for this paper. The data can be obtained free of charge from the Cambridge Crystallographic Data Centre via http://www.ccdc.cam.ac.uk/getstructures.

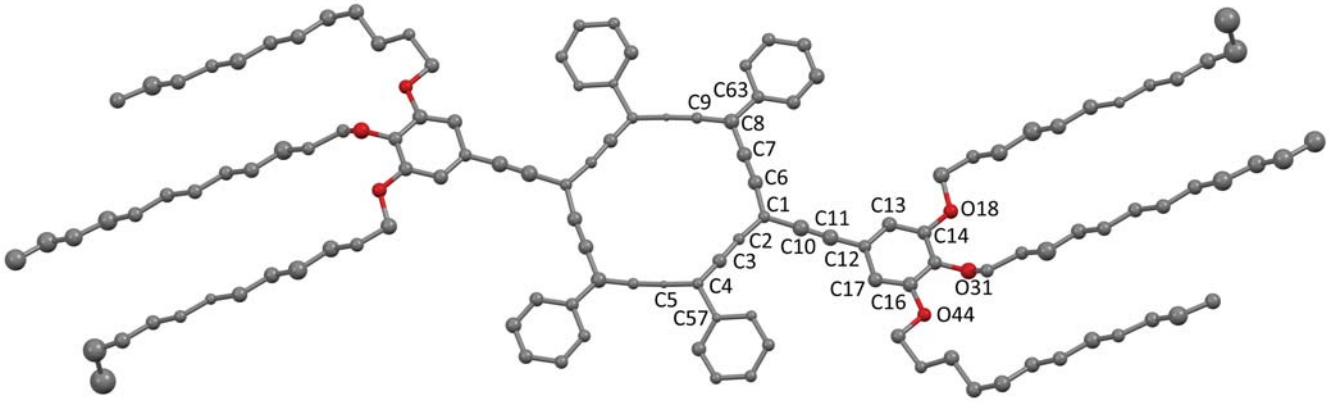

Figure 1. Molecular view of the X-ray crystal structure of 1a, with thermal ellipsoids drawn at 30 % probability level. For clarity, hydrogen atoms are omitted.

8. References

[1] J. Wu, M. D. Warson, L. Zhang, Z. Wang and K. Müllen, *J. Am. Chem. Soc*. 2004, **50**, 177-186.

[2] R. I. Cooper, R. O. Gould, S. Parsons and D. J. Watkin, *J. Appl. Cryst*. 2002, **35**, 168-174.

Chapter 5

Carbo-bi- and -ter-phenyls: OPE ring *carbo*-mers

Introduction & Summary

After Ratner's initial theoretical report in 1974,[1] molecular electronics became a hot research topic, which considerably attracted the interest of the scientific community.[2] It is today well known that π-conjugated organic molecules having small HOMO-LUMO gap can potentially find applications in molecular electronic devices.[3] Over the past few decades, many efforts were thus devoted to the development of novel organic molecules as alternative components in electronic devices aiming at miniaturization of integrated circuits in replacement of silicon-based circuits.[4] As compared to traditional inorganic semiconductors (silicon), π-conjugated organic molecules including oligomers and polymers have many advantages: a) low production costs, b) easy processability, and c) tunable optical and electronic properties through modifications of the molecular structures.[5]

Oligo(phenylene-ethynylene)s (OPEs) molecular wires were considered as model compounds to give insight into the structural and electronic properties of the corresponding poly(phenylene-ethynylene)s (PPEs) polymers.[6] Due to their remarkable optical and electronic properties, OPEs also found applications in a wide range of domains such as in organic light-emitting devices,[7] chemosensors,[8] molecular electronic switches,[9] and nonlinear optical materials.[10] Though numerous studies on the synthesis and charge transport properties of OPEs were implemented in the past decades,[6b, 9, 11] fabricating a molecular integrated circuit applicable in devices still remains today challenging. Charge transport properties of molecular wires hinge not only on physical factors, such as temperature, molecule-electrode interfaces, but also on the chemical nature of the molecule, including its conjugation, redox characteristics, molecular length and substitution.[12] In general, the charge transport is enhanced for molecules having a flat and rigid organic core with an extended π-conjugation and a low redox potential.[6,13]

The 18-π-electrons *carbo*-benzene ring, three times larger but three times less energetically aromatic than its parent 6-π-electrons benzene ring,[14] was recently shown, through the study of the quadrupolar *p*-dianilinyl-*carbo*-benzene, to exhibit an unprecedented ten times higher single molecule conductance (SMC) than comparable molecules of similar size.[15] This high conductance, but also the rigidity, flatness, and π-electron-richness of *carbo*-benzenes encouraged the design of a series of ring *carbo*-mers of oligo(phenylene-ethynylene)s (*carbo*-OPEs). The preparation of one *carbo*-OPE_2 (skeleton *carbo*-mer of biphenyl) and two *carbo*-OPE_3 (skeleton *carbo*-mers of terphenyl) were thus envisaged. In

order to enhance the predicted low solubility of these *carbo*-OPEs, two *n*-octyl substituents were introduced at the two ends of the *carbo*-OPEs backbone, and the four phenyl groups of the central C_{18} macrocycle of one *carbo*-OPE_3 were additionally replaced by four *para*-*n*-pentylphenyl groups.[16]

Synthetic routes based on mono-addition processes onto the key [6]pericyclynedione precursor were applied to the preparation of the three *carbo*-OPEs. The *carbo*-OPE_2, made of two *carbo*-benzene units connected to each other by an ethynyl bridge, was first synthesized with 7 % global yield from the [6]pericyclynedione (Scheme 1.). Two *carbo*-OPE_3 derivatives, first examples to date of molecules made of three *carbo*-benzene rings, were prepared through two different strategies. These three molecules were fully characterized by ^{1}H, ^{13}C NMR and UV-visible spectroscopy, HRMS (MALDI-TOF technique), and electrochemistry. Two *carbo*-OPEs were also characterized by X-ray diffraction analysis of single crystals deposited from chloroform. The *carbo*-OPE_3 compounds were found to exhibit very low first reduction potentials (-0.42 ± 0.03 V/SCE), unprecedented in the *carbo*-mer series. Additionally, theoretical investigations of the aromaticity of the *carbo*-benzene rings of this series of *carbo*-OPEs (s = 1 - 4) were also carried out by DFT calculations of the NICS values at the center of each macrocycle.

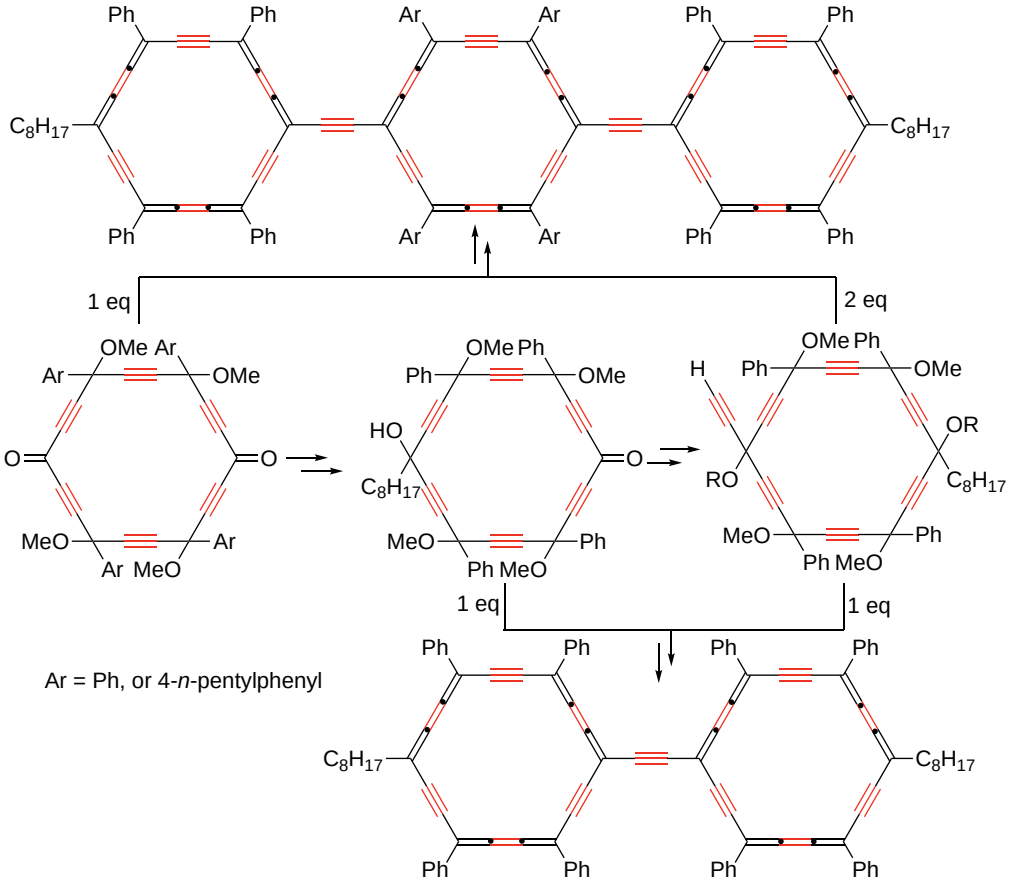

Scheme 1. The designed synthetic routes for preparation of *carbo*-OPEs

Reference

1. A. Aviram, M. A. Ratner, *Chem. Phys. Lett*., **1974**, *29*, 277-283.

2. a). N. Robertson, C. A. McGowan, *Chem. Soc. Rev*., **2003**, *32*, 96-103; b). A. C. Benniston, *Chem. Soc. Rev*., **2004**, *33*, 573-578; c). R. Klajn, J. F. Stoddart, B. A. Grzybowski, *Chem. Soc. Rev.*, **2010**, *39*, 2203-2237.

3. C. R. Parker, E. Leary, R. Frisenda, Z. Wei, K. S. Jennum, E. Glibstrup, P. B. Abrahamsen, M. Santella, M. A. Christensen, E. A. Della Pia, T. Li, M. T. Gonzalez, X. Jiang, T. J. Morsing, G. Rubio-Bollinger, B. W. Laursen, K. Nørgaard, H. van der Zant, N. Agrait, M. Brønsted Nielsen, *J. Am. Chem. Soc*., **2014**, *136*, 16497-16507.

4. a). M. D. Watson, A. Fechtenkötter, K. Müllen, *Chem. Rev*., **2001**, *101*, 1267-1300; b). J. Wu, W. Pisula, K. Müllen, *Chem. Rev*., **2007**, *107*, 718-747; c). K. Müllen, J. P. Rabe, *Acc. Chem. Res*., **2008**, *41*, 511-520.

5. D. A. M. Egbe, B. Carbonnier, E. Birckner, U. W. Grummt, *Progr. Polym. Sci*., **2009**, *34*, 1023-1067.

6. a). J. M. Tour, *Chem. Rev*., **1996**, *96*, 537-554; b). U. H. F. Bunz, *Chem. Rev*., **2000**, *100*, 1605-1644; c). W. Hu, N. B. Zhu, W. Tang, D. H. Zhao, *Org. Lett*., **2008**, *10*, 2669-2672; d). Q. Lu, K. Liu, H. M. Zhang, Z. B. Du, X. H. Wang, F. S. Wang, *ACS Nano*, **2009**, *3*, 3861-3868.

7. Y. Yamaguchi, Y. Matsubara, T. Ochi, T. Wakamiya, Z. Yoshida, *J. Am. Chem. Soc*., **2008**, *130*, 13867-13869.

8. S. W. Thomas, G. D. Joly, T. M. Swager, *Chem. Rev*., **2007**, *107*, 1339-1386.

9. a). Z. J. Donhauser, B. A. Mantooth, K. F. Kelly, L. A. Bumm, J. D. Monnell, J. J. Stapleton, D. W. Price, A. M. Rawlett, D. L. Allara, J. M. Tour, P. S. Weiss, *Science*, **2001**, *292*, 2303-2307; b). G. K. Ramachandran, T. J. Hopson, A. M. Rawlett, L. A. Nagahara, A. Primak, S. M. Lindsay, *Science*, **2003**, *300*, 1413-1416; c). P. A. Lewis, C. E. Inman, Y. X. Yao, J. M. Tour, J. E. Hutchison, P. S. Weiss, *J. Am. Chem. Soc*., **2005**, *127*, 17421-17426.

10. a) Y. M. Zhao, Y. Shirai, A. D. Slepkov, L. Cheng, L. B. Alemany, T. Sasaki, F. A. Hegmann, J. M. Tour, *Chem. Eur. J*., **2005**, *11*, 3643-3658; b) B. Babgi, L. Rigamonti, M. P. Cifuentes, T. C. Corkery, M. D. Randles, T. Schwich, S. Petrie, R. Stranger, A. Teshome, I. Asselberghs, K. Clays, M. Samoc, M. G. Humphrey, *J. Am. Chem. Soc*., **2009**, *131*, 10293-10307.

11. a). J. M. Tour, A. M. Rawlett, M. Kozaki, Y. X. Yao, R. C. Jagessar, S. M. Dirk, D. W. Price, M. A. Reed, C. W. Zhou, J. Chen, W. Y. Wang, I. Campbell, *Chem. Eur. J*., **2001**, *7*, 5118-5134; b). J. M. Tour, L. Cheng, D. P. Nackashi, Y. Yao, A. K. Flatt, S. K. S. Angelo, T. E. Mallouk, P. D. Franzon, *J. Am. Chem. Soc*., **2003**, *125*, 13279-13283; c). P. A. Lewis, C. E. Inman, Y. Yao, J. M. Tour, J. E. Hutchison, P. S. Weiss, *J. Am. Chem. Soc.*, **2004**, *126*, 12214-12215; d). C. D. Zangmeister, S. W. Robey, R. D. van Zee, Y. Yao, J. M. Tour, *J. Am. Chem. Soc.*, **2004**, *126*, 3420-3421; e). C. Wang, A. S. Batsanov, M. R. Bryce, *J. Org. Chem.*, **2006**, *71*, 108-116.

12. X. Xiao, L. A. Nagahara, A. M. Rawlett, N. Tao, *J. Am. Chem. Soc*., **2005**, *127*, 9235-9240.

13. A. M. Moore, A. A. Dameron, B. A. Mantooth, R. K. Smith, D. J. Fuchs, J. W. Ciszek, F. Maya, Y. X. Yao, J. M. Tour, P. S. Weiss, *J. Am. Chem. Soc*., **2006**, *128*, 1959-1967.

14. a). C. Godard, C. Lepetit, R. Chauvin, *Chem. Commun*. **2000**, 1833-1834; b) C. Lepetit, C. Godard, R. Chauvin, *New J. Chem*., **2001**, *25*, 572-580; c) C. Lepetit, B. Silvi, R. Chauvin, *J. Phys. Chem. A* **2003**, *107*, 464-473; d). R. Chauvin, C. Lepetit, V. Maraval, L. Leroyer, *Pure Appl. Chem*., **2010**, *82*, 769-800.

15. a). A. Rives, I. Baglai, V. Malytskyi, V. Maraval, N. Saffon-Merceron, Z. Voitenko, R. Chauvin, *Chem. Commun*., **2012**, *48*, 8763-8765; b). Z. Li, M. Smeu, A. Rives, V. Maraval, R. Chauvin, M. A. Ratner, E. Borguet, *Nat. Commun.*, **2015**, *6*, 6321-6329.

16. a) C. W. Zhu, A. Rives, C. Duhayon, V. Maraval, R. Chauvin, *J. Org. Chem*., **2017**, *82*, 925-935; b) K. Cocq, N. Saffon-Merceron, Y. Coppel, C. Poidevin, V. Maraval, R. Chauvin, *Angew. Chem. Int. Ed*. **2016**, *55*, 15133-15136.

Article 6

(C. Zhu, A. Poater, C. Duhayon, B. Kauffmann, A. Saquet, V. Maraval, R. Chauvin, *Angew. Chem.*, under review.)

WILEY-VCH

COMMUNICATION

Carbo-bi- and -ter-phenyls: OPE ring *carbo*-mers

Chongwei Zhu,[a,b] Albert Poater,[c] Carine Duhayon,[a,b] Brice Kauffmann,[d] Alix Saquet,[a,b] Valérie Maraval,*[a,b] Remi Chauvin*[a,b]

Abstract: Ring *carbo*-mers of oligo(phenylethynyl)enes (OPE*n*, *n* = 0-2), made of C_2-catenated C_{18} *carbo*-benzene rings, have been synthesized and characterized by NMR and UV-vis spectroscopy, crystallography and voltammetry. Analyses of crystal and DFT-optimized structures show that the C_{18} rings preserve their individual aromatic character according to structural and magnetic criteria (NICS indices). *Carbo*-terphenyls (*n* = 2) are reversibly reduced at much higher potential $E_{1/2}^{red1}$ (≈ -0.42 V/SCE) than the corresponding *carbo*-benzene (-0.83 V/SCE), thus revealing salient inter-ring π-conjugation. An accurate linear fit of $E_{1/2}^{red1}$ *vs* the DFT LUMO energy suggests a notably higher value (-0.30 V/SCE) for a *carbo*-quaterphenyl congener (*n* = 3). Increase with *n* of the effective π-conjugation is also evidenced by a red shift of two of the three main visible light absorption bands, all being assigned to TDDFT-calculated excited states, one of them restricting to a HOMO→LUMO main one-electron transition.

Oligo(*p*-phenylene)s (OPP*n*)[1] and oligo(*p*-phenylethynylene)s (OPE*n*)[2] (*n* > 0) are π-conjugated hydrocarbon ribbon-wires widely used in the design of molecular materials with topical electronic properties, such as electrical conductance at the molecular level.[1d,2a] Their common phenylene brick provides stability, but also local insulating character due to its intrinsic aromaticity. The latter can however be "diluted" by embedding OPP sections within polycylic aromatic scaffolds, such as pyrene or hexabenzocoronene (HBC) cores also bringing enhanced rigidity ("super-OPP").[3] Such rigid extension can also be achieved by replacing phenylene rings of OPEs by porphyrinylethynylene moieties.[4] In either case, the macrocyclic framework is filled by smaller C_6-benzenic or C_4N-pyrrolic circuits. In a homogeneous series of bis-dianilinyl derivatives, the hollow C_{18} *carbo*-benzene macrocycle has been shown to provide a much higher conductivity (106 nS over 2.0 nm) than the diethynylbenzene, HBC or porphin congeners (10 ± 4 nS over 1.7 ± 0.3 nm).[5] This specificity can be attributed to the three time weaker energetic aromaticity of the *carbo*-benzene ring as compared to benzene parent.[6] Beyond this, the accessibility of OPP *carbo*-mers, or OPE *ring carbo*-mers, appears as a natural challenge (Figure 1). After a recent report of the first molecule containing two *carbo*-benzene rings in the fused mode, a *carbo*-naphthalene,[7] counterparts in the catenated mode through acetylene linkers are thus devised from the known *carbo*-benzene **1**,[8] as the *carbo*-biphenyl and *carbo*-terphenyl targets **2** and **3**. The *n*-octyl ends, and *n*-pentyl lateral chains of **3b**, were selected with the view to enhancing solubility and processability. Beyond known dioctyl-OPP*n* parents,[9,10] dioctyl-OPE2 was employed for the syntheses of substituted acenes and blue-emitting conjugated polymers applicable in organic semiconducting materials.[11,12] Liquid crystal and charge carrier properties of dioctyl-OPE3 were also reported.[13]

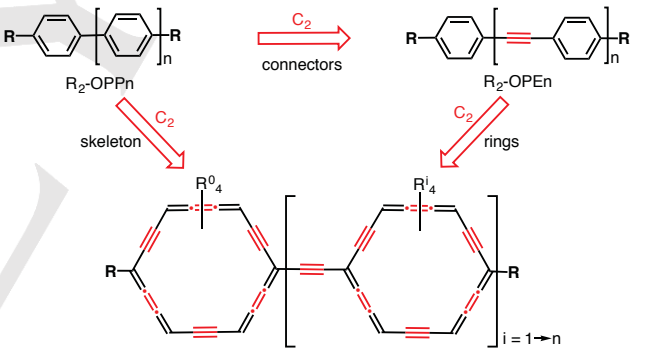

Figure 1. Target design: R^i = stabilizing/solubilizing substituents at four sp^2 vertices.

The synthesis of **2** was undertaken from the [6]pericyclynedione **4**[14] and octyl-[6]pericyclynone **5** using procedures previously implemented for the preparation of **1**.[8] In parallel, similar methods were applied to the sequential preparation of the ethynyl-[6]pericyclynol **6**, [6]pericyclynediol **7** and dimethyl diether **8**, isolated in 42 % yield over three steps by the optimized route (see ESI). Deprotonation of **8** with LiHMDS in the presence of **5** led to crude bis-[6]pericyclynediol **9** as an intractable mixture of isomers, which, under treatment with $SnCl_2$/HCl, afforded the *carbo*-biphenyl **2** as a stable black solid, with 18 % yield over two steps.

[a] C. Zhu, C. Duhayon, A. Saquet, V. Maraval, R. Chauvin
CNRS, LCC (Laboratoire de Chimie de Coordination)
205 route de Narbonne, BP44099, 31077 Toulouse Cedex 4 (France)
E-mail: valerie.maraval@lcc-toulouse.fr, chauvin@lcc-toulouse.fr
[b] C. Zhu, C. Duhayon, A. Saquet, V. Maraval, R. Chauvin
Université de Toulouse, UPS, ICT-FR 2599
31062 Toulouse Cedex 9 (France)
[c] A. Poater
Institut de Química Computacional i Catàlisi and
Departament de Química, Universitat de Girona
Campus Montilivi, 17003 Girona, Catalonia (Spain)
[d] B. Kauffmann
Université de Bordeaux, CNRS, INSERM, UMS3033/US001
Institut Européen de Chimie et Biologie, F-33607 Pessac (France)

Supporting information for this article is given via a link at the end of the document.

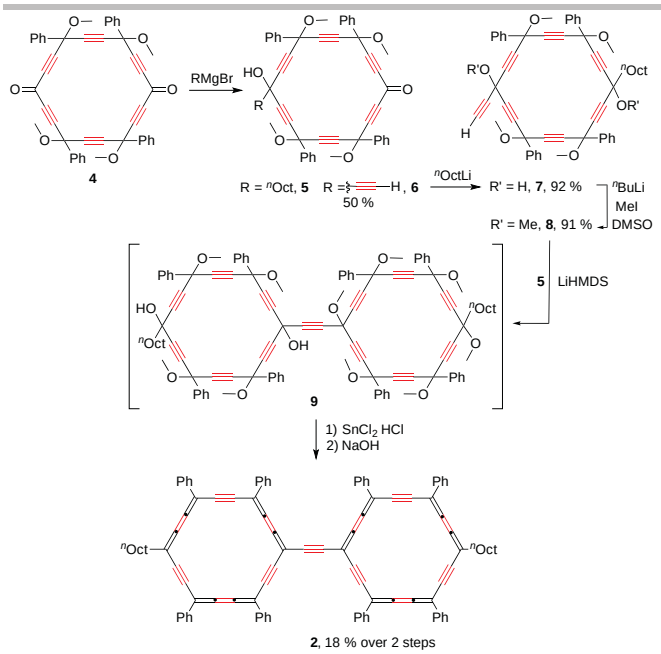

Scheme 1. Synthesis of a *carbo*-biphenyl.

The synthesis of *carbo*-terphenyls **3a**-**b** was addressed *via* a similar strategy first aiming at the preparation of the respective tris-[6]pericyclynic precursors **10a**-**b** (Scheme 2).

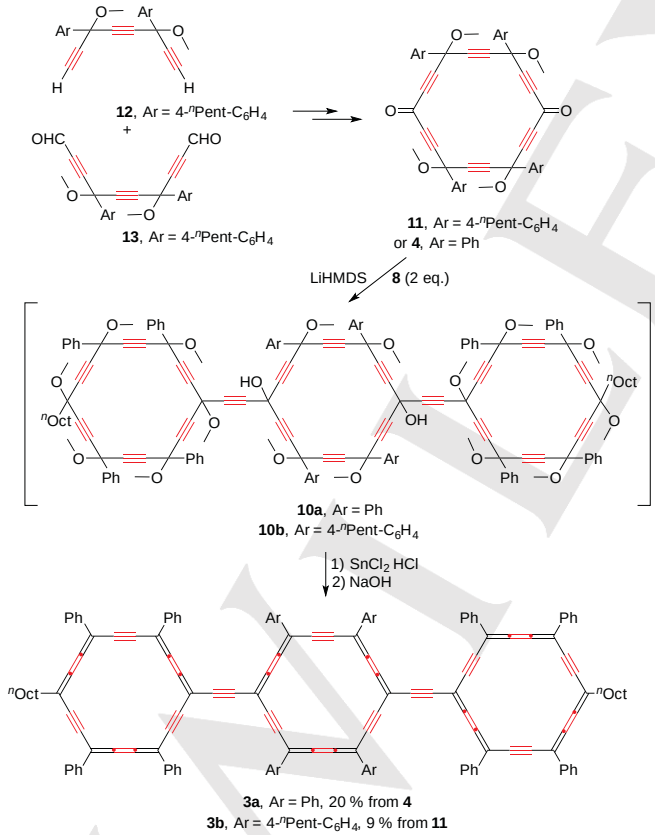

Scheme 2. Synthesis of *carbo*-terphenyls (HMDS = hexamethyldisilazane).

The most efficient method implemented for the preparation of **10a** (see ESI) was resumed for the preparation of **10b**. The pentylphenyl [6]pericyclynedione **11** was first obtained from the known triyne **12** and dialdehyde **13** by a two-step procedure adapted from the one used for the phenyl congener **4** (see ESI).[7] In the presence of LiHMDS, addition of two equivalents of **8** to **4** and **11** thus afforded the respective primary targets **10a** and **10b**. The latter could not be isolated in pure form, but their direct treatment with $SnCl_2$/HCl, gave **3a** and **3b** as poorly soluble black solids in 20 % and 9 % yields over two steps, respectively.

The three *carbo*-OPEs **2** and **3a**-**b** were found to be stable under air at room temperature for at least several weeks. As expected, **3b** was found to be significantly more soluble than **3a**.

In all the cases, the ^{1}H NMR signals of the *ortho*-H nuclei of the aryl substituents are highly deshielded in two separate sets: those of the external phenyl groups (adjacent to octyl substituents) resonate at $\delta \approx 9.5$ ppm as in the *carbo*-benzene **1**,[8] while those of the internal aryl groups occur at lower field ($\delta \approx 9.8$ ppm). This extra-deshielding can be attributed to the combined effects of the diatropic ring currents of both the geminal and vicinal C_{18} rings. The signals of the octyl CH_2 groups resonate at similar chemical shifts as in **1**.[8] The magnetic aromaticity of **1**, **2** and **3a**-**b** was further analyzed in a systematic manner by calculation of nucleus independent chemical shifts (NICS;[15] see below).

The structure of **2** and **3b** were confirmed by X-ray diffraction (XRD) analyses of single crystals obtained by slow evaporation of nitrobenzene or chloroform solutions (Figure 2 and ESI).[16]

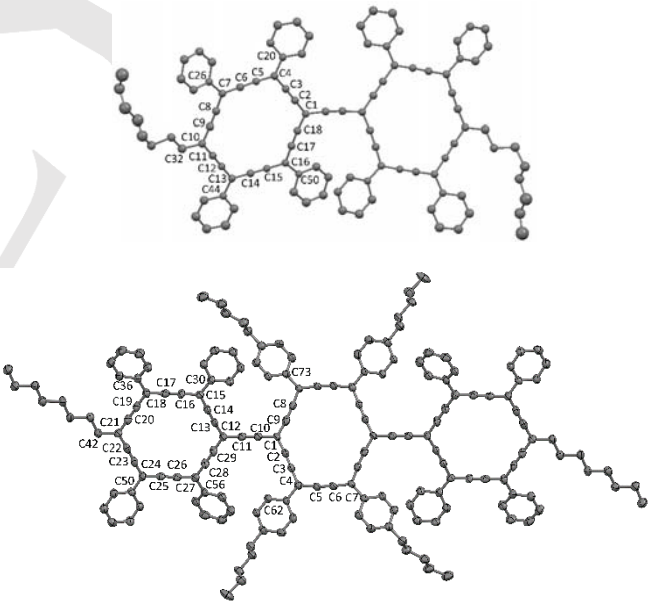

Figure 2. Crystallographic molecular views of **2** (from nitrobenzene: top, ellipsoid shown at 30 % probability) and **3b** (from chloroform: bottom, ellipsoid shown at 50 % probability).[16] For XRD analysis of crystals of **2** deposited from chloroform, see ESI.

In the *carbo*-biphenyl **2**, the two C_{18} rings are quite puckered, with deviation from the mean planes, Δ, up to 0.17 Å. These mean planes form an angle of 34.5(1)° through a bent C_4 acetylenic bridge of *ca* 4.05 Å long (bending angle *ba* = 169.8°). The C1-C10 diagonal of one macrocycle forms an angle of 24.3° with the projection of the C1'-C10' diagonal of the other macrocycle in the mean plane of the former (see ESI). In the *carbo*-terphenyl **3b** the

three C_{18} ring are closer to planarity (Δ = 0.05 Å and 0.09 Å for the central and external rings, respectively), with dihedral angles values θ = 35.63(3)° and 0° (parallel external C_{18} mean planes). The C_4 bridges (4.03 Å) are also closer to linearity (*ba* = 177.9°), while the three C_{18} centroids are perfectly aligned. The central macrocycle displays a significantly shrunk C1-C1' axial diagonal (7.23(1) Å *vs* 8.21± 0.10 Å for C7-C7' and C4-C4'), while the external counterparts are more regular hexagons (diagonal distances = 7.98 ± 0.11 Å). Crystallographic features of **2** and **3b** were found preserved in the isolated state by DFT calculation (see below).

The UV-vis absorption spectra of **2**, **3a** and **3b** exhibit three main absorption bands, one of them in the far red-region (661-743 nm). These spectra are thus quite different from those of **1** (Figure 2), with, however, a similar intense band between 435 and 457 nm (447 nm for **1**), the maximum molar extinction coefficient remaining around 200 000 L.mol^{-1}.cm^{-1}. While the spectrum of **2** presents two bands of identical intensities at 435 and 542 nm, the weaker most blue-shifted band of **3a** and **3b** is actually split in two shoulders of similar intensities.

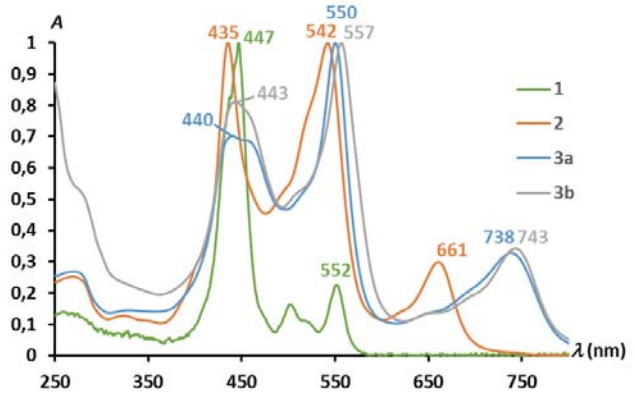

Figure 3. UV-vis absorption spectra of **1**, **2**, **3a**-**b** ($CHCl_3$ solutions).

The *carbo*-OPEs **2** and **3a**-**b** were also studied by cyclic voltammetry (CV) and square-wave voltammetry (SWV) (Table 1). They were found to be much more readily reduced than the reference *carbo*-benzene **1**, the first and second absolute reduction potentials decreasing regularly with the global π-conjugation extent, up to $E_{1/2}$ = -0.39 V for **3a** (*vs* -0.83 V for **1**).

Table 1. Voltammetric data for the three *carbo*-OPEs **1**, **2**, **3a** and **3b**.

	Reduction				Oxidation
	E_p red4[b]	E_p red3[b]	$E_{1/2}$ or E_p red2	$E_{1/2}$ red1[a]	$E_{1/2}$ or E_p
1			-1.31[b]	-0.83	1.20[a]
2		-1.20	-0.76[a]	-0.58	1.22[b]
3a[c]	-1.10	-0.89	-0.49[a]	-0.39	1.14[b]
3b[c]	-1.04[d]	-0.87[d]	-0.52[d]	-0.45	1.16[b]

Note: supporting electrolyte: $CHCl_3$ + 0.1 mol/L [TBA][PF_6]; scan rate: 0.2 V/s; half-wave potential $E_{1/2}$ = (E_p^{red} + E_p^{ox})/2 in V/SCE. [a] Reversible process. [b] Irreversible process. [c] Measurements performed after deposition of the compound on the working electrode by dipping it in a DCM solution of **3a** or **3b** (see section 3 in ESI). [d] Observed by SWV only.

In contrast, increasing the π-conjugation extent from **1** to **3a**-**b** has a negligible effect on the first oxidation potential, remaining in the range 1.18 ± 0.04 V. The first reduction process is reversible in all cases, while the first oxidation is reversible for the *carbo*-benzene **1** only.

The structures of **1**, **2** and **3a** in vacuum were optimized at the B3PW91/6-31G(d,p) DFT level without symmetry constraint (see ESI) in the singlet spin state (the singlet-triplet gap still mounting to 20 kcal/mol for **2**). The long known [6]pericyclynedione **4** [14b] has also been calculated for the first time (as a *trans*-*cis*-*trans*, stereoisomer: see ESI, Figure S8). A tractable model of **3b** was devised by truncating the four central pentyl chains to four methyl groups in **3b'**. Calculated bond lengths and C_{18}–Ph dihedral angles reproduced crystallographic data within experimental errors, fitting with current values in the *carbo*-benzene series (C*sp*–C*sp* ≈ 1.236 ± 0.003 Å, C*sp*-C*sp*^{2} ≈ 1.382 ± 0.005 Å, C–Ph ≈ 1.480 ± 0.002 Å). Perfectly linear C_4 bridges are found 0.05 Å longer (4.05 Å) than the C_{18} ring edges, with shorter C*sp*–C*sp* (1.220 Å) and longer C*sp*–C*sp*^{2} (1.417 Å) bonds. The calculated structure of the quaterphenyl **14** (n = 3, R^i = Ph in Figure 1) exhibits similar features, confirming the structural "*carbo*-aromatic" character of the individual macrocycles.[6] All the C_{18} rings were found nearly planar ($\Delta \leq$ 0.053 Å) in a staggered conformation: θ = 29.9° for **2**, θ = 30.8° for **3a** with external rings staggered by 2θ = 61.6° (θ = 38.5 ±0.5° for the parent OPEs), deviation from co-planarity being due to steric repulsion between phenyl substituents (replacing the Ph groups of **2**, **3a**-**b** and **14** by H atoms leads to equilibrium structures of perfect C_{2h} symmetry). Successive C_{18} rings are calculated to be quite free-rotating about the C_4 bridges, with a barrier of *ca* 1.7 kcal/mol through both orthogonal ($\theta \approx 90°$) and eclipsed ($\theta \approx 0°$) transition states (see full conformational analysis in ESI). Planar rigidification of the *carbo*-biphenyl core of **2** has also been theoretically envisaged by double Ph–Ph oxidative coupling and by embedding in a *carbo*-pyrene frame (see section 4.6.3 in ESI and Figure S13).

The magnetic aromaticity of the macrocycles can be appraised by the NICS values calculated at either the ring center (NICS(0)) or 1 Å above (NICS(1)). As previously reported, starting from $C_{18}H_6$ or $C_{18}{}^t Bu_6$, the NICS(0) value decreases upon substitution with phenyl groups from *ca* -18 ppm to -13.5 ppm for $C_{18}Ph_6$, through -14.6 ppm for $C_{18}Ph_4{}^t Bu_2$.[17] The values -14.9 ppm for $C_{18}Ph_4Oct_2$ **1** (Tables 2 and S6) is thus consistent with this trend. In **3a**, **3b'** and **14**, the NICS values are *ca* 1 ppm higher for the central rings than for the external counterparts, which is consistent with the general trend (both CC-C_{18} and Ph substituents are π-conjugating). The C_{18} rings thus preserve their intrinsic magnetic anisotropy/aromaticity in *carbo*-OPE wires.

As in all the *carbo*-benzenes calculated to date, the near-frontier MOs (NFOs) are of out-of-plane π symmetry (Table S9, Figures S4-S7). For **3a-b'**, while the HOMO and LUMO are delocalized over the three macrocycles, six NFOs of higher or lower energy are localized on either the central or external macrocycles ("central MOs" or "external MOs", respectively; Figure S6). Consistently with the donating character of alkyl substituents, the energies of the central NFOs increase by *ca* 0.005 Ha (0.14 eV) from **3a** to **3b'** (or a vertical model thereof), while their rank changes from HOMO-3 to HOMO-1 and from LUMO+1 to LUMO+4 (Figure S6, Table S10). In contrast, the energy variation of the external NFOs is negligible (0.02 eV) and that of the delocalized NFOs is intermediate (0.07 eV), with the same HOMO-LUMO gap for **3a** and **3b'** (1.7 eV).

Calculation of the excited states |Si> (i = 1-50) at the TDDFT level shows that the three excitations of greatest oscillator strengths correlate with the observed spectra as $\lambda_{exptl} \approx 0.76\ \lambda_{calcd}$ + 94 nm (Table 2, Table S8, Figure S3A). The wavelength of the most red-sifted band also correlates quite accurately with the

HOMO→LUMO gap over the series (Figure S3B): this is confirmed by the CI expansion of the corresponding excitation consisting mainly in a HOMO→LUMO one-electron transition (62 % of |S2> for **1**, 67 % of |S3> for **2**, 70% of |S1> for **3a**, **3b'** and **14**: see section 4.8 in ESI). The intermediate band of **2**, **3a** and **3b** (in the range 542-557 nm) is assigned to a more complex excitation (|S9>, |S19 and |S24>, respectively). As previously reported for other *carbo*-benzenes,[18] the interpretation of the most blue-shifted band (around 450 nm) within the Gouterman model (devised for porphyrins) applies to **1** and can be generalized to **2**, **3a** and **3b** (excitations involving two one-electron transitions from {HOMO-1, HOMO} to {LUMO, LUMO+1}).[19] Although not experimentally detected, fluorescence properties have also been calculated (Table S8). The *carbo*-quaterphenyl target **14** is thus predicted to exhibit strong absorption and emission propensity in the near infrared region (at 937 and 1254 nm, with $f \approx 3$ and 4.8, respectively).

Table 2. DFT calculated electronic and magnetic properties of **1, 2, 3a**, **3b** or **3b'**, and **4** (B3PW91/6-31G(d,p) level) *vs* experimental data.

	E_{HOMO} [a]	E_{LUMO} [a]	$-E_{red1}$ [b]	$1/\eta$ [c]	λ_{expt} [d]	λ_{calcd} (f) [e]	-NICS(0)/-NICS(1) [f]	
							ext. C_{18}	centr. C_{18}
1	-0.190	-0.106	-0.83	539	552	606.9 (0.3)	14.9 /13.6	
				462	447*	465.7 (2.8)		
						446.6 (1.3)		
2	-0.189	-0.117	0.58	632	661	734.3 (0.8)	13.7 /12.5	
				536	542*	579.9 (2.4)		
					435*	463.6 (3.5)		
3a	-0.187	-0.124	0.39	727	738	858.5 (2.0)	13.6/12.4	12.5/11.4
				541	550*	580.8 (1.0)		
					455	465.2 (0.7)		
					440	461.2 (3.4)		
3b' [•]	-0.185	-0.122	0.45	724	743	858.6 (2.0)	13.7/12.5	12.4/11.3
				565	557*	598.6 (2.3)		
					443	462.8 (3.2)		
14	-0.186	-0.128	(0.30)	786	-	937.4 (3.0)	13.6/12.4	12.4/11.3

a) HOMO and LUMO energies in Ha (see complete NFO data in Table S9); b) first reduction potential in V/SCE (Table 1), extrapolated value in brackets; c) chemical hardness $\eta = E_{LUMO} - E_{HOMO}$, in a.u. (Table S5); d) observed strongest absorptions in nm (Figure 3), stars (*) denote λ_{max} values; e) in nm for TDDFT-calculated excited states, f = absorption oscillator strength (Table S8); f) calculated in ppm within the GIAO formalism. The NICS(0) and NICS(1) values of the phenyl substituents vary in the ranges -6.3 ± 0.4 and -8.4 ± 0.4 ppm, respectively, *vs* -9.8 and -11.4 ppm for benzene (see Tables S6-S7).

Finally, a remarkable linear fit of the first reduction potential with the LUMO energy of **1**, **2**, **3a**-**b'** is evidenced (Figure 4): $E_{1/2red} = -3.32 - 23.52\ E_{LUMO}$ (in V/SCE *vs* a.u.). By extrapolation, a reduction potential of -0.30 V is thus predicted for the *carbo*-quaterphenyl **14** (E_{LUMO} = -0.128642 a.u.).

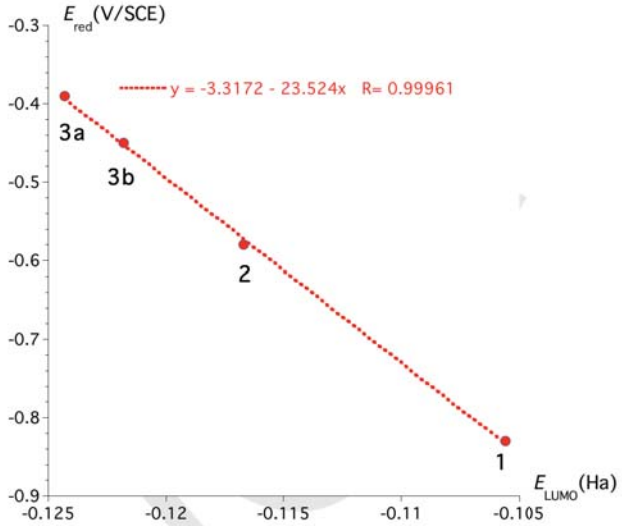

Figure 4. Linear fit of the measured first (reversible) reduction potential with the DFT-calculated LUMO eigenvalue.

Along the lines developed in the Introduction, the availability and stability of the *carbo*-OPEs **2**, **3a** and **3b** open natural prospects in molecular electronics, in particular for comparison with parent OPE wires and accessing longer wires such as **14**. On this occasion, first compounds containing three *carbo*-benzenes rings were isolated (**3a**-**b**). Functionalization of the *carbo*-OPE termini, e.g. by amino groups, is the next challenge.

Acknowledgements

C. Z. thanks the China Scholarship Council for his Ph.D. scholarship. The authors thank the Toulouse IDEX Emergence program 2014 (*Carbo*-device project) and the Centre National de la Recherche Scientifique for funding. In the framework of the CNRS ЯÉCIPROCS network, this work has benefited from the X-ray facility of the Biophysical and Structural Chemistry platform at IECB, CNRS UMS 3033, INSERM US 001, Bordeaux University.

Keywords: alkynes • aromaticity • bi-/ter-phenyl • *carbo*-benzenes • OPEs

[1] For early and recent articles on OPPs, see for example: a) W. Ried, D. Freitag, *Angew. Chem. Int. Ed*. **1968**, *7*, 835-844; b) E. Zojer, J. Cornil, G. Leising, J. L. Brédas, *Phys. Rev. B* **1999**, *59*, 7957-7968; c) O. S. Weng, *J. Chem. Soc. Rev*. **2011**, *40*, 3538-3550; d) Z. Xie, I. Baldea, C. E. Smith, Y. Wu, C. D. Friesbie, *ACS Nano* **2015**, *9*, 8022-8036; e) M. Fang, J. Huang, S.-J. Chang, Y. Juang, W.-Y. Lai, W. Huang, *J. Mater. Chem. C* **2017**, *5*, 5797-5809.

[2] For electronic properties of OPEs, see: a) Q. Lu, K. Liu, H. Zhang, Z. Du, X. Wang, F. Wang, *ACS Nano* **2009**, *3(12)*, 3861-3868; b) Q. Lu, C. Yao, X. Wang, F. Wang, *J. Phys. Chem. C* **2012**, *116*, 17853-17861; c) C. R. Parker, E. Leary, R. Frisenda, Z. Wei, K. S. Jennum, E. Glibstrup, P. B. Abrahamsen, M. Santella, M. A. Christensen, E. A. Della Pia, T. Li, M. T. Gonzalez, X. Jiang, T. J. Morsing, G. Rubio-Bollinger, B. W. Laursen, K. Nørgaard, H. van der Zant, N. Agrait, M. Brønsted Nielsen, *J. Am. Chem. Soc.* **2014**, *136*, 16497-16507. For fluorescence properties of OPEs, see: d) W. Hu, N. Zhu, W. Tang, D. Zhao, *Org. Lett.* **2008**, *10*, 2669-2672; e) V. Ervithayasuporn, J. Abe, X. Wang, T. Matsushima, H. Murata, Y. Kawakami, *Tetrahedron* **2010**, *66*, 9348-

9355; f) S. Yin, V. Leen, C. Jackers, D. Beljonne, B. Van Averbeke, M. Van der Auweraer, N. Boens, W. Dehaen, *Chem. Eur. J*. **2011**, *17*, 13247-13257.

[3] J. Wu, M. D. Watson, N. Tchebotareva, Z. Wang, K. Müllen, *J. Org. Chem*. **2004**, *69*, 8194-8204.

[4] G. Sedghi, V. M. Garcia-Suarez, L. J. Esdaile, H. L. Anderson, C. J. Lambert, S. Martin, D. Bethell, S. J. Higgins, M. Elliott, N. Bennett, J. E. Macdonald, R. J. Nichols, *Nat. Nanotechnol*. **2011**, *6*, 517-523.

[5] a) Z. Li, M. Smeu, A. Rives, V. Maraval, R. Chauvin, M. A. Ratner, E. Borguet, *Nat. Commun*. **2015**, *6*, 6321-6329. For the synthesis of the *p*-dianilinyl-carbo-benzene see: b) A. Rives, I. Baglai, V. Malytskyi, V. Maraval, N. Saffon-Merceron, Z. Voitenko, R. Chauvin, *Chem. Commun*. **2012**, *48*, 8763-8765.

[6] K. Cocq, C. Lepetit, V. Maraval, R. Chauvin, *Chem. Soc. Rev*. **2015**, *44*, 6535-6559.

[7] K. Cocq, N. Saffon-Merceron, Y. Coppel, C. Poidevin, V. Maraval, R. Chauvin, *Angew. Chem. Int. Ed*. **2016**, *55*, 15133-15136.

[8] C. Zhu, A. Rives, C. Duhayon, V. Maraval, R. Chauvin, *J. Org. Chem*. **2017**, *82*, 925-935.

[9] See for example: J. Kuwabara, M. Sakai, Q. Zhang, T. Kanbara, *Org. Chem. Front*. **2015**, *2*, 520-525.

[10] A. Bramborg, T. Linker, *Adv. Synth. Catal*. **2010**, *352*, 2195-2199.

[11] T. Fukutani, K. Hirano, T. Satoh, M. Miura, *J. Org. Chem*. **2011**, *76*, 2867-2874.

[12] M. Saleh, M. Baumgarten, A. Mavrinskiy, T. Schäfer, K. Müllen, *Macromolecules* **2010**, *43*, 137-143.

[13] T. Yatabe, H. Okumoto, Y. Kawanishi, T. Inoue, *Chem. Lett*. **2013**, *42*, 764-766.

[14] For an early reference on pericyclynes see: a) L. T. Scott, G. J. DeCicco, J. L. Hyunn, G. Reinhardt, *J. Am. Chem. Soc*. **1985**, *107*, 6546-6555; for the [6]pericyclynedione **4** see: b) L. Leroyer, C. Zou, V. Maraval, R. Chauvin, *C. R. Chim*. **2009**, *12*, 412-419.

[15] P. v. R. Schleyer, C. Maerker, A. Dransfeld, H. J. Jiao, J. R. V. Hommes, *J. Am. Chem. Soc*. **1996**, *118*, 6317-6318.

[16] CCDC 1559540 (**2**) and 1553845 (**3b**) contain the supplementary crystallographic data for this paper. These data can be obtained free of charge from The Cambridge Crystallographic Data Centre.

[17] D. Listunov, C. Duhayon, A. Poater, S. Mazères, A. Saquet, V. Maraval, R. Chauvin, *manuscript in preparation*.

[18] a) L. Leroyer, C. Lepetit, A. Rives, V. Maraval, N. Saffon-Merceron, D. Kandaskalov, D. Kieffer, R. Chauvin, *Chem. Eur. J.* **2012**, *18*, 3226-3240; b) I. Baglai, M. de Anda-Villa, R. M. Barba-Barba, C. Poidevin, G. Ramos-Ortíz, V. Maraval, C. Lepetit, N. Saffon-Merceron, J.-L. Maldonado, R. Chauvin, *Chem. Eur. J*. **2015**, *21*, 14186-14195.

[19] M. Gouterman, *J. Chem. Phys*. **1959**, *30*, 1139-1161.

Supporting Information

69451 Weinheim, Germany

Carbo-bi- and -ter-phenyls: OPE ring *carbo*-mers

Chongwei Zhu,[a,b] Albert Poater,[c] Carine Duhayon,[a,b] Brice Kauffmann,[d] Alix Saquet,[a,b] Valérie Maraval*[a,b] and Remi Chauvin*[a,b]

[a] *CNRS, LCC (Laboratoire de Chimie de Coordination), 205 route de Narbonne, BP44099, 31077 Toulouse Cedex 4 (France)*

[b] *Université de Toulouse, UPS, ICT-FR 2599, 31062 Toulouse Cedex 9 (France)*

[c] *Institut de Química Computacional i Catàlisi and Departament de Química, Universitat de Girona, Campus Montilivi, 17003 Girona, Catalonia (Spain)*

[d] *Université de Bordeaux, CNRS, INSERM, UMS3033/US001, Institut Européen de Chimie et Biologie, F-33607 Pessac (France)*

Abstract: Ring *carbo*-mers of oligo(phenylethynyl)enes (OPEs) containing C_2-catenated C_{18} *carbo*-benzene rings have been synthesized from a key [6]pericyclynedione, and characterized by ^{1}H, ^{13}C NMR and UV-vis absorption spectroscopy, X-ray diffractometry, and voltammetry. Analyses of crystal and DFT-optimized structures show that the C_{18} rings preserve their individual *carbo*-aromatic character according to both structural and magnetic criteria (NICS indices). *Carbo*-terphenyls are however found to be reversibly reduced at much higher potential $E_{1/2}^{red1}$ (-0.42 ± 0.03 V/SCE) than the parent mono-*carbo*-benzene (-0.83 V/SCE). Over the series, an accurate correlation between $E_{1/2}^{red1}$ and the DFT-calculated LUMO energy, suggests an even lower value for a theoretical *carbo*-quaterphenyl congener (0.30 V/SCE). Extended π-conjugation is also revealed by three main absorption bands from the blue to the far-red regions, two of which can be interpreted, by single one-electron excitations in frontier orbitals, and by TDDFT-calculated low lying excited states.

DOI: 10.1002/anie.2016XXXX

Table of Content

1. Experimental Procedures

1.1. General remarks

THF, diethyl ether (Et_2O), pentane and dichloromethane (DCM) were dried with a PureSolv-MD-5 Innovative Technology system for the purification of solvents. All other reagents were used as commercially available. In particular, commercial solutions of LiHMDS were 1 M in THF, solutions of *n*-BuLi were 2.5 M in hexane and 1.6 M in THF, solutions of *t*-BuLi were 1.6 M in pentane, solutions of ethylmagnesium bromide were 3 M in THF, solutions of octylmagnesium bromide were 3 M in THF, solutions of ethynylmagnesium bromide were 0.5 M in THF, solutions of HCl were 2 M in diethyl ether, $SnCl_2$ was anhydrous. Silica gel (60 Å, C.C 70-200 µm) was used for column chromatography. Silica gel thin layer chromatography plates (60F254, 0.25 mm) were revealed under UV-light and/or by treatment with an ethanolic solution of phosphomolybdic acid (20%). The following analytical instruments were used, 1D (^1H, ^{13}C) and 2D (^1H-^{13}C HSQC, ^1H-^{13}C HMBC) NMR: Avance 300, Avance 400, Avance 400 HD and Avance 600 spectrometers; Mass spectroscopy: Quadrupolar Nermag R10-10H spectrometer; UV-Visible: Perkin-Elmer UV-Vis Win-Lab Lambda 950; All the ^1H and ^{13}C signals were assigned according to chemical shifts, spin-spin coupling constants, splitting patterns, signal intensities, and 2D NMR experiments; NMR chemical shifts are given in ppm with positive values to high frequency relative to the tetramethylsilane reference. Coupling constants *J* are in Hertz. UV-Visible extinction molar coefficient ε is in $L{\cdot}mol^{-1}{\cdot}cm^{-1}$ and wavelengths λ in nm.

1.2. Synthesis and characterization of new compounds

1-octyl-10-[2-(10-octyl-4,7,13,16-tetraphenylcyclooctadeca-1,2,3,7,8,9,13,14,15-nonaen-5,11,17-triyn-1-yl)ethynyl]-4,7,13,16-tetraphenylcyclooctadeca-1,2,3,7,8,9,13,14,15-nonaen-5,11,17-triyne (2)

A solution of crude dodecaoxy-[6,6]peribicyclyne **9** (40 mg) in DCM (40 mL) was treated with anhydrous $SnCl_2$ (98 mg, 0.514 mmol) and HCl (0.51 ml, 1.023 mmol) at -78 °C. The reaction mixture was stirred at -78 °C for 15 min, then at room temperature for 20 min. After treatment with a 2 M aqueous NaOH solution (0.51 mL), the solution was filtrated through celite®. The organic layer was washed with brine, dried over $MgSO_4$ and concentrated under reduced pressure. The residue was purified on silica gel by column chromatography (pentane/DCM 3:1, then 2:1) to give **2** (12 mg, 0.009 mmol, 18 % over 2 steps) as a black solid.

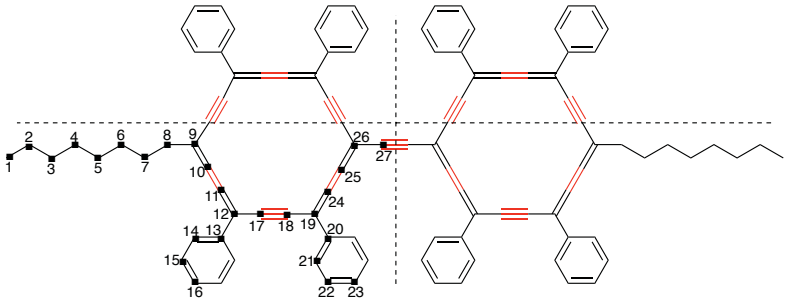

^1H NMR (600 MHz, $CDCl_3$) δ 9.80 (d, *J* = 7.4 Hz, 8H, H^{21}), 9.50 (d, *J* = 7.4 Hz, 8H, H^{14}), -8.00 (t, *J* = 7.4 Hz, 8H, H^{22}), 7.96 (t, *J* = 7.4 Hz, 8H, H^{15}), 7.74 (t, *J* = 7.1 Hz, 4H, H^{23}), 7.67 (t, *J* = 7.1 Hz, 4H, H^{16}), 4.68 (t, *J* = 7.6 Hz, 4H, H^8), 3.01 (quint., *J* = 7.7 Hz, 4H, H^7), 1.96 (quint., *J* = 7.6 Hz, 4H, H^6), 1.73 (quint., *J* = 7.6 Hz, 4H, > H^5), 1.48 (quint., *J* = 7.4 Hz, 4H, H^4), 1.35 (m, 8H, H^3, H^2), 0.89 (t, *J* = 7.0 Hz, 6H, H^1).
$^{13}C\{^1H\}$ NMR (151 MHz, $CDCl_3$) δ 139.7 (C^{13}), 139.6 (C^{20}), 130.3 (C^{15}, C^{21}), 130.0 (C^{16}), 129.9 (C^{14}, C^{22}), 129.5 (C^{23}), 122.3 (C^{10}), 10-8.8 (C^9), 105.8 (C^{19}), 103.7 (C^{12}), 99.7 (C^{26}), 82.9 (C^{27}), 120.6, 120.5, 119.3, 117.1, 113.7 ($C^{11, 17, 18, 24, 25}$), 40.9 (C^8), 32.0 (C^7), 31.8 (C^6), 29.8 (C^5), 29.6 (C^4), 29.4 (C^3), 22.7 (C^2), 14.1 (C^1).
HRMS (MALDI-TOF/DCTB): *m/z*: $[M]^+$ calculated for $C_{102}H_{74}$: 129-8.5791, found: 129-8.5802.
UV−vis ($CHCl_3$): λ = 435 (ε 191000), 542, 661.

1,10-bis[2-(10-octyl-4,7,13,16-tetraphenylcyclooctadeca-1,2,3,7,8,9,13,14,15-nonaen-5,11,17-triyn-1-yl)ethynyl]-4,7,13,16-tetraphenylcyclooctadeca-1,2,3,7,8,9,13,14,15-nonaen-5,11,17-triyne (3a)

A solution of crude octadecaoxy-[6,6,6]peritricyclyne **10a** (50 mg) in DCM (50 mL) was treated with anhydrous $SnCl_2$ (120 mg, 0.630 mmol) and HCl (0.63 mL, 1.260 mmol) at -78 °C. The reaction mixture was stirred at -78 °C for 15 min, then at room temperature for 20 min. After treatment with a 2 M aqueous NaOH solution (0.630 mL), the solution was filtrated through celite®. The organic layer was washed with brine, dried over $MgSO_4$ and concentrated under reduced pressure. The residue was purified on silica gel by column chromatography (pentane/DCM 3:1 then pure $CHCl_3$), the elution was collected and evaporated under rotovap, the product was rinsed with pentane and Et_2O on glass fiber to give pure **3a** (13 mg, 0.007 mmol, 20 % from **4**), as a black solid.

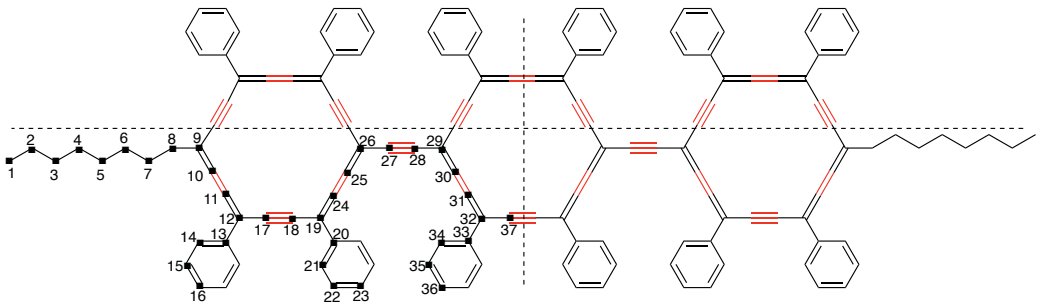

^1H NMR (400 MHz, $CDCl_3$) δ 9.86 – 9.72 (dd, *J* = 7.5 Hz, 16H, H^{21}, H^{34}), 9.53 – 9.47 (d, *J* = 7.5 Hz, 8H, H^{14}), -8.05 – 7.95 (m, 24H, H^{15}, H^{22}, H^{35}), 7.79 – 7.77 (t, *J* = 6 Hz, 4H, H^{36}), 7.74 – 7.71 (quint., *J* = 6 Hz, 4H, H^{16}, H^{23}) 4.69 (t, *J* = 7.5 Hz, 4H, H^8), 3.02 (quint., *J* = 7.6 Hz, 4H, H^7), 1.96

(quint., J = 7.7 Hz, 4H, H^6), 1.74 (quint., J = 7.4 Hz, 4H, H^5), 1.49 – 1.45 (m, 4H, H^4) 1.37 – 1.34 (m, 8H, H^3, H^2), 0.90 – 0.88 (m, 6H, H^1).
$^{13}C\{^1H\}$ NMR (151 MHz, $CDCl_3$) δ 139.9 (C^{33}), 139.8 (C^{20}), 139.6 (C^{13}), 130.5 – 130.4 (C^{34}, C^{21}, C^{22}), 130.2 – 130.0 (C^{14}, C^{15}, C^{23}, C^{35}, C^{36}), 129.7 (C^{16}), 122.5 (C^{10}), 109.1 (C^9), 10-6.4 (C^{19}), 10-6.1 (C^{32}), 103.9 (C^{12}), 120.9 – 113.8 ($C^{11, 17, 18, 24, 25, 30, 31, 37}$), 94.6 ($C^{29}$), 8-8.6 ($C^{26}$), 83.5 – 81.8 ($C^{27}$, C^{28}), 41.1 (C^8), 32.1 (C^7, C^6), 31.9 (C^5), 29.9 (C^4), 29.5 (C^3), 22.9 (C^2), 14.3 (C^1).
HRMS (MALDI-TOF/DCTB): *m/z*: $[M+Na]^+$ calculated for $C_{146}H_{94}Na$: 1869.7253, found: 1869.7404.
UV−vis ($CHCl_3$): λ = 440, 550 (ε 218000), 73-8.

Alternative strategy for the synthesis of 3a.
The *carbo*-terphenyl **3a** was also prepared by the procedure outlined in Scheme S1a.

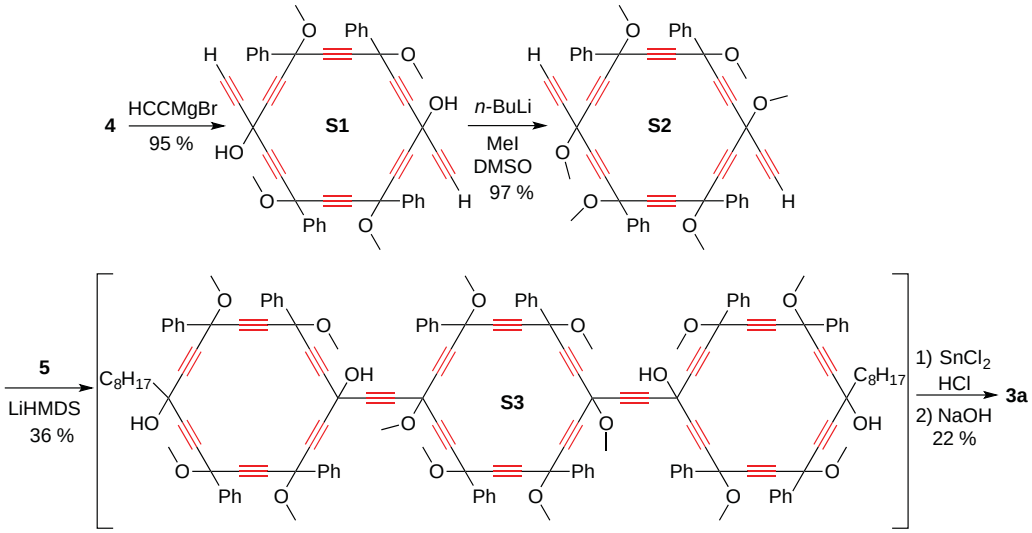

Scheme S1a. Alternative synthesis of the *carbo*-OPE **3a**.

1,10-bis[2-(10-octyl-4,7,13,16-tetraphenylcyclooctadeca-1,2,3,7,8,9,13,14,15-nonaen-5,11,17-triyn-1-yl)ethynyl]-4,7,13,16-tetraphenylcyclooctadeca-1,2,3,7,8,9,13,14,15-nonaen-5,11,17-triyne (3a)
A solution of crude **S3** (17 mg) in DCM (50 mL) was treated with anhydrous $SnCl_2$ (40 mg, 0.210 mmol) and HCl (0.21 mL, 0.042 mmol) at -78 °C. The reaction mixture was stirred at -78 °C for 15 min, then at room temperature for 20 min. After treatment with a 1 M aqueous NaOH solution (0.630 mL), the solution was filtrated through celite®. The organic layer was washed with brine, dried over $MgSO_4$ and concentrated under reduced pressure. The residue was purified with the identical manipulations as above to give **3a** (3.5 mg, 0.002 mmol, 8 % from **S2**) as a black solid.

1,10-diethynyl-4,7,13,16-tetramethoxy-4,7,13,16-tetraphenylcyclooctadeca-2,5,8,11,14,17-hexayne-1,10-diol (S1)

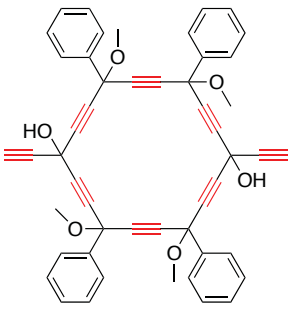

A solution of **4** (130 mg, 0.191 mmol) in THF (30 mL) was treated with ethynylmagnesium bromide (0.8 mL, 0.400 mmol,) at 0 °C. The solution was stirred for 1 h at 0 °C, then overnight at room temperature. After treatment with saturated aqueous NH_4Cl, the aqueous layer was extracted with EtOAc, and the combined organic layers were dried over $MgSO_4$ and concentrated under reduced pressure. The residue was purified by chromatography over silica gel (pentane/EtOAc 3:1) to give **S1** (133 mg, 0.182 mmol, 95%) as a pale yellow solid foam.
^1H NMR (400 MHz, $CDCl_3$) δ 7.76 – 7.66 (m, 8H, *o*-C_6H_5), 7.41 – 7.33 (m, 12H, *m*-, *p*-C_6H_5), 3.72 – 3.03 (m, 14H, -OCH_3, -OH), 2.90 – 2.52 (m, 2H, -C≡CH).
$^{13}C\{^1H\}$ NMR (101 MHz, $CDCl_3$) δ 139.0 – 13-8.8 (*i*-C_6H_5), 129.2 – 129.0 (*p*-C_6H_5), 12-8.6 – 12-8.5 and 12-6.5 – 12-6.4 (*o*-, *m*-C_6H_5), 84.5 – 79.8 (-C≡C-), 72.5 – 72.4 (-C≡CH), 71.8 (>C(OMe)Ph), 60.4 (>C(OH)C≡CH), 54.0 – 53.5 (-OCH_3).
HRMS (MALDI-TOF/DCTB): *m/z*: $[M+Na]^+$ calcd for $C_{52}H_{40}O_6Na$: 783.2723, found: 783.2764.

3,12-diethynyl-3,6,9,12,15,18-hexamethoxy-6,9,15,18-tetraphenylcyclooctadeca-1,4,7,10,13,16-hexayne S2

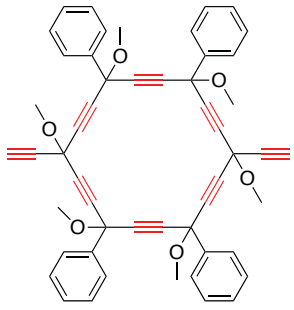

A solution of **S1** (183 mg, 0.250 mmol) in THF (30 mL) was treated with *n*-BuLi (0.31 mL, 0.500 mmol) at -78 °C. The reaction mixture was stirred for 10 min before addition of MeI (0.093 mL, 1.500 mmol) at the same temperature. The solution was slowly warmed up to -25 °C before addition of anhydrous DMSO (0.035 mL, 0.500 mmol). Then the reaction was allowed to slowly warm up to room temperature under stirring overnight. After treatment with the distilled water, the aqueous layer was extracted with Et_2O, the combined organic layers were dried over $MgSO_4$, and concentrated under reduced pressure. The residue was purified by silica gel column chromatography (pentane/EtOAc 4:1) to give **S2** (185 mg, 0.243 mmol, 97%) as a pale yellow foamed solid.

^{1}H NMR (400 MHz, $CDCl_3$) δ 7.77 – 7.70 (m, 8H, *o*-C_6H_5), 7.41 – 7.35 (m, 12H, *m*-, *p*-C_6H_5), 3.66 – 3.37 (m, 18H, -OCH_3), 2.75 – 2.69 (m, 2H, -C≡C*H*).
^{13}C{^{1}H} NMR (101 MHz, $CDCl_3$) δ 139.2 – 13-8.9 (*i*-C_6H_5), 129.2 – 129.0 (*p*-C_6H_5), 12-8.6 – 12-8.5 and 12-6.5 – 12-6.4 (*o*-, *m*-C_6H_5), 84.8 – 77.9 (-C≡C-), 73.3 – 73.0 (-C≡CH), 71.9 – 71.8 (>C(OMe)), 53.6 – 53.0 (-OCH_3).
HRMS (MALDI-TOF/DCTB): *m/z*: $[M]^+$ calculated for $C_{50}H_{36}O_6$: 732.2512, found: 732.2499.

1-(2-{10-[2-(1,10-dihydroxy-4,7,13,16-tetramethoxy-10-octyl-4,7,13,16-tetraphenylcyclooctadeca-2,5,8,11,14,17-hexayn-1-yl)ethynyl]-1,4,7,10,13,16-hexamethoxy-4,7,13,16-tetraphenylcyclooctadeca-2,5,8,11,14,17-hexayn-1-yl}ethynyl)-4,7,13,16-tetramethoxy-10-octyl-4,7,13,16-tetraphenylcyclooctadeca-2,5,8,11,14,17-hexayne-1,10-diol (S3)
To a solution of **S2** (29 mg, 0.038 mmol) in THF (15 mL) was added LiHMDS (0.228 ml, 0.228 mmol) at -78 °C. After stirring for 1h at this temperature, a solution of **5** (60 mg, 0.076 mmol) in THF (10 mL) was added at -78 °C. The resulting mixture was stirred for 1 h at -78 °C and overnight at room temperature. After treatment with a saturated aqueous solution of NH_4Cl, the aqueous layer was extracted with EtOAc, and the combined organic layers were dried over $MgSO_4$ and concentrated under reduced pressure. The residue was purified by silica gel column chromatography (pentane/EtOAc 4:1 then 3:1), to give a fraction of not pure **S3** (32 mg, *ca* 36% yield) as a yellow solid foam.

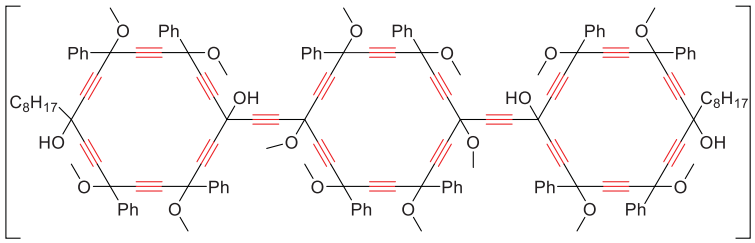

^{1}H NMR (400 MHz, $CDCl_3$) δ 7.72 – 7.64 (m, 24H, *o*-C_6H_5), 7.36 – 7.26 (m, 36H, *m*-, *p*-C_6H_5), 3.91 – 3.03 (m, 42H, -OCH_3), 2.89 – 2.56 (m, 4H, -O*H*), 2.08 – 1.90 (m, 4H, >CCH_2), 1.69 – 1.58 (m, 4H, >CCH_2CH_2), 1.27 (m, 20H, -$(CH_2)_5$-CH_3), 0.88 (m, 6H, -CH_3).
^{13}C{^{1}H} NMR (101 MHz, $CDCl_3$) δ 139.3 – 13-8.9 (*i*-C_6H_5), 129.2 – 129.0 (*p*-C_6H_5), 12-8.6 – 12-8.2 (*m*-C_6H_5), 12-6.4 (*o*-C_6H_5), 87.4 – 81.7 (-C≡C-), 73.3 – 73.2 (>C(OH)-C≡C-(OMe)C<), 71.8 (>C(OMe)Ph), 64.6 – 63.5 (>C(CH_2)), 53.5 – 53.0 (-OCH_3), 43.0 (>CCH_2OMe), 31.9 (>CCH_2CH_2), 30.3 – 29.2 (>C$(CH_2)_2(CH_2)_3$), 24.5 (-$CH_2CH_2CH_3$), 22.7 (-CH_2CH_3), 14.1 (-CH_2CH_3).
HRMS (MALDI-TOF/DCTB): *m/z*: $[M+Na]^+$ calculated for $C_{160}H_{140}O_{18}Na$: 2371.9937, found: 2371.999-8.

1,10-bis[2-(10-octyl-4,7,13,16-tetraphenylcyclooctadeca-1,2,3,7,8,9,13,14,15-nonaen-5,11,17-triyn-1-yl)ethynyl]-4,7,13,16-tetrakis(4-pentylphenyl)cyclooctadeca-1,2,3,7,8,9,13,14,15-nonaen-5,11,17-triyne (3b)
A solution of crude octadecaoxy-[6,6,6]peritricyclyne **10b** (40 mg) in DCM (40 mL) was treated with anhydrous $SnCl_2$ (86 mg, 0.451 mmol) and HCl (0.45 ml, 0.903 mmol) at -78 °C. The mixture was stirred at -78 °C for 15 min, then at room temperature for 20 min. After treatment with aqueous 1 M NaOH (0.45 mL), the reaction mixture was filtrated through celite®. The organic layer was washed with brine, dried over $MgSO_4$, and concentrated under reduced pressure. The residue was purified by silica gel column chromatography (pentane/DCM 3:1 then 3:2) to give **3b** (-6.5 mg, 0.003 mmol, 9 % from **11**) as a black solid.

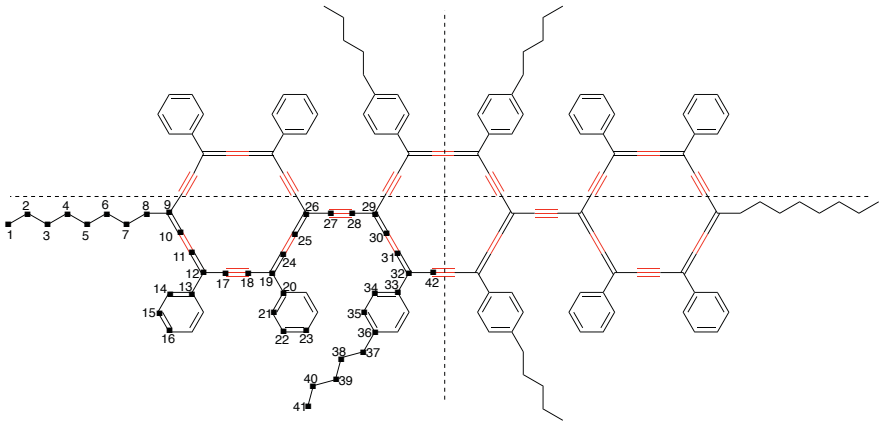

^{1}H NMR (600 MHz, $CDCl_3$) δ 9.84 (d, *J* = 7.5 Hz, 8H, H^{21}), 9.70 (d, *J* = 7.6 Hz, 8H, H^{34}), 9.52 (d, *J* = 7.5 Hz, 8H, H^{14}), -8.01 (dt, *J* = 7.5, 7.2 Hz, 16H, H^{15}, H^{22}), 7.81 (d, *J* = 7.5 Hz, 8H, H^{35}), 7.76 (t, *J* = 7.0 Hz, 4H, H^{23}), 7.70 (t, *J* = 7.0 Hz, H^{16}), 4.70 (t, *J* = 7.7 Hz, 4H, H^{8}), 3.02 (quint., *J* = 7.7 Hz, 4H, H^{7}), 2.89 (t, *J* = -8.1 Hz, 8H, H^{37}), 1.97 (t, *J* = 7.6 Hz, 4H, H^{6}), 1.87 (t, *J* = 7.3 Hz, 8H, H^{38}), 1.76 – 1.73 (m, 4H, H^{5}), 1.49 (2t, *J* = 7.0 Hz, 20H, H^{4}, H^{39}, H^{40}), 1.35 (dd, *J* = -6.9, 3.4 Hz, 8H, H^{3}, H^{2}), 1.01 (t, *J* = -6.9 Hz, 12H, H^{41}), 0.89 (m, 6H, H^{1}).
^{13}C{^{1}H} NMR (151 MHz, $CDCl_3$) δ 145.6 (C^{36}), 139.8 (C^{13}), 139.7 (C^{20}), 137.2 (C^{33}), 130.5 (C^{35}), 130.3 (C^{15}, C^{21}), 130.2 (C^{34}), 129.9 (C^{14}, C^{16}, C^{22}), 129.6 (C^{23}), 122.3 (C^{10}), 10-8.9 (C^{9}), 10-6.0 (C^{32}), 105.8 (C^{19}), 103.7 (C^{12}), 120.6 (C^{11}), 120.4, 120.3, 119.5, 119.4, 117.2, 114.1, 113.6 ($C^{17, 18, 24, 25, 30, 31, 42}$), 105.1 ($C^{29}$), 100.3 ($C^{26}$), 83.8 ($C^{27}$), 82.9 ($C^{28}$), 40.9 ($C^{8}$), 3-6.2 ($C^{37}$), 32.0 ($C^{7}$), 31.8 ($C^{38}$), 31.0 ($C^{6}$), 29.5 ($C^{39}$), 29.8 ($C^{5}$), 29.7 ($C^{4}$), 29.4 ($C^{39}$), 22.9 29.7 ($C^{2}$, C^{40}), 14.2 (C^{1}, C^{41}).
HRMS (MALDI-TOF/DCTB): *m/z*: calculated for $[M]^+$ $C_{166}H_{134}$: 2127.0486, found: 2127.0403
UV−vis ($CHCl_3$): λ= 442, 557 (ε 224000), 743.

10-ethynyl-10-hydroxy-4,7,13,16-tetramethoxy-4,7,13,16-tetraphenylcyclooctadeca-2,5,8,11,14,17-hexayn-1-one (6)

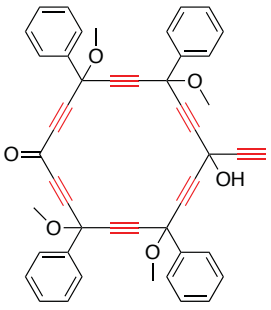

A solution of [6]pericyclynedione **4** (350 mg, 0.515 mmol) in THF (60 mL) was treated with ethynylmagnesium bromide (1.13 mL, 0.566 mmol) at 0°C. The mixture was stirred for 1 h at 0 °C, then overnight at r. t. After addition of water, the aqueous layer was extracted with Et_2O, the combined organic layers were dried over $MgSO_4$ and concentrated under reduced pressure. The residue was purified by chromatography over silica gel (pentane/EtOAc 4:1, then 3:1, then 2:1) to give **6** (180 mg, 0.255 mmol, 50%), the di-adduct **S1** (30 mg, 0.040 mmol, 8%) and unreacted **4** (150 mg, 0.220 mmol), as pale yellow solid foams.

^{1}H NMR (400 MHz, $CDCl_3$) δ 7.82 – 7.60 (m, 8H, *o*-C_6H_5), 7.53 – 7.28 (m, 12H, *m*-, *p*-C_6H_5), 3.69 – 3.37 (m, 13H, -OCH_3, -OH), 2.88 – 2.58 (m, 1H, -C≡CH).
^{13}C{^{1}H} NMR (101 MHz, $CDCl_3$) δ 159.2 – 159.0 (>C=O), 139.0 – 137.7 (*i*-C_6H_5), 129.7 – 12-8.6 (*p*-C_6H_5), 12-8.8 – 12-6.4 (*o*-, *m*-C_6H_5), 89.7 – 79.9 (-C≡C-), 72.5 – 72.4 (-C≡CH), 72.0 – 71.8 (>C(OMe)Ph), 60.5 (>C(OH)C≡CH), 53.9-53.5 (-OCH_3).
HRMS (MALDI-TOF/DCTB): *m/z*: $[M+Na]^+$ calculated for $C_{48}H_{34}O_6Na$: 729.2253, found: 729.231-6.

1-ethynyl-4,7,13,16-tetramethoxy-10-octyl-4,7,13,16-tetraphenylcyclooctadeca-2,5,8,11,14,17-hexayne-1,10-diol (7)

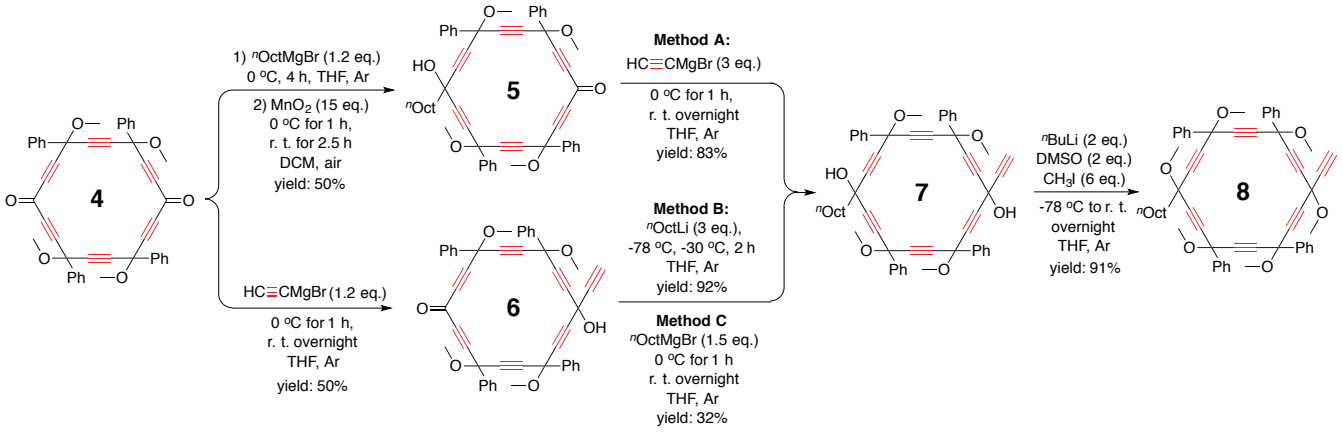

Scheme S1b. Alternative routes and methods to **7** and **8** from **4**.

Method A (Scheme S1b). To a solution of **5** (118 mg, 0.148 mmol) in THF (15 mL) was added ethynylmagnesium bromide (0.88 mL, 0.444 mmol) at 0 °C. The mixture was stirred for 1 h at 0 °C and overnight at room temperature. After treatment with a saturated aqueous solution of NH_4Cl, the aqueous layer was extracted with EtOAc, and the combined organic layers were dried over $MgSO_4$ and concentrated under reduced pressure. The residue was purified by silica gel column chromatography (pentane/EtOAc 3:1) to give **7** (100 mg, 0.123 mmol, 83%) as a pale yellow foamed solid.

Method B (Scheme S1b). A solution of **6** (180 mg, 0.255 mmol) in THF (40 mL) was treated with freshly prepared *n*-$C_8H_{17}Li$ (0.765 mmol in Et_2O) at -78 °C. The reaction mixture was slowly warmed up to -30 °C in 2 h under stirring. After treatment with a saturated aqueous solution of NH_4Cl, the aqueous layer was extracted with EtOAc, and the combined organic layers were dried over $MgSO_4$ and concentrated under reduced pressure. The residue was purified by silica gel column chromatography (pentane/EtOAc 3:1) to give **7** (192 mg, 0.233 mmol, 92%) as a pale yellow foamed solid.

Preparation of *n*-$C_8H_{17}Li$. To a solution of $C_8H_{17}I$ (0.362 mL, 2mmol) in Et_2O (4 mL) was added dropwise *t*-BuLi (2.4 mmol, 1.5 ml, 1.6 M) at -78 °C. The reaction mixture was stirred for 1 h at -78 °C and 0.5 h at room temperature. The resulting solution was used directly without further purification.[1]

Method C (Scheme S1b). A solution of **6** (90 mg, 0.128 mmol) in THF (10 mL) was treated with *n*-$C_8H_{17}MgBr$ (0.1 mL, 0.2 mmol) at 0 °C. The mixture was stirred for 1 h at 0°C and overnight at room temperature. After treatment with a saturated aqueous NH_4Cl, the aqueous layer was extracted with EtOAc, and the combined organic layers were dried over $MgSO_4$ and concentrated under reduced pressure. The residue was purified by silica gel column chromatography (pentane/EtOAc 3:1) to give **7** (33 mg, 0.040 mmol, 32%) and the reduced compound **S4** (62 mg, 0.087 mmol, 68%) as pale yellow solid foam.

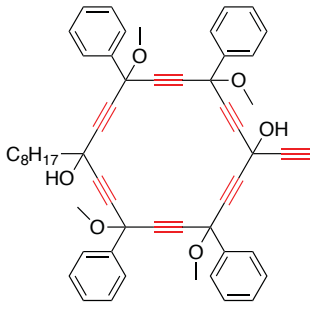

^{1}H NMR (400 MHz, $CDCl_3$) δ 7.86 – 7.65 (m, 8H, *o*-C_6H_5), 7.50 – 7.28 (m, 12H, *m*-, *p*-C_6H_5), 4.07 – 2.81 (m, 14H, -OCH_3, -OH), 2.80 – 2.60 (m, 1H, -C≡CH), 2.04 (m, 2H, >CCH_2), 1.77 – 1.50 (m, 2H, >CCH_2CH_2-), 1.38 – 1.26 (m, 10H, -$(CH_2)_5$-CH_3), 0.92 (m, 3H, -CH_3).
^{13}C{^{1}H} NMR (101 MHz, $CDCl_3$) δ 139.6 – 13-8.9 (*i*-C_6H_5), 129.2 – 129.0 (*p*-C_6H_5), 12-8.6 – 12-6.4 (*o*-, *m*-C_6H_5), 87.6 – 80.0 (-C≡C-), 72.5 – 72.2 (-C≡CH), 71.9 – 71.8 (>C(OMe)Ph), 63.7 – 63.6 (>C(OH)Oct), 60.7 (>C(OH)C≡CH), 54.0 – 53.3 (-OCH_3), 43.2 – 43.0 (>CCH_2), 31.9 (>CCH_2CH_2), 29.7 – 29.2 (>$C(CH_2)_2(CH_2)_3$), 24.6 – 24.5 (-$CH_2CH_2CH_3$), 22.7 (-CH_2CH_3), 14.2 (-CH_2CH_3).
HRMS (MALDI-TOF/DCTB): *m/z*: $[M+Na]^+$ calculated for $C_{48}H_{36}O_6Na$: 843.3662, found: 843.370-8.

1-ethynyl-4,7,13,16-tetraphenylcyclooctadeca-2,5,8,11,14,17-hexayne-1,10-diol (S4)

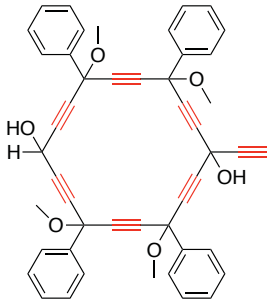

Side-product of the synthesis of **7** by the **method C**.
^{1}H NMR (400 MHz, $CDCl_3$) δ 7.82 – 7.63 (m, 8H, *o*-C_6H_5), 7.50 – 7.29 (m, 12H, *m*-, *p*-C_6H_5), 5.43 – 5.20 (m, 1H, >CHOH), 3.86 – 3.08 (m, 13H, -OCH_3, -OH), 2.99 – 2.30 (m, 2H, -C≡CH, -OH).
^{13}C{^{1}H} NMR (101 MHz, $CDCl_3$) δ 139.1 (*i*-C_6H_5), 129.2, 129.1 (*p*-C_6H_5), 12-8.6 – 12-8.5 (*m*-C_6H_5), 12-6.5 – 12-6.4 (*o*-C_6H_5), 8-8.4 – 80.5 (-C≡C-), 72.4 (-C≡CH), 71.8 (>C(OMe)Ph), 53.5, 53.4 (-OCH_3), 52.3 (>CHOH).
HRMS (MALDI-TOF/DCTB): *m/z*: $[M+Na]^+$ calculated for $C_{48}H_{36}O_6Na$: 731.2410, found: 731.2405.

3-ethynyl-3,6,9,12,15,18-hexamethoxy-12-octyl-6,9,15,18-tetraphenylcyclooctadeca-1,4,7,10,13,16-hexayne (8)

A solution of **7** (190 mg, 0.231 mmol) in THF (30 mL) was treated with *n*-BuLi (0.29 mL, 0.460 mmol) at -78 °C. The mixture was stirred for 10 min at this temperature before addition of MeI (0.083 mL, 1.340 mmol). The solution was slowly warmed up to -25 °C before addition of anhydrous DMSO (0.033 mL, 0.463 mmol). Then, the mixture was allowed to warm up to room temperature under stirring overnight. After treatment with the distilled water, the aqueous layer was extracted with Et_2O, and the combined organic layers were dried over $MgSO_4$, and concentrated under reduced pressure. The residue was purified by silica gel column chromatography (pentane/EtOAc 5:1) to give **8** (178 mg, 0.210 mmol, 91%) as a pale yellow foamed solid.

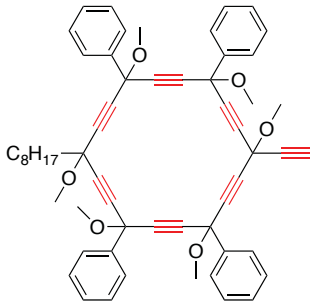

^{1}H NMR (400 MHz, $CDCl_3$) δ 7.88 – 7.64 (m, 8H, *o*-C_6H_5), 7.43 – 7.35 (m, 12H, *m*-, *p*-C_6H_5), 3.73 – 3.30 (m, 18H, -OCH_3), 2.83 – 2.60 (m, 1H, -C≡C*H*), 2.02 (m, 2H, >CCH_2), 1.77 – 1.54 (m, 2H, >CCH_2CH_2-), 1.31 (m, 10H, -$(CH_2)_5$-CH_3), 0.91 (m, 3H, -CH_3).

^{13}C{^{1}H} NMR (101 MHz, $CDCl_3$) δ 139.7 – 139.0 (*i*-C_6H_5), 129.2 – 129.0 (*p*-C_6H_5), 12-8.6 – 12-6.4 (*o*-, *m*-C_6H_5), 85.6 – 77.9 (-C≡C-), 73.3 – 73.1, 70.7 – 70.6 (-C≡CH), 72.0 – 71.9 (>C(OMe)Ph), 73.1 (>C(OMe)Oct), 70.6 – 70.5 (>C(OMe)C≡CH), 53.6 – 52.9 (-OCH_3), 42.3 – 42.0 (>CCH_2), 31.9 (>CCH_2CH_2), 29.7 – 29.2 (>C$(CH_2)_2(CH_2)_3$), 24.5 – 24.4 (-$CH_2CH_2CH_3$), 22.7 (-CH_2CH_3), 14.2 (-CH_2CH_3).

HRMS (MALDI-TOF/DCTB): *m/z*: $[M+H]^+$ calculated for $C_{58}H_{57}O_6$: 849.4155, found: 849.4164.

1-[2-(1,4,7,10,13,16-hexamethoxy-10-octyl-4,7,13,16-tetraphenylcyclooctadeca-2,5,8,11,14,17-hexayn-1-yl)ethynyl]-4,7,13,16-tetramethoxy-10-octyl-4,7,13,16-tetraphenylcyclooctadeca-2,5,8,11,14,17-hexayne-1,10-diol (9)

To a solution of **8** (60 mg, 0.071 mmol) in THF (15 mL) was added LiHMDS (0.21 mL, 0.212 mmol) at -78 °C. After stirring for 1 h at this temperature, the mixture was treated with a solution of **5** (44 mg, 0.055 mmol) in THF (5 mL) at -78 °C. The solution was stirred for 1 h at this temperature and overnight at room temperature. After treatment with a saturated aqueous solution of NH_4Cl, the aqueous layer was extracted with EtOAc, and the combined organic layers were dried over $MgSO_4$ and concentrated under reduced pressure. The residue was purified by silica gel column chromatography (pentane/EtOAc 4:1) to afford a fraction of not pure **9** (41 mg, about 48% yield) as a yellow solid foam.

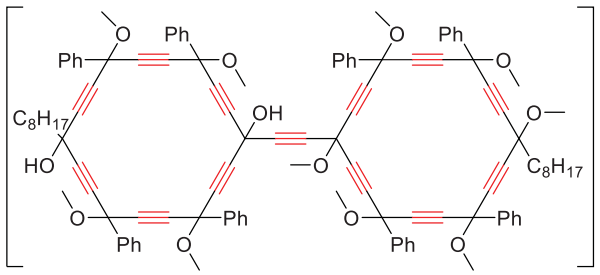

^{1}H NMR (400 MHz, $CDCl_3$) δ 7.87 – 7.57 (m, 16H, *o*-C_6H_5), 7.47 – 7.17 (m, 24H, *m*-, *p*-C_6H_5), 4.02 – 3.12 (m, 30H, -OCH_3), 3.13 – 2.21 (m, 2H, -O*H*), 1.99 (m, 4H, >CCH_2), 1.67 – 1.48 (m, 4H, >CCH_2CH_2-), 1.33 – 1.24 (m, 20H, -$(CH_2)_5$-CH_3), 0.91 – 0.85 (m, 6H, -CH_3).

^{13}C{^{1}H} NMR (101 MHz, $CDCl_3$) δ 139.5 – 139.0 (*i*-C_6H_5), 129.1 – 129.0 (*p*-C_6H_5), 12-8.6 – 12-8.3 (*m*-C_6H_5), 12-6.5 – 12-6.3 (*o*-C_6H_5), 87.5 – 80.8 (-C≡C-), 71.9 – 71.8 (>C(OMe)Ph), 70.6 (>C(OH)-C≡C-(OMe)C<), 63.7 (>C(Oct)), 60.7 (>C(OH)-C≡C-(OMe)C<), 53.6 – 52.3 (-OCH_3), 43.0 (>C(OH)CH_2), 42.1 (>C(OMe)CH_2), 31.9 (>CCH_2CH_2), 30.3 – 29.2 (>C$(CH_2)_2(CH_2)_3$), 24.5 – 24.4 (-$CH_2CH_2CH_3$), 22.7 – 22.6 (-CH_2CH_3), 14.1 (-CH_2CH_3).

HRMS (MALDI-TOF/DCTB): *m/z*: $[M+Na]^+$ calculated for $C_{112}H_{106}O_{12}Na$: 1665.7582, found: 1665.7700.

1,10-bis[2-(1,4,7,10,13,16-hexamethoxy-10-octyl-4,7,13,16-tetraphenylcyclooctadeca-2,5,8,11,14,17-hexayn-1-yl)ethynyl]-4,7,13,16-tetramethoxy-4,7,13,16-tetraphenylcyclooctadeca-2,5,8,11,14,17-hexayne-1,10-diol (10a)

To a solution of **8** (60 mg, 0.071 mmol) in THF (15 mL) was added LiHMDS (0.085 mL, 0.085 mmol) at -78 °C. After stirring for 1 h at this temperature, the mixture was treated with a solution of **4** (24 mg, 0.035 mmol) in THF (5 mL) at -78 °C. The resulting solution was stirred for 1 h at this temperature and overnight at room temperature. After treatment with a saturated aqueous solution of NH_4Cl, the aqueous layer was extracted with EtOAc, and the combined organic layers were dried over $MgSO_4$ and concentrated under reduced pressure. The residue was purified by silica gel column chromatography (pentane/EtOAc 4:1, then 3:1) to give a fraction of not pure **10a** (52 mg, about 62% yield) as a yellow foamed solid.

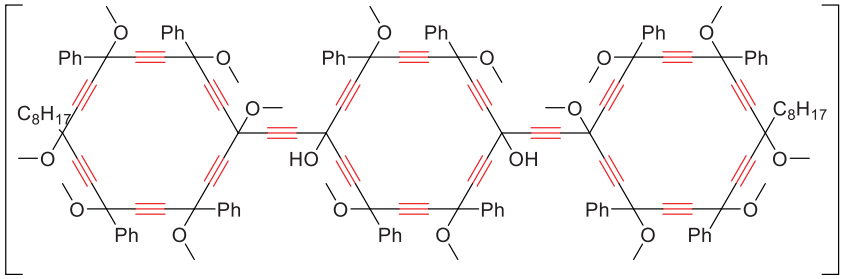

^{1}H NMR (400 MHz, $CDCl_3$) δ 7.80 – 7.54 (m, 24H, *o*-C_6H_5), 7.42 – 7.19 (m, 36H, *m*-, *p*-C_6H_5), 3.79 – 3.01 (m, 50H, -OCH_3, -O*H*), 2.07 – 1.92 (m, 4H, >CCH_2), 1.71 – 1.52 (m, 4H, >CCH_2CH_2), 1.26 (m, 20H, -$(CH_2)_5$-CH_3), 0.90 – 0.87 (m, 6H, -CH_3).

^{13}C{^{1}H} NMR (101 MHz, $CDCl_3$) δ 139.4 – 13-8.9 (*i*-C_6H_5), 129.1 (*p*-C_6H_5), 12-8.6 – 12-8.4 (*m*-C_6H_5), 12-6.4 – 12-6.3 (*o*-C_6H_5), 85.4 – 82.5 (-C≡C-), 71.9 – 71.7 (>C(OMe)Ph), 70.7 – 70.5 (>C(OH)-C≡C-(OMe)C<), 64.7 (>C(Oct)), 60.8 – 60.6 (>C(OH)-C≡C-(OMe)C<), 53.5 – 53.0 (-OCH_3), 42.1 (>CCH_2), 31.9 (>CCH_2CH_2), 30.2 – 29.2 (>C$(CH_2)_2(CH_2)_3$), 24.4 (-$CH_2CH_2CH_3$), 22.7 (-CH_2CH_3), 14.1 (-CH_2CH_3).

HRMS (MALDI-TOF/DCTB): *m/z*: $[M+Na]^+$ calculated for $C_{162}H_{144}O_{18}Na$: 2400.0250, found: 2400.0361.

1,10-bis[2-(1,4,7,10,13,16-hexamethoxy-10-octyl-4,7,13,16-tetraphenylcyclooctadeca-2,5,8,11,14,17-hexayn-1-yl)ethynyl]-4,7,13,16-tetramethoxy-4,7,13,16-tetrakis(4-pentylphenyl)cyclooctadeca-2,5,8,11,14,17-hexayne-1,10-diol (10b)

To a solution of **8** (68 mg, 0.080 mmol) in THF (15 mL) was added LiHMDS (0.100 mL, 0.100 mmol) at -78 °C. After stirring for 1 h at this temperature, the mixture was treated with a solution of **11** (35 mg, 0.036 mmol) in THF (10 mL) at -78 °C. The resulting solution was stirred for 1 h at the same temperature and overnight at room temperature. After treatment with a saturated aqueous solution of NH_4Cl, the aqueous layer was extracted with EtOAc, and the combined organic layers were dried over $MgSO_4$ and concentrated under reduced pressure. The residue was purified by silica gel column chromatography (pentane/EtOAc 5:1 then 3:1) to give a fraction of not pure **10b** (42 mg, about 41% yield) as a yellow foamed solid.

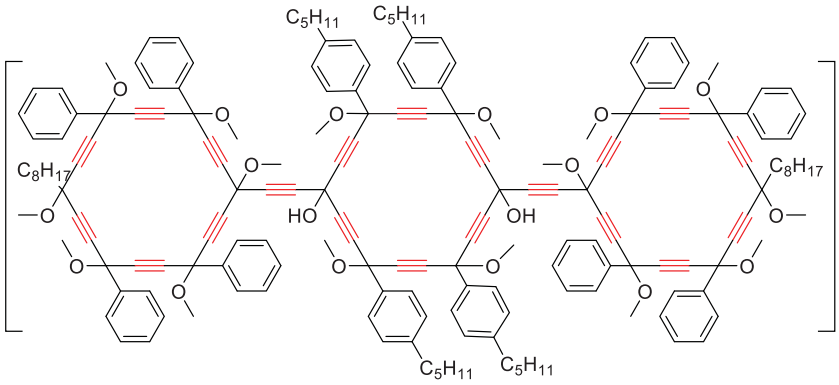

^{1}H NMR (300 MHz, $CDCl_3$) δ 7.78 – 7.51 (m, 24H, *o*-C_6H_5, *o*-C_6H_4), 7.47 – 7.19 (m, 24H, *m*-, *p*-C_6H_5,), 7.15 – 7.02 (m, 8H, *m*-C_6H_4), 3.99 – 2.74 (m, 50H, -OCH_3, -OH), 2.58 – 2.47 (m, 8H, $C_6H_4CH_2$), 2.04 – 1.94 (m 4H, >CCH_2), 1.63 – 1.48 (m, 12H, $C_6H_4CH_2CH_2$, >CCH_2CH_2), 1.27 (brs, 36H, -$(CH_2)_5$-CH_3, $C_6H_4CH_2CH_2(CH_2)_2$), 0.87 (brs, 18H, -CH_3).
^{13}C{^{1}H} NMR (75 MHz, $CDCl_3$) δ 144.0 (*p*-C_6H_4), 139.6 – 139.3 (*i*-C_6H_5, *i*-C_6H_4), 129.1 (*p*-C_6H_5), 12-8.5 (*m*-C_6H_5, *m*-C_6H_4), 12-6.4 (*o*-C_6H_5, *o*-C_6H_4), 85.3 – 79.1 (-C≡C-), 71.9 – 71.6 (>C(OMe)Ph), 70.7 – 70.6 (>C(OH)-C≡C-(OMe)C<), 63.2 (>C(Oct)), 53.5 (-OCH_3), 42.1 (>CCH_2), 35.6 ($C_6H_4CH_2$), 31.9 (>CCH_2CH_2), 31.5 ($C_6H_4CH_2CH_2$), 31.0 ($C_6H_4CH_2CH_2CH_2$), 30.3 – 29.2 (>$C(CH_2)_2(CH_2)_3$), 24.5 – 24.4 (-$CH_2CH_2CH_3$), 22.7 (-CH_2CH_3), 22.5 ($C_6H_4(CH_2)_3CH_2$), 14.1 (-CH_2CH_3), 14.0 ($C_6H_4(CH_2)_4CH_3$).
HRMS (MALDI-TOF/DCTB): *m/z*: $[M+Na]^+$ calculated for $C_{182}H_{184}O_{18}Na$: 2680.3380, found: 2680.349-6.

Two step synthesis of the tetrapentylated [6]pericyclynedione 11

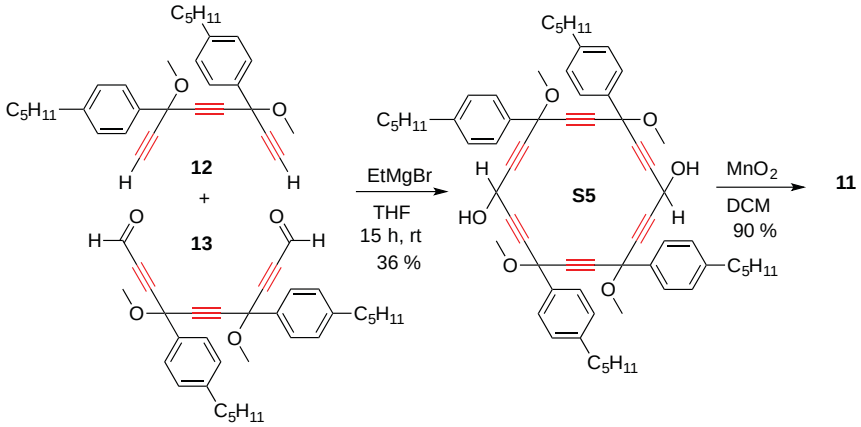

Scheme S2. Synthesis of the tetrapentylated [6]pericyclynedione **11**.

4,7,13,16-tetramethoxy-4,7,13,16-tetrakis(4-p ent ylphenyl)cyclooctadeca-2,5,8,11,14,17-hexayne-1,10-diol (S5)

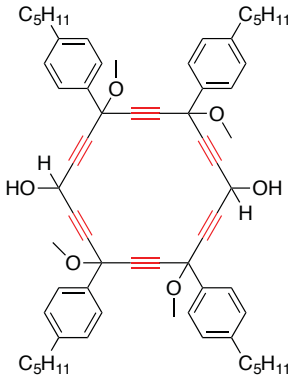

To a solution of triyne **12** [2](355 mg, 0.780 mmol) in THF (50 mL) was added EtMgBr (0.52 mL, 1.560 mmol) at 0 °C. The mixture was stirred for 15 min at 0 °C, then for 2 h at r. t. The resulting solution, and a solution of dialdehyde **13** [2] (400 mg, 0.780 mmol) in THF (50 mL) were added simultaneously (addition rate: 6 mL/h) into a 1 L round bottom flask containing THF (400 mL) under stirring at room temperature. The mixture was stirred for 15 h at room temperature before treatment with a saturated aqueous solution of NH_4Cl. The aqueous layer was extracted with EtOAc, and the combined organic layers were dried over $MgSO_4$ and concentrated under reduced pressure. The residue was purified by silica gel column chromatography (pentane/Et_2O 3:1 then 2:1) to give **S5** (269 mg, 0.279 mmol, 36 %) as a pale yellow solid foam.
^{1}H NMR (400 MHz, $CDCl_3$) δ 7.77 – 7.50 (m, 8H, *o*-C_6H_4), 7.18 (m, 8H, *m*-C_6H_4), 5.44 – 5.16 (m, 2H, >CHOH), 3.64 – 3.31 (m, 12H, -OCH_3), 2.88 – 2.43 (m, 10H, -CH_2, -OH), 1.61 (m, 8H, -CH_2-CH_2), 1.38 – 1.28 (m, 16H, -$(CH_2)_2$-), 0.89 (m, 12H, -CH_2CH_3).
^{13}C{^{1}H} NMR (101 MHz, $CDCl_3$) δ 144.1 – 144.0 (*p*-C_6H_4), 13-6.6 – 13-6.4 (*i*-C_6H_4), 12-8.6 – 12-6.4 (*o*-, *m*-C_6H_4), 84.3 – 82.1 (-C≡C-), 71.7 (>C(OMe)Ph), 53.4 – 53.3 (-OCH_3), 52.4 – 52.3 (>CHOH), 35.6 (-CH_2), 31.5 (-CH_2CH_2), 31.0 (-$CH_2CH_2CH_2$), 22.5 (-CH_2CH_3), 14.0 (-CH_2CH_3).
HRMS (MALDI-TOF/DCTB): *m/z*: $[M+Na]^+$ calculated for $C_{66}H_{76}O_6Na$: 987.5540, found: 987.5599.

4,7,13,16-tetramethoxy-4,7,13,16-tetrakis(4-pentylphenyl)cyclooctadeca-2,5,8,11,14,17-hexayne-1,10-dione (11)

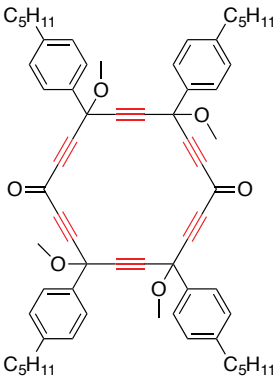

To a solution of **S5** (200 mg, 0.207 mmol) in DCM (50 mL) was added MnO_2 (600 mg, -6.218 mmol) at 0 °C. The reaction mixture was stirred for 1 h at 0 °C and for 2.5 h at room temperature. After filtration through celite®, the solution was concentrated under reduced pressure to give **11** (180 mg, 0.186 mmol, 90%) as a pale yellow foamed solid.

^{1}H NMR (400 MHz, $CDCl_3$) δ 7.70 – 7.50 (m, 8H, *o*-C_6H_4), 7.28 – 7.15 (m, 8H, *m*-C_6H_4), 3.66 – 3.42 (m, 12H, -OCH_3), 2.63 (m, 8H, -CH_2), 1.62 (m, 8H, -CH_2-CH_2), 1.33 (m, 16H, -$(CH_2)_2$-), 0.93 – 0.89 (m, 12H, -CH_2CH_3).

^{13}C{^{1}H} NMR (101 MHz, $CDCl_3$) δ 159.2 (>*C*=O), 144.9 – 144.8 (*p*-C_6H_4), 135.1 – 134.8 (*i*-C_6H_4), 12-8.9 – 12-6.4 (*o*-, *m*-C_6H_4), 89.3 – 84.1 (-*C*≡*C*-), 72.0 – 71.9 (>*C*(OMe)Ph), 53.9 – 53.8 (-O*C*H_3), 35.6 (-*C*H_2), 31.5 (-CH_2*C*H_2), 31.0 (-CH_2CH_2*C*H_2), 22.5 (-*C*H_2CH_3), 14.0 (-CH_2*C*H_3).

HRMS (MALDI-TOF/DCTB): *m/z*: $[M+Na]^+$ calculated for $C_{66}H_{72}O_6Na$: 983.5227, found: 983.5170.

1.3. Copies of ^{1}H, ^{13}C, ^{1}H-^{13}C HSQC, and ^{1}H-^{13}C HMBC NMR spectra

1D (^{1}H, $^{13}C\{^{1}H\}$) and **2D (^{1}H - ^{13}C HSQC** and **HMBC)** NMR spectra of **2** in $CDCl_3$

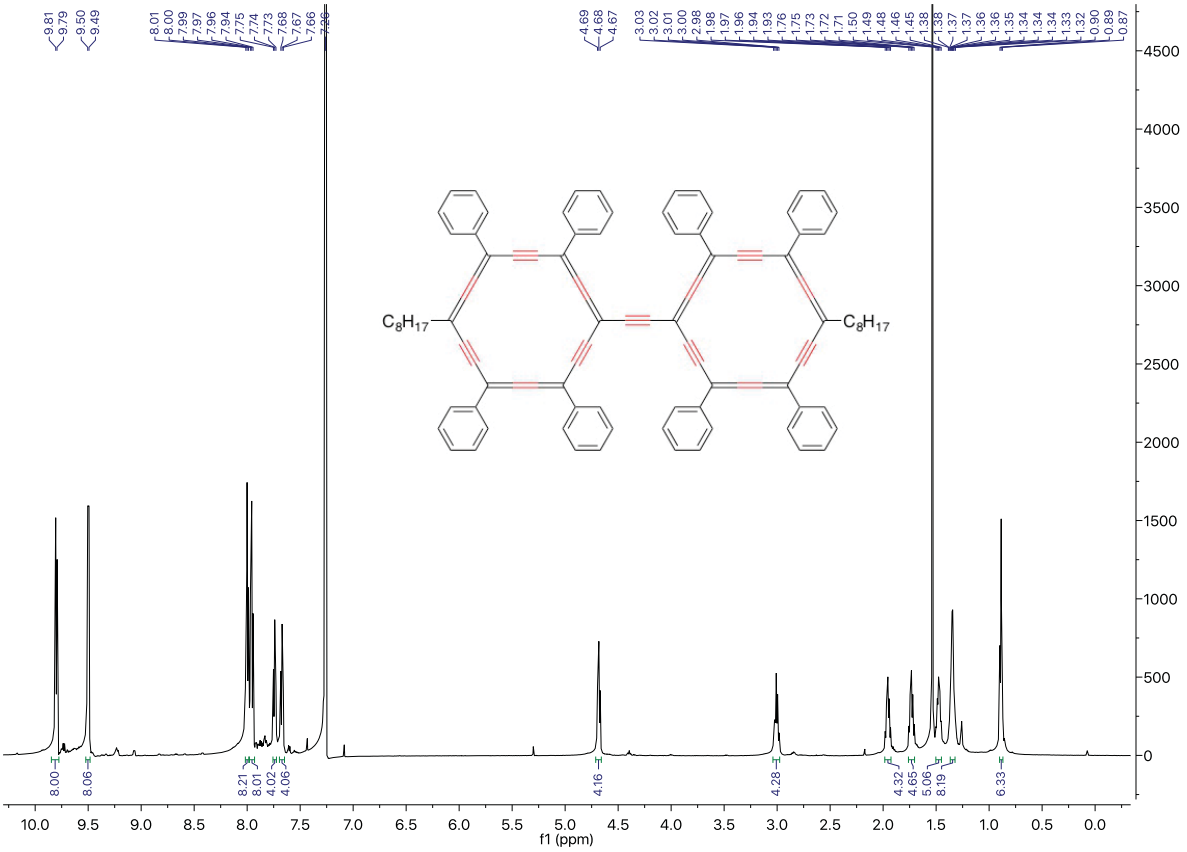

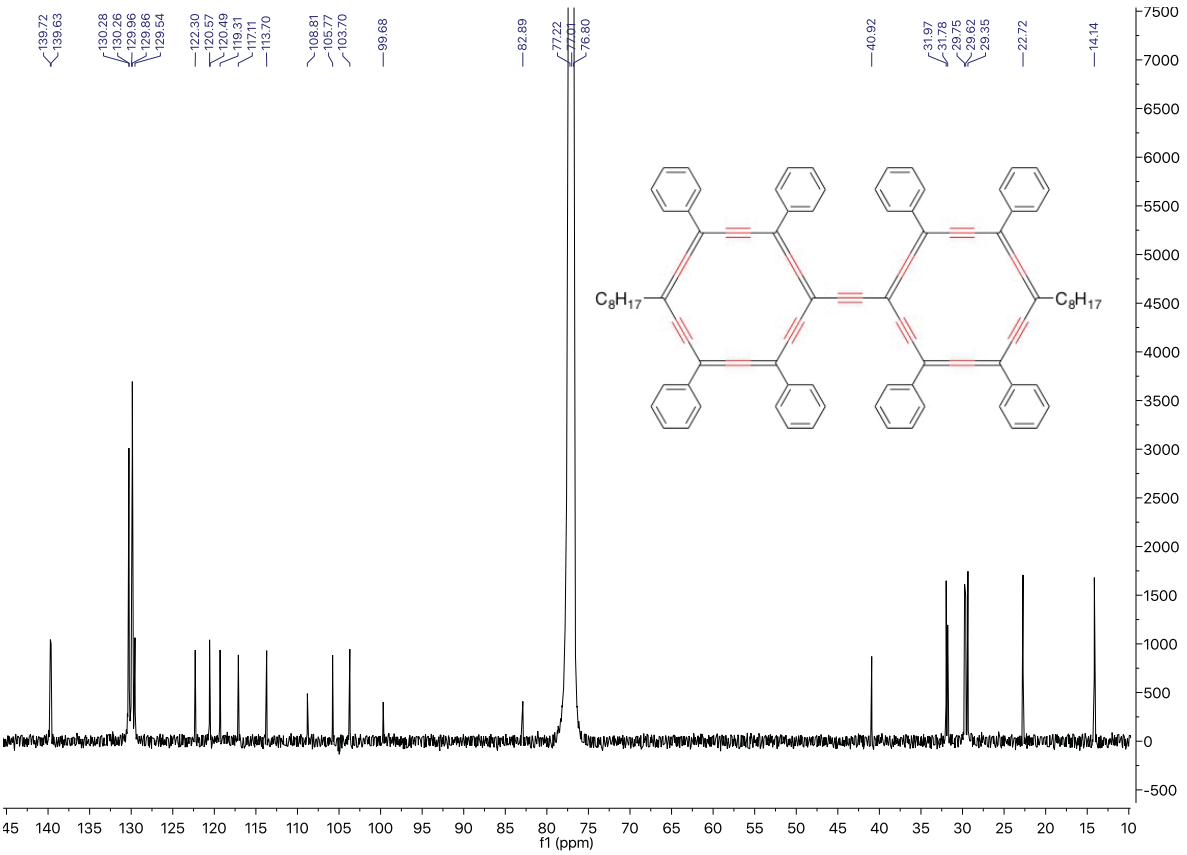

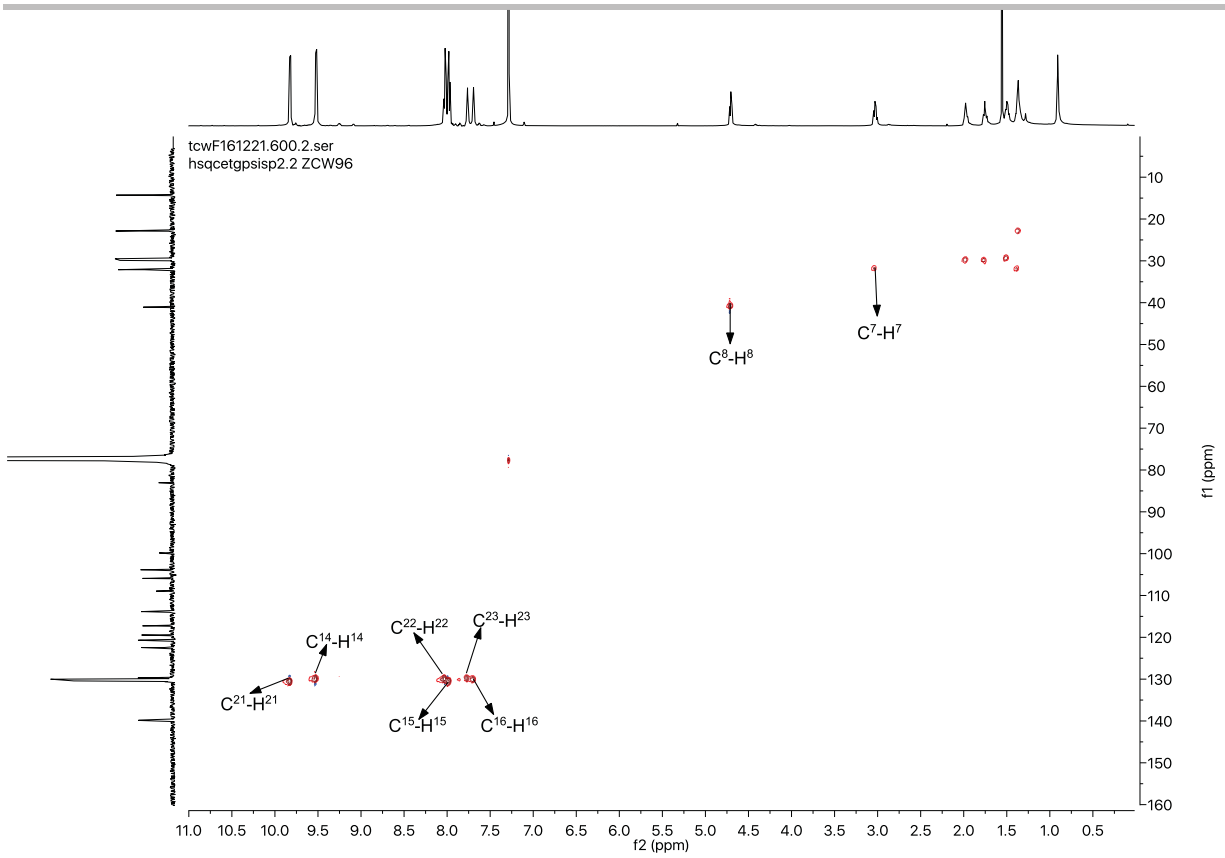
tcwF161221.600.2.ser
hsqcetgpsisp2.2 ZCW96
C8-H8
C7-H7
C14-H14
C21-H21
C22-H22
C23-H23
C15-H15
C16-H16
f2 (ppm)
f1 (ppm)

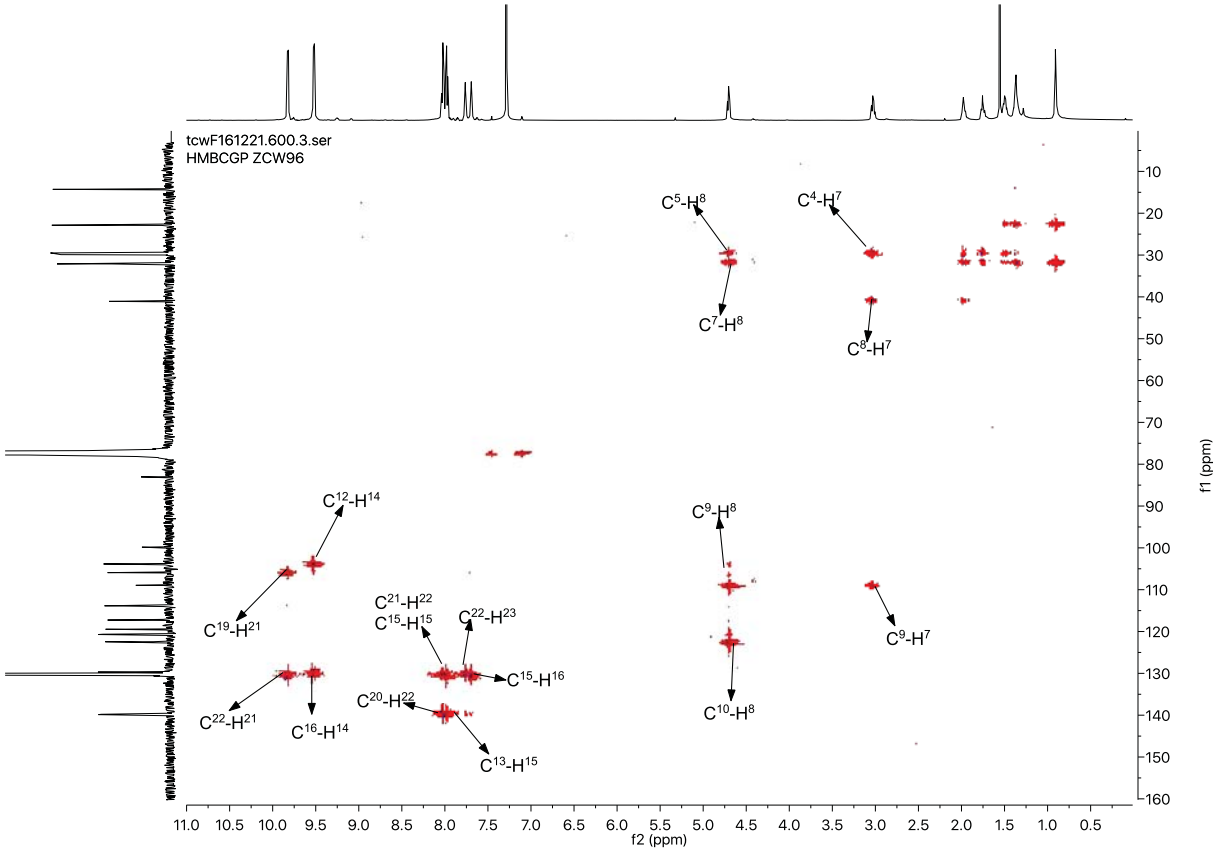
tcwF161221.600.3.ser
HMBCGP ZCW96
C5-H8
C7-H8
C4-H7
C8-H7
C12-H14
C19-H21
C22-H21
C16-H14
C21-H22
C15-H15
C22-H23
C15-H16
C20-H22
C13-H15
C9-H8
C10-H8
C9-H7
f2 (ppm)
f1 (ppm)

1D (^{1}H, ^{13}C{^{1}H}) and **2D (^{1}H - ^{13}C HSQC** and **HMBC)** NMR spectra of **3a** in $CDCl_3$

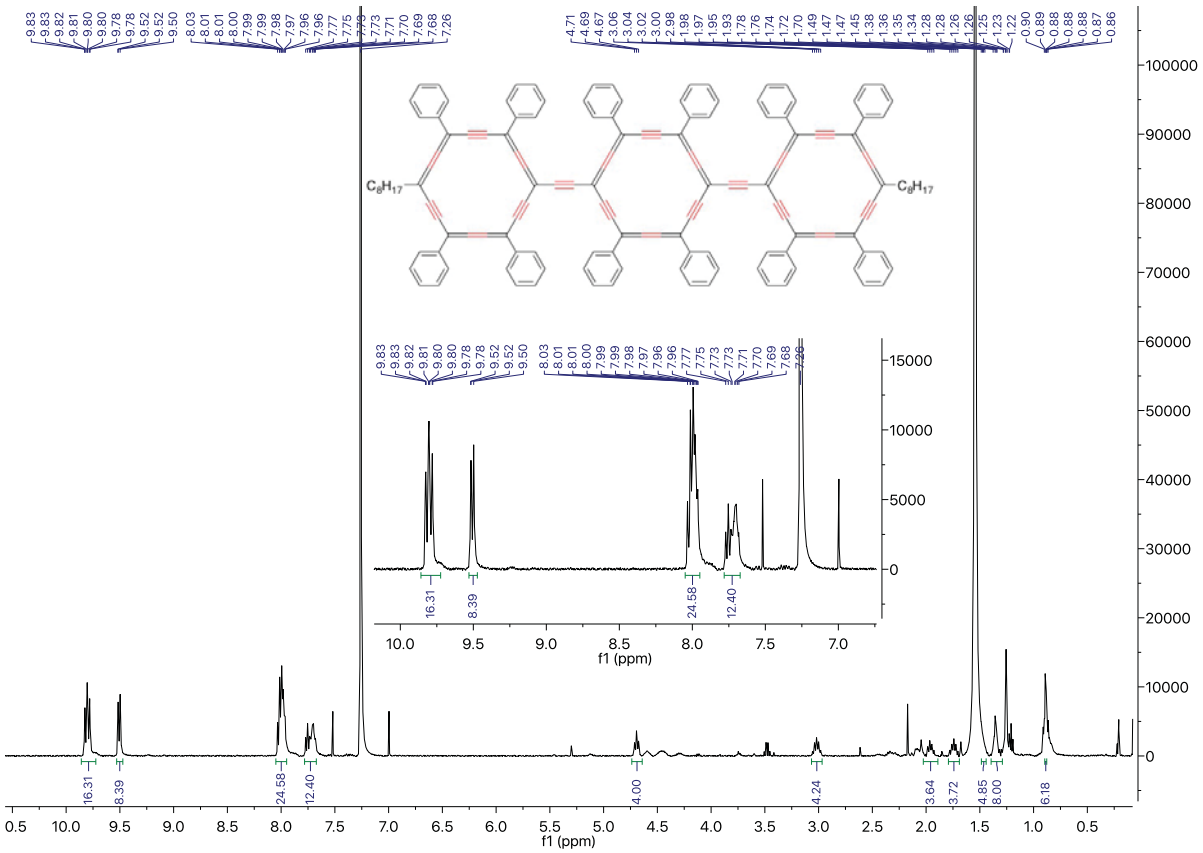

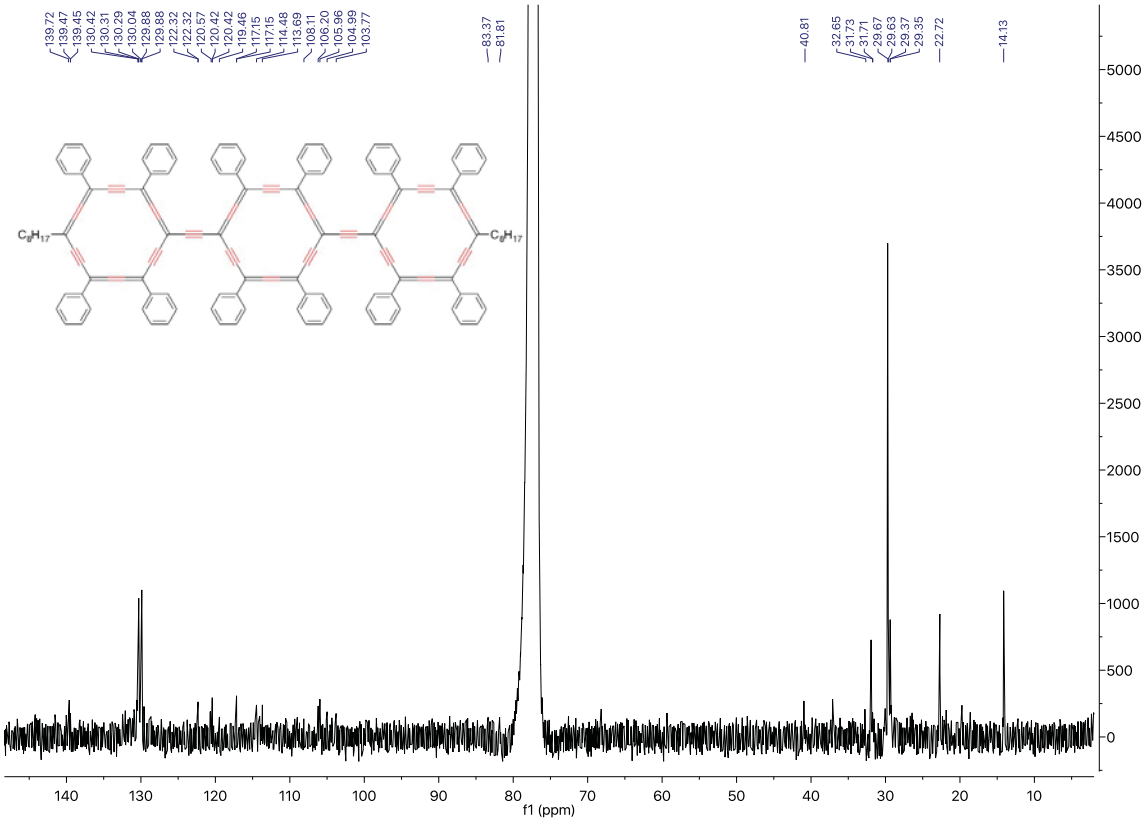

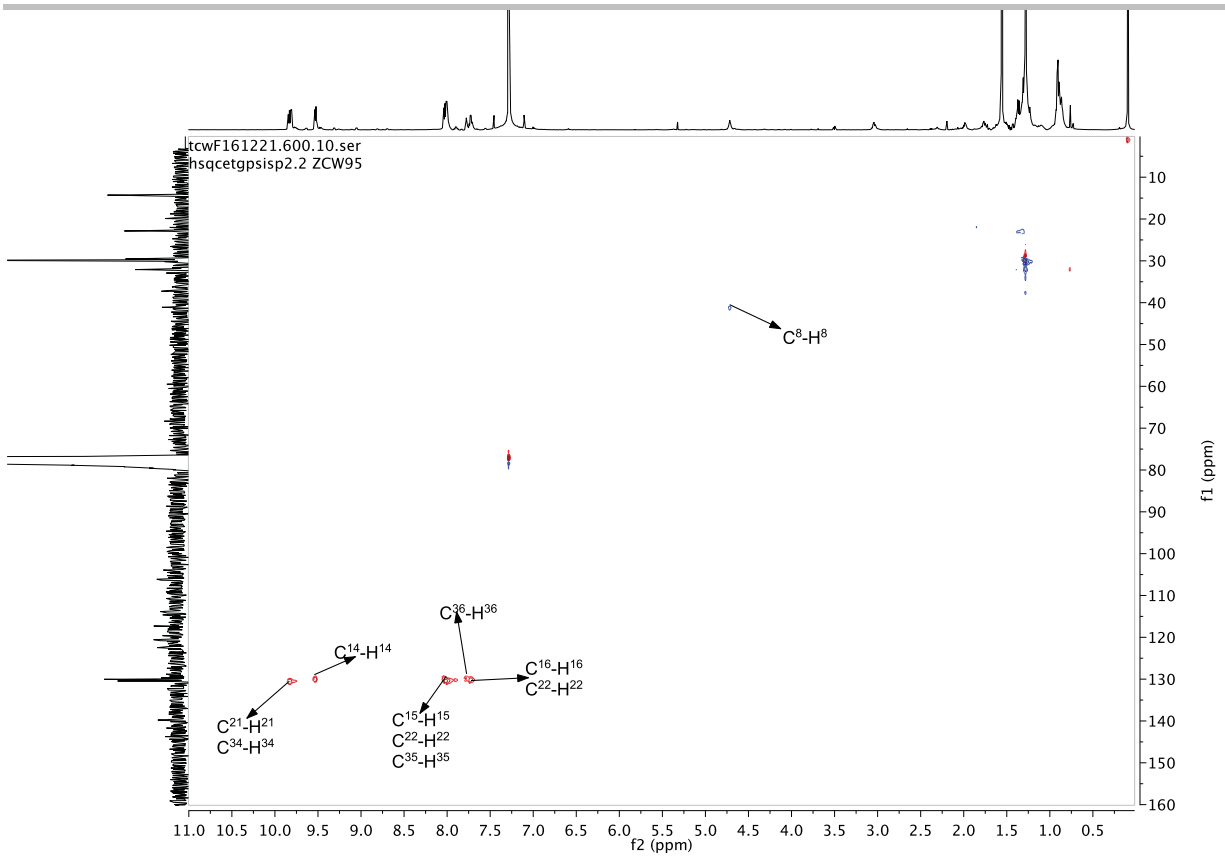
tcwF161221.600.10.ser
hsqcetgpsisp2.2 ZCW95
C8-H8
C36-H36
C14-H14
C16-H16
C22-H22
C21-H21
C34-H34
C15-H15
C22-H22
C35-H35
f2 (ppm)
f1 (ppm)

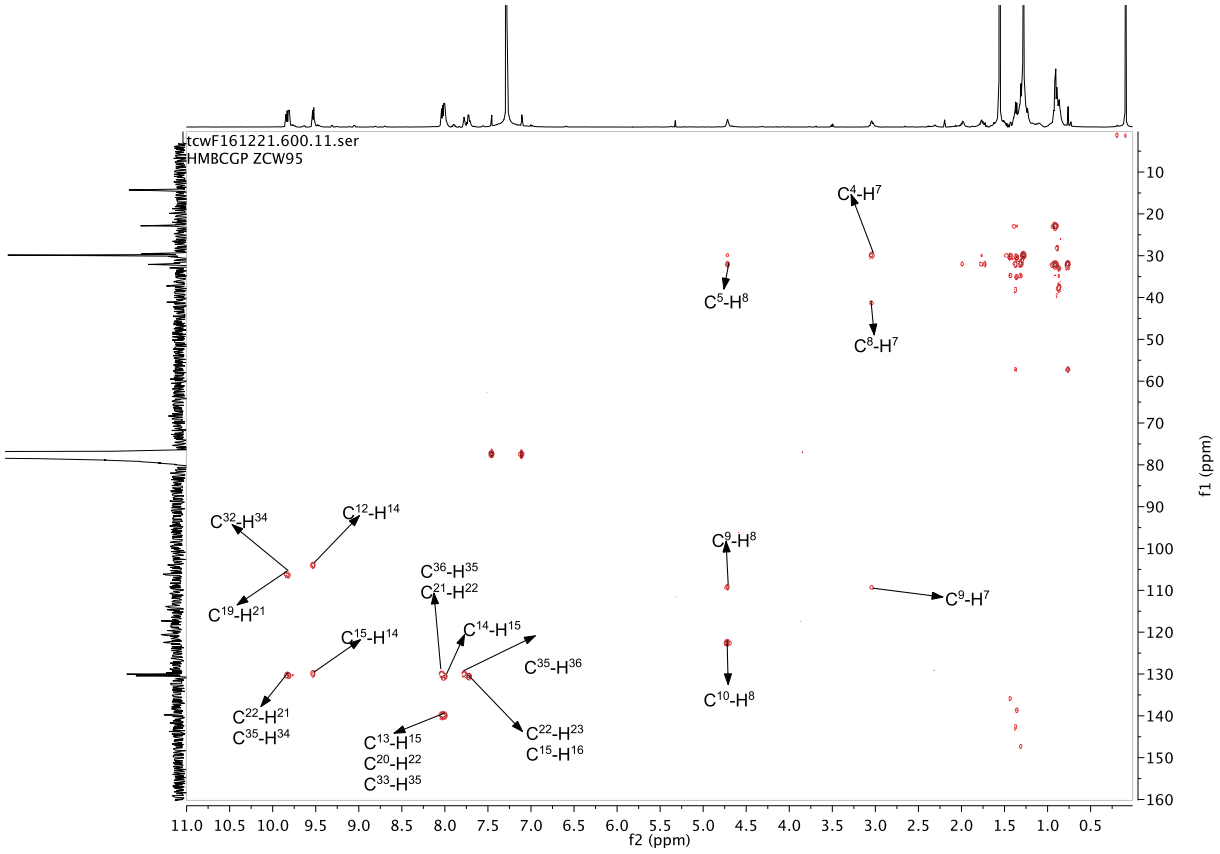
tcwF161221.600.11.ser
HMBCGP ZCW95
C4-H7
C5-H8
C8-H7
C32-H34
C12-H14
C19-H21
C36-H35
C21-H22
C14-H15
C15-H14
C35-H36
C22-H21
C35-H34
C13-H15
C20-H22
C33-H35
C22-H23
C15-H16
C9-H8
C9-H7
C10-H8
f2 (ppm)
f1 (ppm)

1D (^{1}H, ^{13}C{^{1}H}) and **2D (^{1}H - ^{13}C HSQC** and **HMBC)** NMR spectra of **3b** in $CDCl_3$

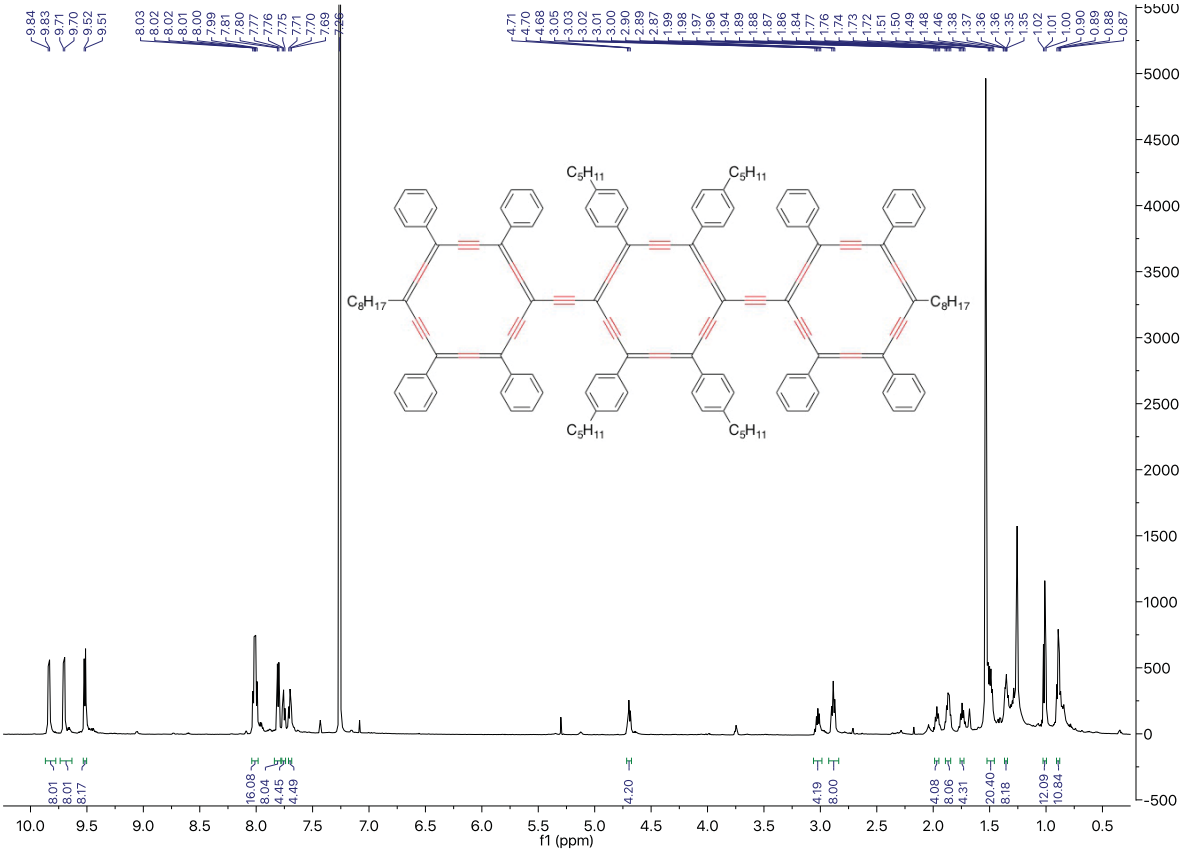

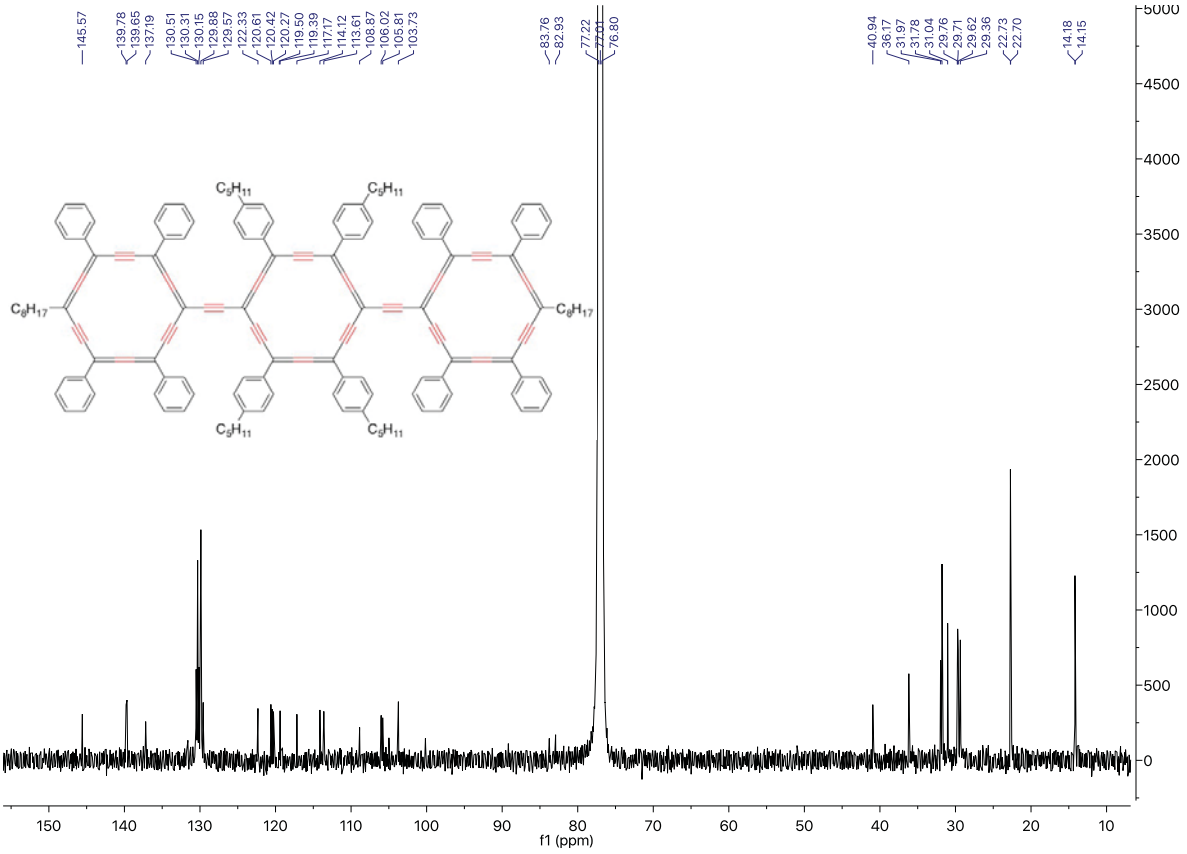

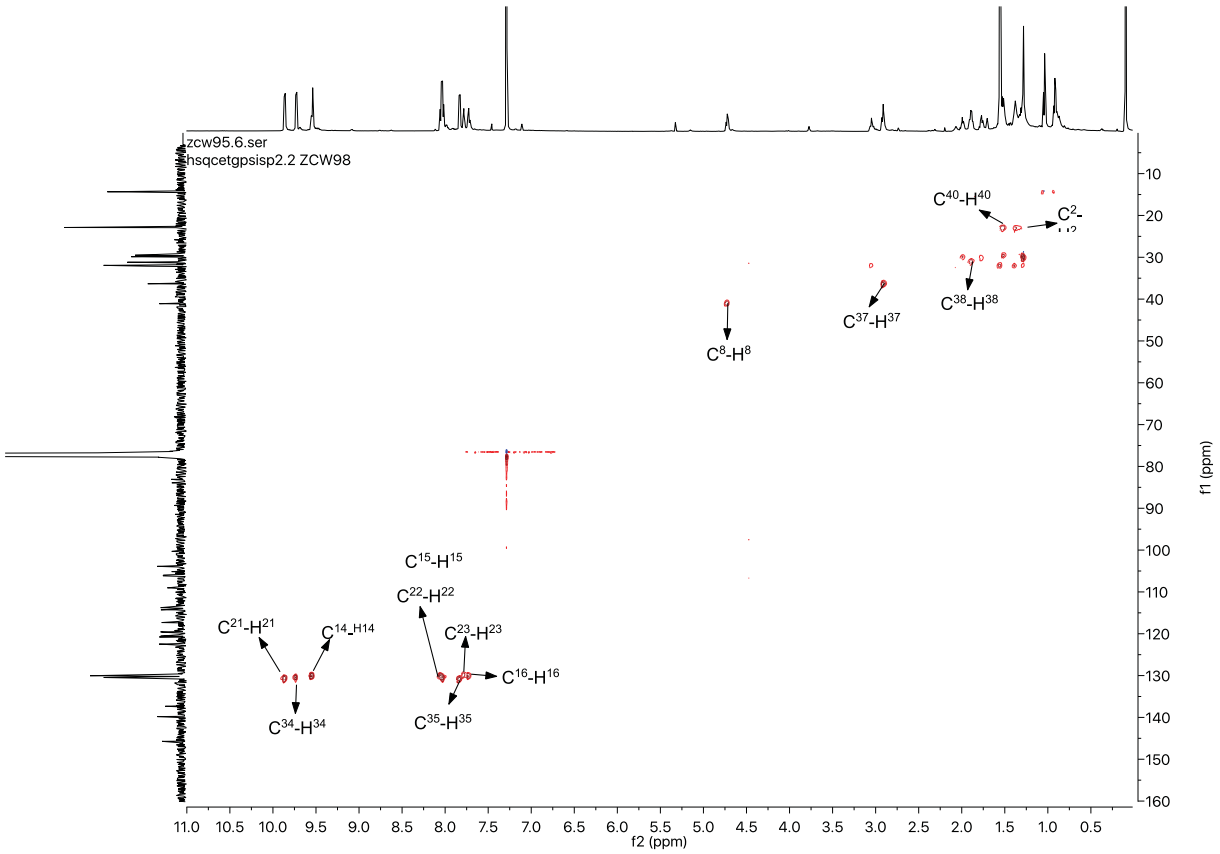
zcw95.6.ser
hsqcetgpsisp2.2 ZCW98
C40-H40
C2-
C38-H38
C37-H37
C8-H8
C15-H15
C22-H22
C21-H21
C14-H14
C23-H23
C16-H16
C34-H34
C35-H35
f1 (ppm)
f2 (ppm)

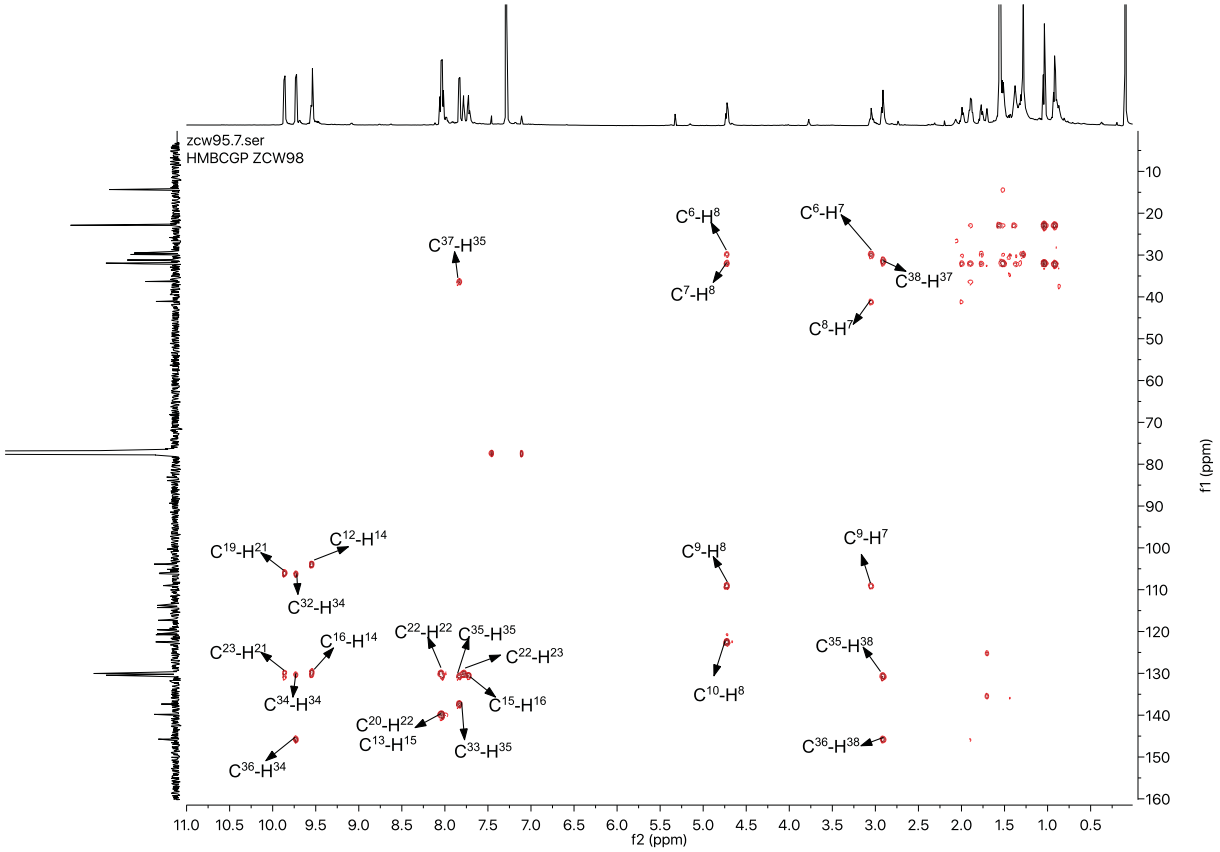
zcw95.7.ser
HMBCGP ZCW98
C37-H35
C6-H8
C6-H7
C7-H8
C38-H37
C8-H7
C19-H21
C12-H14
C32-H34
C9-H8
C9-H7
C23-H21
C16-H14
C22-H22
C35-H35
C22-H23
C34-H34
C15-H16
C10-H8
C35-H38
C20-H22
C13-H15
C33-H35
C36-H34
C36-H38
f1 (ppm)
f2 (ppm)

2. X-ray diffraction analysis

2.1. General remarks

Data collections were performed on a high flux microfocus Rigaku FRX rotating anode at the copper kα wavelength equipped with a Dectris Pilatus 200K hybrid detector at low temperature. The diffractive power of the crystals was quite low for these very small crystals. The structures were solved using SUPERFLIP, and refined by means of least-squares procedures on F using the programs of the PC version of CRYSTALS. Atomic scattering factors were taken from the international tables for X-ray crystallography. Absorption correction was performed by using a multiscan procedure.

For **3b**, all non-hydrogen atoms were refined anisotropically. For the two structures of **2** (**2**•$CHCl_3$ and **2**•$PhNO_2$), due to the weak diffraction intensities and low resolution, non-hydrogen atoms could be refined only with isotropic displacement parameters.

For the crystals of **2**•**$CHCl_3$**, phenyl rings were refined as rigid groups and it was not possible to resolve diffuse electron-density residuals (enclosed solvent molecules). Treatment with the SQUEEZE facility from PLATON resulted in a smooth refinement.[3] Hydrogen atoms were refined using a riding model. Absorption corrections were introduced using the program MULTISCAN.

2.2. Crystallographic data and refinement parameters for 2 (from $CHCl_3$ or $PhNO_2$) and 3b

Table S1. Crystallographic data for **2**•**$CHCl_3$**, **2**•**$PhNO_2$** and **3b.**

	2•**$CHCl_3$**	**2**•**$PhNO_2$**	**3b**
CCDC number	1553844	1559540	1553845
Empirical formula	C_{103} H_{75} Cl_3	$C_{108}H_{79}NO_2$	C_{168} H_{138} Cl_4
Formula moiety	$C_{102}H_{74}$, $CHCl_3$	$C_{102}H_{74}$, $C_6H_5NO_2$	$C_{166}H_{134}$, $2(CH_2Cl_2)$
Formula mass	1419.09	1422.82	229-8.59
Crystal system	Triclinic	Monoclinic	Monoclinic
Space group	P -1	P 2/n	P 2_1/c
T [K]	120	100	100
a [Å]	-8.1955(13)	10.2922(6)	30.1179(12)
b [Å]	19.272(2)	15.7255(9)	7.8989(3)
c [Å]	2-6.297(3)	24.6284(16)	2-8.8304(14)
α [°]	83.460(10)	90	90
β [°]	8-8.563(11)	93.702(5)	10-6.047(5)
γ [°]	84.463(11)	90	90
V [$Å^3$]	410-6.8(5)	3977.8(3)	6591.5(3)
D_c	1.148	1.188	1.158
Z	2	2	2
μ[mm^{-1}]	1.365	0.530	1.218
Refl. measured	14978	16633	23360
Refl. unique/R_{int}	5067 (0.148)	4211 (0.064)	6944(0.055)
Refinement on	F	F	F
Refl. with $I > n\,?(I)$	1985 (n=1.7)	2485 (n=2.7)	5092 (n=2)
Nb parameters	329	241	775
R	0.1655	0.1100	0.1021
R_w	0.1674	0.1316	0.1074
GooF	1.110	1.098	1.070
$\Delta\rho_{max}/\Delta\rho_{min}$ [$e.Å^{-3}$]	1.44/-0.65	0.51/-0.51	0.93/-0.98

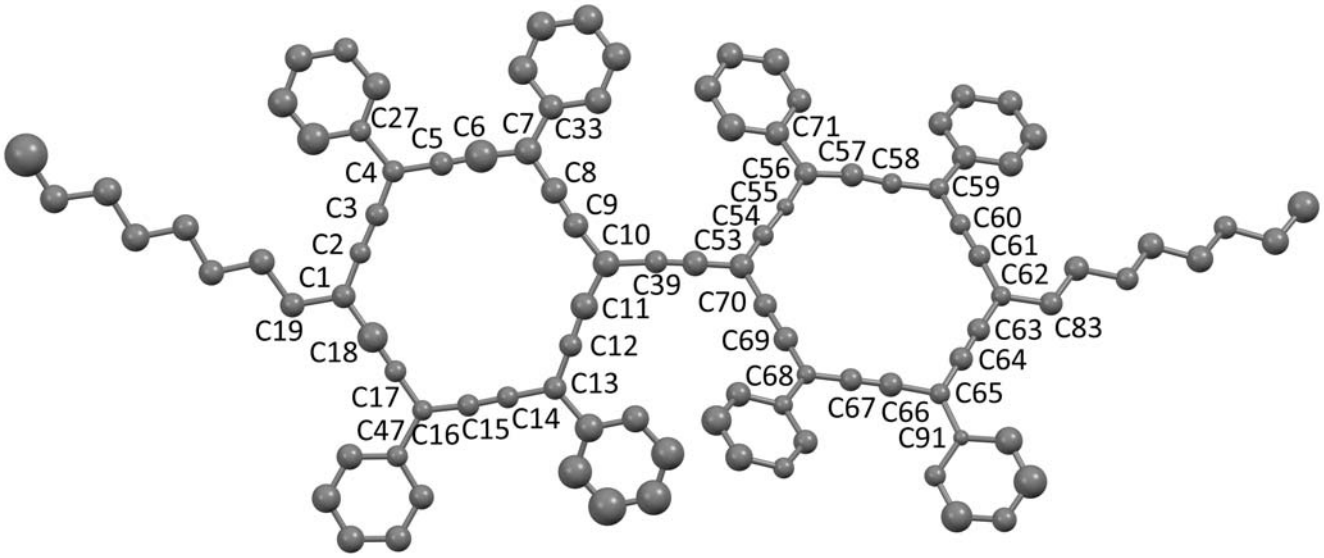

Figure S1. XRD molecular view of **2** crystallized from chloroform (**2•CHCl$_3$**); ellipsoids shown at 50 % probability.

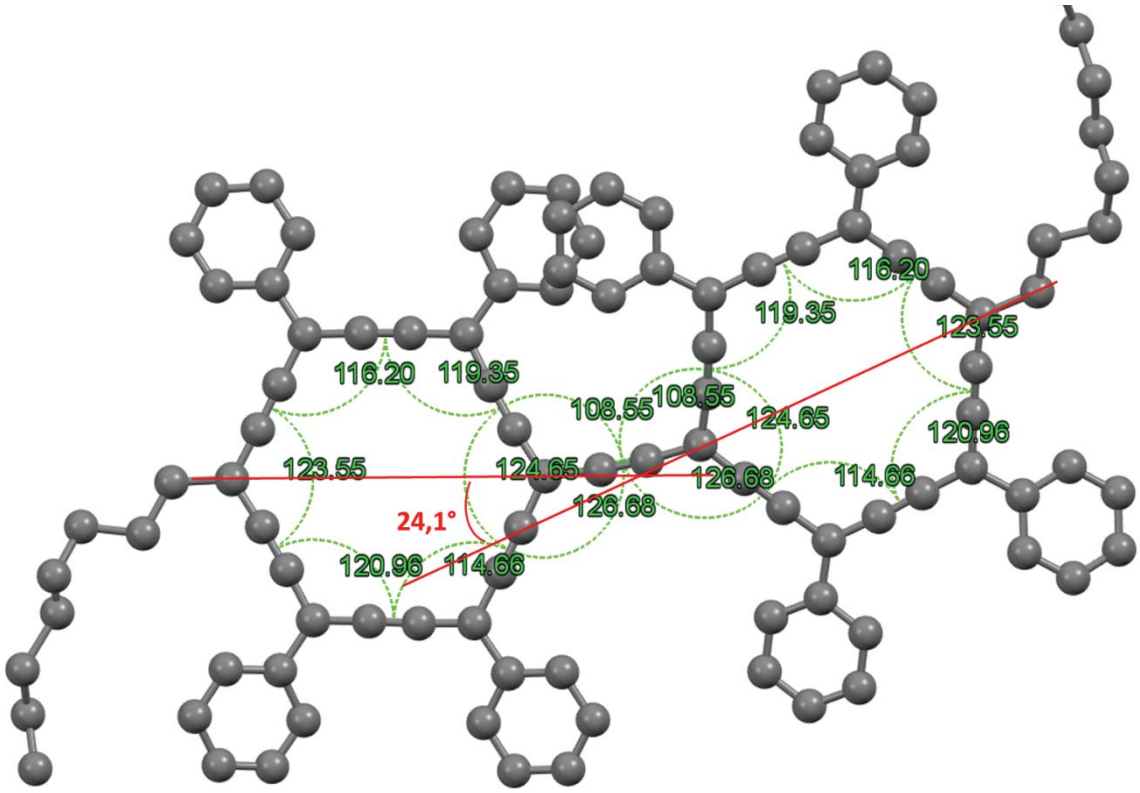

Figure S2. XRD view of **2** crystallized from nitrobenzene (**2•PhNO$_2$**) showing the bending between principal axes of the two C_{18} rings, due to the combined effects of both the non-co-planarity of the rings and non-linearity of the C-ethynylene-C link.

Table S2. Crystal data for 2 crystallized from nitrobenzene (2•$PhNO_2$)

a = 10.2922(6) Å α = 90°
b = 15.7255(9) Å β = 93.702(5)°
c = 24.6284(16) Å γ = 90°

Volume	3977.8(3) Å³	Crystal Class	monoclinic
Space group	P 1 2/n 1	Z =	2
Formula	C_{108} H_{79} N_1 O_2	M_r	1422.82
Cell determined from	3607 reflections	Cell θ range =	3 - 51°
Temperature	100K		
Shape	plate		
Colour	black red	Size	0.00 × 0.02 × 0.02 mm
D_x	1.19	F000	1500.000
μ	0.530 mm^{-1}		
Absorption correction	multi-scan		
T_{min}	0.76	T_{max}	1.00

Data Collection for 2•$PhNO_2$

Diffractometer	multi-scan
Scan type	2θ/ω scans
Reflections measured	16633
Independent reflections	4211
Rint	0.0636
θ_{max}	51.0919
h =	-10 → 9
k =	-15 → 14
l =	-24 → 24

Refinement for 2•$PhNO_2$

$\Delta\rho_{min}$ =	-0.51 e $Å^{-3}$
$\Delta\rho_{max}$ =	0.51 e $Å^{-3}$
Reflections used	2485
Cutoff: I >	2.70σ(I)
Parameters refined	241
S =	1.10
R-factor	0.110
weighted R-factor	0.132
Δ/σ_{max}	0.0002
Refinement on	F
w =	$w' \times [1 - (\Delta F_{obs} / 6 \times \Delta F_{est})^2]^2$
w′ =	$[P_0T_0'(x) + P_1T_1'(x) + ...P_{n-1}T_{n-1}'(x)]^{-1}$, where P_i are the coefficients of a Chebychev series in $t_i(x)$, and $x = F_{calc}/F_{calcmax}$.
P_0 - P_{n-1} =	24.6 2-6.3 21.6 7.46

Table S3. Crystal data for 2 crystallized from chloroform (2•$CHCl_3$).

a = -8.1955(13) Å α = 83.460(10)°

b = 19.272(2) Å β = 8-8.563(11)°

c = 2-6.297(3) Å γ = 84.463(11)°

Volume	410-6.8(5) Å³	Crystal Class	triclinic
Space group	P -1	Z =	2
Formula	C_{103} H_{75} Cl_3	M_r	1419.09
Cell determined from	1531 reflections	Cell θ range =	2 - 40°
Temperature	120K		
Shape	block		
Colour	red	Size	0.02 × 0.02 × 0.10 mm
D_x	1.15	F000	148-8.000
μ	1.365 mm^{-1}		
Absorption correction	multi-scan		
T_{min}	0.85	T_{max}	0.97

Data Collection for 2•$CHCl_3$

Diffractometer	multi-scan
Scan type	2θ/ω scans
Reflections measured	14978
Independent reflections	5067
Rint	0.1476
θ_{max}	40.7733
h =	-6 → 6
k =	-15 → 16
l =	0 → 22

Refinement for 2•$CHCl_3$

$\Delta\rho_{min}$ =	-0.65 e $Å^{-3}$
$\Delta\rho_{max}$ =	1.44 e $Å^{-3}$
Reflections used	1985
Cutoff: I >	1.70σ(I)
Parameters refined	329
S =	1.11
R-factor	0.165
weighted R-factor	0.167
Δ/σ_{max}	0.0000
Refinement on	F
w =	$w' \times [1 - (\Delta F_{obs} / 6 \times \Delta F_{est})^2]^2$
w′ =	$[P_0T_0'(x) + P_1T_1'(x) + ...P_{n-1}T_{n-1}'(x)]^{-1}$, where P_i are the coefficients of a Chebychev series in $t_i(x)$, and $x = F_{calc}/F_{calcmax}$.
P_0 - P_{n-1} =	5.47 4.86 4.34 0.994

Table S4. Crystal data for 3b

a = 30.1179(12) Å α = 90°

b = 7.8989(3) Å β = 10-6.047(5)°

c = 2-8.8304(14) Å γ = 90°

Volume	6591.5(3) Å³	Crystal Class	monoclinic
Space group	P 1 2_1/c 1	Z =	2
Formula	C_{168} H_{138} Cl_4	M_r	229-8.75
Cell determined from	6075 reflections	Cell θ range =	3 - 51°
Temperature	100K		
Shape	needle		
Colour	dark violet	Size	0.05 × 0.07 × 0.20 mm
D_x	1.16	F000	242-8.000
μ	1.218 mm^{-1}		
Absorption correction	multi-scan		
T_{min}	0.55	T_{max}	0.94

Data Collection for 3b

Diffractometer	multi-scan
Scan type	2θ/ω scans
Reflections measured	23360
Independent reflections	6944
Rint	0.0549
θ_{max}	51.1798
h =	-30 → 25
k =	-7 → 7
l =	-28 → 26

Refinement for 3b

$\Delta\rho_{min}$ =	-0.98 e $Å^{-3}$
$\Delta\rho_{max}$ =	0.93 e $Å^{-3}$
Reflections used	5092
Cutoff: I >	2.00σ(I)
Parameters refined	775
S =	1.07
R-factor	0.102
weighted R-factor	0.107
Δ/σ_{max}	0.0003
Refinement on	F
w =	$w' \times [1 - (\Delta F_{obs} / 6 \times \Delta F_{est})^2]^2$
w′ =	$[P_0T_0'(x) + P_1T_1'(x) + ...P_{n-1}T_{n-1}'(x)]^{-1}$, where P_i are the coefficients of a Chebychev series in $t_i(x)$, and $x = F_{calc}/F_{calcmax}$.
P_0 - P_{n-1} =	13.5 13.2 11.9 3.76

3. Electrochemical data

Voltammetric measurements were carried out with a potentiostat Autolab PGSTAT100. Experiments were performed at room temperature in a homemade airtight three–electrode cell connected to a vacuum/argon line. The reference electrode consisted of a saturated calomel electrode (SCE) separated from the solution by a bridge compartment. The counter electrode was a platinum wire of ca 1 cm² apparent surface. The working electrode was a Pt microdisk (0.5 mm diameter). The supporting electrolyte [^{n}Bu$_4$N][PF$_6$] (Fluka, 99% puriss electrochemical grade) was used as received and simply degassed under argon. HPLC grade chloroform was used. The solutions used during the electrochemical studies were typically 10^{-3} M in compound and 0,1 M in supporting electrolyte. Before each measurement, the solutions were degassed by bubbling Ar and the working electrode was polished with a polishing machine (Presi P230).

Compounds **3a** and **3b** being very poorly soluble in chloroform and more soluble in DCM, a small amount of these *carbo*-OPEs was dissolved in few drops of DCM and deposited on the platinum working electrode by dipping. The covered electrode was then immersed in a chloroform solution of the supporting electrolyte just before running the measurement.

SW voltammograms for 1:

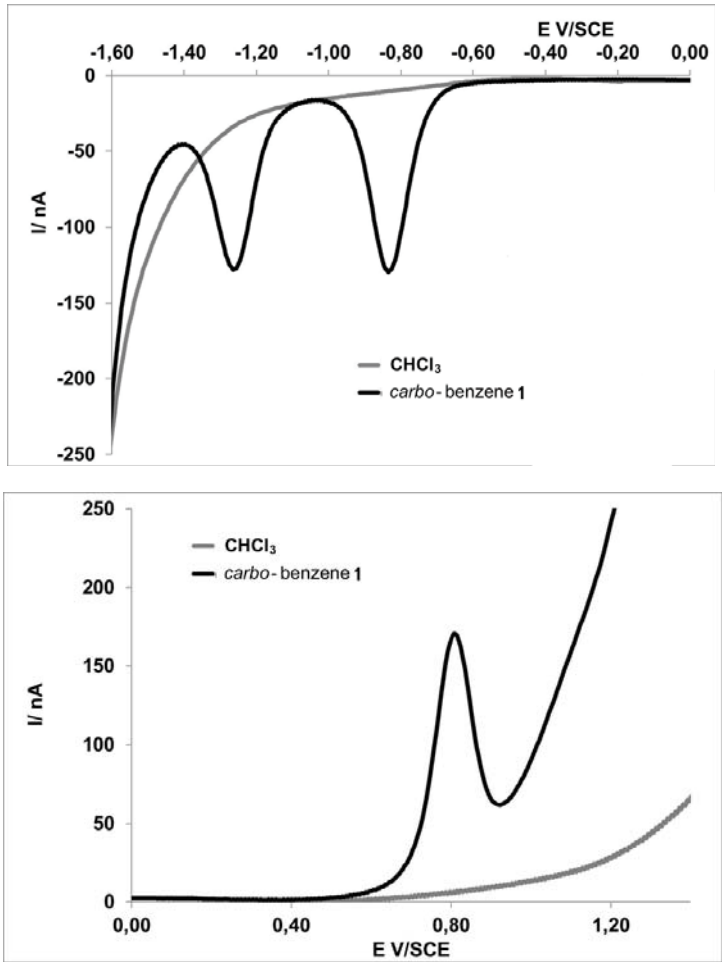

Cyclic voltammogram for 1:

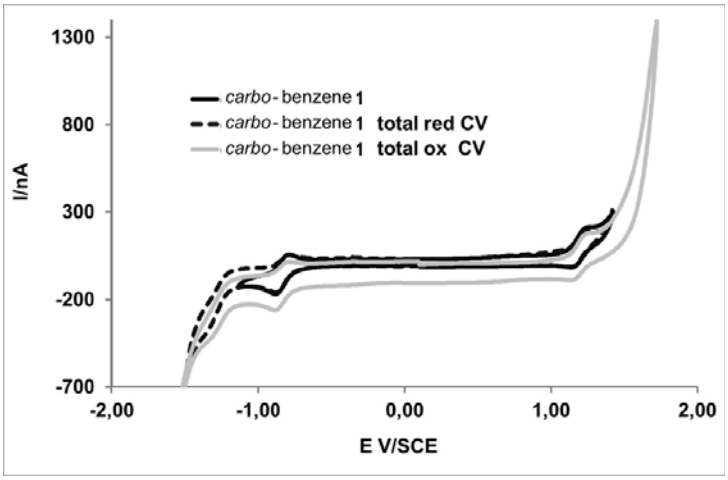

SWV voltammograms for 2:

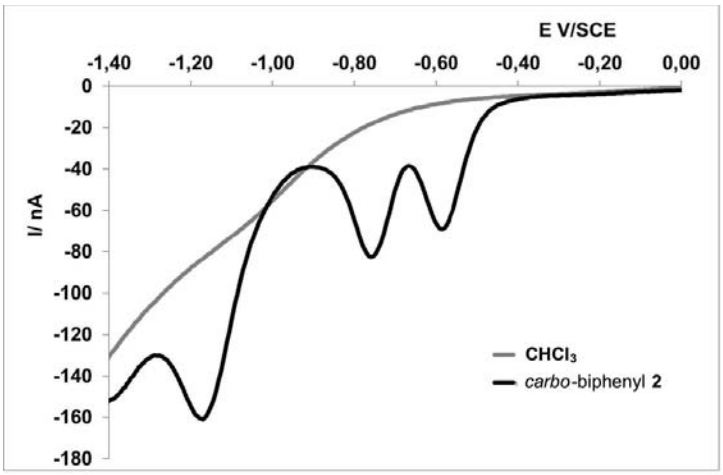

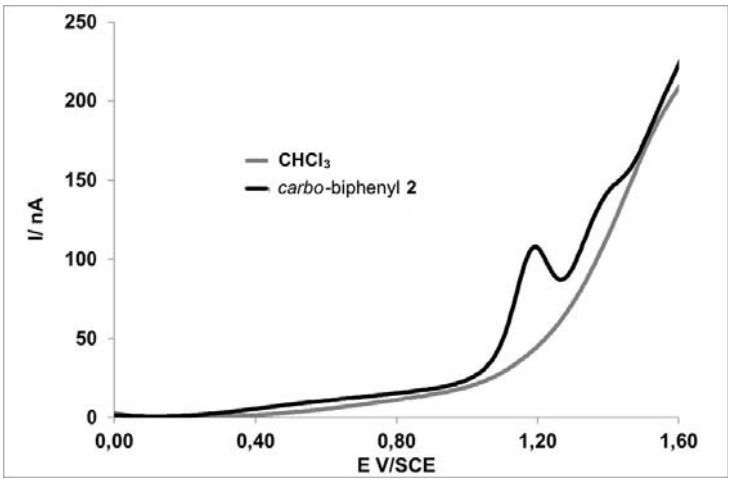

Cyclic voltammogram for 2:

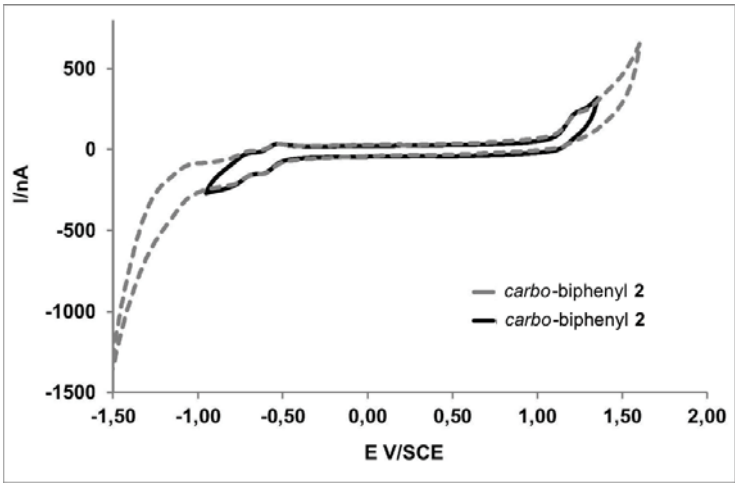

SWV voltammograms for 3a:

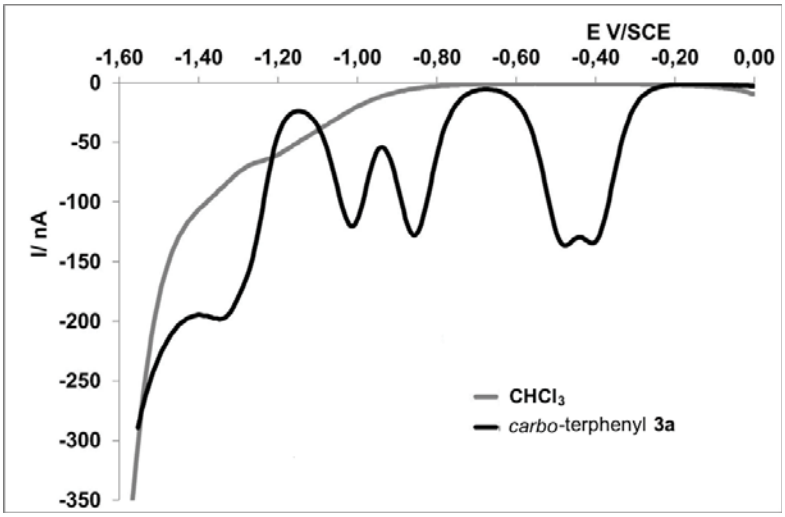

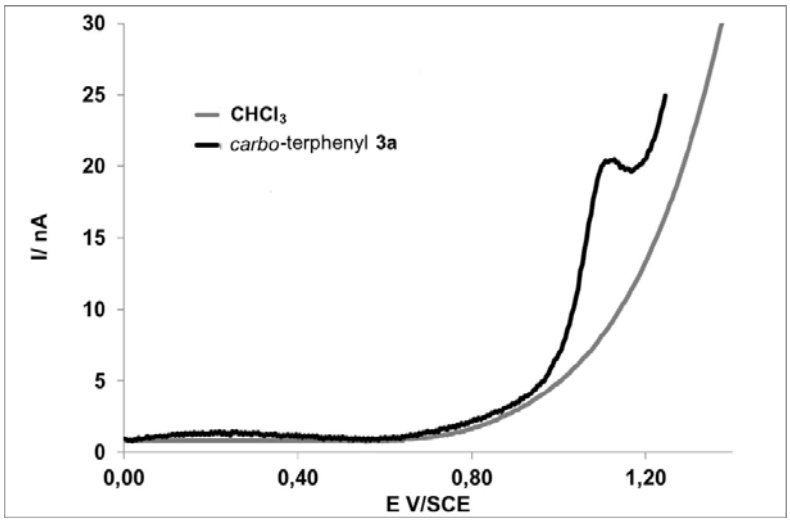

CV voltammograms for 3a:

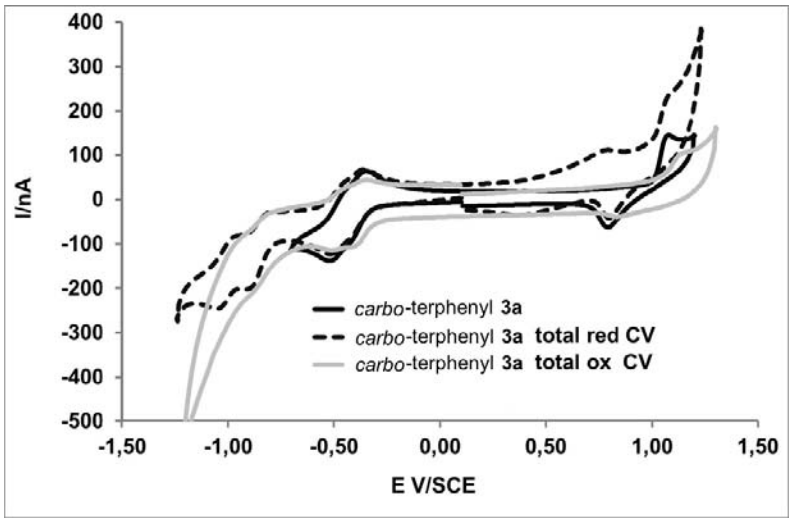

SWV voltammograms for 3b:

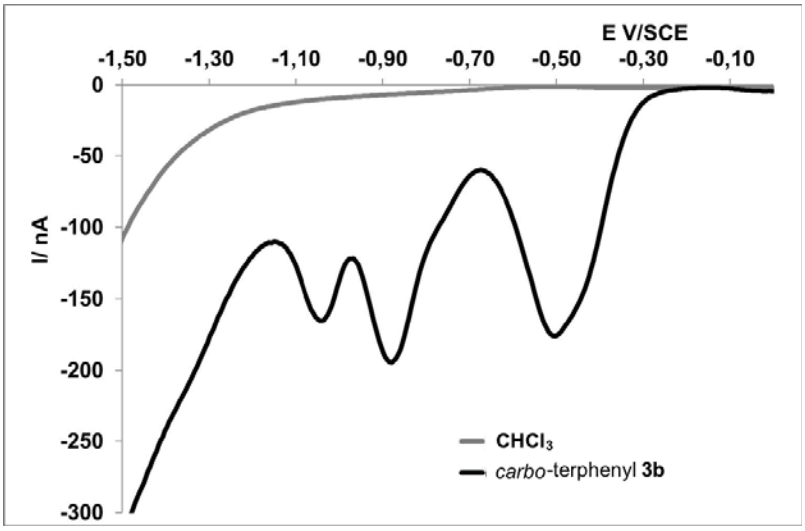

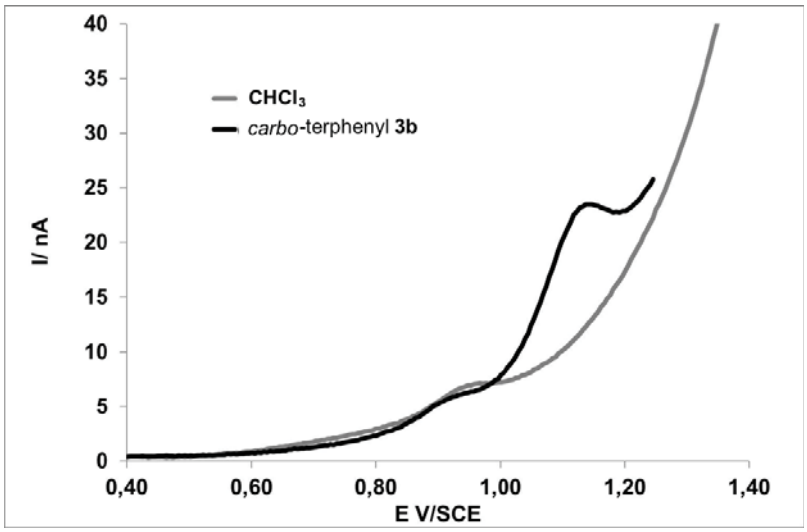

4. DFT-computational studies and theoretical analyses

4.1. Computational details

All the DFT static calculations have been performed at the GGA level with the Gaussian09 set of programs,[4] using the B3PW91 functional of Becke, Perdew and Wang.[5] The electronic configuration of the molecular systems was described with the 6-31G(d,p) basis set for H, C, and O (6-31G** keyword in Gaussian) during geometry optimizations performed without symmetry constraint.[6] The isolated stationary points were characterized by analytical frequency calculations. All NICS and UV-vis absorption or emission calculations were calculated with the same 6-31G(d,p) basis set.

Time dependent density functional theory (TDDFT) calculations were focused on singlet excited states. Both the DFT and TDDFT geometry optimization of the singlet ground state and singlet first excited state were performed without symmetry constraints, in vacuum for the DFT ground state. Solvent effects, based on the polarizable continuum solvation model PCM using dichloromethane as a solvent, were taken into account in the TDDFT calculation of UV-vis absorption or emission spectra.[7] The atomic contribution of single atoms to the molecular orbitals was performed in the framework of the Mulliken population analysis.

Bearing on conceptual DFT,[8] the chemical potential μ for a *N*-electron system of total electronic energy *E* is defined as the first derivative of *E vs N* at a fixed external (nuclear) potential *v*: $\mu = (\partial E/\partial N)_v$; it is identified to the negative of electronegativity χ ($\mu = -\chi$). The molecular hardness η is defined as the corresponding second derivative: [9] $\eta = (\partial^2 E/\partial N^2)_v$ (on the basis of the Taylor expansion of *E vs n*, a factor 1/2 was originally proposed in the alternative definition $\eta' = 1/2\ (\partial^2 E/\partial N^2)_v$).[10] In numerical applications, μ (the Fermi level) and η (the HOMO-LUMO gap) are calculated by finite difference formulas, which, at the first order, are equivalent to the Koopmans' approximation for ionization potential and electron affinity:[11]

$$\mu \equiv \left(\frac{\partial E}{\partial N}\right)_v \cong \frac{1}{2}(\varepsilon_L + \varepsilon_H), \qquad \eta \equiv \left(\frac{\partial^2 E}{\partial N^2}\right)_v \cong \varepsilon_L - \varepsilon_H$$

where ε_H and ε_L denote the energies of the highest occupied molecular orbital (HOMO) and lowest unoccupied molecular orbital (LUMO), respectively.

Electrophilicity ω is the ratio of the chemical potential squared to twice the hardness; a principle of electrophilicity equalization of the constituting atoms within a molecule has been proposed:[12]

$$\omega = \frac{\mu^2}{2\eta}$$

4.2. Chemical potential, hardness and electrophilicity (Table S5)

Table S5. HOMO, LUMO and corresponding electronic indices in the Koopmans' approximation.

Energies in a.u.	HOMO ε_H	LUMO ε_L	chemical potential μ	chemical hardness η	electrophilicity ω
Unsubstituted *carbo*-benzene **$C_{18}H_6$**	-0.21411	-0.10637	-0.1602	0.1077	0.1192
1	-0.19017	-0.10562	-0.1479	0.0846	0.1294
2	-0.18878	-0.11666	-0.1527	0.0721	0.1617
3a	-0.18701	-0.12429	-0.1557	0.0627	0.1931
3b'	-0.18467	-0.12199	-0.1533	0.0627	0.1875
14	-0.18642	-0.12835	-0.1574	0.0581	0.2133
[6]pericyclynedione **4**	-0.25109	-0.09387	-0.1725	0.1572	0.0946

As outlined in the main text, data listed in Table S5 show that the chemical hardness, or HOMO-LUMO gap, decreases very regularly with *n* ($\eta \approx 0.102 - 0.019\ n + 0.002\ n^2$, $R = 1.000$).

The electrophilicity is found to be mainly determined by the LUMO energy ($\omega \approx -0.261 - 3.67\ \varepsilon_L$, $R = 0.994$), i.e. the electron affinity as measured by the first reduction potential $E_{1/2}^{red1}$ (which is indeed shown to vary linearly with *n*: see main text). Electrophilicity also varies in the opposite sense of electronegativity: the decrease of electronegativity *vs n* can be interpreted as a decrease of the *global* aromaticity, while the local aromaticity of the C_{18} rings, as quantified by NICS(0) values, remains the same over the series (see below).

As expeccted, the pericyclynedione **4** with restricted π-conjugation appears highly electrophilic and hard.

4.3. Nucleus-independent chemical shifts (NICS)

The aromaticity of the C_{18} cores and C_6 rings of **1**, **2**, **3a**-**b'** and **14** were evaluated by the corresponding NICS(0)/NICS(±1) values (section 4.1, Table S6) and compared with the bare *carbo*-benzene reference ($C_{18}H_6$).

Table S6. Calculated NICS values (in ppm) for the C_{18} and C_6 rings of the *carbo*-OPEs **1**, **2**, **3a**-**b'**, **14** and the unsubstituted reference $C_{18}H_6$, at the B3PW91-6-31G(d,p) level (GIAO formalism).

rings	**1**		**2**		**3a**		**3b'**		**14**		**unsubstituted *carbo*-benzene** ($C_{18}H_6$)	
	NICS(0)	NICS(±1)	NICS(0)	NICS(±1)	NICS(0)	NICS(±1)	NICS(0)	NICS(±1)	NICS(0)	NICS(±1)	NICS(0)	NICS(±1)
C_{18}	-14.9	-13.6 -13.6	-13.7	-12.5 -12.5	-13.6	-12.4 -12.4	-13.7	-12.5 -12.5	-13.6	-12.4 -12.4	-1-8.3	-1-6.8 -1-6.8
C_{18}			-13.7	-12.5 -12.5	-12.5	-11.4 -11.4	-12.4	-11.3 -11.3	-12.4	-11.3 -11.3		
C_{18}						-12.4 -12.4	-13.7	-12.5 -12.5	-12.4	-11.3 -11.3		
C_{18}									-13.6	-12.4 -12.4		
C_6	-6.4	-8.5 -8.7	-6.5	-8.5 -8.7	-6.5	-8.7 -8.5	-6.4	-8.7 -8.5	-6.5	-8.7 -8.5		
C_6	-6.4	-8.7 -8.5	-5.9	-8.4 -8.0	-5.9	-7.9 -8.4	-6.7	-8.9 -8.6	-5.9	-7.9 -8.4		
C_6	-6.6	-8.7 -8.8	-6.7	-8.9 -8.7	-6.7	-8.7 -8.9	-5.9	-7.9 -8.4	-6.0	-8.3 -8.2		
C_6	-6.6	-8.8 -8.7	-6.0	-8.3 -8.2	-6.0	-8.3 -8.2	-6.0	-8.3 -8.2	-6.7	-8.9 -8.7		
C_6			-6.0	-8.3 -8.2	-6.0	-8.0 -8.4	-5.8	-8.2 7.9	-6.0	-8.4 -8.0		
C_6			-6.7	-8.9 -8.7	-6.0	-8.0 -8.4	-6.0	-8.2 -8.1	-6.1	-8.3 -8.2		
C_6			-6.5	-8.7 -8.5	-6.1	-8.3 -8.3			-5.9	-8.4 -8.0		
C_6			-5.9	-8.0 -8.4	-6.1	-8.3 -8.3			-6.1	-8.3 -8.3		
C_6					-6.0	-8.3 -8.2			-6.1	-8.3 -8.3		
C_6					-6.7	-8.9 -8.7			5.9	-8.4 -8.0		
C_6					5.9	-8.4 -7.9			-6.0	-8.5 -8.0		
C_6					-6.5	-8.7 -8.5			-6.1	-8.3 -8.3		
C_6									-5.9	-8.4 -7.9		
C_6									-6.0	-8.2 -8.3		
C_6									-6.4	-8.7 -8.5		
C_6									-6.4	-8.7 -8.5		

As previously observed,[13] substitution of the "bare *carbo*-benzene" $C_{18}H_6$ results in an increase of the NICS(0) value, albeit much weaker by alkyl groups than by phenyl group: +0.15 ppm per ^{t}Bu or ^{i}Pr group *vs* +0.77 ppm per Ph group (+0.03 ppm per F atom), at the B3PW91/6-31+G (d,p) level. Assuming the same coefficient for ^{n}Oct groups, the predicted value for **1** would be –14.7 pm, so very close to the calculated value of –14.9 ppm at the B3PW91/6-31G (d,p) level.

Upon increasing the number of C_{18} units in the *carbo*-OPE*n* from *n* = 2 to *n* = 4, the external rings exhibit lower NICS values (*ca* –13.7/–12.5 ppm) than the central rings (*ca* –12.4/–11.4 ppm). The phenyl substituents display similar values whatever the*n* value, but are slightly more deshielded (at *ca* –6.0 ppm) in external position (in γ position from the *n*-octyl chains) than in internal positions (at *ca* –6.5 ppm).

For comparison, the NICS(0)/NICS(±1) values of the unsubstituted OPE parents were also calculated. As in the *carbo*-OPE series, the external rings exhibit lower NICS values (≤ –9.0/–10.7 ppm) than the central rings (*ca* –8.3/–10.1 ppm).

Perfluorination of the OPE parents was also considered. As previously observed, fluorination of the benzene ring results in a dramatic decrease of the NICS(0) value (down to –17 ppm), along with a negligible decrease of NICS(1) value due to a decrease of the paratropic ring current in the sigma system induced by the electron-withdrawing effect of the fluorine atoms (Table S7).[13b,14] Although the NICS value increases again quickly upon further partial defluorination, for *n* ≥ 2, the external rings exhibit lower NICS values (≤ –15.2/–11.0 ppm) than the central rings (*ca* –13.5/–10.3 ppm).

Table S7. Calculated NICS values (in ppm) for the C_6 rings of unsubstituted OPEn, Ph–[C≡C-4-C_6H_4]$_n$–H, and perfluorinated F_{6+4n}-OPEn, C_6F_5–[C≡C-4-C_6F_4]$_n$–F, n = 0-3, at the B3PW91-6-31G(d,p) level (GIAO formalism).

	OPE0 benzene		**OPE1 biphenyl**		**OPE2 terphenyl**		**OPE3 quaterphenyl**		**F_6-OPE0**		**F_{10}-OPE1**		**F_{14}-OPE2**		**F_{18}-OPE3**	
	NICS(0)	NICS!1)	NICS(0)	NICS(1)	NICS(0)	NICS(1)	NICS(0)	NICS(1)	NICS(0)	NICS(1)	NICS(0)	NICS(1)	NICS(0)	NICS(1)	NICS(0)	NICS(1)
C_6	-9.8	-11.4	-9.1	-10.8	-9.0	-10.7	-9.0	-4.5	-17.1	-11.9	-15.3	-11.0	-15.2	-11.0	-15.2	-11.0
		-11.4		-10.8		-10.7		-4.5		-11.9		-11.0		-11.0		-11.0
C_6			-9.1	-10.8	-8.4	-10.1	-8.3	-4.2			-15.3	-11.0	-13.5	-10.3	-13.4	-10.3
				-10.8		-10.1		-4.2				-11.0		-10.3		-10.3
C_6					-9.0	-10.7	-8.3	-4.2					-15.2	-11.0	-13.4	-10.3
						-10.7		-4.2						-11.0		-10.3
C_6							-9.0	-4.5							-15.2	-11.0
								-4.5								-11.0

4.4. Excited states and UV-vis absorption/emission spectra

Data for the first fifty excited states of the *carbo*-OPEn **1**, **2**, **3a**, **3b'**, **14**, and [6]pericyclynedione **4** are detailed in section 4.8. As a general trend both the absorption and emission wavelengths of maximum oscillator strength *f,* and the corresponding *f* values themselves, increase with *n* (Table S8).

Table S8. TDDFT-calculated absorption and emission spectra of **1**-**4**, **14** (B3PW91/6-31G(g,p)). See section 4.8.

• Overall spectral data:

	1		**2**		**3a**		**3b'**		**14**		***carbo*-benzene $C_{18}H_6$**		**[6]pericyclynedione 4**	
	λ (nm)	*f*	λ (nm)	*f*	λ (nm)	*f*	λ (nm)	*f*	λ (nm)	*f*	λ (nm)	*f*	λ (nm)	*f*
Absorption	606.9	0.3	734.3	0.8	858.5	2.0	858.6	2.0	937.4	3.0	356.5	1.7	256.9	0.2
	465.7	2.8	602.6	0.5	627.2	0.4	634.2	0.4	621.5	0.2	356.5	1.7		
	446.6	1.3	579.9	2.4	596.2	0.7	598.6	2.3	587.1	4.8				
			463.6	3.5	593.3	0.7	587.5	0.3	522.6	0.3				
					580.8	1.0	549.3	0.8						
					546.9	0.9	533.1	0.6						
					461.2	3.4	462.8	3.2						
Emission	638.1	0.5	887.9	1.7	1049.2	2.9	1045.8	2.8	1093.8	3.7	393.0	2.0	273.0	0.2
	520.1	3.2	648.0	1.5	702.7	0.2	888.9	0.2	639.8	1.1	393.0	2.0		
	484.8	1.4	591.4	2.3	670.1	1.0	704.9	0.3	602.7	1.0				
			488.9	3.3	612.9	0.4	672.8	0.9	584.0	3.0				
					590.9	1.7	602.6	2.4	551,7	0.5				
					570.0	0.8	574.5	0.9	549.8	0.6				
					550.3	1.4	552.0	1.5	522.1	0.4				
					507.5	0.9	513.6	0.6	…	…				
					478.2	0.8	506.8	0.5						
					473.7	1.1	476.0	2.1						

• Main one-electron transition contributions for excited states of highest oscillator strength:

	Absorption			Emission		
	λ_{abs} (nm)	*f* (osc. str.)	One-electron transitions (weight 40% or higher)	λ_{em} (nm)	*f* (osc. str.)	One-electron transitions (weight 40% or higher)
$C_{18}H_6$	356.5	1.7	H→L & H-1→L+1	393.0	2.0	H→L & H-1→L+1
	356.5	1.7	H→L+1 & H-1→L	393.0	2.0	H→L+1 & H-1→L
1	606.9	0.3	H→L	638.1	0.5	H→L
	465.7	2.8	H→L+1 & H-1→L	520.1	3.2	H→L+1 & H-1→L
	446.6	1.3	H→L & H-1→L+1	484.8	1.4	H→L & H-1→L+1
2	734.3	0.8	H→L	887.9	1.7	H→L
	579.9	2.4	H-2→L+2 & H-1→L+1	648.0	1.5	H-1→L & H→L+1
	463.6	3.5	H-3→L+ & H-2→L+3	591.4	2.3	H-3→L+2 & H-2→L+2
				488.9	3.3	H-1→L+1 & H-2→L+3
3a	858.5	2.0	H→L	1049.2	2.9	H→L
	580.8	3.4	H→L+5	590.9	1.7	H-3→L+4
	461.2	3.4	H-5→L+2	550.3	1.4	H-4→L+2
				473.7	1.1	H-5→L+3
3b'	858.6	2.0	H→L	1045.8	2.8	H→L
	598.6	2.3	H-1→L+4	602.6	2.4	H-1→L+4
	462.8	3.2	H-5→L+1	552.0	1.5	H-4→L+2
				476.0	2.1	H-5→L+4
14	937.4	3.0	H→L	1093.8	3.7	H→L
	587.1	4.8	H-5→L+2	584.0	3.0	H-5→L+2
4	256.9	0.2	H-15→L+1	273.0	0.2	H-15→L+1

The claimed correlation between the wavelengths of the experimental three main bands and those calculated for the three highest oscillator strengths (Table 2 in the main text) is shown in Figure S3A. Figure S3B displays the correlation between the observed most bathochromic wavelength of each compound and the reciprocal of the corresponding HOMO-LUMO gap.

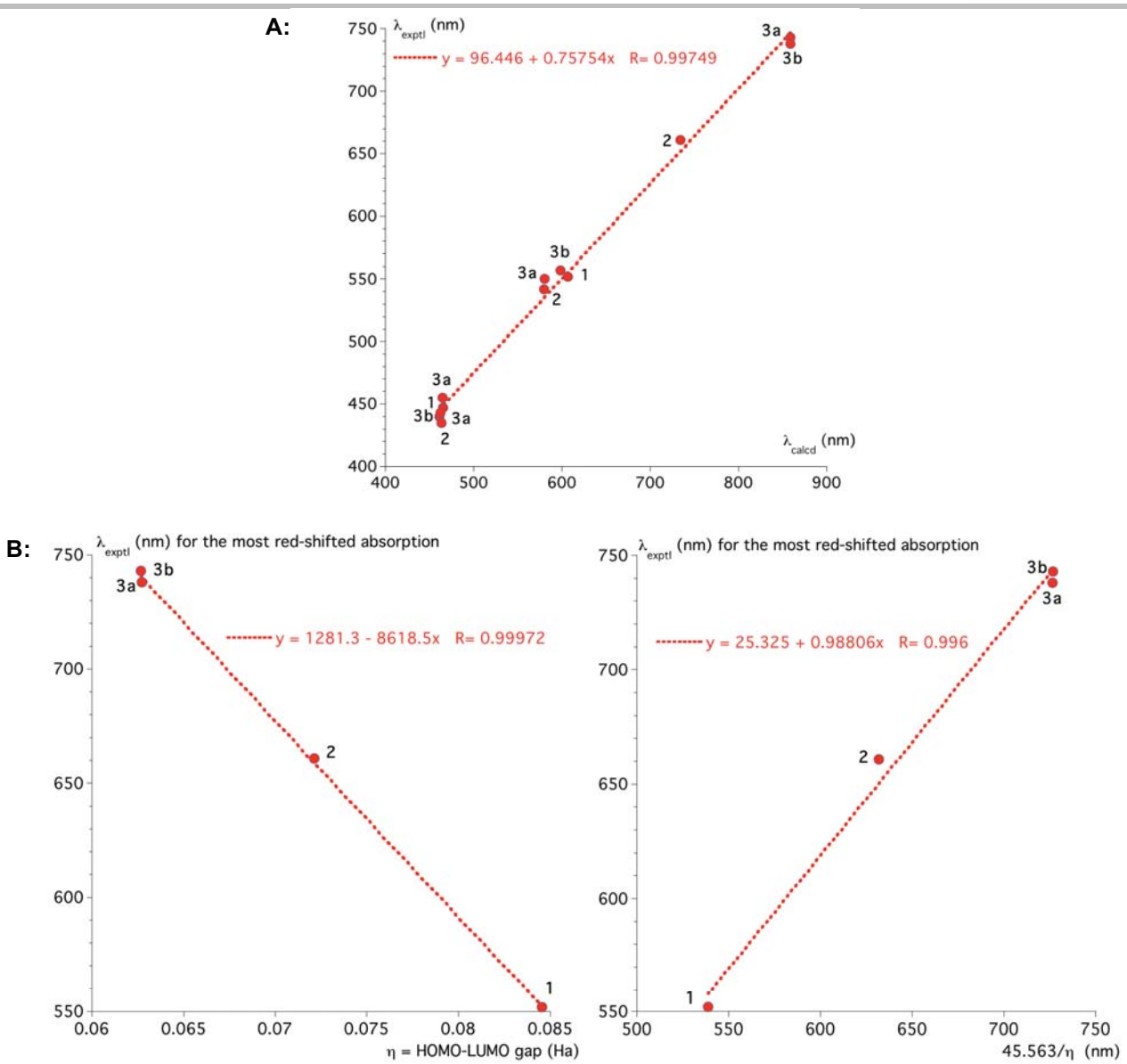

Figure S3. Correlations between **A:** the wavelengths of the experimental three main bands and those calculated for the three highest oscillator strengths (*top*), and **B:** the observed most bathochromic wavelength of each compound and the molecular HOMO-LUMO gap η in Ha (*bottom left*) or the reciprocal of η in nm (*bottom right*).

4.5. Near-frontier molecular orbitals (NFOs)

- **Eigenvalues of ground state NFOs of equilibrium structures** (Table S9)

Table S9. Eigenvalues of NFOs for the bare *carbo*-benzene, **1**-**4** and **14**, in a. u. (B3PW91/6-31G(g,p) level).

	D_{6h} **$C_{18}H_6$**	**1**	**2**	**3a**	**3b'**	**14**	**4**
L+4	0.01036	-0.00831	-0.06569	-0.10874	-0.10617	-0.11051	-0.02950
L+3	-0.01127	-0.01304	-0.09617	-0.10967	-0.10755	-0.11122	-0.03212
L+2	-0.03599	-0.05563	-0.10853	-0.10981	-0.10893	-0.11126	-0.03672
L+1	-0.10637	-0.09700	-0.10855	-0.11030	-0.10905	-0.11731	-0.08949
L	-0.10637	-0.10562	-0.11666	-0.12429	-0.12199	-0.12835	-0.09387
H	-0.21411	-0.19017	-0.18878	-0.18701	-0.18467	-0.18642	-0.25109
H-1	-0.21411	-0.19568	-0.19345	-0.19453	-0.18961	-0.19440	-0.25159
H-2	-0.27533	-0.23008	-0.19355	-0.19460	-0.19383	-0.19515	-0.26045
H-3	-0.28147	-0.25754	-0.20803	-0.19542	-0.19388	-0.19526	-0.26066
H-4	-0.28147	-0.25780	-0.22839	-0.19903	-0.19746	-0.19645	-0.26212

• **Ground state NFOs of *carbo*-benzene 1 and *carbo*-biphenyl 2** (Figure S4)

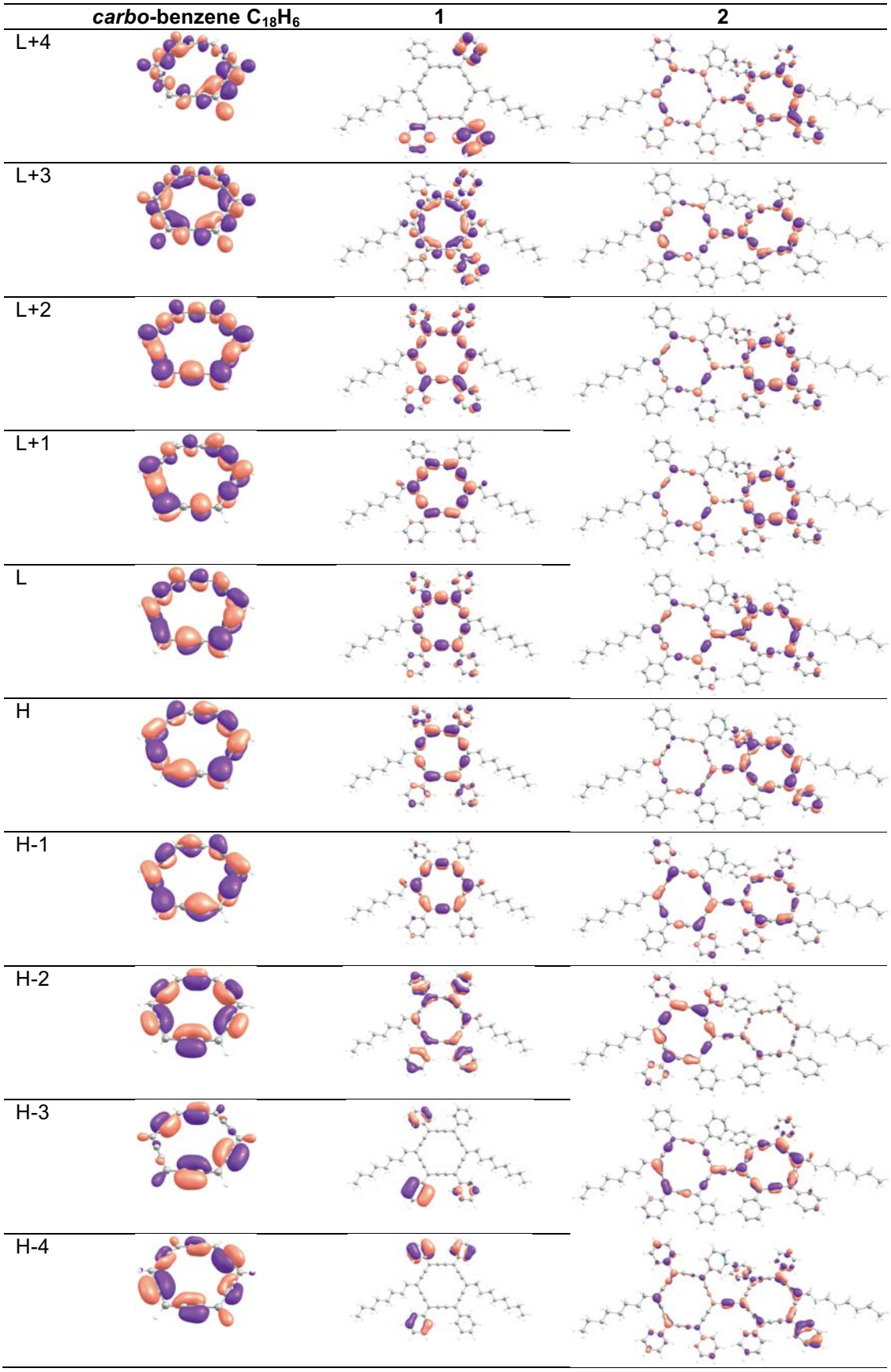

Figure S4. FMOs of unsubstituted *carbo*-benzene $C_{18}H_6$ (D_{6h}) and **1**, and *carbo*-biphenyl **2** (B3PW91-6-31G(d,p).

• Ground state NFOs of *carbo*-terphenyls 3a and 3b (Figure S5)

While the HOMO and LUMO of **3a** are found delocalized over the three C_{18} rings, six NFOs are strongly localized on either the central or external C_{18} rings, and thus called "central" or "external" NFOs, respectively. Substituting the four central phenyl rings of **3a** by methyl groups in **3b'** (instead of pentyl chains in **3b**) results in a shift of the ranks of central FMOs: HOMO-1 and LUMO+4 in **3b'** are thus placed as HOMO-3 and LUMO+1 in **3a**, respectively. The relative energy shift is as expected from the electron-donating effect of the methyl groups.

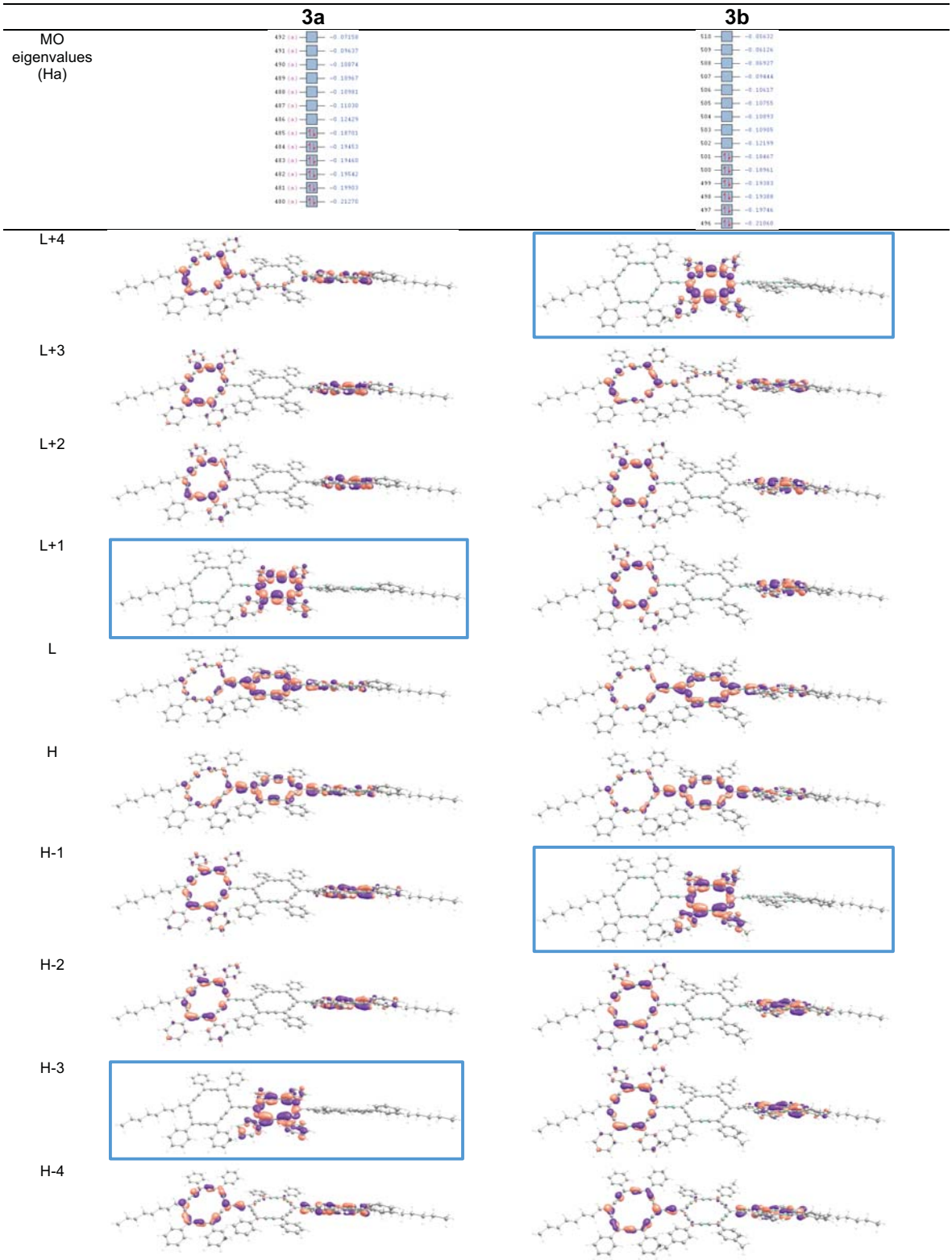

Figure S5. FMOs of **3a** and **3b** (B3PW91-6-31G(d,p)); in the boxes: central NFOs with shifted rank from **3a** to **3b'**.

With the view to appraising the pure electronic effect of alkyl-substitution independently from conformational effects, a vertical model **3b*** of **3b'** (and **3b**) was devised by truncating the four pentyl chains of **3b** to methyl groups in the calculated equilibrium conformation of **3a**. As observed above for the equilibrium structures of **3a** and **3b'**, the energies of the occupied and unoccupied central NFOs increase by *ca* 0.005 Ha (0.14 eV) from **3a** to **3b'**, while their rank changes from HOMO-3 to HOMO-1 and LUMO+1 to LUMO+4, respectively (Table S10).. In contrast, the energy variation of the external MOs is negligible (0.02 eV), while that of the delocalized MOs is intermediate (0.07 eV). The HOMO-LUMO gaps of **3a** and **3b'** are the same (1.7 eV).

Table S10. FMOs of **3a** the vertical model **3b*** of **3b'** (and **3b**) is the same conformation as **3a** (B3PW91-6-31G(d,p) level), showing the electronic origin of the rank shifting of the central NFOs from **3a** to **3b**$^{(',*)}$.

	3a			**3b'**		
	MO no	eigenvalue	de/localization	MO no	eigenvalue	de/localization
LUMO+4	490	-0.1087	delocalized 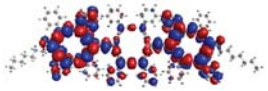	506	-0.1057	central 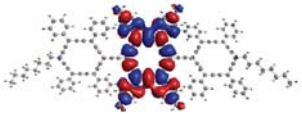
LUMO+3	489	-0.1097	external 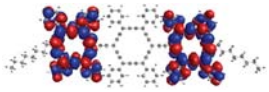	505	-0.1075	delocalized 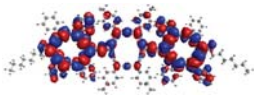
LUMO+2	488	-0.1098	external 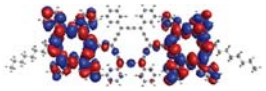	504	-0.1089	external 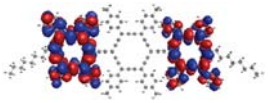
LUMO+1	487	-0.1103	central 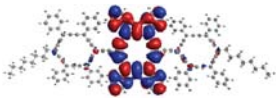	503	-0.1090	external 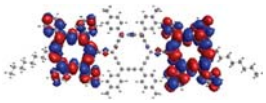
LUMO	486	-0.1243	delocalized 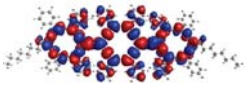	502	-0.1218	delocalized 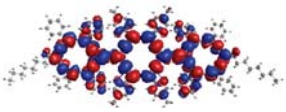
HOMO	485	-0.1870	delocalized 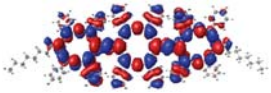	501	-0.1847	delocalized 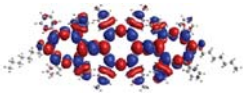
HOMO-1	484	-0.1945	external 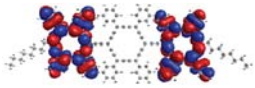	500	-0.1896.	central 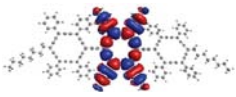
HOMO-2	483	-0.1946	external 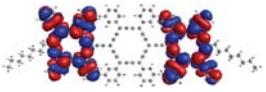	499	-0.1938	external 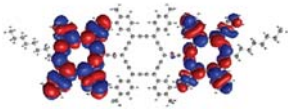
HOMO-3	482	-0.1954	central 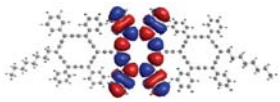	498	-0.1939	external 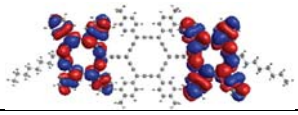
HOMO → LUMO = 0.0627 Ha = 726.68 nm HOMO-1 → LUMO = 0.0702 Ha = 649.05 nm HOMO → LUMO+1 = 0.0767 Ha = 594.05 nm HOMO-1 → LUMO+1 = 0.0842 Ha = 541.13 nm				HOMO → LUMO = 0.0629 Ha = 724.38 nm HOMO-1→LUMO = 0.0678 Ha = 672.03 nm HOMO → LUMO+1 = 0.0757 Ha = 601.89 nm HOMO-1→ LUMO+1= 0.0806 Ha = 565.30 nm		

The change in spatial distribution of the NFOs of **3b'** upon excitation (in the first excited state) is illustrated in Figure S6.

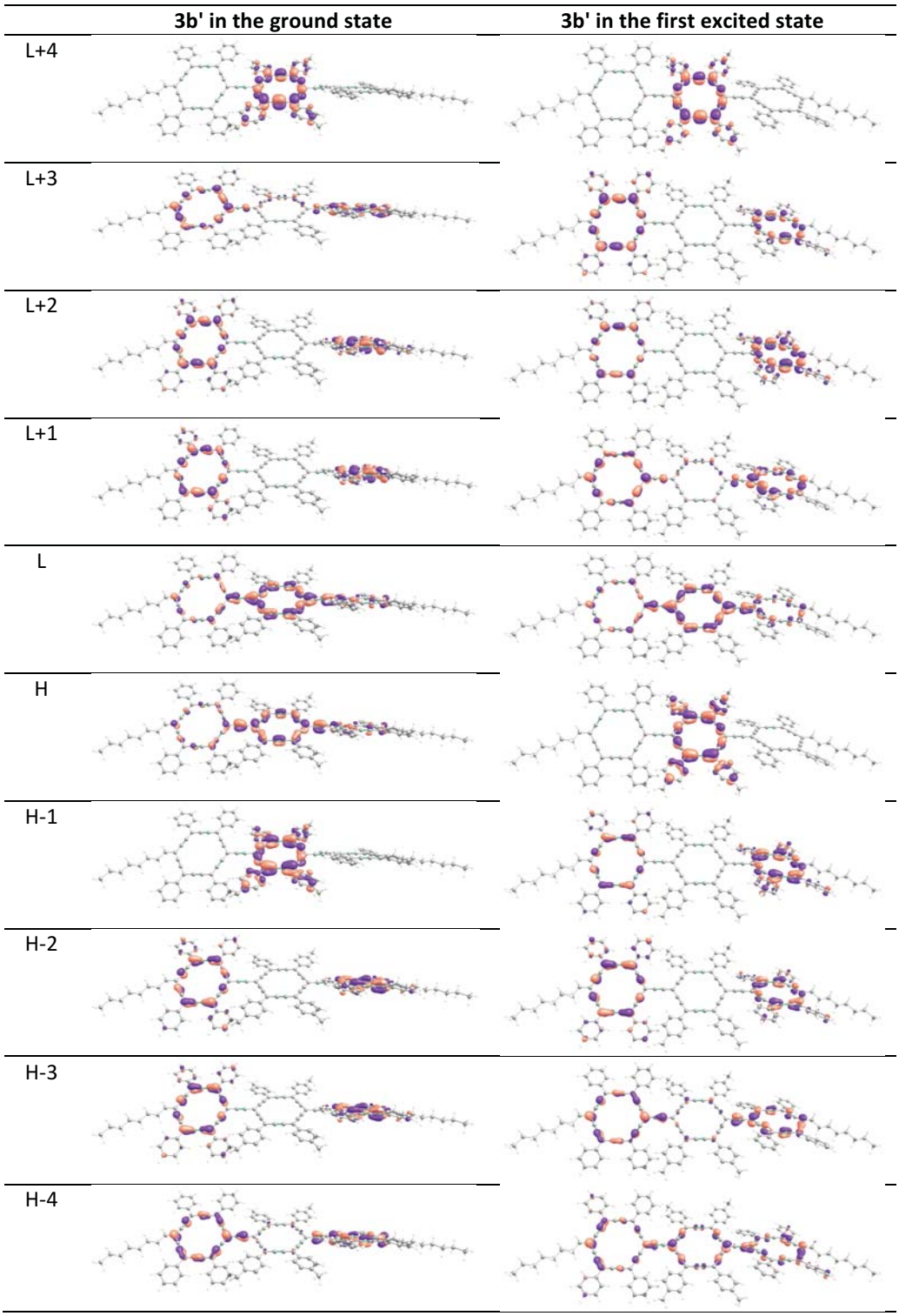

Figure S6. FMOs of the ground and first excited states of the *carbo*-terphenyl **3b'** (TDDFT B3PW91-6-31G(d,p)).

• **NFOs of the *carbo*-quaterphenyl 14** (Figure S7)

	14
L+4	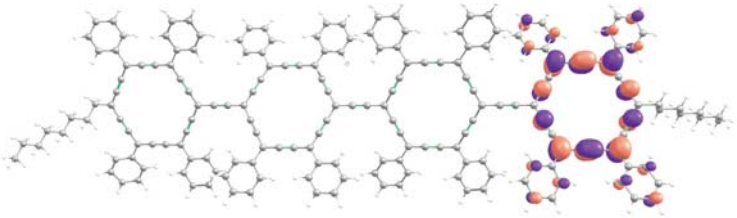
L+3	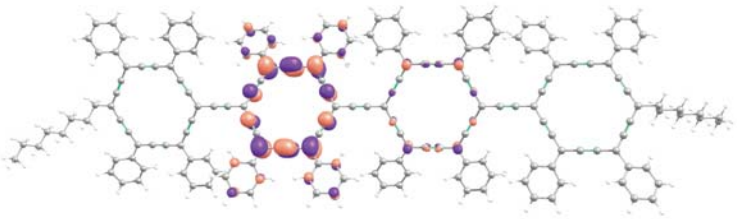
L+2	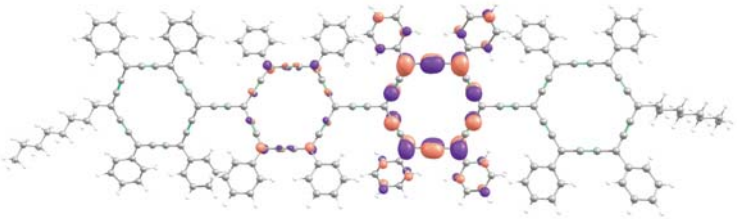
L+1	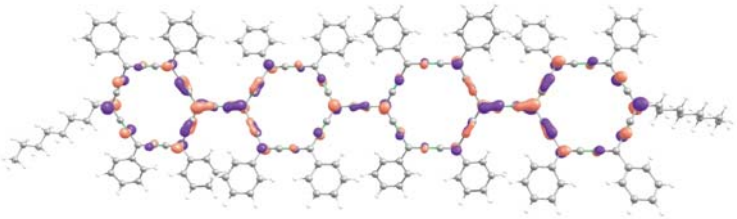
L	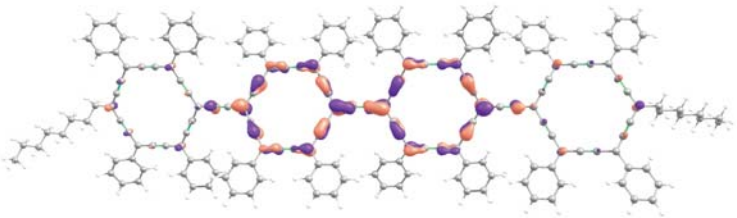
H	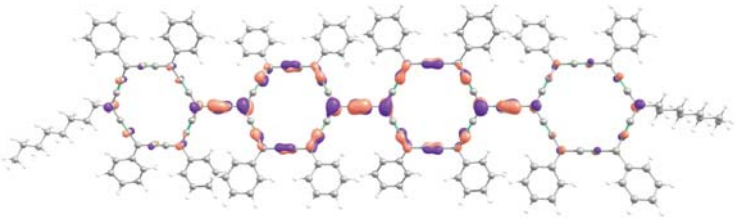
H-1	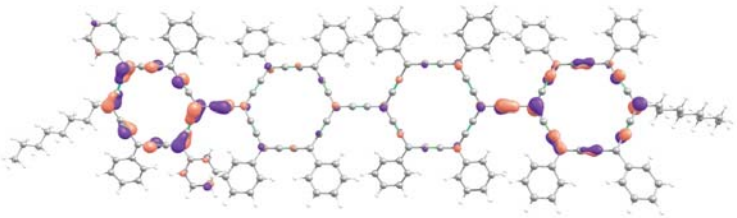

H-2	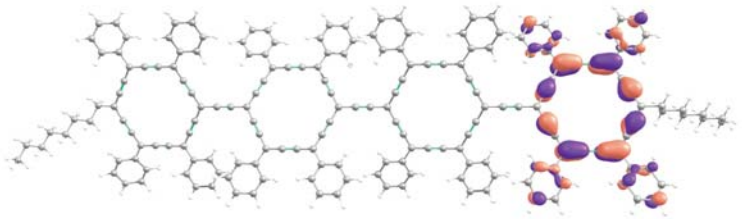
H-3	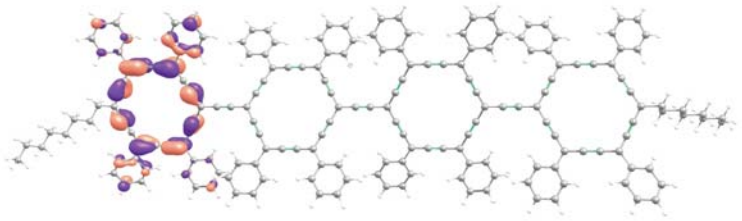
H-4	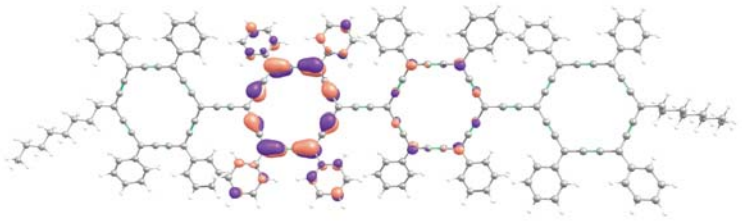

Figure S7. FMOs of the *carbo*-quaterphenyl **14** (B3PW91-6-31G(d,p) level).

• NFOs of the [6]petricyclynedione 4

The [6]pericyclynedione **4** has long been used as a pivotal precursor of quadrupolar tetraphenyl-*carbo*-benzenes. The gas-phase equilibrium structure of one of its stereoisomers (*trans-cis-trans*, the most stable one, among five) has been calculated for the first time; its structure and NFOs are displayed Figure S8.

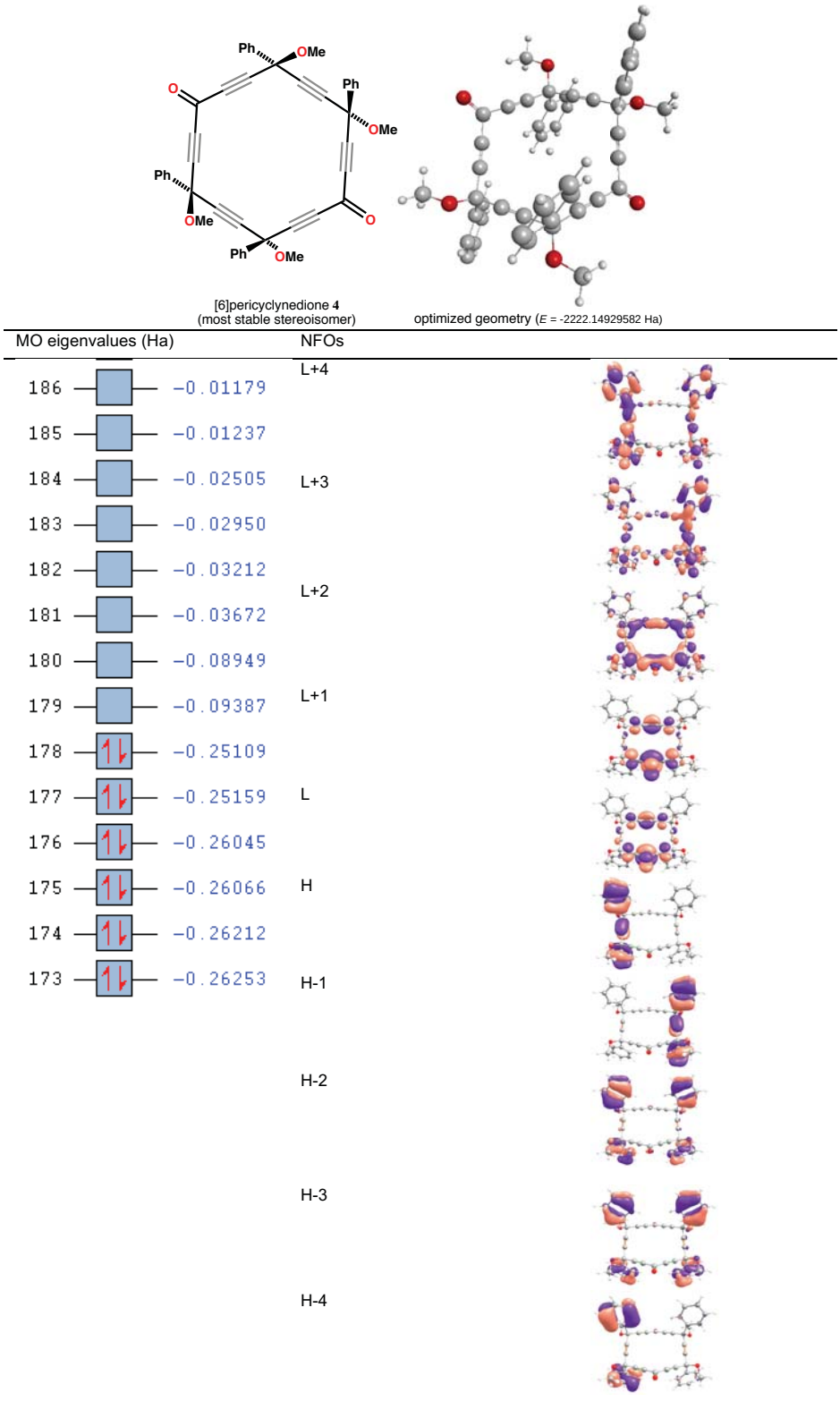

Figure S8. FMOs of the most stable stereoisomer of the *carbo*-[6]pericyclynedione **4** (B3PW91-6-31G(d,p) level).

4.6. Conformational analysis and comparison between catenation and fusion of *carbo*-benzene rings.

4.6.1. Conformational analysis of the *carbo*-biphenyl 2

In the nearly C_2-symmetric equilibrium geometry of **2**, optimized without symmetry constraint, the *carbo*-benzene rings are nearly planar but not coplanar, with a dihedral angle of ca $\theta_{eq} \approx 30°$ (see main text). The rotation about the ethynylene linker, monitored through the dihedral angle variable θ for a *sp***C**–*sp*^{2}**C**-(*sp*C)$_2$-*sp*^{2}**C**–*sp***C** sequence, is quite free, with a barrier of *ca* 1.7 kcal/mol for two quasi-iso-energetic transition states TS1 and TS2, at $\theta_{TS1} = 0°$ (E_{TS1} = 1.8 kcal/mol) and $\theta_{TS2} \approx 90°$ (E_{TS2} = 1.6 kcal/mol: see Figure S9). In TS1, it is noteworthy that the macrocycle mean planes are almost parallel but not the same (non-coplanar C_{18} rings): the mean distances between the eighteen C atoms of a ring and the mean plane of the other ring are 0.82289 Å and 0.82267 Å, so almost equal, as also indicated by the angle between the mean planes of 0.66° only (Figure S9).

The partial de-conjugation between the C_{18} rings (slanting of the axis of the almost perfectly linear C_4 connector *sp*^{2}C–*sp*C–*sp*C–*sp*^{2}C by 9.3° out of the C_{18} ring mean) is actually due to a folding by 7.7° of the prow and stern of the C_{18} rings in a half-chair-like conformation. The latter thus undergo some intrinsic structural de-aromatization dictated by steric repulsion between the facing *ortho*-phenyl substituents (the dihedral angles of *ca* 19° between the corresponding C_6 mean planes and the attached C_{18} ring mean plane indeed guaranty stabilizing residual π-conjugation between them).

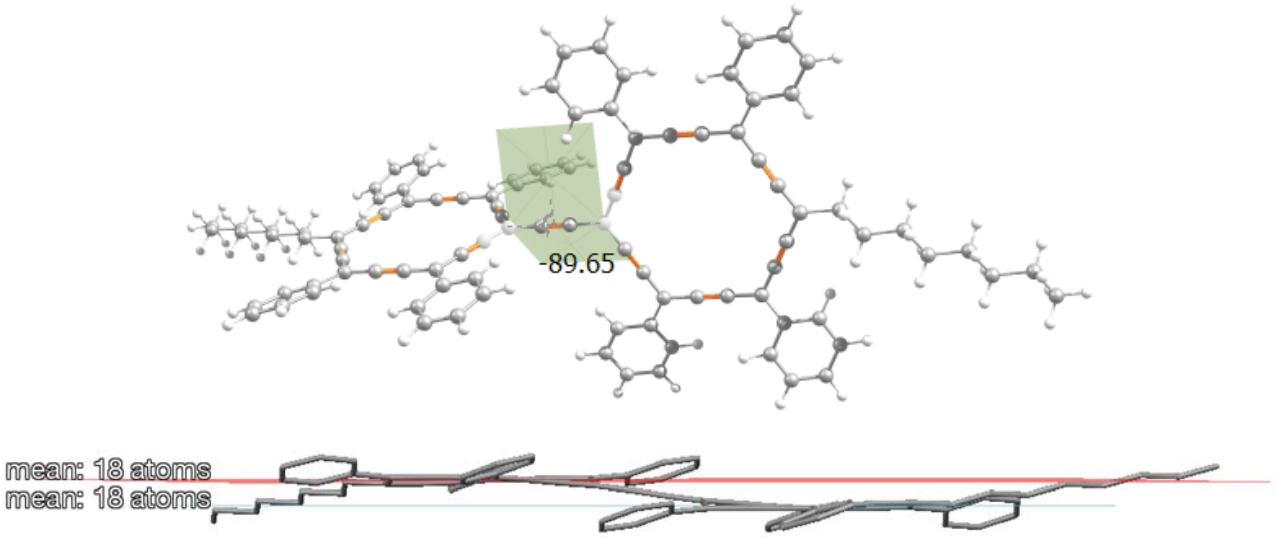

Figure S9. Views of the rotation transition states about the ethynylene linkers in the *carbo*-biphenyl **2**. *Top*: orthogonally staggered TS2 ($\theta_{TS2} \approx 90°$, E_{TS2} = 1.6 kcal/mol); *bottom*: pseudo-eclipsed TS1 ($\theta_{TS2} = 0°$, E_{TS2} = 1.8 kcal/mol) with a local average distance between the two C_{18} ring mean planes of *ca* 0.82 Å.

The complete rotation profile (*E vs* θ) displays no other local extremum (Figure S10), showing that the leading energy costs are equivalently due to steric repulsion between the four internal phenyl groups (in TS1) and complete disruption of π-conjugation trough the C_2 connector (in TS2).

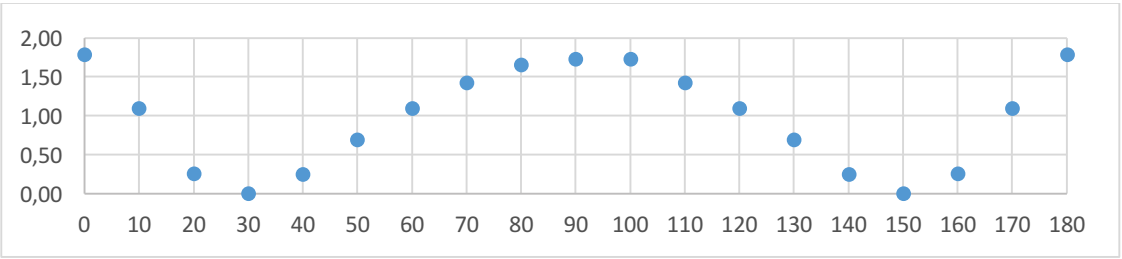

Figure S10. Rotation profile about the ethynylene linkers of the *carbo*-biphenyl **2** (*E* in kcal/mol *vs* a dihedral angle θ defined as shown in Figure S9)

The same features were observed from the calculation of the rotation about the ethynylene linkers of the *carbo*-terphenyl **3a**.

For comparison, the parent OPEn, Ph–[C≡C-4-C_6H_4]$_n$–H, display similar equilibrium dihedral angles (39.1 for n = 2, 38.0º for n = 3). As expected, even on the basis of steric effects only, the perfluorinated parents F_{6+4n}-OPEn, C_6F_5–[C≡C-4-C_6F_4]$_n$–F exhibit greater dihedral angles (56.6° for n = 2, 56.0º for n= 3).

4.6.2. Steric effects *vs* inter-ring π-conjugation in *carbo*-OPEs

Geometry optimization while constraining dihedral angles between all the successive C_{18} rings to vanish in a "co-flip" TS-like eclipsed conformation gave destabilizations of 1.7, 3.0 and 5.7 kcal/mol *vs* the respective equilibrium structures of **2**, **3a** and **14**. Under such a constraint, as observed for **2**, the C_{18} rings are neither coplanar nor individually planar: the central C_{18} rings of **3a** and **14** adopt a chair-like conformation where the prow and the stern, in quasi-parallel mean planes, are folded by ca 4.0-4.5° from the central square bearing the four phenyl groups (see section 4.6.1, and Figures S9 and S11). This gives an average cost of 1.7 kcal/mol per C_{18} ring pair for the steric effects to compete with π-conjugation through the C_2 connectors.

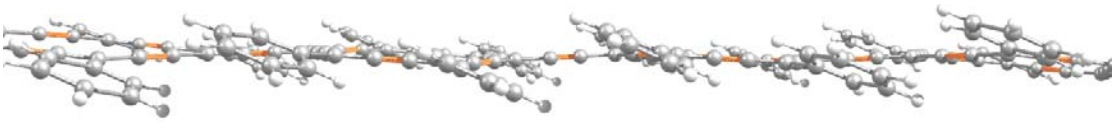

Figure S11. Side view of the TS-like pseudo-eclipsed conformation of the *carbo*-terphenyl **3a** (optimized under the constraint of simultaneously vanishing particular dihedral angles between successive C_{18} rings).

The NICS(0)/NICS(1) values of the corresponding planar structures **2-eclipsed**, **3a-eclipsed** and **14-eclipsed** were found to not change significantly (i.e. by 0.1-0.2 units) from the values of the equilibrium geometry for **2**, **3a** and **14**, respectively (see section 4.3 and Tables S6 and S11).

Table S11. NICS values (in ppm) for the C_{18} rings of the *carbo*-OPEs **1**, **2**, **3a** **14** with constrained eclipsing C_{18} rings (vanishing dihedral angles), calculated at the B3PW91-6-31G(d,p) level with the GIAO formalism.

	constrained geometry with co-planar C_{18} rings (*vs* equilibrium geometry)					
	2-eclipsed (*vs* **2** at equil.)		**3a-eclipsed** (*vs* **3a** at equil.)		**14- eclipsed** (*vs* **14** at equil.)	
rings	-NICS(0)	-NICS(±1)	-NICS(0)	-NICS(±1)	-NICS(0)	-NICS(±1)
C_{18}	13.6 (13.7)	12.4 (12.5)	13.5 (13.6)	12.4 (12.4)	13.5 (13.6)	12.4 (12.4)
		12.5 (12.5)		12.3 (12.4)		12.3 (12.4)
C_{18}	13.6 (13.7)	12.4 (12.5)	12.5 (12.5)	11.4 (11.4)	12.4 (12.4)	11.3 (11.3)
		12.5 (12.5)		11.4 (11.4)		11.3 (11.3)
C_{18}			13.5 (13.6)	12.4 (12.4)	12.4 (12.4)	11.3 (11.3)
				12.3 (12.4)		11.3 (11.3)
C_{18}					13.5 (13.6)	12.4 (12.4)
						12.2 (12.4)

Addressing the issue of the through-ring π-conjugation driving force in the absence of steric counter-effect, the phenyl rings of **2**, **3a** and **14** have been replaced by simple hydrogen atoms in **2H**, **3H** and **14H**, respectively: starting optimization without any symmetry constraint led to equilibrium structures of perfect C_{2h} symmetry. For **14H** (Figure S12), the external and internal NICS(0)/NICS(1) values are –16.5/–15.1 and –15.2/–13.9 ppm, respectively.

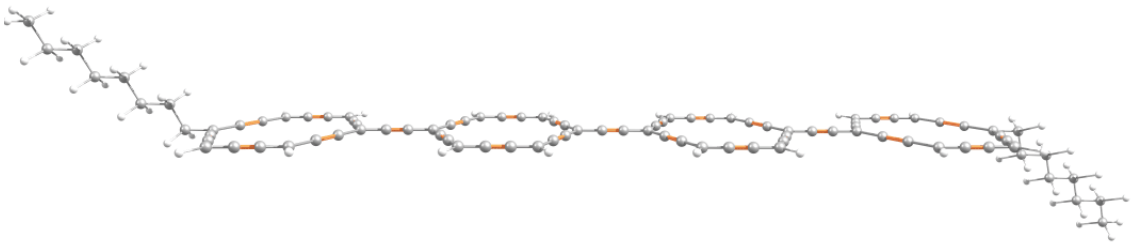

Figure S12. Perfectly C_{2h}-symmetric equilibrium geometry of the *carbo*-quaterphenyl **14H** without phenyl substituent; level of calculation: B3PW91-6-31G(d,p).

4.6.3. From *carbo*-biphenyl to *carbo*-pyrene

With the view to appraising the experimental possibility to force co-planarity between the C_{18} ring of *carbo*-terphenyl **2**, the theoretical tetra-dehydrogenated Scholl product **2-H$_4$** was calculated (see Figure S13).

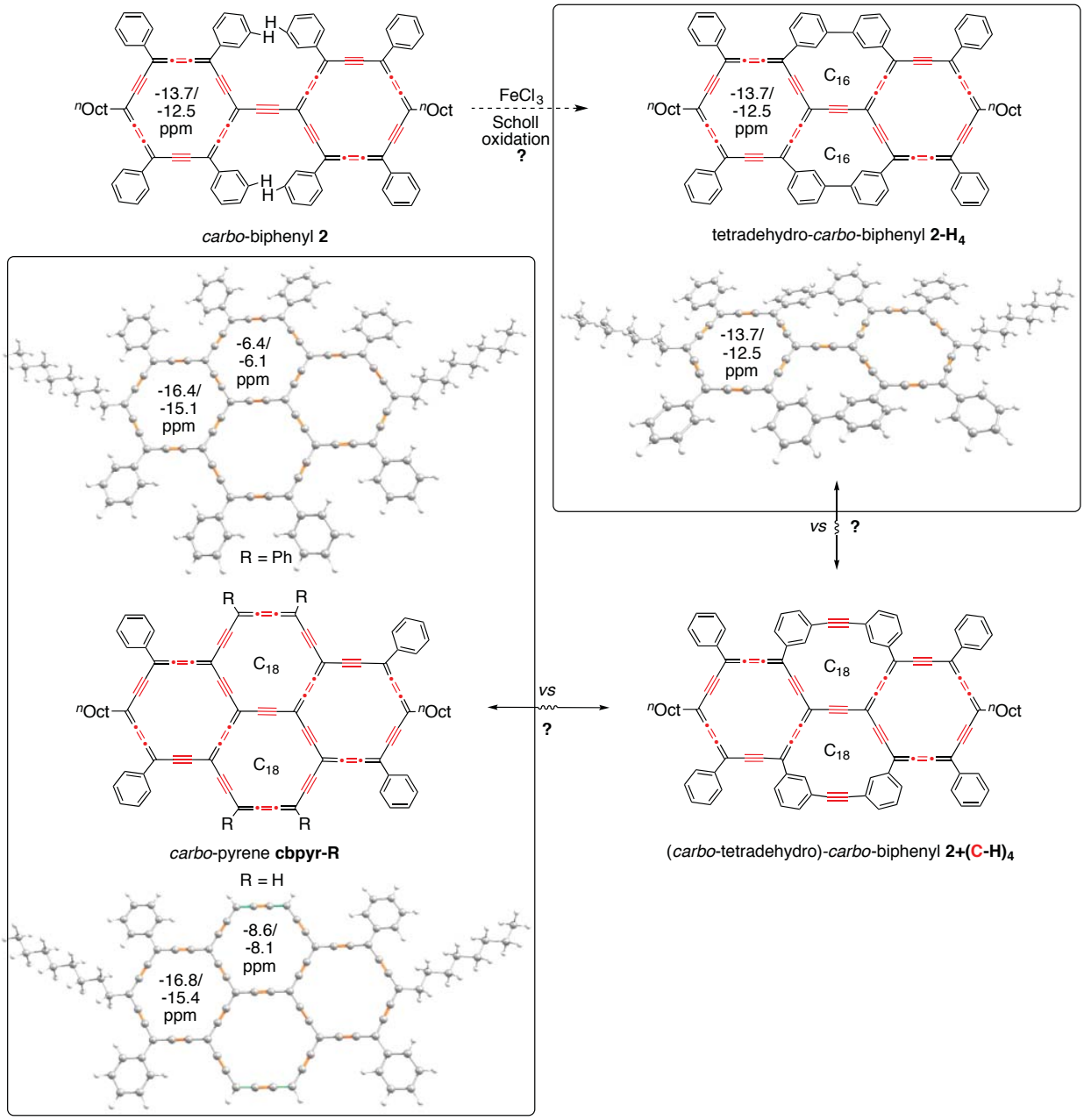

Figure S13. Embedding the free-rotating C_{38} *carbo*-OPE1 motif of *carbo*-biphenyl **2** in the C_{54} core of *carbo*-pyrenes. Calculated equilibrium structures at the B3PW91/6-31G(d,p) level. NICS(0)/NICS(1) values, calculated at the same level, are indicated for the C_{18} rings (see Table S12).

The resulting C_{16} cyclo-meta-phenyleneethynylene rings were however found to remain non-planar - albeit more than in **2**, see section 4.2 -, with unchanged NICS(0)/NICS(1) values of the C_{18} rings (–13.7/–12.5 ppm: Table S12).

To restore a Hückel aromaticity count in the added peri-condensed rings, the C_{16} macrocycles were formally replaced by C_{18} macrocycles in **2+(C-H)$_4$** and *meta*-benzannelation was finally deleted in *carbo*-pyrenes derivatives **cbpyr-R**, R = Ph, H. The NICS(0)/NICS(1) values of the original catenated (distal) C_{18} rings decrease significantly to –16.4/–15.1 ppm for R = Ph and –16.8/–15.4 ppm for R = H (Table S12). Meanwhile, the NICS(0)/NICS(1) values of the added fused (central) C_{18} rings are more than twice smaller, at –6.4/–6.1 ppm for R = Ph and –8.6/–8.1 ppm for R = H, witnessing a very weak *carbo*-aromatic character.

Eigenvalues of DFT-calculated NFOs of the ground state in vacuum are listed in Table S13, and TDDFT-calculated absorption and emission spectra in dichloromethane (using the PCM method) are reported in Table S14.

Table S12. Calculated NICS values (in ppm) for the C_{18} and C_6 rings of the *carbo*-OPEs **1**, **2**, **3a**-**b'**, **14** and the unsubstituted reference $C_{18}H_6$, at the B3PW91-6-31G(d,p) level (GIAO formalism).

rings	**2-H$_4$**		**cbpyr-H**		**cbpyr-Ph**	
	NICS(0)	NICS(±1)	NICS(0)	NICS(±1)	NICS(0)	NICS(±1)
C_{18}	-13.7	-12.5 -12.5	-16.8	-15.4 -15.4	-16.4	-15.0 -15.1
C_{18}	-13.7	-12.5 -12.5	-16.8	-15.4 -15.4	-16.4	-15.0 -15.1
C_{18}			-7.1	-6.8 -6.8	-6.4	-6.1 -6.1
C_{18}			-8.6	-8.1 -8.1	-7.8	-7.4 -7.4
C_6	-5.7	-8.0 -7.7				
C_6	-5.7	-8.0 -7.7				
C_6			-4.7	-7.1 -7.1	-4.7	-7.0 -7.2
C_6	-6.3	-8.6 -8.5				
C_6					-7.1	-6.8 -6.8
C_6	-6.6	-8.6 -8.7				

Table S13. Eigenvalues of NFOs for the Scholl oxidation product and *carbo*-pyrenes of Figure S12, in a. u. (B3PW91/6-31G(g,p) level).

	2-H$_4$	**cbpyr-H**	**cbpyr-Ph**
L+4	-0.06644	-0.09101	-0.09196
L+3	-0.09478	-0.10867	-0.10784
L+2	-0.10932	-0.10926	-0.11095
L+1	-0.11020	-0.11999	-0.11863
L	-0.11759	-0.13268	-0.13171
H	-0.18818	-0.18334	-0.17923
H-1	-0.19367	-0.19776	-0.19571
H-2	-0.19524	-0.20831	-0.20005
H-3	-0.20926	-0.21067	-0.20599
H-4	-0.22964	-0.21826	-0.21410

Table S14. TDDFT-calculated absorption and emission spectra of the Scholl oxidation product and *carbo*-pyrenes of Figure S12 (B3PW91/6-31G(g,p)).

• Overall spectral data:

	Absorption			Emission		
	λ_{abs} (nm)	*f*	Transition (weight 40% or higher)	λ_{abs} (nm)	*f*	Transition (weight 40% or higher)
2-H$_4$	755.9	0.6	H→L	890.8	1.4	H→L
	578.9	2.4	H-2→L+2	653.1	1.7	H-1→L & H→L+1
	458.0	3.6	H-2→L+3 & H-3→L+2	600.7	1.9	H-1→L+1
				484.9	3.6	H-3→L+2 & H-2→L+3
cbpyr-H	992.8	1.2	H→L	1179.8	2.2	H→L
	717.2	0.8	H-1→L & H→L+1	776.5	1.7	H-1→L & H→L+1
	635.7	2.8	H-1→L+1	649.8	2.7	H-1→L+1
	522.5	1.2	H-2→L+3 & H-3→L+2	537.2	1.2	H-2→L+3 & H-3→L+2
	458.3	3.0	H-2→L+3 & H-3→L+2	515.5	1.2	H-5→L
				492.4	2.4	H-3G? Excited→L+3
cbpyr-Ph	1061.1	1.2	H→L	1269.2	2.1	H→1
	750.7	0.8	H-1→L	814.0	2.1	H-1→L
	653.1	1.4	H-1→L+1	663.0	1.7	H-1→L+1
	565.8	2.8	H-2→L+2	607.2	2.7	H-2→L+2
	525.6	2.2	H-2→L+3 & H-3→L+2	561.1	3.4	H-3→L+2 & H-2→L+3

• Main one-electron transition contributions for excited states of highest oscillator strength:

	2-H$_4$		**cbpyr-H**		**cbpyr-Ph**	
	λ_{abs} (nm)	*f*	λ_{abs} (nm)	*f*	λ_{abs} (nm)	*f*
Absorption	755.9	0.6	992.8	1.2	1061.1	1.2
	578.9	2.4	717.2	0.8	752.0	0.4
	458.0	3.6	635.7	2.8	750.7	0.8
			522.5	1.2	653.1	1.4
			492.6	0.6	565.8	2.8
			458.3	3.0	525.6	2.2
			409.8	0.7	474.3	0.7
Emission	890.8	1.4	1179.8	2.2	1269.2	2.1
	653.1	1.7	776.5	1.7	814.0	2.1
	600.7	1.9	649.8	2.7	663.0	1.7
	484.9	3.6	537.2	1.2	607.6	2.7
			515.5	1.2	561.1	3.4
			492.4	2.4		

5. References

1. J. Wu, X. Yang, Z. He, X. Mao, T. A. Hatton, T. F. Jamison, *Angew. Chem. Int. Ed.* **2014**, *53*, 8416-8420.
2. K. Cocq, N. Saffon-Merceron, Y. Coppel, C. Poidevin, V. Maraval, R. Chauvin, *Angew. Chem. Int. Ed*. **2016**, *55*, 15133-1513-6.
3. P. v. d. Sluis, A. L. Spek, *Acta Cryst*. **1990**, *A46*, 194-201.
4. Gaussian 09, Revision A.01, M. J. Frisch, G. W. Trucks, H. B. Schlegel, G. E. Scuseria, M. A. Robb, J. R. Cheeseman, G. Scalmani, V. Barone, B. Mennucci, G. A. Petersson, H. Nakatsuji, M. Caricato, X. Li, H. P. Hratchian, A. F. Izmaylov, J. Bloino, G. Zheng, J. L. Sonnenberg, M. Hada, M. Ehara, K. Toyota, R. Fukuda, J. Hasegawa, M. Ishida, T. Nakajima, Y. Honda, O. Kitao, H. Nakai, T. Vreven, J. A. Montgomery, Jr., J. E. Peralta, F. Ogliaro, M. Bearpark, J. J. Heyd, E. Brothers, K. N. Kudin, V. N. Staroverov, R. Kobayashi, J. Normand, K. Raghavachari, A. Rendell, J. C. Burant, S. S. Iyengar, J. Tomasi, M. Cossi, N. Rega, J. M. Millam, M. Klene, J. E. Knox, J. B. Cross, V. Bakken, C. Adamo, J. Jaramillo, R. Gomperts, R. E. Stratmann, O. Yazyev, A. J. Austin, R. Cammi, C. Pomelli, J. W. Ochterski, R. L. Martin, K. Morokuma, V. G. Zakrzewski, G. A. Voth, P. Salvador, J. J. Dannenberg, S. Dapprich, A. D. Daniels, Ö. Farkas, J. B. Foresman, J. V. Ortiz, J. Cioslowski, and D. J. Fox, Gaussian, Inc., Wallingford CT, **2009**.
5. a) A. D. Becke, *J. Chem. Phys.* **1993**, *98*, 5648-5652; b) J. P. Perdew, Y. Wang, *Phys. Rev. B* **1992**, *45*, 13244-13249.
6. a) R. Ditchfield, W. J. Hehre, J. A. Pople, *J. Chem. Phys.* **1971**, *54*, 724; b) T. Clark, J. Chandrasekhar, G. W. Spitznagel, P. v. R. Schleyer, *J. Comp. Chem.* **1983**, *4*, 294-301.
7. a) M. Cossi, V. Barone, R. Cammi, J. Tomasi, *Chem. Phys. Lett.* **1996**, *255*, 327-335; b) J. Tomasi, M. Persico, *Chem. Rev.* **1994**, *94*, 2027-2094; c) V. Barone, M. Cossi, M. *J. Phys. Chem. A* **1998**, *102*, 1995-2001.
8. R. G. Parr, L. von Szentpaly, S. Liu, *J. Am. Chem. Soc.* **1999**, *121*, 1922-1924.
9. P. Geerlings, F. De Proft, W. Langenaeker, *Chem. Rev.* **2003**, *103*, 1793-1873.
10. a) R. G. Parr, W. Yang, *Density Functional Theory of Atoms and Molecules*, Oxford University Press: New York, 1989; b) R. G. Parr, R. A. Donnelly, M. Levy, W. E. Palke, *J. Chem. Phys.* **1978**, *68*, 3801-3807; c) R. G. Parr, R. G. Pearson, *J. Am. Chem. Soc.* **1983**, *105*, 7512-751-6.
11. T. Koopmans, *Physica* **1934**, *1*, 104-113.
12 . P. K. Chattaraj, S. Giri, S. Duley, *J. Chem. Phys. Lett*. **2010**, *1*, 1064-1067.
13. a) K. Cocq, N. Saffon-Merceron, A. Poater, V. Maraval, R. Chauvin, *Synlett*, 2016, **27**, 2105-2112; b) D. Listunov, C. Duhayon, A. Poater, S. Mazères, A. Saquet, V. Maraval, R. Chauvin, *unpublished results*.
14. J. J. Torres-Vega, A. Vasquez-Espina, L. Ruiz, M. A. Fernandez-Herrera, L. Alvarez-Thon, G. Merino, W. Tiznado, *ChemistryOpen* **2015**, *4*, 302-307.

Chapter 6

From endo-aromatic hemi-butatriene to bridging [3]cumulene units: *carbo*-barrelenes and *carbo*-stilbenes

Introduction & Summary

Over the past few decades, π-conjugated polyacetylenic macrocyclic chromophores drew chemist's attention for their peculiar structural, electronic, and optical properties.[1] In *carbo*-mer chemistry, besides the most studied *carbo*-benzenes, the design and synthesis of new types of expanded molecules belonging to this family are still active. Very recently, the multi-step synthesis of a *carbo*-naphthalene, the smallest fused polycyclic fragment of α-graphyne (or *carbo*-graphene),[2] was reported by our group.[3] In this context, the design and synthesis of tricyclic *carbo*-mers of the strained barrelene (bicyclo[2.2.2]-2,5,7-octatriene) was envisaged, the parent barrelene being indeed a fascinating structure with potential applications in various domains. Since the first report of barrelene by Zimmerman in 1960,[4] many of its derivatives were described and studied for their structural and electronic properties,[5] and substituted representatives were also used as ligands in catalysis,[6] or for their ability to trigger photo-generated rearrangements.[7]

The expanded *carbo*-barrelene, with its triple π-electron-rich conjugated system, is attractive not only for its possible optical and electronic properties, but also because its three-dimensional hollow structure can be viewed as a shape-persistent organic cage that could encapsulate small molecules or ions. In the recent years, the use of molecular containers as hosts able to encapsulate small guests[8] have attracted a great interest due to the wide range of related applications such as the stabilization of unstable species,[9] molecular recognition and separation,[10] discrimination of chiral molecules,[11] reactors,[12] sensors,[13] crystal growth,[14] and catalysis.[15] Cage compounds are generally categorized into two classes: (i) supramolecular cages built by self-organization of small molecules;[16] (ii) covalent cages built by organic synthesis. This second class is much less exemplified than the first one, whose prominent representatives are metal-organic frameworks (MOFs) fabricated by coordination between metal ions and rigid organic ligands,[17] and supramolecular cages assembled through hydrogen bonding.[18]

Covalent organic cage molecules are relatively rare as compared to their supramolecular counterparts,[19] their construction indeed requiring multistep synthesis with low overall yields sometimes. In spite of this drawback, their hollow rigid structures still remain attractive because of the higher stability of these covalent assemblies, which could find applications in the domain of molecular recognition of chiral guests,[20] as receptors or sensors.[21] Fullerene C_{60}

and its derivatives were for example largely studied as covalent cages for the encapsulation of dihydrogen.[22]

Here, the synthesis of cage-like *carbo*-barrelenes made of three dialkynylbutatriene moieties covalently connected to each other through two sp^3 hybridized vertices was envisaged. The synthetic strategy designed for the preparation of these tricyclic compounds is based on the cyclizing double nucleophilic addition of one equivalent of triyne to the key [6]pericyclynedione in the presence of LiHMDS as base, followed by a reductive and acidic treatment under optimized conditions. Two *carbo*-barrelenes and a partially reduced bis-butatrienic derivative were isolated as highly soluble brown-yellow chromophores and sufficiently stable to be fully characterized by ^1H, ^{13}C NMR and UV-visible spectroscopy, HRMS (MALDI-TOF technique), and by square-wave and cyclic voltammetry. They were also shown to crystallize at low temperature, and single crystals of three molecules deposited from *n*-heptane were found to be suitable for X-ray diffraction analysis. In addition, one of the isolated *carbo*-barrelene was selected as a model molecule for the study of its encapsulation ability. The small NH_4^+ cation was first envisaged as a guest, despite the absence of clear experimental evidence of encapsulation up to now, theoretical calculations suggested that an interaction should occur between these two partners (ΔE_{tot} = - 44.4 kcal/mol). Further experiments are in progress in order to study the ability of *carbo*-barrelene cage as host for small molecules or ions.

Inspired by the isolation of a side-product from the addition of the triyne to the [6]pericyclynedione (see Figure 1), the synthesis of expanded stilbenes, or *carbo*-stilbenes, was envisioned. The photo-isomerization property of the parent stilbene (1,1-diphenylethylene), leading to a large number of applications as dyes, in optical devices,[23] and even in biomedicine, [24] indeed motivated the synthesis and study of the expanded π-conjugated *carbo*-stilbene, which could also exhibit interesting electronic and optical properties. Two *carbo*-stilbenes could be prepared through an optimized synthetic strategy, but their unexpected extremely poor solubility prevented their full characterization. Nevertheless, they could be characterized by ^1H NMR and UV-visible spectroscopy, HRMS (MALDI-TOF technique), and square-wave and cyclic voltammetry. The ^1H NMR spectra and DFT calculations revealed the formation of a mixture of the *trans*- and *cis*- isomers for this two *carbo*-stilbenes, but no evidence of *cis*-*trans* interconversion were observed by variable temperature ^1H NMR experiments in the range 25 ^oC to 55 ^oC.

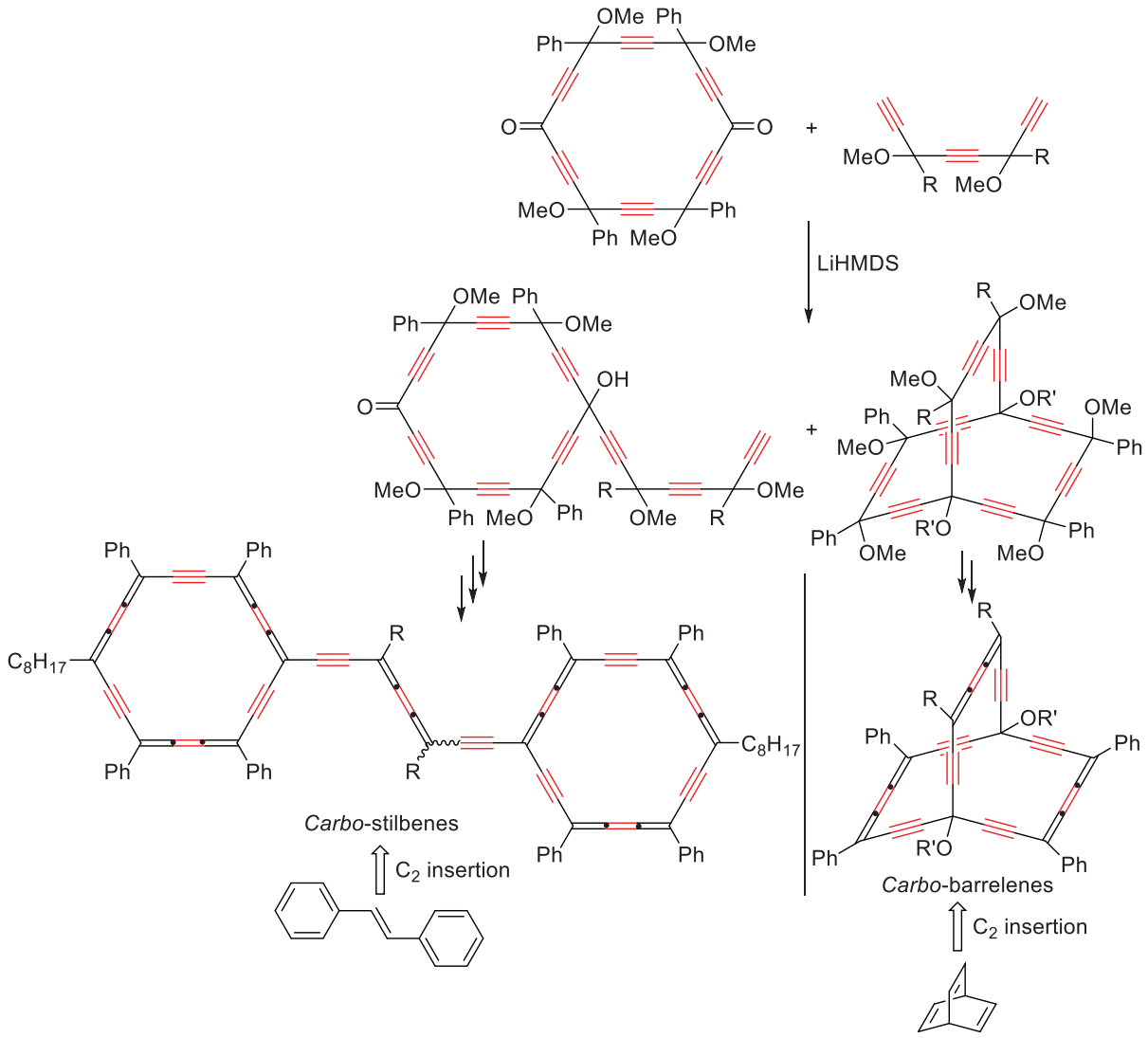

Figure 1. The designed synthetic routes of *carbo*-barrelenes and *carbo*-stilbenes.

Reference

1. For recent examples see: a) S. Ramsaywack, S. Karaca, M. Gholami, A. H. Murray, F. Hampel, R. McDonald, N. Elmaci, H. P. Lüthi, R. R. Tykwinski, *J. Org. Chem*., **2014**, *79*, 10013-10029; b) M. Desroches, J.-F. Morin, *RSC Adv.,* **2017**, *7*, 17117-17121; c) N. Takahashi, S.-i. Kato, M. Yamaji, M. Ueno, R. Iwabuchi, Y. Shimizu, M. Nitani, Y. Ie, Y. Aso, T. Yamanobe, H. Uehara, Y. Nakamura, *J. Org. Chem*., **2017**, *82*, 8882-8896.

2. For references on a-graphyne see: a) R. H. Baughman, H. Eckhardt, M. Kertesz, *J. Phys Chem.,* **1987**, *87(11)*, 6687-6699; b) J-M. Ducéré, C. Lepetit, R. Chauvin, *J. Phys. Chem. C*, **2013**, *117*, 21671-21681.

3. K. Cocq, N. Saffon-Merceron, Y. Coppel, C. Poidevin, V. Maraval, R. Chauvin, *Angew. Chem. Int. Ed*., **2016**, *55*, 15133-15136.

4. H. E. Zimmerman, R. M. Paufler, *J. Am. Chem. Soc*., **1960**, *82*, 1514-1515.

5. a). C. G. Krespan, B. C. McKusick, T. L. Cairns, *J. Am. Chem. Soc.,* **1961**, *83*, 3428-3432; b). R. G. Miller, M. Stiles, *J. Am. Chem. Soc.,* **1963**, *85*, 1798-1800; c). H. E. Zimmerman, G. L. Grunewald, R. M. Paufler, M. A. Sherwin, *J. Am. Chem. Soc.,* **1969**, *91*, 2330-2338; d). M. W. Wagaman, E. Bellmann, M. Cucullu, R. H. Grubbs, *J. Org. Chem.,* **1997**, *62*, 9076-9082; e). M. W. Wagaman, R. H. Grubbs, *Macromolecules,* **1997**, *30*, 3978-3985.

6. a). M. A. Esteruelas, L. A. Oro, *Coord. Chem. Rev*., **1999**, *193-195*, 557-618; b). T. Nishimura, T. Kawamoto, M. Nagaosa, H. Kumamoto, T. Hayashi, *Angew. Chem. Int. Ed*., **2010**, *49*, 1638-1641; c). R. Shintani, M. Takeda, T. Nishimura, T. Hayashi, *Angew. Chem. Int. Ed.,* **2010**, *49*, 3969-3971; d) M. Schlesinger, M. Hofmann, T. Rüffer, D. Schaarschmidt, H. Lang, S. Theilacker, M. Schürmann, K. Jurkschat, M. Mehring, *Eur. J. Inorg. Chem.,* **2013**, 2930-2939.

7. H. E. Zimmerman, D. Armesto, *Chem. Rev.,* **1996**, *96*, 3065-3112.

8. a). D. J. Cram, *Nature,* **1992**, *356*, 29-36; b). M. Frank, M. D. Johnstone, G. H. Clever, *Chem. Eur. J.,* **2016**, *22*, 14104-14125.

9. a). D. Fiedler, R. G. Bergman, K. N. Raymond, *Angew. Chem. Int. Ed.,* **2006**, *45*, 745-748; b). A. Galan, P. Ballester, *Chem. Soc. Rev*., **2016**, *45*, 1720-1737.

10. a). F. Vögtle, W. M. Müller, U. Werner, H. W Losensky, *Angew. Chem. Int. Ed. Engl.,* **1987**, *26*, 901-903; b). D. Fiedler, D. H. Leung, R. G. Bergman, K. N. Raymond, *Acc. Chem. Res.,* **2005**, *38*, 349-358; c). A. Bouchet, T. Brotin, M. Linares, H. Ågren, D. Cavagnat, T.

Buffeteau, *J. Org. Chem.,* **2011**, *76*, 4178-4181; d). I. A. Riddell, M. M. J. Smulders, J. K. Clegg, J. R. Nitschke, *Chem. Commun*., **2011**, *47*, 457-459.

11. K. Wu, K. Li, Y. J. Hou, M. Pan, L. Y. Zhang, L. Chen, C. Y Su, *Nat. Commun*., **2016**, *7*, 10487.

12. a). M. Yoshizawa, Y. Takeyama, T. Kusukawa, M. Fujita, *Angew. Chem. Int. Ed*., **2002**, *41*, 1347-1349; b). M. Yoshizawa, S. Miyagi, M. Kawano, K. Ishiguro, M. Fujita, *J. Am. Chem. Soc*., **2004**, *126*, 9172-9173; c). H. Takezawa, T. Murase, M. Fujita, *J. Am. Chem. Soc.,* **2012**, *134*, 17420-17423.

13. a). P. D. Frischmann, V. Kunz, F. Würthner, *Angew. Chem. Int. Ed*., **2015**, *54*, 7285-7289; b). S. Shanmugaraju, P. S. Mukherjee, *Chem. Eur. J*., **2015**, *21*, 6656-6663.

14. W. Xiao, C. Hu, M. D. Ward, *Cryst. Growth Des.,* **2013**, *13*, 3197-3200.

15. a). V. Marcos, A. J. Stephens, J. Jaramillo-Garcia, A. L. Nussbaumer, S. L. Woltering, A. Valero, J. F. Lemonnier, I. J. Vitorica-Yrezabal, D. A. Leigh, *Science*, **2016**, *352*, 1555-1559; b). W. Cullen, M. C. Misuraca, C. A. Hunter, N. H. Williams, M. D. Ward, *Nat. Chem*., **2016**, *8*, 231-236; c). M. D. Levin, D. M. Kaphan, C. M. Hong, R. G. Bergman, K. N. Raymond, F. D. Toste, *J. Am. Chem. Soc*., **2016**, *138*, 9682-9693; d). P. Howlader, P. Das, E. Zangrando, P. S. Mukherjee, *J. Am. Chem. Soc*., **2016**, *138*, 1668-1676.

16. B. H. Northrop, Y. R. Zheng, C. H. I. Ki-Whan, P. J. Stang, *Acc. Chem. Res.,* **2009**, *42*, 1554-1563.

17. S. Kitagawa, R. Kitaura, S. I. Noro, *Angew. Chem*., **2004**, *116*, 2388-2430; *Angew. Chem. Int. Ed*., **2004**, *43*, 2334-2375.

18. a). K. Swaminathan Iyer, M. Norret, S. J. Dalgarno, J. L. Atwood, C. L. Raston, *Angew. Chem*., **2008**, *120*, 6462-6466; *Angew. Chem. Int. Ed*., **2008**, *47*, 6362-6366; b). F. Hof, S. L. Craig, C. Nuckolls, J. Rebek, Jr., *Angew. Chem*., **2002**, *114*, 1556-1578; *Angew. Chem. Int. Ed*., **2002**, *41*, 1488-1508.

19. M. Mastalerz, *Angew. Chem. Int. Ed.,* **2010**, *49*, 5042-5053.

20. a). A. P. Bisson, V. M. Lynch, M. K. C. Monahan, E. V. Anslyn, *Angew. Chem. Int. Ed. Engl*., **1997**, *36*, 2340-2342; b). K. E. Jelfs, X. Wu, M. Schmidtmann, J. T. A. Jones, J. E. Warren, D. J. Adams, A. I. Cooper, *Angew. Chem. Int. Ed.,* **2011**, *50*, 10653-10656.

21. a). A. P. Davis, *Org. Biomol. Chem*., **2009**, *7*, 3629-3638; b) S. Kubik, *Angew. Chem. Int. Ed*., **2009**, *48*, 1722-1725.

22. a). Y. Murata, M. Murata, K. Komatsu, *J. Am. Chem. Soc.,* **2003**, *125*, 7152-7153; b). M. Murata, Y. Murata, K. Komatsu, *J. Am. Chem. Soc.,* **2006**, *128*, 8024-8033; c). G. C. Vougioukalakis, M. M. Roubelakis, M. Orfanopoulos, *Chem. Soc. Rev.,* **2010**, *39*, 817-844.

23. a). G. Likhtenshtein in Stilbenes: *Applications in Chemistry, Life Sciences and Materials Science*, Wiley-VCH, Weinheim, **2009**, pp. 159-188; b). For a recent reference see: b) M. Cao, X. Chen, K. Yi, D. Wei, *J. Phys. Chem. C,* **2017**, *5*, 9597-9601.

24. a). G. Likhtenshtein in Stilbenes: *Applications in Chemistry, Life Sciences and Materials Science*, Wiley-VCH, Weinheim, **2009**, pp. 189-223; b). Y. Wang, Y. Jiang, X. Fan, H. Tan, H. Zeng, Y. Wang, P. Chen, M. Huang, H. Bi, *Toxicol. Lett*., **2015**, *236*, 82-89.

Article 7

(The first draft)

From endo-aromatic hemi-butatriene to bridging [3]cumulene units: *carbo*-barrelenes and *carbo*-stilbenes

C. Zhu,[a,b] C. Duhayon,[a,b] B. Kauffmann,[c] A. Saquet,[a,b] X. Cui,[d] V. Maraval,*[a,b] R. Chauvin*[a,b]

[a]*CNRS, LCC (Laboratoire de Chimie de Coordination), 205 route de Narbonne, BP 44099, 31077 Toulouse Cedex 4, France*

[b]*Université de Toulouse, UPS, ICT-FR 2599, 118 route de Narbonne, 31062 Toulouse Cedex 9, France*

[c]*Université de Bordeaux, CNRS, INSERM, UMS 3033 / US 001, Institute Europen de Chimie et Biologie, F-33607 Pessac, France*

[d]

Abstract. The synthesis and spectroscopic, diffractometric and electrochemical properties of novel types of bis-C_{18}-bicyclic derivatives of *carbo*-benzene, *carbo*-barrelenes and *carbo*-stilbenes, are described. The possible cage behaviour of *carbo*-barrelenes is explored for various guest candidates, in particular among H-bond donors.

Introduction

[n]Cumulenes are fascinating molecules that were particularly studied for their bond-length alternation (BLA), and for the decrease *vs* n of the barrier of rotation about their cumulenic axis, corresponding to a *R*/*S* enantiomerization for even n, to a *cis* (*Z*)/*trans*(*E*) stereo-conversion for odd n.[1] The [3]cumulene, or butatriene, motif, *carbo*-mer of the alkene motif, has been more largely considered because of its higher stability as compared to longer homologues.[2] The stability of isolated di- and tetra-alkynylbutatrienes was shown to be highly substituent-dependent, in particular with respect to the steric bulkiness.[3] In the series of n-oligobutatrienylethynylenes (OBEs),, ω-dialkynyl-*carbo*-butadienes (OBE2) were also shown to be quite stable when protected by bulky silyl groups,[4] while ω-dialkynyl-*carbo*-hexatrienes (OBE3) could be isolated and stored in the solid state only.[5] In *carbo*-mers of benzene, the alternating butatriene and butyne edges of the resonating Kekule forms are further stabilized by their resulting globally hemi-butatrienic character.[4] In non-aromatic *carbo*-mers of 1,3-cyclohexadienes,[6] two butatrienes are "simply" conjugated to each other through the ethynylene linker as in *carbo*-butadienes, with a similar moderate stabilizing

effect.. In this report, the use of the ethynylbutatrienylethynylene (EBE) motif as a bridging unit was envisaged in two kinds of *carbo*-meric targets: (i) *carbo*-barrelenes, in which three EBEs bridge two sp^3-C vertices in a pericondensed bimacrocycle, and (ii) *carbo*-stilbenes, in which a a single EBE bridges two sp^2-C vertices of two *carbo*-benzene rings. The parent barrelene molecule, first described by Zimmerman in 1960,[7] was later studied in diversely substituted versions for structural and electronic properties,[8] but also for uses as a ligand in catalysis [9] and for its ability to undergo photo-generated rearrangements.[10] The *carbo*-barrelene derivatives targeted hereafter are attractive for their possible electronic properties, their three conjugated bridges being indeed promising of high charge transport properties, even through the sp^3-C bridgehead junctions.[11] The hollow three-dimensional *carbo*-barrelene framework also suggest possible cage behavior for hosting small molecules or ions, e.g. by several H-bonds to triple bonds to prevent too facile escape through the relatively wide apertures of the capsule of elongated triangular bipyramidal shape.. In spite of tricky synthesis, rigid covalent cages remain indeed attractive for their higher stability as compared to supramolecular counterparts.[12] Regarding the carbo-stilbene targets, the parent stilbene molecules have been thoroughly studied for their chromophoric and photo-isomerization properties, allowing prospects of applications in optical devices and in biomedicine, for example. [13] Upon replacement of the central ethenylene C_2 unit of stilbene by an EBE C_8 unit in the *carbo*-stilbene, conditions of isomerization should *a priori* require milder conditions. Dialkynylbutatrienes are indeed known to undergo rather facile *Z*/*E* isomerization and to exhibit minor thermodynamic preference for either the *E* or *Z* isomer due to the absence of steric interactions between remote substituents in δ positions,[3c, 14] Consequently, the anchorage effect of two very large tetraphenyl-*carbo*-benzenic substituents on either phenomena deserves to be studied.

Results and discussion

The preparation of the *carbo*-barrelenes **1** and **2** was envisaged from the [6]pericyclynedione **3**,[15] key precursor of the synthesis of *para*-disubstituted *carbo*-benzenes.[16] Various bases were tested for the formation of the intermediate tricyclic diol **4a**, by di-addition of the triyne dinucleophile **5** to the macrocyclic diketone **3** (Scheme 1). While the use of ethylmagnesium bromide and *n*-butyllithium failed to produce the diol **4a**, it could be isolated with 31 % yield using LiHMDS. This base was thus applied to the preparation of the tricyclic diol **4b**,

obtained by addition of the triyne **6** to the same diketone **3**. This optimal procedure led however to the formation of the monocyclic side-products **7a,b** and/or **8a,b**.

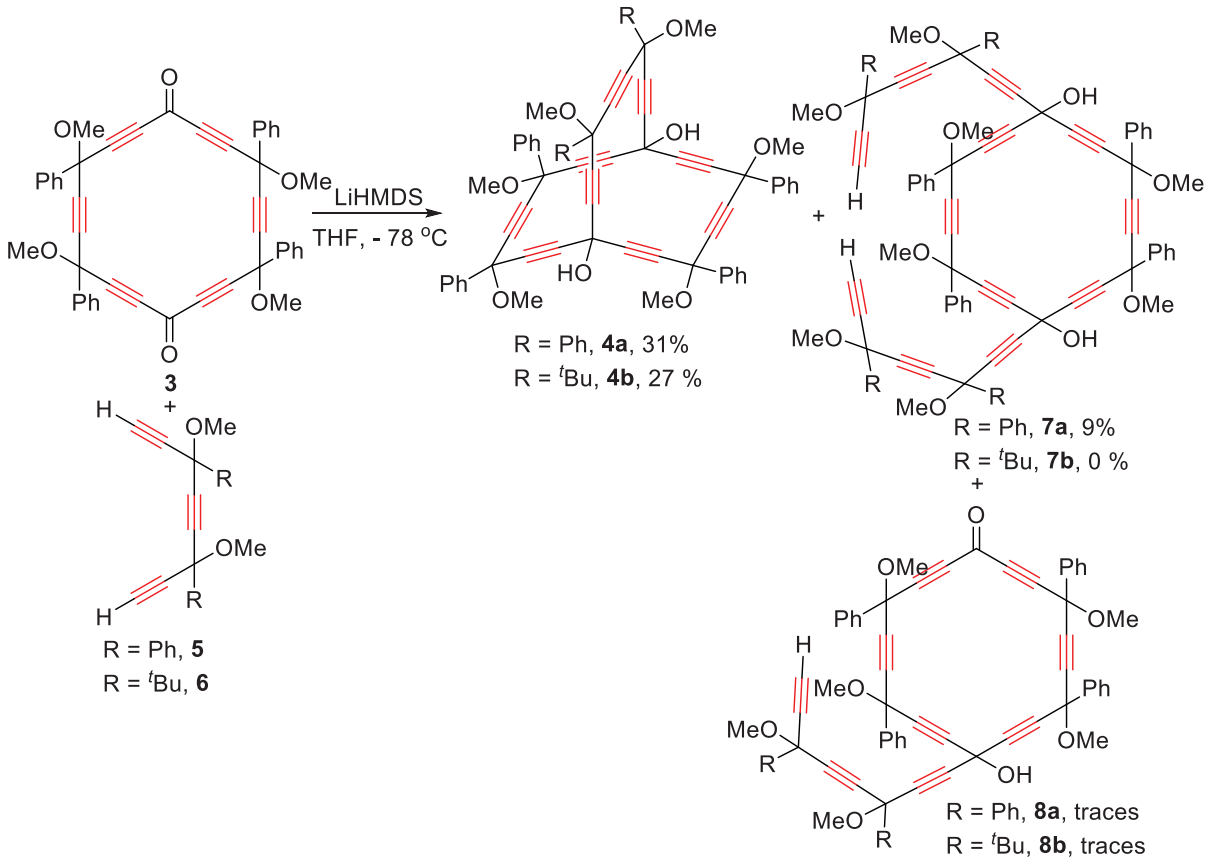

Scheme 1. Synthesis of the tricyclic precursors **4a** and **4b** of *carbo*-barrelenes**.**

The treatment of **4a** with $SnCl_2$ and HCl in dichloromethane at low temperature allowed isolating, after optimization of the amounts of reagents, temperature and reaction time, the *carbo*-barrelene **1** with 28 % yield, as a brown solid. The moderate stability of this first *carbo*-barrelene, possibly due to its two trialkynylcarbinol vertices, motivated their prior transformation into the corresponding methyl ethers in **9a,b**. The treatment of this diethers with the optimal reductive and acidic conditions devised for the preparation of **1** allowed obtaining the *carbo*-barrelene **2** and the partially reduced compound **10**, isolated with 30 % and 17 % yield respectively (Scheme 2). All attempts at formation of the third butatriene unit of the dissymmetrical *carbo*-barrelene **11** by using either a large excess of $SnCl_2$ and HCl, or harsher reaction conditions failed. The donating *tert*-butyl groups make more difficult the formation of the corresponding butatriene moiety, as it was previously observed for the synthesis of *tert*-butyl substituted *carbo*-benzenes,[17] and is here competing with the decomposition of the targeted *carbo*-barrelene **11**, which could not be obtained.

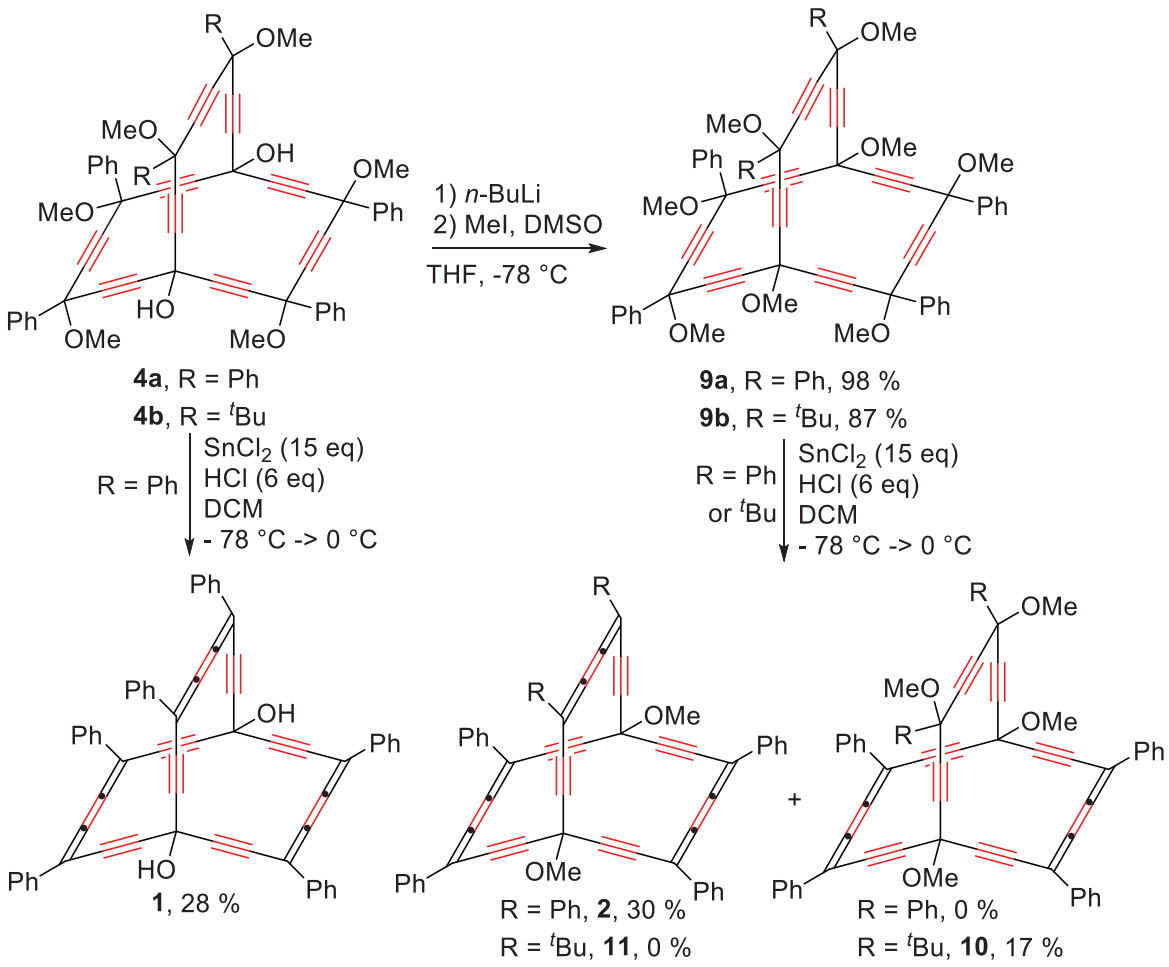

Scheme 2. Synthesis of the *carbo*-barrelenes **1** and **2**, and of the partially reduced derivative **10**.

The three isolated tricyclic compounds **1**, **2** and **10** were found to be highly soluble in most of the classical organic solvents, allowing their full characterization by ^{1}H and ^{13}C NMR spectroscopies in solution. The two *carbo*-barrelenes **1** and **2** display comparable ^{1}H NMR spectral profile in the aromatic region, the six equivalent phenyl groups giving a doublet for the *ortho*-H and two triplets for the *meta*- and *para*-H resonating between 7.8 and 7.3 ppm, namely in the classical range for aromatic H-nuclei on isolated butatrienes, and thus much less deshielded than the signals of aromatic H-nuclei on butatriene units included into a *carbo*-benzene ring. In the proton NMR spectrum of the partially reduced compound **10**, the four phenyl groups are also equivalent and give signals at similar chemical shifts as in **1** and **2**, but two types of methoxy groups are observed, a singlet at 3.74 ppm counting for six protons and corresponding to the two equivalent methoxy groups occupying the vertices of the tricycle, and two singlets at 3.57 and 3.56 ppm also counting for six protons and corresponding to the methoxy groups of the two diastereoisomers of the non-reduced di-*tert*-butyl-dimethoxy-

butyne edge of **10**. The full assignment of the ^{1}H and ^{13}C spectra could be performed by 2D-NMR experiments (see ESI).

The absorption properties of the three tricyclic chromophores were studied in chloroform solutions. The two *carbo*-barrelenes **1** and **2** exhibit identical UV-visible spectra, with a main intense absorption band at λ_{max} = 401 nm, while the one of **10** is slightly bathochromically shifted at λ_{max} = 418 nm, these values being consistent with the maximum absorption wavelengths of previously reported isolated dialkynyldiphenylbutatrienes (Figure 2).[3d] These three derivatives are much less chromophoric than *carbo*-benzenes (ε often higher than 200 000 $L.mol^{-1}.cm^{-1}$), with molar extinction coefficients lower than 100 000 $L.mol^{-1}.cm^{-1}$.

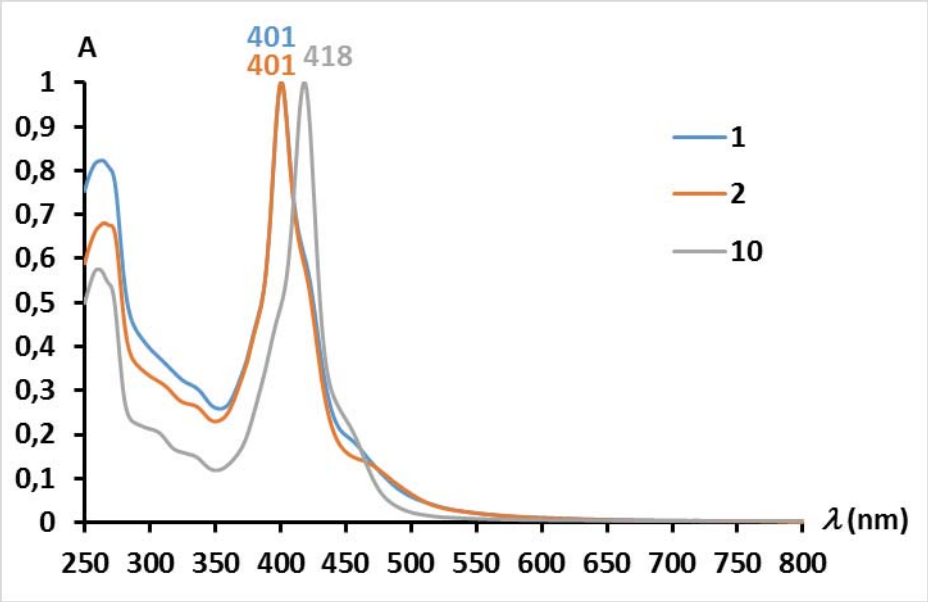

Figure 2. Normalized UV-vis absorption spectra of the bis- and tris-butatrienic derivatives **1**, **2** and **10** in chloroform solutions.

The *carbo*-barrelenes **1** and **2**, and the partially reduced derivative **10** were also characterized by X-ray diffraction analysis of single crystals deposited from *n*-heptane or DCM solutions (Figure 3). Solvent molecules were found in the crystal lattice of **1** and **2**, but not at the center of the tricyclic cage, the DCM molecule being too large to enter inside the hole of the *carbo*-barrelene host. A disorder was observed in the structure of the partially reduced derivative **10**, due to the presence of the two diastereoisomers related to the non-reduced edge in the crystal.

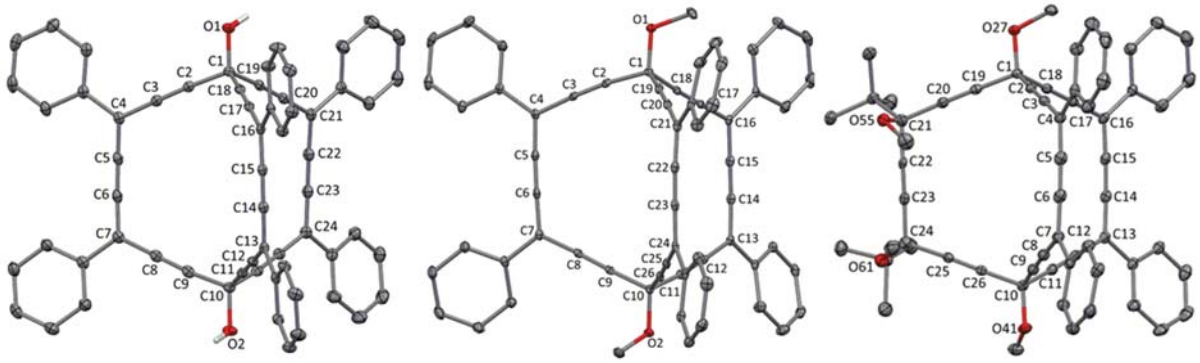

Figure 3. Molecular views of the X-ray crystal structures of the *carbo*-barrelenes **1** and **2**, and of the partially reduced derivative **10**. Thermal ellipsoids at the 30 % probability level. For clarity, unnecessary hydrogen atoms and solvent molecules (for **1** and **2**) are omitted (for more details see ESI).

The electrochemical behavior of **1** and **10** was studied by cyclic and square-wave voltammetry in chloroform solution (Table 1). The two products exhibited two reduction processes and one oxidation process, none of them being reversible. The values of the reduction and oxidation potentials being quite different for the two products, the processes probably occur at different locations of the molecules. The partially reduced *carbo*-barrelene derivative **10** was found to be both the most difficult to reduce and the most difficult to oxidize, with higher values of potentials in absolute value as compared to **1**.

	Reductions			Oxidations		
	Red_1, E_p	Red_2, E_p	Red_3, E_p	Ox_1, E_p	Ox_2, E_p	Ox_3, E_p
1	- 0.87	- 1.20	-	1.45	-	-
10[a]	- 1.11	- 1.28	-	1.61	-	-

Table 1. Voltammetric data for the three *carbo*-barrelene derivatives **1** and **10** in V/SCE. Supporting electrolyte: $CHCl_3$ + 0.1 mol/L [TBA][PF_6]; scan rate: 0.2 V/s; [a] Measurements performed after deposition of the compound on the working electrode by dipping it in a DCM solution of **10** (see SI for more details).

The isolation of traces amounts of the side-products **8a** and **8b** during the synthesis of the tricyclic precursor of *carbo*-barrelenes **4a** and **4b** motivated the search for a more efficient way to produce these monocyclic adducts, which can be seen as intermediates of the preparation of *carbo*-mers of stilbene **12a** and **12b**. The straightforward addition of two equivalents of the known [6]pericyclynone **13** to one equivalent of the triyne **5** or **6** giving

only traces amounts of the bicyclic product **14a** and **14b**, the use of a sequential synthetic strategy, through the intermediates **8a** and **8b** was envisaged (Scheme 3).[8c]

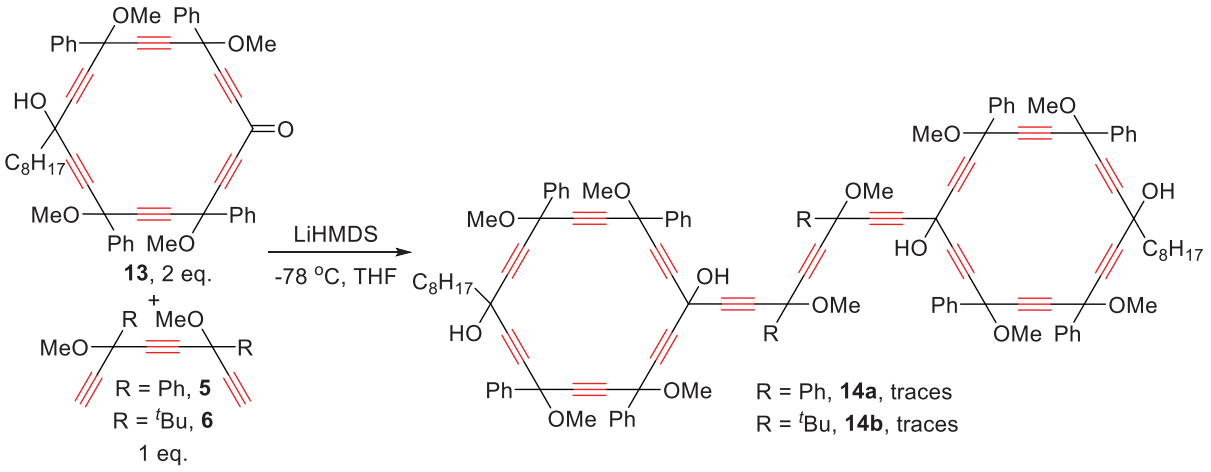

Scheme 3. Attempts at straightforward synthesis of *carbo*-stilbene precursors **14a,b**.

The optimal use of 1.5 equivalent of triyne **5** or **6** and 1.1 equivalent of EtMgBr as base for one equivalent of **3** allowed obtaining the targeted monoadducts **8a** and **8b** as main products, accompanied by small quantities of the diadducts **7a** and **7b**, along with some unreacted **3** and **5** or **6**. The monoketones **8a** and **8b** were then treated with n-octyllithium to give the diols **15a** and **15b**, which were subsequently dimethylated into **16a** and **16b** respectively. Finally, addition of these precursors to the monoketone **13** in the presence of LiHMDS allowed isolating with reasonable yields the bis-macrocyclic precursors **17a** and **17b**, and the corresponding *carbo*-stilbenes **12a** and **12b** after a reductive and acidic treatment with $SnCl_2$ and HCl (Scheme 4). These two *carbo*-stilbenes were isolated as black solids and were found to be very poorly soluble, despite the presence of an octyl chain, previously shown to be an efficient solubilizing substituent,[16c] at each side of the molecule, and the presence of two t-butyl groups on the central butatriene unit of **12b**, also recently described to increase the solubility of *carbo*-benzenes.[17]

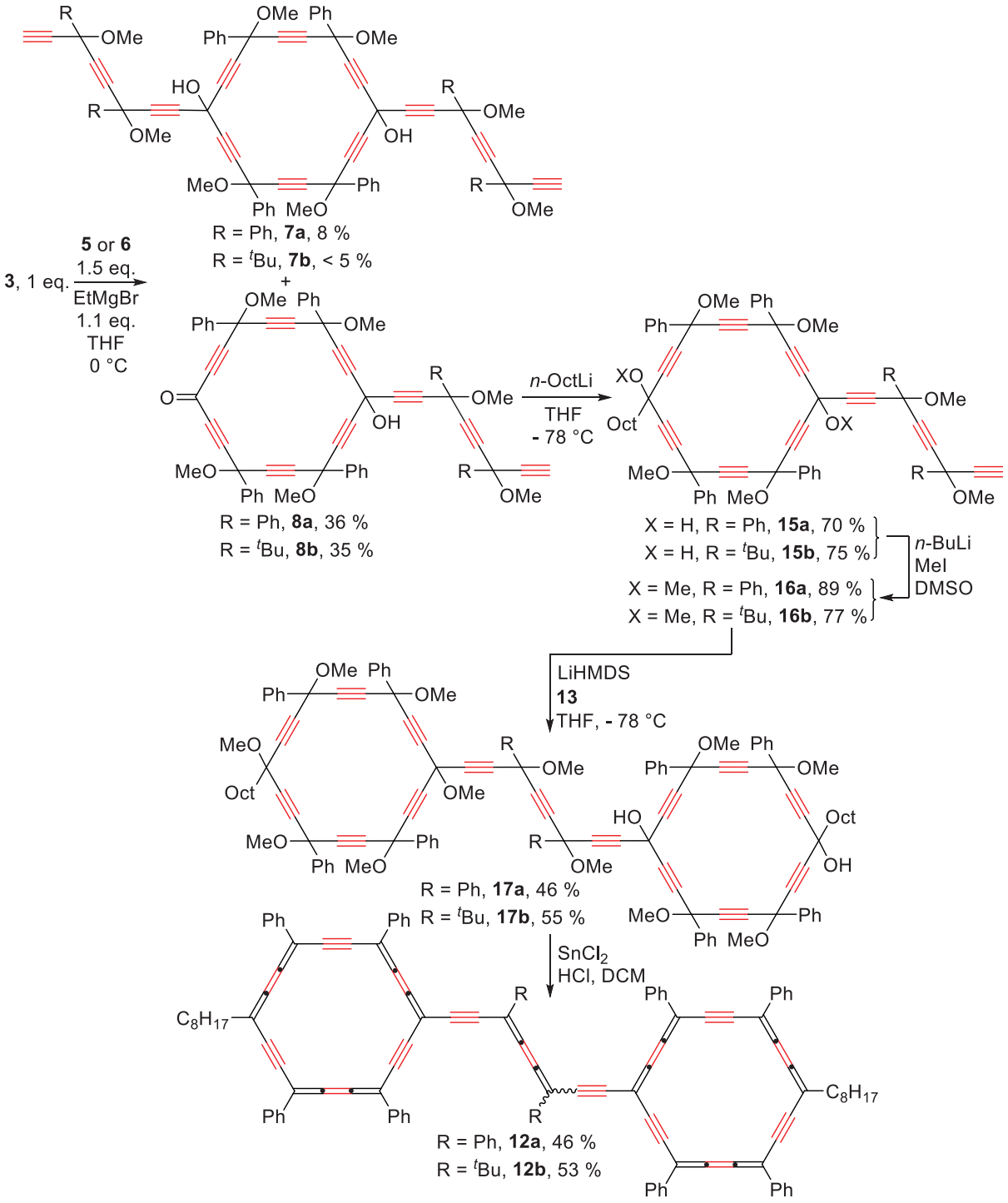

Scheme 4. Synthesis of the *carbo*-stilbenes **12a** and **12b**.

The very low solubility of these two *carbo*-stilbenes **12a** and **12b** prevented their full characterization. In particular, it was almost impossible to record ^{13}C NMR spectra of sufficient quality to be described. Nevertheless, ^{1}H and COSY ^{1}H-^{1}H NMR of the two compounds could be performed, and ^{1}H-^{13}C HSQC and HMBC experiments at 600 MHz at 45 °C were also realized on the slightly more soluble derivative **12b**, thus allowing to propose an assignment of the ^{1}H NMR signals, although it was made difficult by the duplication of all the

signals due to the presence in both samples of a mixture of the *cis* and *trans* isomers of the central butatriene unit of the *carbo*-stilbenes, the ratio between the *trans* and *cis* isomers being about 52:48 for **12a** and 56:44 for **12b** (Figure 4 and ESI).

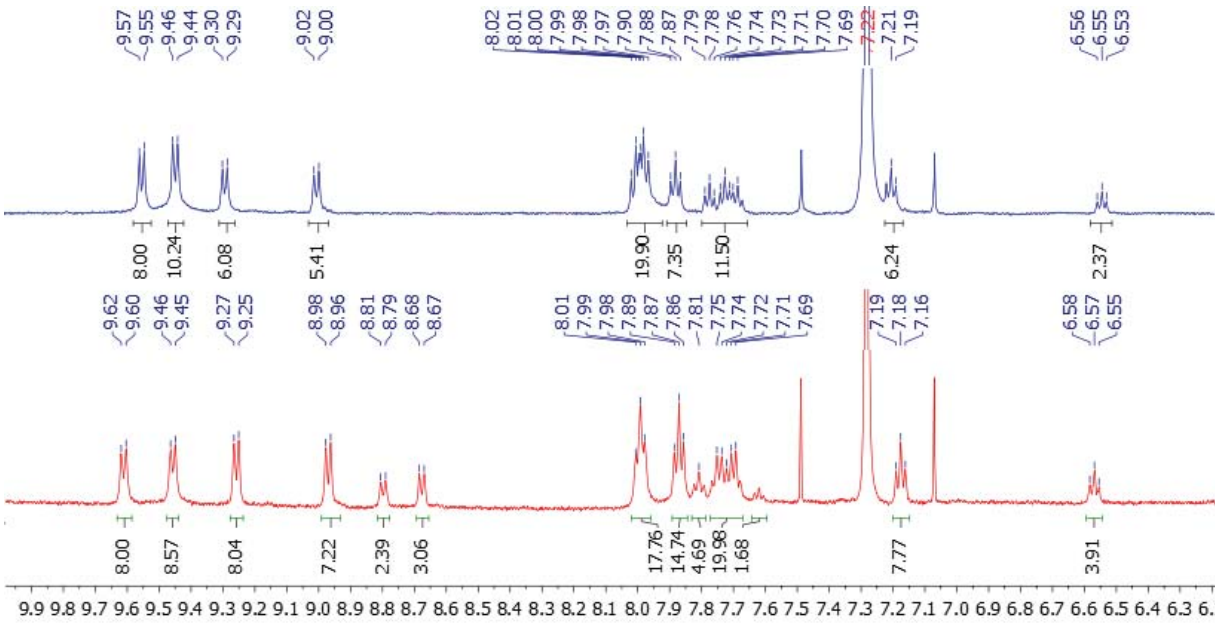

Figure 4. Aromatic region of the ^{1}H NMR of the *carbo*-stilbenes **12a** (*bottom*) and **12b** (*top*) in $CDCl_3$ (500 MHz; 55 °C).

In both spectra, some highly deshielded signals above 9 ppm, characteristics of the *ortho* H-nuclei of the aryl substituents of *carbo*-benzenes, were observed, but a shielded triplet at 6.5 ppm also appeared. This latter signal was attributed to the *cis*-isomer of *carbo*-stilbenes, some of the phenyl substituents of one *carbo*-benzene ring being indeed in this isomer in the shielding cone of the other aromatic macrocycle, and *vice-versa*. This phenomenon being observed for both *carbo*-stilbenes, these shielded signals cannot be assigned to the phenyl substituents on the butatriene unit.

The absorption properties of the two *carbo*-stilbenes **12a** and **12b** were studied in chloroform solutions. They exhibit comparable UV-visible spectra with two intense absorption bands at 459 ± 4 and 550 ± 3 nm followed by a smaller band at higher wavelength (Figure 5). These spectral profiles are very similar to that of the *carbo*-biphenyl **19**,[18] in which the two *carbo*-benzenes are conjugated to each other not through a diethynylbutatriene

linker, but through a short ethynyl linker (Figure 5). As expected, the longer π-conjugated linker of the *carbo*-stilbenes **12a** and **12b** induce a bathochromic shift of their absorption bands as compared to those of the *carbo*-biphenyl **19**. The stronger effect was observed on the small absorption bands at high wavelength with a red shift of 74 nm from the *carbo*-biphenyl **19,** having the shortest π-conjugated skeleton, to the *carbo*-stilbene **12a** exhibiting the largest π-conjugated system through additional delocalization with the two phenyl substituents of the central butatriene bridge as compared to **12b**.

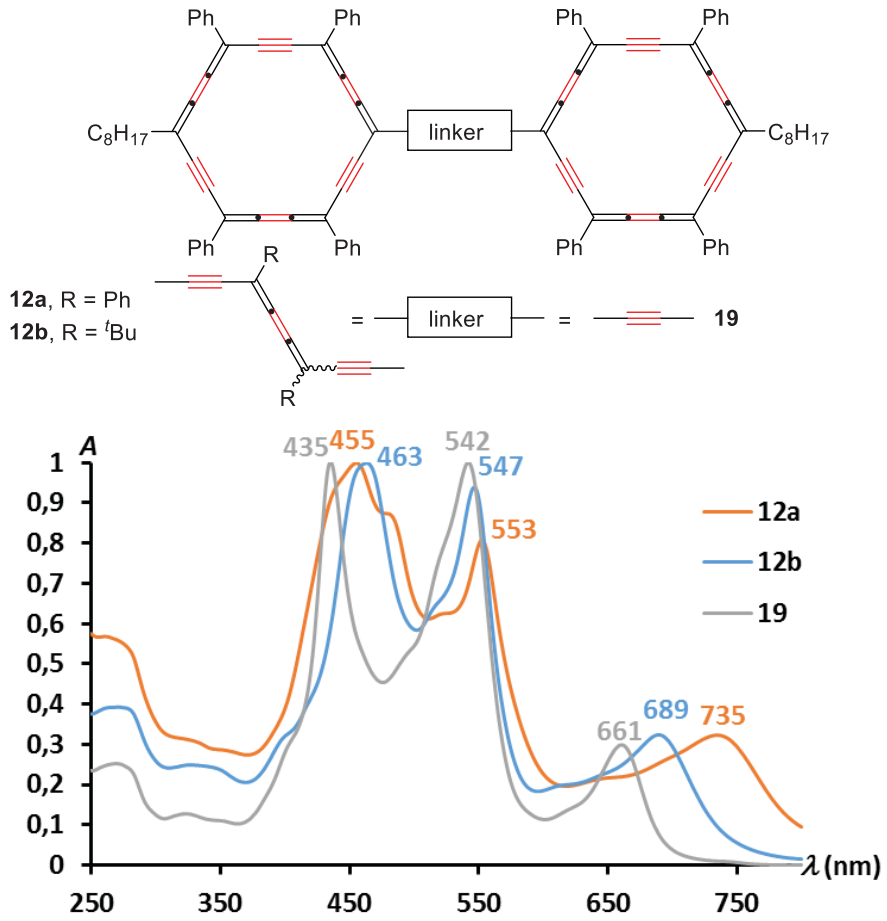

Figure 5. Normalized UV-visible absorption spectra of the two *carbo*-stilbenes **12a** and **12b** and of the *carbo*-biphenyl **19** in chloroform solutions.

The electrochemical behavior of the *carbo*-stilbene **12b** was also studied by square-wave and cyclic voltammetry, while **12a** appeared to be too poorly soluble to give satisfactory results. For solubility reasons, the measurements were performed after deposition of the compound on the working electrode by dipping in a DCM solution of **12b**. Because of this unconventional method of analysis, will the first oxidation and reduction potentials only be

discussed. In these conditions, a quasi-reversible reduction process was observed at $E_{1/2}$ = – 0.65 V/SCE, and an irreversible oxidation was evidenced at 1.11 V/SCE. These results are in agreement with those previously obtained for the *carbo*-biphenyl **19**, exhibiting a first reduction potential at - 0.58 V/SCE.[18] The low reduction potentials of both **12b** and **19** are consistent with their extended π-conjugated systems.

References

1. a) J. A. Januszewski, D. Wendinger, C. D. Methfessel, F. Hampel, R. R. Tykwinski, *Angew. Chem. Int. Ed.* **2013**, *52*, 1817-1821 ; b) D. Wendinger, R. R. Tykwinski, *Acc. Chem. Res*. **2017**, *50*, 1468-1479.
2. L. Leroyer, V. Maraval, R. Chauvin, *Chem. Rev*. **2012**, *112*, 1310-1343.
3. a) J.-D. van Loon, P. Seiler, F. Diederich, *Angew. Chem. Int. Ed*. **1993**, *32*, 1187-1189; b) A. Auffrant, F. Diederich, C. Boudon, J.-P. Gisselbrecht, M. Gross, *Helv. Chim. Acta* **2004**, *87*, 3085-3094; c) A. Auffrant, B. Jaun, P. D. Jarowski, K. N. Houk, F. Diederich, *Chem. Eur. J.* **2004**, *10*, 2906-2911; d) V. Maraval, L. Leroyer, A. Harano, C. Barthes, A. Saquet, C. Duhayon, T. Shinmyozu, R. Chauvin, *Chem. Eur. J.* **2011**, *17*, 5086-5100.
4. For references on *carbo*-mers, see: a) R. Chauvin, *Tetrahedron Lett*. **1995**, *36*, 397-401; b) V. Maraval, R. Chauvin, *Chem. Rev*. **2006**, *106*, 5317-5343; c) K. Cocq, C. Lepetit, V. Maraval, R. Chauvin, *Chem. Soc. Rev*. **2015**, *44*, 6535-6559.
5. a) A. Rives, V. Maraval, N. Saffon-Merceron, R. Chauvin, *Chem. Eur. J*. **2012**, *18*, 14702-14707; b) A. Rives, V. Maraval, N. Saffon-Merceron, R. Chauvin, *Chem. Eur. J*. **2014**, *20*, 483-492.
6. A. Rives, I. Baglai, C. Barthes, V. Maraval, N. Saffon-Merceron, A. Saquet, Z. Voitenko, Y. Volovenko, R. Chauvin, *Chem. Sci*. **2015**, *6*, 1139-1149.
7. H. E. Zimmerman, R. M. Paufler, *J. Am. Chem. Soc*., **1960**, *82*, 1514-1515.
8. a). C. G. Krespan, B. C. McKusick, T. L. Cairns, *J. Am. Chem. Soc.,* **1961**, *83*, 3428-3432; b). R. G. Miller, M. Stiles, *J. Am. Chem. Soc.,* **1963**, *85*, 1798-1800; c). H. E. Zimmerman, G. L. Grunewald, R. M. Paufler, M. A. Sherwin, *J. Am. Chem. Soc.,* **1969**, *91*, 2330-2338; d). M. W. Wagaman, E. Bellmann, M. Cucullu, R. H. Grubbs, *J. Org. Chem.,* **1997**, *62*, 9076-9082; e). M. W. Wagaman, R. H. Grubbs, *Macromolecules,* **1997**, *30*, 3978-3985.
9. a). M. A. Esteruelas, L. A. Oro, *Coord. Chem. Rev*., **1999**, *193-195*, 557-618; b). T. Nishimura, T. Kawamoto, M. Nagaosa, H. Kumamoto, T. Hayashi, *Angew. Chem. Int. Ed*., **2010**, *49*, 1638-1641; c). R. Shintani, M. Takeda, T. Nishimura, T. Hayashi, *Angew. Chem. Int. Ed.,* **2010**, *49*, 3969-3971; d) M. Schlesinger, M. Hofmann, T. Rüffer, D. Schaarschmidt, H. Lang, S. Theilacker, M. Schürmann, K. Jurkschat, M. Mehring, *Eur. J. Inorg. Chem.,* **2013**, 2930-2939.
10. H. E. Zimmerman, D. Armesto, *Chem. Rev.,* **1996**, *96*, 3065-3112

11. The macro-aromatic *carbo*-benzene ring was reported to exhibit an unprecedented single molecule conductance as compared to molecules of similar length. The conductance being known to be higher for non aromatic molecules, and to increase with the number of parallel p-conjugated systems, the non aromatic *carbo*-barrelene presenting three parallel conduction pathways of similar structure as those of the *carbo*-benzene appears thus as a very promising target for the study of charge transport properties. a) Z. H. Li, M. Smeu, A. Rives, V. Maraval, R. Chauvin, M. A. Ratner, E. Borguet, *Nat. Commun*., **2015**, *6*, 6321; b) H. Vazquez, R. Skouta, S. Scheebeli, M. Kamenetska, R. Breslow, L. Venkataraman, M. S. Hybertsen, *Nature Nanotech*. **2012**, *7*, 663-667; c) W. Chen, H. Li, J. R. Widawsky, C. Appayee, L. Venkataraman, R. Breslow, *J. Am. Chem. Soc*. **2014**, *136*, 918-920.
12. M. Mastalerz, *Angew. Chem. Int. Ed.,* **2010**, *49*, 5042-5053.
13. For applications in optical devices see for example: a) G. Likhtenshtein in Stilbenes: *Applications in Chemistry, Life Sciences and Materials Science*, Wiley-VCH, Weinheim, **2009**, pp. 159-188; b). For a recent reference see: b) M. Cao, X. Chen, K. Yi, D. Wei, *J. Phys. Chem. C,* **2017**, *5*, 9597-9601. For applications in biomedecine, see for example: c) G. Likhtenshtein in Stilbenes: *Applications in Chemistry, Life Sciences and Materials Science*, Wiley-VCH, Weinheim, **2009**, pp. 189-223; d) Y. Wang, Y. Jiang, X. Fan, H. Tan, H. Zeng, Y. Wang, P. Chen, M. Huang, H. Bi, *Toxicol. Lett*., **2015**, *236*, 82-89.
14. a) P. D. Jarowski, F. Diederich, K. N. Houk, *J. Phys. Chem. A* **2006**, *110*, 7237-7246; b) P. Gawel, Y.-L. Wu, A. D. Finke, N. Trapp, M. Zalibera, C. Boudon, J.-P. Gisselbrecht, W. B. Schweizer, G. Gescheidt, F. Diederich, *Chem. Eur. J*. **2015**, *21*, 6215-6225.
15. a) L. Maurette, C. Tedeschi, E. Sermot, M. Soleilhavoup, F. Hussain, B. Donnadieu, R. Chauvin, *Tetrahedron* **2004**, *60*, 10077-10098; b) L. Leroyer, C. Zou, V. Maraval, R. Chauvin, *C. R. Chimie*, **2009**, *12*, 412-419. For early references on pericyclynes see: c) L. T. Scott, G. J. DeCicco, J. L. Hyun, G. Reinhardt, J. *Am. Chem. Soc*. **1983**, *105*, 7760-7761; d) L. T. Scott, G. J. DeCicco, J. L. Hyun, G. Reinhardt, *J. Am. Chem. Soc*. **1985**, *107*, 6546-6555.
16. a) L. Leroyer, C. Lepetit, A. Rives, V. Maraval, N. Saffon-Merceron, D. Kandaskalov, D. Kieffer, R. Chauvin, *Chem. Eur. J*. **2012**, *18*, 3226-3240 ; b) I. Baglai, M. de Anda-Villa, R. M. Barba-Barba, C. Poidevin, G. Ramos-Ortiz, V. Maraval, C. Lepetit, N. Saffon-Merceron, J.-L. Maldonado, R. Chauvin, *Chem. Eur. J*. **2015**, *21*, 14186-14195; c) C. Zhu, A. Rives, C. Duhayon, V. Maraval, R. Chauvin, *J. Org. Chem*. **2017**, *82*, 925-935; d) C. Zhu, T.-H. Wang, C.-J. Su, S.-L. Lee, A. Rives, C. Duhayon, B. Kauffmann, V. Maraval, C.-h. Chen, H.-F. Hsu, R. Chauvin, *Chem. Commun*. **2017**, *53*, 5902-5905.
17. D. Listunov, C. Duhayon, A. Poater, A. Saquet, V. Maraval, R. Chauvin, *submitted for publication*.
18. C. Zhu, C. Duhayon, B. Kauffmann, A. Poater, A. Saquet, V. Maraval, R. Chauvin, *submitted for publication*.

Supplementary information

From endo-aromatic hemi-butatriene to connecting [3]cumulene motifs: *carbo*-barrelenes and *carbo*-stilbenes

C. Zhu,[a,b] C. Duhayon,[a,b] B. Kauffmann,[c] A. Saquet,[a,b] X. Cui,[d] V. Maraval,*[a,b] R. Chauvin*[a,b]

[a] *CNRS, LCC (Laboratoire de Chimie de Coordination), 205 route de Narbonne, BP44099, 31077 Toulouse Cedex 4, France*

[b] *Université de Toulouse, UPS, ICT-FR 2599, 118 route de Narbonne, 31062 Toulouse Cedex 9, France*

[c] *Université de Bordeaux, CNRS, INSERM, UMS3033/US001, Institut Européen de Chimie et Biologie, F-33607 Pessac, France*

[d]

Table of contents

1. General remarks

THF, diethyl ether (Et_2O), pentane and dichloromethane (DCM) were dried with a PureSolv-MD-5 Innovative Technology system for the purification of solvents. All other reagents were used as commercially available. In particular, commercial solutions of LiHMDS were 1 M in THF, solutions of *n*-BuLi were 2.5 M in hexane and 1.6 M in THF, solutions of HCl were 2 M in diethyl ether, $SnCl_2$ was anhydrous. Silica gel (60 Å, C.C 70-200 μm) was used for column chromatography. Silica gel thin layer chromatography plates (60F254, 0.25 mm) were revealed under UV-light and/or by treatment with an ethanolic solution of phosphomolybdic acid (20%). The following analytical instruments were used, ^1H and ^{13}C NMR: Avance 300, Avance 400, Avance 400 HD, Avance 500 and Avance 600 spectrometers; Mass spectroscopy: Quadrupolar Nermag R10-10H spectrometer; UV-Visible: Perkin-Elmer UV-Vis Win-Lab Lambda 950; IR: Perkin-Elmer Spectrum 100 FT-IR spectrometer; Dual Syringe Infusion Pump was used for macrocyclization reactions. All the ^1H and ^{13}C signals were assigned according to chemical shifts, spin-spin coupling constants, splitting patterns, signal intensities, and 2D NMR experiments; NMR chemical shifts are given in ppm with positive values to high frequency relative to the tetramethylsilane reference. Coupling constants *J* are in Hertz. UV-Visible extinction molar coefficient ε is in $L \cdot mol^{-1} \cdot cm^{-1}$ and wavelengths λ in nm. IR frequency ν in cm^{-1}.

2. Experimental procedures and characterizations

2.1. General procedure A for the preparation of 9a and 9b.

A solution of diol **4a** or **4b** (1 eq.) in THF was treated with *n*-BuLi (2 eq. 1.6 M in THF) at -78 °C. The reaction mixture was stirred at this temperature for 10 min before addition of MeI (6 eq.). The solution was slowly warmed up to -25 °C, and then anhydrous DMSO (2 eq.) was added. The resulting mixture was warmed up to room temperature and stirred overnight. After treatment with distilled water, the aqueous layer was extracted with Et_2O, the combined organic layers were dried over $MgSO_4$ and concentrated under reduced pressure. The residue was purified by silica gel column chromatography.

2.2. General procedure B for the preparation of 4a and 4b.

A solution of triyne **5** or **6** (1 eq.) in THF was treated with LiHMDS (4eq. 1 M in THF) at -78 ^{o}C. The reaction mixture was stirred for 1 h at this temperature. This solution, and a solution of [6]pericyclynedione **3** (1eq.) in THF were added simultaneously to a round-bottom flask (500 ml) filling with THF at -78 ^{o}C (rate of addition: 20 mL/h). The resulting mixture was slowly warmed up to room temperature and stirred overnight. After treatment with a saturated solution of NH_4Cl, the solution was carefully concentrated under reduced pressure, and then extracted with EtOAc. The organic layer was dried over $MgSO_4$ and concentrated under reduced pressure, before purification of the residue by silica gel column chromatography.

2.3. General procedure C for the preparation of *carbo*-barrelene derivatives.

A solution of **4a**, **9a** or **9b** (1 eq.) in DCM was treated with anhydrous $SnCl_2$ (15 eq.) and HCl (6 eq., 2 M in Et_2O) at -78 ^{o}C. The reaction mixture was stirred for 15 min at this temperature, and then slowly warmed up to -10 ^{o}C during 1.5 h and stirred at this temperature for more 1 h. After addition of aqueous NaOH (6 eq., 2 M), the reaction mixture was filtrated through celite® and washed with a saturated NaCl solution. The organic layer was dried over $MgSO_4$ and concentrated under reduced pressure, before purification of the residue by flash silica gel column chromatography to give **1**, **2** and **10** respectively.

2.4. General procedure D for the preparation of 8a and 8b.

A solution of triyne **5** or **6** (1.5 eq.) in THF was treated with EtMgBr (1.1 eq., 1 M) at 0 ^{o}C. The mixture was stirred for 15 min at this temperature and 2 h at room temperature, and dropwise added to a solution of [6]pericyclynedione **3** (1 eq.) in THF at 0 ^{o}C. The reaction mixture was stirred overnight at room temperature. After treatment with the distillated water, the aqueous layer was extracted with Et_2O, the combined organic layers were dried over $MgSO_4$ and concentrated under reduced pressure. The residue was purified by silica gel column chromatography.

2.5. General procedure E for the preparation of 15a and 15b.

To a solution of **8a** or **8b** (1 eq.) was slowly added freshly prepared octyllithium (4 eq.) at -78 °C. The mixture was stirred for 30 min at -78 °C and then slowly warmed up to -30 °C during 2 h. After treatment with a saturated aqueous NH_4Cl solution, the aqueous layer was extracted with EtOAc, and the combined organic layers were dried over $MgSO_4$ and concentrated under reduced pressure. The residue was purified by silica gel column chromatography.

2.6. General procedure F for the preparation of 16a and 16b.

A solution of **15a** or **15b** (1 eq.) in THF was treated with *n*-BuLi (2 eq.) at -78 °C. The reaction mixture was stirred for 10 min and then MeI (6 eq.) was added at the same temperature. Anhydrous DMSO (2 eq.) was added at -25 °C, and the reaction mixture was warmed up to room temperature and stirred overnight. After treatment with the distillated water, the aqueous layer was extracted with Et_2O, the combined organic layers were dried over $MgSO_4$ and concentrated under reduced pressure. The residue was purified by silica gel column chromatography.

2.7. General procedure G for the preparation of 17a and 17b.

A solution of **16a** or **16b** (1 eq.) in THF was treated with LiHMDS (6 eq.) at -78 ^oC. The reaction mixture was stirred for 1 h at this temperature, and then transferred to a solution of **13** (1.2 eq.) in THF at -78 ^oC. The resulting solution was slowly warmed up to room temperature and then stirred overnight. After treatment with a saturated aqueous NH_4Cl solution, the aqueous layer was extracted with EtOAc, and the combined organic layers were dried over $MgSO_4$, and concentrated under reduced pressure. The residue was purified by silica gel column chromatography.

2.8. General procedure H for the preparation of 12a and 12b.

A solution of **17a** or **17b** (1 eq.) in DCM was treated with anhydrous $SnCl_2$ (25 eq.) and HCl (50 eq.) at -78 ^oC. The reaction mixture was stirred for 20 min at this temperature and then for 2 h at 0 ^oC. After neutralization with aqueous NaOH solution (50 eq.), the mixture was filtrated through celite®, and then washed with a saturated NaCl solution.0Tthe organic layer was dried over $MgSO_4$, and concentrated under reduced pressure. The residue was purified by washing with pentane and Et_2O and filtration through glass fiber to give **12a** or **12b** respectively as black solids.

1,10-dimethoxy-4,7,13,16,21,24-hexaphenylbicyclo[8.8.8]hexacosa-4,5,6,13,14,15,21,22,23-nonaen-2,8,11,17,19,25-hexayne (1)

Prepared from **4a** following the general procedure C. Elution mixture: Pentane/acetone 3:1. Yield: 28 %. Brown solid.

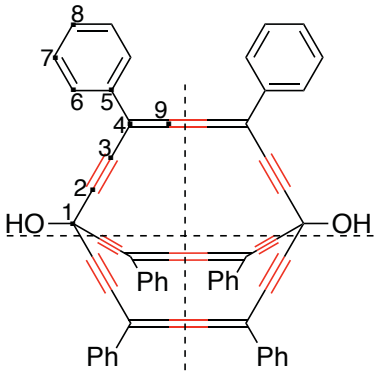

^{1}H NMR (400 MHz, CD_2Cl_2) δ 7.78 (d, J = 7.3 Hz, 12H, H^6), 7.46 (*pseudo*-t, J = 7.5 Hz, 12H, H^7), 7.38 (t, J = 7.3 Hz, 6H, H^8), 3.46 (s, 2H, -O*H*).

^{13}C{^{1}H} NMR (101 MHz, CD_2Cl_2) δ 150.7 (C^9), 134.9 (C^5), 129.5 (C^8), 128.9 (C^7), 127.2 (C^6), 103.8 (C^4), 94.5 (C^2), 79.9 (C^3), 57.2 (C^1).

HRMS (MALDI-TOF/DCTB): *m/z*: calculated for $[M]^+$ $C_{62}H_{32}O_2$: 808.2402, found: 808.2543.

UV−vis ($CHCl_3$): λ_{max} = 401 nm (ε = 31000).

FT-IR: ν: 3397-3270 (O-H); 2922, 2853 (C-H); 1710 (C=C=C=C); 1451 (C=C, Ph); 1259, 1078, 1014 (C-O).

hexaphenylbicyclo[8.8.8]hexacosa-4,5,6,13,14,15,21,22,23-nonaen-2,8,11,17,19,25-hexayne-1,10-diol (2)

Prepared from **9a** following the general procedure C. Elution mixture: Pentane/EtOAc 4:1. Yield: 31 %. Brown solid.

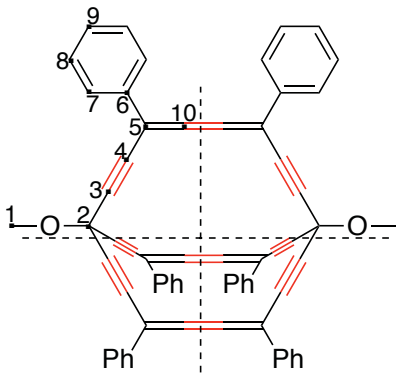

^{1}H NMR (400 MHz, CD_2Cl_2) δ 7.78 (d, J = 7.5 Hz, 12H, H^7), 7.47 (*pseudo*-t, J = 7.6 Hz, 12H, H^8), 7.38 (t, J = 7.3 Hz, 6H, H^9), 3.81 (s, 6H, H^1).

^{13}C{^{1}H} NMR (101 MHz, CD_2Cl_2) δ 150.7 (C^{10}), 135.0 (C^6), 129.5 (C^9), 128.9 (C^8), 127.1 (C^7), 103.8 (C^5), 92.9 (C^3), 81.1 (C^4), 63.4 (C^2), 54.3 (C^1).

HRMS (MALDI-TOF/DCTB): *m/z*: calculated for $[M]^+$ $C_{64}H_{36}O_2$: 836.2715, found: 836.2813.

UV−vis ($CHCl_3$): λ_{max} = 401 nm (ε = 21000).

FT-IR: *v*: 2921, 2852 (C-H); 1712 (C=C=C=C); 1453 (C=C, Ph); 1073, 1025 (C-O).

4,7,13,16,21,24-hexamethoxy-4,7,13,16,21,24-hexaphenylbicyclo[8.8.8]hexa-cosa-2,5,8,11,14,17,19,22,25-nonayne-1,10-diol (4a)

Prepared from **5** and **3** following the general procedure B. Elution mixture: Pentane/EtOAc 3:1. Yield: 31 %. Yellow solid.

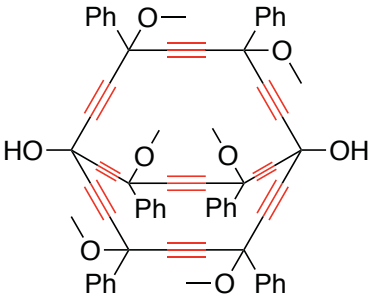

^{1}H NMR (400 MHz, $CDCl_3$) δ 7.88 - 7.55 (m, 12H, *o*-C_6H_5), 7.54 - 7.11 (m, 18H, *m*-, *p*-C_6H_5), 3.97 - 3.12 (m, 20H, -OCH_3, -O*H*).

^{13}C{^{1}H} NMR (101 MHz, $CDCl_3$) δ 139.0 - 138.7 (*i*-C_6H_5), 129.3 - 128.9 (*p*-C_6H_5), 128.6 - 128.5 (*m*-C_6H_5), 126.5 - 126.2 (*o*-C_6H_5), 84.9 - 83.7 (C(OH)($C{\equiv}C$)$_3$), 81.4 - 80.2 ($C{\equiv}C$), 72.0 - 71.6 ($C(OCH_3)$Ph), 54.2 - 54.0 (C(OH)(C≡C)$_3$), 53.6 - 53.3 (-OCH_3).

HRMS (MALDI-TOF/DCTB): *m/z*: $[M+Na]^+$ calculated for $C_{68}H_{50}O_8Na$: 1017.3403, found: 1017.3395.

4,7-di-tert-butyl-4,7,13,16,21,24-hexamethoxy-13,16,21,24-tetraphenylbicyclo[8.8.8]hexacosa-2,5,8,11,14,17,19,22,25-nonayne-1,10-diol (4b)

Prepared from **6** and **3** following the general procedure B. Elution mixture: Pentane/EtOAc 5:1. Yield: 27 %. Yellow solid.

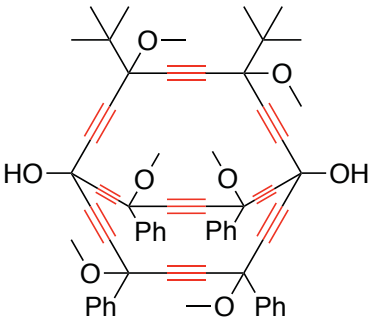

^{1}H NMR (400 MHz, $CDCl_3$) δ 7.86 - 7.53 (m, 8H, *o*-C_6H_5), 7.48 - 7.24 (m, 12H, *m*-, *p*-C_6H_5), 3.70 - 3.04 (m, 20H, -OCH_3, -O*H*), 1.19 - 0.99 (m, 18H, -C(CH_3)$_3$).

^{13}C{^{1}H} NMR (101 MHz, $CDCl_3$) δ 139.2 - 138.6 (*i*-C_6H_5), 129.3 - 129.0 (*p*-C_6H_5), 128.6 - 128.4 (*m*-C_6H_5), 126.5 - 126.2 (*o*-C_6H_5), 84.5 - 77.6 ($C{\equiv}C$), 71.87 - 71.84 (-$C(OCH_3)$Ph), 60.5 (-$C(OCH_3)$(t-Bu)), 54.1 - 54.0 (COH), 53.8 - 53.2 (-OCH_3), 40.3 - 39.8 (-$C(CH_3)_3$), 25.0 - 24.9 (-C(CH_3)$_3$).

HRMS (MALDI-TOF/DCTB): *m/z*: $[M+Na]^+$ calculated for $C_{64}H_{58}O_8Na$: 977.4029, found: 977.4022.

1,10-bis(3,6-dimethoxy-3,6-diphenylocta-1,4,7-triyn-1-yl)-4,7,13,16-tetramethoxy-4,7,13,16-tetraphenylcyclooctadeca-2,5,8,11,14,17-hexayne-1,10-diol (7a)

Side product isolated from the preparation of **4a** by the general procedure B. Yield: 9 %. Yellow solid.

Or,

Side product isolated from the preparation of **8a** by the general procedure D. Yield: 8 %. Yellow solid.

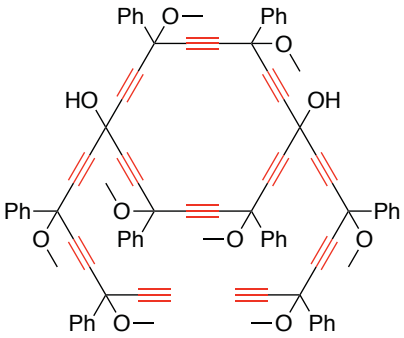

^{1}H NMR (400 MHz, $CDCl_3$) δ 7.71 (m, 16H, *o*-C_6H_5), 7.43 - 7.23 (m, 24H, *m*-, *p*-C_6H_5), 3.77 - 3.14 (m, 26H, -OCH_3, -OH), 2.85 - 2.57 (m, 2H, -C≡CH).

^{13}C{^{1}H} NMR (101 MHz, $CDCl_3$) δ 139.5 - 138.8 (*i*-C_6H_5), 129.2 - 129.0 (*p*-C_6H_5), 128.6 - 128.5 (*m*-C_6H_5), 126.5 - 126.4 (*o*-C_6H_5), 85.0 - 83.2, 81.0 - 80.6 (-C≡C-), 75.5 (-C≡CH), 71.8 - 71.7 (-C(OCH_3)Ph), 54.3 - 54.2 (>COH), 53.6 - 53.3 (-OCH_3).

HRMS (MALDI-TOF/DCTB): *m/z*: $[M+Na]^+$ calculated for $C_{90}H_{68}O_{10}Na$: 1331.4710, found: 1331.4541.

10-(3,6-dimethoxy-3,6-diphenylocta-1,4,7-triyn-1-yl)-10-hydroxy-4,7,13,16-tetramethoxy-4,7,13,16-tetraphenylcyclooctadeca-2,5,8,11,14,17-hexayn-1-one (8a)

Side product isolated from the preparation of **4a** by the general procedure B. Yield: nd. Yellow solid.

Or,

Product obtained by the general procedure D. Elution mixture: Pentane/EtOAc 4:1. Yield: 36 %. Yellow solid.

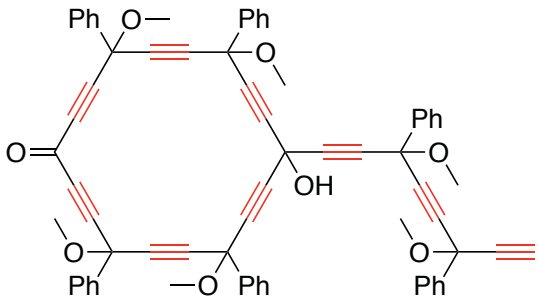

^{1}H NMR (400 MHz, $CDCl_3$) δ 7.90 - 7.60 (m, 12H, *o*-C_6H_5), 7.54 - 7.29 (m, 18H, *m*, *p*-C_6H_5), 3.75 - 3.26 (m, 19H, -OCH_3 and OH), 2.94 - 2.61 (m, 1H, -C≡CH).

^{13}C{^{1}H} NMR (101 MHz, $CDCl_3$) δ 159.1 (C=O), 139.4 - 137.7 (*i*-C_6H_5), 129.7 - 126.4 (*o*-, *m*-, *p*-C_6H_5), 89.5 - 80.6 (-C≡C-), 75.5 (-C≡CH), 71.2 - 71.8 (>C(Ph)(OCH_3)), 53.9 - 53.8 (>COH), 53.6 - 53.3 (-OCH_3).

HRMS (MALDI-TOF/DCTB): *m/z*: $[M+Na]^+$ calculated for $C_{68}H_{50}O_8Na$: 1017.3403, found: 1017.3376.

10-(3,6-di-tert-butyl-3,6-dimethoxyocta-1,4,7-triyn-1-yl)-10-hydroxy-4,7,13,16-tetramethoxy-4,7,13,16-tetraphenylcyclooctadeca-2,5,8,11,14,17-hexayn-1-one (8b)

Side product isolated from the preparation of **4b**. Yield: nd. Yellow solid.

Or,

Product obtained by the general procedure D. Elution mixture: Pentane/EtOAc 6:1. Yield: 35 %. Yellow solid.

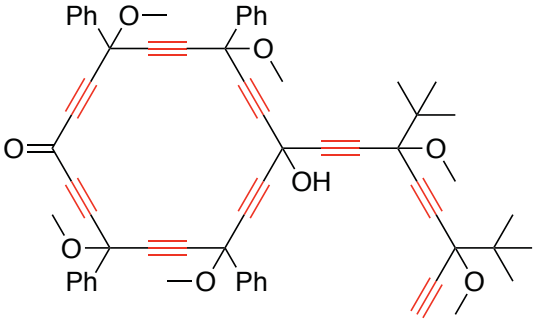

^{1}H NMR (400 MHz, $CDCl_3$) δ 7.81 - 7.60 (m, 8H, *o*-C_6H_5), 7.49 - 7.30 (m, 12H, *m*, *p*-C_6H_5), 3.87 - 3.37 (m, 18H, -OCH_3), 3.36 - 3.19 (m, 1H, -O*H*), 2.58 - 2.42 (m, 1H, -C≡C*H*), 1.21 - 1.04 (m, 18H, -$C(CH_3)_3$).

^{13}C{^{1}H} NMR (101 MHz, $CDCl_3$) δ 159.1 (*C*=O), 139.0 - 137.7 (*i*-C_6H_5), 129.7 - 129.2 (*p*-C_6H_5), 128.8 - 128.6 (*m*-C_6H_5), 126.5 - 126.4 (*o*-C_6H_5), 89.4 - 77.7 (-*C*≡*C*-), 74.0 (-C≡*C*H), 72.0 - 71.8 (>*C*(Ph)(OCH_3)), 54.2 - 54.1 (>*C*OH), 53.9 - 53.5 (-O*C*H_3), 40.8, 40.1 (-*C*$(CH_3)_3$), 25.1 - 25.0 (-C(*C*$H_3)_3$).

HRMS (MALDI-TOF/DCTB): *m/z*: $[M+Na]^+$ calculated for $C_{68}H_{50}O_8Na$: 1017.3403, found: 1017.3348.

1,4,7,10,13,16,21,24-octamethoxy-4,7,13,16,21,24-hexaphenylbicyclo[8.8.8]-hexacosa-2,5,8,11,14,17,19,22,25-nonayne (9a)

Prepared from **4a** following the general procedure A. Elution mixture: Pentane/EtOAc 4:1. Yield: 98 %. Light yellow solid.

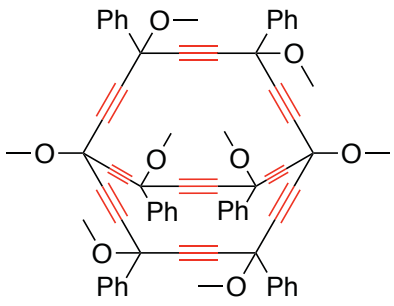

^{1}H NMR (400 MHz, $CDCl_3$) δ 7.91 – 7.52 (m, 12H, *o*-C_6H_5), 7.51 – 7.10 (m, 18H, *m*-, *p*-C_6H_5), 3.79 – 3.12 (m, 24H, -OCH_3).

^{13}C{^{1}H} NMR (101 MHz, $CDCl_3$) δ 139.1 - 138.5 (*i*-C_6H_5), 129.4 - 128.9 (*p*-C_6H_5), 128.7 - 128.5 (*m*-C_6H_5), 126.5 - 126.2 (*o*-C_6H_5), 84.9 - 84.2 (*C*≡*C*), 82.9 - 81.5 (C(OH)(*C*≡*C*)$_3$), 72.1 - 71.8 (-*C*(OCH_3)Ph), 60.9 - 60.8 (*C*(OCH_3)(C≡C)$_3$), 53.6 - 53.2 (-O*C*H_3).

HRMS (MALDI-TOF/DCTB): *m/z*: $[M+Na]^+$ calculated for $C_{70}H_{54}O_8Na$: 1045.3716, found: 1045.3668.

4,7-di-tert-butyl-1,4,7,10,13,16,21,24-octamethoxy-13,16,21,24-tetraphenylbicyclo[8.8.8]hexacosa-2,5,8,11,14,17,19,22,25-nonayne (9b)

Prepared from **4b** following the general procedure A. Elution mixture: Pentane/EtOAc 7:1. Yield: 87 %. Light yellow solid.

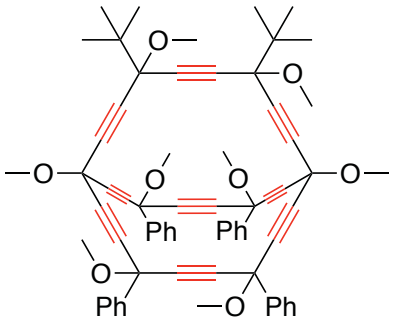

^{1}H NMR (400 MHz, $CDCl_3$) δ 7.86 - 7.56 (m, 8H, *o*-C_6H_5), 7.51 - 7.11 (m, 12H, *m*-, *p*-C_6H_5), 3.77 - 2.99 (m, 24H, -OCH_3), 1.23 - 1.00 (m, 18H, -$C(CH_3)_3$).

^{13}C{^{1}H} NMR (101 MHz, $CDCl_3$) δ 139.3 - 138.8 (*i*-C_6H_5), 129.3 - 129.0 (*p*-C_6H_5), 128.6 - 128.4 (*m*-C_6H_5), 126.5 - 126.2 (*o*-C_6H_5), 84.5 - 76.7 (-$C{\equiv}C$-), 72.0 - 71.8 (-$C(OCH_3)Ph$), 60.8 - 60.7 (-$C(OCH_3)$(t-Bu)), 53.7 - 53.0 (-OCH_3), 40.3 - 39.6 (-$C(CH_3)_3$), 25.1 - 24.9 (-$C(CH_3)_3$).

HRMS (MALDI-TOF/DCTB): *m/z*: $[M+Na]^+$ calculated for $C_{66}H_{62}O_8Na$: 1005.4342, found: 1005.4313.

4,7-di-tert-butyl-1,10-dimethoxy-13,16,21,24-tetraphenylbicyclo[8.8.8]hexa-cosa-4,5,6,13,14,15,21,22,23-nonaen-2,8,11,17,19,25-hexayne (10)

Prepared from **9b** following the general procedure C. Elution mixture: Pentane/EtOAc 8:1. Yield: 17 %. Yellow solid.

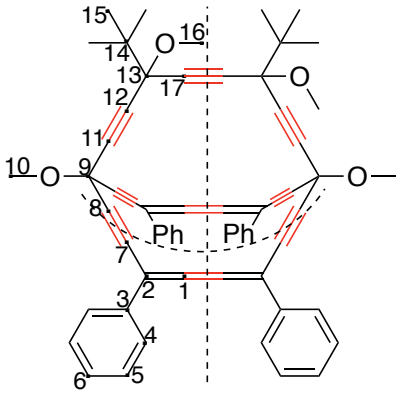

^{1}H NMR (400 MHz, CD_2Cl_2) δ 7.78 (d, J = 7.7 Hz, 8H, H^4), 7.47 (*pseudo*-t, J = 7.6 Hz, 8H, H^5), 7.38 (t, J = 7.3 Hz, 4H, H^6), 3.74 (s, 6H, H^{10}), 3.57 (2s, 6H, H^{16}), 1.16 (s, 18H, H^{15}).

^{13}C{^{1}H} NMR (101 MHz, CD_2Cl_2) δ 150.7 - 150.5 (C^1), 135.7 - 135.6 (C^3), 130.0 (d, C^6), 129.5 (C^5), 127.7 (d, C^4), 104.6 - 104.5 (C^2), 93.5 - 93.0 (C^7, C^8), 83.7 - 82.5 (C^{17}), 81.3, 81.1 (C^{11}, C^{12}), 78.6 (d, C^{13}), 63.1 (C^9), 54.4 (C^{10}), 54.1 (C^{16}), 40.9, 40.7 (C^{14}), 25.4 (C^{15}).

HRMS (MALDI-TOF/DCTB): *m/z*: calculated for $[M]^+$ $C_{62}H_{50}O_4$: 858.3709, found: 858.3640.

UV−vis ($CHCl_3$): λ_{max} = 418 nm (ε = 73000).

FT-IR: *v*: 2922, 2852 (C-H); 1731 (C=C=C=C); 1453 (C=C, Ph); 1260, 1069, 1023 (C-O).

1-octyl-10-[8-(10-octyl-4,7,13,16-tetraphenylcyclooctadeca-1,2,3,7,8,9,13,14,15-nonaen-5,11,17-triyn-1-yl)-3,6-diphenylocta-3,4,5-trien-1,7-diyn-1-yl]-4,7,13,16-tetraphenylcyclooctadeca-1,2,3,7,8,9,13,14,15-nonaen-5,11,17-triyne (12a)

Prepared from **17a** following the general procedure H. Yield: 46 %

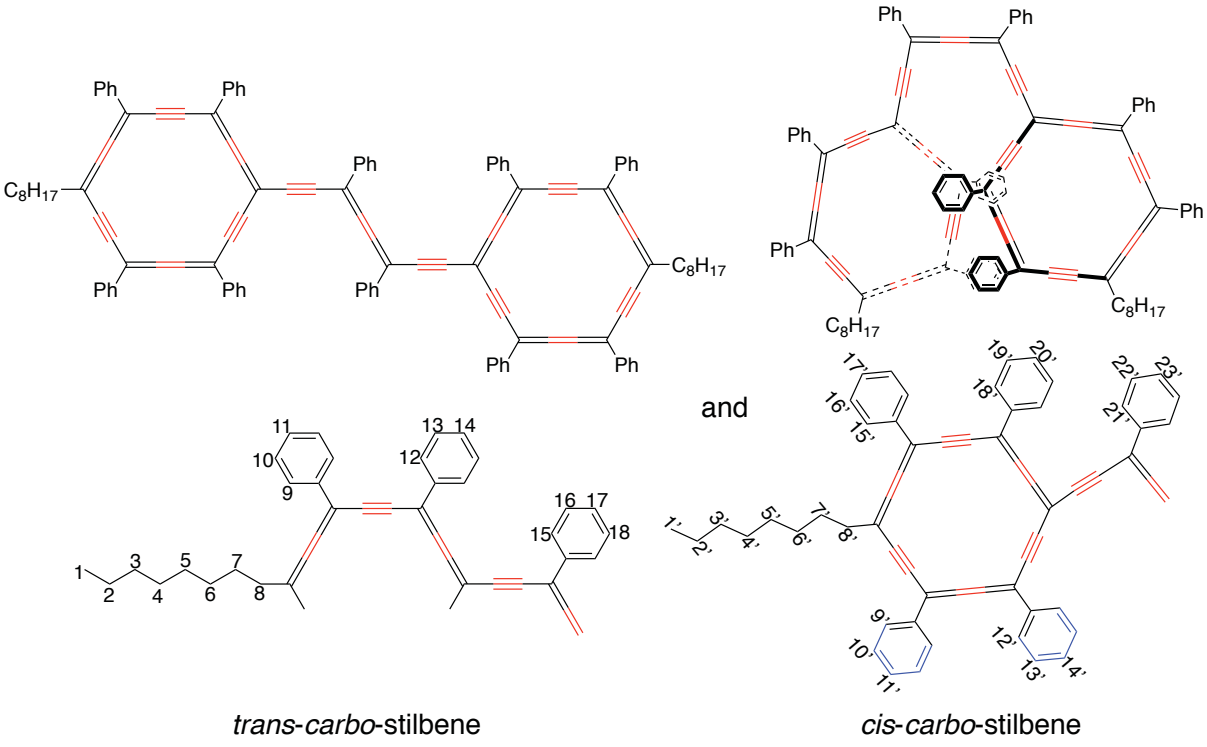

trans-carbo-stilbene *cis-carbo*-stilbene

^{1}H NMR (500 MHz, $CDCl_3$) δ 9.59 (d, *J* = 7.6 Hz, 8H, H^{12}), 9.43 (d, *J* = 7.1 Hz, 8H, H^{9}), 9.24 (d, *J* = 7.3 Hz, 9H, $H^{15'}$, $H^{18'}$), 8.95 (d, *J* = 7.4 Hz, 9H, $H^{9'}$, $H^{12'}$), 8.78 (d, *J* = 7.1 Hz, 4H, H^{15}), 8.65 (d, *J* = 7.7 Hz, 4H, $H^{21'}$), 7.99 - 7.95 (m, 18H, H^{10}, H^{13}, H^{16}), 7.85 (t, *J* = 7.5 Hz, 13H, $H^{16'}$, $H^{19'}$, $H^{22'}$), 7.79 (t, *J* = 7.7 Hz, 2H, H^{18}), 7.73 (t, *J* = 7.6 Hz, 4H, H^{11}, H^{14}), 7.68 (q, *J* = 7.6 Hz, 7H, $H^{17'}$, $H^{20'}$, $H^{23'}$), 7.60 (t, *J* = 6.9 Hz, 2H, H^{17}), 7.15 (t, *J* = 7.2 Hz, 8H, $H^{10'}$, $H^{13'}$), 6.55 (t, *J* = 7.2 Hz, 4H, $H^{11'}$, $H^{14'}$), 4.69 (t, *J* = 7.5 Hz, 4H, $H^{8'}$), 4.63 (t, *J* = 7.3 Hz, 4H, H^{8}), 3.08 - 3.00 (m, 4H, $H^{7'}$), 3.00 - 2.94 (m, 4H, H^{7}), 2.03 (q, *J* = 7.8 Hz, 4H, $H^{6'}$), 1.95 (q, *J* = 7.2 Hz, 4H, H^{6}), 1.82 - 1.70 (m, 8H, $H^{5'}$, H^{5}), 1.41 - 1.38 (m, 16H, $H^{4'}$, $H^{3'}$, H^{4}, H^{3}), 1.37 - 1.34 (m, 8H, $H^{2'}$, H^{2}), 0.89 (m, 12H, $H^{1'}$, H^{1}).

HRMS (MALDI-TOF/DCTB): *m/z*: $[M+Na]^+$ calculated for $C_{120}H_{84}Na$: 1547.6471, found: 1547.6619.

UV−vis ($CHCl_3$): λ = 464 (ε = 102000), 553 (ε = 84000), 735 (ε = 36000).

1-[3,6-di-tert-butyl-8-(10-octyl-4,7,13,16-tetraphenylcyclooctadeca-1,2,3,7,8,9,13,14,15-nonaen-5,11,17-triyn-1-yl)octa-3,4,5-trien-1,7-diyn-1-yl]-10-octyl-4,7,13,16-tetraphenylcyclooctadeca-1,2,3,7,8,9,13,14,15-nonaen-5,11,17-triyne (12b)

Prepared from **17b** following the general procedure H. Yield: 53 %.

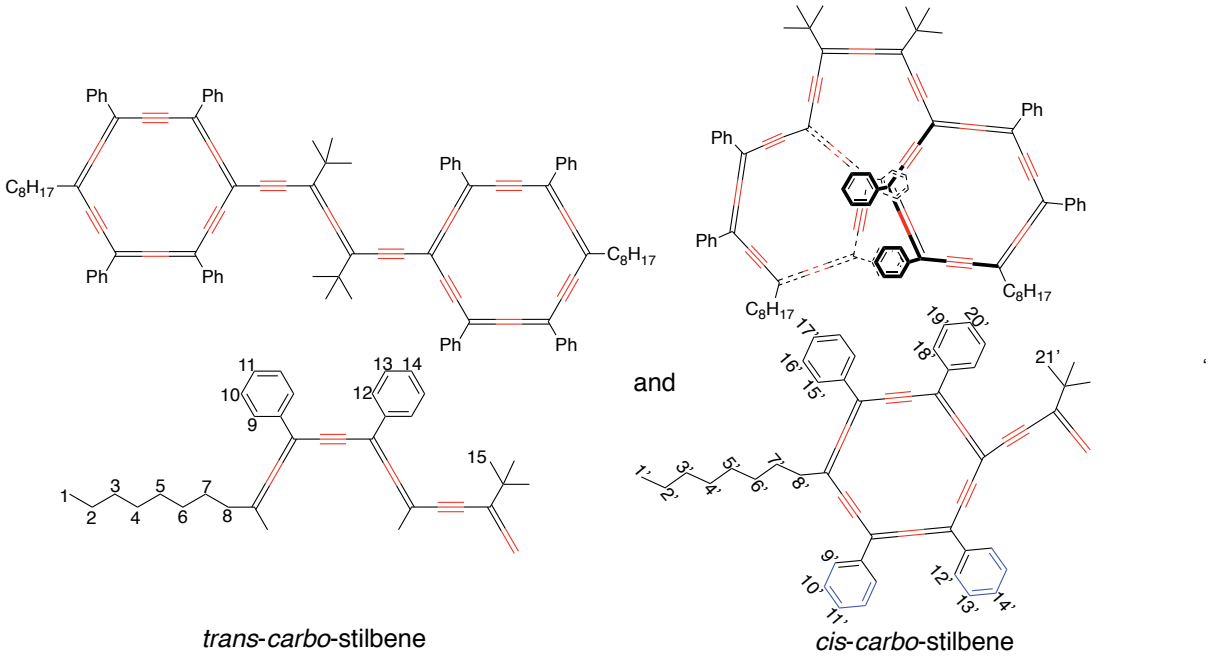

^{1}H NMR (500 MHz, $CDCl_3$) δ 9.56 (d, J = 7.3 Hz, 8H, H^{12}), 9.45 (d, J = 7.3 Hz, 8H, H^{9}), 9.30 (d, J = 7.3 Hz, 8H, $H^{12'}$, $H^{18'}$), 9.01 (d, J = 7.3 Hz, 8H, $H^{9'}$, $H^{15'}$), 8.03 - 7.96 (m, 16H, H^{10}, H^{13}), 7.88 (t, J = 7.6 Hz, 7H, $H^{16'}$, $H^{19'}$), 7.78 (t, J = 7.2 Hz, 4H, H^{14}), 7.73 (t, J = 7.3 Hz, 4H, H^{11}), 7.69 (t, J = 7.1 Hz, 4H, $H^{17'}$, $H^{20'}$), 7.21 (t, J = 7.6 Hz, 8H, $H^{10'}$, $H^{13'}$), 6.55 (t, J = 7.1 Hz, 4H, $H^{11'}$, $H^{14'}$), 4.70 (t, J = 7.6 Hz, 4H, $H^{8'}$), 4.65 (t, J = 7.5 Hz, 4H, H^{8}), 3.07 - 3.02 (m, 4H, $H^{7'}$), 3.01 - 2.97 (m, 4H, H^{7}), 2.09 (s, 16H, H^{15}), 1.98 (s, 16H, $H^{21'}$), 1.96 - 1.87 (m, 8H, $H^{6'}$, H^{6}), 1.83 - 1.77 (m, 4H, $H^{5'}$), 1.77 - 1.72 (m, 4H, H^{5}), 1.42 - 1.39 (m, 16H, $H^{4'}$, H^{4}, $H^{3'}$, H^{3}), 1.37 (m, J = 3.6 Hz, 8H, $H^{2'}$, H^{2}), 0.91 - 0.88 (m, 12H, $H^{1'}$, H^{1}).

HRMS (MALDI-TOF/DCTB): *m/z*: $[M+Na]^+$ calculated for $C_{116}H_{92}Na$: 1507.7097, found: 1507.7180.

UV−vis ($CHCl_3$): λ = 455 (ε = 160000), 547 (ε = 150000), 690 (ε = 51600).

1-(3,6-dimethoxy-3,6-diphenylocta-1,4,7-triyn-1-yl)-4,7,13,16-tetramethoxy-10-octyl-4,7,13,16-tetraphenylcyclooctadeca-2,5,8,11,14,17-hexayne-1,10-diol (15a)

Prepared from **8b** following the general procedure E. Elution mixture: Pentane/EtOAc: 6:1. Yield: 70 %. Yellow solid.

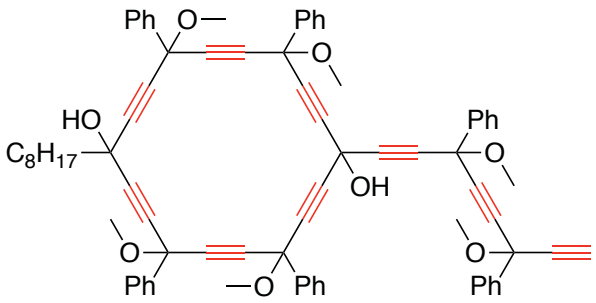

^{1}H NMR (300 MHz, $CDCl_3$) δ 7.84 - 7.60 (m, 12H, *o*-C_6H_5), 7.44 - 7.25 (m, 18H, *m*, *p*-C_6H_5), 3.85 - 3.19 (m, 19H, -OCH_3, -O*H*), 3.15 - 2.84 (m, 1H, -O*H*), 2.81 - 2.58 (m, 1H, -C≡C*H*), 2.06 - 1.93 (m, 2H, >CH_2), 1.60 (m, 2H, >CH_2-CH_2), 1.28 (m, 10H, -$(CH_2)_5$), 0.89 (m, 3H, -CH_3).

^{13}C{^{1}H} NMR (75 MHz, $CDCl_3$) δ 139.5 - 138.9 (*i*-C_6H_5), 129.2 - 129.0 (*p*-C_6H_5), 128.6 - 128.50 (*m*-C_6H_5), 126.5 - 126.4 (*o*-C_6H_5), 87.5 - 80.6 (-C≡C-), 75.5 (-C≡CH), 71.9 - 71.8 (>C(Ph)(OCH_3)), 63.6 (>C(Oct)(OH)), 54.3 - 54.2 (>C(OH)(C≡C)), 53.6 - 53.3 (-OCH_3), 43.1 - 43.0 (>CH_2), 31.9 (>CH_2CH_2), 29.4 - 29.2 (-$(CH_2)_3$-), 24.6 - 24.5 (-$CH_2CH_2CH_3$), 22.7 (-CH_2CH_3), 14.13 (-CH_3).

HRMS (MALDI-TOF/DCTB): *m/z*: $[M+Na]^+$ calculated for $C_{76}H_{68}O_8Na$: 1131.4812, found: 1131.4805.

1-(3,6-di-tert-butyl-3,6-dimethoxyocta-1,4,7-triyn-1-yl)-4,7,13,16-tetramethoxy-10-octyl-4,7,13,16-tetraphenylcyclooctadeca-2,5,8,11,14,17-hexayne-1,10-diol (15b)

Prepared from **8b** following the general procedure E. Elution mixture: Pentane/EtOAc: 6:1. Yield: 75 %. Yellow solid.

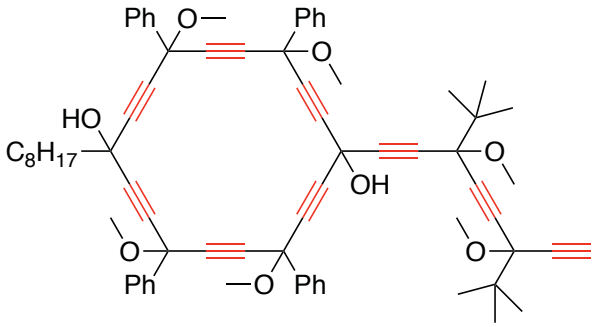

^{1}H NMR (400 MHz, $CDCl_3$) δ 7.82 - 7.62 (m, 8H, *o*-C_6H_5), 7.44 - 7.29 (m, 12H, *m*, *p*-C_6H_5), 3.67 - 3.39 (m, 19H, -OCH_3, -O*H*), 3.31 - 2.81 (m, 1H, -O*H*), 2.58 - 2.33 (m, 1H, -C≡C*H*), 2.14 - 1.91 (m, 2H, >CH_2), 1.73 - 1.49 (m, 2H, >CH_2-CH_2), 1.26 (m, 10H, -

(CH_2)$_5$), 1.17 - 1.07 (m, 18H, -C(CH_3)$_3$-, 0.90 (m, 3H, -CH_3).

^{13}C{^{1}H} NMR (101 MHz, $CDCl_3$) δ 139.5 - 138.9 (*i*-C_6H_5), 129.2 - 129.0 (*p*-C_6H_5), 128.6 - 128.5 (*m*-C_6H_5), 126.5 - 126.4 (*o*-C_6H_5), 87.6 - 77.7 (-C≡C-), 74.0 (-C≡CH), 71.9 - 71.8 (>C(Ph)(OCH_3)), 63.6 (>C(Oct)(OH)), 54.2 - 54.1 (>C(OH)(C≡C)), 53.9 - 53.3 (-OCH_3), 43.1 - 43.0 (>CH_2), 40.8 - 40.0 (-C(CH_3)$_3$), 31.9 (>CH_2CH_2), 29.7 - 29.2 (-(CH_2)$_3$-), 25.1 - 25.0 (-C(CH_3)$_3$), 24.6 - 24.4 (-$CH_2CH_2CH_3$), 22.7 (-CH_2CH_3), 14.1 (-CH_3).

HRMS (MALDI-TOF/DCTB): *m/z*: [M+Na]$^+$ calculated for $C_{72}H_{76}O_8Na$: 1091.5438, found: 1091.5386.

3-(3,6-dimethoxy-3,6-diphenylocta-1,4,7-triyn-1-yl)-3,6,9,12,15,18-hexamethoxy-12-octyl-6,9,15,18-tetraphenylcyclooctadeca-1,4,7,10,13,16-hexayne (16a)

Prepared from **15a** following the general procedure F. Elution mixture: Pentane/EtOAc: 5:1. Yield: 89 %. Yellow solid.

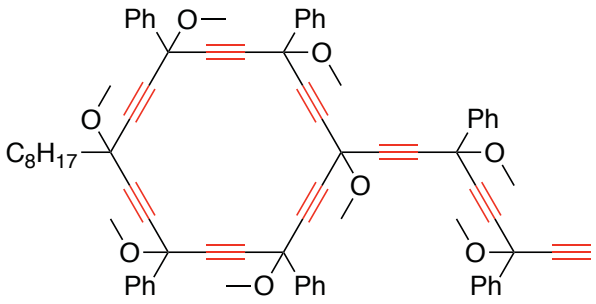

^{1}H NMR (400 MHz, $CDCl_3$) δ 7.80 - 7.63 (m, 12H, *o*-C_6H_5), 7.44 - 7.26 (m, 18H, *m*, *p*-C_6H_5), 3.69 - 3.24 (m, 24H, -OCH_3), 2.84 - 2.65 (m, 1H, -C≡CH), 2.06 - 1.91 (m, 2H, >CH_2), 1.57 (s, 2H, >CH_2-CH_2), 1.31 - 1.20 (m, 10H, -(CH_2)$_5$), 0.91 - 0.86 (m, 3H, -CH_3).

^{13}C{^{1}H} NMR (101 MHz, $CDCl_3$) δ 139.6 - 139.0 (*i*-C_6H_5), 129.2 - 129.0 (*p*-C_6H_5), 128.6 - 128.5 (*m*-C_6H_5), 126.5 - 126.3 (*o*-C_6H_5), 85.4 - 80.6 (-C≡C-), 75.5 (-C≡CH), 71.9 - 71.8, 70.7 - 70.6 (>C(Ph)(OCH_3)), 60.8 - 60.7 (>C(C≡C)(OCH_3)), 53.6 - 53.3 (-OCH_3(Ph)), 53.0 (-OCH_3), 42.3 - 42.0 (>CH_2), 31.9 (>CH_2CH_2), 29.7 - 29.2 (-(CH_2)$_3$-), 24.5 - 24.3 (-$CH_2CH_2CH_3$), 22.7 (-CH_2CH_3), 14.1 (-CH_3).

HRMS (MALDI-TOF/DCTB): *m/z*: [M+Na]$^+$ calculated for $C_{78}H_{72}O_8Na$: 1159.5125, found: 1159.4938.

3-(3,6-di-tert-butyl-3,6-dimethoxyocta-1,4,7-triyn-1-yl)-3,6,9,12,15,18-hexamethoxy-12-octyl-6,9,15,18-tetraphenylcyclooctadeca-1,4,7,10,13,16-hexayne (16b)

Prepared from **15b** following the general procedure F. Elution mixture: Pentane/EtOAc: 8:1. Yield: 77 %. Yellow solid.

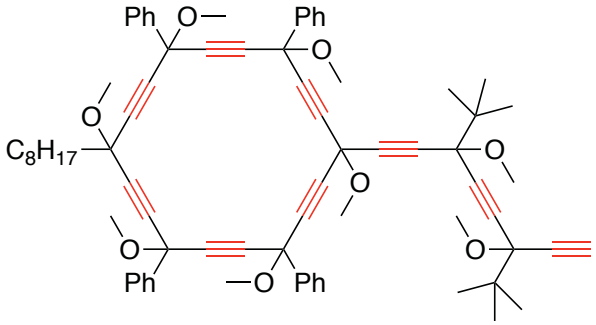

^{1}H NMR (400 MHz, $CDCl_3$) δ 7.79 - 7.62 (m, 8H, *o*-C_6H_5), 7.35 (m, 12H, *m*, *p*-C_6H_5), 3.78 - 3.18 (m, 24H, -OCH_3), 2.60 - 2.36 (m, 1H, -C≡C*H*), 2.09 - 1.85 (m, 2H, >CH_2), 1.76 - 1.56 (m, 2H, >CH_2-CH_2), 1.26 (h, *J* = 9.3, 8.4 Hz, 10H, -(CH_2)$_5$), 1.20 - 1.01 (m, 18H, -C(CH_3)$_3$), 0.91 - 0.85 (m, 3H, -CH_3).

^{13}C{^{1}H} NMR (101 MHz, $CDCl_3$) δ 139.6 - 139.1 (*i*-C_6H_5), 129.1 - 128.9 (*p*-C_6H_5), 128.5 (*m*-C_6H_5), 126.5 - 126.4 (*o*-C_6H_5), 85.5 - 77.8 (-C≡C-), 73.9 (-C≡CH), 71.9 - 70.6 (>C(Ph)(OCH_3)), 53.8 - 53.3 (-OCH_3), 52.9 (>C(C≡C)(OCH_3)), 42.3 - 42.0 (>CH_2), 40.7 - 40.0 (-C(CH_3)$_3$), 31.9 (>CH_2CH_2), 29.7 - 29.2 (-(CH_2)$_3$-), 25.0 (-C(CH_3)$_3$), 24.5 - 24.3 (-$CH_2CH_2CH_3$), 22.7 (-CH_2CH_3), 14.1 (-CH_3).

HRMS (MALDI-TOF/DCTB): *m/z*: $[M+Na]^+$ calculated for $C_{74}H_{80}O_8Na$: 1119.5751, found: 1119.5930.

1-[8-(1,4,7,10,13,16-hexamethoxy-10-octyl-4,7,13,16-tetraphenylcyclooctadeca-2,5,8,11,14,17-hexayn-1-yl)-3,6-dimethoxy-3,6-diphenylocta-1,4,7-triyn-1-yl]-4,7,13,16-tetramethoxy-10-octyl-4,7,13,16-tetraphenylcyclooctadeca-2,5,8,11,14,17-hexayne-1,10-diol (17a)

Prepared from **16a** following the general procedure G. Elution mixture: Pentane/EtOAc: 6:1 then 3:1. Yield: 46 %. Yellow solid.

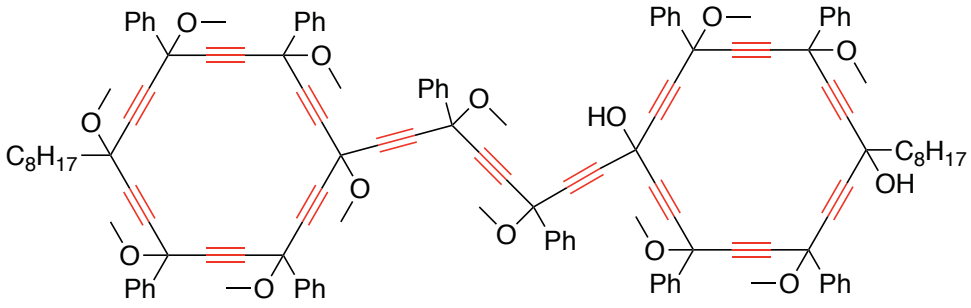

^{1}H NMR (400 MHz, $CDCl_3$) δ 7.82 - 7.59 (m, 24H, *o*-C_6H_5), 7.42 - 7.25 (m, 36H, *m*, *p*-C_6H_5), 3.66 - 3.26 (m, 42H, -OCH_3), 3.05 - 2.50 (m, 2H, -O*H*), 1.98 (m, 4H, >CH_2), 1.61 - 1.49 (m, 4H, >CH_2-CH_2), 1.27 (m, 20H, -(CH_2)$_5$), 0.90 - 0.86 (m, 6H, -CH_3).

^{13}C{^{1}H} NMR (101 MHz, $CDCl_3$) δ 139.5 - 139.1 (*i*-C_6H_5), 129.1 - 129.0 (*p*-C_6H_5), 128.6 - 128.5 (*m*-C_6H_5), 126.5 - 126.3 (*o*-C_6H_5), 87.3 - 80.7 (-C ≡ C-), 71.9 - 71.8, 70.6 (>C(Ph)(OCH_3)), 63.6 (>C(Oct)), 54.3 - 54.1 (>C(C≡C)), 53.5 - 53.0 (-OCH_3), 43.0 - 41.9

(>CH_2), 31.9 (>CH_2CH_2), 29.7 - 29.2 (-(CH_2)$_3$-), 24.5 - 24.3 (-$CH_2CH_2CH_3$), 22.7 (-CH_2CH_3), 14.1 (-CH_3).

HRMS (MALDI-TOF/DCTB): *m/z*: $[M+Na]^+$ calculated for $C_{132}H_{122}O_{14}Na$: 1953.8732, found: 1953.8358.

1-[3,6-di-tert-butyl-8-(1,4,7,10,13,16-hexamethoxy-10-octyl-4,7,13,16-tetraphenylcyclooctadeca-2,5,8,11,14,17-hexayn-1-yl)-3,6-dimethoxyocta-1,4,7-triyn-1-yl]-4,7,13,16-tetramethoxy-10-octyl-4,7,13,16tetraphenylcyclooctadeca-2,5,8,11,14,17-hexayne-1,10-diol (17b)

Prepared from **16b** following the general procedure G. Elution mixture: Pentane/EtOAc: 6:1 then 3:1. Yield: 55 %. Yellow solid.

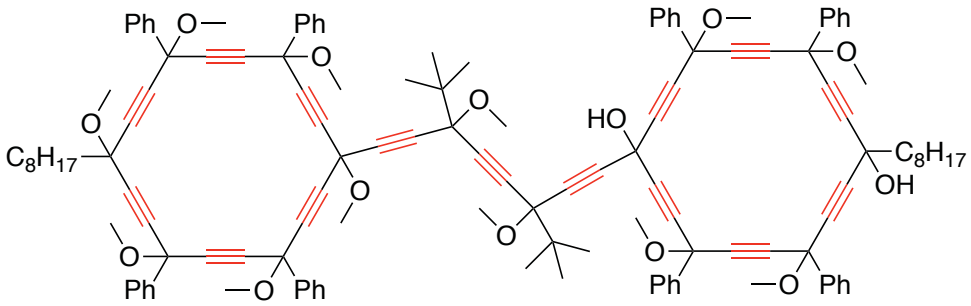

^{1}H NMR (400 MHz, $CDCl_3$) δ 7.81 - 7.57 (m, 16H, *o*-C_6H_5), 7.45 - 7.27 (m, 24H, *m*, *p*-C_6H_5), 3.64 - 3.27 (m, 36H, -OCH_3), 3.09 - 2.71 (m, 2H, -O*H*), 1.97 (m, 4H, >CH_2), 1.68 (s, 4H, >CH_2-CH_2), 1.28 (m, 20H, -(CH_2)$_5$), 1.17 - 0.98 (m, 18H, -C(CH_3)$_3$), 0.89 - 0.86 (m, 6H, -CH_3).

^{13}C{^{1}H} NMR (101 MHz, $CDCl_3$) δ 139.5 - 139.0 (*i*-C_6H_5), 129.2 - 128.8 (*p*-C_6H_5), 128.5 (*m*-C_6H_5), 126.4 (*o*-C_6H_5), 87.7 - 77.8 (-C≡C-), 71.9, 70.6 (>C(Ph)(OCH_3)), 63.6 (>C(Oct)), 53.9 - 53.3 (-OCH_3), 53.0 - 52.9 (>C(C≡C)), 43.20 - 42.0 (>CH_2), 40.8 - 40.4 (-C(CH_3)$_3$), 31.9 (>CH_2CH_2), 29.7 - 29.2 (-(CH_2)$_3$-), 25.0 (-C(CH_3)$_3$), 24.6 - 24.4 (-$CH_2CH_2CH_3$), 22.7 (-CH_2CH_3), 14.1 (-CH_3).

HRMS (MALDI-TOF/DCTB): *m/z*: $[M]^+$ calculated for $C_{128}H_{130}O_{14}Na$: 1913.9358, found: 1913.8297.

3. X-ray diffraction analysis

X-ray data were collected at low temperature on APEX2 Bruker or Gemini Oxford Diffraction diffractometers. The structures were solved using SUPERFLIP, and refined on F by means of least-squares procedures on F using the programs of the PC version of CRYSTALS. Atomic scattering factors were taken from the international tables for X-ray crystallography. Absorption correction was performed by using a multiscan procedure. All non-hydrogen atoms were refined anisotropically. The H atoms were refined using riding constraints. For **10**, the non-reduced butyne edge is disordered, permitting the presence of the two enantiomers in the asymmetric unit.

	1	**2**	**10**
CCDC number			
Empirical formula	$C_{67}H_{46}Cl_6O_4$	$C_{66.50}H_{41}Cl_5O_2$	$C_{62}H_{50}O_4$
Formula moiety	$C_{62}H_{32}O_2$, 3(CH_2Cl_2), C_2H_6O, H_2O	$C_{64}H_{36}O_2$, 2.5(CH_2Cl_2)	$C_{62}H_{50}O_4$
Formula mass	1127.82	1049.32	859.08
Crystal system	Monoclinic	Monoclinic	Triclinic
Space group	P 2_1/c	P 2/c	P -1
T [K]	135	100	100
a [Å]	12.8510(5)	19.5176(12)	12.6902(9)
b [Å]	22.5045(10)	12.4822(7)	15.0361(9)
c [Å]	19.6919(10)	22.4823(14)	15.8198(10)
α [°]	90	90	67.7739(19)
β [°]	91.450(4)	94.348(3)	67.1247(19)
γ [°]	90	90	76.4991(19)
V [Å^3]	5693.2(3)	5461.4(3)	2561.3(3)
D_c	1.316	1.276	1.114
Z	4	4	2
μ[mm^{-1}]	3.141	0.311	0.068
Refl. measured	45645	134670	41130
Refl. unique/R_{int}	8719/0.024	10877/0.049	9368/0.057
Refl. with $I > n\sigma(I)$	7761 (n=3=	8510 (n=3)	4893 (n=2.6)
Nb parameters	694	667	604
R	0.0350	0.0566	0.0400

R_w	0.0443	0.0585	0.0405
GooF	1.025	1.078	1.109
$\Delta\rho_{max}/\Delta\rho_{min}$ [e.Å^{-3}]	0.31/-0.39	1.73/-1.31	0.24/-0.18

4. 2D and variable temperature ^{1}H NMR for the *carbo*-stilbene 12a and 12b.

4.1 Variable temperature ^{1}H NMR (500 MHz) spectra of 12a

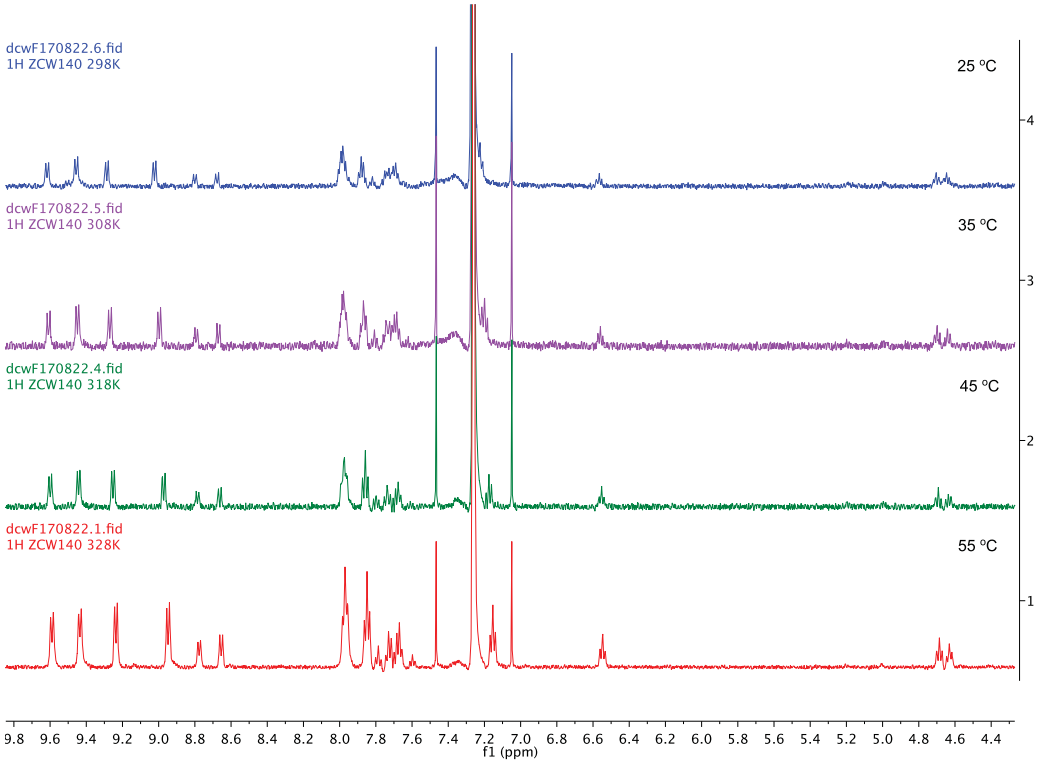

^{1}H – ^{1}H HSQC NMR (600 MHz) spectrum of 12a at 55 °C:

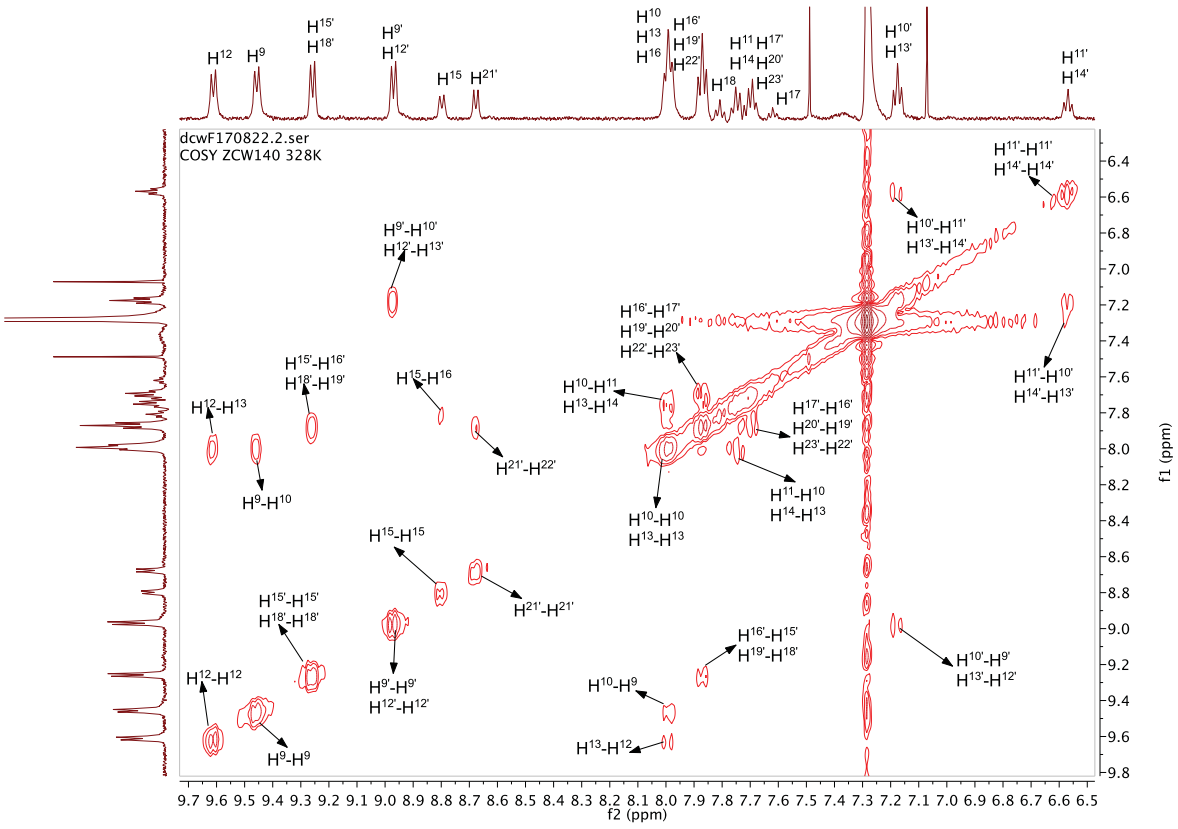

4.2 Variable temperature ^{1}H NMR (500 MHz) spectra of 12b

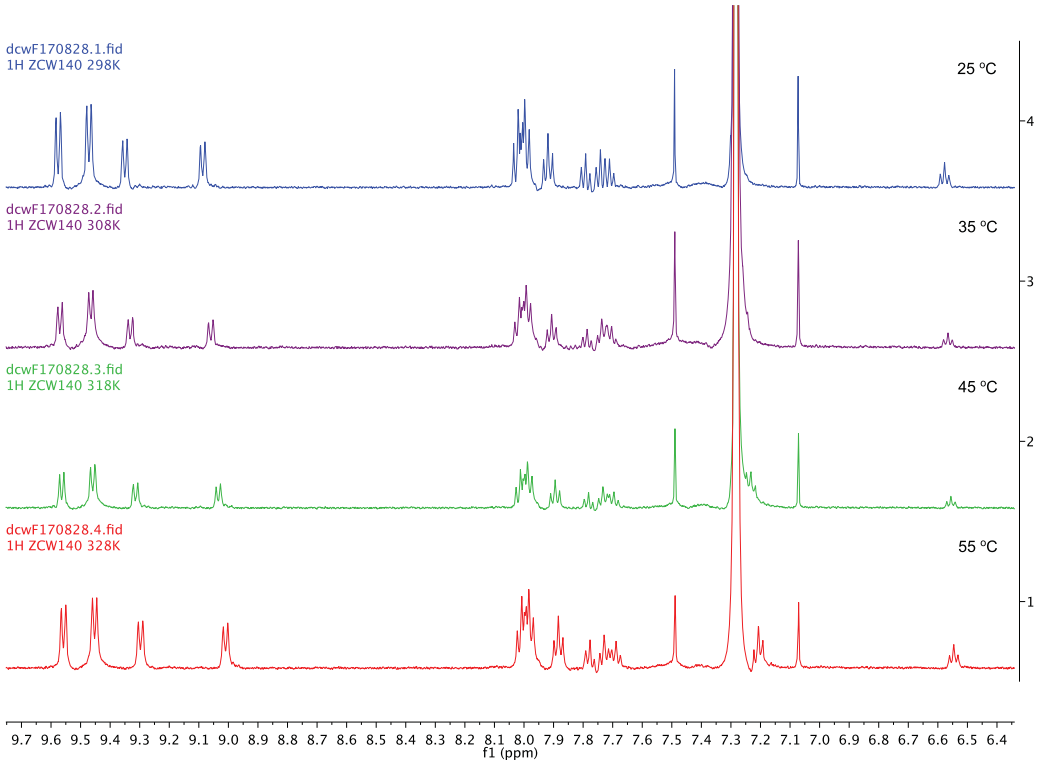

^{1}H - ^{13}C HSQC NMR (600 MHz) spectrum of 12b at 45 ^{o}C:

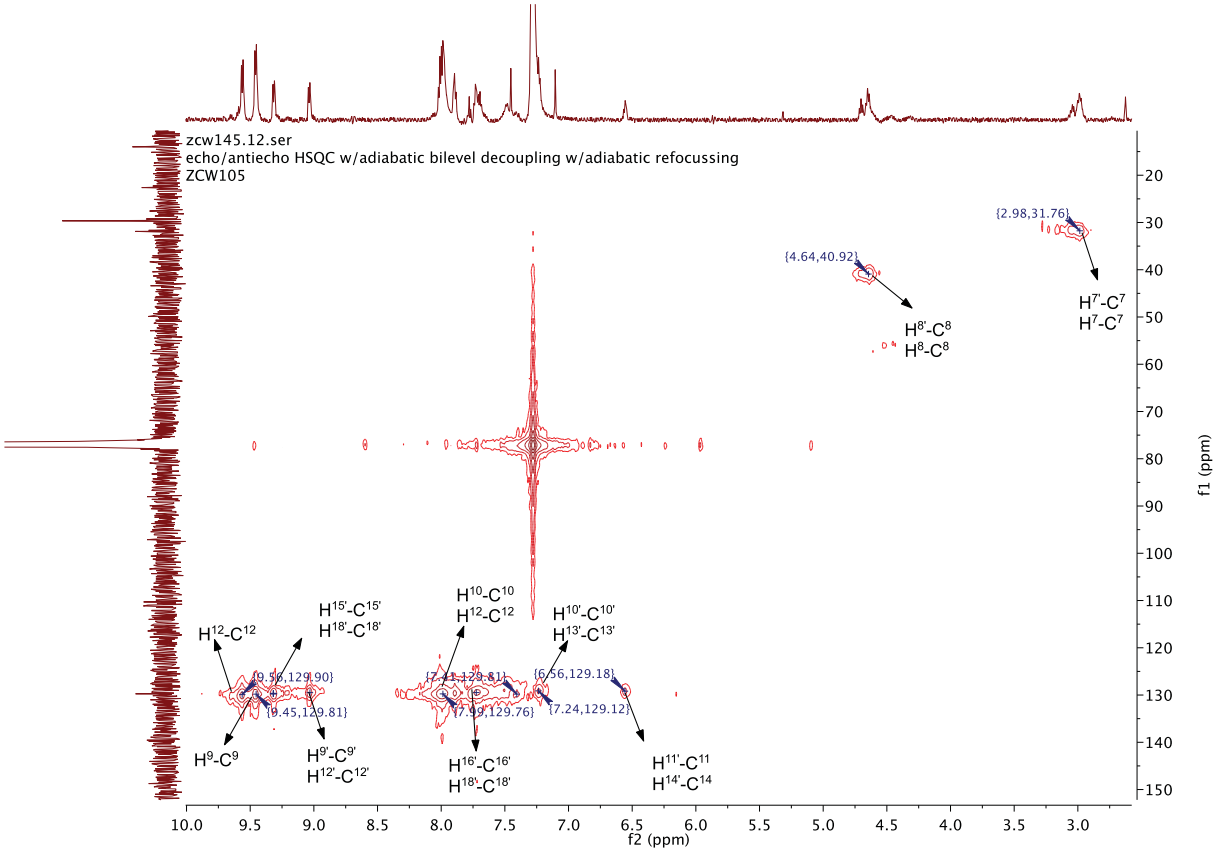

The ^{1}H - ^{13}C HMBC NMR (600 MHz) spectrum of 12b at 45 ^{o}C:

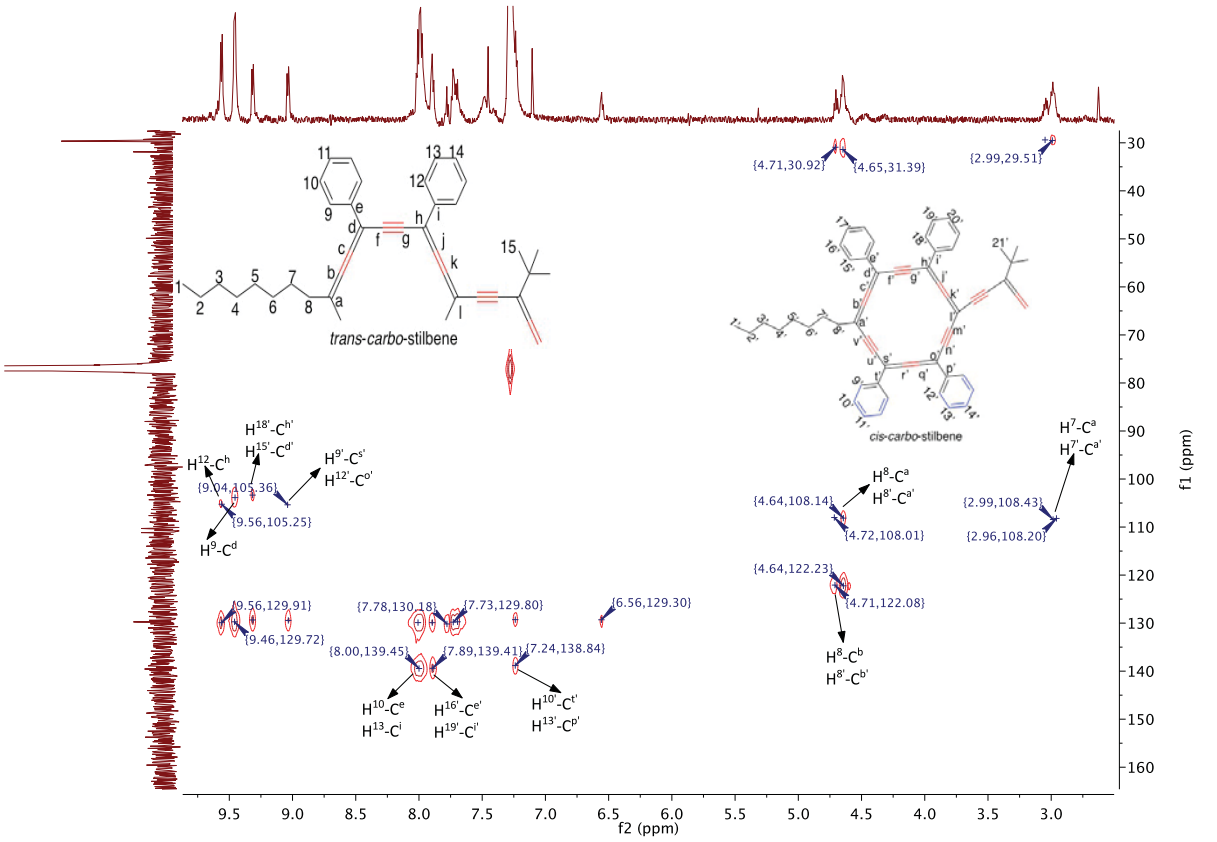

General Conclusion

General Conclusion

As proposed in the General Introduction, the thesis has been divided into two independent parts and six chapters. In a consistent summary, the first part mainly focused on the synthesis of nitro-aromatic phosphines and their coordination chemistry in Rh^I complexes, while the second part described the synthesis of a series of aliphatic *carbo*-benzenes derivatives, the physico-chemical properties of which were investigated systematically with a view to related applications.

More precisely, in the first part and first chapter, an efficient strategy based on the use of LDA as an optimal base was developed for the preparation of nitro-aromatic phosphines, this method might be extended to the preparation of other nitro-substituted heteroaromatic phosphines, e.g. containing a O- or S-heterocycle. In a set of Rh^I complexes of such nitro-substituted (*N*-phenyl-benzimidazol-1-yl)diphenylphosphines L, the moderate but systematic variations of the C=O IR stretching frequency and ^{103}Rh NMR chemical shift of *trans*-$L_2Rh^ICl(CO)$ complexes revealed that neutral nitro-aromatic phosphines are weakly σ-donating P-ligands. As an unexpected observation, crystals of dinuclear side-products $Rh_2Cl_2(\mu\text{-}CO)(\mu_{N,P}\text{-}L)_2$ happened to be organometallic clathrates with high solvent content (dichloromethane), opening options in the design of organometallic frameworks for host-guest chemistry. In the future, Rh^I complexes of the newly designed nitro-aromatic phosphines, or simpler versions thereof such as tris(nitrophenyl)phosphines, e.g. $(4\text{-}NO_2\text{-}C_6H_4)_3P$, would deserve to be tested in homogeneous catalysis.

In the second part of the thesis dealing with *carbo*-mer chemistry, the second chapter describes the synthesis of the long known hexaphenyl-*carbo*-benzene, and its previously unknown *p*-bis-3,5-di-*tert*-butylphenyl homologue, through an [8+10] macro-cyclization strategy (instead of [14+4] or [11+7]) allowing a dramatic improvement of the global yield from 1 % to 8 %. Accurate crystallographic and electrochemical data completed the characterization of the hexaphenyl *carbo*-benzene reference. Attachment of four *tert*-butyl

groups on two phenyl substituents of the C_{18} macrocycle was found to have a very limited effect on the solubility of *carbo*-benzenes, the low solubility being the main general drawback limiting the processability, and thus applications, of *carbo*-benzenes. Application in organic photovoltaics was also envisaged in collaboration with Mexican partners, but the remaining very poor solubility of the tetra *tert*-butyl homologue of the $C_{18}Ph_6$ standard prevented the formation of the required high quality thin films, thus stimulating the search for more efficient solubilizing substituents; in this context, the design of dialkyl-*carbo*-benzenes was proposed in the next section.

The third chapter discloses the synthesis and physical properties of *p*-dialkyl-tetraphenyl-*carbo*-benzenes bearing two *n*-aliphatic chains R = C_nH_{2n+1}, directly anchored to the C_{18} ring (n = 2, 4, 8, 14, 20). The addition of RMgBr nucleophiles to the [6]pericyclynedione resulted in the simultaneous formation of the di-adduct and reduced mono-adduct, thus allowing the parallel synthesis of the quadrupolar dialkyl- and dipolar monoalkyl-*carbo*-benzenes. The use of RMgCl or RLi/$CeCl_3$ nucleophiles was found to prevent the formation of the reduced derivatives. A remarkable enhancement of the solubility of the two series of mono- and di-alkylated *carbo*-benzenes was observed for $n \geq 8$. In the crystal state, the first evidence of direct π-stacking of *carbo*-benzene rings was observed for the diethyl and bis-tetradecyl-derivatives, thus providing experimental evidence of possible attractive arrangement of α-graphyne layers into the theoretical 3D carbon allotrope α-graphityne. In the dialkyl series, a linear decrease of the melting-decomposition temperatures *vs* n was observed. Furthermore, even if slanted, the columnar arrangements of dialkyl-*carbo*-benzenes in the crystalline state suggest that discotic mesophases and liquid crystals could be obtained upon structural tuning of candidate *carbo*-benzenic mesogens.

The fourth chapter focuses on the design of mesogenic *carbo*-benzenes and exploration of their liquid crystal (LC) properties. Two hexaalkoxy-di(phenylethynyl)-tetraphenyl-*carbo*-benzenes bearing six alkyl chains R = C_nH_{2n+1} (n = 12, 18) were synthesized and fully characterized, including by X-ray diffraction analysis of a single crystal for one of them. The mesogenic behavior of the more soluble hexadodecyl-substituted *carbo*-benzene was studied

in depth by Taiwanese collaborators. The formation of a rectangular columnar mesophase at 115 ^{o}C was evidenced by POM, DSC, PXRD and HR-STM experiments. These results pave the way for the development of a new generation of discotic columnar LCs based on the large, rigid and hollow C_{18} *carbo*-benzene core. Improvement of LC properties by modifications of the length and number of aliphatic chains, and/or substitution pattern of the hexagonal macrocycle (quadrupolar *vs* octupolar), can henceforth be confidently envisaged.

In the fifth chapter, a multi-step synthesis of *carbo*-OPE_2 and *carbo*-OPE_3 wire models, composed of two or three *carbo*-benzene rings catenated though ethylene linkers, was described. Despite a limited solubility, they could be fully characterized, including by single crystal XRD analysis and electrochemistry. The *carbo*-OPE_3, or "*carbo*-terphenyls", were found to exhibit the lowest first reduction potential ever measured in the *carbo*-mer family (-0.42 ± 0.03 V/SCE). Results of computational studies at the DFT level, undertaken by a Spanish collaborator, allowed appraisal of the magnetic aromaticity of *carbo*-OPEs: calculated NICS values revealed that the C_{18} rings preserve their individual *carbo*-aromatic character in such oligomers. The more extented *carbo*-quaterphenyl was also calculated and predicted to have an extremely low first reduction potential (-0.31 V/SCE) and an extremely wide UV-vis absorption range (440-738 nm). These results open natural prospects of applications of *carbo*-OPE wires in molecular electronics.

In the last chapter, the synthesis of two new types of skeletal *carbo*-mers, derivatives of *carbo*-benzenics as containing two butatrienic C_{18} rings, aromatic or not, in the peri-condensed fused mode or catenated mode, namely *carbo*-barrelenes and *carbo*-stilbenes, respectively. They were prepared by double addition of triyne dinucleophiles to one or two equivalents of the key tetraphenyl-[6]pericyclynedione, acting as a di- or mono-electrophile, respectively. In the peri-condensed case, two shape-persistent *carbo*-barrelenes and a partially reduced bis-butatrienic derivative were obtained upon treatment of the peribicyclic bis-adducts with $SnCl_2$. Although sensitive to temperature, they were found sufficiently stable to be kept for a few weeks at ambient temperature without decomposition, and to be fully characterized, in particular by single crystal XRD analysis. The ability of such hollow 3D

organic structures to encapsulate NH_4^+ guest was explored both computationally and experimentally: though clear experimental evidence of encapsulation is still missing, investigations are still in progress, and attempts at encapsulation of other small guests, amongst X–H…πC hydrogen bond donors, are envisaged. In the catenated case, two *carbo*-stilbene compounds bearing phenyl or *tert*-butyl substituents at the butatrienic unit bridging the two *carbo*-benzene rings were prepared. Their extremely poor solubility prevented a full characterization, but ^{1}H NMR spectroscopy allowed evidencing the formation of mixtures of *cis* (*Z*) and *trans* (*E*) isomers in ratios close to 1:1. Studies of the photo-isomerization propensity of *carbo*-stilbenes will be implemented in the future.

In summary, the thesis work covers two quite distinct research fields: organometallic coordination chemistry and acetylenic organic synthesis. About 40 final products, including 33 organic compounds and 7 Rh^I complexes were obtained, isolated and characterized, the structures of 27 of them having been determined by X-ray crystallography. Noteworthy as a formal meeting point of the two fields, the sterically hindered bases LDA and LiHMDS played pivotal roles in the preparation of both nitro-aromatic phosphines and *carbo*-benzene derivatives, *carbo*-OPEs, *carbo*-barrelenes, and *carbo*-stilbenes. In terms of synthesis versatility, 24 *carbo*-benzenes were synthesized from the key [6]pericyclynedione precursor. The observed enhancement of solubility upon direct substitution of the C_{18} macrocycle by *n*-alkyl chains also paves the way for improving the processability in solution of larger *carbo*-meric molecules, such as long *carbo*-OPE wires.

Finally, the disclosed results open prospects of applications in many various fields as: catalysis, clathrate and host-guest chemistry, organic photovoltaics, liquid crystal design, electro-conductive molecular electronics, and photochemistry.

Résumé en français

Résumé en français

La thèse est divisée en deux parties portant sur des spécialités expérimentales distinctes, à savoir la chimie du phosphore et de coordination d'une part (pour la catalyse homogène) et d'autre part la chimie organique acétylénique des composés riches en carbone (pour la physique).

La première partie, correspondant au premier chapitre, concerne la conception de nouveaux types de ligands pour des applications spécifiques en catalyse homogène. La famille des ligands faiblement électro-donneurs a été considérée, avec une focalisation sur les phosphines pauvres en électrons et leur coordination avec des centres Rh(I) acides de Lewis. L'étude des nitro-arylphosphines, très peu développée, a donc été initiée avec la synthèse de N-aryl benzimidazolodiphénylphosphines nitrées sur différentes positions des substituants aryle et/ou benzimidazolyle, ainsi que leur complexation avec du Rh(I). La rétro-donation π des ligands ciblés dans les complexes de Rh(I) a été évaluée par des méthodes analytiques complémentaires que sont le blindage en RMN du ^{103}Rh et la fréquence d'élongation CO en infra-rouge.

La seconde partie, correspondant aux chapitres 2 à 6, porte sur la chimie des acétyléniques et en particulier sur les dérivés macro-aromatiques à motifs cumulènes de types *carbo*-mères tels que les *carbo*-benzènes,[1] avec l'objectif de fournir de nouvelles connaissances fondamentales et des perspectives d'applications de ces dérivés. Plus précisément, les efforts ont été dirigés vers la mise en évidence du rôle des interactions supramoléculaires soit au niveau local dans des complexes hôte-invité, soit à longue distance dans des auto-assemblages de dérivés de *carbo*-benzènes. Différentes cibles ont donc été imaginées dans cet objectif, et sont présentées dans les 5 chapitres composant la deuxième partie du manuscrit.

1. Les phosphines nitroaromatiques comme ligands faiblement P-donneurs : la série N-aryl-benzimidazolyle dans des complexes RhCl(CO)

Les ligands peuvent être classés en deux catégories : les ligands pauvres et les ligands riches en électrons. Alors que les ligands phosphines riches en électrons, tels que les arylphosphines à substituants électro-donneurs,[2] les alkylphosphines,[3] les imidazol-2-ylidènaminophosphines[4] ou les phosphinophosphinidènes,[5] ont été beaucoup étudiés, les représentants pauvres en électrons n'ont été que peu explorés. L'efficacité spécifique des ligands phosphane déficients en électrons dans des réactions catalysées par des métaux de transitions, comme la métathèse

des oléfines ou l'hydroformylation, a pourtant longtemps attiré l'attention des chimistes.[6] Les P-ligands pauvres en électrons sont généralement conçus suivant différentes approches :

- substitution du squelette des triarylphosphines par des groupements accepteurs tels que CF_3 ou CN,[7]
- introduction de liaisons P-O exerçant un effet électro-accepteur sur l'atome de phosphore libre ou complexé par effet inductif (-I),[8]
- introduction d'une charge positive au voisinage de l'atome de phosphore, rendant ainsi sa paire libre moins disponible,[9]
- remplacement des substituants aryle des phosphines neutres par des groupes hétéroaryle pouvant exercer un effet électro-attracteur (–M) sur l'atome de phosphore par π-donation de la paire libre du P dans l'orbitale antiliante π* de l'hétérocycle.[10]

Dans l'objectif d'augmenter encore le caractère pauvre en électrons d'hétéroarylphosphines tout en conservant leur caractère neutre, l'utilisation de substituants accepteurs a été considérée à travers l'étude du cas du groupement nitro. Une série de (*N*-phényl-benzimidazol-1-yl)diphénylphosphines portant un nombre variable de groupes NO_2 sur les cycles phényle ou benzimidazolyle a donc été préparée en présence de LDA comme base optimale, et les complexes *trans*-$L_2Rh^ICl(CO)$ correspondants ont été obtenus suivant deux stratégies (Schéma 1).

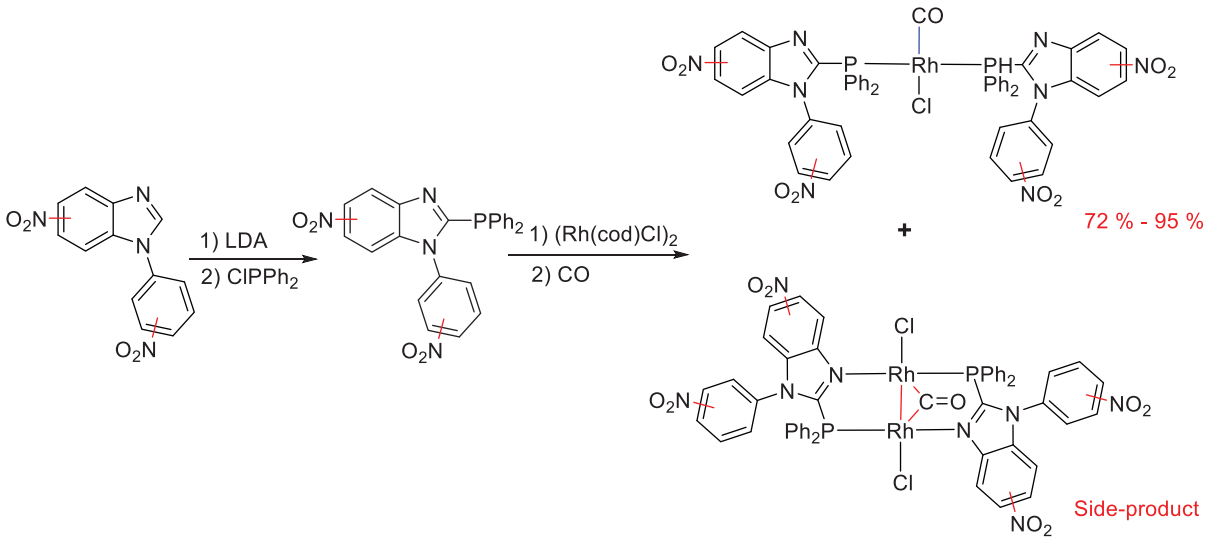

Schéma 1. Méthode générale de préparation des ligands (N-phényl-benzimidazol-1-yl)diphénylphosphine à substituants nitro et des complexes de Rh(I) correspondants.

La fréquence d'élongation de la bande C=O en spectroscopie infra-rouge et le déplacement chimique en RMN du ^{103}Rh ont été utilisés comme sondes pour mesurer le caractère électro-donneur des ligands phosphorés synthétisés, qui se sont avérés être très faiblement σ-donneurs

en comparaison des ligands non-nitrés correspondants et des dérivés cationiques N-méthyl-benzimidazolium.[11]

2. Les hexaaryl-*carbo*-benzènes revisités : nouvelle voie de synthèse, donnés cristallographiques et comportement électrochimique

L'élément carbone est d'une importance primordiale dans la construction chimique de la vie sur Terre et il est également à la base de la chimie organique. Environ 10^7 molécules organiques et polymères ont été synthétisés par les chimistes, leur diversité structurale étant basée sur des liaisons C-C et C-X stables, et accompagnée par de nombreuses propriétés chimiques et physiques. Leurs applications sont très variées, allant des médicaments aux matériaux.

Les premières études sur les matériaux carbonés ont principalement porté sur deux allotropes du carbone : le graphite et le diamant, correspondant à des réseaux d'atomes de carbone hybridés sp^2 et sp^3 respectivement. La structure tridimensionnelle en couches du graphite lui confère des applications comme lubrifiant solide et comme additif pour renforcer les fibres de carbone.[12] Le diamant, avec sa dureté et son indice de réfraction élevé, est quant à lui principalement utilisé en joaillerie et dans les têtes de forage pour l'exploration géologique.[13] Ces différentes applications, basées sur les propriétés chimiques et physiques distinctes de ces deux allotropes du carbone, ont attiré l'attention de la communauté scientifique vers le développement de nouveaux matériaux carbonés.

Après la première synthèse en 1985 du Buckminster fullerene,[14] formé de 60 atomes de carbone équivalents hybridés sp^2, les nanotubes de carbone, composés d'atomes de carbone de même hybridation, ont commencé à être étudiés en 1991.[15] Plus récemment, le « parent » de ces deux allotropes du carbone, un feuillet de graphène, a été synthétisé pour la première fois par Geim et al.[16] Ce réseau bidimensionnel d'atomes de carbone arrangés en nid d'abeilles a été étudié notamment pour ses propriétés électroniques, mais il présente également des propriétés mécaniques et thermiques exceptionnelles.[17] Les structures des graphynes, composés d'atomes de carbone hybridés sp et sp^2, proposées par Baughman en 1987,[18] ont été largement étudiés au niveau théorique. Ces graphènes expansés sont formellement obtenus par insertion d'unités C_2 dans toutes les liaisons covalentes du graphène (α-graphyne) ou dans une partie d'entre elles (γ-graphyne), et peuvent donc être formellement obtenus par le processus de *carbo*-mérisation, défini en 1995, et consistant en l'insertion d'unités C_2 dans toutes les liaisons covalentes, ou dans une partie topologiquement définie des liaisons d'une structure de Lewis parente.[19] L'α-graphyne peut donc être considéré comme le *carbo*-mère du graphène,

ou *carbo*-graphène, dont les motifs constitutifs de base sont des cycles *carbo*-benzènes, largement étudiés dans l'équipe depuis 20 ans. La symétrie D_{6h}, le caractère discotique creux, l'aromaticité magnétique et le système conjugué riche en électrons π du cycle *carbo*-benzène le rend attractif pour de possibles applications dans de nombreux domaines tels que l'optique non linéaire[20] ou la conductivité électrique.[21] Bien que le représentant non substitué $C_{18}H_6$ soir encore inconnu, plus de 30 *carbo*-benzènes diversement substitués ont été décrits.[1]

Tous les *carbo*-benzènes sont préparés à partir de précurseurs hexaoxy[6]péricyclynes,[22] dont les six substituants hydroxyle ou alkoxyle sont éliminés dans des conditions acides et réductrices dans une dernière étape conduisant à la formation du macrocycle aromatique en C_{18}.[1] Différentes voies de synthèse, toutes basées sur une étape clé de macrocyclisation notée [X+Y] entre un dinucléophile X et un diélectrophile Y, ont été envisagées pour préparer ces hexaoxy[6]péricyclynes (Schéma 2).[23]

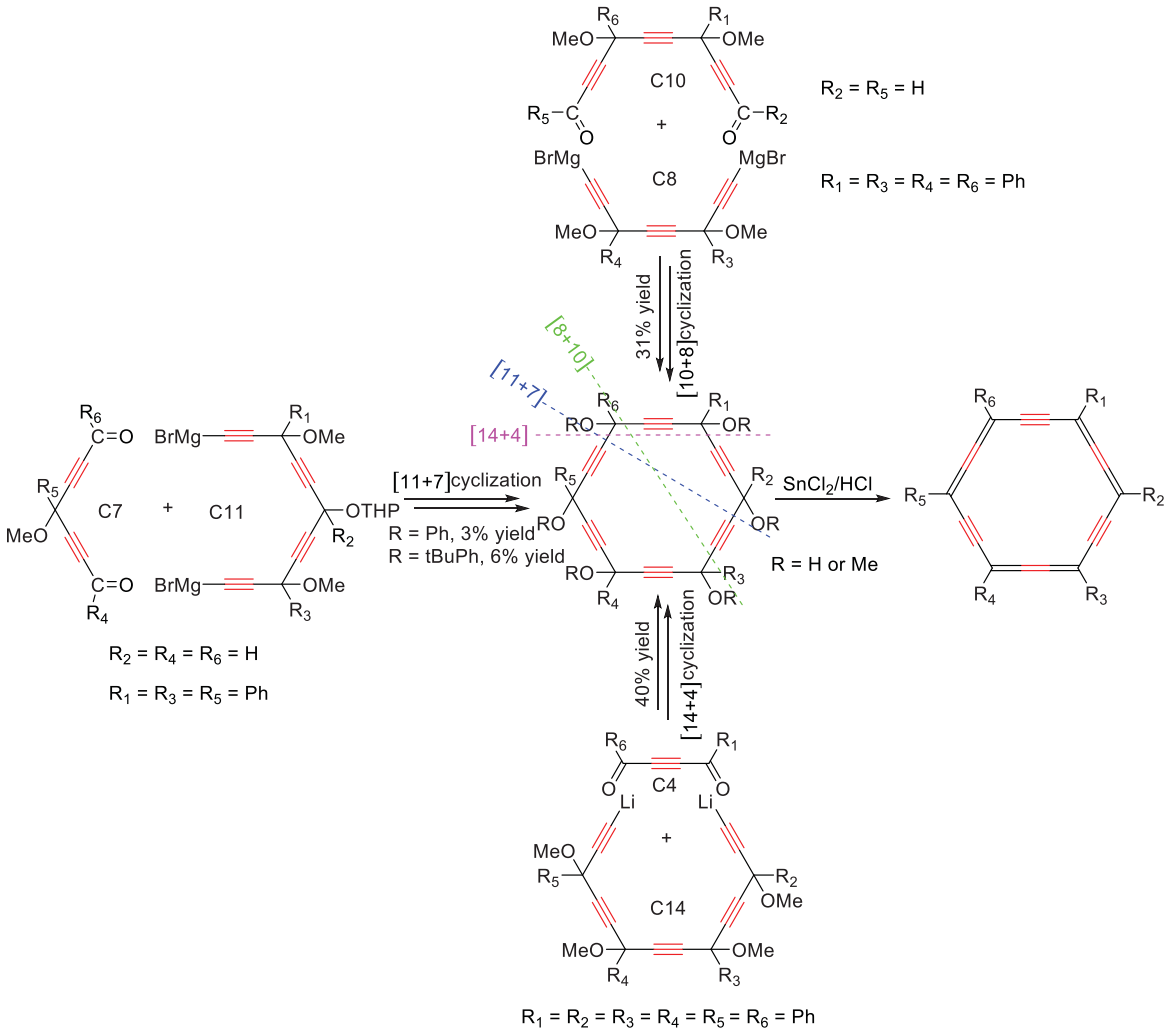

Schéma 2. Différentes stratégies de macrocyclisation développées pour la synthèse des précurseurs hexaoxy[6]péricyclynes de *carbo*-benzènes.

Les premiers exemples de *carbo*-benzènes dont le représentant hexaphénylé de référence, décrits par Ueda *et al*, ont été obtenus par une stratégie de cyclisation de type [11+7].[24] En 2007, une nouvelle voie d'accès à l'hexaphényl-*carbo*-benzène basée sur une macrocyclisation [14+4] a été proposée,[23] avant la mise au point de l'approche [8+10], qui a été montrée comme étant la plus efficace pour préparer les *carbo*-benzènes quadripolaires, via la synthèse d'un [6]péricyclynediol clé résultant de l'addition d'un triyne dinucléophile en C_8 sur un dialdéhyde diélectrophile en C_{10}.[25] Le diol macrocyclique ainsi obtenu peut facilement être oxydé en dicétone, qui peut alors conduire en deux étapes, une addition nucléophile suivie d'une aromatisation réductrice, à de nombreux *carbo*-benzènes quadripolaires (Schéma 3).[1]

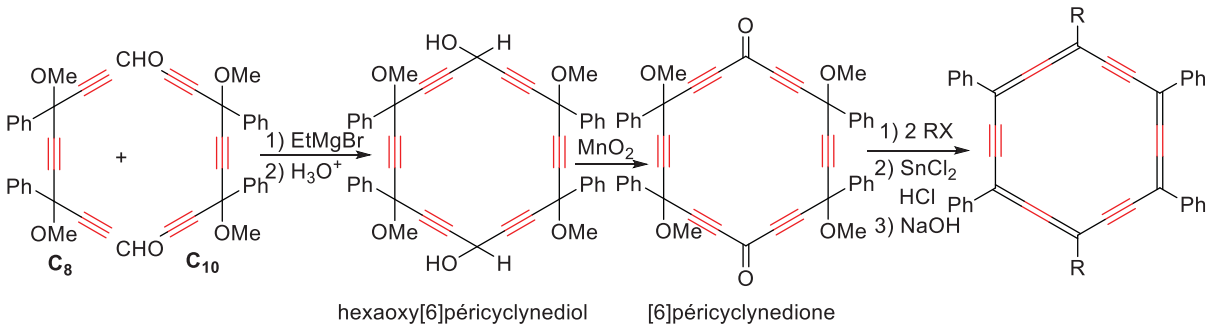

Schéma 3. Méthode générale de synthèse des *carbo*-benzènes quadripolaires.

La plupart des *carbo*-benzènes souffrent d'une solubilité limitée réduisant le champ d'applications possibles. La recherche de substituants permettant d'augmenter la solubilité de cette famille de molécules riches en carbone devient donc aujourd'hui d'une importance cruciale. L'hexaphényl-*carbo*-benzène a donc été re-préparé afin de définir la solubilité de cette molécule de référence, ce qui a permis de compléter sa caractérisation qui n'avait été que partiellement décrite par Ueda et Kuwatani,[24] mais également d'augmenter le rendement global de sa synthèse tout en diminuant le nombre d'étapes.[26] La préparation d'un analogue *a priori* plus soluble à substituants 3,5-di-*tert*-butylphényle a été effectuée en deux étapes à partir de la [6]péricyclynedione, et il a également été entièrement caractérisé, mais l'effet de ces substituants sur la solubilité des *carbo*-benzènes s'est avérée très faible.[26]

3. *Carbo*-benzènes lipidiques : sondes moléculaires de l'anisotropie magnétique et des propriétés d'empilement de l'α-graphyne

La recherche de substituants solubilisants efficaces a été amorcée récemment dans le cadre de la synthèse d'un *carbo*-naphtalène dont la solubilité avait été anticipée comme très faible. Sa préparation a donc été entreprise en version octa-substituée par des groupements 4-

pentylphényle, [27] mais l'effet de ces derniers sur la solubilité est apparu limité, tout comme celui des groupements 3,5-di-*tert*-butylphényle.[26] L'introduction de chaînes alkyles sur les substituants phényle des *carbo*-benzènes ayant peu d'influence sur leur solubilité, l'insertion directe de chaînes aliphatiques sur le cycle en C_{18} a alors été envisagée. Alors que les substituants *iso*-propyl n'améliorent pas la solubilité,[28] les groupements *tert*-butyl directement insérés sur le macrocycle ont récemment été montrés augmenter de façon significative la solubilité des *carbo*-benzènes dans les solvants organiques.[29]

Sur la base de ces résultats préliminaires, l'insertion directe de chaînes alkyles linéaires de longueurs variables sur les positions *para* des *carbo*-benzènes a été envisagée comme nouvelle approche visant à améliorer la solubilité de ces molécules. Une série de longueurs de chaînes (n = 2, 4, 8, 14, 20) a été proposée, et les *carbo*-benzènes correspondants ont été préparés suivant la méthode classique en deux étapes à partir de la [6]péricyclynedione. L'utilisation de réactifs bromures d'alkyl magnésium a conduit à la formation de mélanges des diadduits ciblés et des mono-adduits réduits, permettant ainsi la préparation parallèle de séries de dialkyl- et de monoalkyl-*carbo*-benzènes (Schéma 4). Le résultat de la réaction en fonction de la nature du nucléophile utilisé a également été exploré afin de déterminer quel réactif conduit à la plus grande sélectivité en diadduit. Trois types de nucléophiles ont été envisagés : alkyl lithien (C^-Li^+), alkyl halomagnésien (C^-MgX^+, X = Cl, Br), et alkyl cérien ($C^-CeCl_2^+$), ce dernier donnant le diadduit avec un rendement élevé, sans formation observée de produit de réduction.[30] Les propriétés physico-chimiques, telles que la solubilité, la température de fusion-décomposition, les propriétés d'absorption, le comportement électrochimique et l'empilement cristallin des dialkyl-*carbo*-benzènes obtenus ont été étudiées et discutées en fonction de la longueur de chaîne.[31]

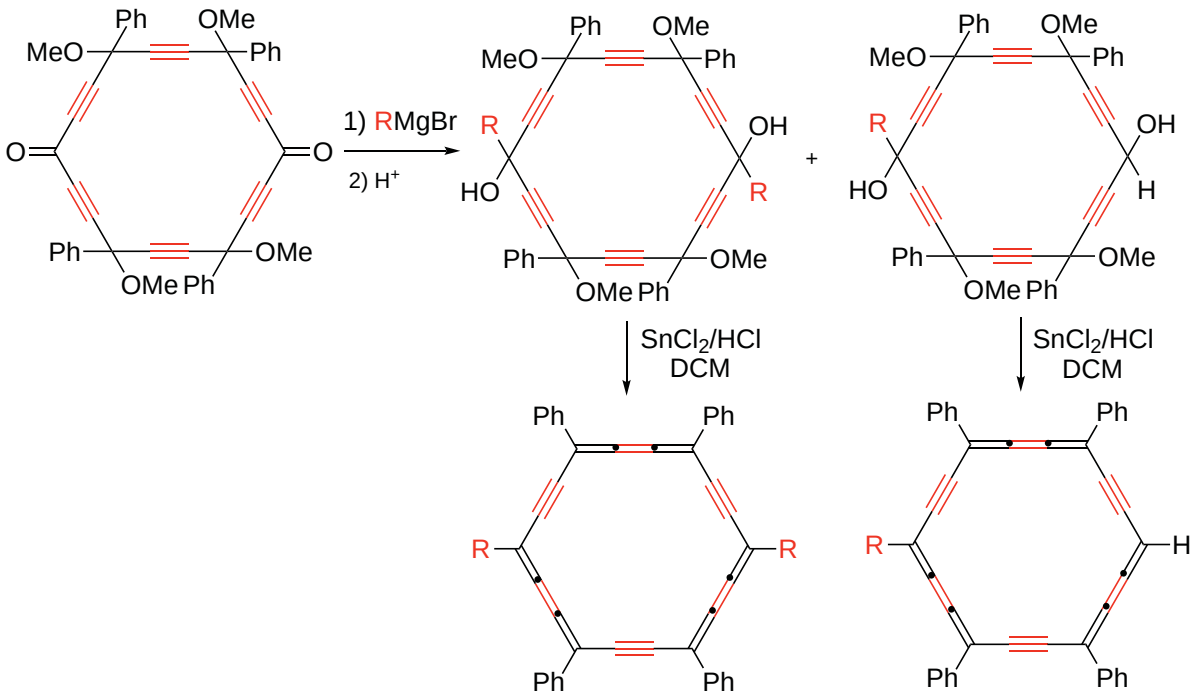

Schéma 4. Synthèse des dialkyl- et monoalkyl-*carbo*-benzènes à partir de la [6]péricyclynedione en utilisant RMgBr comme base.

4. Assemblages supramoléculaires 3D et 2D et comportement thermotropique d'un mésogène de type *carbo*-benzène

Les cristaux liquides sont présents dans de nombreux dispositifs électroniques faisant partie intégrante de notre vie quotidienne, comme les smartphones, les ordinateurs portables et les écrans de télévision. La phase cristal liquide, qui est un état intermédiaire entre l'état cristallin et l'état amorphe, est formée par l'auto-organisation spontanée de molécules mésogènes. Suivant la forme de ces molécules mésogènes, les cristaux liquides sont communément classés en deux catégories : calamitiques (mésogènes en forme de bâtonnets)[32] et discotiques (mésogènes en forme de disque).[33] Les premières mésophases calamitiques ont été décrites par Reinitzer au début du 20ème siècle,[34] et depuis, le comportement cristal liquide de mésogènes linéaires en forme de bâtonnet a été largement étudié et a conduit à des applications concrètes, notamment dans les affichages à cristaux liquides (LCD).[35]

Les cristaux liquides discotiques sont connus depuis que Chandrasekhar a décrit la formation de mésophases de ce type par des mésogènes de type benzène hexasubstitué il y a une quarantaine d'années.[36] Récemment, les cristaux liquides discotiques ont fait l'objet d'intenses recherches pour leurs applications potentielles dans les transistors organiques à effet de champ, dans les diodes électroluminescentes organiques et dans les dispositifs photovoltaïques organiques.[33,37] Les mésogènes discotiques présentent typiquement un cœur

rigide et plat aromatique décoré par plusieurs chaînes aliphatiques flexibles, et ils conduisent à la formation de deux principaux types de mésophases : nématiques et colonnaires.[33,35] Des mésophases lamellaires, dont la structure reste ambigüe encore aujourd'hui, peuvent aussi être formées par des mésogènes discotiques.[38] Dans les mésophases colonnaires, les mésogènes s'organisent en colonnes parallèles, dont la formation est induite par des interactions coopératives à la fois des cœurs aromatiques centraux et des chaînes latérales qui les entourent. Dans ces mésophases, les distances cœur-cœur intra-colonnaires sont généralement courtes (environ 3,5 Å), permettant un recouvrement des orbitales π de deux mésogènes adjacents, alors que les distances inter-colonnaires sont généralement plus grandes (de l'ordre de 20 à 40 Å) et dépendent de la longueur des chaînes flexibles. Les cœurs aromatiques les plus communément utilisés pour l'élaboration de cristaux liquides à mésophases colonnaires sont des dérivés macro-polycycliques pouvant contenir des hétéro-atomes (N, O, S) tels que les porphyrines, les phtalocyanines, les hexaazatriphénylènes (HAT),[39] les triphénylènes ou les hexa-péri-hexabenzocoronènes (HBC).[40] De façon générale, les cœurs aromatiques étendus plans permettant un bon recouvrement des orbitales π sont susceptibles de renforcer la stabilité de l'arrangement colonnaire et l'ordre supramoléculaire. Les chaînes dispersives attachées au cœur central jouent aussi un rôle important dans la formation des mésophases colonnaires. La nature, le nombre et la position de ces chaînes sur le cœur mésogène peuvent fortement modifier les températures de transition de phase, la solubilité des molécules mésogènes, les distances inter-colonnaires et l'ordre intra-colonnaire des mésophases. Les chaînes flexibles les plus utilisées sont des chaînes alkyles linéaires ou branchées, des groupes alkylphényle ou alkoxyphényle.

Alors que les macro-poly-hétérocycles aromatiques tels que les porphyrines ont été largement considérés comme cœur mésogène, aucune attention n'a été portée aux macro-mono-cycles aromatiques. En particulier, le cycle *carbo*-benzène en C_{18}, dont le caractère macro-aomatique est souvent comparé aux circuits en $C_{16}N_2$ à 18 électrons π des porphyrines, n'avait jamais été envisagé comme cœur mésogène avant ce travail. Pourtant, le cycle *carbo*-benzène à 18 électrons π délocalisés, analogue trois fois expansé du benzène, représente un nouveau type de cœur attractif pour l'élaboration de cristaux liquides discotiques. De plus, la forme hexagonale des *carbo*-benzènes en font une plateforme idéale sur laquelle il est possible d'insérer des chaînes alkyles sur différentes positions. Les *para*-dialkyl-*carbo*-benzènes lipidiques portant deux chaînes alkyle linéaires récemment décrits ne présentent pas de comportement cristal liquide, suggérant que la présence de deux chaînes sur le cœur mésogène

n'est pas suffisante pour induire la formation de mésophases.[31] Deux *para*-trialkoxyphényléthynyl-*carbo*-benzènes ayant différentes longueurs de chaînes ont donc été préparés (*n*-$C_{12}H_{25}$ et *n*-$C_{18}H_{37}$), et le comportement mésogène de l'un d'entre eux a été étudié. La formation d'une mésophase colonnaire rectangulaire à 115 °C a été mise en évidence par microscopie optique à lumière polarisée (POM), par calorimétrie différentielle à balayage (DSC), par diffraction des rayons X sur poudre (PXRD) et par microscopie à effet tunnel (STM). Les constantes mesurées pour le réseau 3D ont été trouvées être en accord avec les images STM du réseau 2D obtenu en déposant une solution de *carbo*-mésogène sur une surface de HOPG (Figure 1).[41]

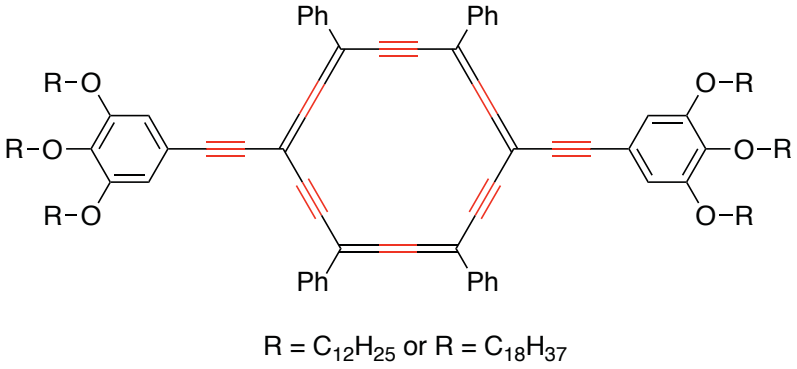

Figure 1. Molécules *carbo*-mésogènes portant des chaînes alkyle de longueurs différentes.

5. *Carbo*-bi- and –ter-phényles : *carbo*-mères de cycle de [n]OPE

Suite au rapport initial par Ratner en 1974,[42] l'électronique moléculaire est devenu un sujet de recherche incontournable qui a considérablement attiré l'intérêt de la communauté scientifique.[43] Il est aujourd'hui reconnu que les molécules organiques π-conjuguées ayant un petit gap HOMO-LUMO peuvent potentiellement trouver des applications dans des dispositifs électroniques moléculaires.[44] Durant les dernières décennies, de nombreux efforts ont porté sur le développement de nouvelles molécules organiques pouvant être utilisées dans des dispositifs électroniques en remplacement des circuits à base de silicium dans le but de miniaturiser les circuits intégrés.[45] Les molécules organiques π-conjuguées parmi lesquels les oligomères et les polymères ont de nombreux avantages tels que de faibles coûts de production, une mise en œuvre simple, et surtout la possibilité de modifier leur structure moléculaire afin de moduler les propriétés optiques et électroniques.[46]

Les fils moléculaires oligo(phénylène-éthynylène)s (OPE) ont été considérés comme modèles pour l'étude des propriétés structurales et électroniques des polymères poly(phénylène-éthynylène) correspondants.[47] Les remarquables propriétés optiques et électroniques des OPE ont conduit à des applications dans de nombreux domaines tels que dans

les diodes organiques électroluminescentes,[48] les chimiosenseurs,[49] les interrupteurs moléculaires[50] ou les matériaux pour l'optique non-linéaire.[51] Malgré les nombreux travaux visant à synthétiser des OPE pour l'étude de leurs propriétés de transport de charge, fabriquer un circuit intégré moléculaire applicable dans des dispositifs reste aujourd'hui un défi.[50,52] Les propriétés de transport de charge de fils moléculaires ne dépendent pas seulement de facteurs physiques tels que la température ou de l'interface molécule-électrode, mais aussi de la nature chimique de la molécule et en particulier de sa conjugaison, de ses caractéristiques redox, de sa longueur et de ses substituants.[53] En règle générale, le transport de charge est amélioré dans les molécules rigides, présentant un système π-conjugué étendu et un potentiel redox faible.[46,54]

Le cycle *carbo*-benzène à 18 électrons π délocalisés, trois fois plus grand mais trois fois moins aromatique au niveau énergétique que son parent benzène à 6 électrons π,[55] a récemment été montré, à travers l'étude du *p*-dianilinyl-*carbo*-benzène, présenter une conductance moléculaire sans précédent de 106 nS, soit dix fois plus grande que celle de molécules comparables de mêmes dimensions.[56] Cette conductance élevée, associée à la rigidité, la planéité et la richesse en électrons π des *carbo*-benzènes, a encouragé l'élaboration d'une série de *carbo*-mères de cycle d'OPE (*carbo*-OPE). La préparation d'un *carbo*-OPE_2 (*carbo*-mère de squelette du biphényle) et de deux *carbo*-OPE_3 (*carbo*-mères de squelette du terphényle) a alors été envisagée. Afin de les rendre solubles, ces trois cibles ont été conçues avec des chaînes *n*-octyle solubilisantes aux deux extrémités de leur squelette π-conjugué. De même, l'un des *carbo*-terphényle a été ciblé avec des chaînes pentyle sur les quatre substituants phényle du macrocycle central.

Des voies de synthèse basées sur des procédés de mono-addition nucléophile sur la [6]péricyclynedione ont été utilisées pour préparer ces *carbo*-OPE (Schéma 4). Le *carbo*-OPE_2 a été synthétisé avec un rendement de 7 % à partir de la [6]péricyclynedione. Les deux *carbo*-OPE_3, premiers exemples de molécules composées de trois cycles *carbo*-benzènes, ont été préparés suivant deux stratégies différentes. Ces trois *carbo*-OPE ont été entièrement caractérisés par RMN ^{1}H et ^{13}C, par spectroscopie UV-visible, par spectrométrie de masse et par électrochimie. Deux d'entre eux ont également été caractérisés par diffraction des rayons-X sur des monocristaux obtenus à partir de solutions dans le chloroforme. Les *carbo*-OPE_3 présentent un très faible potentiel de première réduction (0,42 ± 0.03 V/SCE), sans précédent en série *carbo*-mère. Des études théoriques ont également été réalisées afin d'évaluer l'aromaticité des cycles *carbo*-benzènes de cette série de *carbo*-OPEn (n = 1 – 4) à travers la détermination des valeurs de NICS au centre de chaque macrocycle (calculs DFT).[57]

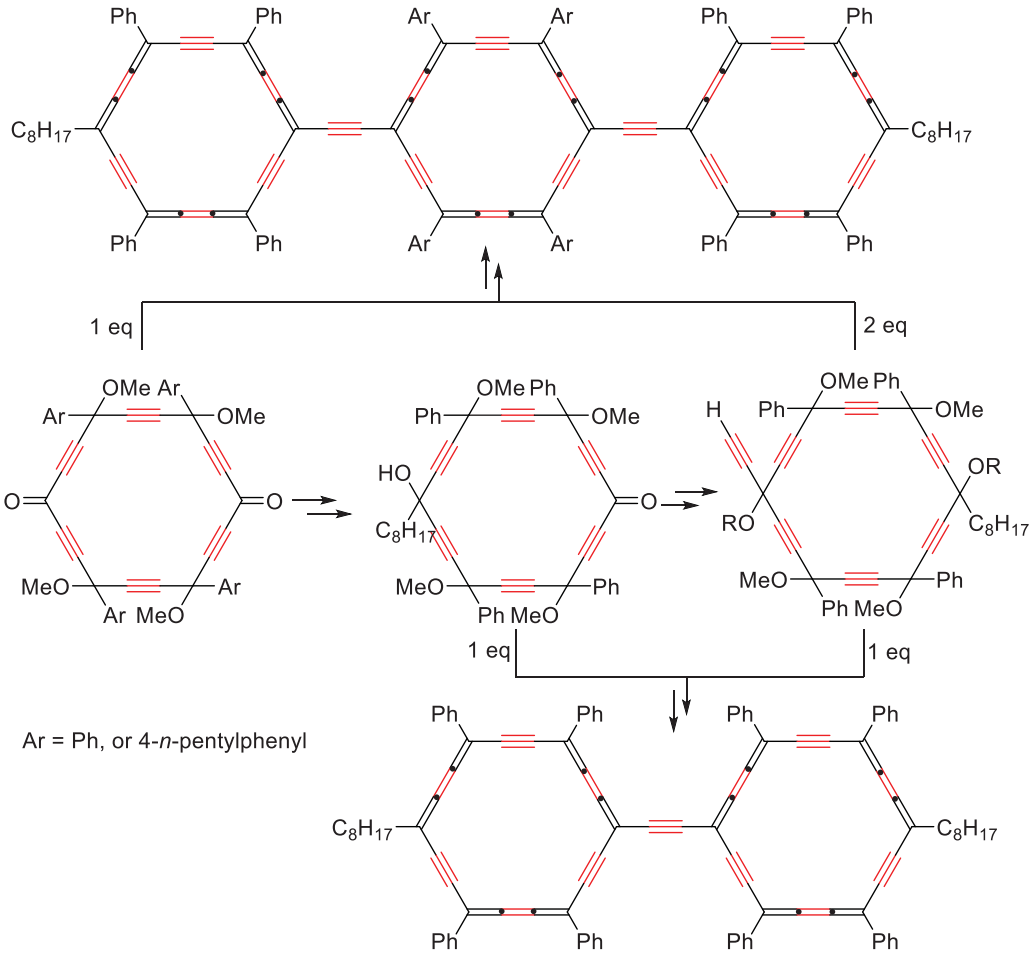

Schéma 4. Stratégies de synthèse des *carbo*-OPE.

6. Des hémi-butatriènes endo-aromatiques aux unités [3]cumulènes pontants : *carbo*-barrélènes et *carbo*-stilbènes

Au cours des dernières décennies, les chromophores macrocycliques polyacétyléniques π-conjugués ont attiré l'attention des chimistes pour leurs propriétés structurales, électroniques et optiques remarquables.[58] En chimie des *carbo*-mères, au-delà des *carbo*-benzènes qui sont les plus étudiés, l'élaboration et la synthèse de nouveaux types de molécules expansées de cette famille est encore aujourd'hui un sujet de recherche active dans l'équipe. Par exemple, la synthèse multi-étapes d'un *carbo*-naphtalène, plus petit fragment polycyclique fusionné d'α-graphyne (ou *carbo*-graphène), a été récemment décrite.[27] Dans ce contexte, la synthèse de *carbo*-mères tricyclique du barrélène tendu (bicyclo[2.2.2]-2,5,7-octatriène) a été envisagée, le barrélène parent étant lui-même attractif, non seulement pour sa structure particulière, mais aussi pour ses possibles applications dans divers domaines. Depuis le premier rapport sur le barrélène par Zimmerman en 1960,[59] de nombreux dérivés du barrélène ont été décrit et étudiés

pour leurs propriétés électroniques,[60] pour leurs applications en catalyse[61] et pour leur capacité à subir des réarrangement photo-induits.[62]

Le *carbo*-barrélène, avec son triple système π-conjugué riche en électrons, est attractif non seulement pour ses possibles propriétés optiques et électroniques, mais aussi parce que sa structure tridimensionnelle creuse peut être considérée comme une cage organique rigide pouvant éventuellement encapsuler de petites molécules ou ions. Ces dernières années, l'utilisation de molécules comme conteneurs hôtes capables d'encapsuler de petits invités a fait l'objet d'intenses recherches,[63] en particulier pour les nombreuses applications qui découlent de cette propriété telles que la stabilisation d'espèces instables,[64] la reconnaissance moléculaire,[65] la discrimination de molécules chirales,[66] la croissance de cristaux[67] ou la catalyse[68] par exemple. Les composés cages sont en général classés en deux catégories : les cages supramoléculaires formées par auto-organisation de petites molécules[69] et les cages covalentes obtenues par synthèse organique.[70] Les cages covalentes, dont la construction requiert des synthèses multi-étapes aux rendements parfois faibles, sont donc plus rares que leurs homologues supramoléculaires. Malgré ce désavantage, les structures creuses rigides covalentes restent attractives pour leur plus grande stabilité ouvrant des possibilités d'applications comme hôte chiral,[71] comme récepteur ou comme capteur.[72] Le fullerène C_{60} et ses dérivés ont été par exemple largement étudiés en tant que cages covalentes pouvant encapsuler le dihydrogène.[73]

Ici, la synthèse de *carbo*-barrélènes, possibles cages covalentes composées de trois unités dialcynylbutatriènes connectées entre elles par deux sommets hybridés sp^3, a été envisagée par double addition nucléophile cyclisante d'un équivalent de triyne sur la [6]péricyclynedione en présence de LiHMDS comme base, suivie d'une étape d'élimination réductrice. Deux *carbo*-barrélènes et un dérivé partiellement réduit bis-butatriénique ont été isolés sous forme de solides brun-jaunes très solubles et suffisamment stables pour pouvoir être caractérisés par RMN, spectroscopie UV-visible, spectrométrie de masse et électrochimie (Schéma 5). Ils ont également été caractérisés par analyse par diffraction des rayons-X sur des monocristaux obtenus à basse température.[74] Le cation NH_4^+ a été envisagé comme invité pour ce nouveau type de cage covalente dans des travaux préliminaires. A ce jour, aucune preuve expérimentale claire d'encapsulation de NH_4^+ dans le *carbo*-barrélène n'a pu être mise en évidence, mais des calculs théoriques suggèrent qu'une interaction stabilisante devrait se produire entre ces deux molécules (ΔE_{tot} = - 44.4 kcal/mol).

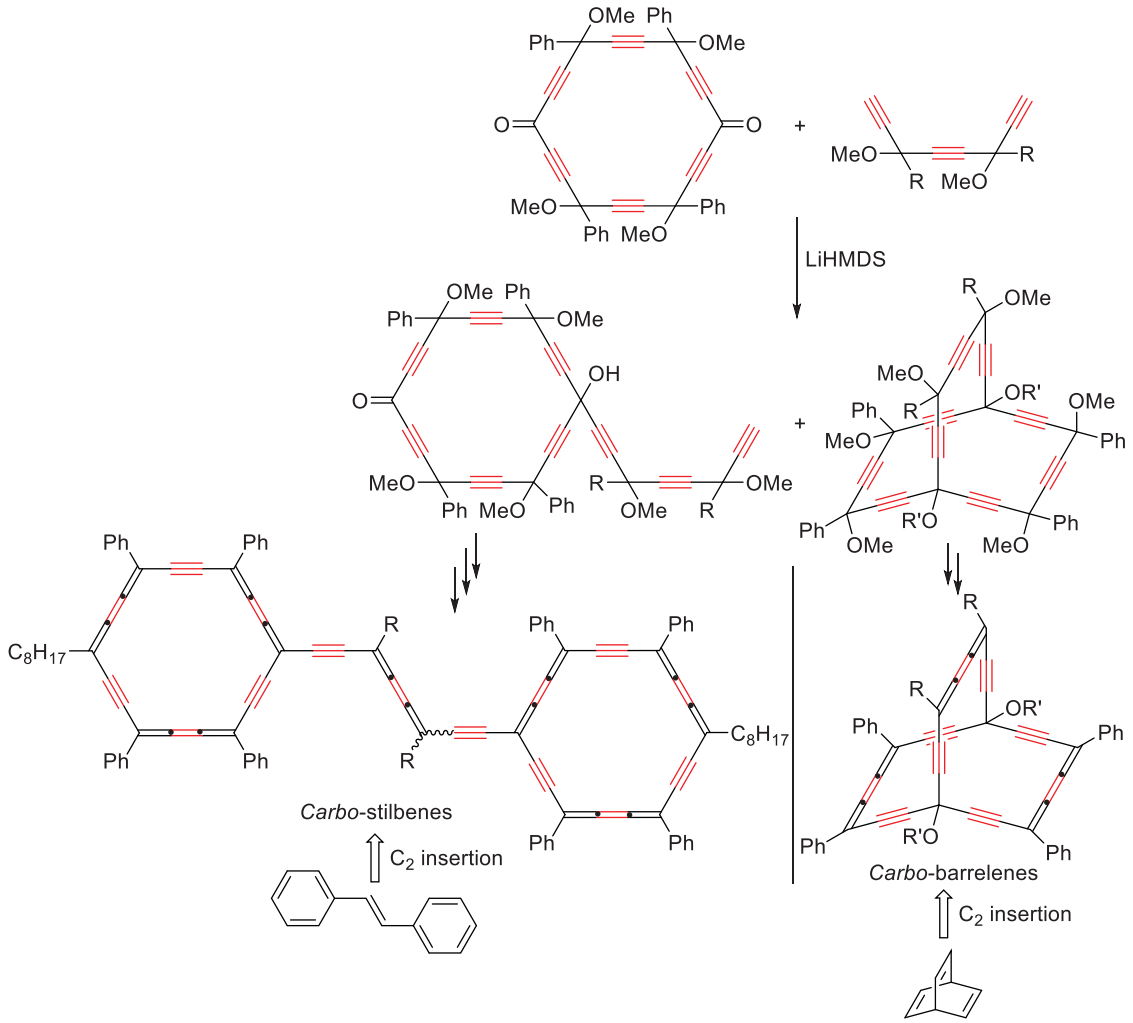

Schéma 5. Stratégies de synthèse des *carbo*-barrélènes et des *carbo*-stilbènes.

Inspirée par la formation d'un produit secondaire lors de la synthèse des *carbo*-barrélènes, la préparation de *carbo*-stilbènes a été envisagée (Schéma 5). La propriété de photo-isomérisation des dérivés du stilbène parent (1,1-diphényléthène), conduisant à de nombreuses applications comme colorant, dans des dispositifs optiques[75] et même en biomédecine,[76] a en effet motivé la synthèse et l'étude de *carbo*-stilbènes, qui pourraient aussi s'avérer présenter des propriétés optiques et électroniques intéressantes. Deux *carbo*-stilbènes ont été préparés suivant une stratégie de synthèse optimisée, mais leur très faible solubilité n'a pas permis leur entière caractérisation. Ils ont cependant pu être caractérisés par RMN ^{1}H, spectroscopie UV-visible, spectrométrie de masse et électrochimie. Les spectres RMN ^{1}H ont montré la formation d'un mélange des deux isomères *cis*- et *trans*- des *carbo*-stilbènes, mais aucune évidence d'interconversion *cis-trans*, souvent observée pour les dialcynylbutatriènes,[77] n'a pu être détectée par RMN à température variable entre 25 et 55 °C.[74]

Ce travail de thèse couvre deux thèmes de recherche distincts : la chimie organométallique de coordination, et la chimie organique de synthèse. Une quarantaine de produits finaux, dont 33 composés organiques et sept complexes de Rh^{I} ont été obtenus, isolés et caractérisés. La structure de 27 d'entre eux a pu être confirmée par analyse par diffraction des rayons X.

On peut remarquer un point commun formel entre ces deux thématiques de recherche, qui est le rôle clé des bases encombrées LDA et LiHMDS dans la préparation des phosphines nitro-aromatiques d'une part, et des *carbo*-benzènes, *carbo*-OPEs, *carbo*-barrélènes et *carbo*-stilbènes d'autre part. En termes de versatilité de synthèse, 24 *carbo*-benzènes ont été préparés à partir du précurseur [6]péricyclynedione clé. L'augmentation de la solubilité observée par substitution directe du macrocycle par des chaînes alkyles devrait permettre de manipuler plus facilement des molécules *carbo*-mères plus étendues, comme de longs films moléculaires *carbo*-OPE.

Enfin, ces résultats ouvrent des perspectives d'applications dans différents domaines tels que la catalyse, la chimie hôte-invité des clathrates, le photovoltaïque organique, l'élaboration de cristaux liquides, l'électronique moléculaire et la photochimie.

Références

1. K. Cocq, C. Lepetit, V. Maraval, R. Chauvin, *Chem. Soc. Rev*., **2015**, *44*, 6535-6559.
2. a). R. Schmid, M. Cereghetti, B. Heiser, P. Schonholzer, H. J. Hansen, *Helv. Chim. Acta.*, **1988**, *71*, 897-929; b). H. Jendralln, C. H. Li, E. Paulus, *Tetrahedron: Asymmetry*, **1994**, *5*, 1297-1320; c). P. Kocovsky, S. Vyskocil, M. Smrcina, *Chem. Rev*., **2003**, *103*, 3213-3245; d). H. Shimizu, I. Nagasaki, T. Saito, *Tetrahedron*, **2005**, *61*, 5405-5432; e). Z, Freixa, P. W.N.M. van Leeuwen, *Coord. Chem. Rev*., **2008**, *252*, 1755-1786.
3. a) M. Bacci, S. Midollini, P. Stoppioni, L. Sacconi, *Inorg. Chem.*, **1973**, *12*, 1801-1805; b) J. R. Görlich, R. Schmutzler, *Phosphorus Sulfur Silicon Relat. Elem.*, **1995**, *102*, 211-215; **1993**, *81*, 141-148; c) M. J. Burk, J. E. Feaster, W. A. Nugent, R. L. Harlow, *J. Am. Chem. Soc*., **1993**, *115*, 10125-10138; d) W. H. Hu, C. C. Pai, C. C. Chen, G. P. Xue, A. S. C. Chan, *Tetrahedron: Asymmetry*, **1998**, *9*, 3241-3246; e) A. Aranyos, D. W. Old, A. Kiyomori, J. P. Wolfe, J. P. Sadighi, S. L. Buchwald, *J. Am. Chem. Soc.*, **1999**, *121*, 4369-4378; f). K. H. Shaughnessy, R. S. Booth, *Org. Lett*., **2001**, *3*, 2757-2759; g) J. S. You, J. G. Verkade, *J. Org. Chem.*, **2003**, *68*, 8003-8007; h) J. S. Huang, G. A. Yu, J. Xie, N. Y. Zhu, C. M. Che, *Inorg. Chem.*, **2006**, *45*, 5724-5726; i) A. J. Kendall, L. N. Zakharov, D. R. Tyler, *Inorg. Chem*., **2016**, *55*, 3079-3090; j) M. Dutartre, J. Bayardon, S. Juge, *Chem. Soc. Rev.*, **2016**, *45*, 5771-5794.
4. a). D. Bourissou, O. Guerret, F. P. Gabbai, G. Bertrand, *Chem. Rev*., **2000**, *100*, 39-91; b). Y. Canac, M. Soleilhavoup, S. Conejero, G. Bertrand, *J. Organomet. Chem*., **2004**, *689*, 3857-3865; c). J. Vignolle, X. Cattoen, D. Bourissou, *Chem. Rev.*, **2009**, *109*, 3333-3384; i). P. L. Arnold, I. J. Casely, *Chem. Rev*., **2009**, *109*, 3599-3611; e). O. Schuster, L. R. Yang, H. G. Raubenheimer, M. Albrecht, *Chem. Rev*., **2009**, *109*, 3445-3478; d). D. J. Nelson, S. P. Nolan, *Chem. Soc. Rev.*, **2013**, *42*, 6723-6753; f). F. E. Hahn, M. C. Jahnke, *Angew. Chem. Int. Ed*., **2008**, *47*, 3122-3172; g). V. Charra, P. Frémont, P. Braunstein, *Coord. Chem. Rev*., **2017**, *341*, 53-176.
5. L. Liu, D. A. Ruiz, D. Munz, G. Bertrand, *Chem.*, **2016**, *1*, 147-153.
6. a). M. P. Magee, W. Luo, W. H. Hersh, *Organometallics*, **2002**, *21*, 362-372; b). R. A. Baber, M. L. Clarke, K. M. Heslop, A. C. Marr, A. G. Orpen, P. G. Pringle, A. Ward, D. E. Zambrano-Williams, *Dalton Trans*., **2005**, 1079-1085; c). Q. Liu, L. P. Wu, I. Fleischer, D. Selent, R. Franke, R. Jackstell, M. Beller, *Chem. Eur. J.*, **2014**, *20*, 6888-6894.
7. a). M. Pomerantz, M. S. Terrazas, Y. Cheng, X. M. Gu, *Phosphorus. Sulfur and Silicon*, **1996**, *109-110*, 505-508; b). F. Berhal, O. Esseiva, C. H. Martin, H. Tone, J. P. Genet, T. Ayad, V. Ratovelomanana-Vidal, *Org. Lett.*, **2011**, *13*, 2806-2809; c). M. H. Shaw, R. A. Croft, W. G. Whittingham, J. F. Bower, *J. Am. Chem. Soc.*, **2015**, *137*, 8054-8057; d). M. J. Stark, M. J. Shaw, A. Fadamin, N. P. Rath, E. B. Bauer, *J. Organomet. Chem.*, **2017**, *847*, 41-53.
8. a) Y. Canac, N. Debono, L. Vendier, R. Chauvin, *Inorg. Chem*., **2009**, *48*, 5562-5568; b) D. Parmar, E. Sugiono, S. Raja, M. Rueping, *Chem. Rev*., **2014**, *114*, 9047-9153.
9. See for examples: a) U. Zoller, *Tetrahedron*, **1988**, *44*, 7413-7426; b) N. Kuhn, M. Goehner, G. Henkel, *Z. Anorg. Allg. Chem*., **1999**, *625*, 1415-1416; c) M. Azouri, J. Andrieu, M. Picquet, P. Richard, B. Hanquet, I. Tkatchenko, *Eur. J. Inorg. Chem*., **2007**, 4877-4883; d) A. A. Tolmachev, A. A. Yurchenko, A. S. Merculov, M. G. Semenova, E. V. Zarudnitskii, V. V.

Ivanov, A. M. Pinchuk, *Heteroatom Chem*., **1999**, *10*, 585-597; e) C. Maaliki, C. Lepetit, C. Duhayon, Y. Canac, R. Chauvin, *Chem. Eur. J*., **2012**, *18*, 16153-16160; f) C. Barthes, C. Lepetit, Y. Canac, C. Duhayon, D. Zargarian, R. Chauvin, *Inorg. Chem*., **2013**, *52*, 48-58; g) Y. Canac, C. Bijani, C. Duhayon, R. Chauvin, *Organometallics*, **2013**, *32*, 4054-4057.

10. a). V. Farina, B. Krishnan, *J. Am. Chem. Soc*., **1991**, *113*, 9585-9595; b). K. Issleib, A. Brack, *Zeitschrift fuer Anorganische und Allgemeine Chemie*, **1957**, *292*, 245-253; c). V. Farina, B. Krishnan, *J. Am. Chem. Soc*., **1991**, *113*, 9585-9595; d). A. A. Tolmachev, A. A. Yurchenko, A. S. Merculov, M. G. Semenova, E. V. Zarudnitskii, V. V. Ivanov, A. M. Pinchuk, *Heteroatom Chem*., **1999**, *10*, 585-597; e). L. H. Zou, Z. B. Dong, C. Bolm, *Synlett*, **2012**, *23*, 1613-1616.

11. C. Zhu, E. Gras, C. Duhayon, F. Lacassin, X. Cui, R. Chauvin, *Chem. Asian J*., **2017**, *12*, 2845-2856.

12. E. Fitzer, *Carbon*, **1989**, *27*, 621-645.

13. F. Diederich, Y. Rubin, *Angew. Chem. Int. Ed. Engl*. **1992**, *31*, 1101-1123.

14. H. W. Kroto, J. R. Heath, S. C. O'Brien, R. F. Curl, R. E. Smalley, *Nature*, **1985**, *318*, 162 −163.

15. S. Lijima, *Nature*, **1991**, *354*, 56-58.

16. K. S. Novoselov, A. K. Geim, S. V. Morozov, D. Jiang, Y. Zhang, S. V. Dubonos, I. V. Grigorieva, A. A. Firsov, *Science*, **2004**, *306*, 666−669.

17. W. Zhou, X. Bai, E. Wang, S. Xie, *Adv. Mater*., **2009**, *21*, 4565−4583.

18. R. H. Baughman, H. Eckhardt, M. Kertesz, *J. Chem. Phys*., **1987**, *87*, 6687-6699.

19. R. Chauvin, *Tetrahedron Lett*., **1995**, *36*, 397-400; *Tetrahedron Lett*., **1995**, *36*, 401-404.

20. I. Baglai, M. Anda-Villa, R. M. Barba-Barba, C. Poidevin, G. Ramos-Ort, V. Maraval, C. Lepetit, N. Saffon-Merceron, J. L. Maldonado, R. Chauvin, *Chem. Eur. J*., **2015**, *21*, 14186-14195.

21. Z. H. Li, M. Smeu, A. Rives, V. Maraval, R. Chauvin, M. A. Ratner, E. Borguet, *Nat. Commun*., **2015**, *6*, 6321.

22. Pour des références sur les péricyclynes voir : a). L. T. Scott, G. J. DeCicco, J. L. Hyunn, G. Reinhardt, *J. Am. Chem. Soc*., **1983**, *105*, 7760-7761; b). K. N. Houk, L. T. Scott, N. G. Rondan, D. C. Spellmeyer, G. Reinhardt, J. L. Hyun, G. J. DeCicco, R. Weiss, M. H. M. Chen, L. S. Bass, J. Clardy, F. S. Jorgensen, T. A. Eaton, V. Sarkosi, C. M. Petit, L. Ng, K. D. Jordan, *J. Am. Chem. Soc*., **1985**, *107*, 6556-6562.

23. a). C. Saccavini, C. Tedeschi, L. Maurette, C. Sui-Seng, C. Zou, M. Soleilhavoup, L. Vendier, R. Chauvin, *Chem. Eur. J*., **2007**, *13*, 4895-4913 ; b) C. Saccavini, C. Sui-Seng, L. Maurette, C. Lepetit, S. Soula, C. H. Zou, B. Donnadieu, R. Chauvin, *Chem. Eur. J*., **2007**, *13*, 4914-4931.

24. a). Y. Kuwatani, N. Watanabe, l. Ueda, *Tetrahedron Lett*., **1995**, *36*, 119-122. b). R. Suzuki, H. Tsukuda, N. Watanabe, Y. Kuwatani, l. Ueda, *Tetrahedron*, **1998**, *54*, 2477-2496.

25. a) L. Leroyer, C. H. Zou, V. Maraval, R. Chauvin, *C. R. Chimie*, **2009**, *12*, 412-429 ; b) L. Leroyer, C. Lepetit, A. Rives, V. Maraval, N. Saffon-Merceron, D. Kandaskalov, D. Kieffer, R. Chauvin, *Chem. Eur. J*., **2012**, *18*, 3226-3240.

26. C. Zhu, C. Duhayon, D. Romero-Borja, J.-L. Maldonado, G. Ramos-Ortíz, A. Saquet, V. Maraval, R. Chauvin, *New. J. Chem*., **2017**, *41*, 3908-3914.

27. K. Cocq, N. Saffon-Merceron, Y. Coppel, C. Poidevin, V. Maraval, R. Chauvin, *Angew. Chem. Int. Ed*., **2016**, *55*, 15133-15136.
28. K. Cocq, N. Saffon-Merceron, A. Poater, V. Maraval, R. Chauvin, *Synlett*., **2016**, *27*, 2105-2112.
29. D. Listunov, C. Duhayon, A. Poater, S. Mazères, A. Saquet, V. Maraval, R. Chauvin, Soumis pour publication.
30. C. Zhu, C. Duhayon, A. Saquet, V. Maraval, R. Chauvin, *Can. J. Chem*., **2017**, *95*, 454-459.
31. C. Zhu, A. Rives, C. Duhayon, V. Maraval, R. Chauvin, *J. Org. Chem*., **2017**, 82, 925-935.
32. M. Hird, *Chem. Soc. Rev*. **2007**, *36*, 2070-2095.
33. T. Wöhrle, I. Wurzbach, J. Kirres, A. Kostidou, N. Kapernaum, J. Litterscheidt, J. C. Haenle, P. Staffeld, A. Baro, F. Giesselmann, S. Laschat, *Chem. Rev*. **2016**, *116*, 1139-1241.
34. D. Vorländer, *Ber. Dtsch. Chem. Ges*. **1907**, *40*, 1970-1972.
35. S. Laschat, A. Baro, N. Steinke, F. Giesselmann, C. Hägele, G. Scalia, R. Judele, E. Kapatsina, S. Sauer, A. Schreivogel, M. Tosoni, *Angew. Chem. Int. Ed*., **2007**, *46*, 4832-4887.
36. S. Chandrasekhar, B. K. Sadashiva, K. A. Suresh, *Pramana*, **1977**, *9*, 471-480.
37. a). S. Sergeyev, W. Pisula, Y. H. Geerts, *Chem. Soc. Rev*., **2007**, *36*, 1902-1929; b). R. J. Bushby, K. Kawata, *Liq. Cryst*. **2011**, *38*, 1415-1426.
38. For a recent example, see: C. W. Ong, Y.-C. Chan, M.-C. Yeh, H.-Y. Lin, H.-F. Hsu, *RSC Adv*. **2013**, *3*, 8657-8659.
39. C. M. Drain, A. Varotto, I. Radivojevic, *Chem. Rev*., **2009**, *109*, 1630-1658; b). B. Roy, N. De, K. C. Majumdar, *Chem. Eur. J*., **2012**, *18*, 14560-14588.
40. a). S. Kumar, *Liq. Cryst*. **2004**, *31*, 1037-1059. b) W. Pisula, X. Feng, K. Müllen, *Adv. Mater*. **2010**, *22*, 3634-3649.
41. C. W. Zhu, T. H. Wang, C. J. Su, S. L. Lee, A. Rives, C. Duhayon, B. Kauffmann, V. Maraval, C. h. Chen, H. F. Hsu, R. Chauvin, *Chem. Commun*., **2017**, *53*, 5902-5905.
42. A. Aviram, M. A. Ratner, *Chem. Phys. Lett*., **1974**, *29*, 277-283.
43. a). N. Robertson, C. A. McGowan, *Chem. Soc. Rev*., **2003**, *32*, 96-103; b). A. C. Benniston, *Chem. Soc. Rev*., **2004**, *33*, 573-578; c). R. Klajn, J. F. Stoddart, B. A. Grzybowski, *Chem. Soc. Rev.*, **2010**, *39*, 2203-2237.
44. C. R. Parker, E. Leary, R. Frisenda, Z. Wei, K. S. Jennum, E. Glibstrup, P. B. Abrahamsen, M. Santella, M. A. Christensen, E. A. Della Pia, T. Li, M. T. Gonzalez, X. Jiang, T. J. Morsing, G. Rubio-Bollinger, B. W. Laursen, K. Nørgaard, H. van der Zant, N. Agrait, M. Brønsted Nielsen, *J. Am. Chem. Soc*., **2014**, *136*, 16497-16507.
45. a). M. D. Watson, A. Fechtenkötter, K. Müllen, *Chem. Rev*., **2001**, *101*, 1267-1300; b). J. Wu, W. Pisula, K. Müllen, *Chem. Rev*., **2007**, *107*, 718-747; c). K. Müllen, J. P. Rabe, *Acc. Chem. Res*., **2008**, *41*, 511-520.
46. D. A. M. Egbe, B. Carbonnier, E. Birckner, U. W. Grummt, *Progr. Polym. Sci*., **2009**, *34*, 1023-1067.
47. a). J. M. Tour, *Chem. Rev*., **1996**, *96*, 537-554; b). U. H. F. Bunz, *Chem. Rev*., **2000**, *100*, 1605-1644; c). W. Hu, N. B. Zhu, W. Tang, D. H. Zhao, *Org. Lett*., **2008**, *10*, 2669-2672; d). Q. Lu, K. Liu, H. M. Zhang, Z. B. Du, X. H. Wang, F. S. Wang, *ACS Nano*, **2009**, *3*, 3861-3868.

48. Y. Yamaguchi, Y. Matsubara, T. Ochi, T. Wakamiya, Z. Yoshida, *J. Am. Chem. Soc*., **2008**, *130*, 13867-13869.
49. S. W. Thomas, G. D. Joly, T. M. Swager, *Chem. Rev*., **2007**, *107*, 1339-1386.
50.). Z. J. Donhauser, B. A. Mantooth, K. F. Kelly, L. A. Bumm, J. D. Monnell, J. J. Stapleton, D. W. Price, A. M. Rawlett, D. L. Allara, J. M. Tour, P. S. Weiss, *Science*, **2001**, *292*, 2303-2307; b). G. K. Ramachandran, T. J. Hopson, A. M. Rawlett, L. A. Nagahara, A. Primak, S. M. Lindsay, *Science*, **2003**, *300*, 1413-1416; c). P. A. Lewis, C. E. Inman, Y. X. Yao, J. M. Tour, J. E. Hutchison, P. S. Weiss, *J. Am. Chem. Soc*., **2005**, *127*, 17421-17426.
51. a) Y. M. Zhao, Y. Shirai, A. D. Slepkov, L. Cheng, L. B. Alemany, T. Sasaki, F. A. Hegmann, J. M. Tour, *Chem. Eur. J*., **2005**, *11*, 3643-3658; b) B. Babgi, L. Rigamonti, M. P. Cifuentes, T. C. Corkery, M. D. Randles, T. Schwich, S. Petrie, R. Stranger, A. Teshome, I. Asselberghs, K. Clays, M. Samoc, M. G. Humphrey, *J. Am. Chem. Soc*., **2009**, *131*, 10293-10307.
52. a). J. M. Tour, A. M. Rawlett, M. Kozaki, Y. X. Yao, R. C. Jagessar, S. M. Dirk, D. W. Price, M. A. Reed, C. W. Zhou, J. Chen, W. Y. Wang, I. Campbell, *Chem. Eur. J*., **2001**, *7*, 5118-5134; b). J. M. Tour, L. Cheng, D. P. Nackashi, Y. Yao, A. K. Flatt, S. K. S. Angelo, T. E. Mallouk, P. D. Franzon, *J. Am. Chem. Soc*., **2003**, *125*, 13279-13283; c). P. A. Lewis, C. E. Inman, Y. Yao, J. M. Tour, J. E. Hutchison, P. S. Weiss, *J. Am. Chem. Soc*., **2004**, *126*, 12214-12215; d). C. D. Zangmeister, S. W. Robey, R. D. van Zee, Y. Yao, J. M. Tour, *J. Am. Chem. Soc.*, **2004**, *126*, 3420-3421; e). C. Wang, A. S. Batsanov, M. R. Bryce, *J. Org. Chem.*, **2006**, *71*, 108-116.
53. X. Xiao, L. A. Nagahara, A. M. Rawlett, N. Tao, *J. Am. Chem. Soc*., **2005**, *127*, 9235-9240.
54. A. M. Moore, A. A. Dameron, B. A. Mantooth, R. K. Smith, D. J. Fuchs, J. W. Ciszek, F. Maya, Y. X. Yao, J. M. Tour, P. S. Weiss, *J. Am. Chem. Soc*., **2006**, *128*, 1959-1967.
55. a). C. Godard, C. Lepetit, R. Chauvin, *Chem. Commun*. **2000**, 1833-1834; b) C. Lepetit, C. Godard, R. Chauvin, *New J. Chem*., **2001**, *25*, 572-580; c) C. Lepetit, B. Silvi, R. Chauvin, *J. Phys. Chem. A* **2003**, *107*, 464-473; d). R. Chauvin, C. Lepetit, V. Maraval, L. Leroyer, *Pure Appl. Chem*., **2010**, *82*, 769-800.
56. a). A. Rives, I. Baglai, V. Malytskyi, V. Maraval, N. Saffon-Merceron, Z. Voitenko, R. Chauvin, *Chem. Commun*., **2012**, *48*, 8763-8765; b). Z. Li, M. Smeu, A. Rives, V. Maraval, R. Chauvin, M. A. Ratner, E. Borguet, *Nat. Commun.*, **2015**, *6*, 6321-6329.
57. C. Zhu, A. Poater, C. Duhayon, B. Kauffmann, A. Saquet, V. Maraval, R. Chauvin, *manuscript en cours de préparation*.
58. Pour des exemples récents, voir: a) S. Ramsaywack, S. Karaca, M. Gholami, A. H. Murray, F. Hampel, R. McDonald, N. Elmaci, H. P. Lüthi, R. R. Tykwinski, *J. Org. Chem*., **2014**, *79*, 10013-10029; b) M. Desroches, J.-F. Morin, *RSC Adv.*, **2017**, *7*, 17117-17121; c) N. Takahashi, S.-i. Kato, M. Yamaji, M. Ueno, R. Iwabuchi, Y. Shimizu, M. Nitani, Y. Ie, Y. Aso, T. Yamanobe, H. Uehara, Y. Nakamura, *J. Org. Chem*., **2017**, *82*, 8882-8896.
59. H. E. Zimmerman, R. M. Paufler, *J. Am. Chem. Soc*., **1960**, *82*, 1514-1515.
60. a). C. G. Krespan, B. C. McKusick, T. L. Cairns, *J. Am. Chem. Soc.*, **1961**, *83*, 3428-3432; b). R. G. Miller, M. Stiles, *J. Am. Chem. Soc.*, **1963**, *85*, 1798-1800; c). H. E. Zimmerman, G. L. Grunewald, R. M. Paufler, M. A. Sherwin, *J. Am. Chem. Soc.*, **1969**, *91*, 2330-2338; d). M.

W. Wagaman, E. Bellmann, M. Cucullu, R. H. Grubbs, *J. Org. Chem.*, **1997**, *62*, 9076-9082; e). M. W. Wagaman, R. H. Grubbs, *Macromolecules*, **1997**, *30*, 3978-3985.
61. a). M. A. Esteruelas, L. A. Oro, *Coord. Chem. Rev*., **1999**, *193-195*, 557-618; b). T. Nishimura, T. Kawamoto, M. Nagaosa, H. Kumamoto, T. Hayashi, *Angew. Chem. Int. Ed*., **2010**, *49*, 1638-1641; c). R. Shintani, M. Takeda, T. Nishimura, T. Hayashi, *Angew. Chem. Int. Ed.*, **2010**, *49*, 3969-3971; d) M. Schlesinger, M. Hofmann, T. Rüffer, D. Schaarschmidt, H. Lang, S. Theilacker, M. Schürmann, K. Jurkschat, M. Mehring, *Eur. J. Inorg. Chem.*, **2013**, 2930-2939.
62. H. E. Zimmerman, D. Armesto, *Chem. Rev.*, **1996**, *96*, 3065-3112.
63. a). D. J. Cram, *Nature*, **1992**, *356*, 29-36; b). M. Frank, M. D. Johnstone, G. H. Clever, *Chem. Eur. J.*, **2016**, *22*, 14104-14125.
64. a). D. Fiedler, R. G. Bergman, K. N. Raymond, *Angew. Chem. Int. Ed.*, **2006**, *45*, 745-748; b). A. Galan, P. Ballester, *Chem. Soc. Rev*., **2016**, *45*, 1720-1737.
65. a). F. Vögtle, W. M. Müller, U. Werner, H. W Losensky, *Angew. Chem. Int. Ed. Engl.*, **1987**, *26*, 901-903; b). D. Fiedler, D. H. Leung, R. G. Bergman, K. N. Raymond, *Acc. Chem. Res.*, **2005**, *38*, 349-358; c). A. Bouchet, T. Brotin, M. Linares, H. Ågren, D. Cavagnat, T. Buffeteau, *J. Org. Chem.*, **2011**, *76*, 4178-4181; d). I. A. Riddell, M. M. J. Smulders, J. K. Clegg, J. R. Nitschke, *Chem. Commun*., **2011**, *47*, 457-459.
66. K. Wu, K. Li, Y. J. Hou, M. Pan, L. Y. Zhang, L. Chen, C. Y Su, *Nat. Commun*., **2016**, *7*, 10487.
67. W. Xiao, C. Hu, M. D. Ward, *Cryst. Growth Des.*, **2013**, *13*, 3197-3200.
68. a). V. Marcos, A. J. Stephens, J. Jaramillo-Garcia, A. L. Nussbaumer, S. L. Woltering, A. Valero, J. F. Lemonnier, I. J. Vitorica-Yrezabal, D. A. Leigh, *Science*, **2016**, *352*, 1555-1559; b). W. Cullen, M. C. Misuraca, C. A. Hunter, N. H. Williams, M. D. Ward, *Nat. Chem*., **2016**, *8*, 231-236; c). M. D. Levin, D. M. Kaphan, C. M. Hong, R. G. Bergman, K. N. Raymond, F. D. Toste, *J. Am. Chem. Soc*., **2016**, *138*, 9682-9693; d). P. Howlader, P. Das, E. Zangrando, P. S. Mukherjee, *J. Am. Chem. Soc*., **2016**, *138*, 1668-1676.
69. B. H. Northrop, Y. R. Zheng, C. H. I. Ki-Whan, P. J. Stang, *Acc. Chem. Res.*, **2009**, *42*, 1554-1563.
70. S. Kitagawa, R. Kitaura, S. I. Noro, *Angew. Chem*., **2004**, *116*, 2388-2430; *Angew. Chem. Int. Ed*., **2004**, *43*, 2334-2375.
71. a). A. P. Bisson, V. M. Lynch, M. K. C. Monahan, E. V. Anslyn, *Angew. Chem. Int. Ed. Engl*., **1997**, *36*, 2340-2342; b). K. E. Jelfs, X. Wu, M. Schmidtmann, J. T. A. Jones, J. E. Warren, D. J. Adams, A. I. Cooper, *Angew. Chem. Int. Ed.*, **2011**, *50*, 10653-10656.
72. a). A. P. Davis, *Org. Biomol. Chem*., **2009**, *7*, 3629-3638; b) S. Kubik, *Angew. Chem. Int. Ed*., **2009**, *48*, 1722-1725.
73. a). Y. Murata, M. Murata, K. Komatsu, *J. Am. Chem. Soc*., **2003**, *125*, 7152-7153; b). M. Murata, Y. Murata, K. Komatsu, *J. Am. Chem. Soc.*, **2006**, *128*, 8024-8033; c). G. C. Vougioukalakis, M. M. Roubelakis, M. Orfanopoulos, *Chem. Soc. Rev.*, **2010**, *39*, 817-844.
74. (a) C. Zhu, C. Duhayon, B. Kauffmann, A. Saquet, V. Maraval, R. Chauvin, *manuscript in preparation (in-template);* (b) C. Zhu, A. Saquet, X. Cui, V. Maraval, R. Chauvin, *manuscript in preparation (in-template).*

75. a). G. Likhtenshtein in Stilbenes: *Applications in Chemistry, Life Sciences and Materials Science*, Wiley-VCH, Weinheim, **2009**, pp. 159-188; b). For a recent reference see: b) M. Cao, X. Chen, K. Yi, D. Wei, *J. Phys. Chem. C,* **2017**, *5*, 9597-9601.
76. a). G. Likhtenshtein in Stilbenes: *Applications in Chemistry, Life Sciences and Materials Science*, Wiley-VCH, Weinheim, **2009**, pp. 189-223; b). Y. Wang, Y. Jiang, X. Fan, H. Tan, H. Zeng, Y. Wang, P. Chen, M. Huang, H. Bi, *Toxicol. Lett*., **2015**, *236*, 82-89.
77. a) A. Auffrant, B. Jaun, P. D. Jarowski, K. N. Houk, F. Diederich, *Chem. Eur. J.* **2004**, *10*, 2906-2911; b) P. D. Jarowski, F. Diederich, K. N. Houk, *J. Phys. Chem. A* **2006**, *110*, 7237-7246; c) V. Maraval, L. Leroyer, A. Harano, C. Barthes, A. Saquet, C. Duhayon, T. Shinmyozu, R. Chauvin, *Chem. Eur. J.* **2011**, *17*, 5086-5100; d) P. Gawel, Y.-L. Wu, A. D. Finke, N. Trapp, M. Zalibera, C. Boudon, J.-P. Gisselbrecht, W. B. Schweizer, G. Gescheidt, F. Diederich, *Chem. Eur. J*. **2015**, *21*, 6215-6225.

Résumé

Le manuscrit est divisé en six chapitres et deux parties indépendantes, la première étant consacrée à l'étude de l'effet de substituants nitro sur des ligands phosphines aromatiques (L). Une série de (N-phényl-benzimidazol-1-yl)diphénylphosphines substituées par 1 à 3 groupes nitro à différentes positions des noyaux N-phényle et benzimidazolyle, a été synthétisée, et comparée au parent non nitré et à l'homologue N-méthyl-benzimidazolium cationique. Dans les complexes trans-$L_2Rh^{I}Cl(CO)$ correspondants, des variations faibles mais systématiques de la fréquence d'élongation C=O IR et du déplacement chimique RMN ^{103}Rh fournissent une quantification empirique des effets régio-spécifiques des substituants nitro sur le caractère donneur global du ligand. Les produits secondaires dinucléaires $(\mu\text{-CO})(LRhCl)_2$ donnent des cristaux de clathrate uniques à teneur élevée (6,7:1) en solvate de dichlorométhane.

La deuxième partie, regroupant cinq chapitres, concerne l'étude de nouveaux types de *carbo*-mères fortement π-conjugués, principalement conçus pour pallier la faible solubilité limitante du noyau *carbo*-benzène. La synthèse et la caractérisation des hexaaryl-*carbo*-benzènes de référence sont revisitées. Une voie de synthèse en 12 étapes améliorée du dérivé hexaphényle connu et de l'homologue *p*-bis-3,5-di-*tert*-butylphényle est décrite. Les deux *carbo*-benzènes ont été entièrement caractérisés, en particulier par analyse par diffraction des rayons X et par électrochimie. Leur utilisation dans les cellules solaires photovoltaïques organiques s'est avérée freinée par leur faible solubilité empêchant la formation de couches minces de haute qualité.

Le troisième chapitre porte sur une série de *p*-dialkyl-tétraphényl-*carbo*-benzènes à deux chaînes aliphatiques $R = C_nH_{2n+1}$, n = 2, 4, 8, 14, 20. Leur synthèse basée sur l'addition nucléophile de RMgBr sur la [6]péricyclynedione clé conduit à la fois aux dialkyl- et mono-alkyl-*carbo*-benzènes réduits, le processus de réduction étant supprimé en utilisant un réactif $RLi/CeCl_3$. Une augmentation spectaculaire de la solubilité dans les solvants chlorés a été observée pour $n \geq 8$. Un empilement π-π direct des cycles en C_{18}, guidé par les forces de dispersions aliphatiques, a été montré pour la première fois dans la structure cristalline du dérivé bis-tétradécyle, appuyant l'existence de l'allotrope du carbone 3D α-graphityne (*carbo*-mère putatif du graphite).

Le quatrième chapitre décrit deux trialkoxyaryléthynyl-tétraphényl-*carbo*-benzènes et l'étude des propriétés mésogènes de l'un d'entre eux. Une mésophase rectangulaire colonnaire, mise en évidence à 115 °C par des analyses DSC, POM et PXRD, ouvre des perspectives pour une étude systématique des cristaux liquides apparentés. Les constantes du réseau 3D sont cohérentes avec les images STM 2D du *carbo*-mésogène sur HOPG.

Le cinquième chapitre décrit trois *carbo*-mères de squelette de bis- et ter-phényles, conçus pour leur relation aux fils moléculaires OPP ou OPE. Un *carbo*-terphényle a montré un très faible potentiel de réduction (-0,39 V/SCE), sans précédent en série *carbo*-mère.

Dans le dernier chapitre, de nouveaux types de *carbo*-mères sont illustrés: les *carbo*-barrélènes et les *carbo*-stilbènes. Leur préparation repose sur l'addition de triyne dinucléophiles sur un ou deux équivalents d'un précurseur [6]péricyclyne(di)one. Dans la série tricyclique, deux *carbo*-barrélènes non macro-aromatiques et un dérivé bis-butatriénique partiellement réduit, se sont révélés suffisamment stables pour permettre une caractérisation complète, y compris par cristallographie. Le rôle de cage d'un *carbo*-barrélène vis-à-vis de petites molécules telles que NH_4^+, même si elle n'a pas encore été clairement établie, a été étudiée théoriquement et expérimentalement. Les *carbo*-stilbènes ont été obtenus sous forme de mélanges. En l'absence d'analyse cristallographique, ils ont été attribués aux diastéréoisomères *cis* et *trans* sur la base de la spectroscopie RMN ^{1}H et des calculs DFT.

Mots clés: ligands phosphine nitroaromatiques, [6]péricyclynes, *carbo*-benzènes aliphatiques, cristaux liquides, *carbo*-barrélène, *carbo*-stilbène, *carbo*-oligo-phénylène(éthynylènes)

Abstract

The manuscript is divided into six chapters and two independent parts, the first part being dedicated to the investigation of the effect of nitro substituents on aromatic phosphine ligands (L). A series of (*N*-phenyl-benzimidazol-1-yl)diphenylphosphines substituted with 1 to 3 nitro groups at different positions of the N-phenyl and benzimidazolyl cores, were synthesized, and compared with the non-nitrated parent and cationic N-methyl-benzimidazolium counterpart. In the corresponding *trans*-$L_2Rh^{I}Cl(CO)$ complexes, prepared in two steps and fully characterized, moderate but systematic variations of the C=O IR stretching frequency and ^{103}Rh NMR chemical shift provide an empirical quantification of regio-specific effects of the nitro-substituents on the global donating character of the P-ligand. Dinuclear $(\mu\text{-CO})(LRhCl)_2$ side-products were shown to give unique clathrate crystals with a high content (6.7:1) of dichloromethane solvate.

The second part, gathering five chapters, concerns the study of new types of highly π-conjugated *carbo*-mers, primarily devised to palliate the limiting poor solubility of the aromatic C_{18} *carbo*-benzene core. The synthesis and characterization of reference hexaaryl-*carbo*-benzenes are revisited. An improved 12-step synthetic route to the long known hexaphenyl derivative and *p*-bis-3,5-di-*tert*-butylphenyl homologue is described. Both *carbo*-benzenes were fully characterized, in particular by X-ray diffraction analysis and electrochemistry. Their use in organic photovoltaic solar-cells was found to be hampered by their very low solubility preventing the formation of high quality thin films.

The third chapter focusses on a series of *p*-dialkyl-tetraphenyl-*carbo*-benzenes with two aliphatic chains $R = C_nH_{2n+1}$, n = 2, 4, 8, 14, 20. The synthetic route based on nucleophilic addition of RMgBr to a key [6]pericyclynedione ultimately led to both the dialkyl- and reduced mono-alkyl-*carbo*-benzenes, the reduction process being found suppressed by using a $RLi/CeCl_3$ reactant. A dramatic enhancement of solubility in chlorinated solvents was observed for $n \geq 8$. A direct π-π stacking of C_{18} rings, driven by aliphatic dispersions forces, could be evidenced for the first time in the X-ray crystal structure of the bis-tetradecyl derivative, giving experimental support to the existence of the α-graphityne 3D carbon allotrope (putative *carbo*-mer of graphite).

The fourth chapter describes two trialkoxyarylethynyl-tetraphenyl-*carbo*-benzenes and the study of the mesogen properties of one of them. A columnar rectangular mesophase, evidenced at 115 ^{o}C by DSC, POM and PXRD analyses, opens prospects for a systematic study of related liquid crystals. The 3D lattice constants are consistent with 2D STM images of the *carbo*-mesogen deposited on HOPG.

The fifth chapter reports on three skeletal *carbo*-mers of bis- and ter-phenyls, devised for their acquaintance with OPP or OPE molecular wires. A *carbo*-terphenyl was found to exhibit a very low first reduction potential (-0.39 V/SCE), unprecedented in the *carbo*-mer series.

In the last chapter, new types of *carbo*-mers are exemplified: *carbo*-barrelenes and *carbo*-stilbenes. Their preparation relies on the addition of triyne dinucleophiles to either one or two equivalents of a [6]pericyclyne(di)one precursor. In the tricyclic series, two non-macroaromatic *carbo*-barrelenes and one partially reduced bis-butatrienic derivative, both containing two sp^3-C bridgeheads, were found to be sufficiently stable to allow full characterization, including by crystallography. The cage-ability of a *carbo*-barrelene toward small molecules such as NH_4^+, albeit not clearly proven yet, was investigated both theoretically and experimentally. The *carbo*-stilbene product was evidenced as an unseparated mixture of two isomers. In the absence of crystal of suitable quality for crystallography, they were assigned to the *cis* and *trans* diastereoisomers on the basis of ^{1}H NMR spectroscopy and DFT calculations.

Key words: nitroaromatic phosphine ligands, [6]pericyclynes, aliphatic *carbo*-benzenes, liquid crystals, *carbo*-barrelene, *carbo*-stilbene, *carbo*-oligo-phenylene(ethynylenes)